DOE/ER/13000--T10

STANFORD SYNCHROTRON RADIATION LABORATORY

DISCLAIMER

ACTIVITY REPORT FOR 1986

DISTRIBUTION OF THIS DOCUMENT IS UNLIMITED

ABOUT THE STANFORD SYNCHROTRON RADIATION LABORATORY

SSRL is a national facility supported primarily by the Department of Energy for the utilization of synchrotron radiation for basic and applied research in the natural sciences and engineering. It is a user-oriented facility which welcomes proposals for experiments from all qualified scientists.

The synchrotron radiation is produced by the 4 GeV storage ring, SPEAR, and the 18 GeV storage ring, PEP, operated by the Stanford Linear Accelerator Center (SLAC). SPEAR is dedicated to the production of synchrotron radiation during 50% of its operations time or about 4 months per year. The remainder of the time synchrotron radiation may be used parasitically during colliding beam runs for high energy physics experiments. Operation on PEP is entirely parasitic.

SSRL currently has 22 experimental stations with 5 more on SPEAR and one more on PEP proposed to be built within the next three to four years. There are 137 active proposals for experimental work from 101 institutions involving approximately 550 scientists. There is normally no charge for use of the facility by experimenters.

Additional information for prospective users is contained in the booklet "SSRL Proposal Guidelines and General Information". This booklet and further information about the facility may be obtained by writing or telephoning Katherine Cantwell at SSRL, SLAC Bin 69, P.O. Box 4349, Stanford, CA 94305 - telephone (415) 854-3300 ext. 3191.

This report summarizes the activity at SSRL for the period January 1, 1986 to December 31, 1986.

SSRL is supported by the Department of Energy, Office of Basic Energy Sciences: and the National Institutes of Health, Biotechnology Resource Program, Division of Research Resource.

TABLE OF CONTENTS

**A separate index for this section starts on page 41*

RESEARCH ACTIVITIES

VUV and Soft X-ray

Vacuum ultra-violet and soft x-ray information on the bonding and orientation of molecules chemisorbed on single crystal metal surfaces can be obtained by the NEXAFS (Near Edge X-Ray Absorption Fine Structure) using the polarization properties of synchrotron radiation. Major advances have been made with this approach and simple molecules, as well as more complex hydrocarbons (carboxylic acids and alcohols), have now been studied, opening access to the field of surface researchers (*801Vp, 1023Vp*).

The electronic and structural properties of metal/semiconductor interfaces and heterostructures have continued to to be the subject of intense efforts. MBE-grown (Molecular Beam Epitaxy) device structures are becoming increasingly important for technological applications. Last year, electronic and atomic properties of the GaAs on Si interface was examined in detail using surface sensitive core-level spectroscopies. The detailed bonding between Ga/As and Si was explored (*908Vp*). Similar detailed studies of Si/GaAs(110) (*935Vp*), Si/GaAs(100) (*959Vp*), CaF_2/Si(111) (*958V*) and Ge/InP(110) (*935Vp*) were performed. The atomic-scale investigations of these and other heterojunctions are making rapid progress. Last year also saw the completion of the first energy-mapping (electron energy vs momentum relations) of strained superlattices (*Letter of Intent Hwang et al*). It also became possible to study the structural arrangement of dopant material in semiconductors by using fluorescence EXAFS (*1013Vp*). The interfacial chemistry and metallurgy of metal/semiconductor systems and their relation to, for instance, Schottky barriers, have been extended to ultralow coverages, 10^{-4} monolayers, as well as including comparisons to bulk standards (*935Vp, 941Vp*). Progress has been excellent in the work on photoelectron spectroscopic studies of metal ion sites for systems which are of interest in catalysis, in particular the role of Cu in ZnO as a methanol synthesis catalyst (*733Vp*).

The localization problem of the 4f (5f) electrons in the lanthanides (actinides) and its relation to the Kondo effect, superconductivity and spin density waves has been studied for many years at SSRL. Last year, resonant photoemission was applied for a heavy-Fermion material, URu_2Si_2, where low temperature data shows a competition between superconductivity and spin density waves (*682Vp*). The 5f spectral weight was also studied in very dilute (2%) uranium-containing metals (also heavy-Fermions). It was inferred from these results that single-site effects, and not lattice interactions, dominate the spectra even for concentrated systems (*1028Vp*).

The basic photoionization process, in particular phenomena for excitation energies close to ionization thresholds, has received continued interest. The energy dependence of the intensity for shake-off peaks and other satellite structures have been examined for low kinetic energy electrons (*943Vp*). Further work has also been preformed in understanding solid state effects in photoionization cross sections (*936V*).

Biotechnology

The past year has been a particularly active one for the Biotechnology Division of the laboratory as reflected in the 26 activity reports in this area. There have been two notable achievements in macromolecular crystallography. In work on the rotation camera (*1A32*), a striking observation was made with regard to crystal lifetimes. In studies of crystalline ribosomal subunits, it was observed that when the crystals were cooled to around 85 K, the lifetime in the beam increased from minutes to many hours enabling excellent data to be collected. The area detector was used to collect data on a biotin complex of streptavidin (*Letter of Intent, Hendrickson et al*) where sulfur in the biotin had been replaced by selenium. Using multiple wavelength anomalous dispersion phasing methods, the selenium atom locations in the electron density map were very dominant and easy to identify. A fully interpretable electron density is expected to follow soon.

Molecular structure at a somewhat lower resolution is being successfully studied by small angle x-ray scattering. Studies of the muscle calcium binding protein, troponin-C, (*852B*) revealed a calcium dependent dimerization of the molecule in solution. Using anomalous small angle x-ray diffraction, details of the electron density and terbium binding site of bacteriorhodopsin were revealed (*1005B*).

INTRODUCTION

FACILITY DEVELOPMENT

1986 was another year of major advances for SSRL as the ultimate capabilities of PEP as a synchrotron radiation source became more apparent and a second PEP beam line was initiated, while effective development and utilization of SPEAR proceeded.

In one day of experimentation, a low emittance operating mode was implemented on PEP and a beam emittance of 120 Å-rad was measured. This corresponds to 67.5 Å-rad at 6 GeV, which is approximately equal to that expected for the Advanced Photon Source (APS) to be constructed at Argonne National Laboratory. Thus, the feasibility of initiating high brilliance experiments immediately on PEP and paving the way for the APS became apparent. Indeed, approximately two weeks of parasitic experimentation using the undulator beam line on PEP demonstrated the effectiveness of high brilliance radiation for high energy resolution inelastic x-ray scattering and for grazing incidence scattering studies of thin amorphous layers.

Subsequently, theoretical studies indicated that it should be possible to reduce PEP's beam emittance gradually to values as low as 5 to 7 Å-rad under operating conditions that allow sufficiently long beam lifetimes. Thus, PEP could bring us, in an evolutionary manner, directly into the operating regime of the generation of storage rings to follow the Advanced Photon Source. These PEP developments have served to define SSRL's anticipated role over the next decade in which the APS and the ALS are being constructed and commissioned.

A major disappointment for SSRL and its users was the news that PEP would not run during fiscal year 1987. Thus, over a year was lost in the exploitation of its unique capabilities. This down time is being used, however, to construct a second beam line, PBL 1B, which will be completed in the summer of 1987 and which also contains a two meter undulator. SSRL does expect both parasitic and dedicated running of PEP in fiscal year 1988.

Given these various PEP developments, SSRL abandoned its plans for a separate diffraction limited ring, as we abandoned our plans for a 6-7 GeV ring of the APS type last year. It has become increasingly apparent that SSRL should concentrate on developing SPEAR and PEP as synchrotron radiation sources. Consequently, initial planning for a 3 GeV booster synchrotron injector for SPEAR was performed in 1986, with a proposal to the Department of Energy resulting. Support for this construction came in the President's fiscal year 1988 budget. We are hopeful that Congress will appropriate the funds for the injector.

As described in Chapter II, the New Rings Group and the Machine Physics Group were combined into one Accelerator Physics Group. This group is focussing mainly on the improvement of SPEAR's operating conditions and on planning for the conversion of PEP into a fourth generation x-ray source. Considerable emphasis is also being given to the training of accelerator physics graduate students. At the same time, several improvements of SSRL's existing facilities were made. These are described in Chapter III.

Chapter IV describes new SSRL beam lines being commissioned. These include the VUV branch of Beam Line VIII, the 18 degree line branch of Beam Line III and Beam Line V.

Chapter V discusses SSRL's present construction projects. These include the second beam line on PEP, the Laboratory-Office-Shop (LOS) building, Beam Line X and, the VUV branch line on the 54 pole Wiggler Beam Line VI.

Chapter VI discusses a number of projects presently underway in the engineering division. These include the beam line control systems, the development of a beam line and storage ring status monitoring system, photon beam steering and stabilization systems, the angiography personnel protection interlock system, portions of the booster synchrotron injector for SPEAR, an in-vacuum hard x-ray monochromator, several thermal-structural analyses and beryllium window studies.

Chapter VII describes SSRL's advisory panels while Chapter VIII discusses SSRL's overall organization.

Important information continues to be obtained from x-ray absorption spectroscopy studies, particularly about metals in biological systems that have previously received little attention. Studies of the manganese and iron atoms in the plant photosynthetic system (*840Bp and LBL-PRT*) revealed the presence of a mu-oxo manganese dimer complex and provided information about the structure of Fe-S clusters. Structrual information has been obtained on technetium and rhenium imaging agents and therapeutic radiopharmaceuticals (*922Bp*) as well as gold-based drugs used in the treatment of rheumatoid arthritis (*922Bp*). The role of nickel in biological systems is also beginning to receive attention (*969Bp*).

X-ray and Materials

Rapid advances in many research areas were reported in 1986, utilizing a wide variety of x-ray techniques at SSRL, broadly grouped about the phenomena of x-ray scattering and x-ray absorption. The intrinsic brilliance of synchrotron radiation beams has engendered strong programs in small angle scattering, grazing incidence surface diffraction, and high angular resolution scattering. The broadband spectrum of the radiation has led to continued advances in edge and extended x-ray absorption fine structure, and to imaging studies of microscopic (tomography) and macroscopic (angiography) subjects.

Utilizing grazing incidence surface scattering, the Si-SiO_2 interface as been probed, to elucidate the structure of the boundary layer in this technologically important material (*743Mp*). Clear evidence for SiO_2 microcrystallites was observed with the α-cristobalite structure, under several distinct preparation techniques. In a similar study (*996M*), the Si(111)/a-Si interface was studied, by collecting a large set (70) of surface scattering structure factors to accurately unfold the surface reconstruction. A preliminary analysis of the data gives evidence of specific stacking faults occurring at the interface region.

High resolution x-ray scattering has been applied to lyotropic liquid crystals, to further elucidate the rich critical phenomena associated with mutlicomponent systems. In particular, the evolution of the correlation lengths above the nematic to lamellar phase transition in CsPFO and water were measured, and found to follow a power law divergence.

Progress in imaging techniques at x-ray wavelengths advanced rapidly in 1986. A computerized micro-tomography system (*979M*) has been developed, for non-destructive elemental and chemical-state characterization of small samples. Utilizing a thermoelectrically cooled CCD array detector, images at 20 micron resolution of test samples were made, and straightforward modifications to improve the resolution by a factor of 20 are in progress. In a related study (*LBL- PRT*), multilayer mirrors have been employed in a microprobe geometery that is capable of resolving picogram quantities of elements at 10 micron resolution, using exposure times of five minutes or less. This probe has been applied to elemental concentration profiles in algae and inclusions in mineral samples.

Extensive developments in the imaging system hardware have culminated in the first images of the coronary arterial system of human subjects with synchrotron radiation (*456Bp*). These developments consisted of an asymmetrically cut silicon monochromator; a new dual-drum x-ray beam chopper which allows scanning speeds at the rate of 12 cm/sec; a new subject support chair with four degrees of freedom; and a personnel protection system to insure the safe exposure of human patients in the synchrotron x-ray beam. These results led to the use this imaging system in May 1986 on three human subjects, each of whom was under treatment for coronary artery disease. Although greater x-ray fluence is needed to provide images of clinical quality, these preliminary images are encouraging. Improvements in the source characteristics and the detector are in progress, with a view toward eventually obtaining images of clinical quality.

- A. Bienenstock
Director

I REVIEW OF LABORATORY OPERATIONS

In 1986 SSRL had two dedicated runs. The first occurred in the spring, mid-April through the end of June. The second started in the fall, November 17, and continued, with a one week Christmas break, through Februray 7, 1987. For the most part information contained in this chapter reflects the run only through December 1986.

SSRL entered the SLC era in 1986. The SLAC Linear Collider Program (SLC) is a High Energy Physics Project aimed at producing head-on collisions between 50 GeV electron and 50 GeV positron beams. It is a single-pass device; i.e., the beams are not recirculated as in a storage ring. New collisions are produced at the repetition rate of the LINAC (up to 180 Hz). Closely spaced electron and positron bunches emerge from the SLAC 3 km LINAC at 50 GeV, after which they are separated and then bent in two independent arcs which bring the beams into head-on collisions. Future linear colliders are envisioned to have two LINACS firing the beams directly at each other.

The project involves major upgrade of the LINAC energy and control system, construction of the arcs, damping rings and a new positron source plus detectors. Various components of the overall system were being commissioned during 1986 and first collisions are expected in the spring of 1987.

The SLC project has placed severe manpower and budgetary constraints on SLAC. A consequence of this was the cancellation of the SPEAR high energy physics program in FY 1987. Hence there has been no "parasitic" time for synchrotron radiation research since 1984. Under normal circumstances SPEAR runs approximately eight months a year, four for high energy physics and four for synchrotron radiation research. Parasitic time is used by synchrotron radiation researchers for training new users and students, testing equipment and performing research, particularly in the VUV, which can utilize the lower energy and shorter lifetimes. Since high energy physics research is performed using a single bunch of electrons, SPEAR's timing characteristics can be used during this type of running. It is anticipated that SLAC will recommence the high energy physics program on SPEAR in October 1987.

A further consequence of the SLAC fiscal situation was that the high energy physics program on PEP was also terminated in March 1986. All synchrotron radiation experimentation on PEP at present is parasitic. The PEP shutdown occurred just after the first PEP beam line for synchrotron radiation (PEP 5B) was commissioned in February 1986. Two short experiments and a brief machine physics test were performed and are described elsewhere in this report. It is anticipated that the PEP program will recommence in October 1987.

The spring dedicated run had some initial difficulties due to poor vacuum. This resulted in short lifetimes and frequent need to "kick" the beam to allow ions to leave the beam area. As the run progressed conditions improved substantially. However, the last three weeks of the run were done in the timing mode (four equally spaced single bunches, rather than about 16 closely spaced bunches as used in normal operation).

The switch between the two modes again caused substantial lifetime and stability problems. Timing mode gives sufficient time in between pulses so that experiments relying on the time structure of the radiation can be performed. This mode is limited to 20% per year since smaller currents and lower lifetimes result. Timing mode in 1986 was run from June 12 to June 30.

To allow SLAC's program to convert the LINAC for SLC operation to progress as rapidly as possible during the fall of 1986, it injection into SPEAR for synchrotron radiation was limited to once every eight hours. Since this was SSRL's first experience running under conditions of limited injection, and due to the poor lifetimes which had been experienced the preceeding spring, it was anticipated that the run would be difficult. Scheduling in the pre-Christmas period was, for the most part, confined to local users and in-house research. In fact, soon after Thanksgiving, the lifetimes were so good that the fill pattern was changed to once every 12 hours. SSRL was beginning to experience some of the best running conditions ever, and this pattern continued until the end of the run. The run was characterized by good current (75-90 mA at injection) with lifetimes ranging from 15 to 20 hours at the start of the fill and up to 40 hours at the bottom of the fill. The current at the bottom of the fill was 25 to 40 mA. Someimes, because of the unavailability of the LINAC, SSRL operated as long as 30 hours on a single fill. The beam was very stable below 60 mA. Above this current beam noise affected some of the more sensitive users. The cooperation of our SLAC colleagues in making this run successul, despite the difficulties under which they were laboring, was great and appreciated.

Limited injection resulted in a decision not to run timing mode during the fall-winter run. Similarly, this injection pattern affected the type of machine physics which could be performed. (See Accelerator Physics chapter.)

The marked improvement in SPEAR performance is partially a result of effective SPEAR management. In the summer of 1986 a detailed cleanup was made of the SPEAR software and many small problems on the ring itself. In addition, an RF cavity structure intended to raise the shunt impedance of the ring had been placed in the ring between the fall 1985 and spring 1986 runs. This device was a major cause of the poor lifetimes experienced in the spring. It was removed before the fall 1986 run.

OPERATIONS DIVISION ACTIVITIES

In 1986, the activities of the Operations Division were, as always, quite varied. During the runs, of course, the activities center around supporting users and ensuring the smooth operation of the beam lines and experimental stations. During shutdowns, the group's activities shift to construcion and maintenance. The increase in construction activities that SSRL has been experiencing over the past few years has allowed the Operations Division to take on more project related responsibilities. In general, a construction project is managed by the Engineering Division while the installation is the responsibility of the Operations Division. By careful planning and suitable expansions in staff, SSRL has, in some cases, been able to assign both shift operators and vacuum technicians to a construction project until its completion.

During the past year, the Operations Division has participated in the construction of a number of beam and branch lines, such as, PEP 5B, PEP 1B, Beam Line V, Beam Line VII, the 18 degree line, and the Beam Line I TGM. In addition, beam line upgrades and routine maintenance are continous. The Operations Division is also responsible for the SSRL large mirror coating facility which has been in operation for several years. During the past year, SSRL has been routinely coating mirrors up to 1 meter in length for the SSRL beam lines as well as for a limited number of outside laboratories which include Frascati, Los Alamos National Lab, and AT&T Bell Labs (the latter two mirrors were for use at NSLS). Finally, the Operations Division has been given the responsibility for plant maintenance and upgrades. Upgrade projects this past year have included a new parking lot and installation of a large liquid nitrogen storage facility.

BEAM AND SPEAR USAGE TABLES

The following tables and graphs contain statistics on SPEAR running, experimental use and characteristics of SSRL stations. For earlier information, consult previous Activity Reports.

Table 1 (and the accompanying graph) show the number of dedicated SPEAR shifts scheduled and delivered since dedicated running commenced in 1979.

Tables 2 and 3 and the accompanying graph illustrate the use of beam at SSRL for experimental purposes.

Table 4 lists the characteristics of the 22 SSRL experimental stations. Table 5 shows the number of shifts requested versus the number of shifts actually assigned for dedicated time.

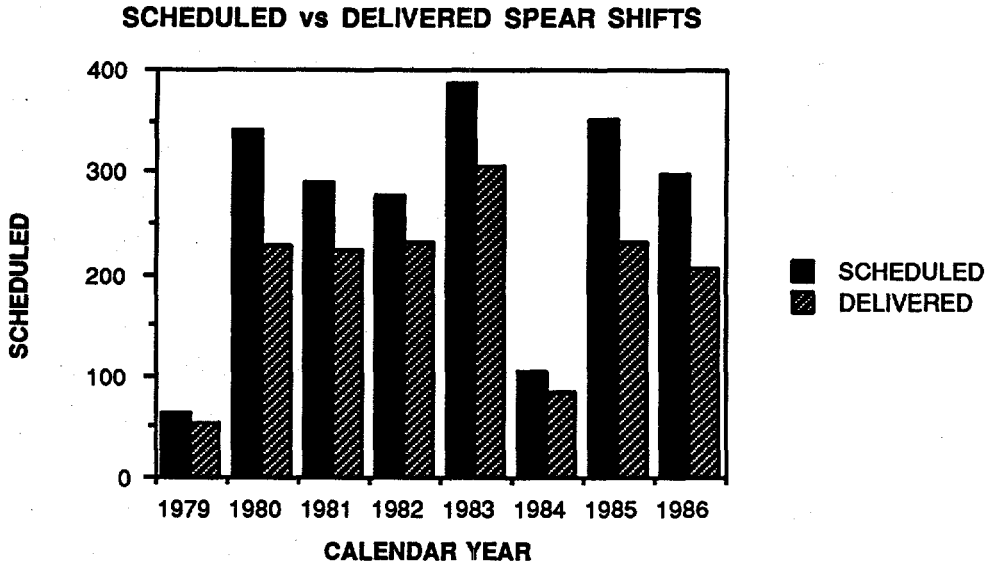

Table 1

Table 1 shows the history of dedicated time at SSRL/SPEAR since its inception in 1979. Delivered SPEAR beams have range from 44% to 85% over the 22 SSRL dedicated runs with an average delivery of 71%. While the delivery rate for the fall of 1986 was average, the quality of the delivered beam was very high.

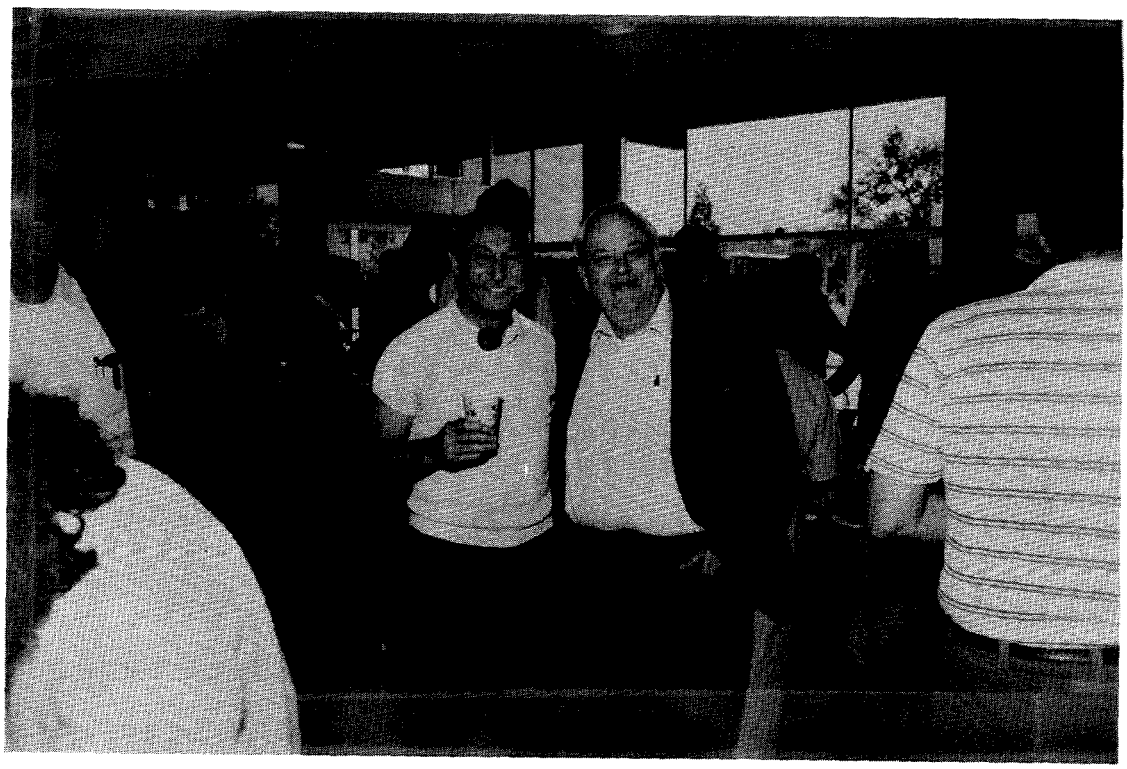

Photo by A. Waldhauer

In April 1986 SSRL and SLAC jointly marked the occasion of Axel Golde's retirement. Axel joined the SLAC staff 25 years ago, transferring to SSRL as one of its original employees. Axel (left) is pictured with Burton Richter, the SLAC Director, at his retirement reception.

TABLE 1

BEAM TIME STATISTICS/DEDICATED TIME

DEDICATED RUN	Scheduled Hours	Delivered Hours	%Del
10/20 to 11/05/79	152	95.3	62%
12/03 to 12/21/79	352	299.4	85%
02/08 to 03/05/80	472	366.3	77%
04/16 to 05/19/80	764	588.2	76%
06/30 to 07/30/80	726	320.4	44%
09/29 to 10/14/80	336	194.9	58%
12/02 to 12/22/80	440	309	70%
01/26 to 03/03/81	792	600.9	76%
05/16 to 06/30/81	988	727	73%
11/18 to 12/21/81	546	363.6	66%
01/8/ to 02/22/82	748	612.5	81%
03/09 to 04/26/82	995	830.9	83%
10/15 to 11/05/82	473	316	66%
12/27 to 02/22/83	1050	825.6	78%
05/09 to 06/30/83	1195	960.3	80%
11/07 to 12/23/83	857	662.8	77%
03/21 to 04/30/84	835	674.3	80%
01/10 to 02/21/85	905	606.6	67%
03/15 to 07/22/85	1502	1056.5	70%
10/14 to 11/11/85	416	203.7	48%
04/11 to 06/30/86	1550	1106.5	71%
11/17 to 12/24/86	752	527	70%

TABLE 2

In 1986 2660 8-hour user-shifts were actually used by experimenters for data taking. Approximately another 20% were used for machine physics studies and beam line check out between experimenters. A total of 303 additional user-shifts were used by SSRL staff and collaborators for facility characterization. In general facility time is used for the upgrading and commissioning of new or modified experimental stations. In 1986 this was the case for stations I-2, V-2 and VIII-2. In addition, facility time is used for continuing developmental studies such as section topography on II-4 and multilayer monochromators on III-4. In the fall run station II-3 was used exclusively for facility development projects (see Chapter III).

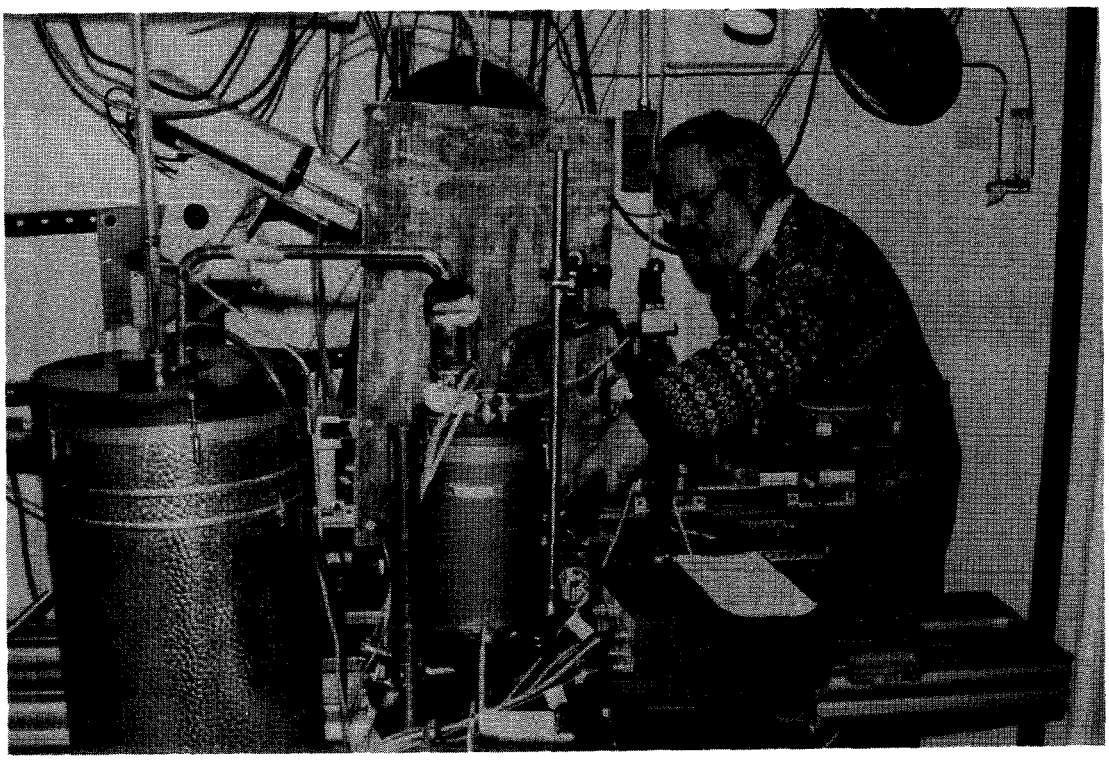

Photo by H. Winick

Hakon Hope (UC Davis) adjusting a liquid nitrogen cryostat beside the rotation camera on BL VII-1. He, in collaboration with other protein crystallographers led by Ada Yonath (Weizmann Institute), successfully collected crystallographic data from a large ribosomal subunit at approximately 85° K.

TABLE 2

USER SHIFTS BY EXPERIMENTAL STATION
Calendar 1986

Experimental Station	04/11/86 06/30/86 Dedicated		11/17/86 12/24/86 Dedicated		Total Shifts per Station	
Beam Line I						
I-1	134		53		187	
I-2	135	(14)**	under development		135	(14)
I-4	41	(25)		(12)	41	(37)
I-5	130		41		171	
Beam Line II						
II-2	129		43		172	
II-3	101			(50)	101	(50)
II-4	132		20	(23)	152	(23)
Beam Line III						
III-1	131		60		191	
III-3	134		53	(6)	187	(6)
III-4	80			(40)	80	(40)
Beam Line IV						
IV-1	124		50		174	
IV-2	108	(8)	54		162	(8)
IV-3	135		65		200	
Beam Line V						
V-2		(90)	under development			(90)
Beam Line VI						
VI-2	130		46		176	
Beam Line VII						
VII-1	117		50	(5)	167	(5)
VII-2	130		51		181	
VII-3	127	(10)	50		177	(10)
Beam Line VIII						
VIII-2	under construction		6	(20)	6	(20)
	TOTALS - Dedicated Running					
	2018 (147)		642 (156)		2660(303)	
PEP 5B Lifetimes Port	8* not used					

**Parasitic Running, February 1986*
***( )= Facility Characterization Shifts*

TABLE 3

SUMMARY of Shifts Used for SSRL Experiments
CALENDAR 1986

RUN PERIODS	04/11/86 to 06/30/86	11/17/86 to 12/24/86	TOTALS for PERIODS
User Shifts (Dedicated)	2018	642	2662
Proposals Run (Dedicated)	115	52	167
Users/Shifts (Dedicated)	14.6	9.4	12.9

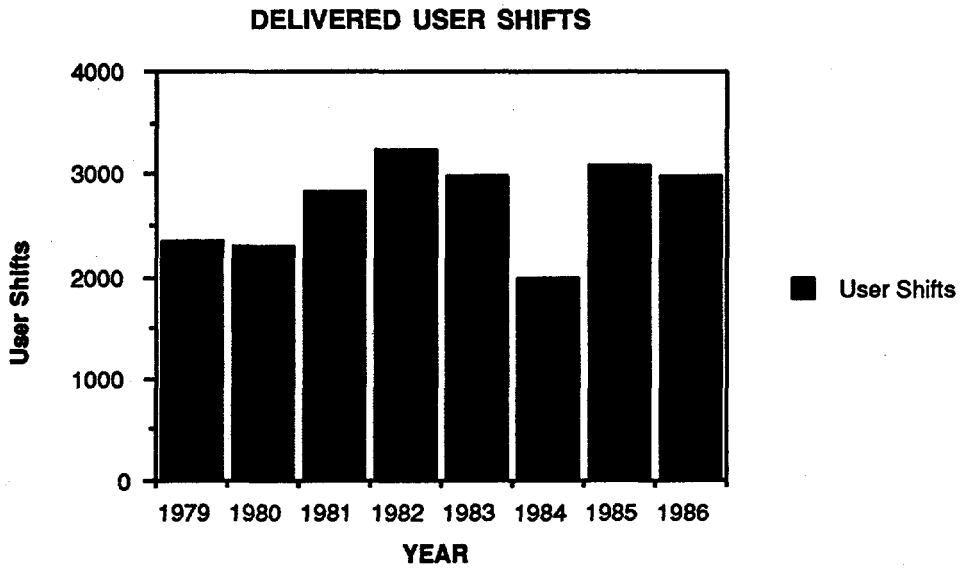

CHARACTERISTICS OF SSRL EXPERIMENTAL STATIONS

TABLE 4

SSRL presently has 22 experimental stations 21 of which are located on SPEAR and one on PEP. Nine of these stations are based on insertion devices while the remainder use bending magnet radiation.

	Horizontal Angular Acceptance (Mrad)	Mirror CutOff (KeV)	Monochromator	Energy Range (eV)	Resolution Δ/E	Approximate Spot Size HgtxWdth	Dedicated Instrumenation (mm)
INSERTION DEVICE STATIONS							
WIGGLER LINES - X-RAY							
End Stations							
IV-2 (8 pole)							
Focused	4.6	10.2	Double Crystal	2800-10200	-5×10^{-4}	2 x 6	
Unfocused	1.0	-	Double Crystal	2800-45000	-10^{-4}	2.0 x 20.0	
VI-2 (54 pole)							
Focused	2.3	22	Double Crystal	2800-21000	-5×10^{-4}	2.0 x 6.0	
Unfocused	1.0	-	Double Crystal	2800-45000	-10^{-4}	2.0 x 20.0	
VII-2 (8 pole)							Six-circle Diffractometer
Focused	4.6	10.2	Double Crystal	2800-10200	-5×10^{-4}	2 x 6	
Side Stations							
IV-1	1.0	-	Double Crystal	2800-45000	-5×10^{-4}	2.0 x 20.0	
IV-3	1.0	-	Double Crystal	2800-45000	-10^{-4}	2.0 x 20.0	Two-circle Diffractometer
VII-1	1.0	-	Curved Crystal	6000-13000	-8×10^{-4}	0.6 x 3.0	Rotation Camera
VII-3	1.0	-	Double Crystal	2800-45000	-10^{-4}	2.0 x 20.0	
UNDULATOR LINES - VUV/SOFT X-RAY							
V-2	1.5	-	Rowland Circle-Multiple Grating	10-1200	≥7%	6.0 x 8.0	Angle Integrated e^- Spectrometer
UNDULATOR LINES - X-RAY							
PEP 5B	Full	15.0	Double Crystal	12000-20000	-10^{-4}	0.6 x 6.0	
BENDING MAGNET LINES							
X-RAY							
I-4	2.0		Curved Crystal	6700-10800	0.3×10^{-3}	0.25 x 0.5	
I-5	1.0	-	Double Crystal	2800-30000	-10^{-4}	3 x 20	Area Detector/CAD-4
II-2 (focused)	4.8	8.9	Double Crystal	2800-8900	-5×10^{-4}	1 x 4	
II-3	1.0	-	Double Crystal	2800-30000	-5×10^{-4}	3 x 20	
II-4	1.0	-	None	3200-30000		3.5 x 18	
Lifetimes Port	1.8	-	None	1-6	Bandpass >10Å	4.0 x .4	
VUV/SOFT X-RAY							
I-1	2.0		Grasshopper	32-1000	Δλ = .1-.2Å	1.0 x 1.0	
I-2	4.0		6m TGM	8-180	Δλ = .06-3Å	TBD	
III-1	2.0		Grasshopper	25-1200	Δλ = .05-2Å	1.0 x 1.0	
III-2	4.0		Seya-Namioka	5-50	Δλ = .2-6Å	TBD	
III-3	8-10	4.5	UHV Double Crystal (Jumbo)	800-4500	0.35-7 eV	2.0 x 4.0	
III-4	0.6		Multilayer	0-3000	White or $\Delta\lambda/\lambda$ = .3%	2 x 8	Vacuum Diffractometer/ Lithography Exposure Station
VIII-1	12		6m TGM	8-180	ΔK = .06-3Å	TBD	Angle Resolved e^- Spectrometer

TABLE 5

Demand for experimental time on the SSRL branch lines varies considerably. In 1986 of the 5593 shifts requested 3688 (65%) were assigned. In general, the wiggler end and side stations and the grasshopper lines, particularly, the new grasshopper, are in the highest demand. Approximately one-half the requests for wiggler side and end station time are accommodated.

The percentage of proposals receiving beam time is often higher than the percentage of shifts accommodated since most experimenters do not receive the full allotment of shifts requested. Demand is also limited by perceived availability of beam time. Experimenters have indicated that they could used much more time if it were available. In addition, many new groups are discouraged from starting programs based on synchrotron radiation since the time available is limited and length of waiting from application (6 months to two years) long.

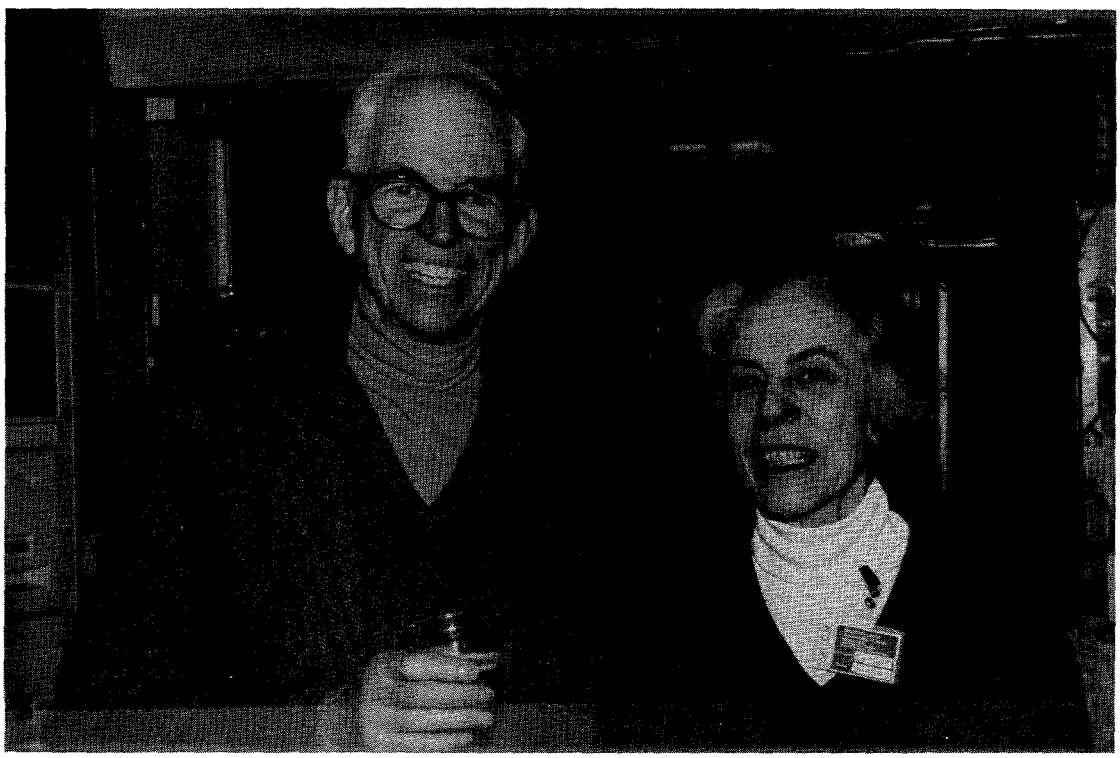

Photo by H. Winick

In December 1986 champagne was served on Experimental Station I-5 to celebrate the ACA Patterson award given to David and Lieselotte Templeton for their work in anomalous scattering.

TABLE 5

DEDICATED DEMAND vs ACCOMMODATION ON SSRL EXPERIMENTAL STATIONS

January 1986-February 1987

Numbers in Bold are Spring dedicated run

Station	Shifts Requested	Shifts Assigned	%Assign	Proposals Requested	Proposals Assigned	%Assign
Bending Magnets						
I-5	***166***	***177***	***106%***	***7***	***7***	***100%***
	252	133	52%	14	6	42%
2-2	***182***	***168***	***92%***	***12***	***10***	***83%***
	170	135	79%	10	8	80%
2-3	***229***	***166***	***72%***	***19***	*12*	*63%*
	used for facility characterization projects					
2-4	***168***	***178***	***105%***	***7***	***7***	***100%***
	174	130	74%	6	6	100%
Wigglers End Stations						
4-2	***201***	***149***	***74%***	***7***	***6***	***85%***
	208	127	61%	9	6	66%
6-2*	***171***	***66***	***38%***	***6***	***3***	***50%***
	56	30	53%	3	2	66%
7-2	***221***	***175***	***79%***	***9***	***8***	***88%***
	222	130	58%	10	6	60%
Side Stations						
4-3	***202***	***181***	***89%***	***9***	***9***	***100%***
	157	150	95%	10	10	100%
7-3, 4-1	***784***	***335***	***42%***	***51***	***27***	***52%***
	598	295	49%	33	17	51%
Grasshoppers						
	624	***354***	***56%***	***15***	***11***	***73%***
	347	278	80%	8	8	100%
Jumbo	***237***	***177***	***74%***	***7***	***6***	***85%***
	224	154	68%	7	5	71%

*** general user time only**

II ACCELERATOR PHYSICS AND SPEAR IMPROVEMENTS

In 1986 the New Rings Group and the Machine Physics Group were combined into one Accelerator Physics Group. The new group is focusing mainly on the improvement of SPEAR's operating conditions and on plans to convert PEP into a next generation x-ray source. Being associated with Stanford University, the SSRL accelerator physics group has become a training center for accelerator physics graduate students. The construction and improvement projects for SPEAR, PEP and the SPRL (Stanford Photon Research Lab) storage rings provide valuable opportunities for students to gain practical experience with accelerator theory, design, construction and operations. This training, presently involves three PhD students. Two others will be supported by SSRL in the future.

During the spring run of SPEAR, a series of machine physics shifts were dedicated to improving the operation of SPEAR for the production of synchrotron light. Specifically, attention was given to significantly reducing the orbit distortion of the beam. This has resulted in much smoother and more reproducible ring operation. It was possible, for example, to fill SPEAR to 80 to 100 mA on demand during the critical period when the method of Digital Subtractive Angiography was applied for the first time to three human subjects.

The improved operating conditions in multibunch mode made the problems encountered during the timing mode with only four bunches all the more obvious. More machine physics is needed to determine the cause of this difference in the SPEAR performance.

Additional efforts have been dedicated to the investigation and cure of beam jitter and movement. To pursue this, new photon beam position monitors have been built.

Silicon Photo-Diode Position Monitors

- Experiments have been done with silicon photodiodes as x-ray position monitors.

Silicon diodes may offer some advantages over split ion chamber type position monitors. For example they do not require a high voltage bias supply, do not require a special gas control system because the detector sensitivity is not affected by gas composition and they can be made two dimensional. There may be other attributes such as spectral and intensitity insensitivity.

Most testing has been done on a commercially made position sensitive PIN diode intended for use with visible light, but modified to allow x-rays to shine directly on the detector surface. It is a monolithic device with a 1 cm square active area. The resistive division of current flow to the edges of the detector are compared to derive the position of the beam on the photodiode.

The detector has been operated in the Beam Line II-4, white radiation beam for a period of two weeks under 3 GeV dedicated conditions. The beam was attenuated with 6.4 mm of aluminum and was collimated horizontally to a width of 3.2 mm. No vertical aperture was imposed. Under these conditions the detector electronics was operated at a factor of 3 to 10 below its maximum gain setting.

The device has performed quite well in tests of sensitivity and linearity. It exhibits the characteristic "pin cushion" response curve which is typical of a detector of this type. This should not alter its usefulness as a steering monitor. Figure 1 is a typical plot of signal vs beam position achieved by scanning the detector across the beam vertically. Typical sensitivity is approximately 1.6 volts per mm for the above beam. Motion increments of 1 micrometer were detectable.

Still to be tested are its radiation damage lifetime and its ability to actually drive a closed loop steering system. The exposure time to date suggests a lifetime of greater than one year at the maximum sensitivity of the detector electronics and typical dedicated beam conditions.

Low Emittance Studies on PEP - The storage ring PEP was available to SSRL for only a short time. During three shifts a low emittance mode of operation was tried at 8 GeV and a beam emittance of 120Å-rad was measured. This corresponds to 67.5 Å at 6 GeV, which is approximately that expected for the 6 GeV Advanced Photon Source. The accelerator physics group intends to establish an operationally reliable low emittance configuration when PEP is available again.

Theoretical studies have been pursued to determine the ultimate capabilities of PEP to produce x-rays with extremely high brilliance. Operating schemes have been identified to gradually reduce the beam emittance to values as low as 5 to 7Å-rad under operating conditions that allow long beam lifetimes.

This small beam emittance, which is an order of magnitude smaller than that of the APS, and would provide a source of spatially coherent radiation in the x-ray regime with a brilliance that is two orders of magnitude higher than that expected for the next generation x-ray storage ring.

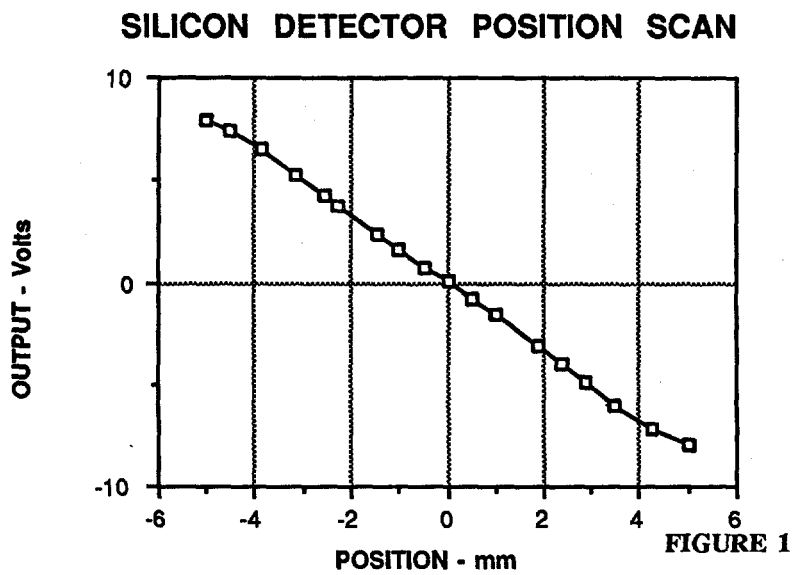

FIGURE 1

III IMPROVEMENTS TO EXISTING FACILITIES

INTRODUCTION

Maintenance and improvement projects are continuous on SSRL's 22 experimental stations, and in the various support laboratories.

X-RAY BEAM LINES

In an on-going program to upgrade the existing x-ray beam lines, significant improvements have been made to each of the scattering beam lines I-4, IV-3, and VII-2. In addition, considerable attention is being given to improving the performance of VI-2 at low x-ray energies, for which the beam line has superb potential. Finally, Branch Line II-3 has been converted to a facility diagnostics port, as part of a program to improve the performance of the optics of every branch line, as well as to diagnose and improve beam stability.

Facility Diagnostics Port - As synchrotron radiation research techniques mature, and as their sophistication increases, greater demands are being placed upon the performance of the storage ring and of the optical systems. In order to accommodate these requirements, SSRL has decided to devote Branch Line II-3 almost exclusively to facility diagnostics. Members of SSRL's scientific and engineering staff have proposed a full schedule of experiments for the December, 1986 - January, 1987 run. By the end of December, experiments had been performed on electron beam positional and angular stability, on novel photon beam detectors, on monochromator glitches, beryllium window characterization, and on intensity levelling schemes. In January, 1987, many of these programs will continue, as well as new ones on beam profiles and noise, monochromator stability, absolute flux calibration, and detector characterization.

Branch Line I-4 - A new elliptical mirror has been installed in Branch Line I-4 replacing the old Cal Tech float glass mirror. The line is designed for small angle scattering. The optical configuration consists of a mirror and crystal in the Kirkpatrick-Baez geometry. The first optical element is a bent mirror focusing in the vertical direction followed by an assymmetrically cut and bent Si(111) crystal focusing in the horizontal direction. Since there is only a single diffracting element the energy range is constrained by the hutch dimensions and is rarely changed. The line was designed to strongly demagnify the source and hence emphasizes intensity over spectral resolution. Photon detection is accomplished with a one dimensional Si photodiode array with a pixel width of 25 microns. The mirror control mechanism is a copy of the design currently being used on Branch Line VII-1. It features four independently operated stepping motors which are controlled manually through four specially modified Joerger stepping motor controllers. Two motors bend the mirror to approximate the shape of an ellipse and the other two motors provide vertical translation and tilt. This mechanism is a major improvement over the previous configuration of 8 independent motors in which all of the above motions were coupled. The mirror itself is a rectangular flat of fused silica polished by Frank Cooke, Inc.

With the cooperation of LBL, the surface roughness of the mirror was measured with a WYCO optical profilometer to be 3 Å RMS over a spatial wavelength range of 2.5 microns to 5 mm. The mirror was subsequently coated with platinum at SSRL and the roughness measurement was repeated at LBL and found to have increased by approximately 1 Å RMS. Since the new mirror is Pt-coated, the increase in critical angle allows the mirror length to be halved while still maintaining the same vertical beam acceptance.

SSRL staff, in collaboration with Tom Russell of IBM, have measured the vertical focal size with a Si photodiode array to be 300 microns (FWHM). Given a demagnification of 0.184, the expected image size for a perfect optic would be 122 microns (FWHM). With the apertures stopped down to reduce the parasitic scattering, a flux of 6.0 x E9 ph/sec was measured with the ring at 3.0 GeV and 80 mA. A 2.0 mm tantalum beam stop has been installed to protect the photodiode array. With a 500 mm sample to detector distance, spatial periodicities of 700-800 Å were observed. With a standard sample in the beam, comparison of photomultiplier tube count rates between the old mirror and the new mirror showed a factor of three increase in scattered flux.

Branch Line IV-3 - Recent work on Branch Line IV-3 is highlighted by an overhaul of the materials diffractometer and refurbishment of the solid state germanium detectors. The mechanical connection between the main shaft and the ring gear has been redesigned and rebuilt. The dewars associated with the Ge detectors were replaced. Re-evacuation of the dewars was not an option because the threads on the dewar neck were too badly stripped. Future plans for IV-3 include a vertically focusing mirror immediately downstream of the monochromator. This mirror will be similar in design to the those currently in use on Branch Line I-4 and VII-2. However, it will be downward reflecting in order to facilitate scattering or diffraction from liquid surfaces.

Branch Line VII-2 - There have been a number of improvements to wiggler end station VII-2 this fall. First among them was the replacement of the doors on the hutch. The new set does not have a sill. The height of the doors was increased and there is over a foot of space between the diffractometer support bearing and the doors, facilitating work in the hutch.

Other improvements to the system include replacing the counterweight on the 2Θ arm so it clears the Θ motor. The present limit to 2Θ is roughly 130 degrees (it runs into the front wall at that point). The Io detector has been remounted under the Io section to eliminate that interference with 2Θ. The Θ and χ circles are now properly counter-balanced and the Φ gearbox has been replaced by a new goniometer with a 180 tooth ring gear which is more robust than the 360 tooth gear on the original system. A 20-to-1 gear reducer has been installed to maintain the same steps/degree as before. There are now separate stepper motor controllers for monochromator and table, which means that the monochromator energy can be changed without major recabling of the CAMAC crate.

There have been software improvements as well. The present program, based on the original SUPER software, is designed for use with a VT-240 terminal. The new version writes separate data files for each scan rather than concatenating scans onto one file. The most recent scan or a previous scan can be plotted on the screen from within the program and a hard-copy of the plot obtained from an LA-50 printer. One of the advantages of using a CRT instead of lineprinter is that the motor positions in degrees and the current HKL values are constantly updated on the screen as the motors move. Thus motor motions can be kept track of without leaving the terminal. Most of the other features of SUPER have been maintained. New EXAFS software has been developed as well. The operating system is still RT-11, but the new software runs interrupt-driven and overlayed, so it is expandable.

VUV BEAM LINES

The number of experimental stations at SSRL devoted to the VUV and soft x-ray region is increasing rapidly. In 1986 there were four VUV branch lines in regular operation. In 1988 10 branch lines in this range will be in use. This year the Seya-Namioka monochromator was moved from Branch Line I-2 to III-2, the 18 degree line, where it now collects a larger fan of radiation, 4.5 mrad, and has higher efficiency input optics. Characterization is currently under way and Beam Line III-2 will be operational for the spring run of 1987. A 6 meter toroidal grating monochromator (TGM) has been installed on Beam Line I-2. It will cover the energy range from 9 to 175 eV and initially collect 3.5 mrad of bend magnet radiation. It has the capability of collecting up to 7 mrad. Commissioning will be done during the 1987 spring run. The experimental station will be ready for users by the fall of 1987.

Many of the new PRT beam lines that are coming on line will be dedicated to VUV and soft x-ray region. Beam Line VIII, the UC/National Labs PRT, has two experimental stations in this spectral range. One has a TGM of the same design as that on Beam Line I-2, and is being commissioned during the current winter run. The other has a spherical grating monochromator (SGM), to operate in the energy range of 50 to 1000 eV. It will be delivered early in 1987. Beam Line V, the Xerox/Stanford/SSRL PRT project, is nearing completion. This beam line has four undulators and a Rowland circle monochromator to cover the energy range form 10 to 1000 eV. The LBL/EXXON/SSRL PRT has started manufacturing components for the VUV branch of Beam Line VI. The source is the 54 pole wiggler and the monochromator will be an SGM that can cover the spectral range from 50 to 1000 eV. (See the sections devoted to each of these beam lines for more information.)

The grasshoppers ran very well during the past year, requiring no repairs and only simple adjustments of mirrors and slits to keep a well focused beam at the sample position. The periodic flux measurements on both grasshoppers have shown little variation over the last year indicating there has been only negligible increase of carbon contamination on the optics. The beam line software was improved during the year to permit existing programs to run on new terminals. Several improvements to the grasshopper lines have been discussed and may be implemented during 1987. These include elliptical focusing mirrors which have been demonstrated at Wiscon-

sin to improve flux by an order of magnitude and new grating(s) which may improve photon energy calibration.

The Toroidal Grating Monochromator (TGM) replacing the Seya on Beam Line I-2 was received October 1, 1986. The new monochromator has a spectral range of 9 to 175 eV (1400 - 70 Å) and will cover that range with higher resolution than previously achieved on SSRL beam lines. The support frame for the TGM is designed to counteract the mechanical instabilities of the Building 120 mezzanine slab where Beam Line I-2 is located. Extra supports for the slab were installed at key points during the summer shutdown. In addition, the input optics to the TGM have been redesigned to enhance the higher photon energy range and improve the transmitted photon flux over this range. The original beam-splitting M0 mirror remains, but a new M1 mirror matched to the TGM with a more grazing angle of incidence and a grasshopper style refocusing mirror have been included in the new line.

Beam Line III-3, Jumbo, continues to perform well. At the sample position of the branch line a pair of slits were used to measure the vertical and horizontal beam size. After optimizing the focal length of the Jumbo mirror the spot size is 1.5 mm FWHM vertically and 2.5 mm FWHM horizontally at an energy of 2300 eV. This has significantly improved the flux density at the sample.

Beam Line III-4, the differentially pumped, white light branch line is now in use for a wide variety of x-ray lithography and x-ray optical experiments. The experimental station is set up for rapid turnaround and flexibility of configuration.

BIOTECHNOLOGY AND COMPUTATIONAL DEVELOPMENT PROJECTS

The research and user support in the Biotechnology Division at SSRL are funded jointly by the NIH Division of Research Resources and the core SSRL operations budget from the DOE. The division also includes oversight for the computer activities of SSRL.

Facilities for Protein Crystallography

- During the past year, the rotation camera facility for protein crystallograhy, mounted on the high intensity wiggler Beam Line VII-1, has continued to be in high demand. In fact, the facility has now become oversubscribed, which will necessitate beam time allocations guided by ratings from the SSRL proposal review biology subpanel rather than the first-come, first-served system. Every attempt will be made to retain simplicity of access.

During the 1986 summer shutdown, a number of improvements were made to the rotation camera system and darkroom. Most significantly, the experimental enclosure was fitted with a "no bars" personnel protection system. This has dramatically improved accessibility to the camera for sample crystal alignment and exchanging film cassettes. The "no bars" system has also greatly improved access for system optics and camera alignment and means that additional peripheral equipment, such as a low temperature cryostat, can be accommodated and adjusted more easily. The "no bars" mode has also eliminated the need to open and close the gate which generated electrical noise on the VII-3 station.

In November 1986, the rotation camera was used for the first time at a wavelength of 1.08Å (11.480 keV). This value has now become the second standard wavelength for data collection on the facility at SSRL, the first being 1.5418Å (8.042 keV). A wavelength of 1.08Å will permit the collection of higher resolution data on our standard flat film cassettes. Also, preliminary experiments have shown that less radiation damage occurs in the protein crystal, which should permit more data to be collected from a given sample crystal.

The area detector facility, used for anomalous dispersion protein crystallography, is undergoing a major upgrade. Previously the data collection rate on this project was limited by the power of the beam line control computer, as was the possibility of simultaneous data collection and analysis. This limitation is being removed by replacing the existing PDP-11/34 computer by a considerably more powerful MicroVAX operating in a networked environment. This will serve as a model for the future of other SSRL beam line control computer systems. The data analysis software has successfully run on a MicroVAX-II workstation for both the Spring and Fall runs of 1986; this has permitted experimenters to leave SSRL with already processed data from the area detector for the first time. Installation of a MicroVAX-I dedicated to equipment control and data collection is in progress. The software developed for this use is designed to be easily transportable to other SSRL beam lines and experimental procedures.

Computational Facilities - Over the last six years the SSRL computer system has expanded to include two large VAX's, several MicroVAX's and PC's, and over 20 PDP-11's for beam line control. This expansion program will continue, both to include support for the ever growing number of beam lines and experimental stations, and to improve the functionality and reliability of the system.

Full implementation of the ETHERNET network at SSRL has been completed during the past year. The network provides inter-machine communications around the laboratory. With the network bridge connection to SPEAR, the local network is connected to a world-wide high energy physics network. This allows our users and staff convenient access to both SSRL computers, and other laboratory computer systems around the world. The network also provides access to many laboratories and universities over the BITNET mail system (the SSRL address is USERNAME@SSRL750).

An ambitious project to convert the beam line data acquisition systems from the current PDP-11's to the large screen MicroVAX-II workstations has begun with the recent installation of the first three of these machines. The aim is to retire the venerable PDP systems, which are becoming increasingly unreliable and expensive to maintain. It is hoped to achieve this conversion over a two year period.

A new billet for a scientific programmer was added to the Computer Group this year. This position will allow, among other tasks, the specification and coding of the new MicroVAX-based data acquisition software.

The expansion of SSRL from its original site around the SPEAR ring to include both the new

LOS building, and an increasing number of PEP beam lines forces a rethinking of the current SSRL computer organization. The scale of the expanded laboratory will require a more distributed computer network, with increased reliance on local intelligence and networking. An expansion of the use of computers for monitoring and control applications will reduce the workload of the operations staff, provide a more careful analysis of long term trends in beam lines and SPEAR, and generally make both SPEAR and PEP more effective sources of synchrotron radiation.

Facilities for X-ray Absorption Spectroscopy - The liquid helium cryostat that was received in the Spring of 1986 has been fully tested and performs well at temperatures down to 4 K. The system has demountable tail pieces with different window thickness. Using the thinner windows (3 mil) the window transmission is sufficiently low that good fluorescence data can be collected in the 7 keV range. The system has been fully utilized by several groups during the Fall-Winter run. A second transfer arm is being purchased that will facilitate the use of the cryostat in stations where the vertical ceiling clearance does not permit easy change of dewar with the current arm.

A new MicroVAX-II workstation system has also been set up. This system is adjacent to Beam Line VII-3 and includes an LN03+ laser printer/plotter and a high quality LVP16 multicolor pen plotter. The system is connected over the network to the VII-3 beam line control 11/34 computer so that data can be transferred directly to the workstation (only when the 11/34 is running the RSX operating system). Programs for full analysis of EXAFS data are available on the MicroVAX workstation. Eventually, this system will replace the 11/34 control computer. A similar system, without the laser printer and plotter, has been installed adjacent to the II-2 beam line.

IV BEAM LINES BEING COMMISSIONED

BEAM LINE VIII

Commissioning of Beam Line VIII began in late 1986. This beam line is being built by a participating research team composed of the University of California, and the Lawrence Livermore, Los Alamos, and Sandia National Laboratories in collaboration with SSRL. The project is funded by the Department of Energy and the University of California with LLNL serving as the lead laboratory. The bending magnet beam line will have two branches: a VUV branch covering the range 8-185 eV and a soft x-ray branch covering the range 60-1100 eV. An assembly drawing of the two branches which are located in Building 120 is shown in Figure 2.

During the March 1986 SPEAR shutdown, the VUV shutter tank was installed, thus completing the alcove section. In the summer the M1 mirror, 6-m toroidal grating monochromator and M2 mirror were installed, performance of the prefocusing optics, mirror movers and control electronics were successfully demonstrated and light through the complete system was obtained on November 18. Monochromator adjustments and tests of the complete VUV branch line using a temporary sample chamber are currently in progress. A permanent 30-port, trilevel UHV experimental chamber is being fabricated by Vacuum Sciences Workshop and is scheduled for delivery in February 1987. Final testing and characterization of the VUV branch of the beam line and preliminary photoemission experiments are planned during the spring running period with full operations commencing in Fall 1987.

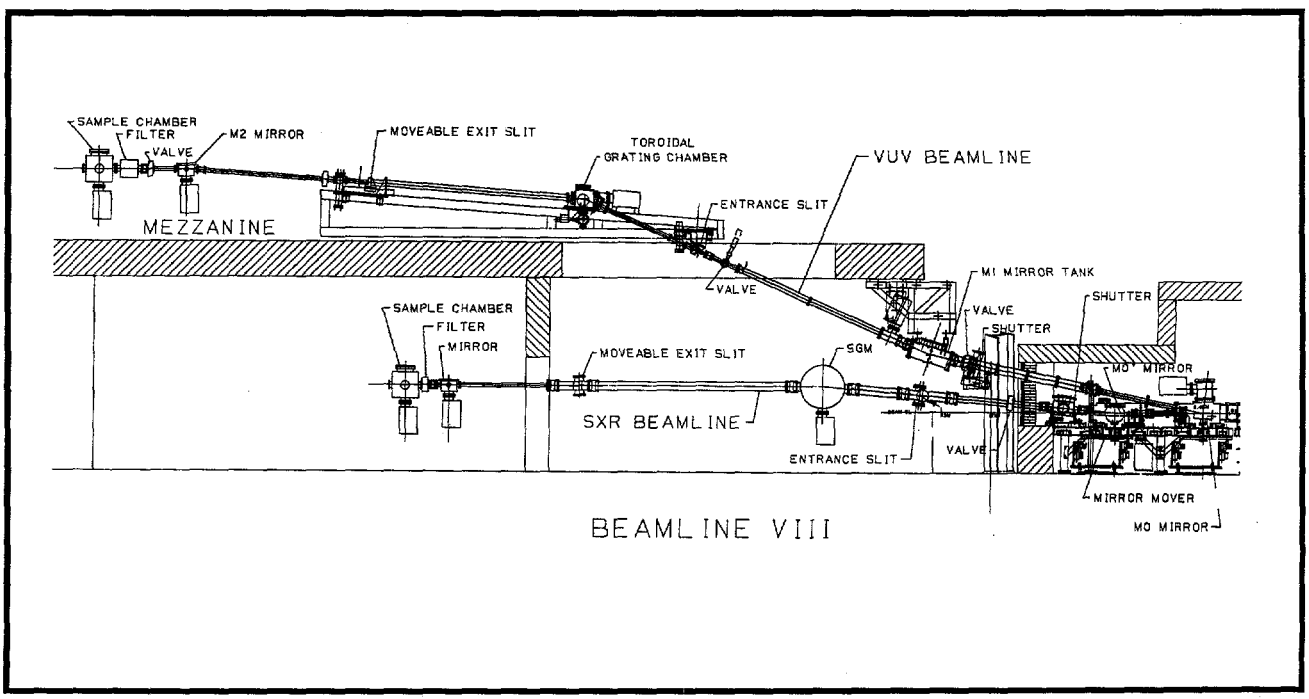

Figure 2
Elevation drawing of the VUV and soft x-ray branch lines on Beam Line VIII.

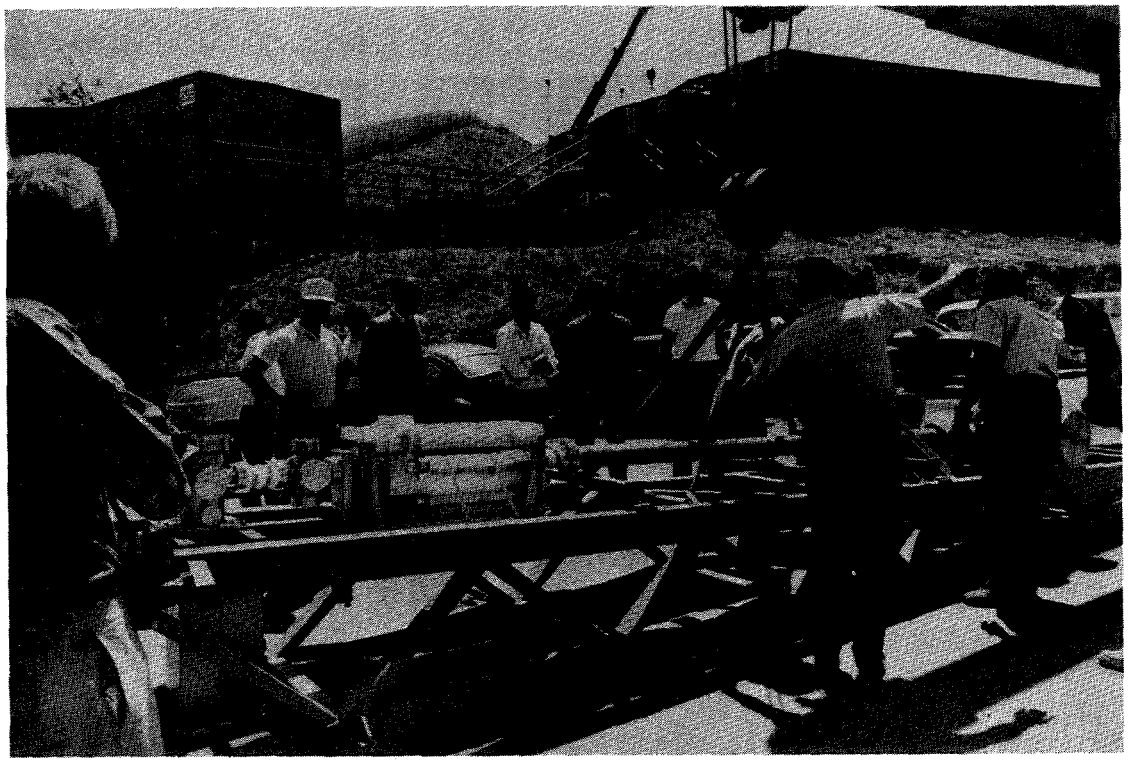

TGM arriving from Acton Research August 21, 1986 *Photo by H. Morales*

The M0' mirror and the shutter tank for the soft x-ray branch and the position monitor beam line were also installed in the summer of 1986. The M0' mirror is a water-cooled, platinum-coated SiC toroid obtained from Frank Cooke. It has a measured rms surface roughness of only 5 Å over its 380 mm length. Final design of the spherical grating monochromator for this branch line was completed and includes three interchangeable holographic gratings and a laser interferometer angle monitor. The gratings are being fabricated by Astron; the monochromator is being build by Acton Research Corporation with delivery scheduled for spring 1987. Commissioning and initial operation of the soft x-ray branch should be completed in 1987.

18 DEGREE LINE COMMISSIONED

The 18 degree line saw its first light on November 14, 1986. The line was designed to cover the photon energy range from 5 to 50 eV with better resolution and flux than was available on the 8 degree branch of Beam Line I. That line was hampered by mechanical instabilities of the mezzanine slab and poor input optics. The design of the 18 degree line incorporates the Seya Namioka monochromator from the 8 degree line, but uses fewer optical elements at more grazing angles of incidence to improve the flux, especially at higher photon energies. In addition, the Building 131 mezzanine slab is thicker and much more stable than the Beam Line I slab, allowing the monochromator to achieve better energy resolution in its new location. It was determined that a silicon

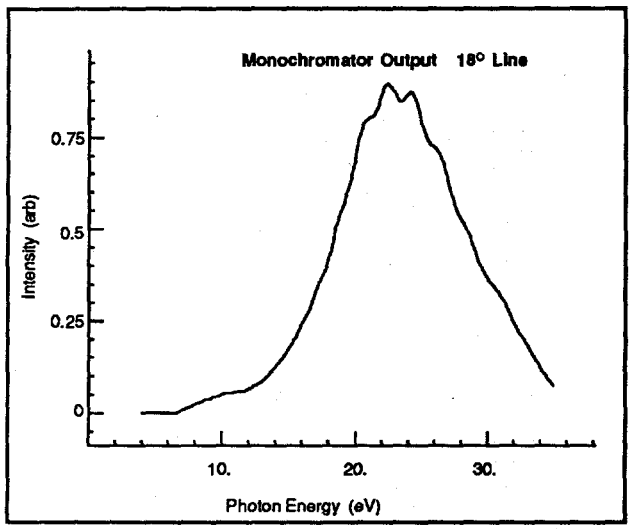

Figure 3
Monochromator output measured with a photodiode on the 18° line

carbide first mirror would best serve the design goals of high reflectivity and temperature stability without the need for water coolng.

In 1986 the 18 degree line progressed from drawings and a few pieces of steel to a working beam line. By March the M1 mirror tank, drift tube section and much cabling were fabricated and installed. After the June dedicated run, the Seya-Namioka monochromator was removed from Beam Line I-2 and installed in place on the Building 131 mezzanine. The M2 refocusing mirror chamber was installed soon after. The silicon carbide M0 mirror was installed in August. By September the beam line hardware was complete and pumped down. By the end of October the vacuum control system and other electronics were complete. On November 14 the beam line was opened to synchrotron light exposing, for the first time at SSRL, a silicon carbide beam splitter mirror. The slow process of working the beam up the line began and when the beam went down on December 24, there was light through the entrance slit of the monochromator. Commissioning will continue during the January run with resolution and energy calibration measurements once the light is past the refocusing mirror. It is anticipated that the line will be opened to users in the first dedicated run of 1987. Figure 3 shows the monochromator output.

BEAM LINE V

The Beam Line V project moved further toward completion in 1986, with the commissioning of the full complement of undulators, the completion of the monochromator design, and the beginning of the final assembly of the monochromator. Since there was an extensive description of the beam line in the 1985 Activity Report, only a brief description of the status of the project, and of some characterization experiments done with the undulator radiation is included here.

The SSRL mechanical design group prepared and checked about 450 monochromator drawings representing some 650 machined parts. As groups of these drawings were signed off, the parts were ordered; this process is now all but complete and the majority of parts were received by the end of the year. The optics for the monochromator are also almost complete. The SiC entrance mirror and the SiC mirrors for the Codling slits have been delivered. The refocusing mirrors were received, though one needed rework. The 5 and 10 meter gratings from Astron were received, and the 1 and 2 meter gratings from Hyperfine are expected soon. The computer system was upgraded with a 28 MB Winchester disk and attached to the SSRL Ethernet.

The main experimental work using Beam Line V this year was a set of x-ray optical experiments performed by R. Tatchyn of SSRL, P. Csonka, H. Kilic, and H. Watanabe from the University of Oregon, A. Toor from Lawrence Livermore, and A. Fuller from Stanford. This group attempted to focus the undulator light with an ellipsoidal mirror, to photograph undulator pulses with a streak camera, to perform lithography with the undulator radiation, and to perform power measurements on the undulator output. Details are included under Proposal 8005 on page 181 of this report.

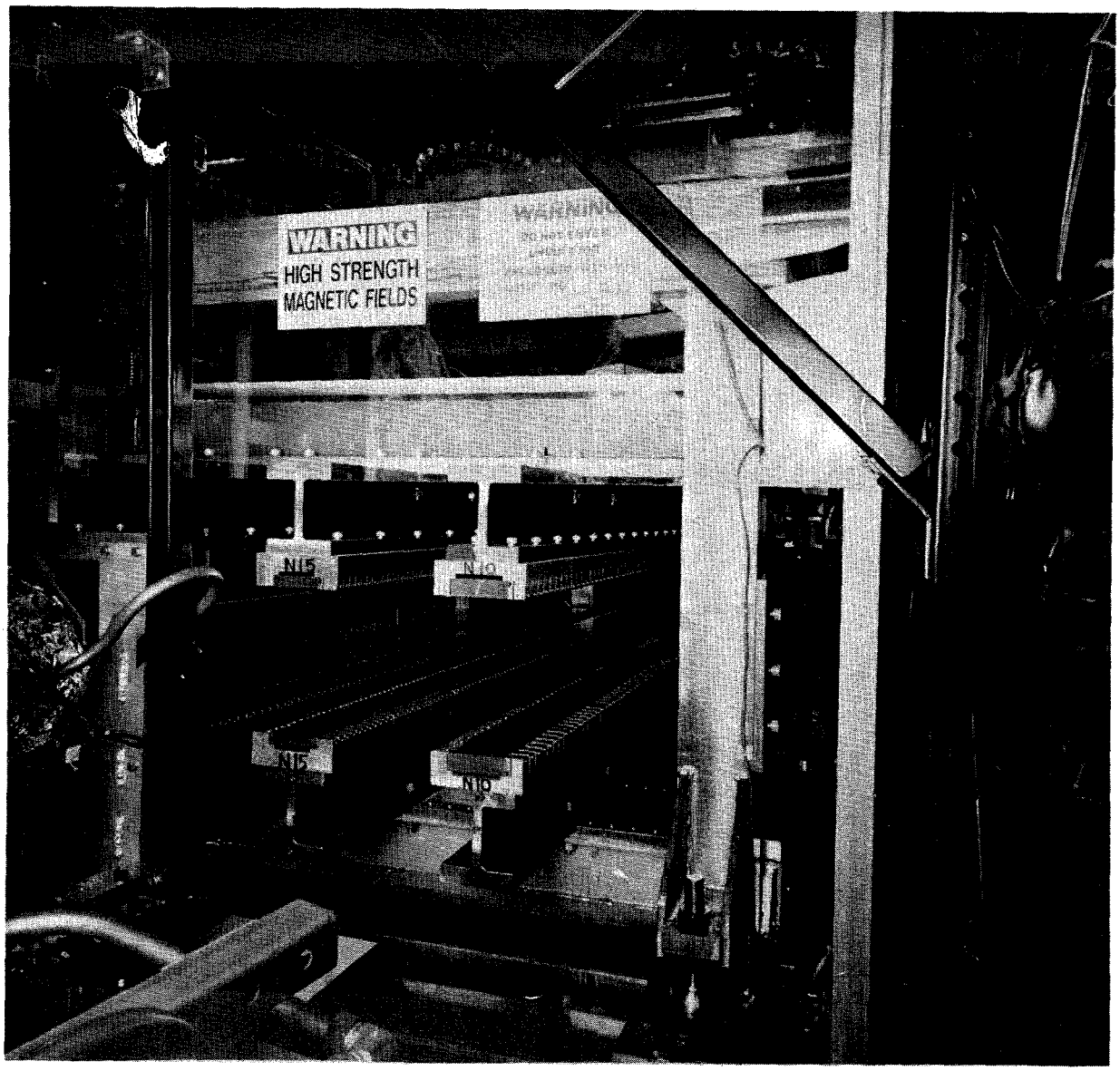

Photo by J. Faust

Beam Line V Multi-undulator Installed in SPEAR

V PRESENT CONSTRUCTION PROJECTS

PEP BEAM LINE 1B

Construction of a second PEP beam line, located at symmetry straight section 1B of PEP, commenced in February, 1986. The unqualified success of the first beam line, located at section 5B, has led SSRL to replicate the optics in 1B, with the exception of a focusing mirror. The details of the optics and the spectrum can be found in the previous year's activity report.

With the completion of PEP 1B, in the fall of 1987, SSRL will have the two brightest x-ray beam lines in the world, in the 12-20 keV spectral range. SSRL intends to scheduled a full program of research utilizing PEP in a parasitic mode, with possible dedicated running as early as FY'88.

An experimental hall is being constructed to house the beam transport and experimental facilities for this second PEP synchrotron radiation port at SSRL. Beneficial occupancy of the building is scheduled for late January, 1987.

SSRL LOS BUILDING

In late 1985, SSRL engaged the architectural firm HED, Inc., to design a 33,000 sq. ft. laboratory-office-shop building, to serve as SSRL's main office building and to house the technical activities being displaced by beam line construction. The facility will be located adjacent to SLAC's computer building, on a site that allows for further expansion of the building at a later date.

Ground was broken for the building in November, 1986, and construction has been progressing smoothly. Barring unusual weather delays, beneficial occupancy is scheduled for December, 1987.

BEAM LINE X

Beam Line X is being constructed for the University of California/National Laboratories PRT in an effort headed by the Lawrence Livermore National Laboratory. The facility will have a high intensity 15-period wiggler source that will achieve 1.4 T at the 2.1 cm operating magnet gap. Design of the wiggler was completed, and fabrication started at the Lawrence Berkeley Laboratory in 1986. Fabrication, magnetic measurements, and installation of the wiggler are to be completed by the end of the summer 1987 SPEAR shutdown.

The Beam Line X wiggler and its magnetic structure, drive, vacuum systems and support frame are shown in Figure 4. The magnetic structure is a steel-hybrid configuration similar to that used in the Beam Line VI 54-pole wiggler but with neodymium-iron rather than rare earth-cobalt as the permanent magnet material. The basic half-period pole assembly consists of a vanadium permendur pole surrounded with eight blocks of Nd-Fe bonded to each side of the pole in the aluminum keeper. End half-period assemblies, consisting of an electromagnetic coil and Nd-Fe, are provided to correct the vertical field integral of the wiggler. Magnetic field adjustment is accomplished by a system of screw shafts driven by a stepping motor with the magnet gap opening controlled through an encoder. The 2.1-m long

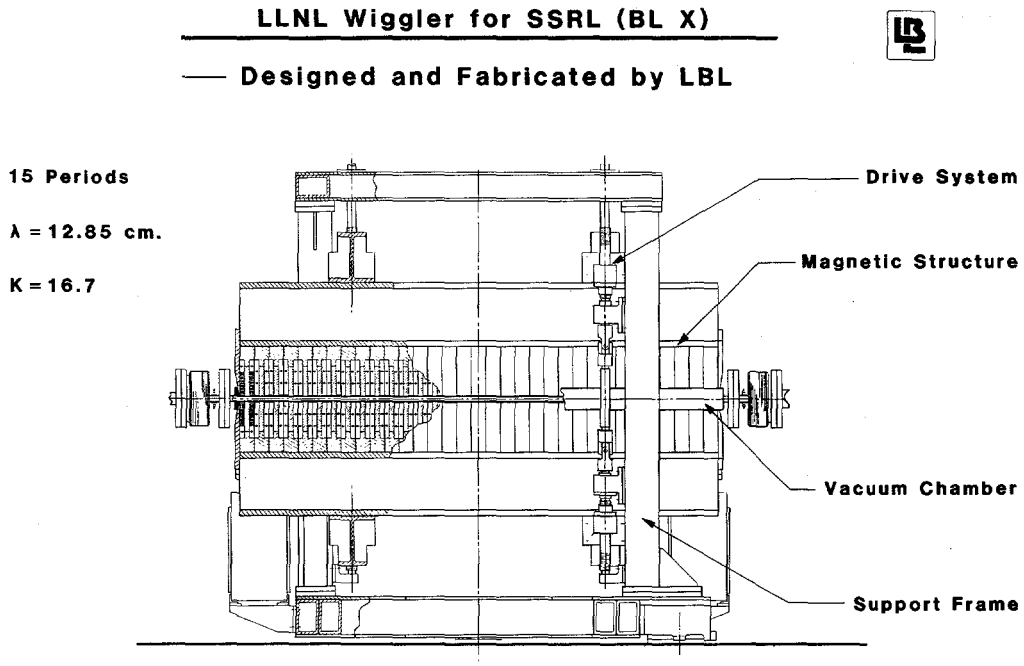

Figure 4
Overall design of 15-period wiggler for Beam Line X.

vacuum chamber will be of 316 L stainless steel and have a beam stay-clear full aperture of 1.8 cm.

A conceptual design task group met in May-June 1986 to recommend a beam line configuration consistent with PRT requirements and cost /schedule constraints. The configuration chosen has a main hard x-ray branch covering the 3-35 keV region. This branch will have a double-crystal monochromator with provisions for operating with a focused or unfocused white beam. The design incorporates the options of adding a soft x-ray side branch via a horizontal reflection from the first mirror tank, and a hard x-ray side branch, either from a horizontal reflection from the first mirror tank or downstream in the vicinity of the main branch focusing mirror.

Much of the instrumentation for the beam line is based on designs and experience gained from handling the heat loads of Beam Line VI, however several studies are underway to improve components and operation. Extension of the low-energy range and increased photon flux are possible by reducing the thickness of the beryllium windows used as vacuum barriers between the SPEAR ring and the beam line. To simulated beam heat fluxes in the Be windows, tests were conducted at LLNL using the Nd:YAG laser welding facility. In 1987, the thermal flux of these laboratory experiments will be increased to produce window damage and 3-D stress analyses will be performed. The results of these investigations will provide input for *in-situ* experiments planned at SSRL on Beam Line VI.

A 3-D thermal stress analysis of the first crystal and crystal holder design for the present Hower-Brown monochromator and 2-D and 3-D analyses of other possible cooling configurations were also performed at LLNL in 1986. In the first half

of 1987 the possibility of direct gas cooling of the crystal surface will be explored and the final design of the monochromator for Beam Line X will be completed.

The wiggler and all in-alcove components for Beam Line X are to be installed during the summer 1987 shutdown. Construction and assembly of beam line components are scheduled to be completed by the end of 1987. End stations on the main branch will provided for tandem x-ray spectroscopy and diffraction experiments. Commissioning of the beam line should commence in early 1988.

VUV BRANCH LINE VI-1

In 1986 many components of the new VUV branch line (LBL/EXXON/SSRL 54 pole wiggler Beam Line VI) passed through the detail design process at LBL and some of them have already been fabricated. The work is being done under the auspices of LBL's Center for X-Ray Optics (CXRO). The front end components are near completion so that the part of the beam line which is inside the alcove can be installed in the summer 1987 shut down. This includes the sophisticated water-cooled first deflection mirror (M0), which can be remotely adjusted for "roll" and "yaw". A twin of this mirror assembly has been successfully installed at Brookhaven National Laboratory by LBL. The plane metal mirror of this device, which contains a water-cooling passage directly under the optical surface, has been very well characterized after polishing of the electroless nickel surface. Measurements with WYKO and Zygo Interferometers proved that surface figure and microroughness are within the required tolerances to ensure good performance. The mirror assembly is shown in Figure 5.

The other major components which go outside the alcove are well along. The detail design of the M1 toroidal mirror assembly is almost finished, and the mirror itself has been ordered and will be delivered in 1987.

A high resolution spherical grating monochromator (SGM) which is suitable for present and future high flux wiggler and undulator synchrotron radiation beam lines, is being developed as part of this branch line. The optical layout of the monochromator which was described last year *(see H. Hogrefe, M.R. Howells and E. Hoyer, "Applications of Spherical Gratings in Synchrotron Radiation Spectroscopy", Proc. SPIE 799, 1987, to be published)* is based on the "Rowland circle" design and features a large radius spherical grating and two movable slits. Table 6 gives the design parameters of the optical system including the condensing mirror M1. The factors which determine the capability of the monochromator to achieve a high resolution are : 1) optical aberrations, 2) fabrication tolerances of the spherical surface figure, 3) distortions due to thermal stresses in the grating and 4) the stability and alignment of the whole slit-grating-slit set-up. While factor 1 is minimized by the chosen layout, careful detail design has been done and will continue through most of 1987 to cope with factors 2-4. The design of the water cooled, adjustable grating blanks and the slit assembly is finished (see Figure 6), leaving the design of the precision drive, the monochromator vacuum chamber, the slide assembly for the slits and the whole support frame for 1987. Also, extensive braze tests for the highly complicated grating blanks have been successful. Parallel to the design work at LBL there has been continuous contact with various optical companies to assure the feasibility of, and to find out the best way to get, holographically

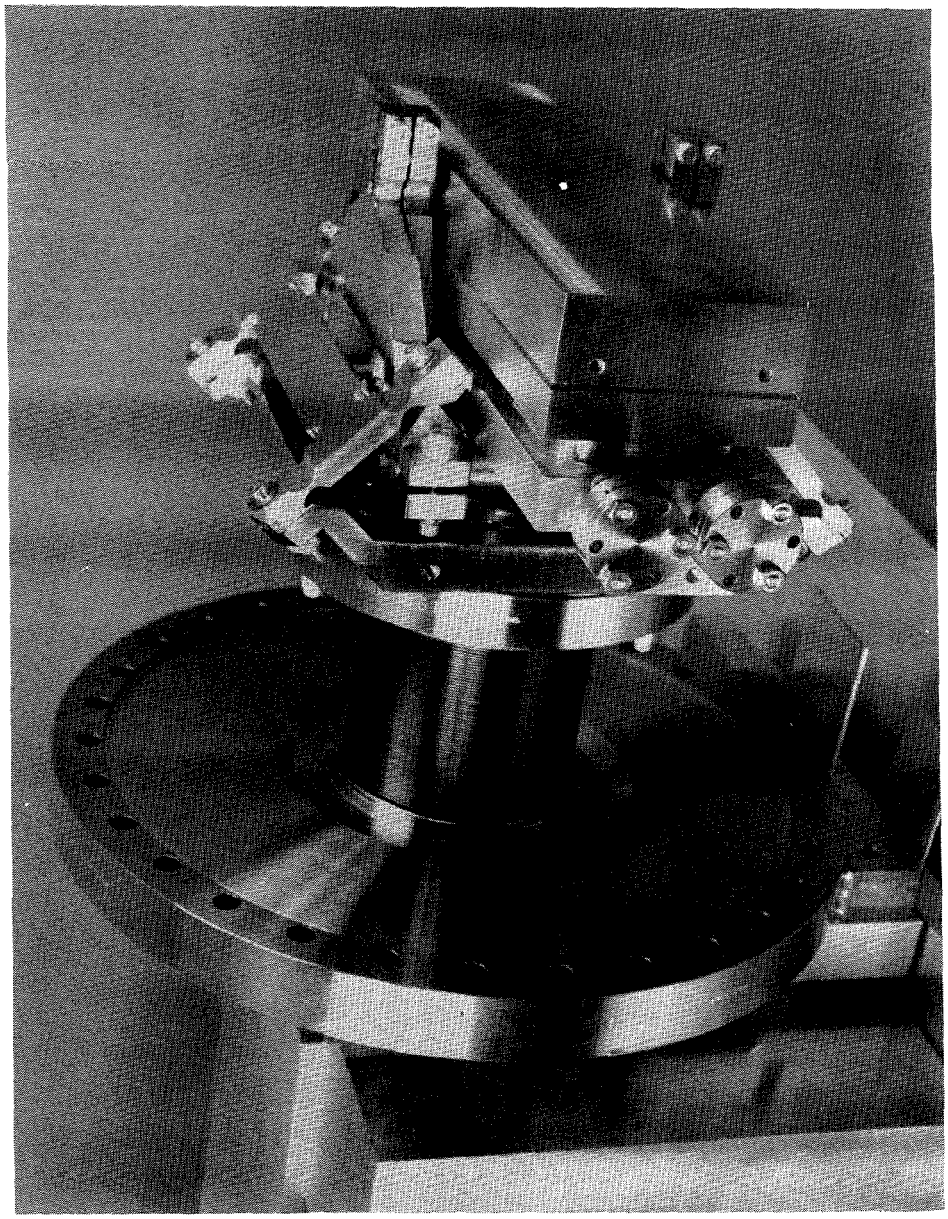

FIGURE 5

Photograph of the adjustable watercooled MO mirror assembly. The device shown here was successfully installed at NSLS. An identical assembly will be used for Beam Line VI at SSRL.

Table 6

Optical Components for Branch Line VI-1

<u>Toroidal mirror</u>	
Source-mirror distance	16.15 m
Mirror-S1 distance	5.35 m
Meridional Radius R_M	184.3 m
Sagittal radius p_M	0.58 m
Angle of incidence	87.5°
Acceptance	1.1 x 1.5 $mrad^2$ (meridional x sagittal)
<u>Spherical grating</u>	
Radius R	55 m
Deflection angle 2Q	174°
Size	178 x 66 mm^2
Grating constant d with G1, G2, G3	1/1100 mm, 1/500 mm, 1/200 mm
Wavelength coverage with G1, G2, G3	~10-35 Å, ~22-80 Å, ~55-200 Å
Slit grating distance:	r = 2.01 - 1.44 m (entrance slit S1)
	r' = 3.68 - ~4.59 m (exit slit S2)

produced gratings with a highly demanding surface figure accuracy for the above mentioned grating blanks. Verification of the optical surface quality with advanced metrology equipment will be required. The order for the gratings will probably be placed early in 1987.

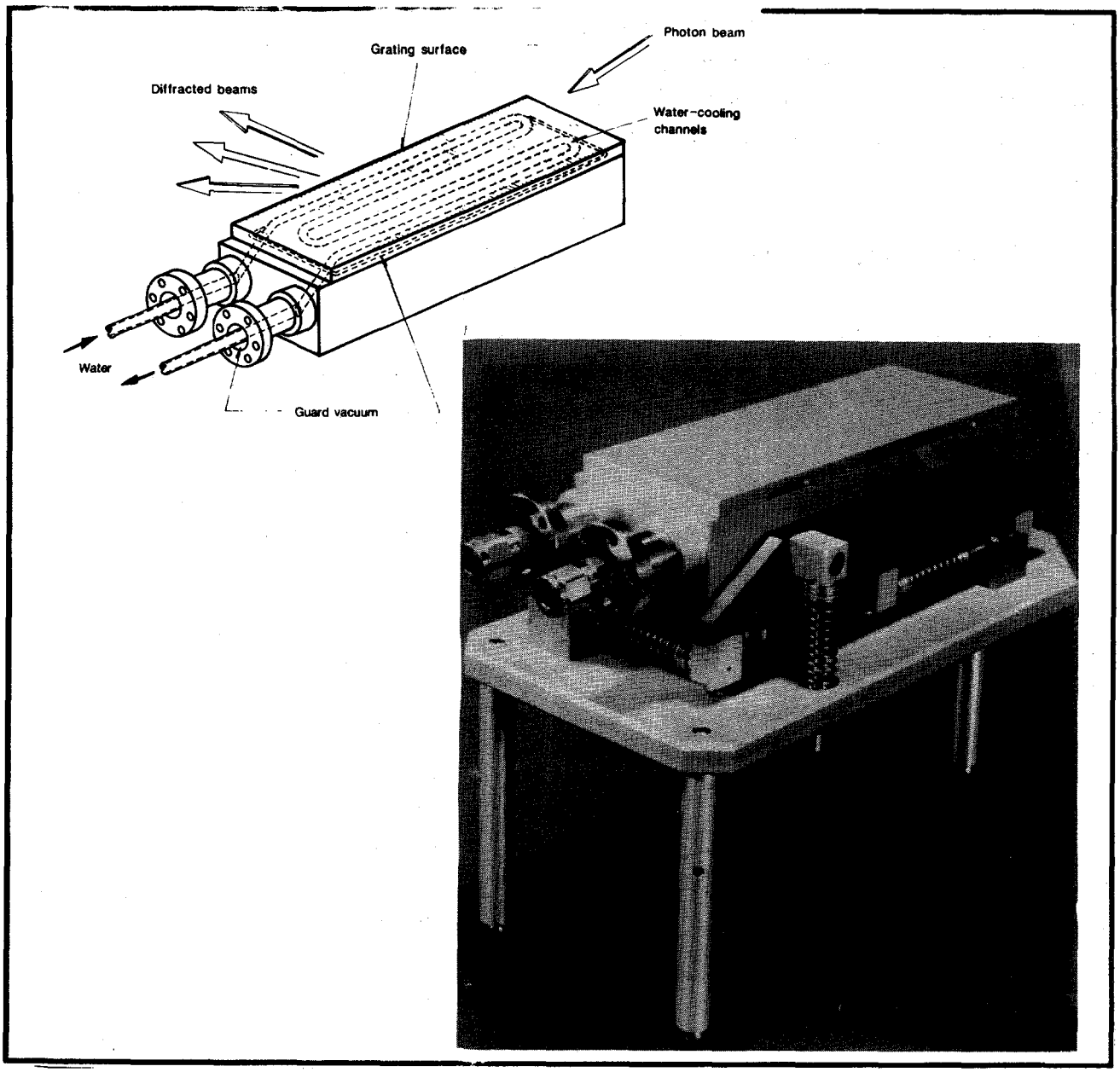

FIGURE 6

Schematic drawing of the actively cooled grating used in the spherical grating monchromator. The complicated blanks include two channel systems: the inner for water cooling, the outer is a rough vacuum to provide security against water leaking into the ultra-high vacuum of the monochromator chamber. On the left a model of the grating assembly is shown. The kinematic mounting system provides sub arc second adjustment of the grating in ultra high vacuum.

VI ENGINEERING DIVISION

The Engineering Division of SSRL provides broad mechanical and electrical engineering support to SSRL staff and users in the operation, maintenance and improvement of the present facility and is heavily involved in the design and construction of new insertion devices, beam lines and related equipment.

ELECTRICAL ENGINEERING

Beam Line Control Systems - A major activity of the EE group is the design, construction, maintenance and improvement of various control systems for SSRL beam lines. These control systems may be divided into the following functional categories: vacuum controls, photon beam steering and stabilization controls, personnel protection interlock systems, communications (audio, video, data), insertion device controls, optical system controls and experimental station electronics.

In 1986 the EE group worked on control systems for the following new beam lines: PEP Beam Line 5B, PEP Beam Line 1B, SPEAR Beam Line III, and SPEAR Beam Line VIII.

Work is continuing to standardize the beam line control systems. The goals of this effort are to simplify the operation and maintenance of these systems and to reduce the training time for technical support personnel.

Development of Beam Line and Storage Ring Status Monitoring System - An effort is continuing to develop a central computer facility for monitoring all SSRL beam line control systems and the SPEAR/PEP ring operating parameters. The purpose of the proposed computer facility is to permit centralized monitoring (and eventually some manipulation) of the beam line control systems. The facility will also act as the interface to the SPEAR/PEP VAX computers for acquisition of storage ring data. The centralized status information will be available to SSRL operators and key personnel, and relevant information will be displayed at each beam line control station and at the main operation console in the SSRL control room. The system will be connected to the SSRL sitewide Ethernet, making the status information available to all network terminals.

Discussions have started as to the functions and topology of the proposed beam line monitoring system. Provisional design envisions a number of intelligent data acquisition systems, based upon CAMAC and a PDP-11/23, each responsible for two or three beam lines. These systems would maintain a data base of parameters that describe the condition of the beam line, and would be connected to the lab-wide Ethernet system. Central coordination of the system would be via a microVAX-II work station placed in SSRL control room.

The central computer would coordinate information from all the data acquisition systems, permitting remote diagnosis of the beam lines from one convenient location. The data acquisition (DA) systems could also be programmed to recognize unusual or fault conditions, and raise alarms. The central computer would collect beam line statistics to investigate long term trends, for example, to identify a slow leak in the vacuum system. The Ethernet connection to the SPEAR VAX would also permit this computer to monitor SPEAR collected information, such as ring current, energy, lifetime, magnet fields and vacuum reading within the ring itself.

Software for the DA systems would be based upon that currently operating on Beam Line VI. Recent hardware improvements in the PDP computers would allow the whole system to be made much smaller and less expensively than the current 11/34 system.

Documentation - In 1986 a computer-aided design (CAD) system was introduced and used to produce drawings and documentation for beam line controls. A library of drawings is stored in the system allowing quick and easy drawing modification. Also, in an effort to improve the existing documentation, a data base was developed which contains information about the various control units. The immediate use of the data base is for construction preparation, expediting, and material planning.

Photon Beam Steering and Stabilization Systems - In 1986 the eighth closed-loop vertical beam steering system was implemented on the SPEAR ring to serve the newly constructed Beam Line VIII. The beam line has a dedicated port for an ion chamber photon position monitor. Thus a narrow-gap version of the monitor was used, achieving a higher degree of response linearity as a function of beam position and intensity than afforded by the wide-gap models employed in lines where the beam must pass unobstructed to downstream experiments. LLNL improved the design of the ion chamber anode and cathode plates by electroplating them with a gold "flash" that will, presumably, greatly reduce the level of long term corrosion or oxidation experienced while in a radiated helium environment. More detailed descriptions of SSRL position monitors and steering systems are given in previous Activity Reports ('82-'85).

Also completed in 1986 was the implementation of SPEAR computer controlled 3-magnet orbital bump configurations for both vertical and horizontal planes at locations all around the ring. The 3-magnet bumps enable localized orbit changes to be made over specific regions in the ring that overlap the beam line source points. Typically two or more different bump configurations will overlap any given source point, each bump affecting orbit position and angle differently. Thus combinations of bumps can be used to obtain virtually any desired combination of orbital position and angle at each source point, within certain limits. These horizontal and vertical "software bumps" are controlled by the SPEAR operator and greatly facilitate orbit adjustment and synchrotron beam alignment during the initial set-up of ring configurations for SSRL operation.

During 1986 work was begun on the replacement of existing prototype steering control units at SPEAR with upgraded, computer-interfaced

units. The new system will enable complete remote control of the steering system, either from the SPEAR control console or even from a remotely located SSRL console, and will provide the SPEAR control program with information from the SSRL position monitors and servo units. This information can then be used to augment and refine the level of automated orbit control in the future. These new systems will be installed in the SPEAR control room during 1987.

Also scheduled for completion in 1987 is the installation of another closed-loop vertical steering system for the new PEP Beam Line 1B, and the continuing development of the 2-loop servo system for PEP beam lines that will correct orbital position and angle independently at the source point (described in the 1985 Activity Report).

Angiography Personnel Protection Interlock System - For use as an angiography station for human subjects in May, 1986, the Beam Line IV-2 hutch was equipped with a personnel protection interlock that would permit a person to receive a controlled dose of synchrotron radiation. An Angiography Personnel Protection Interlock (APPI) was configured that would:

o permit safe access to the patient exposure area while the synchrotron radiation beam was illuminating the upstream dual-energy monochromator (to preserve thermal stability of the monochromator);

o allow a patient to be radiated by the monochromatized beam under the supervision of a radiologist, with scan chair motion and precision shutter actuation regulated by an angiography control computer, while providing a suitable number of safeguards against accidental radiation exposure;

o have different modes of operation to accommodate equipment set-up, test, and calibration and patient exposure;

o ensure the quick extinction of the beam in access areas if a potentially unsafe condition was detected.

The Beam Line IV-2 hutch was divided into two sections, front and rear, with a set of panels. The front hutch contained the dual-energy monochromator and other ancillary equipment, as well as a pair of redundant fast-acting beam shutters that controlled beam exposure to the rear hutch. The rear hutch served as the angiography exposure area and was equipped with the computer controlled scan chair.

Access to the front hutch was supervised by the standard SSRL hutch protection system (HPS): keyed interlock panel, lockable doors, and upstream redundant beam stoppers ("hutch stoppers"). The rear hutch was fitted with a pair of swinging doors with no locks, allowing quick access or egress in case of medical emergency; access was supervised by the new APPI system. Primary radiation protection for the rear hutch was provided by the fast-acting pair of "safety shutters".

When a human heart scan was to be performed, the APPI was operated in "patient" mode. A "diagnostic" mode was also provided to allow equipment set-up, alignment, calibration, etc., in the rear hutch to be quickly carried out without having to satisfy the complete patient mode interlock. In patient mode, the safety shutters could not be opened unless:

o both swinging doors were closed;

o a hand-held "scan switch" was depressed by the radiologist during a key-started timer interval, and was held depressed during the entire patient scan period;

o the scan chair was moving faster than a certain speed determined by a redundant set of motion detectors, so as to prevent patient overexposure during changes in direction as well as in the event of motion malfunction; and

o a redundant pair of "exposure timers", triggered by the initial computer-generated request to open the safety shutters and intended to limit the overall scan period to an interval determined by the radiologist, were active.

An APPI system fault would be generated if either safety shutter was not closed and one or more of the above conditions were not satisfied, or if either one of two "scan stop" buttons were pressed, or if the APPI detected an internal logic fault. An APPI fault would close both safety shutters and hutch stoppers, but would not cause the loss of stored beam in SPEAR.

The APPI system was subjected to hundreds of operational tests before being used for the human scan experiments. During the human patient experimental run, extensive system checkouts were carried out each morning before patient exposure was allowed. The successful functioning of the APPI system during these tests enabled the human angiography experiment to be performed at SSRL. By the same token, the barrage of tests and "hands on" experience has led to the identification of a number of items in the system, prototypical in nature, that could be improved or refined for future regular use. Among these are more polished designs for the safety shutters and chair motion detectors, and a more convenient means for converting the Beam Line IV-2 hutch from its normal operational mode to the angiography mode. Implementation of these changes is planned before the next human angiography experiment at SSRL.

MECHANICAL ENGINEERING

New Beam Lines Including Monochromators and Insertion Devices - The ME group has a major involvement in the design, construction and installation of the many components of a beam line. This activity ranges from full responsibility for the design and construction of beam lines that are fully funded by DOE through SSRL to varying lesser degrees of involvement in beam lines funded in other ways by Participating Research Teams (PRT's). Assembly, test and installation of beam line components is often carried out primarily by others (e.g. SSRL vacuum and operations groups) with advice, assistance and supervision by the ME group.

In 1986 the ME group, in cooperation with other groups worked on the following new beam lines and monochromator systems: PEP Beam Line 5B, PEP Beam Line 1B, SPEAR Beam Line III-2, SPEAR Beam Line VIII, SPEAR Beam Line X, Beam Line V monochromator, plus 24 and 30 period undulator installation in Beam Line V.

Booster Synchrotron Injector for SPEAR - Design studies were begun for components of a proposed new injector for SPEAR, in cooperation with the SSRL Accelerator Physics Group. Layouts have been made for the bend, quadupole, and sextupole magnets, magnet assembly fixturing and alignment devices, and the vacuum system.

In-Vacuum Hard X-Ray Monochromator- Design studies have begun for a cooled crystal monochromator that would operate in the beam line vacuum upstream of the beryllium windows. Such a device would greatly reduce the thermal loading, and hence thickness requirements, of the beryllium windows and permit operation of the beam line at lower photon energies. The work is being carried out in collaboration with the SSRL X-Ray Group and Lawrence Livermore Laboratories.

Thermal-Structural Analysis - Thermal-structural analysis based upon classical methods and handbook formulae has become inadequate to predict temperatures and stresses encountered in the high power beam lines under development at SSRL. Analytical methods used in the past led to conservative design of beam line components, resulting in large safety factors, uncertainty of performance, and limitations on the types of experiments that could be performed.

Mechanical Engineering has begun to use the "finite element method" to refine its calculations of temperatures and stresses in beam line components. This method allows an accurate geometric model of an item to be built, thermal and structural loads applied, and temperatures, stresses, and deformations calculated. The analyses are performed by a highly optimized program, NASTRAN, running on the VAX 11-780. Components analyzed include the Beam Line V monochromator vacuum vessel and granite support block, masks, mirrors, beryllium windows, shutters, crotches, and bend magnet synchrotron radiation heat absorbers.

NASTRAN is a large and complex program, and at present only one engineer at SSRL is trained in its use. In 1987 SSRL will purchase a simpler program that will run on PC's, microVAXs, and the VAX 11-780. The model building portion of this program can be used by designers to reduce the amount of time that engineers must spend in the tedium of model building. This program will also accept models built with Cadkey, the computer aided design package used in the design group. The integration of design and analysis activities will allow thermal-stress predictions to be made more quickly and efficiently.

Beryllium Window Studies - Scientists at SSRL and elsewhere have become interested in using Beam Line VI in undulator mode to produce tightly collimated x-ray beams at lower photon energies. Since the carbon filters and beryllium windows absorb photons of the desired spectral range, interest has been shown in reducing the amount of carbon and beryllium traversed by the x-ray beam. Reducing either material thickness causes the temperature and stresses in the window to increase. Effort has therefore been spent to reduce the amount of conservatism in the thermal analyses, and to measure the thermal response of the window to heat loads.

In 1986 Mechanical Engineering at SSRL and Lawrence Berkeley Laboratories determined ring and insertion device parameters that allowed the reduction of thickness of the second 0.0254 cm window to 0.0127 cm and potential removal of most of the carbon in the filter set. In addition, a test program was initiated at SSRL and Livermore to measure the temperature distribution on the first beryllium window. At present Livermore is heating a 0.0127 cm window with an optical laser heat source, and measuring the

temperature distribution with an infrared camera. Planned for 1987 is a test on Beam Line VI where the temperature distribution on the first window will be measured *in situ*. This effort is a collaboration of SSRL, Lawrence Berkeley, and Lawrence Livermore Laboratories. Results will enable SSRL to set realistic limits on the use of the beam line with minimized thicknesses of carbon filters and beryllium in the windows. A permanent method of monitoring window temperature may be installed. Further analysis may lead to the reduction of thickness of the first window.

Also planned for 1987 is a survey of the limits imposed on SPEAR energy and current by ring components (particularly crotches on wiggler lines) and beam line components such as masks and beryllium windows. This survey will be accomplished in part by use of finite element analysis techniques.

Computer Aided Design - SSRL currently has one CAD system running on an IBM PC/AT clone, driving a large, E-size plotter. Even though this system has been in service only a short time, significant work has been accomplished with it. In the past, drawing layouts of potential beam lines on SPEAR or PEP was a very time consuming process. Drawings were not easily modified, and often required complete redrawing if components were to be added in the middle of a line, or the beamline had to be moved to a different location.With CAD, this exasperating process is greatly simplified. The CAD system produces drawings in as many as fifteen colors, which increases the utility of complicated drawings.

In 1987 Mechanical Engineering will make CAD available to several of the design staff. The designers will not only use these systems for conventional design tasks, but will use the drafting programs for building structural models to be used in finite element analysis.

VII SSRL ADVISORY PANELS

PROPOSAL REVIEW PANEL

A main task of the Proposal Review Panel is the review and rating of scientific proposals to SSRL based largely on reports obtained from outside (non-panel) referees. The panel met on January 17 and 18, 1986 and on July 18 and 19, 1986 at SSRL and rated the new proposals which had been received in September, 1985 and March, 1986, respectively.

As of December 31, 1986 SSRL had received a total of 1061 proposals of which 137 are presently active.

The Proposal Review Panel meets twice yearly, generally in June and January. Deadlines for receipt of proposals for full consideration at the next meeting are the first of September and the first of March of each year.

The panel members in 1986 were:

Biology Sub-panel
Charles Cantor, Columbia University (Chairperson)
Wayne Hendrickson, Columbia University
William Orme-Johnson, MIT

Materials Sub-panel
Boris Batterman, Cornell University
Howard Birnbaum, University of Illinois
Russell Chianelli, Exxon
Denis McWhan, AT&T Bell Laboratories

VUV Sub-panel
Bernd Crasemann, University of Oregon
Charles Fadley, University of Hawaii
Warren Grobman, IBM Watson Research Center

Dr. Hugh Harnsburger left the panel after the July 1986 meeting. He was replaced by Dr. Russell Chianelli.

SCIENCE POLICY BOARD

The Science Policy Board reviews all aspects of SSRL operation, development and plans for the future. It reports to Stanford University President Donald Kennedy. The Board met once during this reporting period, on June 8 and 9, 1986. The members at the time of the meeting were:

P.A. Wolff, MIT (Chairperson)
Wm. Brinkman, Sandia Laboratories
Wm. Orme-Johnson, MIT
B. McDaniel, Cornell University
E. Ginzton, Varian Laboratories
W. Kohn, University of California

The June meeting marked the end Dr. Brinkman's term. A replacement for Dr. Brinkman, as well as several additional members have been appointed for 1987.

SSRL USERS ORGANIZATION

Members of the Executive Committee of the SSRLUO were appointed at the Thirteenth Annual SSRL Users Group Meeting as follows:

Jo Stohr, IBM (Chairperson)
Bob Bachrach, Xerox
Paul Citrin, AT&T Bell Laboratories
Robert Greegor, Boeing Company
Jeff Kortright, LBL
Scott List, Stanford University
Marjorie Olmstead, UC-Berkeley
Tom Russell, IBM Research Laboratory
Lane Wilson, Stanford University
Joe Wong, Lawrence Livermore National Laboratory
Steve Cramer, Schlumberger-Doll Research (Past-Chairperson)
Katherine Cantwell, SSRL (Secretary)

The Users Organization Executive Committee meets periodically throughout the year to consider and advise on matters pertinent to user interests at the Laboratory.

THIRTEENTH ANNUAL SSRL USERS GROUP MEETING

The Users Group Meeting was held this year on October 23 and 24, 1986. The SSRLUO Executive Committee is responsible for organizing the Users Group Meeting jointly with a representative of the SSRL scientific staff. Approximately 138 people were in attendance. The program for the meeting and the authors' abstracts are available as SSRL Report Number 86/02.

Co-Chairpersons for the meeting were Joachim Stohr for the Users Organization and Britt Hedman for the SSRL scientific staff. Reports on individual experiments were presented in poster sessions.

VIII SSRL ORGANIZATION

The chart on the following page depicts the functional organization of SSRL as January 1987. The SSRL administration is divided into seven functional areas each headed by a senior staff member. These are : X-ray, VUV, Biotechnology, Accelerator Physics, Operations, Engineering and Administrative Services. Responsibility for each experimental station and piece of facility equipment is assigned to a staff scientist. The charts below detail these assignments as well as responsibilities for major SSRL development projects.

SSRL CHART OF RESPONSIBILITIES

BRANCH LINE	RESPONSIBLE SCIENTIST/ENGINEER
BL I-1 *(4^o VUV)*	I. LINDAU/A. WALDHAUER
BL 1-2 *(8^o VUV)*	I. LINDAU/M. ROWEN
BL 1-4 *(BEND -X-RAY)*	S. BRENNAN/H. TOMPKINS
BL 1-5 *(BEND -X-RAY)*	G. BROWN/T. TROXEL
BL II-2 *(BEND X-RAY)*	G. BROWN/T. TROXEL
BL II-3 *(BEND X-RAY)*	G. BROWN/T. TROXEL
BL II-4 *(WHITE RADIATION-X-RAY)*	Z. REK
BL III-1 *(4^o VUV)*	I. LINDAU/A. WALDHAUER
BL III-2 *(18^o VUV)*	I. LINDAU/A. WALDHAUER
BL III-3 *(2^o SXR)*	I. LINDAU/M. ROWEN
BL III-4 *(3^o SXR)*	P. PIANETTA
BL IV-1 *(WIGGLER)*	G. BROWN/T. TROXEL
BL IV-2 *(WIGGLER)*	G. BROWN/T. TROXEL
BL IV-3 *(WIGGLER)*	S. BRENNAN/H. TOMPKINS
BL VI-2 *(WIGGLER)*	D. MONCTON *(EXXON)*, J. KORTRIGHT *(LBL)* J. ARTHUR *(SSRL)* /T. TROXEL
BL VII-1 *(ROTATION CAMERA)*	P. PHIZACKERLEY
BL VII-2 *(WIGGLER)*	S. BRENNAN/H. TOMPKINS
BL VII-3 *(WIGGLER)*	G. BROWN/T. TROXEL
BL VIII *(TGM)*	I. LINDAU/M. ROWEN
LIFETIMES PORT *(90^o VUV)*	UNSUPPORTED
PEP BEAM LINE 5	G. BROWN/T. TROXEL

INSTRUMENTATION/FACILITY RESPONSIBILITIES

MATERIALS DIFFRACTOMETER:	S. BRENNAN/H. TOMPKINS
VACUUM SAMPLE CHAMBERS:	A. WALDHAUER
AREA DETECTOR:	P. PHIZACKERLEY
CAD-4:	E. MERRITT
COMPUTER SYSTEMS:	T. COX
VII-2 SPECTROMETER:	S. BRENNAN/H. TOMPKINS
BIOCHEMISTRY LABORATORY:	B. HEDMAN
DARKROOMS:	P. PHIZACKERLEY, Z.REK
BEAM LINE STEERING:	R. HETTEL
EXAFS EQUIPMENT/SOFTWARE:	B. HEDMAN
SAS CAMERA:	S. WAKATSUKI
EXAFS CONSULTANT:	B. HEDMAN
SCATTERING CONSULTANT:	S. BRENNAN
RT-11 SOFTWARE CONSULTANT:	S. BRENNAN

SSRL DEVELOPMENT PROJECTS - RESPONSIBLE PERSONNEL

PROJECTS PRESENTLY UNDERWAY

BEAM LINE V - I. LINDAU (SSRL)/R.BACHRACH (XEROX)/B.YOUNGMAN (SSRL)

BEAM LINE VIII - C. POPPE (LLNL)/A. MARADUDIN (UC)
SSRL PROJECT MANAGER - J. CERINO

BEAM LINE X - C. POPPE (LLNL)/A. MARADUDIN (UC)/S. BRENNAN (SSRL)
SSRL PROJECT MANAGER - J. CERINO

STATION VI-1 - R. TATCHYN (SSRL)/H. HOGREFE (LBL)
R. YOTAM (SSRL)/ J. CHIN (LBL)

LITHOGRAPHY STATION - P. PIANETTA (SSRL)

PEP BEAM LINE 1B - G. BROWN (SSRL)/R. BOYCE (SSRL)/R. HETTEL (SSRL)

PEP BEAM LINE FACILITY 1B - G. BROWN (SSRL)/M. OBERGFELL (SLAC)

LAB-OFFICE-SHOP-BUILDING - G. BROWN (SSRL)/O. PIERON (Stanford)

PROJECT IN INITIAL STAGES

3 GeV SPEAR INJECTOR - H. WIEDEMANN (SSRL)/ J. CERINO (SSRL)

PEP BEAM LINE 12 - G. BROWN (SSRL)/R. BOYCE (SSRL)

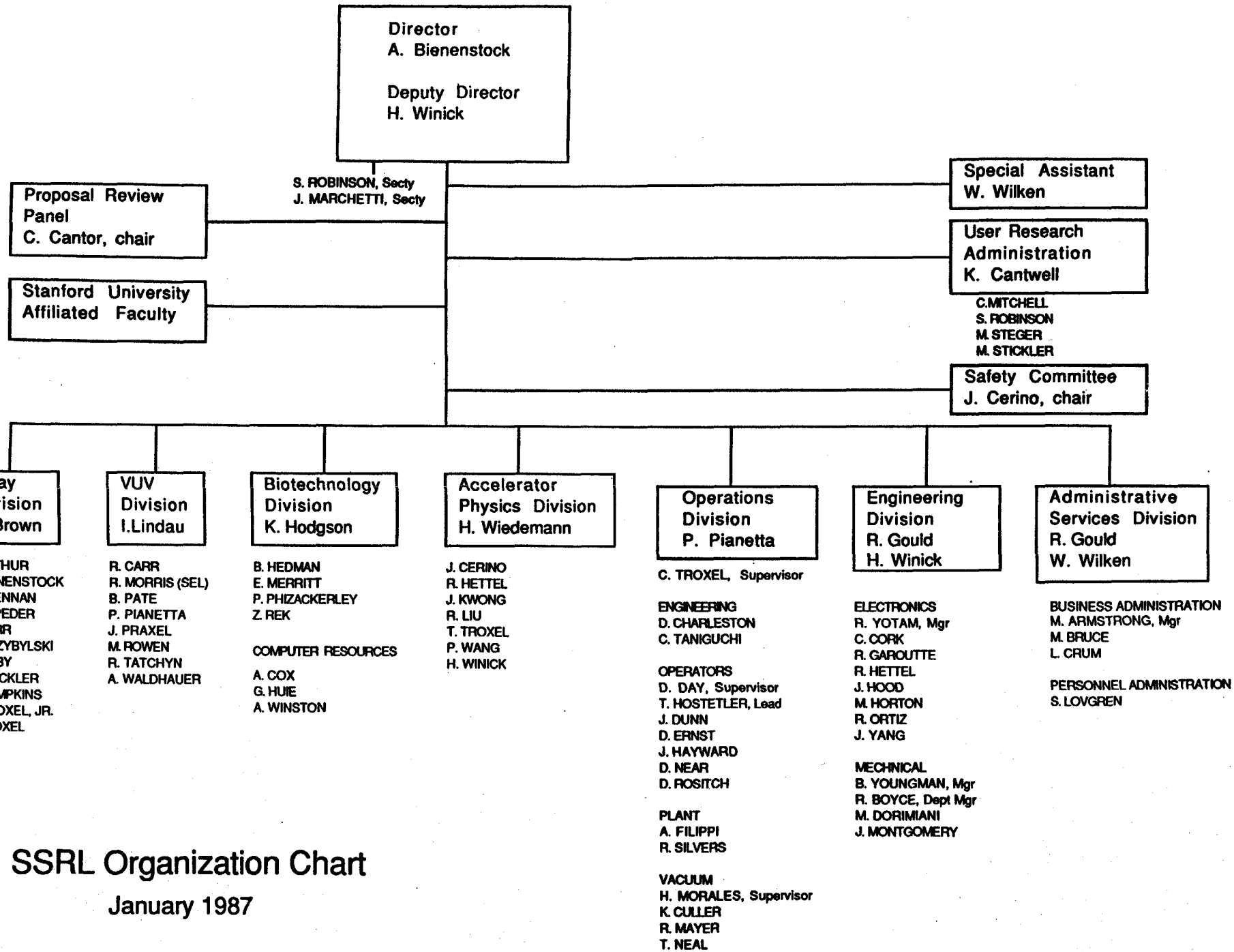

SSRL Organization Chart

January 1987

IX EXPERIMENTAL PROGRESS REPORT

X-RAY ABSORPTION STUDIES OF DISORDERED SYSTEMS

E.D. Crozier, N. Alberding, A.J. Seary, K.R. Bauchspiess, D. Jiang
Physics Department, Simon Fraser University
Burnaby, B.C., Canada V5A 1S6

R. Ingalls and B. Houser
Physics Department, University of Washington
Seattle, Wash., 98195, U.S.A.

X-RAY ABSORPTION AT HIGH PRESSURES

Low Temperature Studies

During this reporting period our x-ray absorption studies were extended to low temperatures (1). This permits the study of pressure-dependent effects that do not occur at room temperature and, through the reduction of thermal motion, has the advantage of providing improved resolution of physical phenomena studied at higher temperatures.

Results were obtained at 77 K for Cu, RbCl and the pressure-induced mixed valent transition in SmSe. The latter is also discussed under proposal number 984. The quality of the data is indicated in the insert of Fig. 1 which shows $k\chi(k)$ for the Se K-edge at 55 kbar and 77 K. The magnitudes of the Fourier transforms of $k\chi(k)$ are also shown for the Se edge at 1 bar, 295 K (dashed line), 37 kbar, 77 K (dot-dash line) and 55 kbar, 77 K (solid line). The Se edge is of particular importance to studying the mixed valent transition because of the enhanced spatial resolution possible. At 77 K the Se EXAFS is still observed at $k = 24$ Å^{-1} due to the onset of the L_2-edge. The large k-space range permits quantitative measurement of the backscattering amplitude for Sm^{2+} (below the transition) and for Sm^{3+} (above the transition). The increase in the EXAFS Debye-Waller factor σ_1^2, which occurs in the middle of the mixed valent transition region, is observed for both Sm and Se edges at room temperature and 77 K. This increase has two components; one, due to normal thermal motion of the atoms and two, due to the breathing mode associated with the valence fluctuation of the Sm ion. The low temperature data permits their separation.

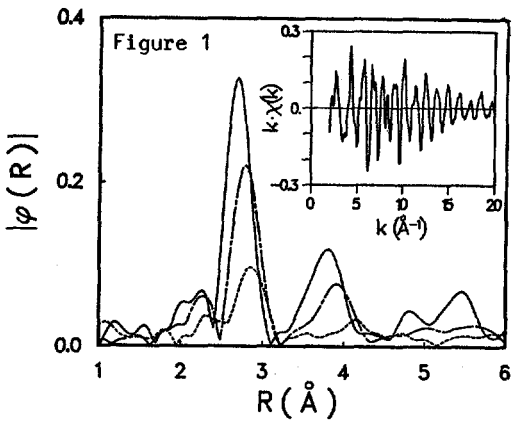

α-Quartz GeO_2

Germanates generally occur in structures similar to the geologically important silicates. Often they will undergo the same pressure-induced transitions as the corresponding silicate, but at lower pressures. As such, they generally model the behavior of silicates at the higher pressures found in deep Earth conditions. However, in contrast to α-quartz SiO_2, our EXAFS measurements indicate that α-quartz GeO_2 does not transform to another phase up to the highest pressure we studied, 59 kbar.

The α-quartz structure is hexagonal with three Ge atoms per unit cell. These sit at the centers of corner-linked GeO_4 tetrahedra. With increasing pressure the EXAFS deduced Ge-Ge distance decreases while the Ge-O distance remains constant. Though we lack the angular resolution to distinguish between cooperative rotations of the tetrahedra and distortions of the tetrahedra which preserve the Ge-O distance, our observations are consistent with the studies of Jorgensen (2), but go to significantly higher pressure. We have used extrapolations of Jorgensen's results to produce the pressure-versus-volume curve for α-quartz GeO_2, and have parameterized it using the Murnaghan equation of state.

Metallic Iron

At standard temperature and pressure, iron is ferromagnetic and has the b.c.c. structure. At higher temperature, it is paramagnetic with the f.c.c. structure, while at high pressures it is h.c.p. with no known magnetic phase down to a few millidegrees Kelvin. X-ray absorption studies were initiated in an attempt to see details of local atomic rearrangements which have not yet been completely determined by x-ray diffraction (3).

X-ray absorption studies of iron at high pressure are difficult because of the low energy of the K-edge (7.1 keV) and high absorption due to the pressure cell. With our pressure cell containing boron carbide anvils, we recently obtained excellent preliminary data on the 120 kbar b.c.c. to h.c.p. transition. The data exhibits a large mixed phase region in which the radial distribution appears to show a continuous change from the one structure to the other. We have also succeeded in studying the h.c.p. phase to over 200 kbar. Further data collection and analysis is planned on this system.

Data have also been obtained on the f.c.c. phase of iron (stabilized as precipitates in a copper matrix) permitting comparison of the XANES of the three phases with each other, and with first-principle calculations.

SURFACES

We have begun a program to study the structure of surfaces and interfacial regions using the grazing incidence EXAFS technique. At angles near the critical angle for total reflection, the x-rays are confined to the interfacial region. Thus the reflected and fluorescence x-rays, as well as the emitted electrons, provide EXAFS spectra with a high signal-to-noise ratio, permitting rapid, in situ measurements.

We have demonstrated that an interface protected by a coating of low atomic number can be examined (4). The

angular dependence of the reflectivity of a multilayer film, 150 Å of Si, 230 Å of Cu and 300 Å of Au deposited on an optical silica window is shown in Fig. 2 for the x-ray energy 11918 eV (Au L_3-edge). The agreement between theory (solid line) and experiment is good for angles greater than 2 mrad. The onset of penetration into the Cu layer occurs at 3 mrad and into the Au layer at 6 mrad. At lower angles the reflectivity is reduced by surface roughness, finite sample thickness and finite beam height. The theoretical curve was calculated using Parratt's formulae (5) and the anomalous scattering factors of Cromer (6). From the reflectivity and the fluorescence yield, which is approximately proportional to 1 - R, it is possible to select accurately the angle to acquire the EXAFS for a specific penetration depth. This was done to examine the Cu and Au layers as a function of depth, with emphasis on the interfacial regions.

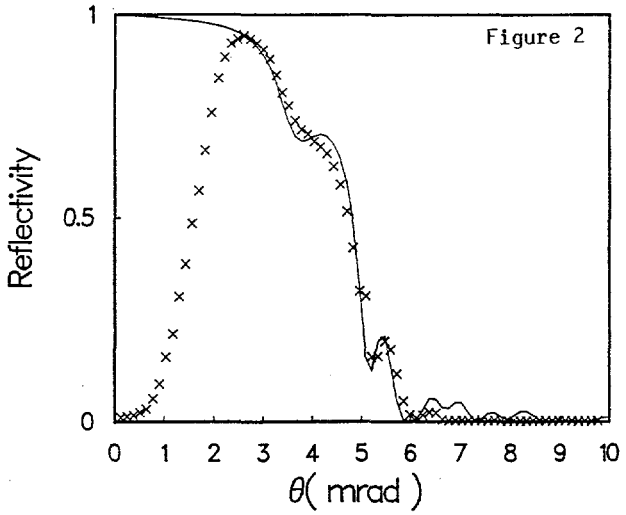

When Ni is grown epitaxially on the (100) face of Fe single crystals, the first 6 layers have the symmetry of bcc. When additional layers are grown, the structure is neither bcc nor the normal fcc structure of Ni (7). In an attempt to determine this structure, we examined a film of Ni, ~ 50 Å thick, which was grown epitaxially on Fe (100) in an ambient pressure of 10^{-10} torr by B. Heinrich. At angles of incidence less than the critical angle, the detected fluorescent x-rays emanated mostly from the top 15 Å of the sample. The EXAFS indicated the film to be a mixture of fcc Ni and NiO. At larger angles of incidence (increasing depth) the percentage of Ni increased (4). Although the sample was maintained in a nitrogen atmosphere, oxidation of the Ni evidently occurred before the EXAFS measurements. In our next experiments, the Ni will be covered with an epitaxially deposited passive film of lower atomic number to prevent oxidation of the Ni, and yet permit determination of the structure of the new phase.

MULTIPLE SCATTERING STUDIES

Pressure-dependent studies of ReO_3 allowed us to obtain spectra exhibiting focussed multiple scattering where the forward scattering angle at 0 could be continuously varied by adjusting the pressure. The angle as a function of pressure is known (8) thus the EXAFS amplitude of the second-neighbor Re shell can be analyzed to give the variation of the oxygen's forward scattering amplitude with scattering angle (9).

In structures such as ReO_3 where focussed multiple scattering occurs, the bending fluctuations of the Re-O-Re angle affect the EXAFS amplitude, but in a manner which is not described by the normal Debye-Waller factor. We have derived expressions to replace the Debye-Waller factor for such cases (10). We have shown that: 1) the individual effects of stretching and bending on the reduction of the EXAFS amplitude can be separated, 2) the effect of the stretching modes is given by the usual Debye-Waller factor and 3) for the bending modes, amplitude reduction factors equivalent to the Debye-Waller factor can be derived.

The near edge structure of the spectra of the cis- and trans- isomers of some platinum compounds has differences in the region just above the L_3 edge white line. In these cases the platinum ligands are Cl and either N, S or Ar. Although the radial distribution functions are similar, the multiple scattering paths Pt-R-R-Pt and Pt-Cl-Cl-Pt exist only in the cis- form. We believe that the spectral differences can be interpreted in terms of the different multiple scattering pathways.

A similar situation exists in ReO_3 where a peak at 3.2 Å can be explained only by Re-O-O-Re scattering via the oxygen atoms of the ReO_6 octahedra. In this case, as with the Pt compounds, the L_3-edge spectra are observed. It has been shown that for the K edge, the multiple scattering signal disappears when the angle between the outgoing and incoming photoelectron is 90 deg. (11). Our empirical evidence is that this cancellation does not occur in L_3-edge spectra. The analysis of the multiple scattering component of the EXAFS allows probing the deformation of the ReO_6 octahedra, as well as their compression and rotation, at the pressure-induced transition at 5.2 kbar.

We also report here the temperature dependence of the EXAFS spectra of another perovskite, Na_xWO_3 (x = .67), in which focussed multiple scattering occurs. It differs from ReO_3 in that it undergoes three separate transitions with increasing temperature (12), and therefore has an additional thermal effect which competes with the effect of the structural transformations. It is simplest to look from the perspective of decreasing temperature. At high temperature (about 130°C), all six W-O-W bonds are linear. At the first transition the WO_6 octahedra undergo a collective rotation about a cubic [100] direction. This transition is second-order, and the order parameter is the deviation of the bond angle from 180 degrees. In this phase, two of the W-O-W bonds remain linear. The second transition is the rotation about the [110] direction, in which all six W-O-W bonds are bent. It is first-order, and occurs slightly above room temperature. The final transition, at about 0°C, results in a net rotation about the [111] direction, actually returning the crystal to cubic symmetry, albeit with a doubling of the unit cell spacings.

EXAFS spectra of Na_xWO_3 were taken at six temperatures from 28°C to 196°C, spanning the three higher-temperature phases. We observed that the changing thermal factor cancels the effects of the changing bond angles, and the W-W peak in the radial distribution function remains nearly unchanged until the transformation to the highest-temperature phase, after which the peak height decreases markedly. We intend to use the EXAFS spectra of ReO_3 to deconvolve these competing effects as Re and W have nearly identical scattering characteristics.

METAL-BASED CHEMOTHERAPEUTIC AGENTS

Knowledge of how metal complexes bind to polynucleotides is important for understanding their ability to inhibit template replication. We have used EXAFS

spectroscopy to examine aspects of $Rh_2(acetate)_4$ binding to purines (13) and have now obtained results on its binding to polyadenylic acid -- a single-stranded DNA chain consisting entirely of adenosine base units. Spectra of rhodium acetate bound to adenosine-monophosphate and bound to polyadenylic acid were taken at room temperature and liquid nitrogen temperature. The Fourier transforms of the spectra of both complexes were very similar at room temperature. The Fourier transform of the spectrum of the rhodium acetate-polyadenylic acid sample taken at liquid nitrogen temperature showed prominent peaks at around 6 Å and 9 Å (see Fig. 3). These peaks were identified to be Rh because the high-k amplitudes of these shells, obtained by Fourier filtering, were much larger than would be expected for other atoms present, O, C, N and P. Analyzing the relative phase of these shells gave distances of 6.3 Å and 9.3 Å. In order to obtain a structural model consistent with these EXAFS results we have used a molecular modelling program that searches for a molecular conformation of minimum energy given a set of intermolecular forces. We have found that the EXAFS distances are reasonable when each rhodium-acetate unit is bound by one Rh atom to a single adenosine. When two rhodium-acetates are bound to consecutive adenosines, the separation between the Rh atoms binding the adenosines is roughly 6 Å. When an unbound adenosine intervenes between two binding sites, distances in the range of 9 Å emerge. Thus we conclude that the binding is monodentate and that binding to adjacent bases is not sterically hindered. The appearance of these high-r Rh shells only at low temperature suggests that low energy bonds are important for stabilizing the structure.

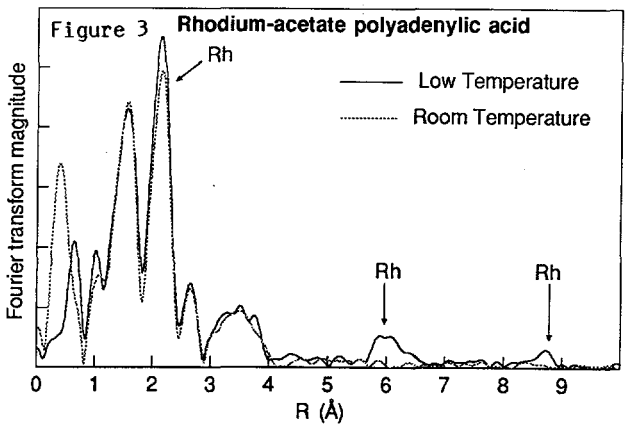

SINGLE LAYER COMPOUNDS

We have continued investigating single layers of MoS_2 which have applications in catalysts and inclusion compounds. A problem encountered last year was the conversion of the suspended phase to an oxidized form. This is now resolved and we have completed a series of EXAFS and XANES measurements on several forms of MoS_2: single layers in water suspension, dry-restacked and samples of intermediate dryness. Crystalline MoS_2 has a first Mo-Mo distance at 3.15 Å, which appears as a clear peak in the Fourier transform (Fig. 4). This peak disappears in the suspension and is replaced by two peaks which we have identified as Mo by analysing the amplitude. These peaks give Mo-Mo distances of 2.8 Å and 3.8 Å respectively. The Mo peak at 6.3 Å disappears in the wet samples suggesting less long-range order. It reappears, however, in the Fourier transform of the restacked form's spectrum. As can be seen in Fig. 4 the intermediate forms can be interpreted as a combination of the crystalline and suspended forms. The near-edge spectra show subtle changes which have not been fully interpreted, but would be consistent with decreased order or loss of symmetry in the Mo ligation which is not completely recovered in the restacked form. By combining the EXAFS results with x-ray diffraction and optical data we have proposed a model in which the lattice is distorted by contact with water molecules. (14)

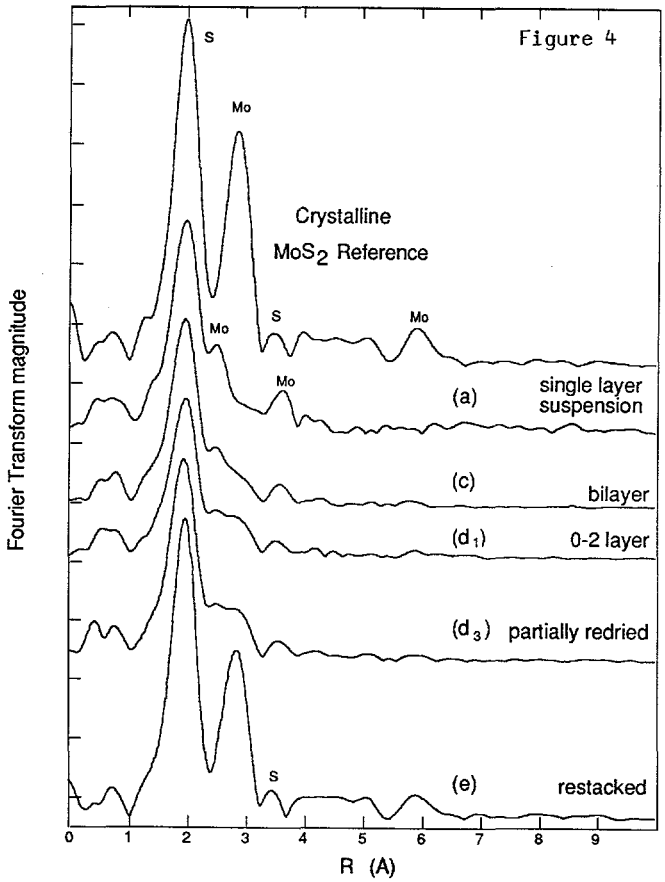

REFERENCES

1. K.R. Bauchspiess, E.D. Crozier and R. Ingalls, J. de Phys. (in press).
2. J.D. Jorgensen, J. Appl. Phys. 49 (1978) 5473.
3. A.P. Jephcoat, H.K. Mao, and P.M. Bell, J. Geoph. Res. 91, (1986) 4677.
4. D. Jiang, N. Alberding, A.J. Seary and E.D. Crozier, J. de Phys. (in press).
5. L.G. Parratt, Phys. Rev. 95 (1954) 359.
6. D.T. Cromer, J. Appl. Cryst. 16 (1983) 437.
7. B. Heinrich, A.S. Arrott, J.F. Cochran, S.T Purcell, K.B. Urquhart, N. Alberding, and C. Liu, in "Thin Film Growth Techniques for Low-dimensional Structures", NATO ASI Series.
8. J.E. Jorgensen, J.D. Jorgensen, B. Batlogg, J.P. Remeika, J.D. Axe, Phys. Rev. B 33 (1986) 4793.
9. N. Alberding, E.D. Crozier, R. Ingalls and B. Houser, J. de Phys. (in press).
10. N. Alberding and E.D. Crozier (submitted).
11. G. Bunker and E.A. Stern, Phys. Rev. Lett. 52 (1984) 1990.
12. R. Clarke, Phys. Rev. Lett., 39 (1977) 1550.
13. N. Alberding, N. Farrell and E.D. Crozier, J. Am. Chem. Soc. 107 (1985) 384.
14. P. Joensen, R. Frindt, E.D. Crozier and N. Alberding (submitted).

SYNCHROTRON RADIATION BASED TRANSVENOUS CORONARY ANGIOGRAPHY

E. Rubenstein[1], G.S. Brown[2], J.C. Giacomini[1], H.J. Gordon[1],
R. Hofstadter[3], R.S. Kernoff[1], W. Thomlinson[5],
A.C. Thompson[4], H.D. Zeman[3]

Department of Medicine, School of Medicine[1],
Stanford Synchrotron Radiation Laboratory[2]
Hansen Laboratories of Physics & Department of Physics[3],
Stanford University, Stanford, California 94305;
and
Lawrence Berkeley Laboratory, University of California[4],
Berkeley, California 94720;
and
National Synchrotron Light Source, Brookhaven Laboratory[5],
Long Island, New York 11973

Substantive improvements were made in the imaging system that has been under development on beam line IV-2. The X-ray fluence was increased by the use of asymmetrically cut monochromator crystals; a new dual-drum X-ray beam chopper was constructed which allows scanning speeds at the rate of 12 cm/sec and decreases the line exposure time; a new subject support system was built and installed; and a personnel protection system was developed and implemented to insure the safe exposure of human subjects in the synchrotron X-ray beam. The enhancements in the X-ray optics resulted in striking improvement in the quality of transvenous canine angiograms compared with those recorded previously.

These results led to the use of this imaging system in May 1986 on three human subjects, each of whom was under treatment for coronary artery disease at the Palo Alto Veterans Administration Hospital at the Stanford University Medical Center [1].

The operating parameters for these studies were: electron beam energy 3.0 GeV; electron beam current 51.5 to 80.4 mA; scanning speed 6 or 12 cm per sec; line exposure time 1.7 or 3.3 msec; interval between exposures 0.4 or 0.8 msec; total time to record one frame (256 lines) 2 sec or 3 sec (including starting and stopping time). The contrast agent (Renografin-76) was injected at rates of 12-15 ml per sec and in volumes of 36 to 50 ml (0.41 to 0.67 ml per kg) by means of a 6.7 French pig-tail catheter, inserted into the internal jugular vein and positioned so that its tip was in the distal superior vena cava or right atrium. The X-ray dose per frame varied from 0.10 to 0.29 rads.

Images were recorded of the left anterior descending coronary artery, the right coronary artery, and of saphenous vein and internal mammary artery grafts. Greater X-ray fluence is needed to provide images of clinical quality. Improvements in the imaging system are now being made to achieve the needed fluence.

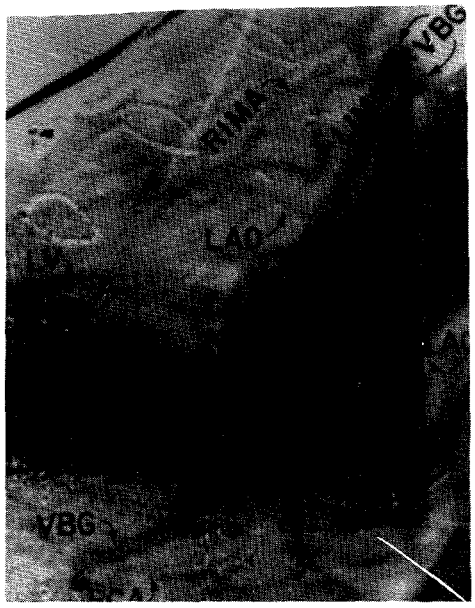

Figure 1. A synchrotron transvenous coronary angiogram done during May 1986 on a 48-year-old man who had undergone coronary artery surgery for diffuse coronary atherosclerosis. The image shows the left internal mammary artery (LIMA) anastamosed to the left anterior descending coronary artery (LAD), and vein bypass grafts (VBG), one of which is anastamosed to the right coronary artery (RCA). Poor postoperative perfusion of the LAD and the RCA are revealed. These findings were corroborated at the time of repeat surgery.

References.

1. E. Rubenstein, R. Hofstadter, H.D. Zeman, A.C. Thompson, J.N. Otis, G.S. Brown, J.C. Giacomini, H.J. Gordon, R.S. Kernoff, D.C. Harrison, W. Thomlinson (1986) Proc. Natl. Acad. Sci. USA 83, 9724

RESONANT PHOTOEMISSION STUDIES OF NARROW BAND MATERIALS

J.W. Allen*, J.-S. Kang*††, W.P. Ellis**, R. Albers**, B.B. Pate†
M.B. Maple††, M.S. Torikachvili††, I. Lindau†, and Y. Lassailly*†

*Xerox Palo Alto Research Center, Palo Alto, CA. 94304
**Los Alamos National Laboratory, Los Alamos, NM. 87545
†Stanford Synchrotron Radiation Laboratory, Stanford, CA. 94305
††University of California, San Diego, La Jolla, CA. 92093

5f SPECTRAL WEIGHT IN HEAVY-FERMION URANIUM MATERIALS

We have recently published combined resonant photoemission (RESPES) and bremsstrahlung isochromat (BIS) spectra for the heavy-Fermion materials UAl_2 [1] ,UPt_3 [1] , and U_2Zn_{17} [2] . We have extended these studies to URu_2Si_2 , a novel material whose low-temperature properties show competition between superconductivity and spin or charge density wave formation [3]. Fig. 1 shows the normalized valence band PES spectra of URu_2Si_2 for several photon energies with 0.8 eV resolution. In the spectrum for photon energy $h\nu = 70$ eV the emission occurring between the Fermi energy E_F and 4 eV is due to Ru 4d states, as shown by the sharp decrease of this emission at higher photon energies approaching the Cooper minimum around $h\nu = 100$ eV. The U emission shows Fano minima at $h\nu = 92$ eV and 102 eV, and Fano maxima at $h\nu = 98$ eV and $h\nu = 108$ eV, arising from the cross-section resonance at the U 5d edge. Fig. 2 shows the complete 5f spectrum obtained by RESPES and BIS. The RESPES part is the result of subtracting the $h\nu = 102$ eV spectrum of Fig. 1 from an $h\nu = 108$ eV spectrum with resolution of 0.4 eV. The general features of the complete 5f spectrum are similar to those of UPt_3, as discussed in more detail in a recent paper

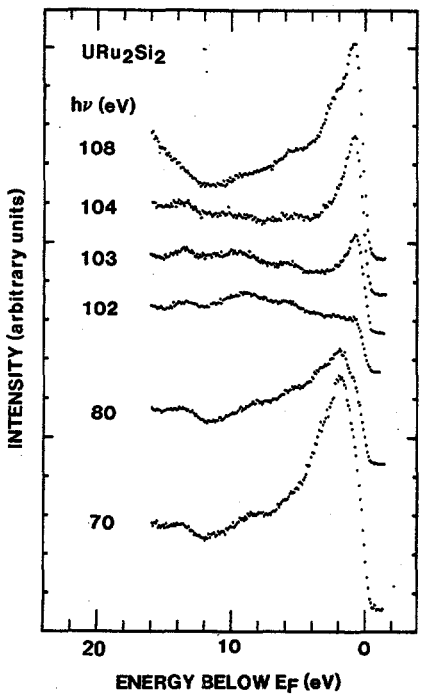

Fig. 1

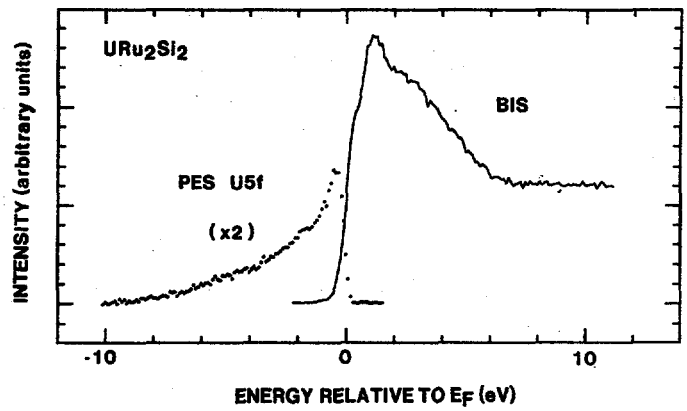

Fig. 2

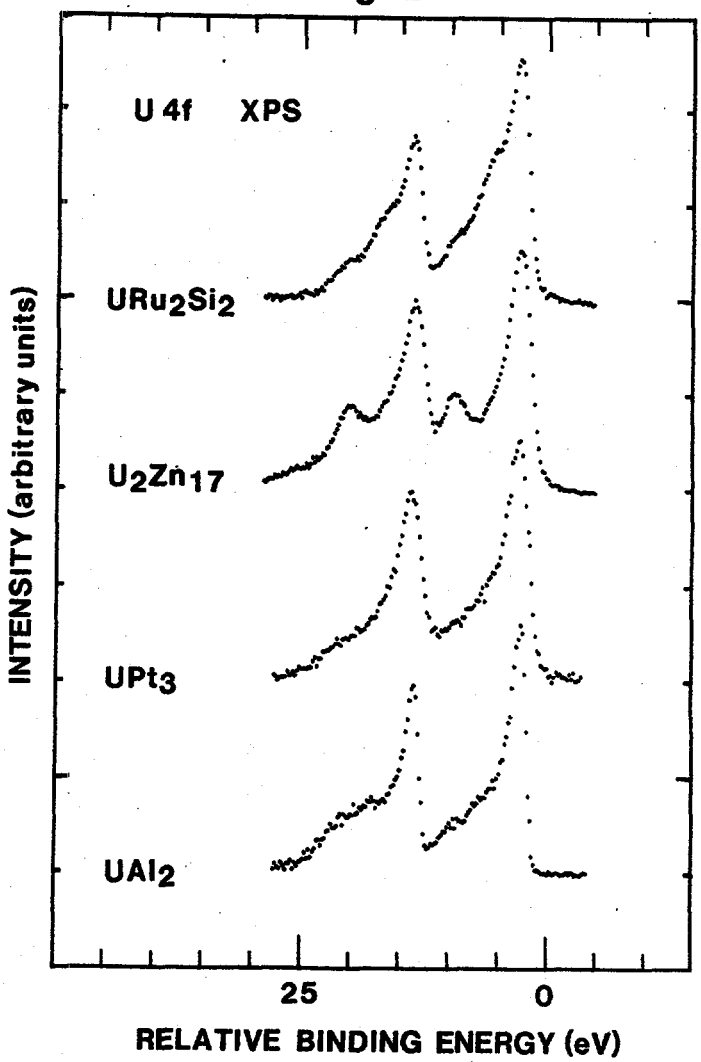

Fig. 3

[4] reporting these results. In Fig. 3 we show the X-ray photoemission U 4f core level spectra for several heavy-fermion U materials. As discussed in Ref. 4, there is not yet a detailed interpretation of such spectra, in contrast to what has been accomplished for Ce materials [5], but the fact that the spectra of Fig. 3 vary from sample to sample is encouraging that they do carry information which can be extracted when a suitable theory is made.

RESONANT VALENCE BAND PHOTOEMISSION IN $Ce(Ru_{1-x}Rh_x)_3B_2$.

$CeRh_3B_2$ and $CeRu_3B_2$ are very interesting materials because the first is a ferromagnet with an anomalously high Curie temperature of 115K, while the second is a superconductor. We have extended previous studies of these two materials to an alloy with $x=0.2$. Efforts to measure an alloy with $x=0.8$ were not successful because the loose grain structure of the polycrystalline samples prevented obtaining clean surfaces by fracturing. Separating the Ce 4f and transition metal 4d emission by using their Fano resonance and Cooper minimum, respectively, was described in the preceding year's SSRL activity report. We have also measured the Ce 4f BIS 3d X-ray photoemission spectra of these materials.

Fig. 4 shows complete 4f spectra for $x=0$, 0.2 and 1, obtained with RESPES and BIS. The Ce 4f emission is typical of that in other cerium materials in having a peak well below E_F and then rising again near E_F. It is also typical in that the more strongly is magnetism suppressed, the greater is the weight at E_F. Fig. 5 shows spectra taken with photon energy $h\nu = 80$ eV, where the transition metal 4d emission dominates. In the region betwen 5eV and 10 eV, the spectra for $x=0$ and 1 have been corrected to remove spurious emission from interstitial carbon (erroneously labeled as boron emission in our previous SSRL report). The $x=0.2$ sample was free of this carbon and we have taken its spectrum in the 5eV to 10eV region as representative.

As we have done previously [5] for many other Ce compounds, we have fit the 4f and 3d spectra using the impurity Anderson Hamiltonian and are preparing a paper reporting all the results. The Ru and Rh 4d spectra are taken to give the conduction band density of states for this analysis, and it is important that the weight at E_F is quite different as x changes. Other workers [6] studying $CeRh_3B_2$ have already pointed out that the low Rh weight does not support a model of itinerant 4d magnetism in $CeRh_3B_2$. In our analysis this weight change strongly affects the fraction of f^0 in the ground state, and the value of the Kondo temperature, which is small for $x=1$ and large for $x=0$. We also find that the spectra for $x=1$ cannot be fit so well as is usual for Ce materials, and we tentatively ascribe this to the occurrence of ferromagnetism in $CeRh_3B_2$.

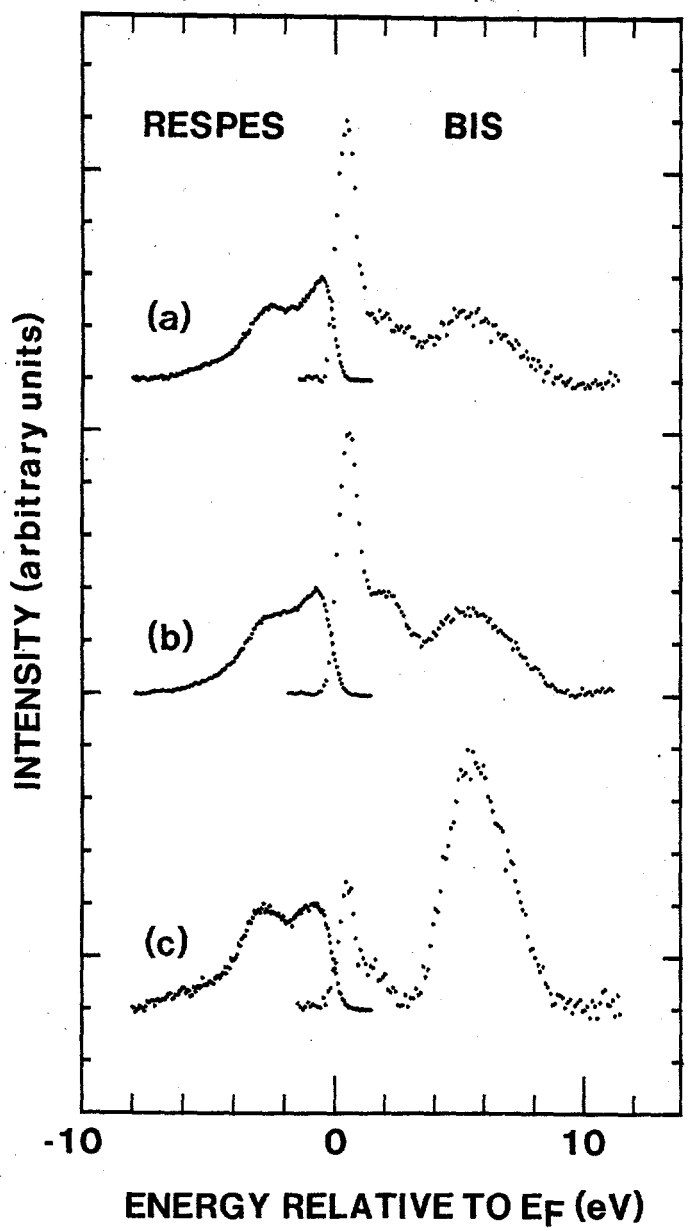

Fig. 4

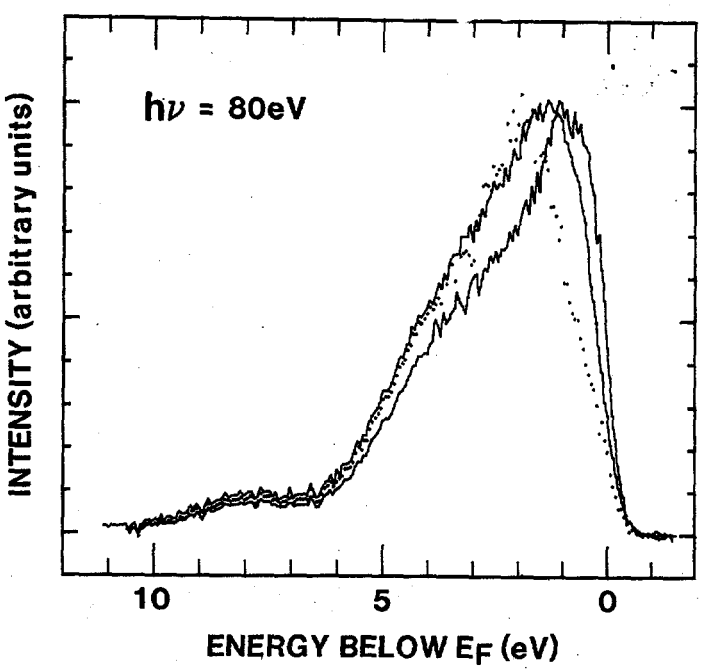

Fig. 5

ELECTRONIC STRUCTURE of TRANSITION METAL COMPOUNDS: NiAs

NiAs is the structural prototype of a large number of binary compounds of transition metals and metalloids, or chalcogenides, some of which we have already studied [7] , including NiSb. Its electronic structure is then generically interesting, and also of importance in understanding compound formation [8] at the interface between Ni and GaAs. Fig. 6 shows the valence band spectrum for a photon energy range which includes the Ni 3p edge, where resonance effects occur. Figures 7 and 8 show CIS spectra for E_F, the main Ni 3d peak and the Ni 3d satellite at 8 eV. Figure 9 shows a higher resolution (0.25 eV) spectrum, in which a shoulder near E_F can be seen.

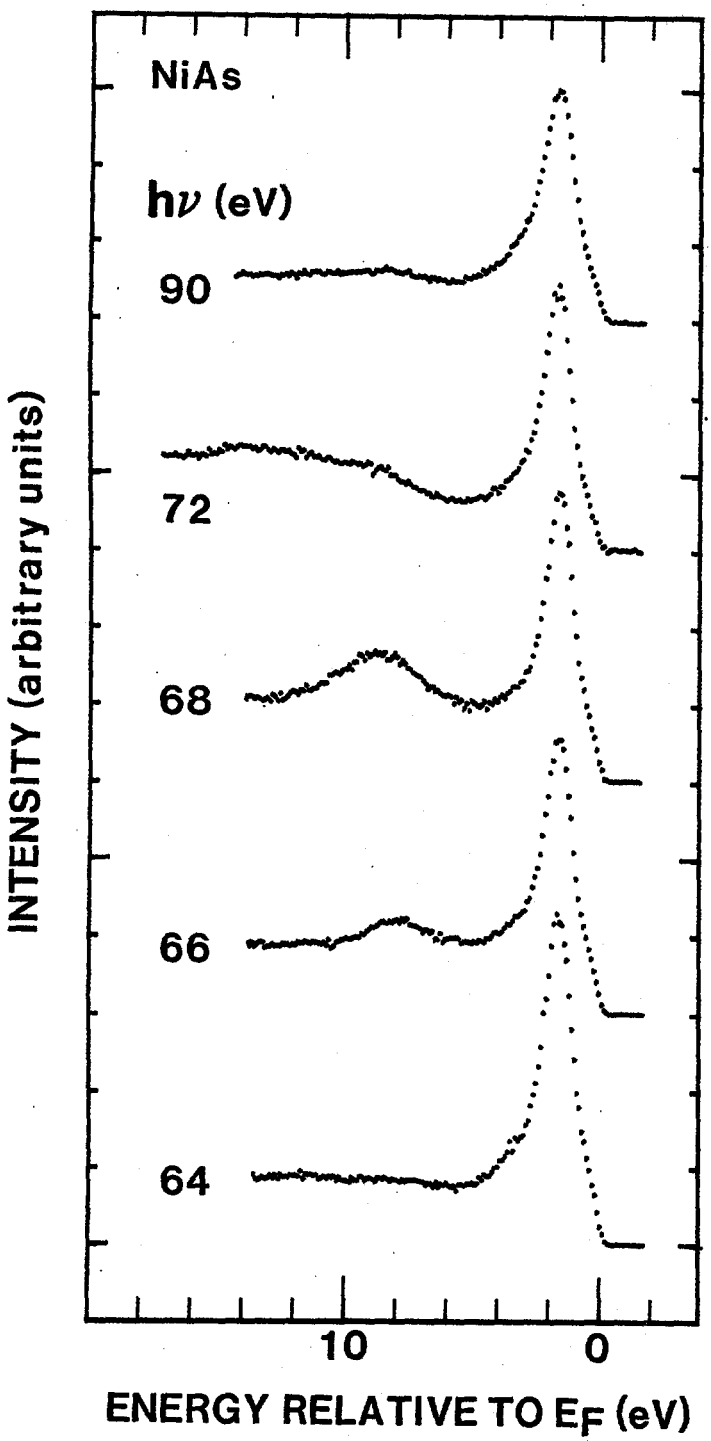

Fig. 6

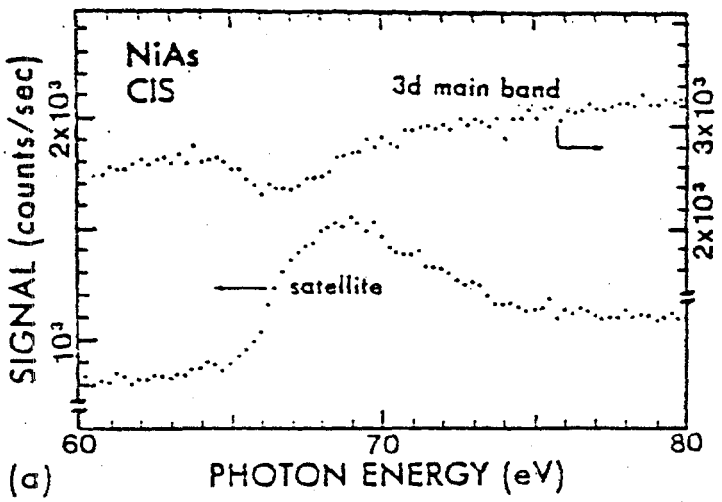

Fig. 7

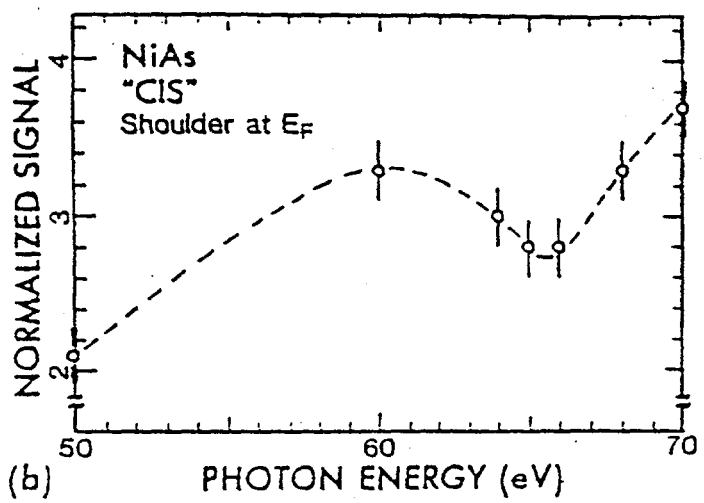

Fig. 8

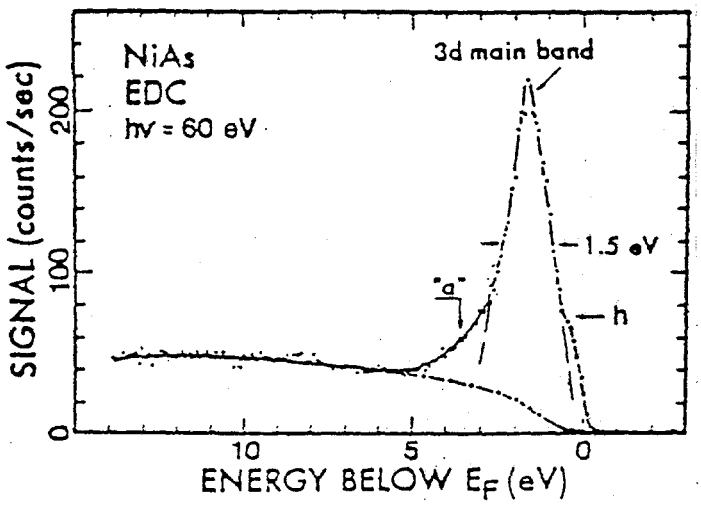

Fig. 9

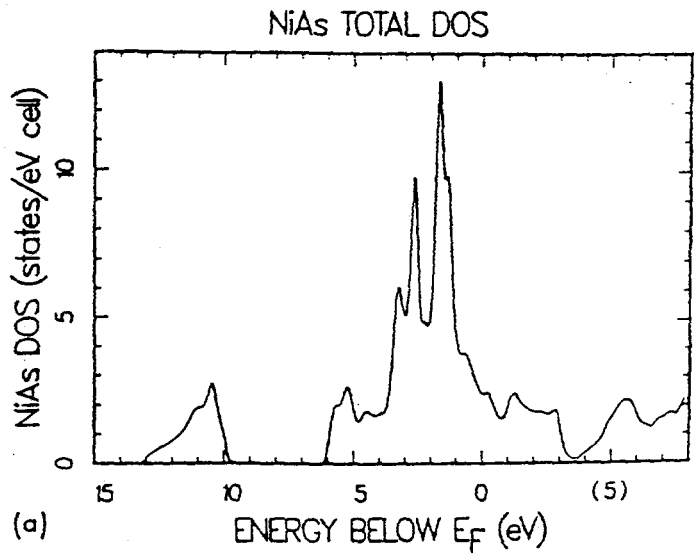

Fig. 10

Figures 10 and 11 show the total and d-projected densities of state obtained in a density-functional calculation for NiAs. As discussed in detail in a recent paper [9] the d-projected result agrees well with the measured spectra, except for the occurence of the satellite at 8 eV, which signals the presence of correlation effects due to 3d Coulomb interactions. It can be concluded that it is the strong p/d hybridization effects (shown by the calculation) rather than the absence of 3d Coulomb effects that causes the material to be nonmagnetic. In particular, relative to Ni metal, 3d weight is pushed by hybridization above E_F, leaving a small density of states at E_F even though the d-shell occupation is similar to that of Ni metal. That the Ni shell is unfilled is also shown by the resonance effects, which require a 3p→3d photon transition, and which reveal 3d states at E_F (see Fig. 8).

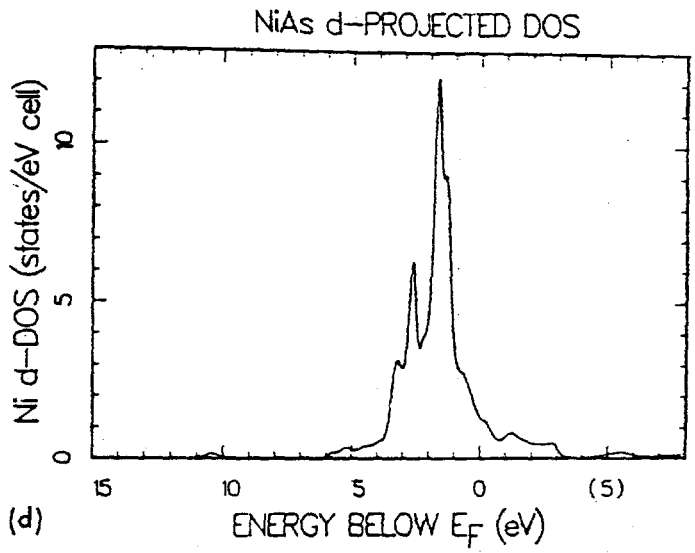

Fig. 11

REFERENCES

1. J.W. Allen, S.-J. Oh, L.E. Cox, W.P. Ellis, M.S. Wire, Z. Fisk, J.L. Smith, B.B. Pate, I. Lindau and A.J. Arko, Phys. Rev. Letters **54**, 2635 (1985).

2. Y. Lassailly, J.W. Allen, W. Ellis, L. Cox, B. Pate, Z. Fisk and I. Lindau, proceedings of the 1986 International Conference on Anomalous Rare Earths and Actinides, to be published in J. Magn. and Mag. Mat.

3. M.B. Maple, J.W. Chen, Y.Dalichaouch, T. Kohara, C. Rossel, M.S. Torikachvili, M.W. McElfresh and J.D. Thompson, Phys. Rev. Letters **56**, 185 (1986).

4. J.W. Allen, J.-S. Kang, Y. Lassailly, M.B. Maple, M.S. Torikachvili, W. Ellis, B. Pate and I. Lindau, Solid State Commun. **61**, 183 (1987).

5. J.W. Allen, S.-J. Oh, O. Gunnarsson, K. Schönhammer, M.B. Maple, M.S. Torikachvili and I. Lindau, Adv. in Physics **35**, 275 (1986).

6. E.V. Sampathkumaran, G. Kaindl, C. Laubschat, W. Krone and G. Wortmann, Phys. Rev. B **31**, 3185 (1985).

7. S.-J. Oh, J.W. Allen, I. Lindau and J.C. Mikkelsen, Phys. Rev. B **26**, 4845 (1982).

8. T. Kendelewicz, M.D. Williams, W.G. Petro, I. Lindau and W.E. Spicer, Phys. Rev. B **32**, 3758 (1885).

9. W. Ellis, R. Albers, J.W. Allen, Y. Laissailly, J.-S. Kang, B. Pate and I. Lindau, Solid State Commun., submitted.

PHOTOELECTRON SPECTROSCOPIC STUDIES OF METAL ION SITES

Stephen V. Didziulus, Kristine D. Butcher, Jian-yi Lin, and Edward I. Solomon
Stanford University, Stanford, California 94305

This past year, we have continued our PES studies of the electronic structure and bonding in metal ion sites related to catalysis, concentrating on the investigation of the role of copper in promoting ZnO, a methanol synthesis catalyst, and the extension of our d^9/d^{10} copper chloride study to d^5 and d^6 iron chlorides. Model catalysts are prepared by evaporating submonolayer coverages of Cu onto ZnO single crystals in UHV. The results presented are for the (0001) and (000$\bar{1}$) surfaces. Valence band PES has been used to study the bonding in the Cu/ZnO system. The Cu 3d band lies to lower binding energy than the Zn 3d, and is most easily observed at Hν = 120 eV due to attenuation of the O2p photoemission. The Cu 3d band shifts to lower binding energy with increasing Cu coverage, indicating a well-dispersed form of Cu on the surface at low coverage. Changes in band-bending and work function on the (000$\bar{1}$) face are consistent with charge donation to the surface. This behavior is not observed for the (0001) face.

Resonant PES was used to probe the system, as the resonance satellite and associated Auger are diagnostic of Cu(I) and Cu metal cluster species (see Fig. 1).[1] In spectra taken at the Cu 3p absorption edge, both the satellite and Auger peak are visible, even at 0.3 monolayer coverages. The energy positions of the satellite and weak auger relative to Cu metal (10 ml coverage) on both surfaces indicate that low coverage Cu is much different from the metallic form, and that charge donation to the surface has occurred.

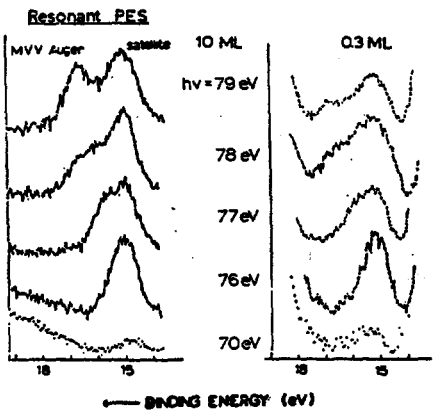

Fig.1

As further perturbation, heating and oxidation studies were performed on both surfaces, with 0.3 ml Cu overlayers. Heating to 200-400° C causes the Cu features to shift to lower binding energy and lose intensity, the more dramatic changes occurring at lower temperature on the (0001) face. These changes are characteristic of more metallic Cu, and three-dimensional clustering. Heating in $1X10^{-6}$ torr ambient O_2 produces a shift in the Cu 3d to deeper binding energy, but no intensity change. Again, the effect is more dramatic on (0001) (Fig. 2). The satellite peak, which is more sensitive to oxidation, shows an increase in off resonance intensity, but less resonance enhancement. The energy positions of the satellite and auger are consistent with Cu(I) formation. Again, the greater effect is observed on the (0001) surface. These data indicate that Cu is more reactive on the Zn face (0001), and that Cu in the dispersed form is more stable at catalytic temperatures on the (000$\bar{1}$) as are the oxidized forms on both surfaces.

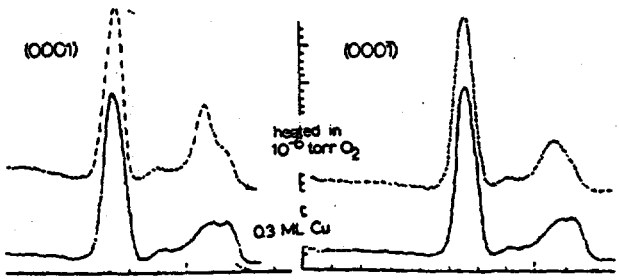

Fig.2

We are currently extending our variable energy PES studies to the d^5 and d^6 iron chlorides. These data (see Fig. 3) exhibit large differences from the $CuCl_4^=$ data, especially at the metal 3p edge.[2] The peak at 4.6 eV binding energy in Fe(III) shows Cl 3p Cooper minimum behavior near 50 eV (absolute intensities not shown), while the effect is less pronounced in Fe(II).

At the Fe 3p absorption edge, the Fe(III) salt shows a strong resonance effect in the peak at 6.1 eV binding energy, which also has significant off-resonance intensity. Resonance enhancement is also observed in the peak to lowest binding energy, and in the region of 11 eV B.E., but the peak is obscured by Cs 5p photoemission. In Fe(II), the dominant resonance effect is observed in the peak at lowest B.E., indicating metal character present. Some resonance is seen in the 7.5 eV B.E. peak also, but at a slightly higher photon energy. Absolute intensity information and comparison to polarized optical absorption studies and Xα-SW calculations gives a preliminary assignment of the peaks at 3.6 eV and 4.7 eV in Fe(III), and 3.8 and 6.1 eV in Fe(II) as predominantly Fe 3d and Cl 3p, respectively. These data are presently being analyzed using methods previously developed for our d^9/d^{10} copper chloride study.

REFERENCES:

1. M.R. Thuler, R.L. Benbow, and Z. Hurych, Phys. Rev. B. 26, 669 (1982).

2. S.L. Cohen, S.V. Didziulis, A.A. Gewirth, and E.I. Solomon, submitted to J.A.C.S.

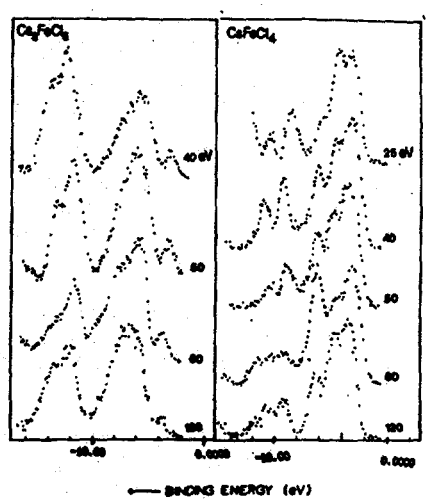

X-Ray Scattering Studies of the Si-SiO_2 Interface

S. Brennan
Stanford Synchrotron Radiation Laboratory, Stanford, CA 94305

P.H. Fuoss and L. Norton
AT&T Bell Laboratories, Holmdel, NJ 07733

A. Fischer-Colbrie
Hewlett-Packard Laboratories, Palo Alto, CA 94304

The Si-SiO_2 interface has unique electronic and structural properties of enormous importance. However, the detailed atomic nature of this interface is essentially unknown. Controversy exists over whether the crystal-amorphous transition is abrupt or whether there is a boundary layer which consists of micro-crystallites which gradually disorder into the amorphous film.

We report here the first direct observation of microcrystallites at the Si-SiO_2 interface. X-ray scattering measurements were made on BL VII-2, using the surface-sensitive grazing incidence scattering geometry, where the incident and scattered wavevectors are at a very glancing angle with respect to the sample surface. There were four samples with SiO_2 thicknesses ranging from 15 to 250 Å. Two of the samples were made by thermal oxidation, one by electron-beam evaporation of SiO_2, and the final was a native oxide. All substrates were Si(100). In all cases we observed sharp diffraction peaks indicating microcrystallites in the SiO_2 layer. The orientational order of these microcrystallites varied greatly according to preparation method.

Fig. 1 shows the scattering from a 150 Å thick thermally grown SiO_2 layer as a function of k for two different grazing angles ϕ. These data, as well as others shown in this report, have been corrected for polarization effects due to the horizontal scattering geometry used and for an angular dependence on the area sampled. At a grazing angle of 0.24^o, ($\sim 0.07^o$ above the critical angle for total external reflection), there are two strong broad peaks. One (the low-K peak) is the scattering of the amorphous film and the other ($3.279\ Å^{-1}$) is diffuse scattering from the Si(220) reflection. (The sample is rotated 10^o from the exact Si(220) azimuth for this scan.) As the grazing angle is reduced to 0.16^o, the penetration depth of the x-rays into the Si substrate is greatly reduced and the Si substrate contributions disappear.

In Fig. 2, the scattering of a 20 Å thermal oxide is shown. There is still a broad low-K peak indicating an amorphous aspect to the film, but in contrast to the thicker film, there are also sharp features indicating microcrystallinity. Also shown in the Fig. are lines marking the α-cristobalite reflections. There is good but not perfect agreement between the two patterns. In particular, significant differences occur at $2.313\ Å^{-1}$ and $3.029\ Å^{-1}$. An azimuthal scan of the peak at $1.52\ Å^{-1}$ (also corresponding to the α-cristobalite (111) reflection), has a very sharp peak which is rotated 58.9^o from a Si substrate (220) reflection. This very sharp peak occurs also at 90 and 120^o azimuthally, but there is no 12-fold symmetry.

Measurements of a 15 Å native oxide film show very weak scattering, with both diffuse and crystalline components. Microcrystalline peaks are at 2.5 and 2.6 $Å^{-1}$ and are sharply peaked azimuthally.

For a 250 Å electron-beam evaporated sample, we find both diffuse and crystalline peaks (Fig. 3). Many, but not all, of the sharp peaks can be indexed using the α-cristobalite structure. The azimuthal scan shows many small, sharp peaks indicating that either there are very few crystallites or they are highly correlated in the plane of the surface (since the resolution in that direction is not particularly high).

These data clearly demonstrate that crystallites, which seem to be closely related to α-cristobalite, are present at or near the SiO_2-Si interface. For the thermally-oxidized Si, they appear to be at the interface. From peak widths, the crystallites are ~90 Å or larger. Peak widths of the diffuse peaks suggests that the structural ordering in the amorphous matrix is greatest for the thermally oxidized films, less for the electron beam evaporated SiO_2 and least for the native oxide.

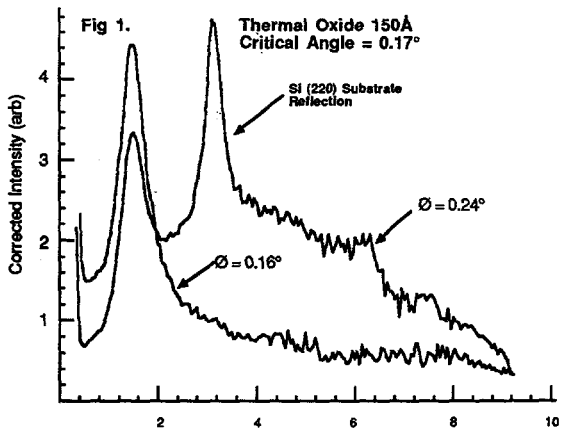

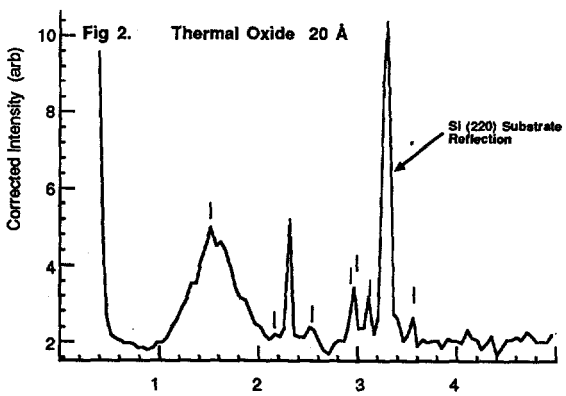

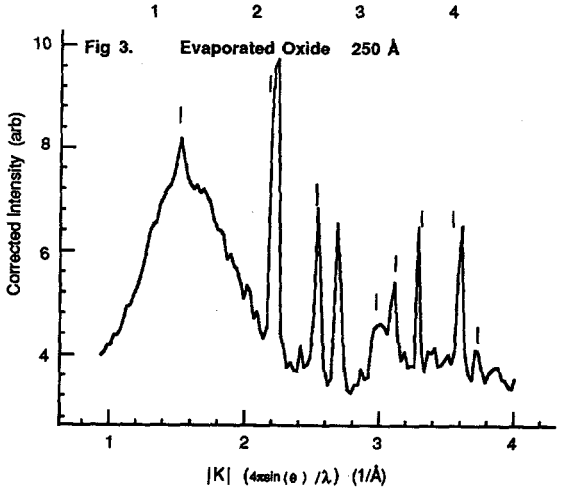

INVESTIGATION OF THE Ta SITE IN ALPHA-RECOIL DAMAGED NATURAL PYROCHLORES BY XAS

R. B. GREEGOR*, F. W. LYTLE*, B. C. CHAKOUMAKOS**, G. R. LUMPKIN**,
R. C. EWING**, C. L. SPIRO*** AND J. WONG***

*The Boeing Company, Seattle, WA 98124

**Department of Geology, University of New Mexico, Albuquerque, NM 87131

***General Electric Company, Schenectady, NY 12345

INTRODUCTION

The pyrochlore structure type $A_{1-2}B_2O_6Y_{0-1}$, predominately cubic and ionic in nature, allows a wide variety of chemical substitution at the A (Ca, Na, U, Th, REE, Y, Ba, Sr, Pb), B (Nb, Ta, Ti, Zr, Sn, Fe), and Y (O, OH, F) sites with vacancies at the A and Y sites. The variable chemistry and large stability field lead to several interesting applications including use as a principal constituent of polycrystalline radioactive waste forms.

The use of pyrochlore phases as potential hosts for radioactive waste has prompted several studies concerning the effects of alpha-decay damage on the structure. Both naturally occurring samples (containing U and Th) and synthetic phases doped with Pu or Cm have been investigated using conventional powder x-ray diffraction and transmission electron microscopy.

We extend these measurements using EXAFS/XANES to Ta in the B-site of pyrochlore group minerals including the microlite subgroup (Ta-rich), the betafite subgroup (Ti-rich) and the pyrochlore subgroup (Nb-rich). These subgroups of pyrochlore minerals are defined by Hogarth [1], and additional examples of natural chemical variations are given by Lumpkin and Ewing [2].

EXPERIMENTAL

The samples reported on here contained 8 to 24 wt.% UO_2 and 2 to 70 wt. % Ta_2O_5. All U was calculated as UO_2 and allocated to the A-site. All the samples in their natural condition were metamict (radiation damaged) and have calculated alpha doses of 4-9 x 10^{17} alpha events/mg. The number of displacements per atom (dpa) range from 49 to 94. Splits of all samples were annealed at 1000° in air for one hour. Standards synthesized for data analysis included Ta_2O_5, $CeTaO_4$, and $KTaWO_6.H_2O$. The mineral maganotantalite ($MnTaNbO_6$) was also included; this sample is a placer nugget from the wall zone of the Harding pegmatite, Taos County, New Mexico.

The EXAFS/XANES experiments were performed at the Stanford Synchrotron Radiation Laboratory (SSRL). At SSRL the side stations of Beam Lines IV-1 and VII-3 were used, with the synchrotron beam at a current of approximately 20 to 60 mA and an energy of 3 GeV. A Si (220) or (333) double crystal monochromator was used.

RESULTS

Results of the normalized XANES measurements at the Ta L_{III} edge (9881.1 eV, zero of energy in the plotted spectra) are shown in Figure 1 for selected reference compounds and in Figure 2 for the metamict and annealed pyrochlore samples.

The normalized XANES spectra for the metamict and annealed samples (Fig. 2) shows that the doublet in the resonance of the annealed samples is less pronounced for the corresponding metamict (radiation damaged) samples and even merges into a single absorption resonance for the metamict microlite sample. The primary resonance of the metamict samples closely resembles that of Ta_2O_5 or manganotantalite, while the primary resonance of the annealed samples most closely matches that of $KTaWO_6.H_2O$ pyrochlore.

The phase corrected Fourier transforms of the Ta L_{III} edge EXAFS for the various reference materials are shown in Figure 3 and the metamict and annealed natural sample transforms are shown in Figure 4 for the pyrochlore and microlite sample. The signal to noise ratio of the EXAFS for the betafite sample was insufficient for a Fourier transform. The average Ta-O bond length for the fully damaged, metamict samples and their annealed, crystalline counterparts was 1.96 ± 0.05 A. In the case of microlite (#153, Ta = 88% of B-site cations) the Ta-O bond is shortened by 0.05 A for the metamict sample compared to the annealed; and for the pyrochlore (#186, Ta = 12% of B-site cations) the Ta-O bond is lengthened by 0.05 A for the metamict sample compared to the annealed. The second major peak at approximately 3.5 A in the Fourier transforms for the annealed samples in Figure 4 is clearly resolved into a shorter and a longer bond in the damaged sample.

DISCUSSION

The XANES and EXAFS (Fourier transforms) results clearly demonstrate that significant changes occur as a result of radiation damage for Ta at the B-site in natural pyrochlore group minerals. The comparison of the spectra of the fully damaged samples (unannealed) and Ta_2O_5 suggests that Ta_2O_5 may be an appropriate topologic model structure for the metamict state. In Ta_2O_5, the Ta-oxygen coordination polyhedra are extremely varied in their Ta-O bond lengths (1.81-2.57 A), coordination number (VI-VII), types of polyhedral distortion (distorted octahedra or pentagonal dipyramids), and the manner in which the polyhedra are connected to one another (e.g. edge-sharing vs. corner-sharing). These variations cause a wide spread in the separation between Ta and atoms in the second coordination sphere (e.g. Ta...Ta or Ta-O...O (Fig. 5)). This distribution is roughly trimodal with corner- and edge-sharing Ta-O-Ta separations being the shortest and Ta-O...O separations being the longest.

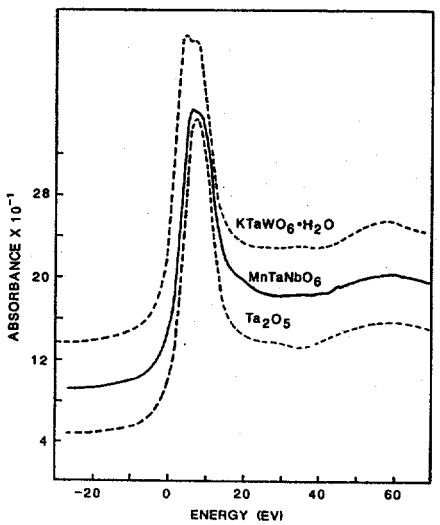

Figure 1. Ta L_{III} edge XANES of standard compounds.

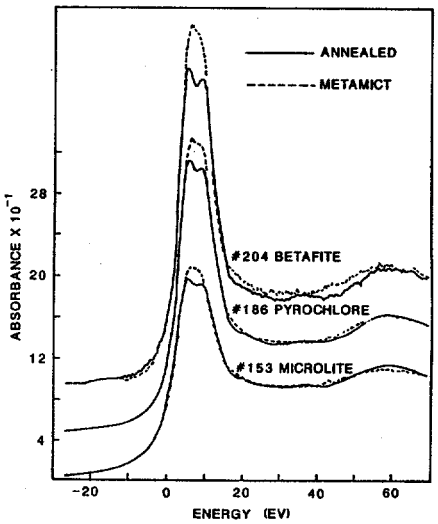

Figure 2. Ta L_{III} edges XANES of metamict and annealed minerals.

With increased alpha-recoil dose, the Fourier transform magnitude of the peak that represents the second coordination sphere decreases an splits into multiple peaks similar to the trimodal distribution observed in the histogram of Ta...X distances in Ta_2O_5 (Figure 5). Thus, with increasing alpha-decay dose and decreasing long-range periodicity, we observe: (1) greater distortion of the primary coordination polyhedron around Ta, (2) a slight increase in the mean second nearest neighbor <Ta...X> distance, and (3) a wider distribution of second nearest-neighbor distances.

ACKNOWLEDGEMENTS

This work was supported by the U.S. Department of Energy, Office of Basic Energy Sciences under Grants DE-FG06-84ER45121 (R. B. Greegor and F. W. Lytle) and DE-FG04-84ER45099 (R. C. Ewing).

REFERENCES

1. D. D. Hogarth, Am. Mineral., 62, 403 (1977).
2. G. R. Lumpkin and R. C. Ewing in Scientific Basis for Nuclear Waste Management - VIII, edited by C. M. Jantzen, J. A. Stone and R. C. Ewing (Materials Research Society, Pittsburg, PA, 1985) pp. 647-654.

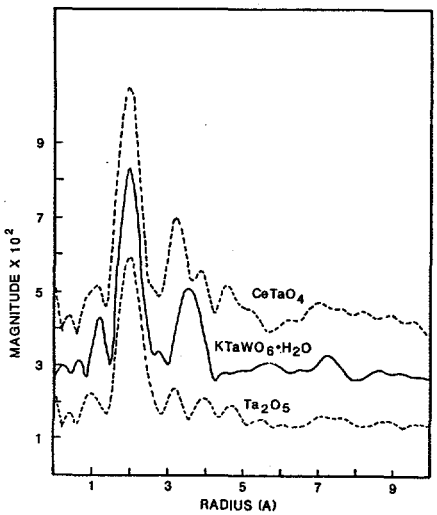

Figure 3. Fourier transforms of Ta L_{III} edge EXAFS of standard compounds.

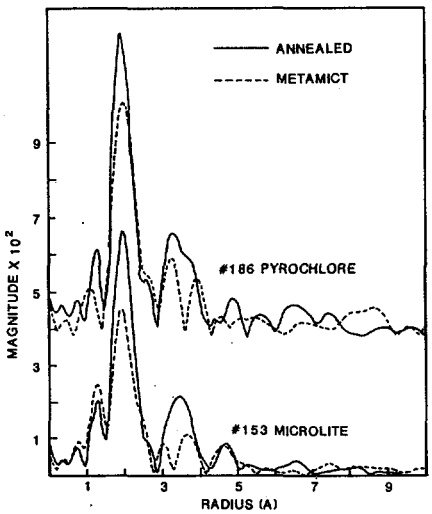

Figure 4. Fourier transforms of Ta L_{III} edge EXAFS of metamict and annealed minerals.

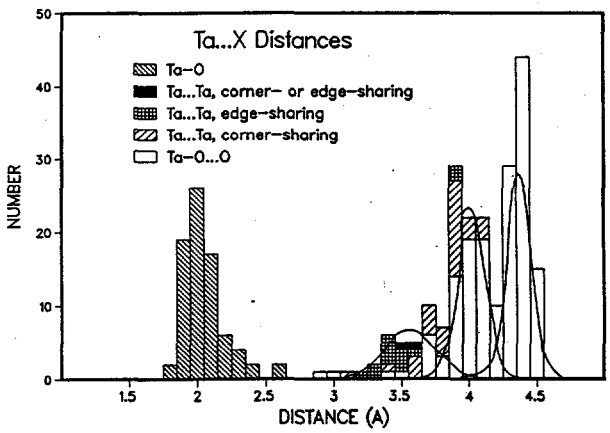

Figure 5. First and second nearest-neighbor atom distances (under 4.5 A) around the tantalum positions in Ta_2O_5. The schematic distribution curves superimposed emphasize the trimodal distribution of the second nearest-neighbors.

XAS Studies of the Active Sites of Cytochrome *c* oxidase

R. A. Scott, R. J. Sullivan
School of Chemical Sciences, University of Illinois, Urbana, IL 61801

S. I. Chan, P. M. Li
Arthur Amos Noyes Laboratory of Chemical Physics, California Institute of Technology, Pasadena, CA 91125

We report Cu EXAFS measurements of three forms of cytochrome *c* oxidase : native (resting state), pHMB-modified, and Cu_A-depleted [1]. Cytochrome *c* oxidase contains four spectroscopically distinct redox-active metal centers. Two iron atoms are present as heme *a* and heme a_3 as well as two copper atoms in the Cu_A and Cu_B sites. Previous Cu EXAFS studies of oxidase have been limited by the convolution of the EXAFS from both of the Cu sites. As a result, it was not possible to distinguish the ligands bound to Cu_A from those bound to Cu_B. To overcome the problem of interfering EXAFS from the two copper sites, we have prepared oxidase samples that have been chemically modified at the Cu_A site. This modification makes possible a probe of the Cu_B site EXAFS alone. Comparison of our present EXAFS results for the Cu_A-depleted, pHMB-modified, and the native enzyme allows the separation of the EXAFS from the Cu_A and Cu_B sites. Our results demonstrate that the Cu sites in oxidase differ in the number of (S, Cl) ligands. The Cu_A center is bound by 2 (N, O) and 2 S atoms whereas the Cu_B site contains 3 (N, O) and 1 (S, Cl) ligating atoms.

Cu EXAFS of the three forms of cytochrome *c* oxidase were measured on beam-line VII-3 under dedicated operating conditions using Si[220] monochromator crytals. Data were collected in the fluorescence mode using a fluorescence detector (EXAFS Co., Seattle) with a Ni filter, and the sample temperature was maintained at 4 K by a continuous flow liquid He cryostat manufactured by Oxford Instruments (model CF1208).

The Fourier transforms (FT's) of the Cu EXAFS of the native, pHMB-modified, and Cu_A-depleted cytochrome *c* oxidase are shown in Figure 1. In accord with our previous work on other preparations of the native enzyme, the FT peak at R' ≅ 1.5 Å is assignable to (N, O) containing ligands and the FT peak at R' ≅ 2.0 Å is assignable to (S, Cl) ligands. In all of the FT's, the amplitude of the peak attributable to (N, O) scatterers is nearly constant, whereas the amplitudes of the FT peaks assigned to (S, Cl) scatterers vary considerably. The two major peaks of each FT were Fourier filtered and the resulting *k* space data were analyzed according to our standard curve-fitting procedures [2]. Curve-fitting results are summarized in the Table and best curve fits are shown in Figure 2.

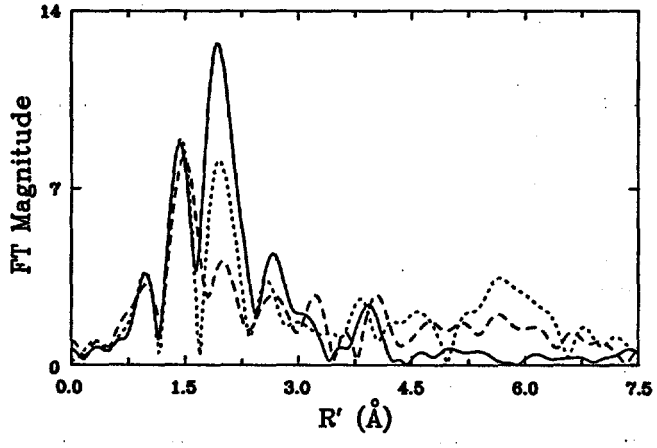

Figure 1. Comparison of Fourier transforms (k = 3.0-13.0 Å^{-1}, k^3 weighting) of Cu EXAFS of cytochrome *c* oxidase samples: native enzyme (—); pHMB-modified (- - -); and Cu_A-depleted (···).

As shown in the Table, Cu_A-depleted oxidase leads to EXAFS analysis of the Cu_B site. Thus 3 (N, O) and 1 (S, Cl) atoms are directly assigned to the inner coordination sphere of Cu_B. Using this ligand set for the Cu_B site in the native enzyme curve fits, we are able to determine the ligands bound to Cu_A. We find that the native enzyme Cu_A site contains 2 (N, O) ligands and 2 S ligands. Cu_A is thought to be bound by S rather than Cl ligands in view of EPR and ENDOR studies on the Cu_A site [3]. Given the fact that pHMB-modification affects only Cu_A [1], the curve-fitting results for the pHMB-modified sample can be interpreted in terms of the (now) known Cu_B coordination. We find the pHMB-modified Cu_A to exist in a site consisting of 4(N, O)-containing ligands, not unlike a type 2 copper, consistent with EPR spectra of this form [1].

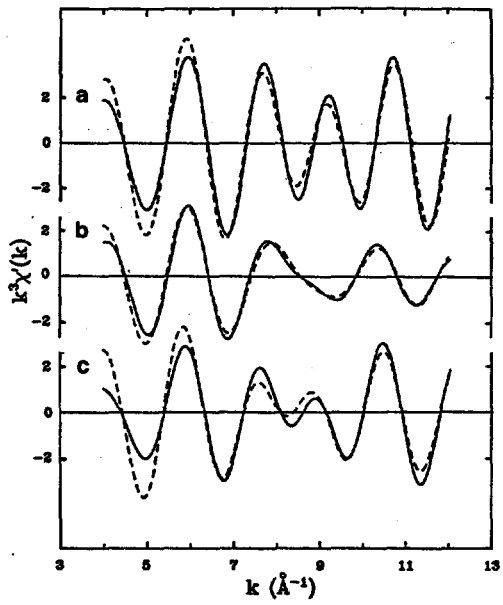

Figure 2. Best-fit simulations of the first coordination sphere Cu EXAFS of cytochrome *c* oxidase samples: (a) native enzyme; (b) pHMB-modified; and (c) Cu_A-depleted. In each, the solid line is the Fourier-filtered EXAFS and the dashed line is the best-fit simulation.

Table. Best-fit EXAFS Derived Coordination Environments for the Copper Sites of Cytochrome *c* Oxidase.

Sample	Coordination Environment			
	Cu_A	Cu_B	Avg. (per Cu)	
Native enzyme	2(N, O)	3(N, O)	2.5(N, O)	@ 1.96 Å
	2(S, Cl)	1(S, Cl)	1.5(S, Cl)	2.28
pHMB-modified	4(N, O)	3(N, O)	3.5(N, O)	1.98
	———	1(S, Cl)	0.5(S, Cl)	2.31
Cu_A-depleted	———	3(N, O)	3.0(N, O)	1.98
	———	1(S, Cl)	1.0(S, Cl)	2.31

References.
1. Li, P. M.; Gelles, J.; Chan,S. I.; Sullivan, R. J.; Scott, R. A. *Biochem.*, submitted for publication.
2. Scott, R. A. *Methods Enzymol.* **1985**, *117*, 414-459.
3. Blair, D. F.; Martin, C. T.; Gelles, J.; Wang, H.; Brudvig, G. W.; Stevens, T. H.; Chan, S. I. *Chemica Scripta* **1983**, *21*, 43-53.

"NO-PASSING" EFFECT IN POST-COLLISION INTERACTION DURING PHOTON-EXCITED COSTER-KRONIG DECAY*

G. Bradley Armen, Stacey L. Sorensen, and Scott B. Whitfield
Department of Physics and Chemical Physics Institute
University of Oregon, Eugene, Oregon 97403

Gene E. Ice and Jon C. Levin
Oak Ridge National Laboratory, Oak Ridge, Tennessee 37830

George S. Brown
Stanford Synchrotron Radiation Laboratory
Stanford, California 94305

Bernd Crasemann
Department of Physics and Chemical Physics Institute
University of Oregon, Eugene, Oregon 97403

In radiationless transitions to atomic inner-shell hole states produced by threshold photoionization, the Auger-electron energy is shifted up by post-collision interaction between the two continuum electrons. According to both semiclassical and quantum-mechanical models, this shift is expected to disappear if the photoelectron energy exceeds that of the Auger electron (the "no-passing" effect).

The no-passing effect was first seen experimentally by Borst and Schmidt[1] in the Xe N_5-$O_{2,3}O_{2,3}$ ($^1S_0$) Auger transition. This involves a very long-lived initial [4d] hole state, of width Γ_i=0.110 eV, and an Auger energy ε_A=29.97 eV which is large in comparison; the theoretically significant dimensionless parameter Γ_A/ε_i is ~272 in this case and the PCI shift near threshold, ~0.1 eV. To test the validity of present theories and seek further experimental verification of the no-passing effect, it is desirable to examine transitions which correspond to other extremes. We have therefore studied the Xe L_2-L_3N_4 (J=3) Coster-Kronig transition, which is very fast (Γ_i=3.06 eV) and has a relatively low energy (ε_A=228 eV; ε_A/Γ_i=75) and large PCI shift (~3.2 eV near threshold).

The Xe L_2-L_3N_4 Coster-Kronig peak was recorded (Fig. 1) as excited by incident x rays of 8 different energies, ranging from 5,153 to 6,007 eV, i.e., from 46 to 900 eV in excess of the Xe L_2 binding energy. This range of E_{exc} thus bracketed the Coster-Kronig-electron energy at which the no-passing effect is expected to set in. At each x-ray energy, several Coster-Kronig spectra were measured and later combined. Typical peak counting rates were ~10-20 Hz, with signal-to-background ratios from 0.4 to 0.5. The energy of the L_2-L_3N_4 diagram-peak centroid was determined, as a function of photon excess energy E_{exc}, by means of a least-chi-square procedure applied with an appropriate fitting function. The quantity of interest is the PCI shift $\Delta(E_{exc})$, which is the (positive) energy shift of the centroid of the L_2-L_3N_4 (J=3) Coster-Kronig diagram line when the transition is excited by photoionization with x rays of energy E_{exc} in excess of the Xe L_2 binding energy.

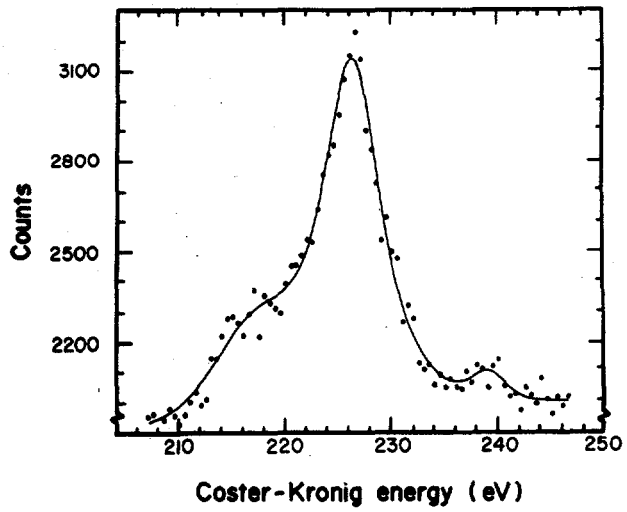

FIG. 1. Measured spectrum of L_2-L_3N_4 Coster-Kronig electrons emitted following $2p_{1/2}$-shell ionization of Xe atoms with 5,204-eV photons.

The experimental results are compared with two theoretical models, the first of which (denoted by I) does not include the no-passing effect and the second of which (labeled NP) does. For the first (shake-down) model, which does not take into account the interaction between photoelectron and Auger electron in the final state, we have used our analytic quantum-mechanical formula[2] with a change of unit charge in the potential experienced by the outgoing photoelectron. For the second model (NP), which takes account of the time required for the Auger electron to overtake the photoelectron, we invoke the semiclassical formula of Russek and Mehlhorn.[3]

The fit of the predictions from the two theories to the experimental data is shown in Fig. 2. The data show that the no-passing effect clearly manifests itself in this case of an exceedingly fast, low-energy Coster-Kronig transition. If the time required for the Coster-Kronig electron to catch up and pass the photoelectron is not taken into account (Model I), the final observed energy of the secondary electron is overestimated; in the present case, the shift is overestimated by 0.5 eV for $E_{exc} = \varepsilon_A$.[3] The Russek-Mehlhorn semiclassical model[3] fits the present data well. It is shown elsewhere[4] that the fully quantum-mechanical theory also adequately accounts for the no-passing effect once dynamic screening is included.

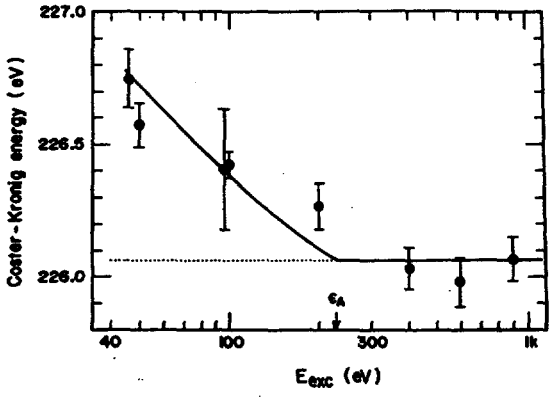

FIG. 2. Measured Xe L_2-L_3N_4 (J=3) Coster-Kronig-electron energies (dots with error bars) as a function of incident-photon excess energy over the L_2 ionization potential. The broken curve (I) represents the prediction of the simple shake-down theory according to Ref. 2; the solid curve (NP), calculated according to the semiclassical formula of Ref. 3, includes the no-passing effect that causes the PCI shift to vanish at $E_{exc}=\varepsilon_A$.

*This research was supported in part in the University of Oregon by the National Science Foundation under Grant No. PHY-85 16788 and the U.S. Air Force Office of Scientific Research through Contract No. F49620-85-C-0040, and in the University of Tennessee by the National Science Foundation under Grant No. PHY-85 06692. The Stanford Synchrotron Radiation Laboratory, where this experiment was performed, is supported by the Department of Energy through the Office of Basic Energy Sciences and by the National Institutes of Health through the Biotechnology Resources Program.

[1]M. Borst and V. Schmidt, Phys. Rev. A 33, 4456 (1986).

[2]J. Tulkki, G. B. Armen, T. Aberg, B. Crasemann, and M. H. Chen, Z. Phys. D (in press).

[3]A. Russek and W. Mehlhorn, J. Phys. B 19 911 (1986).

[4]G. B. Armen, J. Tulkki, T. Aberg, and B. Crasemann (to be published).

THE BONDING AND ORIENTATION OF DICARBON, ETHYLENE AND ACETYLENE ON Ag(110)

P. Stevens and R.J. Madix*
J. Stöhr**

*Department of Chemical Engineering, Stanford University, Stanford, CA 94305
**IBM Almaden Research Center, 650 Harry Road, San Jose, CA 95120

Dicarbon (C_2) differs from other diatomic molecules comprised of elements of the first row of the periodic table. Contrary to expectations based on simple molecular orbital schemes, its ground state is a singlet and the lowest unoccupied molecular orbital is a bonding orbital of σ symmetry [1]. Because of this, C_2 has a high electron affinity; further, the bond length of C_2^- is close to that of C_2 itself. This aspect of C_2 contrasts to that for O_2 which possesses antibonding orbitals of π symmetry as frontier orbitals. The comparison of the bonding and structure of these two diatomics thus provides important basic knowledge on bonding at surfaces. In previous work we have synthesized C_2 on Ag(110) using preadsorbed atomic oxygen to selectively activate the C-H bonds of acetylene to form gaseous water, leaving the C-C bond intact. The integrity of the C-C bond was verified by the titration of the species with deuterated acetic acid, which produced the C_2D_2 isotope only [2]. Since the reaction between surface oxygen and acetylene is quantitative, C_2 can be produced at coverages up to one-third monolayer. As the coverage is increased a series of well-ordered two dimensional structures are indicated by low energy electron diffraction. The origin of the long range order of these structures is not understood, nor is the local bonding of the C_2 species. We have undertaken studies of the fine structure at the C(1s) absorption edge at beam line I-1 at SSRL to determine the local structure and bonding of adsorbed C_2.

The near edge spectra for the dicarbon species on Ag(110) show both azimuthal and polar angle dependence on the angle of incidence of the radiation. In fig. 1 are shown the spectra for normal incidence at four different azimuths varied from along the [001] direction to along [$\bar{1}$10]. The σ* resonance is most intense when the electric field vector is along the [$\bar{1}$10] direction and vanishes along the [001], clearly showing that the species is aligned along the close-packed direction on the surface. Similarly, the π* resonance is sharply diminshed in the [$\bar{1}$10] azimuth, as expected when the vector points along the internuclear axis. The spectra at glancing incidence support this conclusion.

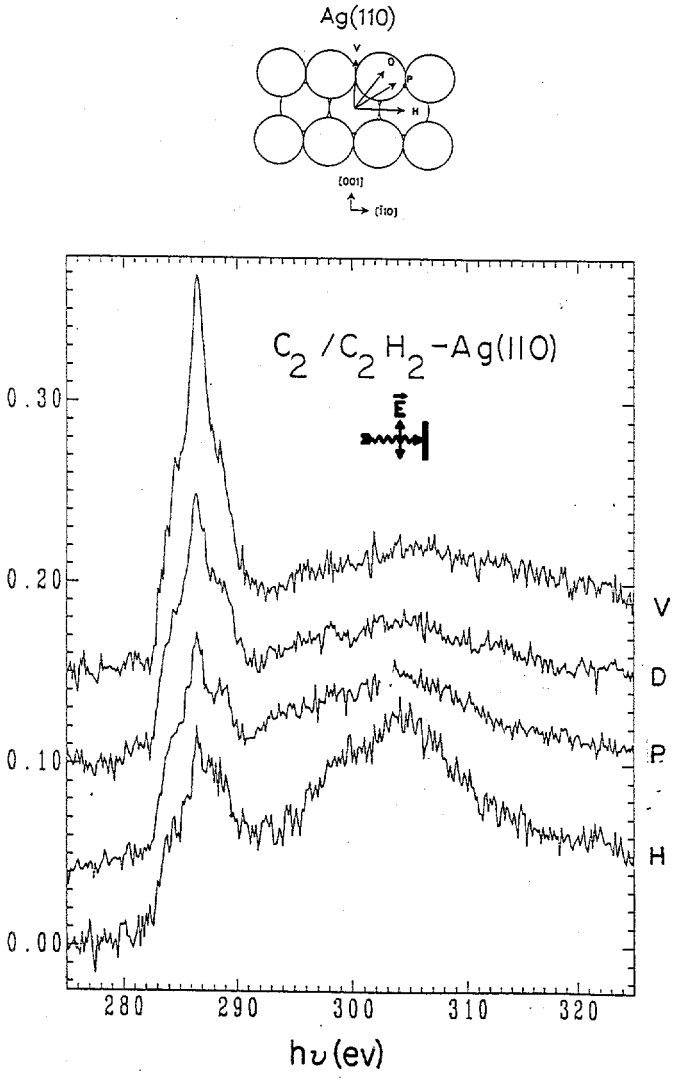

Figure 1.

The near edge spectra for acetylene and ethylene on Ag(110) were taken to provide fiducial points for the correlation between the C-C bond length and the σ^* resonance energy. Figure 2 shows the spectra obtained at normal incidence for ethylene (a) and acetylene (b), which are both known to adsorb as molecules on this surface with negligible perturbation of the intramolecular bonding [3,4]. The position of the σ^* resonances at 301 and 310 eV agree well with that expected from their respective bond lengths of 1.34 and 1.20 Å based on published correlations between the resonance position and the bond length [5]. The bond length for the dicarbon species is 1.30 Å. This bond length compares to those of gaseous C_2 (1.24 Å), C_2^- (1.27 Å), and C_2^+ (1.30 Å). The closeness of the bond lengths for C_2^- and C_2^+ make it difficult to assign the direction of charge transfer.

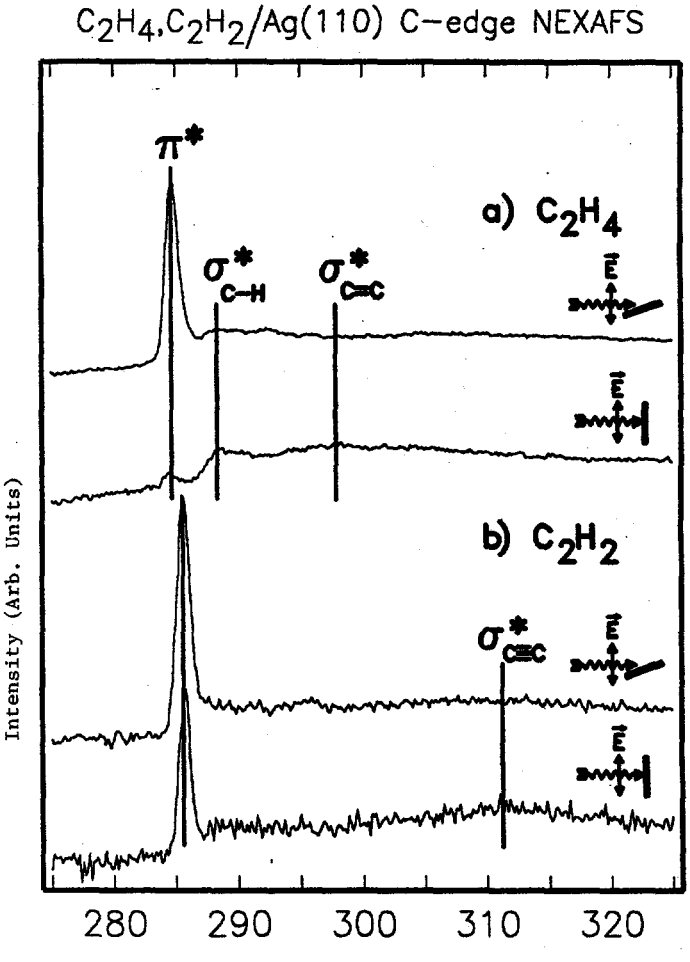

Figure 2

Some aspects of the spectra and the bonding are incompletely understood at this time. In order to clarify spectral features, such as the broad π^* resonance, we have undertaken ab initio theoretical calculations, which will allow us to contrast the bonding of both O_2 and C_2 to this surface.

[1] Herzberg, Lagerquist, Malmberg, Can. J. Phys. 47 (1969) 2735. Meinel, Can. J. Phys. 50 (1972) 158.

[2] M.A. Barteau and R.J. Madix, Surf. Sci. 115 (1982) 355.

[3] M.A. Barteau and R.J. Madix, Surf. Sci. 103 (1980) L171.

[4] E. Stuve, R.J. Madix and B.A. Sexton, Surf. Sci. 123 (1982) 491.

[5] F. Sette, J. Stöhr and A.P. Hitchcock, J. Chem. Phys. 81 (1984) 4906.

NEXAFS STUDIES OF UNSATURATED CARBOXYLIC ACIDS AND ALCOHOLS

D.A. Outka*, J.Stöhr*, R.J. Madix**,
H.H. Rotermund*, B. Hermsmeier***, J. Solomon**

*IBM Almaden Research Center, 650 Harry Road, San Jose, CA 95120
**Department of Chemical Engineering, Stanford University, Stanford, CA 94305
***Department of Chemistry, University of Hawaii, Honolulu, HI 96822

Near-edge X-ray absorption fine structure (NEXAFS) has been shown recently to be a probe of the structure, orientation, and electronic state of molecules either in the gas phase or adsorbed on surfaces [1,2]. In the NEXAFS technique, a K-shell electron is excited to unoccupied orbitals near the ionization threshold. Since the properties of these unoccupied orbitals, in molecules, are determined to a large extent by the bonding in the molecule, NEXAFS is sensitive to certain molecular properties such as those listed above. For example, transitions to the following empty states are easily identified C-C σ^*, C=C σ^*, C=C π^*, C≡C σ^*, C≡C π^*, C-O σ^*, C=O σ^*, C=O π^*, C≡O σ^*, and C≡O π^*, based upon their energies and peak shapes [2]. NEXAFS can thus serve to identify these functional groups in unknown species.

In this study NEXAFS is extended beyond simple monofunctional molecules to molecules containing more than one functional group. In most cases the NEXAFS spectra of such molecules can be described as a superposition of features from the individual functional groups. An important exception, however, is observed for molecules with alternating π orbitals which results in distinct changes in the π^* resonances.

CONDENSED ALCOHOLS

The NEXAFS spectra of the complex alcohols examined here can be attributed to the superposition of features expected of their constituent functional groups. To establish this principle, the condensed layers of the simplest alcohol, methanol, were used to provide a prototype for the alcohol group. Two primary resonances were observed, the C-H π^* resonance at 289.4 eV and the C-O σ^* resonance at 293.0 eV (figure 1).

Condensed layers of the first complex alcohol, allyl alcohol, ($CH_2=CH_2OH$) has the features of methanol plus those of ethylene (C_2H_4) (figure 1). As in methanol the alcohol features, C-H π^* and C-O σ^*, are observed at 289.4 and 293.0 eV, respectively. The alkene features are the C=C π^* resonance at 285.0 eV and the C=C σ^* resonance at approximately 300 eV. The last two are similar to the gas phase spectrum of ethylene which has the corresponding peaks at 284.8 eV and 302 eV [3].

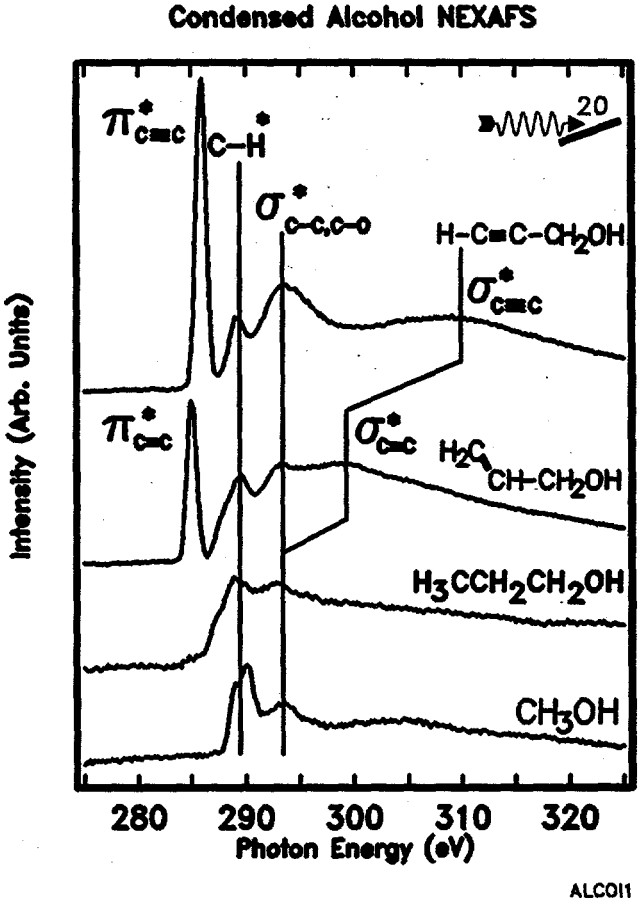

Figure 1: Comparison of the carbon K edge NEXAFS spectra of various condensed alcohols.

Condensed layers of propargyl alcohol, ($HC\equiv CCH_2OH$), also illustrate the superposition principle for NEXAFS spectra (figure 1). The features attributed to the alcohol function are the C-H π^* peak at 289.2 eV and the C-O σ^* resonance which contributed to the peak at 293.7 eV. The latter is not resolved from the σ^* peak for the C-C single bond expected in the same region. Two additional peaks are expected from the C≡C bond by comparison to acetylene (HC≡CH) [3,4]. These are the sharp C≡C π^* peak at 285.7 eV in propargyl alcohol, in reasonable agreement with the 286.1 eV location in acetylene, and the C≡C σ^* peak at 310 eV which is at the same location as in acetylene.

CONDENSED CARBOXYLIC ACIDS

Most of the features of the NEXAFS spectra of the condensed carboxylic acids could also be attributed to the superposition of features expected for these molecules from the functional groups they contained. The π^* features of molecules containing more than one π orbital, however, did not follow this principle. Instead, because the π orbitals were conjugated, interaction occurred among them which altered the NEXAFS spectra. It is these interactions among the π orbitals which will be the focus of this discussion.

Condensed layers of formic acid (HCOOH) provide the prototype for the unperturbed C=O π orbital in a carboxylic acid (figure 2). A single C=O π^* peak was observed at 288.6 eV. Such a peak was observed for all of the carboxylic acids near this position. For example, the C=O π^* resonance was observed for propionic acid ($CH_3CH_2CO_2H$) at 288.5 eV, for acrylic acid ($CH_2=CHCO_2H$) at 288.5 eV, and for propiolic acid ($HC\equiv CCO_2H$) at 288.9 eV. Thus the C=O π^* resonance appears to follow the superposition principle.

The simplest complex carboxylic acid, acrylic acid, also appears to follow the superposition principle in its π^* resonances. In addition to the C=O π^* peak already mentioned it also exhibited a C=C π peak at 284.4 eV (figure 2) which is reasonably near the location of this same resonance in allyl alcohol and gaseous ethylene which are 285.0 and 284.8 eV, respectively.

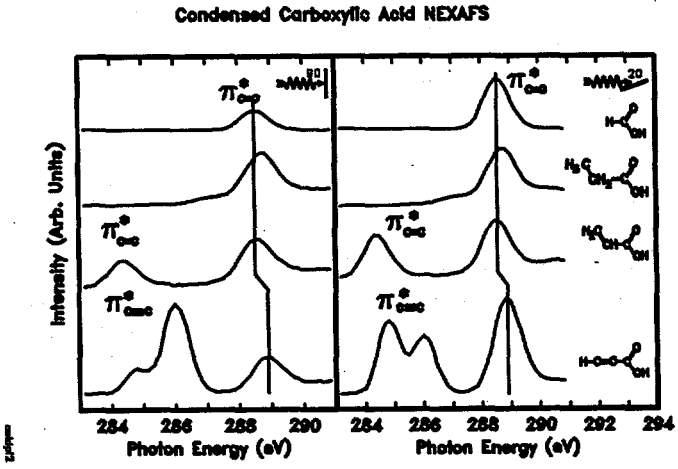

Figure 2: Comparison of the π^* regions of the carbon K edge NEXAFS spectra of various condensed carboxylic acids.

The π^* peaks of propiolic acid show profound differences from the superposition principle, however. For example, the superposition principle predicts that only two π^* peaks will be observed, one for the C=O π^* resonance and one for the C≡C π^* resonance. Experimentally, three peaks are observed, however (figure 2). In particular, rather than a single C≡C π^* resonance being observed at 285.7 eV as in propargyl alcohol, two π^* peaks are observed in this region.

The angular dependence of these peaks identify them as resulting from the removal of the degeneracy of the two π components of the C≡C bond. The condensed layers of propiolic acid have a preferred orientation with the plane of the OCO group nearly parallel to the surface. This is apparent in the NEXAFS spectra as a more intense C=O π^* peak under glancing X-ray incidence as compared to normal incidence (figure 2). The two C≡C π^* peaks also exhibit an angular dependence. In particular, the 284.8 eV peak shows the same angular dependence as the C=O π^* resonance, while the 286.0 eV peak exhibits the opposite angular dependence. Therefore, the 284.8 eV resonance is that component of the C≡C π bond which is parallel to the C=O π bond while the 286.0 eV resonance is that component which is perpendicular to the C=O π bond.

CONCLUSIONS

This study illustrates the application of NEXAFS to the analysis of complex molecules containing more than one functional groups. In many cases the assignment of the NEXAFS transitions follows directly from the spectra of simple monofunctional molecules. Interaction between functional groups can alter the NEXAFS spectra from these simple considerations, however, as in the case of conjugated π orbitals considered here.

REFERENCES

1. J.Stöhr and R.Jaeger, *Phys. Rev. B*, **26**, 4111 (1982).
2. F.Sette, J.Stöhr, and A.P.Hitchcock, *J. Chem. Phys.*, **81**, 4906 (1984).
3. J.A.Horsley, J.Stöhr, and R.J.Koestner *J. Chem. Phys.*, **83**, 3146 (1985).
4. A.P.Hitchcock and C.E.Brion *J. Electron Spectrosc.*, **22**, 283 (1981).

NEXAFS STUDY OF THE ORIENTATIONS OF MOLECULAR OXYGEN ADSORBED ON Ag(110)

D.A. Outka, W. Jark and J. Stöhr*
R.J. Madix, P. Stevens and J. Solomon**

*IBM Almaden Research Center, 650 Harry Road, San Jose, CA 95120
**Department of Chemical Engineering, Stanford University, Stanford, CA 94305

Oxygen was first shown to adsorb molecularly on metal surfaces by the simultaneous adsorption of $^{18}O_2$ and $^{16}O_2$ on Ag(110) [1]. The absence on the mixed isotope in the low temperature desorption state of O_2 clearly indicated that the O-O bond was not broken in this binding state. Subsequent studies of this species with vibrational spectroscopy revealed an unusually low O-O stretching frequency, indicative of substantial charge transfer from the metal to the molecule and a reduction of the bond order from two to one or less [2,3]. The molecule has been proposed to lie in the troughs on this surface, though there is no published evidence to establish this feature. Since this oxygen-metal complex is the precursor to oxidation of the surface, its bonding and strucutre is of considerable importance. We have examined this system with NEXAFS, since this spectroscopy affords the determination of the orientation and bond lengths of molecules containing elements of low atomic number [4]. The experiments were performed on beam line I-1 at SSRL.

The spectra taken at the oxygen edge at 90K for adsorbed O_2 are shown in the accompanying figure. The XPS binding energy was determined previously in our laboratory. The raw spectra were normalized by the incident beam flux to correct for the changes in X-ray intensity of the source. Spectra taken in the absence of adsorbed dioxygen were then subtracted to obtain the features due to adsorbed O_2 only. The buildup of subsurface oxygen makes this correction necessary and difficult. The figure shows the oxygen K edge absorption spectra for angles of incidence of the light of 90 and 10 degrees with respect to the surface tangent for the [001] and [1$\bar{1}$0] azimuths. Whereas resonances with both the π and σ antibonding orbitals are observed for gas phase O_2, only one major feature is observed for the adsorbed species, and this resonance at 532.6 eV is assigned to the transition from the O(1s) core level to the unfilled antibonding σ orbital of the O-O bond. The absence of the π^* resonance shows that this orbital is fully occupied and that the bond order is reduced to one or less in the surface complex. The bond order can be estimated from the position of the peak to be 1.45 Å [5]. Furthermore, the σ^* resonance observed here is even lower than that for CF_3OOCF_3, consistent with the reduced bond order.

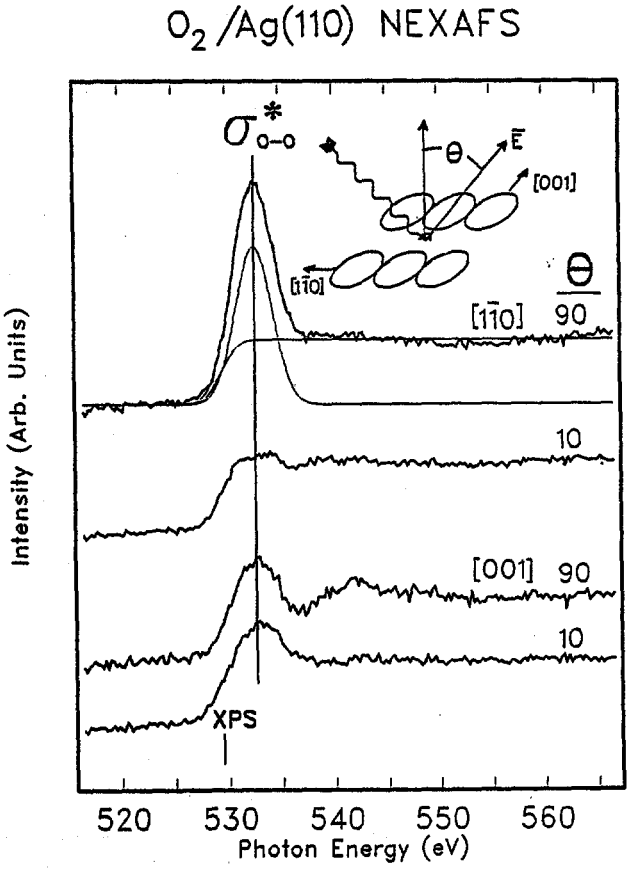

The angular dependence of the intensity of the σ^* resonance shows that the molecule lies with both oxygens in the plane of the surface with the internuclear bond axis along the [1$\bar{1}$0] direction. This is clearly seen from the absence of significant intensity in all but the 90 degree incidence spectrum with the electric field vector along the close-packed direction. The residual intensity in the other azimuths is due to incomplete polarization of the beam.

[1] M.A. Barteau and R.J. Madix, Surf. Sci. 97 (1980) 101.
[2] B.A. Sexton and R.J. Madix, Chem. Phys. Letts. 76 (1980) 294.
[3] C. Backx, C.P.M. de Groot and P. Biloen, Surf. Sci. 104 (1981) 300.
[4] J. Stöhr and R. Jaeger, Phys. Rev. B 26 (1982) 4111.
[5] F. Sette, J. Stohr and A.P. Hitchcock, J. Chem. Phys. 81 (1984) 4905.

XASEGS: X-RAY ABSORPTION SPECTROSCOPY OF ELECTROCHEMICALLY GENERATED SPECIES, A NEW TECHNIQUE

R.C. Elder and William R. Heineman
Department of Chemistry
University of Cincinnati
Cincinnati, OH 45221-0172

Introduction:

We have continued in the development and implementation of EXAFS spectroelectrochemistry for preparing and characterizing solutions of transition metal and biological complexes in varied oxidation states. In the process, thin-layer spectroelectrochemistry generates and maintains materials in a particular oxidation state easily and quantitatively while X-ray absorption spectra are recorded. X-ray spectra are analyzed in terms of their coordination numbers, interatomic distances, excitation state, and ligand identity. With the development of this hybrid technique, we have eliminated some of the weak points of each individual analysis tool, e.g., the lack of definite chemical identification in spectroelectrochemistry and the limited number of stable oxidation states which can be generated by chemical reductants and oxidants for analysis by conventional X-ray absorption spectroscopy.

This report focuses on our efforts in three areas toward the development and evaluation of EXAFS spectroelectrochemistry for the determination of local structure of electrogenerated species. First, a sensitivity study to evaluate the ability to obtain high quality EXAFS spectra of solution species is presented. Next, results using a new cell designed to study materials in nonaqueous solution are reported. Finally, our extension of the EXAFS spectroelectrochemistry technique to the examination of redox active metal complexes incorporated on polymer modified electrodes is described.

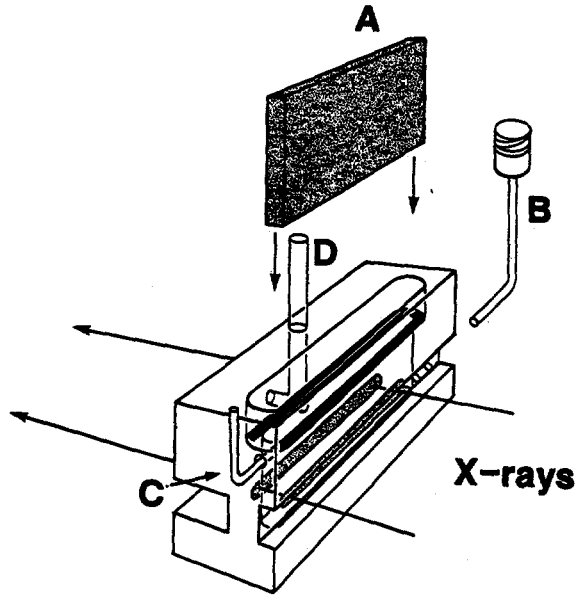

Figure 1: EXAFS spectroelectrochemical cell: (A) RVC working electrode, (B) Pt syringe needle inlet port and electrical contact; (C) Pt wire auxiliary electrode; (D) Ag/AgCl (3M NaCl) reference electrode. Cell body: Plexiglas G. X-ray window material: 0.0005 in. polyimide Kapton tape.

Experimental

The construction of the spectroelectrochemical cell used for the aqueous sensitivity and polymer modified electrode studies has been reported and is shown in Figure 1 (1). The cell was assembled with reticulated vitreous carbon as the working electrode. The platinum syringe needle served both as the filling port and the electrical contact to the RVC. The platinum wire auxiliary electrode was shaped like an opened paper clip and encased in an ion-exchange tubing (Nafion). The reference electrode was Ag/AgCl (3M NaCl). The X-rays passed through the region (l = 30 mm, h = 3 mm) marked with the double arrows. Polyimide Kapton tape was the X-ray window cover material.

The cell used for the nonaqueous EXAFS spectroelectrochemistry studies also followed the design shown in Figure 1, with some of the materials used for the construction of the cell modified such the experiments using nonaqueous solutions could be performed. The cell body was machined from Macor ceramic and the polyimide Kapton windows were sealed with a fast-setting epoxy. Silicone rubber was used to seal electrode ports.

Polymer coated electrodes were prepared by coating the bare RVC electrode surface with a solution of polymer, followed by crosslinking techniques using gamma radiation, as required. The electroactive species were incorporated into the polymer coated RVC electrode using immersion, with stirring, of the electrode in a solution of the complex. Once rinsed with supporting electrolyte and dried, EXAFS spectra were taken of the metal complex incorporated, polymer modified electrodes in the cell illustrated in Figure 1. Addition of supporting electrolyte to the cell with application of the appropriate potential allowed for the generation of alternative oxidation states.

Results and Discussion:

One of the major difficulties in obtaining EXAFS spectra of good quality on solution species is sensitivity. In order to obtain adequate signal/noise, experiments are preferably performed on solutions that are typically 0.1 M and higher in concentration. This is a very high concentration for electrochemical experiments such as thin-layer cyclic voltammetry and thin-layer spectroelectrochemistry where the resulting large currents exacerbate the IR drop problem. More importantly, many species of interest are not soluble to this extent. Consequently, a series of experiments was performed on various concentrations of $Ru(NH_3)_6Cl_3$ in order to establish a concentration range over which workable EXAFS spectra can be obtained in the RVC cell. The effect of a deteriorating signal-to-noise ratio for data collected in both transmission (A) and fluorescence (B) modes for 100 mM, 10 mM and 1 mM $Ru(NH_3)_6Cl_3$ is shown in Figure 2. The EXAFS multiplied by k^2 vs. k data have been plotted. The decrease in quality for the transmission data is much more pronounced (2). The Fourier transform of the fluorescence data (Figure 2C) exhibits one major peak for the Ru-N absorber-scatterer pair. Back-transformation of the peak generated the Fourier filtered data shown in Figure 2D.

Curve fitting of the filtered data with empirical parameters derived from the solid model were internally consistent. The calculated Ru(II)-N bond distances are within $\pm$0.02 Å of agreement with crystal structure results. More importantly, these results do not change significantly as the concentration is lowered. Calculated coordination numbers and goodness of fit values are also reasonable and do not vary significantly

with concentration. An increase in coordination number on

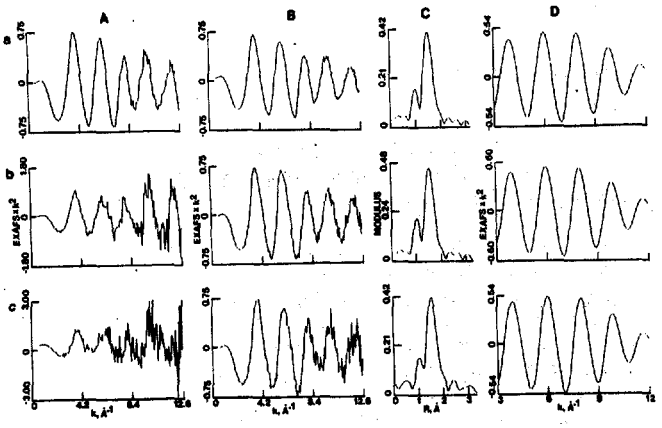

Figure 2: EXAFS spectra of $Ru(NH_3)_6Cl_3$ in 1M sodium acetate: Concentrations (a) 100mM; (b) 10mM; (c) 1mM; (A) transmission mode; (B) Fluorescence mode; (C) Fourier Transforms of B, K = 3-12 $Å^{-1}$, E_o = 22139.3 eV; (D) Fourier Filters of C, R = 1.239-2.129 Å; applied potential +0.2 V vs. Ag/AgCl. Fluorescence filter 0.025-mm Mo Foil.

dissolution was observed and may arise from a lower static disorder in the solution phase. Considering these EXAFS results, which are for single scans without the benefit of signal averaging, it appears that ruthenium solutions of 10^{-4} M could be examined readily. This is highly desirable for study of many bioinorganic complexes which exhibit low solubility or for which little sample is available. Also, the problem associated with the high currents that accompany the higher concentrations is minimized.

Our efforts to extend EXAFS-spectroelectrochemistry to study materials in nonaqueous solution include two examples. We have investigated trans-$[Re(DEPE)_2Cl_2]PF_6$, (where DEPE represents 1,2-bis(diethylphosphino)ethane) and $(Et_4N)_2[W_2(CO)_8(S\text{-benzyl}_2]$. Our interest in the rhenium complex is as a non-radioactive analogue of a technetium complex which might serve as a heart imaging agent (3). Tc and Re are congeners; analogous complexes should provide insight on the role of the oxidation-reduction potential of complexes in determining biological behavior. The Re complexes are typically 200 mV more difficult to reduce than the Tc analogues. We have measured EXAFS spectra on the solid complex and on the solution species. The Fourier transform exhibits one main peak foo both the Re-P and Re-Cl interactions. A distance of 2.44 A for Re-P and 2.35 Å for Re-Cl has been obtained.

We also have investigated the complex $(Et_4N)_2[W_2(CO)_8(S\text{-benzyl})_2]$. The interest in thiolate complexes of tungsten and molybdenum is related to their possible implication in the structure and function of molybdoenzymes (4). The W(0) dimer undergoes a single two-electron oxidation to the W(I) dimer and is accompanied by the formation of a W-W bond with extensive structural reorganization. The Fourier transform of the EXAFS spectra for the W(0) dimer exhibits multiple peaks which can be attributed to W-C, W-O, W-S, and W-W interactions. Multi-shell curve fitting analyses are in progress.

Immobilization of a polymer coating on the surface of the electrode offers a convenient means for modifying the electrode surface to incorporate the metal ion or complex of interest and control its behavior electrochemically. Although an extensive variety of experiments can be performed to study the redox chemistry of electroactive components incorporated in a polymer coated electrode, little has been done to evaluate the molecular structure of these redox speies (5). The EXAFS spectroelectrochemical approach which we have developed for solution studies offers a new and powerful approach to the structural characterization of various redox species incorporated in a polymer immobilized on the electrode surface.

In order to ascertain the feasibility of making EXAFS measurements on redox species in polymer films coated on electrodes, we performed preliminary EXAFS spectroelectrochemistry experiments on three different metal complexes incorporated into two types of polymer coated electrodes. Systems studied consisted of crosslinked poly (diallyl dimethyl ammonium chloride) (DMDAAC) into which $Fe(CN)_6^{4-/3-}$ was loaded and Nafion into which either $Ru(bpy)_3^{2+/3+}$ or $Co(sep)^{3+/2+}$ was loaded. Analysis of the EXAFS spectra taken before and after the application of an appropriate potential to effect electrolysis gave the following results. Spectra obtained for both $Fe(CN)_6^{4-}$ and electrogenerated $Fe(CN)_6^{3-}$ in DMDAAC exhibited an absorption edge shift and gave metal-ligand Fe-C bond distances changes comparable to these that we have reported for this system in aqueous solution (6). Analysis of spectra obtained for $Ru(bpy)_3^{2+}$ and electrogenerated $Ru(bpy)_3^{3+}$ in Nafion resulted in Ru-N bond distances comparable to those known for the solid and those we have previously measured in aqueous solution. These experiments demonstrated that EXAFS spectroelectrochemistry can be used to explore redox systems incorporated in polymer films on electrode surfaces. Continued investigations in this area include modifications in cell design specific to the special needs for the study of polymer modified electrodes and studies on diverse types of chemical systems.

Individuals working on this project include Drs. H.D. Dewald, D.M. Caster, and C.E. Lunte. Support for this project is provided by NSF Grant CHE 8401525.

References

1) Dewald, H.D.; Watkins II, J.W.; Elder, R.C.; Heineman, W.R. Anal. Chem. 1986, 58, 2968-2975.

2) Elder, R.C.; Tepperman, K.G.; Eidsness, M.; Heeg, M.J. Proceedings of Bioinorganic Chemistry of Gold Coordi-nation Compounds, Nov. 16-17, 1981, Smith Kline & French Laboratories, Philadelphia, 1983, pp. 124-142.

3) Vanderheyden, J.-L.; Heeg, M.J.; Deutsch, E. Inorg. Chem. 1985, 24, 1666-1673.

4) Zhuang, B.; McDonald, J.W.; Schultz, F.A.; Newton, W.E. Inorg. Chim. Acta 1985, 90, L29-L31.

5) R.W. Murray in "Electroanalytical Chemistry" A.J. Bard, Ed: Marcell Dekker: New York, 1984, Vol. 13, 191-368.

6) Smith, D.A.; Elder, R.C.; Heineman, W.R. Anal. Chem. 1985, 57, 2361-2365.

THE OFF CENTER DISPLACEMENT OF CATIONS IN ALKALI HALIDES

Frank Bridges and Gina Dimino
Physics Department, University of California
Santa Cruz, CA 95064
and
J. B. Boyce
Xerox Palo Alto Research Center
Palo Alto, CA 94304

We outline briefly our progress in measuring the local structure about an off-center Cu^+ ion in NaCl and KCl. Some instrumentation development to improve the S/N in these dilute systems is also discussed.

A. Off-Center Studies

When a small anion (such as Li^+, Cu^+, or Ag^+) replaces a larger host ion in an alkali halide crystal, the defect ion does not always sit at the center of symmetry. Instead, it can occupy an off-center position, displaced along one of the symmetry axes of the crystal. The off-center position produces an electric dipole moment; consequently such systems are called paraelectric systems.

In Li^+ doped crystals, theoretical results,[1] confirmed by experiments,[2] show that an isolated Li^+ ion is off-center along <111> in KCl, but moves on-center in the larger anion systems KBr and KI. Ag^+ systems, however, have off-center wells which become deeper as the anion size is increased,[3] suggesting, perhaps, that a different mechanism is involved.

Cu^+ systems are more problematical, since the Cu^+ ions are frozen off-center at low temperatures, making measurements more difficult. Nevertheless, the data available[4] suggest they resemble Ag^+ systems.

We have made EXAFS measurements of NaCl:Cu and KCl:Cu systems at the Cu K-edge in order to determine the Cu^+ local environment. KCl:Cu is known to be off-center but its orientation has not been definitively determined.[4] NaCl:Cu has heretofore been considered an on-center defect.

The fourier transform of $k\chi(k)$ of an averaged set of NaCl:Cu (Cu^+ concentration of 500ppm) runs is compared with a CuCl standard in Fig. 1 (upper trace CuCl, lower trace NaCl:Cu). Attempts to fit the first neighbor peak (from 1.3 to 2.6A) to a single CuCl standard resulted in poor fits. Two gaussian fits were not much better, and required considerable broadening of the standard. Three or more gaussians were needed to obtain a reasonably good fit.

To minimize the number of free parameters, we included constraints on the fits, assuming that the Cu^+ cation is displaced along one of the symmetry axes of a cube. For instance, a defect off-center along the <110> axis would show three near neighbor peaks with equal broadenings and amplitudes. A <111> defect would show two such peaks.

An additional unbroadened and unshifted CuCl standard was required because of unavoidable CuCl precipitate in the samples. The amplitude of the CuCl peak is constrained, since Cu^+ has four nearest neighbor Cl atoms in CuCl, while it has six in NaCl:Cu.

To test for a <111> defect, we made three gaussian fits, which yielded two shifted gaussians (at shifts -.133A and .334A with $\Delta\sigma^2$ = .00072 and amp. = .532), and a CuCl peak of amp = .621. We obtained good fits, but the free parameters changed significantly as we included some or all of the constraints discussed above. We then tested for a <110> defect, with four gaussian fits. The results were similar, but the center peak was decomposed into a smaller (amp = .259) undistorted CuCl and a third gaussian. The gaussians were located at shifts -.142H, .041A and .34A. Introducing the above constraints did not cause large changes in the fit parameters in this case.

Regardless of whether the defect is <111> or <110>, we obtain surprising information from the EXAFS data. First, Cu^+ does appear to go off-center in NaCl:Cu systems, contrary to what was previously supposed. Secondly, the near neighbor distances correspond more closely to the CuCl distance (2.34A) than to the distance calculated using the ionic radii (.96A + 1.81A = 2.77A). Thirdly, one of the distances (2.21A) is even smaller than the CuCl distance.

This indicates considerable distortion of the near neighbor anion shell about the Cu^+, as well as distortion of the Cu^+ itself. It suggests that Cu^+ may move off-center in such a way that its environment is closer to the tetrahedral coordination of CuCl. Note that for a <110> off-center Cu^+ displacement, the four closest Cls form a distorted tetrahedron.

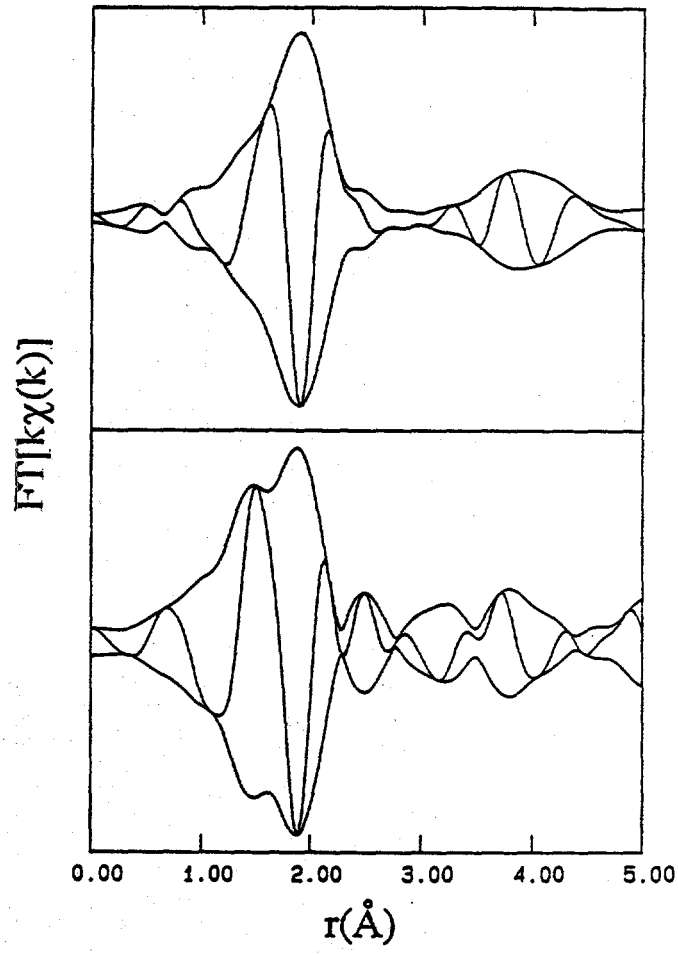

Fig. 1. The fourier transform of $k\chi(k)$ for CuCl (upper) and NaCl:Cu (lower).

B. Development of an Incident Flux Leveling Circuit

The fluorescence signal in these dilute samples is very weak and small intensity variations in the X-ray source and/or monochrometer glitches can introduce small steps in the EXAFS data that cannot be reliably removed.

To compensate for variations in the incident beam I_0, the transmission I_T or fluorescence I_F is usually normalized by taking the ratio with I_0 (I_0/I_T or I_F/I_0). However, an exact cancellation of variations in I_0 is possible only if the two detectors have the same response (i.e., both exactly linear and no geometric effects) as a function of energy and count rate. In general this not possible; consequently many of our early traces had to be rejected.

For our experiments, we designed a leveling control feedback system to keep I_0 constant using the existing instrumentation on beamlines IV-1 or VII-3, without modifications to the monochrometer or detectors.

We controlled I_0 by varying the voltage V_p applied to the piezoelectric cell on one of the crystals in the monochrometer. This device determines the relative angle $\Delta\beta$ ($\Delta\beta \propto V_p$) between the two monochrometer crystals. The rocking curve (the variation of transmitted flux as a function of V_p) is shown schematically in Fig. 2. For stable leveling, the piezoelectric voltage must be kept within the range V_1 to V_2 (or V_3 to V_4). In addition, it is important that the range V_1 to V_2 be low enough (or V_3 to V_4 high enough) that harmonics are not present in the output beam. Since the change in I_o increases with voltage in the first range but decreases with voltage in the second, it is important that V_p does not increase above a certain value, otherwise unstable operation results. This is particularly true during the time in which the monochrometer is stepped to a new energy and the output flux varies wildly. Our feedback control circuit uses voltage clamps on V_p to ensure stable operation.

The effectiveness of this leveling feedback system is illustrated in Fig. 3, at the Cu K-edge for a very low concentration sample -- 100 ppm of Cu in KCl. Here the overall S/N is improved by about a factor of 2, even where clear glitches are not observed in I_o.

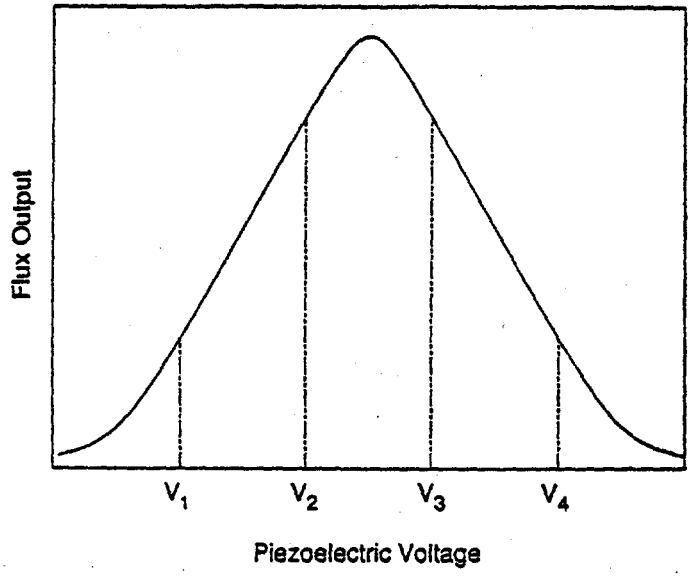

Fig. 2. The rocking curve for a double monochrometer as a function of the applied piezoelectric voltage V_p.

One important advantage of the leveling feedback method that is not so obvious in the brief discussion above is the improvement in the settling of the monochrometer after it is stepped to a new energy. If the mechanical resonances that are generated in a step have a frequency within the bandwidth of the feedback loop, the piezoelectric cell will compensate for the mechanical motion. In our experiments this is best observed in the short energy range about the K-edge in which we use 1eV steps, with 1 second for settling and 1 second for data collection. Often there is an oscillation of I_o which suggests a mechanical resonance with a frequency of roughly 1-2 Hz. This increased variation of I_o with energy about the K-edge is often observed in unleveled operation but is not observed when the leveling curcuit is used.

Additional details of this circuit[5] and a comparison with other servo loop systems will be published shortly.

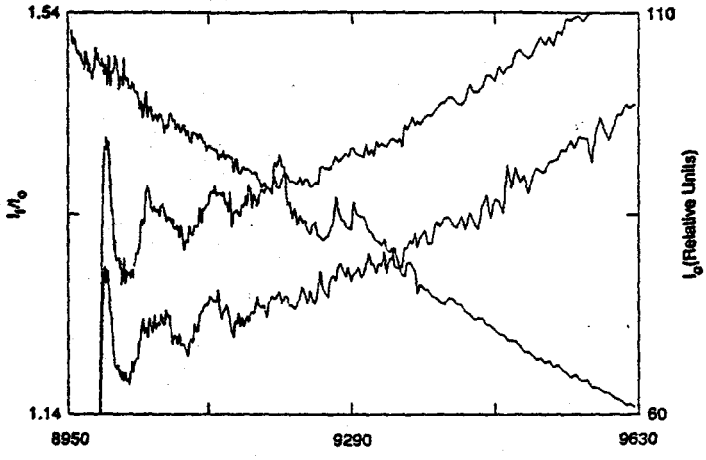

Fig. 3. A comparison of the fluorescence EXAFS signal with (upper trace) and without (lower trace) leveling over the energy range 8950 to 9630 eV. A plot of I_0 (decreases with energy) is included for reference.

1. M.J.L. Sangster and A.M. Stoneham, Phys. Rev. B26, 1028 (1982); C.R.A. Catlow, K.M. Diller, M.J. Norgett, J. Corish, B.M.C. Parker, and P.W.M. Jacobs, Phys. Rev. B18, 2739, (1978).

2. N.E. Byer and H.S. Sack, Phys. Rev. Lett. 17, 72 (1966); J. Phys. Chem Solid 29, 677 (1968); F. Bridges, Crit. Rev. Solid State Sci. 5, 1 (1975).

3. R.V. Jiminez, F. Luty, M. Sin Lu, and M. deSouza, Phys. Stat. Sol (b)106, 683(1981).

4. U. Holland and F. Luty, Ferroelectrics 17 377(1977); U. Holland PhD thesis, Utah, 1976.

5. F. Bridges, Nuclear Instr. and Meth. (1987).

EXAFS OF RHODIUM SUPPORTED ON ALUMINA

D.J. Sajkowski, E.S. Birnbaum, and M. Boudart
Department of Chemical Engineering
Stanford University
Stanford, CA 94305

This work shows the utility of using EXAFS to estimate the size of supported metallic clusters when such estimates are not possible by using conventional techniques such as chemisorption.

We have prepared rhodium clusters supported on alumina. Our intent was to prepare supported clusters containing less than 20-30 atoms; this corresponds to a nearest neighbor coordination number N_1 of less than about 7. Such clusters are of interest because of their potential for exhibiting novel catalytic properties.

The preparation procedure followed that of previously published work (1,2). Values of N_1, the average interatomic distance between nearest neighbors R_1, and the change in the Debye-Waller factor $\Delta\sigma^2$ are shown for two Rh/Al_2O_3 samples and the reference material, Rh powder, in the table below. These parameters were obtained from EXAFS data collected on samples at room temperature and atmospheric pressure of dihydrogen. Also shown is the amount of chemisorbed H atoms (H/Rh) and CO molecules (CO/Rh) per Rh atom contained in the sample. These values were obtained from isotherms at room temperature. The value of N_1 = 5 indicates clusters containing roughly a dozen atoms.

It is important to note that the H/Rh and CO/Rh ratios do not permit a quantitative estimate of the size of such small clusters. In the case of dihydrogen chemisorption, the stoichiometry of adsorption is unknown, while for CO it is known that the clusters are destroyed due to the formation of isolated $Rh(CO)_2$ species bound to the surface of the alumina (2). On the other hand, for the sample with a value of N_1 = 10, indicating clusters containing about 150 atoms, the H/Rh and CO/Rh ratios agree. Moreover, the value of 67-69% metal exposed is consistent with the estimate of the cluster size from the measured value of N_1 = 10. It appears that at large cluster sizes the adsorption stoichiometry for CO and H per Rh atom is, in both cases, 1:1. In addition, the larger rhodium clusters do not break up in the presence of CO.

Characterization of Rh/Al_2O_3 Samples

$\%Rh/Al_2O_3$	H/Rh	CO/Rh	N_1	R_1(pm)	$\Delta\sigma^2$(pm^2)
0.45	1.47	1.93	5	271	49
3.66	0.69	0.67	10	267	15
Rh powder	--	--	12	269	0

Acknowledgment

D.J. Sajkowski acknowledges support from NSF Grant CBT 8219066. E.S. Birnbaum acknowledges support from the National Science Foundation in the form of a Graduate Fellowship.

References

(1) G.H. Via, G. Meitzner, F.W. Lytle, and J.H. Sinfelt, J. Chem. Phys. 79, 1527 (1983).

(2) J.B.A.D. van Zon, D.C. Koningsberger, H.F.J. van't Blik, and D.E. Sayers, J. Chem. Phys. 82, 5742 (1985).

High Resolution X-Ray Scattering from the Lyotropic Liquid Crystal Cesium Perfluoro-Octanoate†

J. Brock, S. Kumar,[a] J. D. Litster, M. Sutton[b]

Department of Physics and Center for Materials Science and Engineering
Massachusetts Institute of Technology, Cambridge, MA 02139

Lyotropic nematic liquid-crystalline phases are formed by the long-range orientational ordering of non-spherical micelles in surfactant and water systems. Some of these nematic materials also have phase transitions, which may be either first or second order, to a lamellar phase. These phases have been discovered relatively recently and are of interest not only to liquid-crystal physicists but also to those concerned with the statistical mechanics of surfactants, micelles, and microemulsions. They appear to have symmetry properties similar to the nematic and smectic A phases of thermotropic liquid crystals, so our knowlege of thermotropics should be a good starting point to understand ordering in surfactant systems. The behavior may be more complex, however, because they are multicomponent systems and involve the ordering of molecular aggregates which may change size and shape.

Our project is to use high resolution x-ray scattering to study the development of lamellar order in nematic lyotropic systems in order to determine the similarities to thermotropic smectic materials and to elucidate the role played by the extra degrees of freedom. Initial studies have been done on the simple binary system of cesium perfluoro-octanoate (CsPFO) and water. CsPFO is a classical soap molecule, but with a fluorocarbon tail.

To obtain alignment, we have been using bulk samples ~ 1 mm thick; thus absorption is a serious problem. We have found it possible to make measurements on beam line VII-2 with an incident energy of 12 keV. Our results show that for samples with mole fraction soap X = 0.026, the lamellar density wave develops continuously in the nematic phase. Figure 1 shows scattering from short-range lamellar order in the nematic phase where the correlation length along the wave has grown to 5000 $\mathring{A}$. The solid line in the figure is a fit to a theoretical expression for the line shape which includes the spectrometer resolution function, shown as dash-dot-dash, and a background, shown dashed. We do not yet understand the origin of the background.

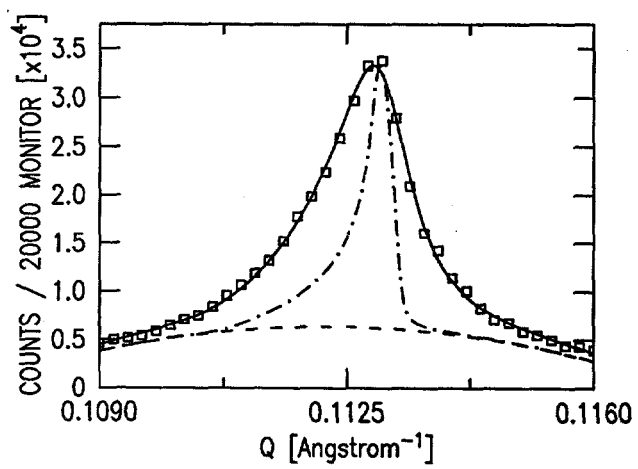

Figure 1. X-ray scattering from lamellar short-range order in CsPFO.

In figures 2 and 3 we show the evolution of the correlation lengths above the nematic to lamellar phase transition. The solid lines are fits to the power law divergence

$$\xi = \xi^0 (T/T_C - 1)^{-\nu}$$

expected if the analogy with thermotropic smectic phases is valid. We find $\nu = 0.76 \pm 0.03$, and 0.88 ± 0.11 for the longitudinal and transverse lengths, respectively. It remains to be determined whether the two exponents are equal, or, as in some thermotropic materials, different.

In future experiments we need to improve sample alignment in order to obtain better measurements of ξ and intend to explore the phase diagram near the tricritical point where the nematic-lamellar transition becomes first order.

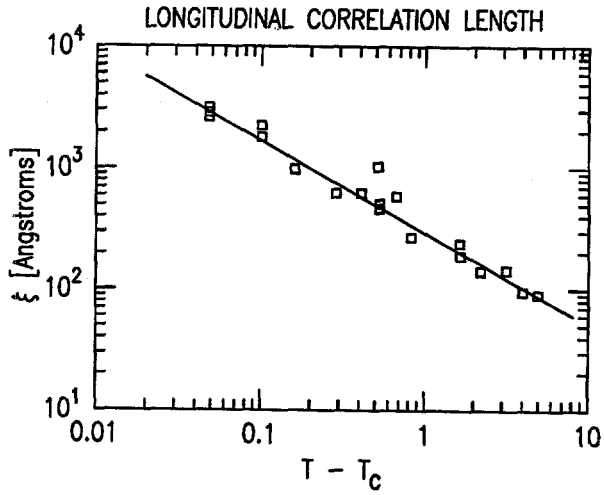

Figure 2. Longitudinal correlation length for lamellar order in nematic CsPFO.

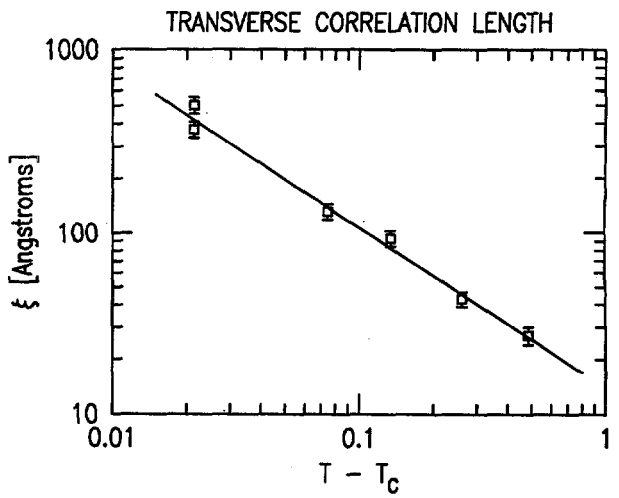

Figure 3. Transverse correlation length for lamellar order in nematic CsPFO.

† Proposal No. 837Mp

(a) Present address: Department of Physics, Kent State University, Kent, OH 44242

(b) Present address: Department of Physics, McGill University, Montreal, Quebec H3A 2T8, Canada

TIME RESOLVED X-RAY DIFFRACTION: THE KINECTICS OF THE THERMAL DECOMPOSITION OF $CdCO_3$ POWDERS

J.R. Schoonover and S.H. Lin
Department of Chemistry, Arizona State University
Tempe, Az 85287

Time resolved x-ray diffraction (TRXD) is the repeated taking of x-ray diffraction patterns of a solid undergoing a reaction[1]. The shape of a x-ray diffraction line is then obtained as a function of time. The shape of the line is determined by the size and shape of the growing crystallite, the strain in the crystallite, disorder, and fault stacking; indeed, most any deviation from that of the perfect solid will affect the line shape. Thus, the evolution of a solid state reaction may be followed.

The most readily available information is the size of the crystals, so that the kinectics of the reaction are easily followed. By observing several diffration lines, the rate of growth in three dimensions msy be obtained. If more than one order is accessible, or that an assumption can be made about the size distribution, a strain distribution can also be found.

TRXD requires that the line shapes be well defined, even when the lines are of low intensity and very broad, as occurrs early in the reaction; of course, the time to collect the diffraction pattern must be short relative to the half life of the reaction. These are necessary, but opposing requirements. For these reasons synchrotron radistion, with it's intense beam in the hard x-ray region, is being used. In addition, only a small region of the diffraction pattern, usually 1-5°, which is only one or two lines, are measured in a given experiment; thus , numerous experiments are required for each temperature. Presently, excellent results are being obtained for reactions that occur in less than thirty minutes, about a 50% improvement over the early results[2].

The thermal decomposition of $CdCO_3$ powders was studied for temperatures between 650k and 725K, in vacuum and in air, on BL IV-3. The oxide (111), (200), (220), and (311) lines have been studied as well as the higher orders (222) and (400); this is the entire diffraction pattern with two theta less than 100°, the lines of greater two theta being of too low intensity and the noise level too high. In addition, the carbonate (104),(001), and (110) lines have been studied. The lines were stepped scanned with intervals of 0.0250° to 0.030°, with collection times of 1 to 3 seconds for each interval depending upon the line width and peak intensity. The time for scans was 1.5 to 5 minutes, with scans 2 to 6 minutes apart.

Early in the reaction there is a decrease in the full width at half maximum (FWHM) of the carbonate lines, which indicates annealing. This was also present in earlier studies with cadmium hydroxide, but the temperature dependence showed that there was also a breaking up of the crystals[2]. In the carbonate system a very much different mechanism is seen; the crystals are breaking up randomly and rapidly so that the size distribution is not greatly affected.

The oxide FWHMdecreases as the reaction proceeds From the variance, with the instrumental variance removed, the size distribution changes tolarger crystallites. The period of crystal growth ends with the end of the decomposition, indicating that the growth does corrospond to development of the produst phase from the reactant. In the early stages of the reaction, fault stacking is seen, but as the size distribution changes, the affects of fault stacking on line shape is minimal. Within the time resolution, the oxide forms rapidly from the carbonate, so that the distribution of carbonate sizes is nearly constant and the oxide developes from stack faulting of the hexagonal carbonate just after loss of CO_2.

There is also a radistion induced phase, the lines of which are found near those of the oxide, and often coinciding with them; they are of low intensity and decay as the reaction proceeds. These lines may be from an oxycarbonate phase.

The results of thse TRXD experiments show very well the possibilities of the technique. Not only arethe results consistent with the theory[1], but promise to yield new insight into solid state reaction kinectics. The results may also aid in understanding radiation damage and how it affects the kinectics from TRXD experiments.

References.

1. T.L. Groy, S.H. Lin, S.K. Porter, R.R. Von Dreele, and L. Eyring (1982) J. Mol. Sci.,2, 93

2. J.R. Schoonover, O. Savborg, S.H. Lin, and 1. Eyring, J. Solid State Chem., in press.

X-RAY ABSORPTION SPECTROSCOPY OF MN AND FE IN THE PHOTOSYNTHETIC APPARATUS

Vittal K. Yachandra, Ann E. McDermott, R. D. Guiles,
R. David Britt, S. L. Dexheimer, James Cole,
Kenneth Sauer and Melvin P. Klein

Laboratory of Chemical Biodynamics, Lawrence Berkeley Laboratory
University of California, Berkeley, CA. 94720 USA

The process of photosynthesis in green plants may be considered as a photoinduced chlorophyll mediated transfer of electrons from water to CO_2 resulting in the formation of carbohydrates and O_2. Strong oxidants produced by photosystem II (PS II) remove electrons from the O_2-evolving complex resulting in water oxidation. Photosystem I (PS I) produces powerful reductants that donate electrons through a series of membrane bound proteins, one of which has been identified as an iron-sulfur protein containing at least three Fe-S clusters, to soluble ferredoxin and NADP, which are ultimately responsible for CO_2 reduction.

The primary focus of our work is directed toward the Mn containing O_2-evolving complex (Mn-OEC) in PS II and the Fe-S acceptor centers A, B and X in PS I.

The State of Manganese in the Photosynthetic Apparatus

The Mn-OEC is the least understood of the light-driven electron transfer protein complexes in chloroplasts, even though it has been the subject of extensive studies. Studies of O_2 evolution using a train of saturating light flashes have given rise to a model for the accumulation of oxidizing equivalents in which some intermediates, labeled S_0-S_4 operate in a cyclic fashion. X-ray spectroscopy using synchrotron radiation has supplied the most detailed information on the structure and oxidation state(s) of the Mn complex in the various S-states. Oxidation state and site symmetry are determined from the edge or XANES region while structural information is obtained from the EXAFS modulations.

The Mn K-edge energy shifts to higher energy upon advancement from the dark-adapted S_1 to the S_2 state prepared by illumination at 140 K, 190 K or at 277 K in the presence of DCMU, indicating that the Mn cluster undergoes oxidation. Illumination at 140 K produces a S_2 state characterized by a g=4.1 EPR signal, and illumination at 190 or 277 K produces a S_2 state characterized by a multiline EPR signal centered about g=2.0 with hyperfine structure characteristic of Mn. The edge results established that Mn is directly involved in the storage of oxidizing equivalents, and that the g=4.1 signal and the multiline EPR signal both arise from the Mn complex in the S_2 state [1-3]. Comparison of the Mn K-edge energies of the PS II preparations with those of multi-nuclear models with single and mixed valence states suggests that the oxidation state(s) of the Mn cluster is +3 or greater in the S_1 and S_2 states. Incubation of PS II particles with 50 μM hydroxylamine in the dark neither oxidizes nor reduces the Mn. Illumination of hydroxylamine treated samples at 190 K causes reduction from the S_1 state to an S_0-like state. The Mn K-edge spectra of samples in the S_0, S_1 and S_2 states is shown in Fig 1. We have not observed any oxidation of the Mn sites upon advancement from the S_2 to an S_3-like state. We conclude that the oxidation state of Mn increases in the transition from S_0 to S_1 and in the transition from S_1 to S_2 but is invariant on advancement from S_2 to S_3.

The salient features of the Mn EXAFS results for the spinach S_1 state and for the S_2 state are a Mn neighbor at ~2.70 Å and two shells of N or O at ~1.75 and 2.00 Å, indicative of a μ-oxo bridged Mn complex. These features are constant for the S_1 state and the S_2 state (Fig 2) suggesting that no major change occurs on advancement from the S_1 to the S_2 state [4,5].

Recently, we have extended our Mn K-edge and EXAFS studies to PS II particles from a thermophilic cyanobacterium *Synechococcus*. The K-edge results indicate that the Mn cluster is oxidized in the S_1 to S_2 transition, but the K-edge inflection point is at a slightly lower energy, suggesting some differences in the coordination sphere of Mn in spinach and *Synechococcus*. The Fourier-transform from *Synechococcus* is shown in Fig 2 and is very similar to that obtained from spinach, in particular the peak labelled III, which is assigned to a Mn scatterer at 2.7 Å and is characteristic of a μ-oxo bridged structure. The edge and EXAFS results from spinach and *Synechococcus* suggest that the basic structure of the Mn center in the OEC is conserved over a period of 2 billion years but subtle changes in terminal ligation are likely.

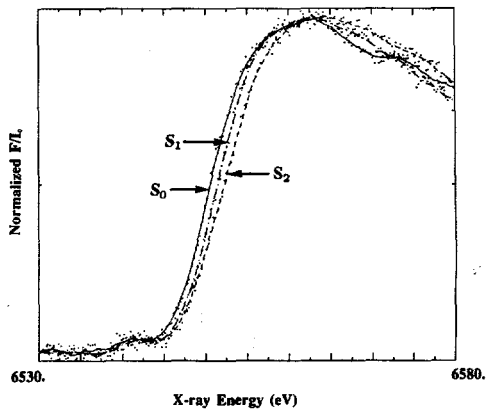

Figure 1. The X-ray absorption K-edge spectra of Mn in the S_0, S_1 and S_2 states of spinach PS II particles. A smoothed curve is drawn through the data points. The small pre-edge features at ~6543 eV are due to the 1s → 3d bound state transition. The K-edge inflection energy for the S_0 state is at 6550.3 eV, the S_1 state at 6551.3 eV and the S_2 state is at 6552.5 eV. The shifts from S_0 to S_1 to S_2 indicate a progressive oxidation of Mn as the Mn-OEC steps through the S-state cycle.

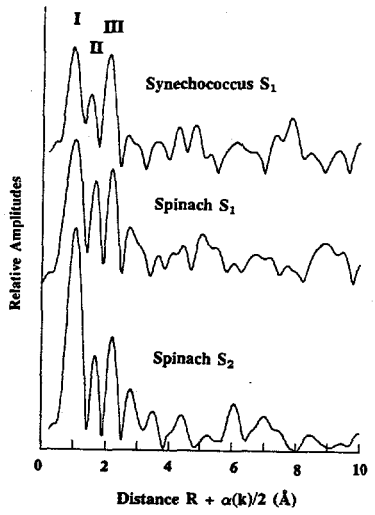

Figure 2. Fourier transforms of the $k^1\chi(k)$ Mn EXAFS data from spinach S_1, spinach S_2 and *Synechococcus*. The peaks labelled I and II are characteristic of bridging and terminal N or O ligands and peak III is due to a neighboring Mn atom and the distances are typical for μ-oxo bridged binuclear Mn clusters.

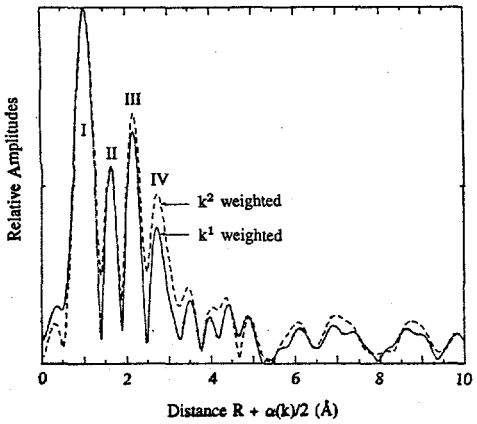

Figure 3. Fourier transform of the sum of the S_1 and S_2 EXAFS data weighted by k^1 and k^2. The solid line is the k^1 weighted data set and the dashed line is the k^2 data set. Note that the third and fourth peaks grow with increasing k-weighting indicating a heavy scatterer like manganese.

There is growing concensus that there are about four Mn atoms per PS II reaction center. Our third R-space Fourier peak fits best to 1-2 Mn atoms at the distance of 2.7 Å. Since there is virtual identity of the EXAFS for spinach PSII particles in the S_1 and S_2 states we added the k-space spectra to improve the S/N. The Fourier transform of the k^1-weighted sum is shown in Fig 3, which shows a fourth R-space peak significantly above the noise level. Also shown in Fig 3 is the Fourier transform of the k^2-weighted data set. The k-weighting suggests that the fourth peak may also be assigned to Mn. A reasonable fit is obtained to the back-transformed data from the fourth peak to one or more Mn atoms at ~3.3 Å or to two low-Z shells, such as C, N or O at 3.0 and 3.2 Å. These data are compatible with two binuclear clusters or an open tetranuclear structure but incompatible with either a regular cubane or adamantane-like structure.

Iron X-ray Absorption Spectra of Acceptors in PS I

The stable electron acceptors in PS I, centers A, B and X, are thought to be [2Fe-2S] or [4Fe-4S] ferredoxins. Their EPR spectra resemble the spectra of the [2Fe-2S] and [4Fe-4S] ferredoxins, having anisotropic signals with g_{ave} <2.0, and their EPR spectra are quite different from the spectra of the [1Fe], [3Fe-4S] or [3Fe-3S] ferredoxins. PS I contains 10-14 Fe and approximately 12 acid labile sulfide per P700, and contains one center A, one center B and one to two X per P700. On the basis of these observations two models of PS I seem likely: 1) PS I contains three [4Fe-4S] ferredoxins or 2) it contains two [4Fe-4S] ferredoxins and two [2Fe-2S] ferredoxins. In this study, we address the nuclearity of centers A, B and X using X-ray absorption spectroscopy [6].

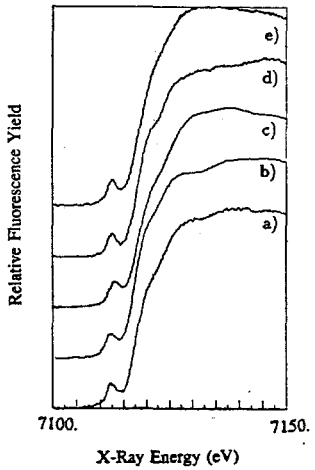

Figure 4. Iron K-edge spectra of oxidized PS I with iron-sulfur models. From the bottom: a) PS I from spinach, b) PS I from *Synechococcus*, c) $(Et_4N)_2Fe_4S_4(S\text{-benzyl})_4$, d) spinach $[2Fe\text{-}2S]^{2+(2+,1+)}$ ferredoxin and e)$(Et_4N)_2Fe_2S_2(S_2\text{-o-xyl})_2$. The pre-edge transition has been assigned as a 1s → 3d transition, and is a good indicator of non-centrosymmetric environments. The PS I from spinach and *Synechococcus* are quite similar to each other and to the [2Fe-2S] soluble spinach ferredoxin.

Fig 4 shows the iron K-edge spectrum of PS I from spinach and *Synechococcus* along with the spectrum of soluble spinach [2Fe-2S] ferredoxin, $(Et_4N)_2$ $Fe_4S_4(S\text{-benzyl})_4$ and $(Et_4N)_2$ $Fe_2S_2(S_2\text{-o-xyl})_2$. The iron K-edges of the PS I preparations are nearly identical to those of the soluble [2Fe-2S] ferredoxin including the size of the 1s → 3d transition, an indicator of the amount of non-centrosymmetric iron. The magnitude of the pre-edge and the shape of the edge are sensitive reporters of ferredoxin content and we estimate that over 90% of the iron in PS I is bound in ferredoxins.

Fig 5 shows the Fourier filtered spinach PS I EXAFS spectrum plotted over spectra from soluble spinach [2Fe-2S] ferredoxin and over data from soluble *Clostridium pasteurianum* [4Fe-4S] ferredoxin. In the region of k=7.5Å^{-1} the [4Fe-4S] and [2Fe-2S] ferredoxin data are out of phase owing to the much greater amount of iron backscattering in the [4Fe-4S] cluster from three equivalent Fe neighbors. The PS I spectrum, while not identical to either spectrum, more nearly resembles the [2Fe-2S] spectrum. Curve fitting analysis suggests that the PS I spectrum is better explained by a sum of two [2Fe-2S] and two [4Fe-4S] ferredoxins than by three [4Fe-4S] ferredoxins. For both our spinach and *Synechococcus* data the fits assuming a mixture of [2Fe-2S] and [4Fe-4S] ferredoxins had least squares errors lower by a factor of more than two and agree much better with the data around k=7.5Å^{-1}. The EXAFS results and some unusual EPR properties of X suggest that X is a strongly coupled pair of [2Fe-2S] clusters and A and B are [4Fe-4S] clusters.

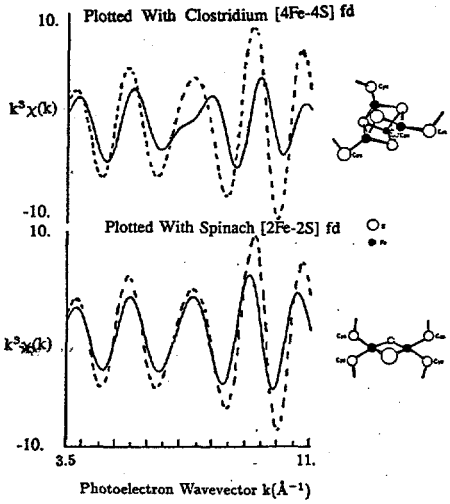

Figure 5. The Fourier filtered k^3-weighted EXAFS spectrum of PS I from spinach (dotted line) plotted with: (a) the spectrum of soluble *Clostridium pasteurianum* [4Fe-4S] ferredoxin and (b) the spectrum of soluble spinach [2Fe-2S] ferredoxin. The beat region around k=7.5Å^{-1} is diagnostic of [2Fe-2S] and [4Fe-4S] ferredoxins. The beat region indicates that PS I is likely to contain some [2Fe-2S] ferredoxins.

Acknowledgements

This work was supported by a grant from the National Science Foundation (PCM 82-16127 and PCM 84-16676) and by the Director, Office of Energy Research, Office of Basic Energy Sciences, Division of Biological Energy Conversion and Conservation of the Department of Energy under contract DE-AC03-76 SF00098. Synchrotron radiation facilities were provided by the Stanford Synchrotron Radiation Laboratory which is supported by the U.S. Department of Energy, Office of Basic Energy Sciences, and by the NIH Biotechnology Program, Division of Research Resources.

References

1. Goodin, D.B., Yachandra, V.K., Britt, R.D., Sauer, K. and Klein, M.P. (1984) Biochim. Biophys. Acta 767, 209-216.
2. Goodin, D.B., Yachandra, V.K., Guiles, R.D., Britt, R.D., McDermott, A., Sauer, K. and Klein, M.P. (1984) in EXAFS and Near Edge Structure III (eds., Hodgson, K.O., Hedman, B. and Penner-Hahn, J.E.), Springer-Verlag, New York, 130-135.
3. Cole J., Yachandra, V.K., Guiles, R.D., McDermott, A.E., Britt, R.D., Dexheimer, S.L., Sauer, K. and Klein, M.P. (1987) Biochim. Biophys. Acta, *in press*.
4. Yachandra, V., Guiles, R., McDermott, A., Britt, R., Dexheimer, S., Sauer, K. and Klein, M.P. (1986) Biochim. Biophys. Acta 850, 324-332.
5. Yachandra, V., Guiles, R., McDermott, A., Cole J., Britt, R.D., Dexheimer, S.L., Sauer, K. and Klein, M.P. *submitted*.
6. McDermott, A.E., Yachandra, V.K., Guiles, R., Britt, R.D., Dexheimer, S., Sauer, K. and Klein, M.P. *submitted*.

A STUDY OF CALCIUM-BINDING PROTEINS IN SOLUTION USING SMALL ANGLE X-RAY SCATTERING

[1]S.R. Hubbard, [1]S. Doniach, [2]K.O. Hodgson, [1]P.C. Leavis
Dept. of [1]Applied Physics and [2]Chemistry, Stanford University, Stanford, CA
[3]Dept. of Muscle Research, Boston Biomedical Research Institute, Boston, MA

We have completed our small angle X-ray scattering experiments (SAXS) on the calcium-binding protein troponin C (TnC). TnC is the calcium-sensitive constituent of the troponin complex responsible for initiating muscle contraction. The protein contains four "EF hand" calcium-binding sites. The work was carried out using the Biotech SAXS camera on BL II-2 and BL IV-2.

Figures 1 and 2 show the scattering curves of TnC with 0, 2 and 4 molar equivalents of calcium (Ca(II)) at a protein concentration of 27mg/ml. Figure 3 shows the scattering curves at 6.5mg/ml. At protein concentrations above 14mg/ml, the curves exhibit Ca(II)-dependent differences in the low S ($S = 2\sin(\theta/2)/\lambda$) region, $S < 0.015$ $Å^{-1}$ (Figure 2). At and below 14mg/ml, this effect is not noticeable (Figure 3). Our interpretation of the data is that the protein in solution undergoes a Ca(II)-dependent dimerization. The dependence of the SAXS curves on the protein concentration is consistent with a monomer/dimer equilibrium. Unlike the equilibrium ultracentrifugation study of TnC[1], in which the Ca(II) effect saturated at a Ca(II)/TnC monomer ratio of about 2:1, we see evidence for further dimerization through a molar ratio of 4:1.

Table 1 gives the radius of gyration (Rg - 2nd moment of the electron density distribution) as a function of concentration and number of Ca(II) equivalents. At the lowest concentration (6.5mg/ml), the 4 Ca(II) sample appears to have a slightly smaller Rg than the 0 Ca(II) sample, although the difference is only roughly one standard deviation. At 14mg/ml, the Rg's for the three Ca(II) stoichiometries are virtually the same. At higher concentrations, Rg[4Ca] > Rg[2Ca] > Rg[0Ca]. A plausible scenario is that when Ca(II) binds to TnC, the protein undergoes a limited (as judged by the SAXS) conformational change; our data suggest a change to a slightly more compact structure. This conformational change alters the association equilibrium constant, resulting in an increase in the dimer content of the solution.

We are attempting to characterize the monomer/dimer equilibrium. To do this, we are studying the interplay between the effects of dimerization (which tends to increase the lowest angle scattering) and that of interparticle interference (which tends to decrease the lowest angle scattering). Work is also underway to determine whether the SAXS data is consistent with the published crystal structure[2]. A computer program has been written to compute SAXS curves from a set of coordinates utilizing a cube method to determine the inaccessible solvent volume and a Monte Carlo approach to approximate the distance distribution functions.

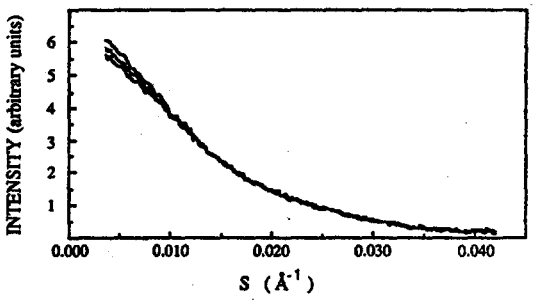

Figure 1 Slit-smeared SAXS curves of 27mg/ml TnC with 0, 2 and 4 molar equivalents of Ca(II).

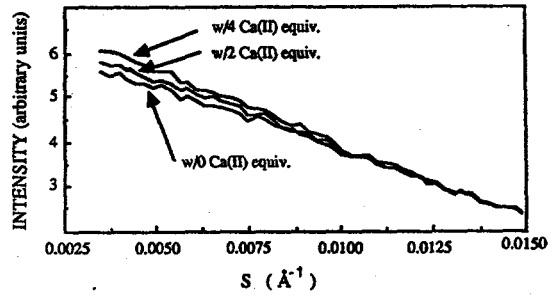

Figure 2 Same as in figure 1 for S < 0.015.

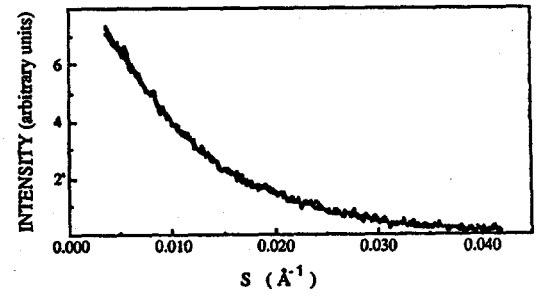

Figure 3 Slit-smeared SAXS curves of 6.5mg/ml TnC with 0, 2 and 4 molar equivalents of Ca(II).

Protein Conc.	Rg w/0 Ca	Rg w/2 Ca	Rg w/4 Ca
6.5 (mg/ml)	22.5 (Å)	22.8	22.1 (~+/- 0.4)
14	20.9	21.0	21.0 (~+/- 0.2)
27	17.8	18.7	19.2 (~+/- 0.1)

Table 1 Rg values derived from Guinier analyses on slit-smeared data. Errors given are based on those obtained from an indirect transformation algorithm.

REFERENCES:
1. S.S. Margossian, W.F. Stafford, Journal of Biological Chemistry, 257, 1160 (1982).
2. O. Herzberg, M.N.G. James, Nature, 313, 653 (1985).

TEMPERATURE DEPENDENT EXAFS OF $Nb_3(Sn,Sb)$ A15 COMPOUNDS

J. B. Boyce
Xerox PARC, Palo Alto, CA 94304

F. C. Bridges
Physics Department, U.C. Santa Cruz, Santa Cruz, CA

T. Claeson
Physics Department, Chalmers Univ. of Techn., 41296 Gothenburg, Sweden

T. H. Geballe
Applied Physics Department, Stanford University, Stanford, CA 94305

G. Hull
AT&T Bell Labs, Murray Hill, NJ

N. Kitamura
Aoyama Gakuin University, Chitosedai, Setagaya-ku, Tokyo 157. Japan

P. Weiss
Lab des materiaux et du génie phys, St Martin d'Hères, France

We have studied the temperature dependence of the Sn-K and Sb-K EXAFS of Nb_3Sn and Nb_3Sb between 4 and 650 K and of $Nb_3(Sn,Sb)$ alloys (of A15 structure) between 4 K and room temperature. A15 compounds give high superconducting transition temperatures, T_c, the highest until the recent discovery of new high T_c superconductors. A wealth of properties has been determined. However, the cause of the high T_c is not fully understood. A theory of Yu and Anderson [1] emphasizes localized ionic vibrations in a two well potential, giving a very high electron-phonon coupling at high temperature, going over into extended phonon states and a renormalized electron-phonon coupling as the temperature is lowered. The atomic displacements are small, but an anomalous temperature dependence of the broadening of the pair distribution function may occur.

Nb_3Sn has a high T_c (18 K) and Nb_3Sb a low one (0.9 K). They form a solid solution with remaining A15 symmetry. Interesting martensitic transformations occur at the Sn-rich side of the phase diagram [2].

No anomalous temperature dependence was noted for the Debye-Waller type broadening of the first near neighbor (Sn-Nb or Sb-Nb) distance. The difference in slopes of $\Delta\sigma^2(T)$ vs $T(\Delta\sigma^2(T) = \sigma^2_{X\text{-}Nb} - \sigma^2_{X\text{-}Nb}(4.2\ K))$ for Nb_3Sn and Nb_3Sb, seen in Fig. 1, can be explained by a larger electron-phonon coupling and lower frequency lattice vibrations in Nb_3Sn (with its substantially higher superconducting transition temperature) as compared to Nb_3Sb. The most striking feature of Fig. 1 is that the $\Delta\sigma^2$'s of Sb-Nb and Sn-Nb distances in the alloys seem not to be identical (for a certain composition and temperature) but rather follow those of the end constituents of the alloy series (Nb_3Sn and Nb_3Sb, respectively). This would emphasize the local correlation between the vibrations of the Sn-Nb and Sb-Nb atom pairs rather than extended, average, phonon modes in the alloy. It should be stressed, however, that the results are preliminary; the differences in the $\Delta\sigma^2$'s fall within the uncertainty of the experiment and have to be confirmed by further analysis and higher temperature measurements.

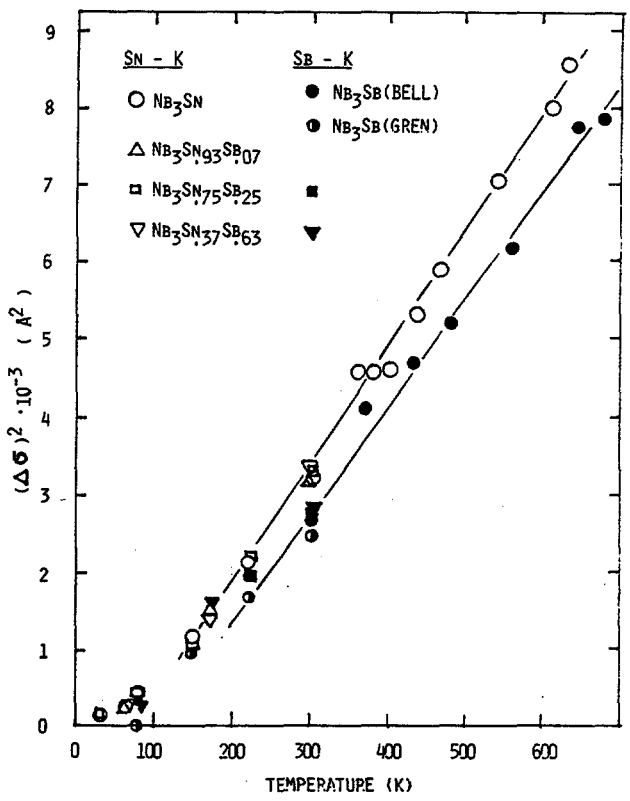

Fig. 1 The temperature dependence of the square of the Debye-Waller-like width of the nearest neighbor distance for Nb_3Sn, Nb_3Sb and alloys of $Nb_3(Sn,Sb)$.

References
1. C. C. Yu and P. W. Anderson, *Phys. Rev.* **29**, 6165 (1984).
2. Y. Fujii, J. B. Hastings, M. Kaplan, G. Shirane, Y. Inada, and N. Kitamura, *Phys. Rev. B* **25**, 364 (1982).

In Situ Surface Extended X-ray Absorption Fine-structure Spectroscopic Study of Lead Monolayer at a Metal/Liquid Interface

Mahesh G. Samant, Gary L. Borges, Joseph G. Gordon II, and Owen R. Melroy

IBM Almaden Research Center, K34/802
650 Harry Road, San Jose, CA 95120

Lesser Blum

Physics Department
College of Natural Sciences
PO Box AT, Rio Piedras, Puerto Rico 00931

Introduction

Structural information on species adsorbed at the electrode/electrolyte interface is essential to any complete understanding of the electrochemical processes. Most surface science techniques (developed for UHV) are based on electron yields and are unsuitable for use in condensed phase as the mean free path of electrons is far too short. Although these UHV techniques applied in a quasi in-situ mode have provided significant insight into the nature of adsorbed species[1], the question of possible changes occurring during transfer from the electrolyte to vacuum remains unanswered. In addition, all information concerning the structure of the solvent is lost. Optical methods such as Raman spectroscopy[2], surface plasmon spectroscopy[3], and surface infrared spectroscopy[4] have been successfully used to study these interfaces but they are unable to provide the desired structural information. The availability of synchrotron radiation has made possible several new techniques. Among them, Surface Extended X-ray Absorption Fine Structure (SEXAFS)[5] seems particularly well suited for probing this interface and by using fluorescence detection, these studies can be made in-situ. We describe here the in-situ SEXAFS study of a monolayer adsorbed at a metal electrode/electrolyte interface.

Experimental

The system chosen for this study was an underpotentially deposited lead monolayer on a silver (111) electrode. The electrode was prepared by epitaxial deposition on a cleaved mica substrate. Lead was deposited in a thin layer cell from an aqueous solution of lead acetate in an sodium acetate/acetic acid electrolyte. The thin layer cell was used to reduce background scattering and to reduce interference from aqueous lead acetate. The SEXAFS data were then collected about the Pb L_{III} absorption edge. The emitted fluorescence was isolated from the background signal by a high purity germanium solid state detector and appropriate filters. The incidence x-ray beam was at grazing incidence to the sample with the polarization perpendicular to the plane of the surface to decrease the background scattering from the electrode.

Results and Discussion

Figure 1 shows the EXAFS function for a Pb monolayer with the electrode potential controlled at -0.53 V (vs. 3M silver/silver chloride). The position of the lead absorption edge in the sample was identical to that of lead foil and 1.2 eV lower than that for aqueous lead acetate indicating that the lead being probed was indeed on the surface and fully reduced. No back-scattering was observed corresponding to a lead silver distance and is probably a result of the large Debye-Waller factor for lead and the incommensurate nature of the lead monolayer. Back-scattering was, however, observed from a low Z element ($Z < 10$) at a well defined distance from the surface. Based on the composition of the solution, this most likely results from either water or acetate ions adsorbed on the lead monolayer. EXAFS can not differentiate between these two possibilities. Lead oxide can be eliminated as the source of oxygen based on absorption edge position. This lead oxygen distance is observed to depend on the electrode potential. Bond distances of 2.33 Å and 2.38 Å were obtained with the electrode polarized at -0.53 V and -1 V respectively. This well defined distance would seem to imply that either the layer of solvent or adsorbed acetate forms an ordered layer at the surface.

Acknowledgements

This work was supported by Office of Naval Research and was performed at SSRL which is supported by the Department of Energy.

References

1. A. Hubbard, Acc. Chem. Res., *13*, 177 (1980); E. Yeager, J. Electroanal. Chem., *128*, 1600 (1981); P. N. Ross, Surf. Sci., *102*, 463 (1981).

2. M. Fleischmann, P. J. Hendra, and A. J. McQuillan, Chem. Phys. Lett., *26*, 173 (1974); D. J. Jeanmaire and R. P. Van Duyne, J. Electroanal. Chem., *84*, 1 (1977).

3. J. G. Gordon and S. Ernst, Surf. Sci., *101*, 499 (1980).

4. S. Pons, J. Electroanal. Chem., *150*, 495 (1983); A. Bewick, J. Electroanal. Chem., *150*, 481 (1983).

5. P. Eisenberger and B. M. Kincaid, Science, *200*, 1441 (1978).

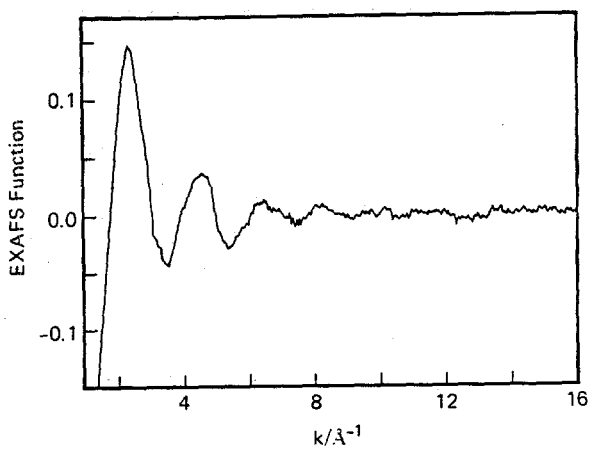

Figure 1.

HIGH COUNT RATE CAPABILITIES OF HGI2 X-RAY DETECTORS*

J.S. Iwanczyk, W.K. Warburton & A.J. Dabrowski

Institute of Physics, USC School of Medicine
4676 Admiralty Way, Suite 932, Marina del Rey, CA 90292

B Hedman & K.O. Hodgson

Stanford Synchrotron Radiation Laboratory
SLAC Bin 69, P.O. Box 4349 Stanford, CA 94305

High Count Rate HgI_2 Detector

A prototype element for an energy dispersive detector array was designed and constructed using a HgI_2 detector. Both the detector and input FET were thermoelectrically cooled, using 0.25W total cooling power. The HgI_2 x-ray detector was especially designed for high counting rate operation, with a front metal shield and guard ring configuration being introduced into the detector fabrication technique. The detector and its ultra-low noise, pulsed optical feedback preamplifier were combined into a small, hand portable unit. At low counting rates and 12 microsec shaping time, this detector system had an energy resolution of 260 eV (FWHM) at 5.9KeV and 225 eV (FWHM) electronic noise level measured by the pulser method.

The detector system's high count rate capabilities were tested at SSRL using characteristic fluorescence from a Cu target. These tests were perfromed with different commercial amplifiers and different combinations of shaping time and pileup rejection. Count rate capability to 200,000 cps was successfully demonstrated with no detrimental effects in the detector response being observed over the entire range of counting rates studied. Throughput and energy resolution at these very high counting rates were found to be determined almost exclusively by the characteristics of the amplifier employed.

Array Detector Tests:

A ten element detector array was fabricated on HgI_2 using a mask originally designed for the development of angiography detectors.[1] While the resulting electrode shapes were not optimized for best performance, study of the resulting detector array was extremely profitable in identifying the areas which will require attention in future designs.

The array was tested in two modes: current and single photon counting. In the current mode, the elements were scanned with a 100 micron wide direct wiggler beam at 10 KeV on BL IV-3 and their current output read directly via Keithley electrometers. By this means both uniformity of positional response and efficiency of charge collection could be determined. The linearity of pixel output currents versus intensity was also measured by detuning the monochromator and comparing integrated pixel outputs to those of an in-line ion chamber. Their response quality suggests that properly patterned arrays might be suitable either as beamline position monitoring devices or angiography detectors.

All pixels were also tested as individual energy dispersive spectrometers. Their performance was degraded in two major ways, compared to single detector HgI_2 spectrometers. First, peak to background ratios were poor, due to charge splitting between neighboring pixels. The solution to this problem will be the same as for single pixels: design pixel shields to keep x-rays from striking close to the pixel boundaries. Energy resolution was also degraded, which is due mostly to excessive capacitance in the unoptimized pixel geometry. These measurements have therefore provided both some strong guide lines to be followed in the design of array elements specifically intended for spectrometric applications and some general encouragement in the development of energy dispersive arrays for fluorescence and diffraction applications.

Acknowledgements:

Supported by the SSRL Biotechnology Program, NSF Contract No. DMB-8415194, NASA Contract No. NSG-7535, and DOE Contract No. DE-AM03-76SF00113.

References:

[1] HgI_2 provided by EG&G Santa Barbara Operations, the mask by Dr. A. Thompson (LBL) and the Stanford Angiography Group.

Sturctural Investigations of Mo-Ge Multilayers Using Anomalous Scattering and EXAFS.

Lane Wilson and Arthur Bienenstock
Department of Applied Physics, Stanford University, Stanford, California 94305

Synchrotron radiation X-ray diffraction and EXAFS were used to study atomic arrangements in amorphous and crystalline sputtered Mo-Ge multilayers over a wide range of compositions and layer thicknesses. Differential anomalous scattering (DAS) and EXAFS techniques, which determine the environment about each atomic species, were used to help separate the local structure of the individual constituent layers and the interfacial regions of the multilayers. Layer thicknesses were varied to examine the new atomic configurations and bonding patterns that appear when the interfacial regions become a substancial portion of the total system. An appreciable area of each substrate was removed so that three dimensional diffraction data and transmission EXAFS on thin film multilayers were easily obtained. As a result of all these techniques, much more complete structural information was obtained than has been previously possible. This includes information about atomic arrangements in thin amorphous layers, crystallite size anisotropies in thicker films, and intermixing at the layer boundaries; as well as observations of a new Ge epitaxial structure. The studies make apparent the great variety of structural forms in the multilayers.

Multilayers were grown on Si (100) substrates by magnetron sputtering with the substrates alternately rotating beneath continuously sputtered Mo and Ge targets.[1] The layer compositions and thicknesses were varied by adjusting deposition rates of the individual targets and substrate rotation speed. Exact composition modulation has not been addressed in this report, rather the local structures that appear as a function of nominal layer thicknesses are examined. The local structures in turn help define the composition modulation. Uncertainties in the individual layer thicknesses do not influence the conclusions about the local structures observed in this work. 10um samples were fabricated and substrates were removed employing techniques developed for the industrial micro-machining of Si wafers.[2] A window in the substrate was etched by immersion of the masked sample in either EDP or KOH for several hours at 100°C. The samples were thus rendered free- standing while retaining a frame of Si which was then inserted into an X-ray diffractometer sample holder. X-ray scattering and EXAFS experiments were carried out at SSRL on the materials diffactometer under dedicated beam time conditions.

As a starting and reference point for structural investigations, a multilayer consisting of thick crystalline (c-)Mo (30Å) and thick amorphous (a-)Ge (30Å) was studied. X-ray scattering from this sample in both transmission and reflection is shown in Fig. 1. Line widths show average Mo crystallite sizes which are at least 250Å in the layer plane but are limited to the Mo layer thickness (30Å)

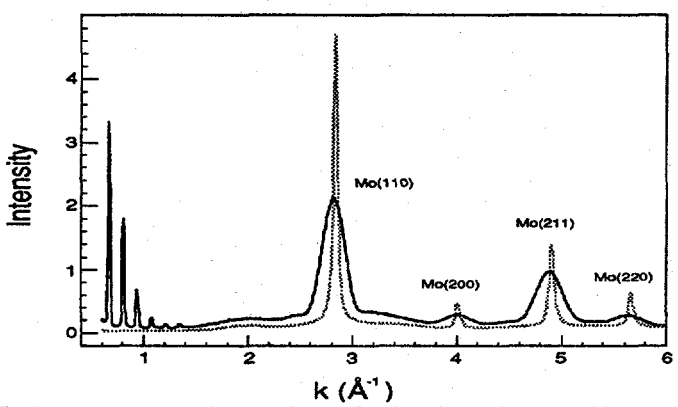

Fig. 1 ----- X-ray scattering intensity as a function of scattering vector (k) perpendicular to the layer plane (dark line) and parallel to the layer plane (light line). Scattering is from a sample of average χ_{Mo}=.49 and nominal layer thicknesses 30Å Mo/30Å Ge. Low angle multilayer reflections (k<1.5Å^{-1}) indicate the bilayer thickness to be 47.0Å. Scattering from an amorphous component, in the Ge layer, to the total scattering is evidenced by the diffuse peaks at k=2.0Å^{-1} and k=3.2Å^{-1}.

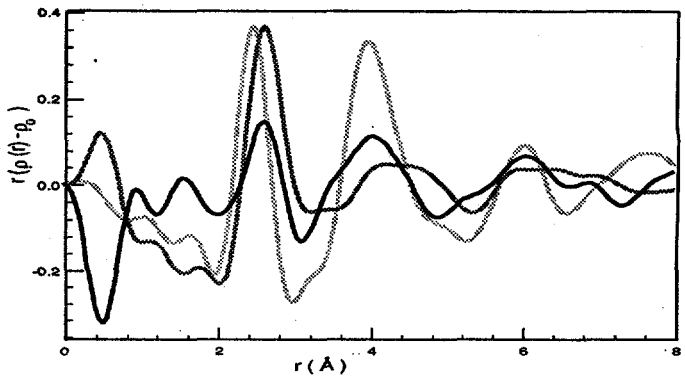

Fig. 2 ----- Ge absorption edge DDF [r(ρ(r)-ρ$_o$)] for multilayer of average χ_{Mo}=.49 and nominal layer thicknesses 30Å Mo/30Å Ge (dark line), amorphous co-sputtered alloy $Mo_{14}Ge_{86}$[4] (medium line), and amorphous sputtered Ge[4] (light line).

perpendicular to the plane. A Ge edge differential distribution function (DDF)[3] (Fig. 2) allows the removal of the Mo-Mo correlations, leaving information about the Ge layer and interfacial structure, even though the c-Mo contributes very strongly to the total scattering (Fig. 1). Comparison of this distribution with that of a-Ge and a 14% a-Mo-Ge alloy[4] (Fig. 2) indicates that the Ge layer has Mo correlations denoting an a-Mo-Ge interfacial region. The DDF from the multilayer has features of both a-Ge and a-Mo-Ge. The broadening and shift of the first peak outward from the a-Ge value is evidence of Mo correlations, as shown by Kortright. On the other hand, the second and third neighbor peaks of a-Ge are still apparent.

In this report distributions are compared in the form r(ρ(r)-ρo). This allows a more detailed comparison of structure at high r. Displayed as r(ρ(r)-ρo) the region below the first peak is especially sensitive to low frequency error in the scattering data. The error is exacerbated in a DDF since it is the transform of a difference between two scattering data sets. However, the DAS technique employed here has resulted in coordination numbers and peak distances accurate to 4% in the region of 2Å to 10Å on a test material $GeBr_4$[5]. The current work was performed employing the same experimental techniques as the DAS test case and therefore similar accuracy can be expected to apply to the DAS results presented here. Indeed, the good agreement at high r between distribution functions from multilayer and alloy samples as well as between those from transmission and reflection geometries is evidence that the errors are limited to the low r region.

The structures of thin Ge layers were investigated by examining

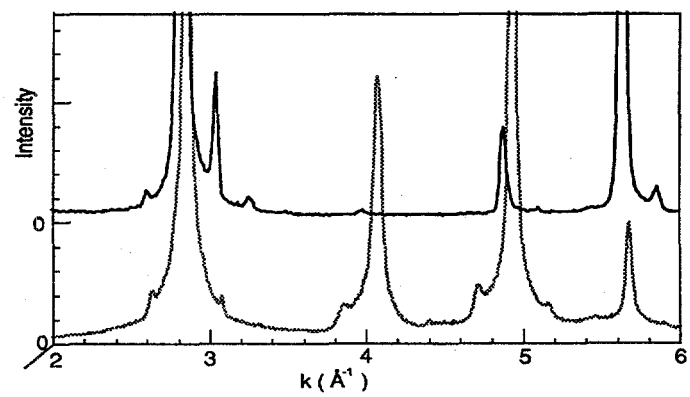

Fig. 3 ----- BCC X-ray reflections and asymmetric satellites from strained epitaxial Mo-Ge multilayers; χ_{Mo}=.87, $d_{(nominal)}$ =30ÅMo/10ÅGe, $d_{(measured)}$ =27.3Å (upper, dark line); and χ_{Mo}=.74, $d_{(nominal)}$ =20ÅMo/10ÅGe, $d_{(measured)}$. -25.6Å (lower, light line).

two samples, each with 10Å Ge layers bounded by relatively thick (≥20Å) Mo layers. Fig. 3 shows parts of the scattering data from the two samples, 30ÅMo/10ÅGe and 20ÅMo/10ÅGe. There is no sign of an amorphous multilayer component in either the total scattering (Fig. 3) or the Ge-edge differential structure factor (not shown). The assymetric side bands about the Mo crystalline peaks indicate that the Ge has assumed a crystalline stucture coherent with the BCC Mo[6]. Simple modeling of the side band modulations indicates that the structure consists of strained multilayers. EXAFS modeling yielded Ge-Ge distances of 2.78Å for the 30Å Mo sample and 2.73Å for the 20Å Mo sample in agreement with the modeling of the assymetric side bands. These distances are much longer than the covalent bond lengths of pure Ge (2.44 Å) and are close to the lengths of metallic Mo (2.74Å). The normal covalent nature of Ge-Ge bonds is modified by the thinness of the layers and their boundary of crystalline Mo layers. Texturing occurs with the BCC (110) planes parallel to the layers and is stronger for the sample with thicker Mo layers.

The structure of thin Mo layers was investigated on a multilayer of 10Å Mo and 40Å Ge. This sample showed no evidence of cystalline Mo nor of any unique amorphous Mo structure. Instead, the stucture

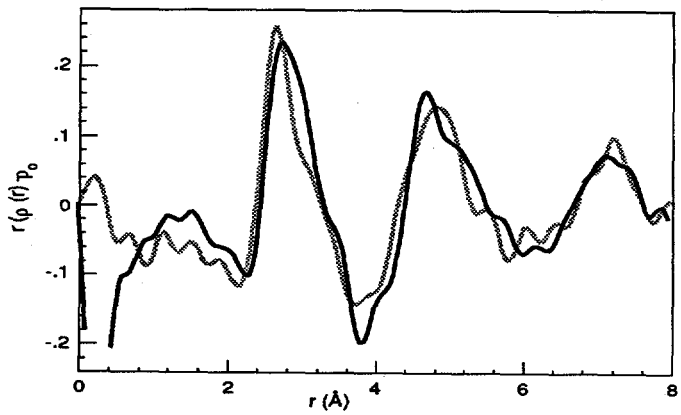

Fig. 4 ------ Mo absorption edge Differential Distribution Function $[r(\rho(r)-\rho_o)]$ for multilayer of average χ_{Mo}=.20, nominal layer thicknesses 10ÅMo/40ÅGe, and measured bilayer thickness 50.5Å (dark line); and amorphous co-sputtered alloy $Mo_{42}Ge_{58}$[4] (light line). Local structure of the Mo layer is in close agreement with that of the amorphous Mo-Ge alloy with χ_{Mo}=.42 indicating that Ge has intermixed with the thin Mo layer.

is characterized by a-Mo-Ge alloy material bounded by layers of a-Ge. The Mo edge DDF is useful in examining the Mo-Ge interfacial region since the scattering contributions of the a-Ge in the thick Ge layer are removed. The Mo DDF (fig. 4) shows good agreement with that of an a-$Mo_{42}Ge_{58}$ alloy.[4] The average sample composition of 20% Mo is periodically modulated between limits of an alloy richer in Mo and a-Ge. The modulation is most simply modelled by a two layer system with an a-Ge layer of 30Å and a 21Å a-$Mo_{42}Ge_{58}$ alloy region. More detailed analysis, using the anomalous scattering data, is underway.

When multilayers of both thin Ge and thin Mo are deposited, the stucture closely resembles that of a-Mo-Ge alloys although a periodic composition modulation is evidenced by the multilayer low angle Bragg reflections. Two compositions were investigated (65%Mo, 10ÅMo/10ÅGe and 45%Mo, 10ÅMo/20ÅGe). The scattering curves and differential structure factors of both are in good agreement with those from the amorphous alloys of their respective compositions. Radial distribution functions (RDF's) from data taken in transmission and reflection are similar for both compositions (shown in Fig. 5 for the 10ÅMo/10ÅGe sample.) The minor differences are currently being examined in more detail with anomalous scattering. The similarity of the amorphous scattering when probed both in the layer plane and perpendicular to the layers is evidence that the local structure is isotropic. Anisotropy of local structure might have been expected to result from the existence of layers or interfacial regions of limited extent on an atomic scale in the layering direction only. This study uncovered no experimental evidence for such anisotropy in the Mo-Ge system. The fact that the structures of the alloys match well the structures of the multilayers supports the conclusion that there are broad compositional ranges where structure is only slowly changing[4];

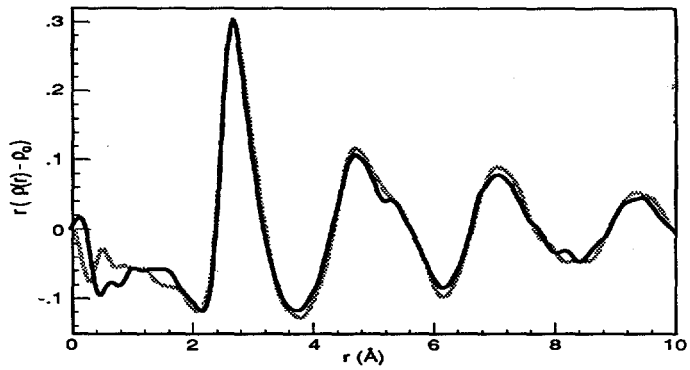

Fig. 5 ------ Radial Distribution Function $[r(\rho(r)-\rho_o)]$ from data taken with the scattering vector (k) perpendicular to the layer plane (dark line) and parallel to the layer plane (light line). Result is from a sample of average χ_{Mo}=.65, nominal layer thicknesses 10Å Mo/10Å Ge and measured bilayer thickness 16.9Å.

thus the multilayers can be structurally homogenous while compositionally modulated.

An intermediate thickness sample (57%Mo, 20ÅMo/20ÅGe) was also examined. Like the thin layer samples just mentioned, multilayer composition modulation exists but the local structure matched the isotropic structure of the Mo-Ge alloy of the overall multilayer composition. Ge added to the epitaxial system of 20ÅMo/10ÅGe not only destroys the crystallinity and epitaxy of the Ge but also prevents the Mo from being crystalline. It is evident that the local structure of each layer type is dependent on both its own thickness and the thickness of the neighboring layer. In general, thin layers (≤20Å) of both Mo and Ge exhibit the isotropic alloy structure but if Ge is decreased to 50% or less of the Mo thickness the tendency of Mo to crystalize results in an epitaxial structure.

A wide range of structure is exhibited by the Mo and Ge layers as thicknesses are varied. Thick layers of Mo (≥30Å) exhibit bulk BCC crystalline structure while thick layers of Ge (≥30Å) exhibit 4-fold coordinated amorphous RTN structure. The interface between such thick layers is not sharp but rather exists as an amorphous Mo-Ge alloy. As the Ge layer is made thinner (10Å) while the Mo remains at least relatively thick (≥20Å), the Ge structure is transformed into a novel form, a metallic, strained BCC structure coherent with the Mo BCC structure. If, however, the Mo layer thickness is decreased (≤10Å) while the Ge layers remain thick, the Mo is no longer crystalline but is incorporated in an interfacial amorphous Mo-Ge alloy separating layers of a-Ge. If both layers are decreased (Mo ≤20Å, Ge ≤20Å), with the Ge thickness equal to or greater than the Mo thickness, only an amorphous Mo-Ge alloy with a layered concentration gradient remains. The amorphous alloys show striking similarities with homogeneously sputtered samples on the scale of local atomic structure. Indeed, data taken with the scattering vector in the layer plane and perpendicular to the layer plane indicate the same distribution function. This demonstrates that the tendency to alloy is strong and bonds are similar in all directions even though the concentration modulation is strong enough to yield multilayer Bragg reflections. There is no evidence of an amorphous Mo structure of concentration greater than 75% in any of the samples.

---

[1]T.W. Barbee and D.L.Keith, in Synthesis and Properties of Metastable Phases, E.S. Machlin and T.J. Rowland, eds., AIME, 93 (1980)

[2]K.E. Petersen, Proceed IEEE 70, 420 (1982).

[3]P.H. Fuoss, P.Eisenberger, W.K. Warburton, and A.I. Bienenstock, Phys. Rev. Lett. 46, 1537 (1981).

[4]J.B. Kortright, Ph.D. Thesis, Stanford Univ., and SSRL Report 84/05, (1984).

[5]K.F. Ludwig, L. Wilson, W.K. Warburton, and A.I. Bienenstock, J. Physique, 46, C8-193 (1985).

[6]D.B. McWhan, in Synthetic Modulated Structures, L.L. Chang and B.C. Giessen, eds., Academic Press, 43-74 (1985).

KINETICS OF DOMAIN ORDERING IN GRAPHITE INTERCALATION COMPOUNDS*

Proposal 903M

Roy Clarke, P. Hernandez and F. Lamelas
Department of Physics
The University of Michigan
Ann Arbor, MI 48109

and

S.K. Sinha and E.B. Sirota
Exxon Research and Engineering Company
Annandale, NJ 08801

The aim of these time-resolved x-ray scattering experiments is to probe the kinetics associated with ordering after quenching below a first-order phase transition. Graphite intercalation compounds (GIC's) represent an interesting class of materials for such studies because the ordering of the intercalant is strongly influenced by competing interactions.[1] For example, the interplay of intercalant-host and intercalant-intercalant forces can give rise to extended defects such as dislocations and stacking faults, and domain walls between locally commensurate regions (discommensurations). The time scales on which such defects migrate out of the structure as it approaches the long-range ordered equilibrium state can be quite long (seconds to even hours).[2]

The present experiments focus on the diffuse scattering associated with the existence of domain walls and other extended defects in the non-equilibrium structure. Results obtained on beamline VII-2 using a Ge(111) monochromator and a linear position sensitive detector (psd) reveal a large diffuse scattering component centered on the reciprocal lattice point of the intercalant superstructure. After quenching from the liquid phase, the diffuse scattering increases rapidly at first and then decays relatively slowly.

We ascribe this behavior to the formation of a large density of domain walls immediately after the quench. As the domain structure subsequently coarsens, the diffuse scattering diminishes.

During the dedicated summer run we obtained a large amount of time-resolved data on HNO_3-GIC ($T_m \approx 250K$). Fig. 1 illustrates the richness of the ordering kinetics in this system. The approach to the equilibrium ordered phase (which is commensurate) appears to proceed in a stepwise fashion marked by the nucleation and subsequent decay of relatively long-lived intermediate phases. The detailed structures of these non-equilibrium phases are unknown at present but the data indicate that they may consist of locally ordered arrays of discommensurations.

The analysis of the time-resolved data is hampered by the limitations of the 1-d p.s.d. which records only a narrow radial slice of the diffraction pattern. We have developed a 2-d version for future experiments which will provide for a full mapping of the in-plane reciprocal lattice as well as the distribution of diffuse scattering.

*This work was supported in part by NSF Low Temperature Physics Grant No. DMR-8404975.

1. R. Clarke, J.N. Gray, H. Homma and M.J. Winokur, Phys. Rev. Lett. 47, 1407 (1981); M.J. Winokur and R. Clarke, Phys. Rev. Lett. 54, 811 (1985).

2. R. Clarke, P. Hernandez, H. Homma and E. Montague, Synthetic Metals 12, 27 (1985).

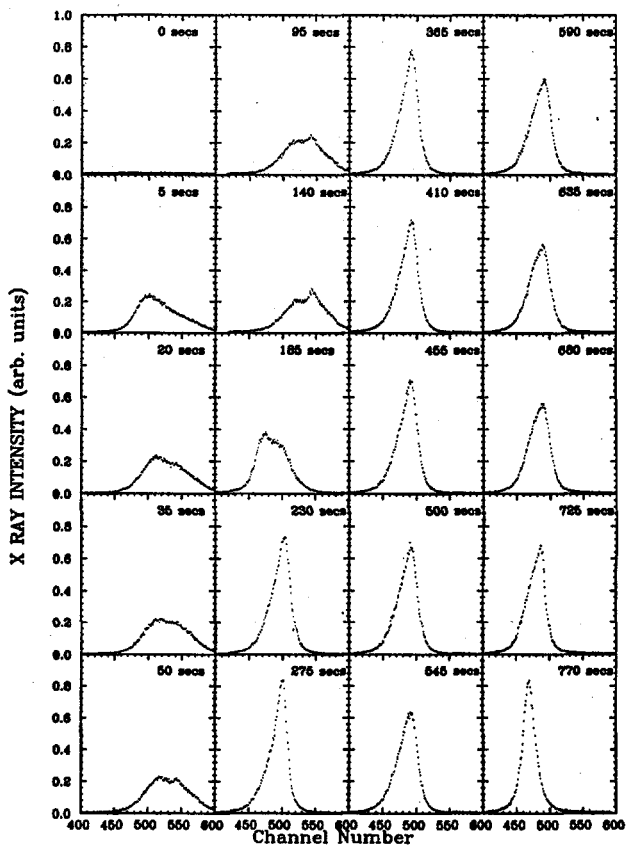

Fig. 1: Time-resolved X-ray scattering data for a single-crystal sample of HNO_3-GIC quenched from 266K to 240K. The collection time for each slice was 5 sec. The superlattice peak that has developed after 770 sec. (lowermost right) is resolution limited, FWHM = 3×10^{-3} Å^{-1}.

CORE LEVEL SPECTROSCOPY OF THE GaAs - ON - Si INTERFACE

R. D. Bringans, M. A. Olmstead*, R. I. G. Uhrberg** and R. Z. Bachrach

Xerox Palo Alto Research Center
3333 Coyote Hill Rd., Palo Alto, CA 94304, USA

INTRODUCTION

There has been a great deal of interest recently in the properties of thick layers of GaAs grown epitaxially on Si[1]. In all heteroepitaxial systems the interface properties play a very important role and it is the aim of the present study to examine the atomic and electronic properties of the GaAs-on-Si interface. Although the bulk properties of both Si and GaAs are well understood, simple estimates of the atomic arrangement at the interface are not reliable. It is not clear, for example, how As and/or Ga atoms are bonded to the Si substrate. In order to address this issue, we have made a comparative study of the energetics of the interface bonding for As, Ga and GaAs with Si(111), Si(100) and Ge(111) surfaces.

RESULTS AND DISCUSSION

Thin layers of GaAs were grown *in situ* by Molecular Beam Epitaxy (MBE) on the clean Si and Ge substrates which were held at temperatures in the range 550 to 580^{o}C. A comparison was made with results for isolated As and Ga layers on the same surface. The ~1 monolayer Ga layer was deposited at room temperature and then annealed at 570^{o}C. The As-terminated surfaces were produced by exposing the substrates, held at temperatures in the range 300-600^{o}C, to an As_4 source. This has been found[2-5] to give highly stable surfaces containing a single monolayer of As. The As-terminated Ge(111)[2], Si(111)[4] and Si(100)[3] surfaces have been studied in great detail experimentally with both angle-resolved photoemission and core level spectroscopy and theoretically using total minimization methods. A review of these results is given in reference 5.

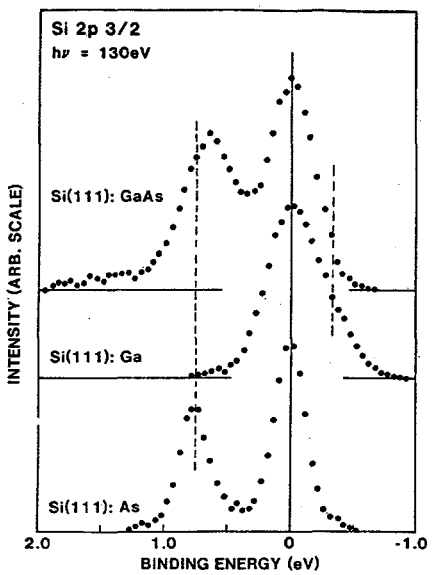

Figure 1. Si 2p 3/2 core-level components for a Si(111) substrate with approximately 1 monolayer of GaAs (uppermost spectrum), Ga (central spectrum) and As (lowermost spectrum). The vertical lines show the locations obtained for chemically-shifted components when the Si(111):As and Si(111):Ga levels are separately fitted with a bulk plus a single shifted component.

Surface sensitive core level spectroscopy measurements were carried out because the chemical shifts for the substrate core levels make it possible to determine the species in the GaAs overlayer which is bonded to the substrate. Results are shown in Fig 1 for Si(111). The Si 2p core level for Si(111):GaAs shows a single component shifted to higher binding energy by 0.62eV with respect to the bulk Si 2p energy. By comparison, the Si 2p level for Si(111):As has a shift in the same direction of 0.75eV whereas Si(111):Ga has a shift in the opposite direction of 0.30eV. This can be seen clearly in Fig 1 which shows only the 3/2 component of the Si 2p spectra. Deconvolution into 3/2 and 1/2 components was carried out using a spin-orbit splitting of 0.600eV and the statistical intensity ratio of 2:1. These results for around one monolayer provide strong evidence that the surface Si atoms are predominantly bonded to As rather than Ga. We also found that these results did not change significantly if Ga was deposited on a room temperature substrate and then As was added at a raised substrate temperature. This indicates that the As atoms were able to move underneath the Ga atoms which had been bonded to the substrate atoms.

At greater thicknesses than those considered here, a bonding arrangement in which the substrate atoms all bond to As atoms is expected to give rise to a prohibitively large dipole at the surface[6] Consequently we expect a transition to another geometry accompanied by defect formation as the lattice mismatch can no longer be accommodated by straining the overlayer.

ACKNOWLEDGEMENTS

We have benefitted greatly from the technical expertise of L. E. Swartz and R. Johnson. Part of this work was performed at SSRL which is supported by the Department of Energy, Office of Basic Energy Sciences. RIGU was partially supported by the U. S. Office of Naval Research through the contract No. N00014-82-C-0244.

REFERENCES

* Present Address: Dept. of Physics, University of California, Berkeley, CA 94720
** Present address: Dept. of Physics and Measurement Technology, Linköping Institute of Technology, S-581 83 Linköping, Sweden.
1. See, for example, R. Fischer, H. Morkoc, D. A. Neumann, H. Zabel, C. Choi, N. Otsuka, M. Longerbone and L. P. Erickson, J. Appl. Phys., 60, 1640 (1986).
2. R. D. Bringans, R. I. G. Uhrberg, R. Z. Bachrach and J. E. Northrup, Phys. Rev. Lett. 55, 533, (1985).
3. R. I. G. Uhrberg, R. D. Bringans, R. Z. Bachrach and J. E. Northrup, Phys. Rev. Lett. 56, 520 (1986).
4. M. A. Olmstead, R. D. Bringans, R. I. G. Uhrberg and R. Z. Bachrach, Phys. Rev. B, 34, 6041 (1986).
5. R. D. Bringans, R. I. G. Uhrberg, M. A. Olmstead, R. Z. Bachrach and J. E. Northrup, Proceedings of the 8th Conf on Vacuum Ultra Violet Radiation Physics, to be published in Physica Scripta.
6. Harrison, W. A., Kraut, E. A., Waldrop, J. R. and Grant, R. W., Phys. Rev. B, 18, 4402 (1978).

X-RAY ABSORPTION SPECTROSCOPY OF IRON-IRON INTERACTIONS: RIBONUCLEOTIDE REDUCTASE

B. Chance, G. Bunker, M. Chance
Institute for Structural & Functional Studies, Philadelphia, PA

L. Petersson, M. Sahlin, A. Ehrenberg
Arrhenius Laboratory, Department of Biophysics, University of Stockholm, Sweden

B.-M. Sjöberg
Swedish University of Agricultural Sciences, Uppsala Biomedical Center, Sweden

The correlation between hemerythrin and hemocyanin as non-enzymatic oxygen transport molecules and ribonucleotide reductase as a key enzyme of the living cell having, however, a metabolic function completely different from that of oxygen transport has afforded a fascinating structure/function example: ribonucleotide reductase is essential to the biosynthesis of DNA. A publication under the authorship of G. Bunker, et al., has been accepted for publication by the Journal of Biochemistry (1) and affords an update on the parameters reported in the previous report. This study has focused upon the third coordination shell which shows an iron-iron distance in the range of 3.26-3.48 Å and a bridging angle between 130° and 150°. This iron-iron distance appears slightly longer than that in the oxidized forms of hemerythrin which ranges between 3.21 and 3.25 Å as determined from X-ray crystallography at 2 Å resolution. Whether this distance is related to the different functions of the two proteins is not known at the present time, however, the remarkably good agreement between the results of this paper and the results from another laboratory (2) suggest that, in this case, the EXAFS data collection and analysis has resulted in a strikingly good agreement.

In recent studies, it has been found that the hydroxyurea treated form which does not contain the radical has an identical structure to the native B2 subunit. However, optical monitoring indicated some sample damage and further studies are needed of the undamaged form.

Future Plan. Further study of the radical free form, improved spectra on the B2 subunit, studies of the holoenzyme, and consideration of the study of reaction kinetics.

Reference

1. Bunker, G. Petersson, L. Sjöberg, B.-M., Sahlin, M., Chance, M., Chance, B. and Ehrenberg, A. EXAFS Studies on the Iron-Containing Subunit of Ribonucleotide Reductase from Escherichia Coli, Biochemistry, (1987) (in press).

2. Scarrow, R.C., Maroney, M.J., Palmer, S.M. and Que, L. J. Am. Chem. Soc. 108, 6836-6834 (1986).

NEXAFS Determination of the Geometry of Stable Intermediates Formed after Chemisorption of Ethylene on a Ni (100) Single Crystal Surface

F. Zaera
Dept. of Chemistry, Univ. of California
Riverside, CA 92521

D.A. Fischer
NSLS, Brookhaven National Laboratory
Upton, NY 11973

R. Carr
SSRL, Stanford, CA 94305

J.L. Gland
Exxon Research and Engineering
Annandale, NJ 08801

The chemisorption of ethylene on Ni (100) at low temperature was studied by using NEXAFS. The experiments were done at beam line III-1 (the new grasshopper) at SSRL. The spectra show the existance of two peaks corresponding to transitions to a π^* and a σ unoccupied orbitals. The dependence of the cross-section for these transition with respect to the angle between the molecular axis and the light polarization vector suggest that the molecule chemisorbs with the C-C bond parallel to the metal surface. Annealing to temperatures about 170K results in the formation of a new species, as determined previously from kinetic measurements using laser induced desorpton techniques (R.B. Hall, S.J. Bares, A.M. De Santolo and F. Zaera, J. Vac. Sci. Technol, A4, 1493 (1986). The NEXAFS data obtained in these experiments suggest that the new moiety retains the C-C double bond but in a tilted configuration. A detail analysis of the data is presently being done.

Near Edge X-ray Absorption Fine Structure Studies of Small Molecules on W(100)-(5x1)-C

Cynthia M. Friend, E.K. Baldwin
Department of Chemistry
Harvard University

P.A. Stevens and R.J. Madix
Department of Chemical Engineering
Stanford University

Roger Carr
SSRL, Stanford University

The adsorption structures of CO, CH_3CN, HCN and HCOOH on W(100)-(5x1)-C were investigated using the near edge X-ray adsorption fine structure method. The energetics for reaction on the W(100)-(5x1)-C surface are known to be qualitatively different than clean W9100).[1] The near edge X-ray adsorption fine structure studies performed in this work were part of an effort to develop an understanding of the molecular level basis for the observed changes in reactivity. In addition, the structural information obtained in the near edge X-ray absorption fine structure experiments is used as input for semi-empirical tight-binding calculations used to describe bonding to the surface.[2] The structural information obtained shows that adsorbed CO is essentially unperturbed compared to the gas phase, while HCN is signficantly rehybridized. Detailed analysis of the formic acid and acetonitrile is still underway.

Near edge data was obtained at the C K-edge for all molecules, with complementary data collected at the N K-edge for HCN and CH_3CN and at the O K-edge for CO and formic acid. Spectra were obtained by measuring the emission of electrons as a function of photon energy using a partial electron yield detector, similar in principal to that described previously.[3] Representative near edge X-ray absorption fine structure data are depicted in Figure 1 for CO at saturation coverage on W(100)-5(5x1)-C maintained at 130 K. The curves were fit using Gaussian line-shapes in order to determine the energy position of the π^* and σ resonances. The π^* is maximum in intensity at normal photon incidence, indicating that the CO bond vector is perpendicular to the surface plane. The absence of the π^* resonance at normal photon incidence further supports this interpretation. The C-O bond length was estimated using the empirical bond length correlation.[4,5] Using this method, the C-O bond length was estimated to be 1.05 Å.

NEXAFS data obtained for HCN consisted of a π^* and σ resonance associated with the C-N bond and a weak resonance tentatively assigned to a C-H resonance. Both the π^* and σ C-N resonance were more intense at normal relative to glancing photon incidence. A bond length of 1.38 Å was estimated from the energy of the transition. This is consistent with a rehybridization of the C-N bond worth vector oriented approximately parallel to the surface. The extremely long bond length is interpreted as a decrease in bond order to approximately 1.5 compared to 3 for the gas phase molecule. These data and conclusions are consistent with vibrational investigatons of HCN: and exceedingly low C-N streiching frequency of 1400 $cm.^{-1}$ was observed.[6]

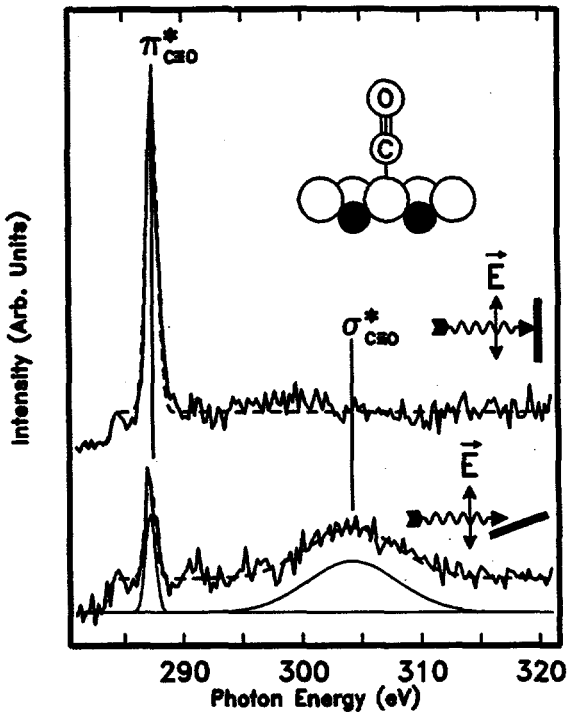

Figure 1: Polarization dependent carbon K-edge near edge X-ray absorption fine structure data for a satuaration coverage of CO on W(100)-(5x1)-C at a surface temperature of 100 K. The proposed bonding structure for CO on the W(100)-(5x1)-C surface is represented schematically in the upper left hand corner of the figure.

REFERENCES

1. See, for example, K.A. Pearlstine, C.M. Friend, J. Phys. Chem., 90, 1986, 4344.

2. S. Jansen, R.S. Hoffmann, C.M. Friend, In Preparation.

3. J. Stohr, R. Jager, Phys. Rev. B, 26. 1982, 4111.

4. J. Stohr, F. Sette, A.L. Johnson, Phys. Rev. Lett., 53, 1984, 1684.

5. F. Sette, J. Stohr, A.P. Hitchcock, J. Chem. Phys., 81, 1984, 4906.

6. C.M. Friend, J.G. Serafin, In Preparation.

EXAFS, WAXS AND DAS OF GOLD-BASED DRUGS USED TO TREAT RHEUMATOID ARTHRITIS

Richard C. Elder* and Katherine Tepperman
Departments of Chemistry and Biological Sciences
University of Cincinnati
Cincinnati, Ohio 45221-0172

We have a long standing interest in the use of synchrotron radiation to study the structural changes of gold-containing antiarthritis drugs that occur when binding in a biological matrix occurs. A new avenue we have been investigating centers upon the ability of algal biomass, a biological matrix prepared from the algae Chlorella vulgaris, to bind heavy metals such as gold.

This biomass has been shown to have a high affinity for both gold(I) and gold(III) species in aqueous solution. The accumulation of gold may approach 10 percent or more of the alga dry-weight. We have used X-ray absorption spectroscopy (EXAFS and XANES) to investigate gold-algae samples prepared from aqueous solutions of the antiarthritic drug Myochrisine (sodium gold(I)thiomalate) and the gold complexes dicyanoaurate(I) and tetracloroaurate(III). The average oxidation state and the immediate coordination environment of the gold in these algae samples has been determined.[1]

X-ray absorption spectra were recorded at SSRL on beam lines IV-1 and IV-3 under dedicated running conditions about the gold L_{III} absorption edge. XANES studies yield the oxidation state information for gold in the samples. Gold-algae samples prepared from aqueous solutions of the gold(I) complexes were found to maintain a +1 oxidation state. Samples prepared from gold(III) tetrachloride, however, were shown to readily undergo reduction to a +1 species. Figure 1 illustrates the change in oxidation state from Au(III) to Au(I) in the gold-algae samples. The Au(III) oxidation state is indicated by the presence of a peak at 11923 eV. Depending upon the concentration of gold in the algae, from 50 to 100 percent of the gold(III) is reduced to gold(I).

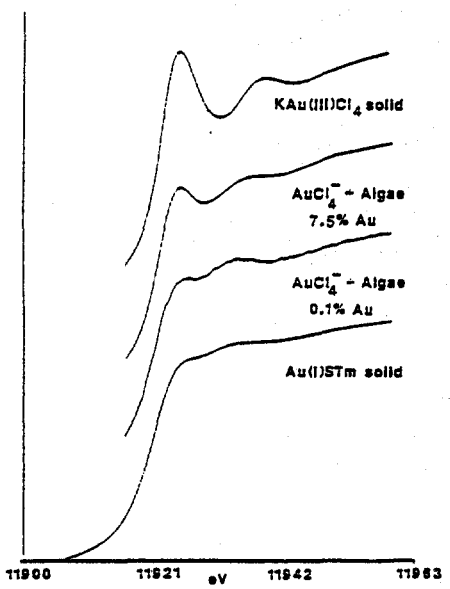

Figure 1: Plots of the XANES region spectra, F/I_o, vs. energy (eV) obtained for solid $KAu(III)Cl_4$ with no algae present, the samples derived from the reaction of $AuCl_4^-$ with algae biomass and an example of an Au(I) XANES spectrum taken from gold(I)thiomalate. The intense band at 11923 eV is characteristic of the Au(III) oxidation state.

Analyses of the EXAFS regions of the spectra provide structural details of the average gold coordination environment. Direct evidence for the complexation of a gold(I) species with algae was obtained from the EXAFS analysis of algae samples prepared from dicyanoaurate(I). The change in the gold coordination environment is apparent in the Fourier transform of the EXAFS data. Figure 2a is the Fourier transform (FT) obtained for the starting material $[Au(CN)]_2^-$. The peaks correspond to Au-C and Au-N absorber-scatterer distances. Figure 2b is the FT obtained for one algae sample treated with dicyanoaurate(I). The changes in the FT indicate a change in the average coordination environment of the gold. Curve fitting of the EXAFS data indicates that some of the gold is now coordinated to sulfur from the algae. Similar envidence

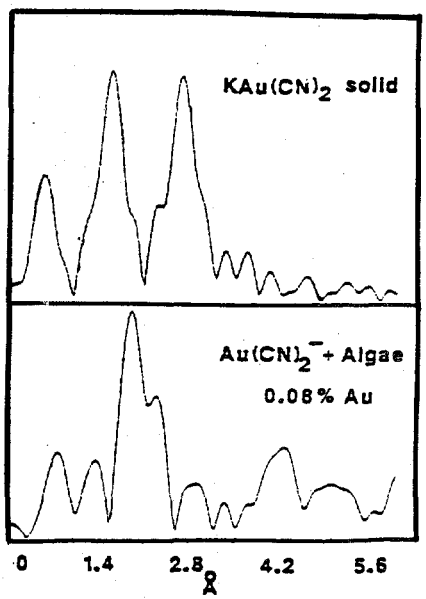

Figure 2: Plots of the modulus of the Fourier transforms vs. radial position (Å) obtained from the EXAFS data of solid $KAu(CN)_2$ with no algae present and a sample derived from the reaction of $Au(I)(CN)_2^-$ with algae (0.08% gold). The changes observed in the FT indicates that some CN is replaced by S in the gold coordination sphere upon binding to the algae.

for the direct coordination of gold to functional groups in the algae was obtained for an algae sample prepared from gold(III) tetrachloride. The gold in this sample was found to coordinate to a nitrogen moiety of the algae. The samples prepared from gold(I) thiomalate were found to maintain a two coordinate geometry with the gold bound to two sulfurs. This geometry is identical with that found for the starting material[2] and is consistent with our findings on the binding of gold(I) complexes with the protein, bovine serum albumin.[3]

Our study thus indicates that both of the gold(I) complexes lead to gold-algae samples where the gold(I) species coordinates to sulfur. This is contrasted with the gold(III) samples where we see evidence for reduction of the gold in the biological matrix as well as an affinity for a nitrogen moiety in the algae.

While the EXAFS analysis provides accurate structural

information for the first coordination shell, it is unsuitable for examining atomic interactions at distances greater than 3 Å. To extract this longer-range structural information, we have continued to develop the use of wide angle X-ray scattering (WAXS) and differential anomalous scattering (DAS) for the structural characterization of these metal-containing complex biological systems.

Of specific interest has been the structural characterization of various metallothioneins. Metallothioneins are thought to be involved in metal transport and heavy metal scavenging. As a mammalian protein, metallothionein is isolated from the kidney tissue of rats and rabbits. Gold from antiarthritis drugs is known to bind to metallothionein, replacing the native zinc. These gold containing aurothioneins have been studied by X-ray absorption spectroscopy.[4] The EXAFS analysis gave details of the immediate coordination environment around the gold, but longer-range distance information was not obtainable. Thus any protein structural changes that occur as a result of gold binding are unknown. We have been involved in developing a differential anomalous scattering analysis for various metallothionein systems to extract the longer-range distance information.

The short supply of metallothioneins requires that data collection be accomplished on small amounts of material. To reduce the amount of material typically used in an X-ray scattering experiment, a transmission geometry is employed. In this mode, the protein sample is pressed into a thin, rigid wafer and placed on a holder so that the beam may pass directly through it. This geometry has enabled us to reduce the sample quantity by a factor of 20 to a size of ca. 15 mg. Figure 3 is a plot of the scattering data obtained for 15 mg of gold-substituted metallothionein.

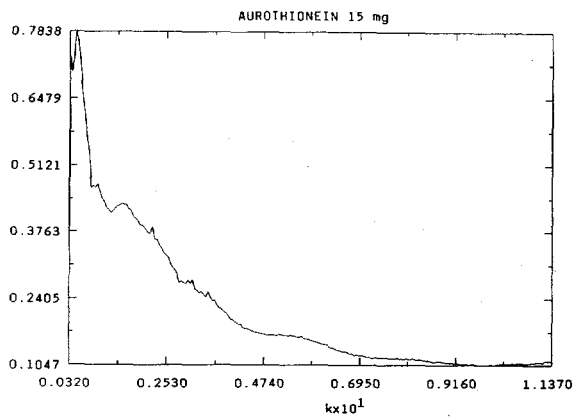

Figure 3: Wide angle X-ray scattering data, I/I_o vs k collected at 11800 eV for gold substituted metallothionein.

The successful data collection achieved for the metallothioneins will make possible a more complete structural characterization. We are currently involved in the calculational process necessary to obtain this information.

The individual working on these projects is John Watkins. Support for this work is from the NIH (GM 35404).

References

1) Watkins, II, J.W.; Elder, R.C.; Greene, B.; Darnall, D.W., Inorg. Chem. in press.

2) Elder, R.C.; Ludwig, K.; Cooper, J.N.; Eidsness, M.K., J. Am. Chem. Soc., **1985**, 107, 5024.

3) Carlock, M.T.; Shaw, III, C.F.; Eidsness, M.K.; Watkins, II, J.W.; Elder, R.C., Inorg. Chem., **1986**, 25, 333.

4) M.K. Eidsness Ph.D. Thesis, University of Cincinnati, 1984.

Technetium and Rhenium Imaging Agents and Therapeutic Radiopharmaceuticals

Richard C. Elder and Edward Deutsch

Department of Chemistry and Radiology and
the Biomedical Chemistry Research Center
University of Cincinnati
Cincinnati, Ohio 45221-0172

Rhenium Palliatives for Metastatic Prostate and Breast Cancer. We have been examining the structures of a series of rhenium diphosphonate complexes formed from hydroxyethylidine diphosphonate (HEDP) or methylene diphosphonate (MDP) ligands. The ligand (O_3P-CRR'-PO_3) is thought to bind through the oxygen atoms of the phosphonate groups to the rhenium. The complex appears to be polymeric with multiple rhenium atoms per unit. The polymeric unit then is assumed to bind to the calcium atoms of growing bone. What actually is known is that these complexes (which are analogous to the widely used technetium bone imaging agents) are preferentially absorbed at sites of bone growth. In the case of early trials with cancer patients, the complexes are taken up at the site of the metastatic bone tumors. These complexes may be synthesized using ^{186}Re or ^{188}Re both of which emit strong γ's (>100 keV) and decay with energetic β^- emission. The hard X-rays may be used with the standard imaging gamma camera to indicate localization of the complexes in a test subject. The β's cause severe local damage resulting in cell death at the localization site. While this is not a broad enough effect to wipe out the tumor completely, it can reduce tumor size significantly and provide pain relief when effective doses of morphine or heroin are so large as to render the patient permanently comatose. Our interest in these systems, then, is to understand the mechanism responsible for the biodistribution found and by using this knowledge to design agents which more specifically bind at tumor sites and function as better palliatives or even as therapeutic agents.

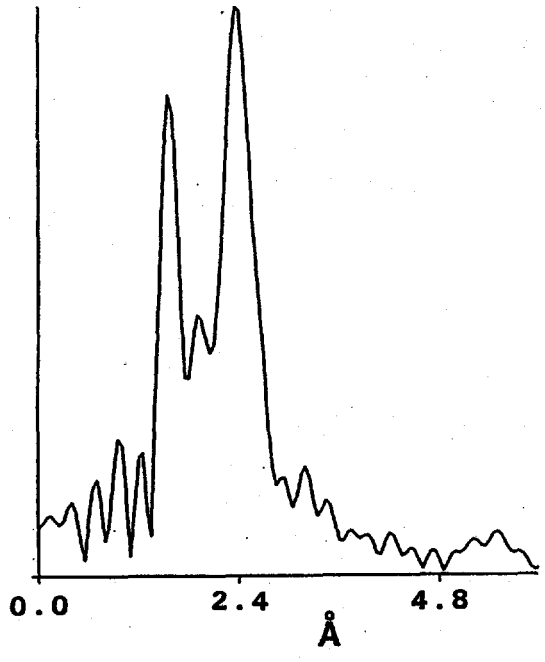

Figure 1

Our initial attempts to determine the structures of these agents have involved two different approaches with studies of non-radioactive complexes synthesized from natural abundance rhenium. We have synthesized $[Re(HEDP)_x]^{n-}_m$ and precipitated the polymeric complexes with various counter ions such as Ca^{2+}, Sr^{2+} and Ba^{2+}. In our first studies we have measured the EXAFS spectra of these materials. In other studies we have used WAXS and DAS to determine longer distance interactions than those found via EXAFS studies. The Fourier transform of a typical Re L_{III} EXAFS spectrum is shown in Figure 1. There are two principal peaks which can be back-transformed independently to yield the filtered data shown in Figures 2a and 2b. The data shown in 2a, from the low R peak in the FT, can be

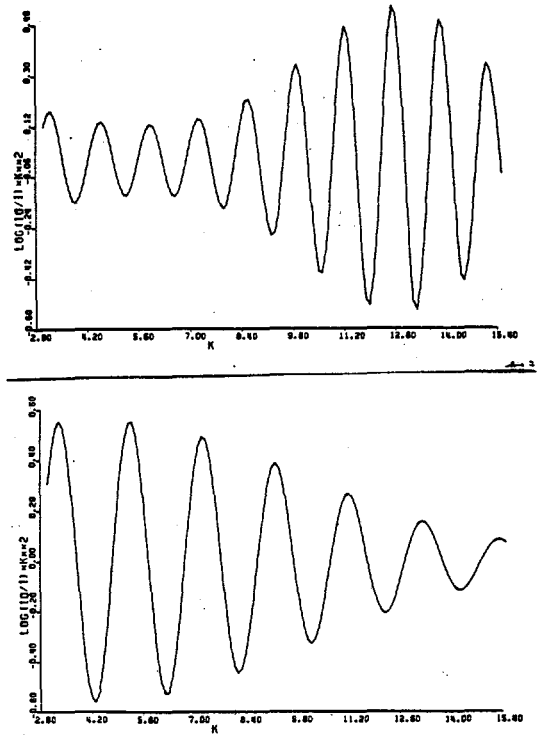

Figure 2a (top) and 2b (bottom)

successfully fit to describe a first shell of oxygen atoms surrounding the rhenium as anticipated. The data from the high R peak back-transform to yield the filtered component shown in 2b. There the amplitude envelope is clearly very different reaching a maximum at 12 to 13 $Å^{-1}$ in these plots weighted by k^2. The envelope shape clearly requires a heavy atom as the back-scatterer. That this second peak occurs regardless whether the precipitating counter ion is Ca^{2+} or Ba^{2+} indicates that the heavy back-scatterer must indeed be a rhenium atom. These findings may be modelled by a nearly square array of two rhenium and two oxygen atoms.

A large sample of the same material (approx. 1.0 g) was mulled with 50% Vaseline and examined by wide angle X-ray scattering (WAXS) in reflection mode. Figure 3 shows

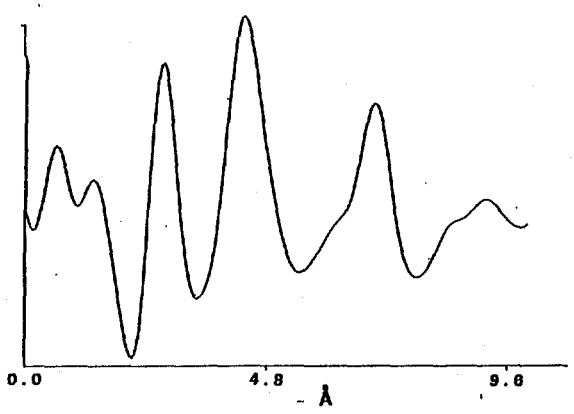

Figure 3

the radial distribution function (RDF) calculated from the scattering data. Most importantly the RDF shows relatively long-range order with major peaks at 4.7 and 7.1 Å. WAXS data for these materials have been measured immediately below the rhenium L_{III} edge and 100 ev further below the edge. The difference between the pair of data sets so measured results from the changing amount of anomalous scatter involving rhenium atoms. The Fourier transform of the difference yields a differential distribution function (DDF). The DDF has a clear advantage over the RDF in that it is somewhat element specfic whereas the RDF represents every possible scattering pair in the sample. Additional calculations are in progress with these data involving improved normalization and more elaborate modelling and will be presented subsequently. At this point the following conclusions appear warranted, rhenium is coordinated by oxygen and bridged into a polymeric structure by oxygen atoms forming a Re_2O_2 nearly square array. This structure is further extended resulting in metal-metal distances of 4.7 and 7.1 Å as well.

Influence of Pi Bonding on Re-P Bond Lengths. In analogy to previous studies with technetium complexes (1), we are able to synthesize rhenium complexes with the ligand bis(dimethylphosphino)-1,2-ethane (dmpe). Complexes can be formed in +1 and +2 oxidation states as $[Re(dmpe)_3]^{n+}$. EXAFS data have been measured on both complexes and fit using theoretical amplitudes and phases to a model with six phosphorous atoms at equal distances. The Re-P distance is 2.44 Å for the +2 oxidation state whereas it is found to contract to a value of 2.39 Å for the +1 oxidation state. An ionic or sigma bonding model would predict a smaller radius for Re^{2+} than for Re^{+} and therefore shorter bonds for the higher oxidation state. That the opposite trend is observed requires invoking a pi-back-bonding interpretation. The donation of sigma electron density results in more of a negative charge accumulation for the +1 oxidation state at rhenium than for the +2 state. This results in back donation of pi symmetry electron density from the metal orbitals to the appropriate phosphorous d orbitals and strengthens and shortens the bonds in the lower oxidation state compared to the higher. This effect is expected to be of some importance in determining the rate of electron exchange reactions between the two species (2).

WAXS and DAS on Techneitum Diphosphonate Complexes. We have developed a transmission measurement technique which utilizes pressed pellets of a 6 by 15 mm area and containing 10 to 20 mg of sample. The pellet may be encapsulated within kapton tape to contain radioactive samples and ensure sample integrity. With this approach we have measured high quality scattering data on technetium diphosphonate complexes and will report on those experiments as well as EXAFS measurements on the same materials in the future.

Individuals working on this project have included John Watkins and Maqsudur Rahman. Support for this project has been from the National Institutes of Health Grants GM35404 and CA 32863.

References

1) J.L. Vanderheyden, et.al. Inorg. Chem. **1984**, 23, 3184.

2) M.N. Doyle, et.al., Inorg. Chem. **1986**, 25, 3367.

Determination of The Oxidation State and Site Structure of Cu Centers

By X-ray Absorption Edge Spectroscopy

Lung-Shan Kau, James E. Penner-Hahn, Darlene J. Spira-Solomon, Britt Hedman, Edward I. Solomon* and Keith O. Hodgson*

Department of Chemistry, Stanford University, Stanford, CA 94305, U.S.A.

Due to the fact that conventional spectroscopic methods can neither probe a $3d^{10}$ cuprous configuration nor distinguish reduced copper from an antiferromagnetically-coupled, EPR-nondetectable cupric pair, it may be difficult to determine the oxidation state and geometry for mamy copper centers. However, cuprous complexes exhibit a strong X-ray absorption edge feature at ~8984 eV, which is absent in Cu(II) complexes.

We have systematically studied a number of model compounds to correlate copper X-ray absorption edge features with oxidation state and geometry [1]. The Cu(I) compounds studied represent different coordination numbers, geometries and degrees of covalency. Most Cu(II) complexes studied have geometries close to tetragonal but with different ligand sets and therefore covalency.

All X-ray absorption edge data were measured at Stanford Synchrotron Radiation Laboratory utilizing several different beam lines. To insure a consistent energy reference, the internal calibration method with Cu foil was used. To allow proper normalization, the absorption was measured for at least 300 eV below and 200 eV above the Cu K edge. These edge spectra were pre-edge background-subtracted and normalized to give an edge jump of 1.0 at 9000 eV.

Using the energy calibration and normalization procedure described above, we find that, in all cases, Cu(II) complexes show no low-energy pre-edge peak below 8985.0 eV and that their absorption intensities in this region are significantly lower than those of Cu(I) complexes, which exhibit a pre-edge maximum in the 8983-8984 eV region. Further, we find that the shape, energy and intensity of the pre-edge maximum varies significantly over the different Cu(I) complexes studied. These Cu(I) pre-edge spectral changes have been correlated systematically with coordination number and geometry of the metal ion and interpreted using a simple ligand field model. This model predicts that the $4p_{x,y,z}$ in the free Cu(I) ion will be split differently by the ligand field associated with different geometries.

Many Cu(II) complexes studied show structure on the absorption edge at energies of 8986-8988 eV. In all complexes studied, this Cu(II) peak is always observed at energies greater than 8985.0 eV. Alternatively, most Cu(II) complexes do exhibit a pre-edge low energy tail through this 8983-8984 eV region, which with few exceptions have quite low intensity over this energy range. The exceptions are for highly covalent Cu(II) complexes (with sulfur ligation) where the higher intensity in the low energy tail appears to be related to the increased covalency.

We have calculated the normalized difference X-ray absorption edge spectra (NDXAES) to further quantify these features by substrating the normalized edge of a representative Cu(II) complex from that of a Cu(I) or from a covalent Cu(II) complex. The difference of properly normalized Cu(I) and Cu(II) edge spectra has a derivative shape with a positive peak at 8983-8984 eV for 2- and 3-coordinate Cu(I) and at 8986 eV for 4-coordinate Cu(I) and a broad negative feature for all Cu(I) complexes at ~8990-9000 eV. The difference edge spectra of covalent Cu(II), although qualitatively similar in shape to those of 2- and 3-coordinate Cu(I), have lower intensity and in particular their maxima are shifted to significantly higher energy.

We have also simulated NDXAES for binuclear Cu(I) systems where each copper can have a different coordination number (2&3, 2&4 and 3&4). From the energy and shape of the NDXAES maxima, we find that it is possible to distinguish 2, 3, 2&3 and 2&4 coordinate Cu(I) complexes from 4 coordinate Cu(I) and covalent Cu(II) systems. However, there is ambiguity in distinguishing between 4 coordinate Cu(I) and covalent Cu(II). Once the approximate geometry of a copper site is known, it is further possible to use the amplitude of the peak maxima of the NDXAES to quantitate the amount of Cu(I) present.

This NDXAES technique has been successfully applied to determine the amount of Cu(I) present in several derivatives of the multicopper oxidase laccase [1,2,3]. The analysis of the Cu(I) edge features has been further applied to interpret the polarized, pH-dependent edge spectra of reduced plastocyanin [4].

1. Kau, L.-S.; Spira-Solomon, D.J.; Penner-Hahn, J.E.; Hodgson, K.O.; Solomon, E.I. submitted to J. Am. Chem. Soc.
2. Hahn, J.E.; Co, M.S.; Spira, D.J.; Hodgson, K.O.; Solomon, E.I. Biochem. Biophys. Res. Comm., **1983**, 112, 737-745.
3. Penner-Hahn, J.E.; Hedman, B.; Hodgson, K.O.; Spira, D.J.; Solomon, E.I. Biochem. Biophys. Res. Comm. **1984**, 119, 567-574.
4. Penner-Hahn, J.E., Ph.D. thesis, Stanford University, Stanford, CA 94305, **1984**.

Research supported by NIH Grant RR 01209 and NSF Grant CHE 85-12129.

X-RAY ABSORPTION STUDIES OF LACCASE DERIVATIVES

Him-Tai Tsang[1] Angela M. Schmidt[2], David R. McMillin[2], and James E. Penner-Hahn[1]

[1]Department of Chemistry, University of Michigan Ann Arbor, Michigan 48109-1055
[2]Department of Chemistry, Purdue University, West Lafayette, IN 47907

Laccase is a multi-copper enzyme containing three distinct copper sites: the mononuclear Type I and Type II sites and the binuclear Type III site. The Type I or "blue" site is characterized by intense visible absorption (λ~600 nm, ε~10,000 $M^{-1}cm^{-1}$) and a small $A_{||}$ hyperfine coupling constant. Spectral evidence suggests that the Type I site in laccase should have a structure similar to that found in other Type I copper proteins, however the presence of multiple Cu sites has prevented selective study of the Type I site using XAS. Recently a new laccase derivative has been prepared in which the Type I Cu(II) is selectively replaced with Hg(II) [1]. This modification makes possible the selective study of only the Type I environment. We have previously reported preliminary measurements of Hg laccase [2]. In the last year these measurements have been extended, including studies of the Cu absorption edge, and are described in greater detail herein.

Crystallographic characterization of plastocyanin [3] and azurins [4] have shown that the Cu is ligated to two histidine nitrogens (Cu-N = 2.0 Å), one cysteine sulfur (Cu-S = 2.15 Å) and one methionine sulfur (Cu-S ca. 3 Å). In azurin, there is also a peptide carbonyl oxygen at > 3 Å. Stellacyanin has not been crystallographically characterized, however since its amino acid sequence lacks methionine, the stellacyanin metal site cannot be identical to those in azurin and plastocyanin.

The Cu XAS of plastocyanin does not show any evidence of the methionine sulfur, even for data measured at 4K [5]. This is believed to be due to largely uncorrelated motion (e.g., weak interaction) of the copper and the methionine sulfur. Since Hg(II) is larger than Cu(II) and since Hg(II) has a greater affinity for sulfur it seemed possible that Hg XAS could detect the presence (or absence) of the methionine ligand. The Hg XANES spectra for plastocyanin, azurin, and stellacyanin are compared in Figure 1. These spectra show small but reproducible differences, demonstrating that Hg XAS, unlike Cu XAS, is capable of distinguishing between these three different Type I sites. Structural interpretation of these XANES differences is difficult, however the EXAFS results (below) offer some preliminary suggestions.

The XANES spectra for laccase, plastocyanin and azurin are compared in Figure 2. These spectra are extremely similar, thus demonstrating that the Hg substituted Type I site in laccase is structurally very similar to the Hg substituted Type I sites in azurin and plastocyanin Hg. The crystal structure of the Hg substituted plastocyanin has recently been reported and is isostructural with the Cu site [6]. Even in the absence of a structural interpretation of the XANES, the present results demonstrate that the Type I sites in these proteins fall into two structural categories: plastocyanin, azurin, and laccase are very similar and distinct from stellacyanin.

The Fourier transforms of the EXAFS data for stellacyanin and laccase are compared in Figure 3. Stellacyanin seems to show additional amplitude at ca. 2.4 Å (corresponding to an atom at ca. 2.8 Å) which is absent in laccase. While preliminary, these results suggest that Hg EXAFS may be able to identify the structural differences between these sites.

References

1. M.M. Morie-Bebel et al., J. Am. Chem. Soc., 1984, 106, 3677-8.
2. J.E. Penner-Hahn et al., SSRL Activity Report, 1985.
3. J.M. Guss and H.C. Freeman, J. Mol. Biol., 1983, 169, 521-63.
4. a) E.T. Adman and L.H. Jensen, Isr. J. Chem., 1981, 21, 8-12. b) G.E. Norris et al., J. Am. Chem. Soc., 1986, 108, 2784-5.
5. J.E. Penner-Hahn et al., submitted.
6. W.B. Church, et al., J. Biol. Chem., 1986, 261, 234-7.

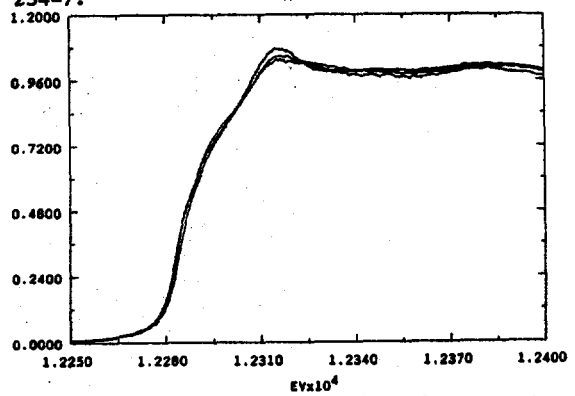

Figure 1. Hg XANES spectra. Light) plastocyanin and azurin. Dark) Stellacyanin.

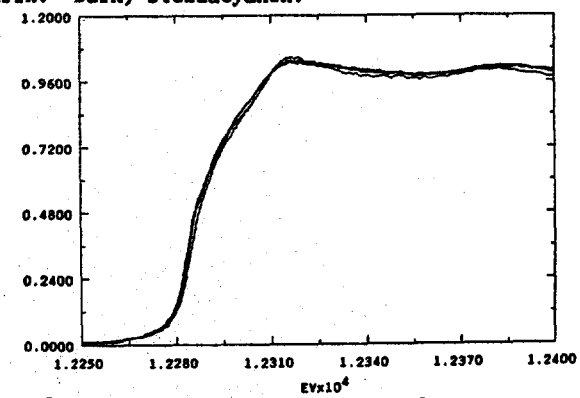

Figure 2. Hg XANES spectra. Light) plastocyanin and azurin. Dark) Laccase.

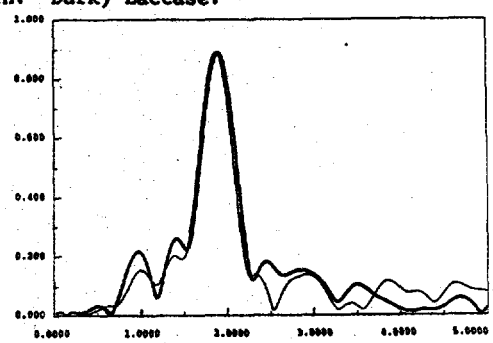

Figure 3. k^3 weighted Fourier transforms of Hg EXAFS spectra. Light) Laccase. Dark) Stellacyanin.

TEMPERATURE EFFECT ON THE INITIAL STAGE BAND BENDING OF AL/GaAs(110)

Renyu Cao, Ken. K. Chin*, Ken Miyano
Ingolf Lindau, and William E. Spicer

Stanford Electronics Laboratories
Stanford University, Stanford, CA 94305

Schottky barrier formation at metal/semiconductor interfaces still remains as a puzzle even after more than four decades of study because the real interfaces are too complicated. To simplify the systems and obtain the clue of the fundamental physics behind the initial stage band bending study at Al/GaAs(110) at room temperature and low temperature (-90°C) was performed. At low temperature more uniform interface can be obtained and the Al cluster formation, which plays an important role in Fermi level pinning at room temperature, is largely inhibited. That is at low temperature Al/GaAs system is much simpler.

The experimental was performed at the beam line I-1 at the Stanford Synchrotron Radiation Laboratory. The surface sensitive photoemission spectroscopy was used to track the band bending of the semiconductor as a function of Al coverage. To perform initial stage band bending study, a low coverage evaporator was employed with evaporation starting from as low as 10^{-4} monolayer (ML).

Evolution of band bendings of n- and p-GaAs as a function of Al coverage are recorded in a band bending diagram in the attached figure. At room temperature n- and p-GaAs bands bend at more or less same rate towards to the final position, similar to many other metal/GaAs systems at room temperature. However, the band bending of GaAs at low temperature shows some interesting features. Compared with room temperature band bending behavior, at a given Al coverage n-GaAs band bending is reduced while p-GaAs band bending is enhanced. p-GaAs also shows a maximum band bending around 0.1 ML, which is larger than its final value. And with thick Al coverage, both n- and p-GaAs tend to move to the final pinning positions same as those of corresponding room temperature systems.

These dramatic difference of Al/GaAs(110) band bending at different temperatures can not be explained by any of current models about Schottky barrier formation at metal/semiconductor interfaces. It strongly suggests that there must exist another mechanism which is responsible for the initial stage band bending as well as Schottky barrier formation at low temperature. It is interesting to note that Al/GaAs is not the only system which shows different band bending behavior upon temperature. Other systems show the similar behavior[2--4]. Those results[2] show that for metal/p-GaAs at low temperature the initial stage band bending is related to the work function of the metals deposited on GaAs surfaces. Because of interface at low temperature has better homogeneity, many actions are slowed down, then a Schottky-like mechanism may play a more important role in determining the surface Fermi level position. With thick metal coverage or higher temperature, or generally more surface disturbance this mechanism breaks down, the room temperature mechanism then takes over. To get an overall picture, more studies are needed.

This work is supported by ONR under contract No. N00014-82-K-0524 and N00014-86-K-0736.

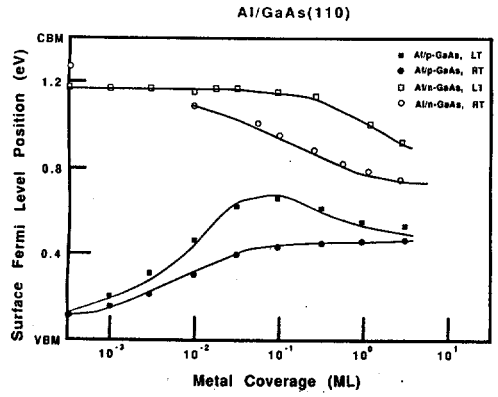

Figure 1. The evolution of surface Fermi level positions vesus Al coverages (in monolayer) at room temperature and low temperature (-90°C) are recorded. Note the difference between room temperature band bending and low temperature band bending.

Refernces:

* Present adress: Department of Physics, University of Notre Dame, Notre Dame, IN 46556

1. K. K. Chin, R. Cao, T. Kendelewicz, K. Miyano, M. D.Williams,S.Doniach, I. Lindau, and W. E. Spicer, MRS 1986, in press.
2. R. Cao, K. Miyano, T. Kendelewicz, K. K. Chin, I.Lindau, and W. E.Spicer, 14th PCSI, in press.
3. K. Stiles, A. Kahn, D. G. Kilday, N. Tache, G. Margaritondo, 33rd AVS, in press.
4. K. Stiles, A. Kahn, D. G. Kilday, G. Margaritondo, 14th PCSI, in press.

METAL/$Hg_{1-x}Cd_xTe$ INTERFACES

D. J. Friedman and I. Lindau

Stanford Electronics Laboratories,
Stanford University, Stanford, CA 94305

In 1986, the study of Metal/$Hg_{1-x}Cd_xTe$ interfaces was continued and extended to a wider range of overlayer metals, including Cu [1] and Pt [2]. This data was found to be very helpful in the overall goal of understanding the driving forces influencing interface morphology and surface Fermi level motion. For instance, it was found that for both Cu and Pt as well as for metals studied previously, the surface Fermi level motion upon overlayer deposition is consistent with the bulk doping properties of the overlayer metal in the semiconductor. Furthermore, analysis of the Pt/MCT overlayer morphology showed that interface reactivity can be affected by reaction with the semiconductor cation as well as with the anion.

REFERENCES

1. D. J. Friedman, G. P. Carey, I. Lindau, and W. E. Spicer, Phys. Rev. B 34, 5329 (1986).
2. D. J. Friedman, G. P. Carey, I. Lindau, and W. E. Spicer, Phys. Rev. B, (1987).

Optically enhanced O_2 and N_2O chemisorption on GaAs(110): Reaction kinetics and mechanism

Proposal 935Vp

K. A. Bertness, T. T. Chiang, C. E. McCants, P. H. Mahowald, A. K. Wahi,
T. Kendelewicz, I. Lindau, and W. E. Spicer
Stanford Electronics Laboratories, Stanford University, Stanford, CA 94305

Using surface sensitive photoemission we have measured oxygen uptake versus gas exposure to N_2O and O_2 on cleaved GaAs(110) surfaces under different conditions of sample surface temperature, sample doping, and intensity of argon ion laser illumination ($h\nu = 2.41$ eV). The chemisorption kinetics as characterized by the sticking coefficient and chemisorption activation energy are then compared to learn which reaction steps are crucial to the overall process. On the basis of recent work at SSRL and with conventional photon sources, we have been able to demonstrate the following key facts about the oxygen chemisorption mechanism: first, that physisorption of gas molecules on the surface dramatically influences the overall reaction kinetics; second, that dissociation of physisorbed O_2 is a major rate-limiting step in O_2 chemisorption; third, that this dissociation is the step enhanced by the presence of visible light; and finally, that both photogenerated electrons and holes are involved in the optical enhancement mechanism.

A general theme in our findings is the importance of the gas molecule physisorption step prior to dissociation and reaction with the surface. It is not possible, for example, to explain the slight decrease we observe in N_2O uptake as the surface temperature increases if one assumes a reaction model in which the gas molecules react upon impact with the surface. This conclusion has implications for other reaction enhancement mechanisms, particularly chemisorption enhanced by thin metal layers or surface disorder, since a dominant part of these enhancements may be due to increasing the physisorbed molecules' residence time rather than speeding up the oxygen reaction *per se*.

As we expected from earlier work, we have found that the breakup of the oxygen molecule is a major rate-limiting step in O_2 chemisorption in the dark. This conclusion is indicated by the increased reactivity displayed by N_2O, a more weakly bound molecule, both in terms of room temperature sticking coefficients (3×10^{-7} and 7×10^{-10} at 0.4 ML for N_2O and O_2, respectively) and chemisorption activation energy (0.15 ± 0.08 eV and 0.47 ± 0.02 eV, respectively). Optically enhanced oxygen chemisorption also has the same activation energy as N_2O, suggesting that the reaction step enhanced by visible light is the breakup of the molecule. This hypothesis is further supported by the absence of a large optical enhancement for N_2O (see figure); a molecule which dissociates readily is not expected to strongly influenced by the opening of additional reaction channels for dissociation.

We are able to eliminate single-carrier optical enhancement mechanisms from sample doping comparisons. Although light-induced changes in surface electron and surface hole concentrations are very different for the two doping types, *n*- and *p*-type GaAs have virtually identical O_2 uptake rates under 1 W/cm^2 illumination. When the laser intensity is increased to 3 W/cm^2 for the *n*-type sample, however, the sticking coefficient increases by a factor of 5 to 10, unlike an earlier study on *p*-type where the enhancement ceased to increase for intensities above 1 W/cm^2. We are currently refining our calculations of surface carrier concentrations to determine whether there is an explanation for this effect.

In addition to these implications concerning reaction mechanisms, we are looking into other differences observed between N_2O and O_2. Nitrous oxide, for example, seems to form more oxides with lower oxygen coordination and displays different surface band bending than molecular oxygen. These differences may be due to variations in surface strain or changes in the amount of energy released by the oxygen reaction. The data from recent runs will also be used to confirm our previous work in which we demonstrated that oxygen chemisorption is primarily a surface phenomenon, with little (if any) oxidation taking place more than two atomic layers below the surface.

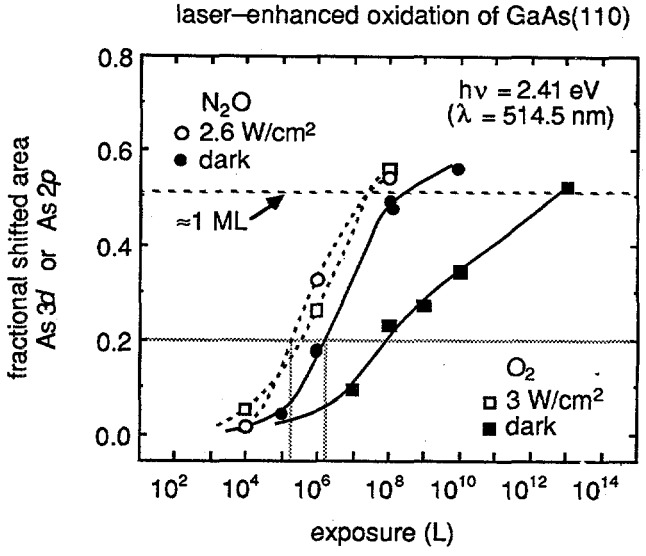

Oxygen uptake vs. gas exposure both in the dark (closed symbols) and with argon ion laser illumination (open symbols). N_2O, a weakly bound molecule, is seen to be much more reactive than O_2 in the dark and displays little laser enhancement relative to O_2, supporting our conclusion that dissociation of O_2 is the reaction step enhanced by visible light.

CHEMICAL REACTION AT THE In ON Ga As (110) INTERFACE - A SYNCHROTRON RADIATION PHOTOEMISSION STUDY

K. K. Chin,* K. Miyano, R. Cao, T. Kendelewicz,
J. Yeh, I. Lindau, and W. E. Spicer

Stanford Electronics Laboratory,
Stanford University, Stanford, CA 94305

We have recently reported a PES study of the chemical reaction at the In on GaAs interface, in which 40.8 eV photons from a Helium discharge lamp were utilized as the light source [1]. Upon annealing the interface above the In melting point, the In 4d spectrum contained a component shifted to 0.8 eV higher binding energy from the unreacted In 4d peak. This component is indicative of In bonded covalently, as in InAs. Consequently, it was suspected that the energetically unfavorable replacement reaction c In + GaAs --> $In_xGa_{1-x}As$ + $In_{c-x}Ga_y$ + (x - y) Ga occurs at the interface. However, Ga 3d signals from the segregated elemental Ga and alloyed Ga reaction products could not be resolved. We suspected that the failure to resolve these signals was due to the proximity in binding energy of the elemental Ga 3d core level and the covalent In 4d core level. At 40.8 eV, the photoionization cross section of In 4d is 7.5 times that of Ga 3d, and hence a potential elemental Ga 3d signal would be washed out by the stronger In 4d. Thus, to study the possibility of a replacement reaction, synchrotron radiation, which allows adjustment in relative signal strength between the In 4d and Ga 3d peaks, was utilized, and the following result was obtained.

The In 4d cross section passes through a Cooper minimum, and as a result, at roughly 140 eV the Ga 3d to In 4d signal ratio is maximized. For comparison, the In 4d Cooper minimum for free elemental In is theoretically calculated to occur at a photon energy of 130 eV [2]. The Ga 3d and In 4d post-anneal spectra at photon energy 140 eV are shown in the figure. The Ga 3d signal from the clean surface at 140 eV is also plotted, with the band bending shift subtracted out. With the In 4d signal minimized, we can see that the Ga 3d spectra from the annealed surfaces have nearly the same width and lineshape as that of the clean surface. The clean surface spectrum has an extra bump on the low binding energy side that can be attributed to nonuniform band bending of the clean surface. The photoemission spectra of the annealed In/n-GaAs (110) interface show no evidence of the elemental Ga reaction product expected for a replacement reaction.

One possible explanation is that the elemental Ga was sufficiently alloyed in In or clustered to be difficult to detect with PES. It must be noted that in the case of Al on n-GaAs such a difficulty does not occur, and the segregated Ga peak is clear in the Ga 3d spectrum [3]. Another possiblity is that upon heat treatment the molten In reacts with excess As, which has been reported to exist in GaAs. We have not detected free As in our PES measurements, but segregated As has been observed at GaAs dislocations by Cullis *et al* [4] and as inclusions in *in situ* cleaved GaAs surfaces by Bartels *et al* [5]. Certainly the existence of significant quantities of excess As in GaAs would have implications on reactions beyond the In /GaAs system under study, and whether the reactions observed in other GaAs systems are consistent with such an excess must be investigated.

This work was supported by the Office of Naval Research (ONR) under Contract No. N00014-82-K-0525.

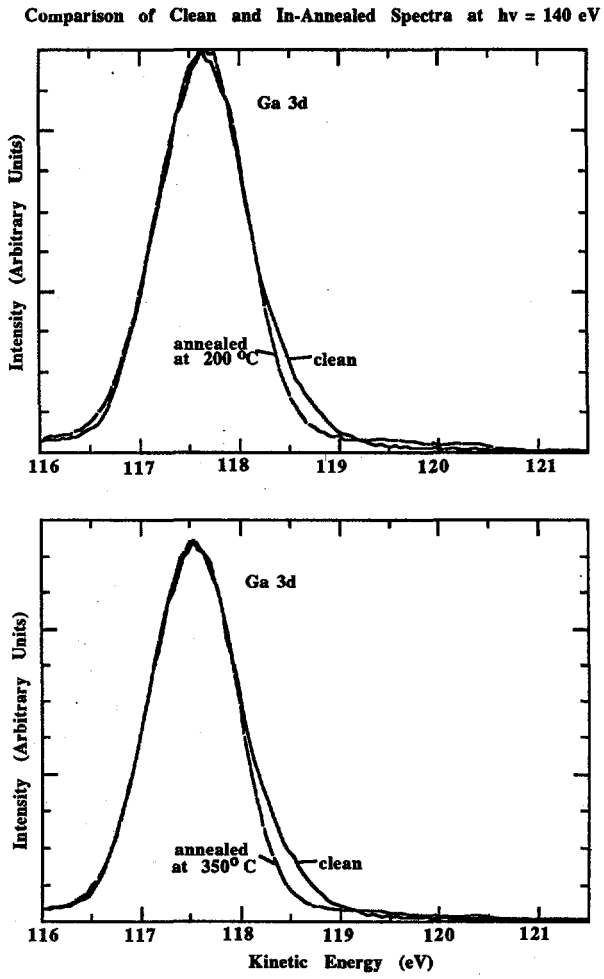

Fig. 1. Ga 3d and In 4d core level spectra taken at photon energy 140 eV (a) following anneal at 200 °C and (b) following anneal at 350 °C. In both cases, the clean surface Ga 3d spectrum is also plotted, with the band bending shift removed.

REFERENCES

*Present address : Department of Physics, University of Notre Dame, Notre Dame, IN 46556.

1. K. K. Chin, T. Kendelewicz, N. Newman, I. Lindau, and W. E. Spicer, J. Vac. Sci. Technol. B **4**, 955 (1986).
2. J. -J. Yeh and I. Lindau, Atomic Data and Nuclear Data Tables **32**, 1 (1985).
3. P. Skeath, I. Lindau, C. Y. Su, and W. E. Spicer, Phys. Rev. B **28**, 7051 (1983).
4. A. G. Cullis, P. D. Augustus, and D. J. Stirland, J. Appl. Phys. **51**, 2556 (1980).
5. F. Bartels, H. J. Clemens, and W. Monch, Physica **117B & 118B**, 801 (1983).

PHOTOEMISSION STUDY OF OXYGEN UPTAKE ON $Hg_{1-x}Zn_xTe$, HgTe, AND $Cd_{1-x}Zn_xTe$

A.K. Wahi, C.K. Shih, I. Lindau, and W.E. Spicer

Stanford Electronics Laboratories
Stanford University, Stanford, CA 94305

The chemical and structural properties of the zinc blende semiconductor alloy $Hg_{1-x}Zn_xTe$ are of interest since it has important potential as a substitute for $Hg_{1-x}Cd_xTe$ in IR detection. In $Hg_{1-x}Cd_xTe$, the weak Hg-Te bond contributes to the poor mechanical properties and the instability of Hg in the lattice. Theoretical predictions [1] and initial experimental evidence [2,3] indicate that substitution of Zn for Cd in the lattice will improve structural properties. Comparitive studies of the surface chemistry and structural (stoichiometric) effects in the near surface region of $Hg_{1-x}Zn_xTe$ should provide more insight into the influence of Hg-bonding on the lattice stability of Hg-based alloys. Studies performed in parallel on related alloys such as $Cd_{1-x}Zn_xTe$ and the relevant binary compounds (e.g., HgTe) provide important reference systems to investigate compositional effects.

OXIDATION OF $Hg_{1-x}Zn_xTe$, HgTe, AND $Cd_{1-x}Zn_xTe$

Comparitive studies of oxygen uptake on the (110) surfaces of $Hg_{1-x}Cd_xTe$, HgTe, and CdTe have been published by Silberman *et al.* [4,5] In these studies, oxygen uptake was activated by oxygen exposure with a hot filament in direct line of sight of the sample surface. Depletion of Hg in the near-surface region occurred during oxide film growth. A correlation was also found between the rate of uptake and the bulk Hg concentration, suggesting the importance of breaking the Hg-Te bonds during oxide formation. Extension of these studies to $Hg_{1-x}Zn_xTe$ and $Cd_{1-x}Zn_xTe$ was undertaken in December. Preliminary results reveal aspects of the oxygen chemistry in these alloys and of the kinetics when excited oxygen is used. Uptake of oxygen is indicated by the onset of O2p emission in the valence band, and later by the emergence of an oxidized Te component in $Hg_{1-x}Zn_xTe$ and $Cd_{1-x}Zn_xTe$. In $Hg_{1-x}Zn_xTe$, the Hg/Zn ratio decreases concurrent with uptake. $Cd_{1-x}Zn_xTe$ was found to oxidize more readily at a lower filament temperature than did $Hg_{1-x}Zn_xTe$ and HgTe. Oxygen uptake rate exhibited a strong dependence on filament temperature. Increased filament temperatures result in oxygen uptake with the sample out-of-line of sight of the hot filament. In the present study, oxygen uptake was not found to be linear with time. Further investigation into the chemistry which occurs, and comparison with the oxidation behavior of $Hg_{1-x}Cd_xTe$ is necessary. Further study may also be necessary to determine the dependence of oxidation kinetics on parameters affecting production of the excited oxygen.

PHOTOIONIZATION CROSS SECTION OF Hg5d, Zn3d, Cd4d

The photon energy dependence of the Hg5d and Zn3d photoionization cross sections was experimentally established using the Synchrotron source. In studies using a He discharge lamp (photon energy 21.2 eV) it was found that the Zn3d level emerges with the $Hg5d_{3/2}$ core level, inhibiting detection of chemical information associated with Zn. Using the tunability of the Synchrotron source, it is possible to separate the Zn3d contribution by minimizing Hg5d emission. This capability is crucial to studying the chemical properties of $Hg_{1-x}Zn_xTe$. It was found that

1. The photoionization cross section of the Hg5d level is decreased substantially between 150 eV and 180 eV photon energy while that of Zn3d is still sufficiently high.

2. The photoionization cross section of Cd4d is decreased substantially between 130 eV and 150 eV photon energy. The Zn3d signal can be well separated from Cd4d at these photon energies.

This work was supported by NASA under Contract No. NAS 1-18232.

REFERENCES

1. A. Sher, A.-B. Chen, W.E. Spicer, and C.-K. Shih, J. Vac. Sci. Technol. A 3 (1) (1985).
2. E.F. Skelton, S.B. Qadri, A.W. Webb, M.W. Schaefer, J. Dinan, D. Chandra, and L. Columbo, Proc. 1986 HgCdTe Workshop.
3. Ariel Sher, D. Eger, and A Zemel, Appl. Phys. Lett. **46**, 59 (1985).
4. J.A. Silberman, D. Laser, I. Lindau, and W.E. Spicer, J. Vac. Sci. Technol. B **2**, 589 (1984).
5. J.A. Silberman, D. Laser, I. Lindau, W.E. Spicer, J.A. Wilson, J. Vac. Sci. Technol. A **3**, 222 (1985).

THERMAL OXIDATION OF GaAs: A STUDY OF OXIDE MORPHOLOGY

Proposal 935Vp

T. Chiang, D. J. Friedman, G. Carey, K. A. Bertness, I. Lindau, and W. E. Spicer
Stanford Electronics Laboratories
Stanford University, Stanford, CA 94305

Recently there has been a resurgence of interest in the morphology of oxide growth on GaAs surface during the initial stage of oxidation and the results have been controversial. The photoemission study by Landgren et al. [1] suggests that the oxide grows nonuniformly in depth with substantial subsurface oxidation. The oxide is best characterized by patches covering a third of a monolayer but extending over ten layers deep. This view is challenged by another photoemission study undertaking by Bertness et al. [2]. That study suggests the oxide grows uniformly, so initial oxidation of GaAs produces an oxide layer of uniform thickness from the first monolayer on up. These two views appear difficult to reconcile, but recent study of the initial stage of thermal oxidation of Si [3] suggests that high temperature oxidation produces nonuniform oxide growth while room temperature oxidation produces uniform oxide growth. Therefore it is interesting to find out if GaAs oxidation behaves in a similar manner as Si oxidation. Synchrotron radiation is the ideal experimental tool to use because the tunable radiation allows one to probe differing depths of the GaAs substrate.

Because GaAs is a compound semiconductor, both Ga and As oxides are formed. As expected, the rate of oxide growth is different for Ga and As. However, it is surprising to discover the As oxide grows in a uniform manner regardless of the exposure temperature. It is harder to resolve out the Ga oxide peak and hence more difficult to follow the Ga oxide growth, but preliminary results suggest the Ga oxide also grows in a uniform manner regardless of the exposure temperature.

[1] G. Landgren et al., J. Vac. Sci. Technol. **B 2**, 351(1984).
[2] K. A. Bertness et al., J. Vac. Sci. Technol. **B 4(4)**, 1102 (1986).
[3] M. Tabe et al., Phys. Rev. B **34**, 2706 (1986).

* This work was supported by the U.S. Office of Naval Research and the U.S. Defense Advanced Research Projects Agency under Contract No. N00014-83-K-0073.

CHEMICAL REACTION AND SCHOTTKY BARRIER FORMATION AT Ti/InP (110) AND Sn/InP (110) INTERFACES: REACTIVE VERSUS NONREACTIVE INTERFACE

T.Kendelewicz, P.H. Mahowald, C. E. McCants, K. A. Bertness, I. Lindau, and W. E. Spicer

Stanford Electronics Laboratories, Stanford University, Stanford, CA 94305

Extensive core level studies of the metal/InP interfaces show that, in general, most of the metallic overlayers react strongly and in a complicated fashion with the InP surface. For transition metal interfaces, the reactions are so profound and complicated that it is difficult to separate the band bending from the chemical shifts [1]. This questions the utility of the photoelectron spectroscopy in Schottky barrier studies. Fortunately, for these interfaces the surface becomes pinned for coverages as low as a fraction of a monolayer, where chemical shifts and band bending can be separated [1,2]. At the other extreme, it is very difficult to find metal which does not react with the InP surface and is growing in a laminar fashion. The later requirement is necessary if one wants to avoid problems with nonuniform pinning possibly causing different pinning levels for n- and p-type crystals. In this work [3], we were able to select such metal-Sn which is not only a little reactive but also forms a uniform overlayer, at least for the first two atomic layers. This is concluded from the exponential decrease of the In 4d and P 2p core level intensities with the escape depth of 3 Å. The surface Fermi level is pinned for both types of doping well at 0.4 eV below the conduction band minimum (CBM) at coverages below 1 ML of Sn. The other part of this study considered a typical reactive Ti/InP interface with complicated morphology. It is shown that the reaction with the InP surface is very strong starting at submonolayer coverages of Ti. A Ti-In alloy (In dispersed in the Ti overalyer) of changing composition and two phases of phosphide are formed [4]. The type of reaction is in many respects similar to that observed on the Ti/GaAs. The pinning at 0.3 eV below the CBM is established at the coverage of 0.5 Å.

It is interesting to compare the pinning behavior of these two different interfaces from the point of view of general models of the Schottky barrier formation. Recently, Ludeke [5] proposed the importance of transition metal derived levels in the pinning at the transition metal/GaAs interfaces. This model can be extended to the similarly behaved Ti/InP interface. However, both of the studied interfaces show such remarkable similar pinning patterns (pinning at the similar level at submonolayer coverages) that one is forced to conclude that metal independent interface states provide a more general understanding of the Schottky barrier formation. However, the role of impurity induced states can be in some cases important.

REFERENCES

1. T. Kendelewicz, N. Newman, R. S. List, I. Lindau, and W. E. Spicer, J. Vac. Sci. Technol. B3, 1206 (1985).
2. T. Kendelewicz, R. S. List, K. A. Bertness, M. D. Williams, I. Lindau, and W. E. Spicer, J. Vac. Sci. Technol. B4, 959 (1986).
3. For details, see T.Kendelewicz, P. H. Mahowald, C. E. McCants, K. A. Bertness, I. Lindau, and W. E. Spicer, Proceedings of 14th PCSI Conference, to be published in J. V. S. T.
4. J. Nogami, T. Kendelewicz, I. Lindau, and W. E. Spicer, Phys. Rev. B 34, 669 (1986), and literature therein.
5. R. Ludeke, and G. Landgren, Phys. Rev. B33, 5526 (1986); R. Ludeke, D. Straub, F. J. Himpsel, and G. Landgren, J. Vac. Sci. Technol. A4, 874 (1986).

CHEMICAL AND ELECTRONIC PROPERTIES OF THE Pt/GaAs(110)INTERFACE

C. E. McCants, T. Kendelewicz, K. A. Bertness, P. H. Mahowald,
M. D. Williams, R. S. List, I. Lindau, and W. E. Spicer

Stanford Electronics Laboratories
Stanford University, Stanford, CA 94305

The near-noble transition metal Pt is an excellent candidate to test models of Fermi-level pinning and examine the role of interfacial chemistry in Schottky barrier formation. In addition to its technological importance as a diffusion barrier metal in Schottky and "ohmic" contacts and use in silicides, Pt is isoelectronic with Pd which should allow for comparisons between the influence of the d-electrons in the Fermi-level pinning and in determining chemical trends in moving down the periodic table. Also, its high electronegativity makes Pt attractive to test the charge transfer correction to the Unified Defect Model [1,2].

In this work, we present the results of bulk- and surface-sensitive core level and valence band studies of the Pt/GaAs interface. Detailed curvefitting analysis is employed to elucidate the room temperature chemistry at and near the interface by separating band-bending shifts from reacted species in the core level spectra. The interfacial chemistry is compared with that seen for other metals which yield a high barrier height on n-GaAs, and the pinning behavior evaluated in terms of current models for Schottky Barrier formation.

The surface sensitive Ga3d spectra remain relatively unchanged during the initial metal depositions. No appreciable changes in either the width or area are observed between 0 and 0.67 ML. The peak then appears to shift smoothly towards lower binding energy (BE) at coverages >1 ML due to the attenuation of the substrate contribution and an increase in a reacted component. The overall width of the peak decreases between 0.13 and 3.33 ML but has still increased from the value for the clean spectrum, suggesting a change in bonding environment. The final energy position of this reacted peak is ~0.4 eV to lower binding energy relative to Ga in GaAs.

Bulk-sensitive Ga 3d spectra taken at hν=32 eV confirm the chemical trends observed for the surface-sensitive case. The first deposition shows a sharpening of the spectra due to the removal of any inhomogeneties in initial pinning; subsequent depositions show little change in the lineshape until a coverage of 1.33 ML. It appears that this coverage represents the threshold for the Pt-Ga reaction as seen at this photon energy. The width of the peak increases at 3.33 ML, and the reaction becomes more pronounced between 6.67 and 13.3 ML with a noticeable decrease in the substrate emission and an increase in emission on the high KE side. At 20 ML, all that remains is this shifted component at an energy 0.37 eV to lower binding energy than the substrate Ga, which agrees well with the surface-sensitive spectra. It appears that almost all of the observed Ga is in this single bonding configuration as there is little evidence of unreacted, i.e., elemental Ga. Analysis of attenuation vs. thickness plots for the substrate contributions shows an exponential dependence for both the bulk- and surface-sensitive cases. Thus, the overlayer growth mode appears to be uniform with little evidence of islanding.

The As 3d shifts smoothly to lower KE as the overlayer thickness is increased, beginning at submonolayer coverages. This suggests that As is being liberated from the lattice and beginning to react with the Pt. We observe an increase in emission on the low kinetic energy side of the peak for the initial coverages of 0.13 and 0.67 ML. This emission becomes more pronounced between 0.67 and 3.33 ML, corresponding to a decrease in the substrate component as evidenced by a slight shift to higher binding energy of the high KE side of the component. Similar to the Ga, the FWHM also decreases steadily with a "plateau" between 0.67 and 3.33 ML before the final decrease to the minimum value. This again suggests changes in the bonding environment of the As at these coverages. The final energy position is 0.3 eV to higher binding energy which is near the value for elemental As [3]. Although the sharpening of the spin-orbit splitting appears to indicate two distinct As *compounds*, curvefitting shows that one component is sufficient to explain the results.

The Ga peak is decomposed into a slowly increasing reacted component and a decreasing substrate contribution. This reacted component is apparent at 0.67 ML; fitting with one component yielded a high residual, and thus a two component fit is used. The FWHM of the reacted component increases between 0.67 and 1.33 ML, suggesting Ga bonding with the Pt. The reacted component shifts slightly to lower binding energy between 0.67 and 1.33 ML and is fairly constant for higher coverages. The subsequent decrease in the FWHM of this component occurs at coverages for which the stabilizing in the final observed binding energy occurs, which suggests a Pt-Ga alloy with a definitive stoichiometry. Calculations performed by Nogami et. al. [4] predict a shift of 0.30 eV to lower binding energy with respect to Ga in GaAs for the dilute limit of Ga in Pt; our data, which show a shift of 0.37, eV agree well with this prediction. This differs from transition metals such as Ti, Cr and V which show a continuous shift to lower binding energy of the reacted Ga 3d towards dilution in the overlayer matrix without establishing a definite energy position before the Ga signal is completely attenuated [5,6]. Since no evidence for unreacted or elemental Ga is observed, and given the agreement in the reacted peak energy between the surface-sensitive and bulk-sensitive data, it appears that the alloy is located near the Pt/GaAs interface. For overlayer thicknesses $\theta \geq$ 6.67 ML, the reacted Ga 3d is modeled with a single component modified by a Doniach-Sunjic parameter of 0.12, which gives good agreement to the raw data. We thus note that Ga in a Pt-Ga alloy dominates at 3.33 ML and the higher coverages studied.

The As chemistry is more complicated than that seen for the Ga and suggests the formation of two Pt-As reaction products--one at a higher binding energy and one at a lower binding energy . For the initial coverages (< 2 ML), one of the reacted components overlaps with the substrate component and the other overlaps with the "surface" component, which must be accounted for when performing the deconvolution. At 0.13 ML, the lower BE contribution is the sum of the fading surface component and the first reacted component. We assume the same decrease in the As substrate contribution from the results of the attenuation vs. thickness profile observed for the substrate Ga component. Thus, at 0.67 ML, the higher BE component is a combination of the substrate contribution and a second As reacted component. By 1.33 ML, the lower BE component is a purely reacted phase, and the second reacted component has shifted slightly to higher binding energy. The final energy position ~0.3 eV to higher binding energy suggests elemental As; however, for these highest coverages, curvefitting shows very good results using a single component modified with a Doniach-Sunjic parameter of 0.12. This leads us to believe that the observed compound becomes more As rich, as fitting with two components yields a very broad component (FWHM >1.0 eV) which did not seem physically meaningful. There is also an increase in the As to Ga intensity ratio for coverages higher than 3.33 ML, as this single bonding configuration dominates at these coverages. The data from the initial stages of interface formation suggests that the observed As diffuses easily through the overlayer to react with the Pt near the overlayer surface.

From this core level data, we believe that the interface consists of a Pt-Ga alloy located near the metal/semiconductor interface, followed by the first Pt-As compound and then the second Pt-As compound. The steady increase in the As to Ga intensity ratio leads us also to believe that ternary $Pt_xGa_yAs_z$

compounds are not important in describing properties of the interface.

In conclusion, we have found that a combination of charge transfer and chemical reactions occur at the Pt/GaAs interface, with charge transfer effects dominating. Core level analysis shows a Pt-Ga alloy with a well defined binding energy 0.4 eV to lower binding energy located near the metal/semiconductor interface. This Ga chemistry is similar to that seen for Au and Cu overlayers. Pt also reacts with the As, forming two $PtAs_x$ compounds, one of which appears to be As moving towards elemental As. The alloy layer appears to be nearest the interface, followed by the two Pt-As compounds, and finally the metallic Pt. The high Schottky barrier of 0.83 eV on n-type and 0.48 eV on p-type substrates are, within experimental error, in good agreement with those observed for the noble metals Au, Ag, and Cu, and for the transition metal Pd. Comparisons with the rare-earth metal Gd and the transition metals Ti and Cr confirm the agreement with the charge-transfer correction to the UDM [1,2] and imply that there are two pinning levels for GaAs. Further studies are planned to characterize the effects of annealing on the Schottky barrier height.

REFERENCES

1. W. E. Spicer, S. Pan, D. Mo, N. Newman, P. Mahowald, T. Kendelewicz, and S. Eglash, J. Vac. Sci. Technol. B **2**, 476 (1984).

2. W. E. Spicer, N. Newman, T. Kendelewicz, W. G. Petro, M. D. Williams, C. E. McCants, and I. Lindau, J. Vac. Sci. Technol. B **3**, 1178 (1985); N. Newman, W. E. Spicer, T. Kendelewicz, and I. Lindau, J. Vac. Sci. Technol. B **4**, 931 (1986).

3. P. Skeath, I. Lindau, C. Y. Su, and W. E. Spicer, Phys. Rev. B **28**, 7051 (1983).

4. J. Nogami, T. Kendelewicz, I. Lindau, and W. E. Spicer, Phys. Rev. B **34**, 669 (1986).

5. M. Grioni, J. J. Joyce, and J. H. Weaver, J. Vac. Sci. Technol. A **4**, 965 (1986).

6. M. D. Williams, T. Kendelewicz, R. S. List, N. Newman, C. E. McCants, I. Lindau, and W. E. Spicer, J. Vac. Sci. Technol. B **3**, 1202 (1985).

THE Si/GaAs (110) HETEROJUNCTION: STRAIN, DISORDER, AND VALENCE BAND DISCONTINUITY

R. S. List, J. C. Woicik, I. Lindau, and W. E. Spicer

Stanford Electronics Laboratories
Stanford University, Stanford, CA 94305

The effects of strain in thin heterojunction overlayers and superlattices have recently gained a great deal of experimental and theoretical interest [1,2]. Specifically, modifications of the strain in the overlayers are thought to change the band offsets and thereby give the electronic device designer an important new degree of freedom. We have studied such effects through a combined photoemission and polarization dependent surface extended x-ray absorption fine structure (SEXAFS) study of thin Si overlayers on the 4% lattice mismatched GaAs (110) substrate. By selectively orienting the heterojunction interface either parallel to or perpendiculat to the x-ray polarization vector, we have independently measured from SEXAFS the Si-Si nearest neighbor bond lengths of bonds lying either in the plane $r_{\parallel}$ or out of the plane of the interface $r_{\perp}$, respectively. The in plane bond lengths were larger by a maximum of 2%. An ideal pseudomorphic overlayer would have a 4% difference between these bond lengths. Near edge x-ray absorption fine structure and low energy electron diffraction were also monitored to characterize the crystalline perfection of the overlayers. Modifications of the growth temperature allowed us to vary the strain in the overlayer and to study the kinetics of epitaxial growth and dislocation formation. Surprisingly, we found no resolvable (>0.05 eV) differences in the valence band discontinuity between Si overlayers which were either crystalline and 2% anisotropically strained, crystalline and unstrained, or amorphous and unstrained. It is important to note that the ideal pseudomorphic calculations do not include the effects of dislocations which were present in large densities at all our interfaces.

This work was supported by the Defence Advanced Research Projects Agency and the Office of Naval Research under Contract No. N00014-83-K-0073. The SEXAFS and NEXAFS experiments were performed on the Jumbo beamline at SSRL.

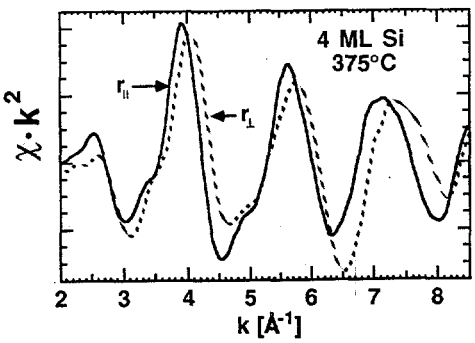

Fig. 1. Polarization dependent SEXAFS spectra for a 4 ML Si overlayer grown at 375°C on the GaAs (110) substrate. $r_{\perp} \Leftrightarrow \hat{\varepsilon} = [110]$ and $r_{\parallel} \Leftrightarrow \hat{\varepsilon} = [1\bar{1}0]$.

REFERENCES

1. D. V. Lang, R. People, J. C. Bean, and A. M. Sergent, Appl. Phys. Lett. 47, 1333 (1985).
2. C. G. Van de Walle and R. M. Martin, J. Vac. Sci. Technol. B 4 (4), 1055 (1986).
3. R. S. List, J. Woicik, P. H. Mahowald, I. Lindau, and W. E. Spicer, J. Vac. Sci. Technol. A, July/August (1987), in press.
4. R. S. List, J. C. Woicik, I. Lindau, and W. E. Spicer, Proceedings of the 14th Physics and Chemistry of Semiconductor Interfaces Conference, January 1987, Salt Lake City, Utah.

THE Ge/InP HETEROJUNCTION

P.H. Mahowald, T. Kendelewicz, and W.E. Spicer

Stanford Electronics Laboratories
Stanford University, Stanford, CA 94305

During this time period, we studied the heterojunction formed when Ge is deposited on an atomically clean, cleaved InP(110) sample. We found that when the Ge is deposited at 280°C, the Ge overlayer valence band is 0.65 ± 0.1 eV higher than that of the InP substrate. This result is in agreement with results previously performed at 20°C (Katnani *et. al.*). The surface Fermi level position is 0.5 ± 0.1 eV below the InP conduction band minimum.

Both of these results rely on the identification of the bulk component of the substrate core levels. Surface shifts occur in the core level energy for substrate atoms near the surface, where the Madelung potential is different from in the bulk. Also, when Ge is deposited, In is freed from the substrate and forms islands of metallic indium on the surface. The surface shift and the chemically shifted indium must be identified to obtain the bulk band bending. Since these components can never be fully resolved, the data must be curve-fitted to an idealized lineshape which then yields the energy and intensity of the shifted components. During this time period, improvements were made to the computer programs used for this function.

The interface was formed at 20°C also, and we found that, although roughly the same amount of In was released from the substrate during overlayer growth, less could intermix with the overlayer because of the lower temperature and more was surface segregated into islands on the surface. The overlayer was less compensated by the indium and consequently heavily doped n-type by the P from the substrate. The doping was heavy enough that the band bending of the substrate-interface region was modified. Furthermore, the metallic indium at the surface had significant photoemission intensity up to the Fermi level which obscured the valence band maximum and made the valence band discontinuity value unavailable for the 20°C growth.

Previous researchers may have missed the excess indium which tends to have compensating effects on the core levels and the valence band maximum, so that the final result for the valence band discontinuity is about the same. When we analyze our data in the same way that we believe they analyzed theirs, we obtain the same answer as they do. However, the correct analysis cannot be performed at 20°C, because the excess indium obscures the valence band maximum.

At both temperatures, the Ge overlayer grows in a laminar fashion up to 2 ML. At higher coverages, islands of metallic indium form, especially when the deposition is performed at 20°C. For 15 ML of Ge coverage, there is only 10% of the substrate atom concentration near the surface, which is almost unchanged for 20°C and 280°C depositions, and the indication is that Ge would be a good encapsulant for InP.

REFERENCES

1. P.H. Mahowald, T. Kendelewicz, K.A. Bertness, C.E. McCants, M.D. Williams, and W.E. Spicer, submitted to PCSI-14 Proceedings, J. Vac. Sci. Technol.

2. A.D. Katnani and G. Margaritondo, Phys. Rev. B **28**, 1944 (1983).

Oxidation Study of Au/Si Interface at Room Temperature

J. - J. Yeh, R. Cao, J. Hwang,
H. Nakamura, and I. Lindau

Stanford Electronics Laboratories,
Stanford University, Stanford, CA 94305

The role of Au atoms on the Si surface during RT Si oxidation process has been investigated by exposing different Au/Si interfaces, ordered or non-ordered, to a wide range of O_2 exposures at RT. In this case, Si oxidation can be conducted through a different channel from its normal oxidation process by introducing Au atoms to the Si surface; this study also offers a different view to the Si oxidation mechanism on a microscopic scale. Four different Au thicknesses, 20 ML, 4 ML, 1ML, and 0.5 ML, corresponding to four different Au/Si interface structures and also different Au-Si bonding relations, are exposed to molecule O_2 from 10^2 L to 10^{10} L. Oxidation of a $\sqrt{3} \times \sqrt{3}$ (R 30°) 1 ML Au covered Si surface was also studied to compare whether the atomic arrangement of Au atoms on the Si surface has any significant effect in the Si oxidation process.

The oxidation results obtained here can all be interpreted by the Au/Si interface model proposed from the study of Au/Si interface at different Au coverages. Experimental evidence obtained in this experiment does not agree with a previously proposed Au/Si interface model which requires a minimum amount of Au atoms to perturb the Si substrate in order to alter the Si oxidation behavior [1]. The passivation [2] of a Si surface to oxidation by an ordered Au layer on the Si(111) surface with a $\sqrt{3} \times \sqrt{3}$ (R 30°) surface reconstruction is found to be an artifact arising from the low sensitivity to the surface oxide formation in that experiment.

A systematic study has been conducted on the oxidation behavior of the Si surfaces with different Au coverages that covers most of the Au/Si interface structures, where each surface is characterized by different Au-Si bond formations and/or Au-Si atomic arrangements. Oxygen exposures from 10^2 L O_2 to 10^{10} L O_2 on the 20 ML, 4 ML, 1 ML and 0.3 ML Au covered Si surfaces have shown that the Au-Si bonding has a strong effect on the Si oxidation at RT. The Au-Si bond is a barrier at the initial stage of oxide formation. After the initial oxide is completed, oxygen atoms can break the covalent bonds easier between oxidized Si atoms and next unoxidized Si atoms easier if the unoxidized Si atoms have already bonded to Au atoms. The Au-Si bonding weakens the Si-Si bond and therefore facilitates further oxide formation. This is why even a 0.3 ML Au covered surface can have thicker oxide than the clean Si surface. This is also the case for 1 ML Au/Si surface with or without $\sqrt{3} \times \sqrt{3}$ (R 30°) surface reconstruction and both surfaces oxidized in a similar manner with only a small difference at low O_2 exposures.

During the oxidation process, Au-Si bonding are broken when oxide is formed regardless of the different Au-Si bonding strengths and concentrations. Si outdiffusion effect has been proposed to explain the increase of the total Si signal on the oxidized Au/Si surfaces with Au coverages not less than 1 ML. No evidence indicates that Au dissociates oxygen molecules during the formation of Si oxide. Oxide creates smaller band bending on the 1 ML Au/Si surfaces than on the 0.3 ML Au/Si surface. It is proposed that Si surface band bending is determined by the areas of oxide and Au occupy on the Si surface.

1. A. Hiraki, Surf. Sci. Rep. **3**, 357 (1984).
2. A. Cros, F. Houzay, G. M. Guichar,and R. Pinchaux, Surf. Sci. Lett. **116**, L232 (1982).

High Temperature Annealing Study of Au/Si Interface

J. - J. Yeh, R. Cao, D. Friedman,
K. Bertness, and I. Lindau

Stanford Electronics Laboratories
Stanford University, Stanford, CA 94305

The Au-Si chemical bonding properties and the kinetics of Au/Si interface growth upon high temperature annealing (≥ 700 °C) were studied by photoemission spectroscopy (PES). High resolution Si 2p and Au 4f core level spectra shows that (sub)monolayer Au on Si(111) surface is very stable. The Au/Si interface morphology after annealing was also studied by tuning the probing depths in PES. It was found that at such a temperature Au islanding is negligible and Au diffusion is the major mechanism which occurred at the Au/Si interfaceBecause of the earlier interest in studying the stability of the Au/Si interface for possible semiconductor applications, there were many elevated temperature annealing studies with general surface study tools like AES and LEED. The common features of these tools are the high sensitivities to Au/Si surface composition or ordering but low or no sensitivity to Au-Si chemical shifts. Because the low resolution makes the studies uncertain about the details of the Au-Si bonding and the limited surface sensitivity makes it difficult to evaluate the loss of Au atoms on the Si surface after annealing, experimental results from these studies therefore created some contradictory conclusions like the existence of the critical thickness for Au film interaction with the Si(111) surface, but that the inert Au layer can remain on the Si surface up to 800 °C.

High resolution Si 2p core level spectra and Au 5d VB spectra have shown that Au and Si exhibit very stable chemical bonds for Au coverage not higher than one monolayer on the Si(111) surface. On a Si(111) - 7 × 7 surface, a (sub)monolayer amount of Au deposited at RT does not perturb the 7 × 7 structure to a great extent so that the 7 × 7 feature (a - 4 eV peak in VB spectra) can still exist. Annealing of this surface has only a minor effect on the Au-Si bonding relation because the Si 2p lineshape and Au 4f spectra are very similar. The Si 7 × 7 structure was preserved after annealing for Au coverage up to 0.5 ML, where the surface has shown 5 × 1 and $\sqrt{3} \times \sqrt{3}$ (*R* 30°) LEED patterns. This structure was removed if Au coverages are 1 ML or higher on a Si(111) - 7 × 7 surface, because the Au 5d's Cooper minimum spectra shows no more Si substrate structure, the same as a 2 × 1 surface. Considering that, when more Au atoms are deposited on the Si surface, the deeper the Au atoms are expected to distort the Si substrate. This -4 eV peak structure is therefore attributed to the formation of a deep lying stacking fault when a Si(111) - 2 × 1 surface transforms into a 7 × 7 surface.

Annealing results of multimonolayer Au on the Si(111) surface show no dependence on the initial Si surface reconstructions. For 1 ML, 6 ML, and 20 ML Au/Si surfaces investigated here, all of the annealed surfaces have the same spectra as that of an as-deposited 1 ML Au on the Si(111) - 2 × 1 surface. The high Au diffusivity in Si makes Au diffusion the most probable mechanism to account for the loss of Au upon annealing. Island formation was considered negligible in this case from the analysis of Au 4f intensities measured from 170 eV and MgKα x-ray source. Au desorptions were also excluded because the temperature 700 °C used was shown not to desorb a measurable amount of Au atom [2]. Compared with the other types of bondings Au may have on the multimonolayer Au/Si surface, Au atoms in the 3-hollow sites form the most stable bonds with their neighboring atoms, the surface Si(111) atoms.

Although annealing of (sub)monolayer Au on the n-Si(111) surface has only minor effects on the Au-Si bonding, the Si surface Fermi level pinning positions are strongly affected. Annealing on a n-Si surface with (sub)monolayer Au tends to pin the Fermi level closer to the valence band but further RT Au deposition will move the Fermi level towards the midgap. Continuous deposition/annealing cycles at low Au coverage therefore induce an oscillatory behavior in the change of the Fermi level pinning positions. Since the Au-Si bonding structures are similar in spite of annealing for Au coverages not higher than 1 ML, this behavior is probably controlled by Au-Au interaction but not Au-Si interaction nor the surface ordering.

1. K. Okuno, T. Ito, M. Iwami, and A. Hiraki, Solid State Commun. **34**, 493 (1980).
2. G. Le Lay and J. P. Faurie, Surf. Sci. **69**, 295 (1977).

3d and 4d photoionization cross section: two studies on Cr and Mo

E. Puppin, Z. X. Shen, I. Lindau
Stanford Electronics Laboratories
Stanford University, USA
B. B. Pate
Jet Propulsion Laboratories, USA
I. Abbati, L. Braicovich
Istituto di Fisica
Politecnico di Milano, ITALY

During 1986 we performed two experiments on beam line 1-I (new grasshopper) in order to study the solid state effect on the photoionization cross section of d-type valence electron in two refractory metals: Mo and Cr.

1) Mo

We have already shown a dramatic effect in the comparison of the cross section of 4d electrons in metallic Mo with the calculated values for the isolated atom [1]. This effect is due to the distortion of the atomic orbitals during the formation of the solid. In this respect an interesting case is encountered when small aggregates of atoms are formed.

This investigation has been done on Mo islands grown at liquid nitrogen temperature on an Al substrate. These islands are 2-3 ML thick i.e. they have a high fraction of surface atoms [2].

Fig. 1shows the cross section we measured for islands compared with the calculated atomic cross section [3](solid line). It is evident that, in the limit of the experimental accuracy [4], there is no difference with respect to the isolated atom. This is despite the fact that the photoemission spectra are closely related to those from bulk Mo [2].

2) Cr

The results for bulk Cr are given in fig. 2. The solid line refers to the isolated atom. It should be observed that in this case the relative minimun observed for Mo is not present in the Cr 3d cross section. This is due to the absence of nodes in the radial wave function (Cooper effect) [5]. It is interesting to observe that the cross section does not change (inside the experimental accuracy) moving from the isolated atom toward situation in which the 3d electrons are deeply involved in the formation of the chemical bond.

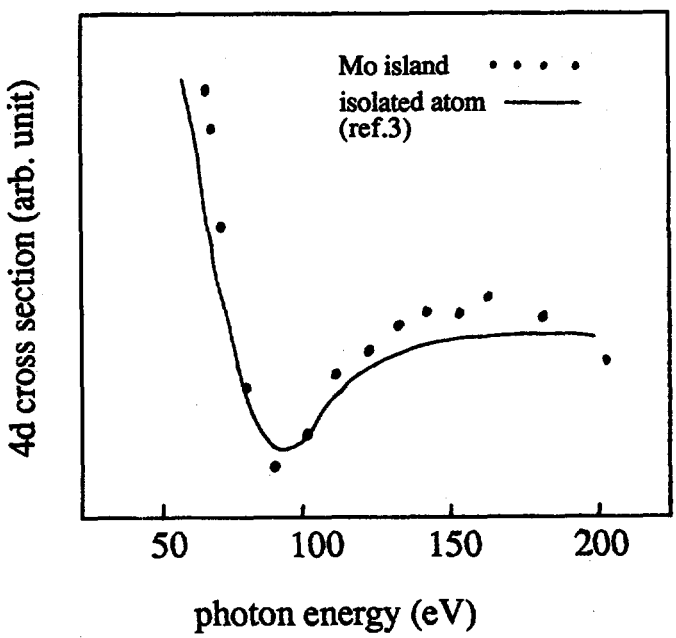

Fig.1: Mo 4d cross section vs. photon energy (exp. points) compared with the calculation (ref.3)for the isolated atom (solid line).

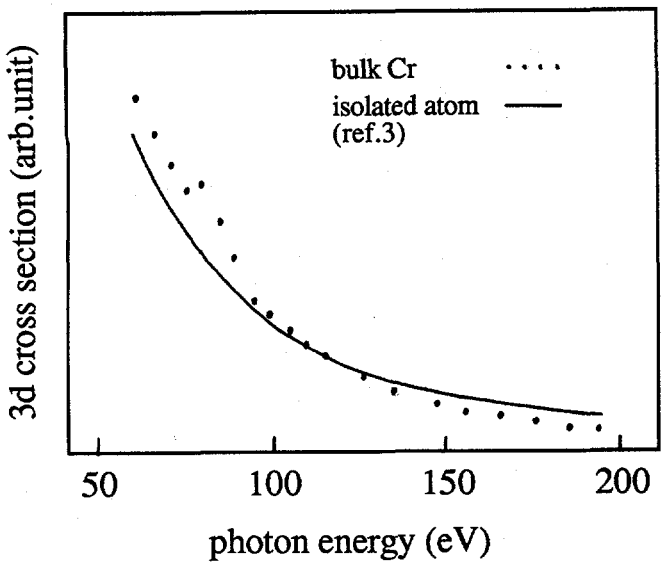

Fig.2: Cr 3d cross section vs.photon energy (exp. points) compared with the calculation (ref.3) for the isolated atom (solid line).

In the first Born approximation the photoionization cross section is related to the Fourier transform of the wave function. Our results therefore indicate that in Mo islands and in Cr metal the d-electrons participate in the formation of the chemical bond without suffering relevant modification in the wave function. In Mo islands this is probably related to the high fraction of surface and subsurface atoms for which the orbital distortion can be smaller compared to the bulk. This result is relevant for cluster physics and is at present under discussion.

REFERENCES

1 I.Abbati *et.al.* Phys. Rev. Lett. **50**,1799(1983)
2 L.Braicovich *et.al* Phys.Rev.B **34**,4398(1986)
3 J.J.Yeh, I. Lindau, At.Data Nucl.Data Tables **32**,1(1985)
4 U. Del Pennino *et.al.* J.El.Spec.and Rel.Phen. **37**,389(1983)
5 J.W.Cooper, Phys.Rev.Lett.**13**,762(1964).

The Silicon-rare earths interaction: interfaces and bulk compounds studied with photoemission spectroscopy

E. Puppin, Z. X. Shen, I. Lindau
Stanford Electronics Laboratories
Stanford University, USA
B. B. Pate
Jet Propulsion Laboratories, USA
I. Abbati, L. Braicovich
Istituto di Fisica
Politecnico di Milano, ITALY

During the last year a considerable amount of data has been collected using the monochromatic light from beam-lines 1-I and 3-I (grasshopper monochromator). We summarize our activity distinguishing between studies on bulk silicides and Si/RE interfaces. For reasons of space we cannot show specific results that will be published in several different papers.

BULK SILICIDES

The research on the rare earth silicides has been centered on the measurement of the photoemission spectra from the whole set of silicides of the Gd-Si phase diagram. The Gd silicides measurements are the first investigation on a RE silicides in which the valence states are directly observable taking advantege of the fact that the 4f signal is about 7 eV below the Fermi level. It has been possible for the first time to assess clearly the contribution of the 5d states to the chemical bond. In particular the shift of the 5d emission to higer binding energies due to the hybridization with the Si p states is particularly evident. The effect is strongly dependend on the stoichiometry and the shift of the d-contribution increases for increasing Si content. This analisys is complementary to the one of Yb silicides where the effect of the chemical bond on the Yb valence fluctuation has been studied and compared with the situation at the interfce [1-4]

INTERFACES

In the field of interfaces three research lines have been followed.

(i) The result on the Gd silicides have been used in conjunction with old and new results on the Si-Gd interface at room temperature. This allows the calibration of the composition of the interface reaction compounds. A rather close correlation with the silicides is found and the first silicides-like compound that forms is related to GdSi (to be published in the PCSI 87 proceedings).

(ii) Photoemission spectroscopy of the Si-RE interfaces grown at liquid nitrogen temperature. This new research can be very useful to elucidate the relative importance of several different growth mechanisms. In particular the new interesting result is that both Si-Yb and Si-Gd interfaces are reactive also at low temperature although the amount of reacted silicon (easily observable in the Si 2p lineshape) is much lower than at RT. The reacted component is observed also at coverages higher than 1monolayer. Since the attenuation of the reacted component is not exponential this means that a true reaction is going on. A clear understanding of the impact of this new results on the knowledge of the interfaces growth requires further investigations and a great effort will be devoted in the future to the interface spectroscopy at low temperature. It is however clear that we have to consider in the discussion also the role of not thermally activated mechanisms.

(iii)The systematic of the Si-RE interfaces grown at room temperature. During 1986 the Si-La interface has been studied. This study adds to the other already published on Si-Yb[1-4],Si-Gd[5],Si-Eu[6]. A wide set of data is now available in order to understand the general feautures of the Si-RE interaction at RT ranging from a system with no 4f-electrons (La) up to Yb where the 4f shell is filled.

REFERENCES

1 L. Braicovich *et al.*, Surf. Sci. **168**, 193 (1986).
2 I. Abbati *et al.*, Phys. Rev. B **34**, 4150 (1986).
3 In press in Sol.St.Comm.
4 Also in press in Sol.St.Comm.
5 C. Carbone *et al.*, JVST **A 3**, 972 (1985).
6 J. Nogami *et al.*, Proceedings 17 Int. Conf. Phys.Semic. (Springer, New York 1985).

Mixed valence behavior in two families of Yb compounds: a NEXAFS study

E. Puppin, Z. X. Shen, I. Lindau
Stanford Electronics Laboratories
Stanford University, USA
M. Sancrotti, I. Abbati
Istituto di Fisica
Politecnico di Milano, ITALY
R. Eggenhoffner, A. Iandelli, G. L. Olcese, A. Palenzona
Dipartimento di Chimica-Fisica
Universita' di Genova, ITALY

Near edge absorption spectroscopy can be used to determine the value of valence of elements that, like Yb and other rare earths (RE), shows mixed valence behavior. In this experiment performed in may 1986 we measured the L_{III} absorption edge in two families of Yb intermetallic compounds. We used the monochromatic light from beam line II-3 and the spectra were taken in total yield mode. The samples were polished by scraping in vacuum (p about 10^{-7} Torr). In these two families, both starting from $YbAl_2$, Yb atoms are gradually replaced by Ca and Sc. The stoichiometry of the samples is $Yb_{1-x}Ca_xAl_2$ and $Yb_{1-x}Sc_xAl_2$, $0 < x < 1$. Recent structural investigations [1] have shown that the lattice parameter decrease repacing Yb with Ca while it increase if the substituent is Sc.

$YbAl_2$	$Yb_{.6}Ca_{.4}Al_2$	$Yb_{.4}Ca_{.6}Al_2$	$Yb_{.2}Ca_{.8}Al_2$
v=2.3	2.26	2.26	2.21
$YbAl_2$	$Yb_{.8}Sc_{.2}Al_2$		$Yb_{.2}Sc_{.8}Al_2$
v=2.3	2.4		2.63

Tab.1 Values of valence determined decomposing the edge in two components divalent and trivalent.

If Yb is divalent (Yb^{2+}), like in the bulk metal, a single edge is observed as shown by the dotted line in fig.1. In the trivalent case (Yb^{3+}) the edge is the same but shifted toward higer binding energies. This is shown in fig.1 by the dashed line. In this case the edge was measured from an $YbAu_2$ sample. The solid line refers to $YbAl_2$. In this compound the valence has a value intermediate between two and three. The

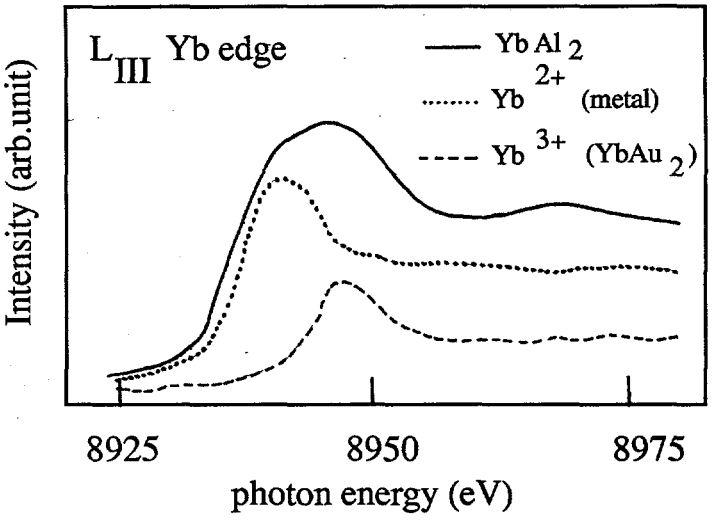

Fig. 1 Absorption edge in a mixed valence compound (solid line) compared with two cases of integer valence.

exact value can be determined deconvolving the spectrum in the two components divalent and trivalent. The values of valence determined in this way are shown in tab.1.

These values clearly show that the mixed valence is a monotonic function of the Yb nearest neighbour distance. In other words the tunnelling probability of a 4f electron into the conduction band is an increasing function of the volume available to the Yb 4f orbitals.

REFERENCES

A. Iandelli, G. L. Olcese, J.Less.Comm.Metals **111**,145 (1985).

Helium Photoelectron Satellites: Low-Energy Behavior of the n=3-5 Lines*

D.W. Lindle,† P.A. Heimann,¶ T.A. Ferrett,† and D.A. Shirley

Materials and Molecular Research Division
Lawrence Berkeley Laboratory
and
Department of Chemistry
University of California
Berkeley, California 94720

Photoelectron satellite branching ratios and asymmetry parameters have been measured for photoionization of atomic He to $He^+(n)$, where n=3-5, at a few photon energies near the satellite thresholds. The photoelectron spectrum in Figure 1 illustrates the different satellite final states of $He^+(n)$ at a photon energy of 80 eV. The n=3 and n=4 satellite branching ratios relative to the n=1 main-line cross section exhibit behavior similar to that previously observed for the $He^+(n=2)$ satellite. The asymmetry parameter β shows progressively more negative values as n_1 increases, supporting a prediction by Greene[1] for the threshold behavior of the He satellites.

*This work was supported by the Director, Office of Energy Research, Office of Basic Energy Sciences, Chemical Sciences Division of the U.S. Department of Energy under Contract No. DE-AC03-76SF00098. It was performed at the Stanford Synchrotron Radiation Laboratory, which is supported by the Department of Energy's Office of Basic Energy Sciences.

†Present address: National Bureau of Standards, Gaithersburg, MD 20899.
¶Present address: Technische Universitat Munchen, D-8046 Garching b, Munchen, W. Germany.

Reference

1. Phys. Rev. Lett. 44, 869 (1980).

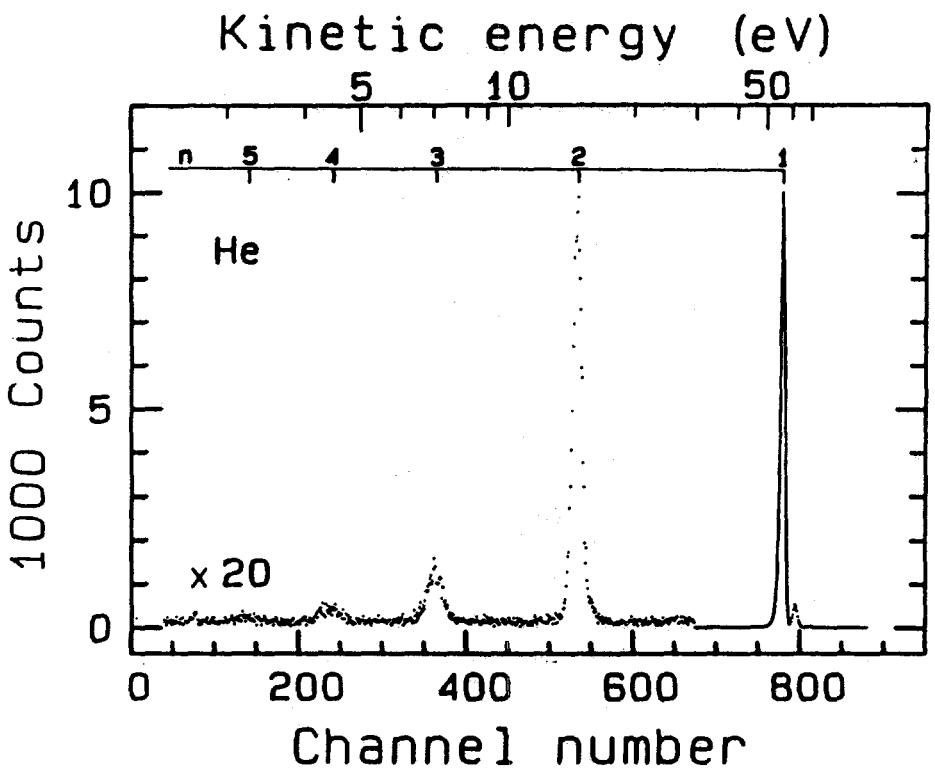

Figure 1. TOF photoelectron spectrum of He at 80 eV photon energy and with θ = 54.7°. The peak label n refers to the principal quantum number of the remaining electron in the He^+ final state. The small peak to the right of the n=1 main line is a result of ringing in the timing circuit, displacing a small fraction of the true counts by a few channels.

Shake-Off on Inner-Shell Resonances of Ar, Kr, and Xe*

P.A. Heimann,§ D.W. Lindle,† T.A. Ferrett,¶ S.H.Liu,
L.J. Medhurst, M.N. Piancastelli,** D.A. Shirley, U. Becker,††
H.G. Kerkhoff,†† B. Langer,†† D. Szostak,†† and R. Wehlitz††

Materials and Molecular Research Division
Lawrence Berkeley Laboratory
and
Department of Chemistry
University of California
Berkeley, California 94720

Synchrotron radiation was used to excite an inner-shell electron into a Rydberg orbital at the Ar 2p → ns, nd, Kr 3d → np, and Xe 4d → np resonances. The resonant decay into shake-off channels was studied by three different electron measurements. First, threshold electron scans were obtained over the resonances and thresholds shown for Kr in Figure 1. On one resonance for each atom, photoelectron spectra were collected. The intensity distribution of low kinetic energy electrons was also determined for a few resonances. Finally, a shake calculation was carried out to compare with the experimental shake-off probabilities. Shake-off is observed to be a strong decay channel for these resonances.

*This work was supported by the Director, Office of Energy Research, Office of Basic Energy Sciences, Chemical Sciences Division of the U.S. Department of Energy under Contract No. DE-AC03-76SF00098. It was performed at the Stanford Synchrotron Radiation Laboratory, which is supported by the Department of Energy's Office of Basic Energy Sciences.

§Present address: Technische Universitat Munchen, D-8046 Garching b, Munchen, Federal Republic of Germany.

†Present address: National Bureau of Standards, Quantum Metrology Group, Physics A141, Gaithersburg, MD 20899.

¶Present address: National Bureau of Standards, Physics A251, Gaithersburg, MD 20899.

**Permanent address: II University of Rome, 00173 Rome, Italy.

††Permanent address: Technische Universitat Berlin, Institut fur Strahlungs- und Kernphysik, Berlin, Federal Republic of Germany.

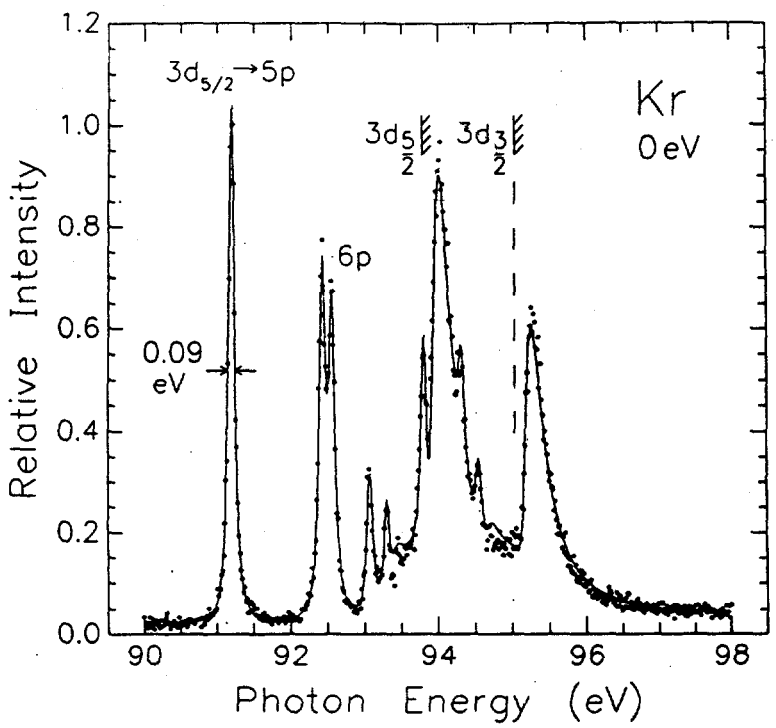

Figure 1. A threshold scan over the Kr $3d^{-1}$ np resonances and 3d thresholds. The curve reproduces a fit.

The Surface Structure of (2x2) S/Ge(111) Determined Using ARPEFS*

S.W. Robey,† C.C. Bahr,¶ Z. Hussain,†† K.T. Leung,**
Ji-ren Lou,¶¶ A.E. Schach von Wittenau, and D.A. Shirley

Materials and Molecular Research Division
Lawrence Berkeley Laboratory
and
Departments of Chemistry and Physics
University of California
Berkeley, California 94720

Measurements of the extended fine structure in the photoemission intensity from the S(1s) core level were performed for a (2x2) overlayer of S on Ge(111). The $\chi(k)$ results are given in Figures 1 and 2. This is the first application of ARPEFS to study an adsorbate on a semiconductor substrate. The adsorption site and local geometry were determined from the ARPEFS using comparisons to multiple-scattering calculations. The results of this analysis indicate adsorption in a 2-fold bridge site 1.03 ± 0.05 Å above the Ge surface. The separation between the first and second Ge layers is contracted by 9 ± 6%, and some Ge-Ge bond lengths between the Ge bilayers are expanded by 8 ± 3%. This adsorption site is different from that determined for another chalcogenide, Te, on the Ge(111) surface on the basis of SEXAFS measurements, but it is the same as those found for Te/Si(111) and Se/Si(111).

*This work was supported by the Director, Office of Energy Research, Office of Basic Energy Sciences, Chemical Sciences Division of the U.S. Department of Energy under Contract No. DE-AC03-76SF00098. It was performed at the Stanford Synchrotron Radiation Laboratory, which is supported by the Department of Energy's Office of Basic Energy Sciences.

†Present address: IBM, T.J. Watson Research Center, Yorktown Heights, NY 10598.

¶Present address: AT&T Laboratories, Princeton, NJ 08540.

††Permanent address: Department of Physics, University of Petroleum and Minerals, Dhahran, Saudi Arabia.

**Permanent address: Department of Chemistry, University of Waterloo, Ontario N2L 3G1, Canada.

¶¶Permanent address: Department of Chemistry, University of British Columbia, Vancouver, B.C., Canada.

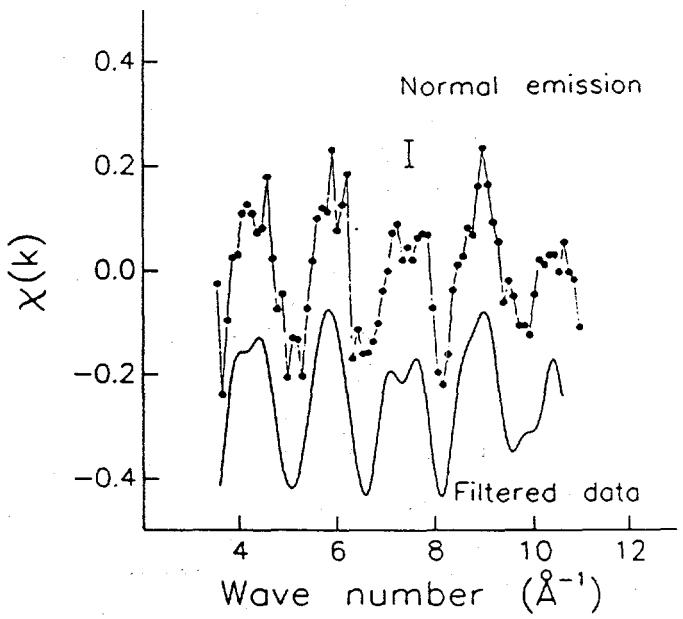

Figure 1. Normal emission $\chi(k)$ data. The upper curve gives the raw data and the lower solid curve represents the same data after Fourier filtering to remove "frequencies" above 10Å. The error bar at the top displays the level of statistical uncertainty in the data. These data represent the average of two normal emission ARPEFS measurements.

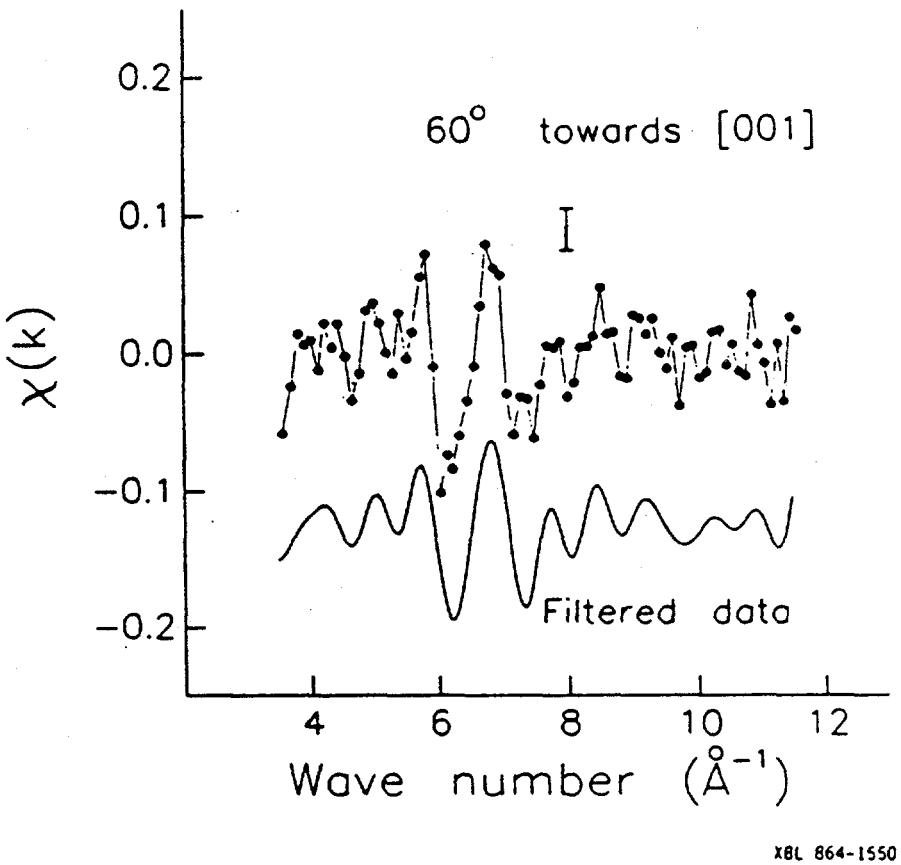

Figure 2. Same as Figure 1 for the off-normal data, except that only one measurement was performed for this geometry.

INVESTIGATION OF GASEOUS CHLORINE COMPOUNDS BY X-RAY ABSORPTION SPECTROSCOPY

F. W. Lytle, R. B. Greegor, E. C. Marques and D. R. Sandstrom
The Boeing Co., Seattle, WA 98124
G. P. Huffman, F. E. Huggins, University of Kentucky, Lexington, KY 40506

We measured the x-ray absorption spectra of gaseous Cl_2, CCl_4, and $H_4C_2Cl_2$. The samples were mixed with He at approximately 1000 ppm concentration and flowed through the detector/sample cell(1). This consisted of a cavity in a 1.3 cm Lucite block covered front and back with 6 μm aluminized Mylar windows. At the center was a thin electron-collecting grid of Ni mesh. The windows were connected to -45 V while the positive battery terminal was connected to the ground of the electrometer. The e-yield signal was collected at 10^8 gain from the center mesh. Absorption and fluorescent mode data were also collected but were much inferior in quality. The Si(111) double crystal monochromator was detuned 80% to reduce harmonics. A 1 mm entrance slit gave an energy resolution $\Delta E/E=0.5$ eV(2). Early data for Cl_2 gas was published by Stephenson et al.(3). Their data was obtained in the absorption mode, cranking the spectrometer and recording the data by hand. Although their first peak was attenuated by the thickness effect, the spectra are comparable with ours to 10 eV. In the region from 10-24 eV we found an interesting double series resonance which is blown up in scale in the inset to Fig. 1. By analogy to N_2 data(4) these features are due to transitions to unfilled orbitals of the molecule in its various charged states.

The data of Fig. 1 were placed absolutely in energy by noting the impurity Ar 1s resonance at 3203.3 eV(5) at the end of each scan. The zero of energy of Fig. 1. is 2833.4 eV. The π resonance peaks were located at -2.6, 0.0 and 0.2 ± 0.2 eV for Cl_2, CCl_4, and $H_4C_2Cl_2$, respectively. The σ resonance energy as defined by Sette et al.(6) moves with bond distance as noted for smaller molecules(6). The Ar K-edge spectrum is shown for comparison, E_o=3203.3 Note that no feature similar to the Ar double electron ionization (1s3p) at 23 eV (the vertical arrow) occurs in the Cl spectra. The EXAFS of Fig. 2 was terminated by the ubiquitous Ar impurity in the x-ray path. Considerably more EXAFS could be measure if this could be corrected. The Cl-Cl phase-corrected

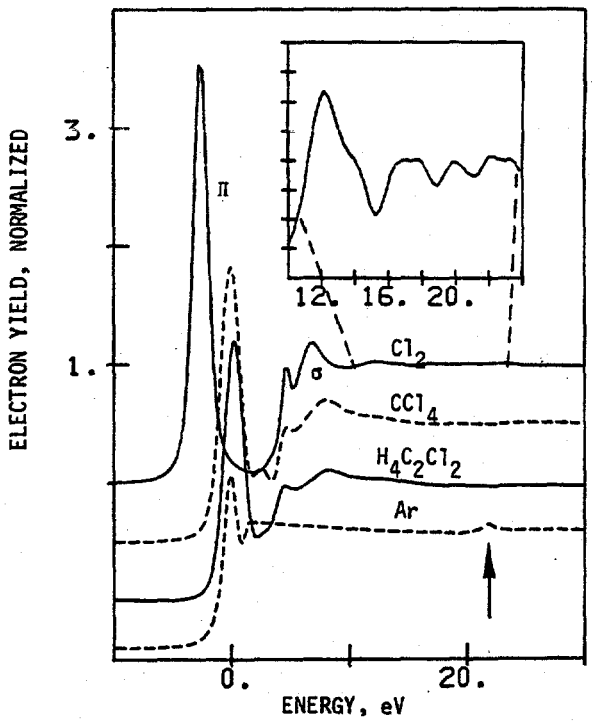

Fig. 1 Near edge spectra of gas phase Cl_2, CCl_4, $H_4C_2Cl_2$ and Ar all normalized to unit edge jump. The π and σ maxima are indicated. The Ar 1s3p edge is marked by the vertical arrow. A region of the Cl_2 spectrum is blown up in the inset to illustrate a double series resonance.

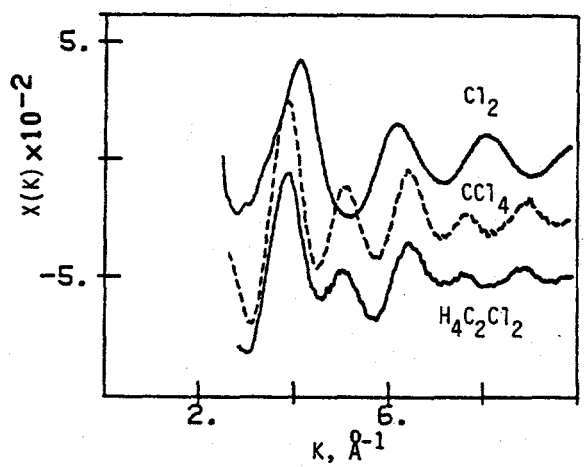

Fig. 2. Normalized EXAFS of gas phase Cl_2, CCl_4 and $H_4C_2Cl_2$.

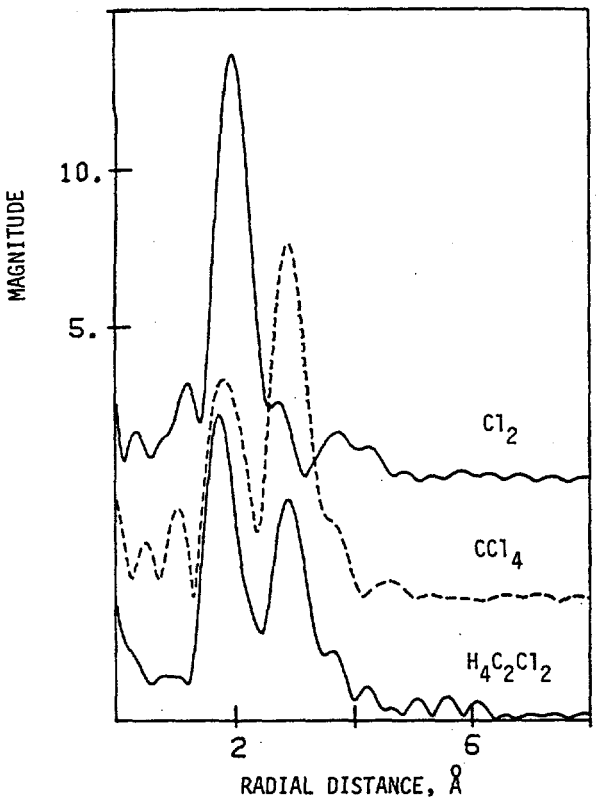

Fig. 3 K^1, Cl-Cl phase corrected Fourier transforms of gas phase Cl_2, CCl_4 and $H_4C_2Cl_2$ all plotted to the same scale.

Fourier transforms are given in Fig. 3. The Cl peaks were found at the expected distances of 1.99, 2.90 and 2.97 Å, top to bottom. The shorter Cl-C bonds are clearly resolved and could easily be analyzed. Any sample with appreciable vapor pressure may be introduced into an ion chamber with a diluent gas. With a long beam path a sensitivity of 1 ppm is possible. This remarkable sensitivity occurs because of the nominal 4π collecting efficiency.

Research funded by NSF and ONR

References

1. F. W. Lytle et al., "GAS PHASE X-RAY ABSORPTION SPECTROSCOPY WITH AN ELECTRON YIELD DETECTOR", presented at IVth Int. EXAFS Conf., Fontevraud, France, July 1986.
2. F. W. Lytle et al., Nucl. Inst. Methods 226, 542 (1984).
3. S. T. Stephenson et al., Phys. Rev. 84,806 (1951).
4. M. Nakamura et al., Phys. Rev. 178, 80 (1969). A. Bianconi et. al., Chem. Phys. Lett. 58, 263 (1978). A. P. Hitchcock et al., J. Elec. Spec. 18, 1 (1980).
5. R. D. Deslattes et al., Phys. Rev. A27, 923 (1983)
6. F. Sette et al., Chem. Phys. Lett. 110, 517 (1984)

RAPID FREEZE EXAFS OF NITROGENASE AND XANTHINE OXIDASE

S. P. Cramer[1,4] L. E. Mortenson[1], M. Eidsness[1], R. C. Bray[2], G. N. George[1], D. Lowe[3], B. Smith[3], R. Thorneley[3], and B. Hales[5]

[1]Exxon Research and Engineering, Annandale, New Jersey 08801
[2]School of Chemistry and M.S., University of Sussex, Brighton, BN1 9RQ UK
[3]AFRC Unit of Nitrogen Fixation, University of Sussex, Brighton, BN1 9RQ UK
[4]Schlumberger-Doll Research, Old Quarry Road, Ridgefield, CT 06877 (current address)
[5]Department of Chemistry, Lousiana State University, Baton Rouge, LA 70803

Although EXAFS has made major contributions to the study of stable bioinorganic structures, the long time required for data collection has precluded study of transient intermediates. Solutions to this problem have included dispersive EXAFS and flash photolysis techniques. We have examined an alternative approach, rapid-freeze EXAFS, in which a chemically generated intermediate is frozen in a few milliseconds in liquid isopentane (1). The enzyme and reactant solutions in syringes are driven through a mixing chamber and shot at a speed of 13m/s into a tube at -140 C. At the bottom of the tube lies the EXAFS cell, and the packed powder is kept cold throughout the process and the spectrum measured by fluorescence detection.

Previous EPR studies on xanthine oxidase have identified a signal called "Very Rapid" corresponding to an intermediate with substrate bound at the Mo site, and various structures have been proposed (2) for this species (Scheme 1). Our rapid-freeze EXAFS of the Mo(IV) transient formed by lumazine with xanthine oxidase reveals that a terminal oxo is present after 600 msec (Figure 1). This time was chosen to maximize the small amount of Mo(V) intermediate in this sample. Recent work by Palmer and coworkers has shown that other intermediates occur on even shorter time scales.

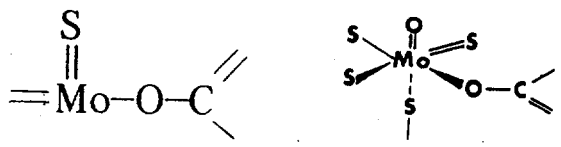

Scheme 1. Alternate structures proposed for "Very Rapid" species, from Ref. 2.

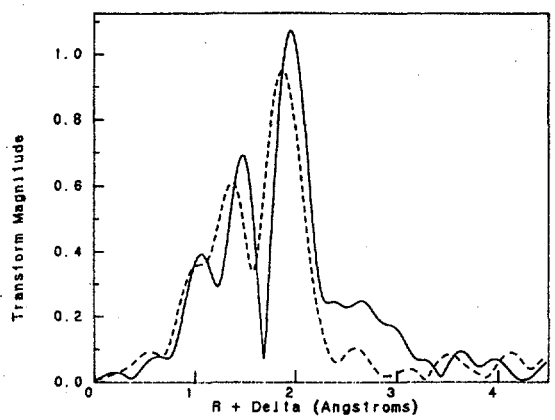

Figure 1. Fourier transform of xanthine oxidase-lumazine product after 600 msec (—), compared to transform for oxidized active enzyme(- - -).

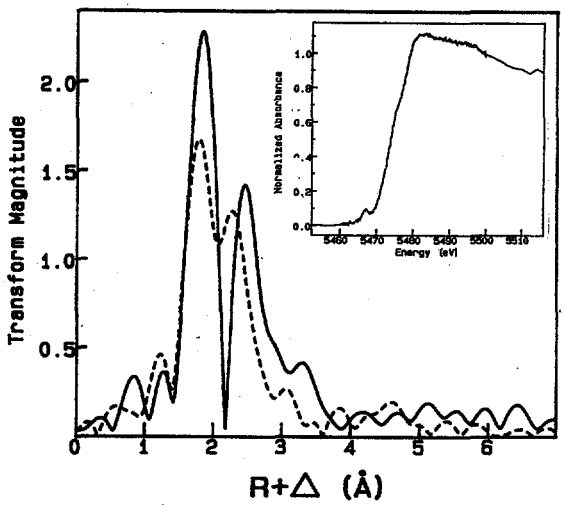

Figure 2. Fourier transform of alternate vanadium nitrogenase from *Azotobacter vinelandii* (—) compared to Mo nitrogenase from *Klebsiella pneumoniae* (- - -). Inset: absorption edge region for V protein.

Our rapid-freeze studies of nitrogenase were designed to detect a Mo-N_2 intermediate. The spectrum of the fixing system trapped at 100 msec shows interesting low R features, but there is no dramatic change in the edge features. We feel that the spectral changes due to dinitrogen may be too subtle to be seen convincingly in the Mo edge spectra.

Because vanadium K edges have higher resolution, the recently discovered vanadium nitrogenases (3,4) may be better suited for spectroscopic detection of bound intermediates. We have obtained preliminary edge and EXAFS spectra of the alternate nitrogenase from *Azotobacter vinelandii* (Figure 2). We find a V-Fe-S cluster similar to the molybdenum nitrogenase Mo-Fe-S cluster. The absorption edge has a well-resolved *1s→3d* transition which should be sensitive to the binding of dinitrogen and other substrates or inhibitors, and our future rapid-freeze studies will emphasize this system.

References:

1. George, G. N.; Bray, R. C.; Cramer, S. P. *Biochem. Soc. Trans.* **1986**, *14*, 561-2.

2. Bray, R. C.; George, G. N. *Biochem. Soc. Trans.* **1985**, *13*, 560-7.

3. Arber, J.M.; Dobson, B. R.; Eady, R. R.; Stevens, P.; Hasnain, S. S.; Garner, C. D.; Smith, B. E. *Nature* **1987**, *325*, 372-4.

4. Hales, B. J.; Case, E. E.; Morningstar, J. E.; Dzeda, M. F.; Mauterer, L. A. *Biochemistry* **1986**, *25*, 7251-5.

EXAFS OF WILD-TYPE AND MUTANT NITROGENASE Mo-Fe PROTEINS

S. P. Cramer[1,4], B. E. Smith[2], M. K. Eidsness[1],
G.N. George[1], C.D. Garner[3], and A. Flood[3]

[1]Exxon Research and Engineering, Annandale, N.J. 08801
[2]AFRC Unit of Nitrogen Fixation, U. Sussex, Brighton, BN1 9RQ, UK
[3]Department of Chemistry, University of Manchester, Manchester, M13 9PL, UK
[4]Schlumberger-Doll Research, Ridgefield, CT 06877 (present address)

One approach to understanding the structure and mechanism of the enzyme nitrogenase is to examine the effects of mutations on these properties. The enzyme from *nif V* mutants in *Klebsiella pneumoniae* is relatively ineffective at dinitrogen reduction, is more efficient than the wild-type at HCN reduction, and has its hydrogen evolution activity inhibited up to 80% by CO (1-3). This altered substrate specificity has been associated with the iron-molybdenum cofactor, FeMo-co, of the enzyme (4). In order to understand whether or not this functional change is associated with the molybdenum site, we have compared resting and dye-oxidized forms of the enzyme at both the Mo K (5) and L edges.

The Mo EXAFS Fourier transforms of Nif V$^-$ and wild-type nitrogenase were found to be nearly identical (Figure 1).

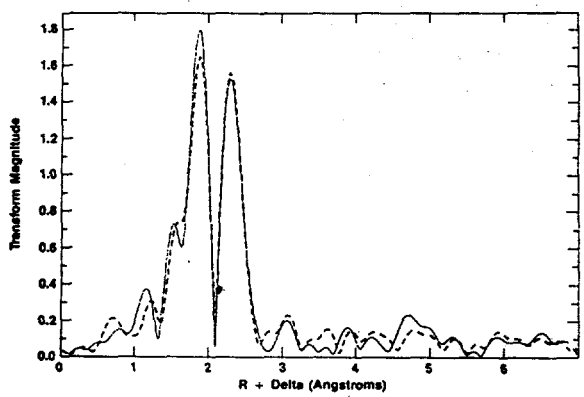

Figure 1. Fourier transforms of Mo EXAFS of Nif V$^-$ Mo-Fe protein (—) and wild type Mo-Fe protein (- - - -).

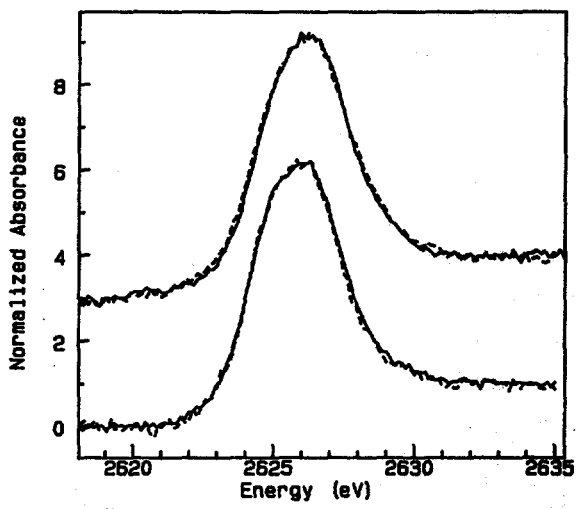

Figure 2. Mo L_2 edge for Nif V$^-$ (- - -) *vs.* wild-type Mo-Fe protein(—). Top - oxidized, bottom - reduced.

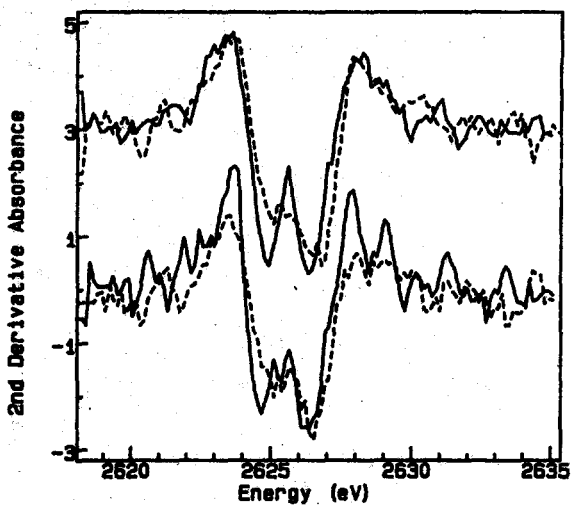

Figure 3. Second derivative comparison of as-isolated (—) *vs.* dye-oxidized (- - - -) Mo-Fe protein. Top - Nif V$^-$, bottom wild-type.

In both cases, the data were consistent with 4-5 Mo-S interactions at 2.37 Å and 3-4 Mo-Fe interactions at 2.69 Å. If there is any difference at the Mo site of the mutant enzyme, it most likely involves non-sulfur ligands. McLean *et al.* have reported changes in the Mo ENDOR signal that may address this perturbation (6).

The Mo L-edges of wild-type and Nif V$^-$ nitrogenase were also compared (Figure 2), in order to exploit the higher resolution of this low energy region. The corresponding wild-type and mutant edges are similar in shape and position, and in both cases, changes are observed upon dye-oxidation of the enzyme (Figure 3). This is the first report of an oxidation state change of the enzyme specifically linked to Mo.

References

1. Liang, Y. C.; Smith, B. E.; *Advances in Nitrogen Fixation*; Veeger, C., Newton, W. E. eds. Martenus Nijhoff/Junk: The Hague, 1984; p. 195.
2. McLean, P. A.; Dixon, R. A.; *Nature*, **1981**, *292*, 655-6.
3. McLean, P. A., Smith; B. E., Dixon, R. A.; *Biochem. J.*, **1983**, *211*, 589-97.
4. Hawkes, T. R.; McLean, P. A.; Smith, B. E.; *Biochem. J.*, **1984**, *217*, 317-21.
5. Eidsness, M. K.; Flank, A. M.; Smith, B. E.; Flood, A. C.; Garner, C. D.; S. P. Cramer; *J. Am. Chem. Soc.*, **1986**, *108*, 2746-7.

X-ray Absorption Spectroscopy of Silica-Supported Ir-Ru Bimetallic Clusters

H. Hamada, M. G. Samant, and M. Boudart
Department of Chemical Engineering
Stanford University
Stanford, CA 94305

Silica-supported Ir-Ru bimetallic catalysts were effective for the selective preparation of C_2-oxygenated compounds from synthesis gas (1). In this system, a strong interaction between Ir and Ru atoms was observed. The structure of similar samples as revealed by XAS is reported here. These bimetallic samples were prepared by co-impregnation of silica (Davison No. 57) with an aqueous solution of $IrCl_4$ and $RuCl_3$ followed by reduction with flowing dihydrogen at 773 K for 3 h. X-ray diffraction patterns of the Ir-SiO_2 showed very broad peaks, suggesting the presence of clusters of $\leq$2 nm. The samples were pressed into self-supporting wafers. The sample wafers were re-reduced at 673 K for 1 h in a controlled atmosphere cell (2) equipped with beryllium windows. The XAS data were obtained with the sample in the cell at room temperature in a dihydrogen atmosphere. Reference materials were Ir and Ru powders. The XAS data were collected in transmission mode at the Stanford Synchrotron Radiation Laboratory. The data were analyzed by the curve-fitting procedure described by Sinfelt et al. (3).

In the case of bimetallic Ir-Ru/SiO_2 samples, the composition of the nearest coordination shell of atoms about Ir or Ru does not agree with a model in which Ir and Ru form a homogeneous alloy. Moreover, for all the samples, the Ru-Ru and Ir-Ru distances (265$\sim$267 ppm) are quite similar and they are different from the Ir-Ir distance (270$\sim$271 pm). These results indicate the presence of two different metal phases, namely, the Ir metal phase and the bimetallic Ir-Ru alloy phase. There is formation of separate particles of Ir and Ir-Ru alloy, or there is segregation of Ir-Ru alloy on the surface of Ir particles. The latter case is more probable, because the previous catalytic study of CO hydrogenation showed an increase in CO conversion and selectivity to hydrocarbons heavier than CH_4 with the increase in Ru/Ir ratio (4). It was concluded that Ir and Ru are homogeneously mixed on the surface and no pure Ir or Ru surface exists.

The magnitude of the absorption threshold resonance is higher for Ir atoms present in Ir/SiO_2 and in Ir-Ru/SiO_2 than for Ir atoms in bulk Ir powder. There was no difference in the magnitude of the absorption threshold resonance between Ir/SiO_2 and Ir-Ru/SiO_2. It can be concluded that Ir on silica appears to be more electron deficient than bulk metallic Ir, and at this point it is not clear why this electron deficiency of Ir is not affected by the presence of Ru.

H. Hamada acknowledges support from the National Chemical Laboratory for Industry, Yatabe, Tsukuba, Ibaraki 305, Japan. Support from NSF Grant CPE 9219066 is acknowledged.

References

(1) H. Hamada, Y. Kuwahara, Y. Kintaichi, T. Ito, K. Wakabayashi, H. Ijima, and K. Sano, Chem. Lett. 1984, 1611.

(2) R.S. Weber, Ph.D. Dissertation, Stanford University, 1985.

(3) J.H. Sinfelt, G.H. Via, and F.W. Lytle, J. Chem. Phys. 72, 4832 (1980).

(4) Y. Sugi, K. Takeuchi, H. Arakawa, Y. Kuwahara, H. Hamada, T. Matsuzaki, Y. Kintaichi, T. Ito, K. Wakabayashi, T. Fukushima, and M. Ichikawa, Proceedings of the Symposium on C_1 Chemistry, Tokyo, P5 (1984).

ANOMALOUS SCATTERING OF X-RAYS

David H. Templeton and Lieselotte K. Templeton
Department of Chemistry, University of California, Berkeley, CA 94720

X-ray Birefringence, Observation of Forbidden Reflections, and Direct Observation of Structure Factor Phases. One effect of X-ray dichroism and birefringence is that the screw-axis and glide-plane rules for absent reflections are not rigorous (1,2). Experiments with sodium bromate near the K edge confirmed the novel dependence of some of these reflections on azimuthal angle and showed that they can give accurate information about structure (3). This year similar measurements were made on some additional forbidden reflections, and it was shown how the shape of one of these curves for 00ℓ gives in a direct way the phase of the 0,0,2ℓ structure factor for the bromine-only part of the crystal structure. A maximum in the intensity at $\psi = 0$ means that the phase of this structure factor is negative. In this way the phases of 00ℓ (ℓ = 2, 6, 10, 14, 18, 22) were shown to be +, −, +, −, −, +, in agreement with those calculated from the known structure (4).

X-Ray Pleochroism and the Anomalous Scattering Tensor of Selenolanthionine. Pleochroism (independent absorption spectra for three directions of polarization) was studied near the Se K edge in two crystal forms of D-selenolanthionine (5), $Se(C_3H_6O_2N)_2$. In this compound Se in site symmetry C_{2v} is bonded to two carbon atoms. A single molecular orientation in the monoclinic (hydrate) crystal permits direct observation of the molecular absorption. Strong absorption lines (at slightly different energies) occur for z-polarization (bisector of bond angle) and y-polarization (C-C direction), but not for x-polarization (perpendicular to plane of bonds). The anomalous scattering tensor for Se, measured by diffraction in tetragonal (anhydrous) crystals shows the same features. It's real and imaginary parts were determined by least-squares refinement in a way similar to anisotropic thermal refinement, but with polarization vectors in place of h vectors in the expressions. This polarization dependence is explained by an elementary molecular-orbital description of the electronic structure. Electrons in B_2 (y) and A_1 (z) orbitals form the bonds. The absorption lines are assigned to transitions to the corresponding antibonding B_2 and A_1 orbitals (which are vacant). No similar vacant orbital is available for x-polarization.

This research was supported by National Science Foundation Grant CHE-8515298 and was done at SSRL which is supported by the Department of Energy, Office of Basic Energy Sciences; and the National Institutes of Health, Biotechnology Resource Program, Division of Research Resources. It used some facilities of the Lawrence Berkeley Laboratory, supported by DOE Contract DE-AC03-76SF00098.

References

1. D.H. Templeton and L.K. Templeton, Acta Cryst. A 36, 237-241 (1980).
2. V.E. Dmitrienko, Acta Cryst. A 39, 29-35 (1983); A 40, 89-95 (1984).
3. D.H. Templeton and L.K. Templeton, Acta Cryst. A 42, 478-481 (1986).
4. D.H. Templeton and L.K. Templeton, Acta Cryst. A in press, 1987).
5. W.A. Hendrickson, Trans. Am. Crystallogr. Assoc. 21, 11-21 (1985).

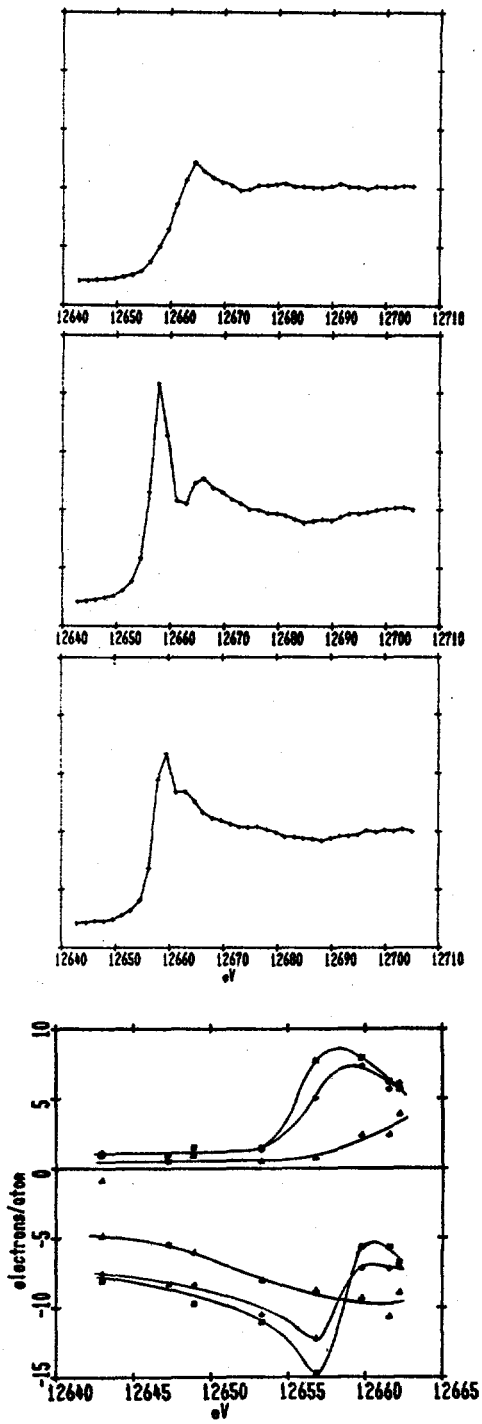

Fig. 1. From top, absorption spectra for x, y, z polarization, monoclinic selenolanthionine; principal values of Se anomalous scattering tensor, imaginary part (upper curves) and real part (lower curves) measured in tetragonal selenolanthionine.

CORE LEVEL STUDY OF THE INTERFACE BETWEEN CaF_2 AND Si(111)

M. A. Olmstead*, R. I. G. Uhrberg**, R. D. Bringans, and R. Z. Bachrach

Xerox Palo Alto Research Center
3333 Coyote Hill Rd., Palo Alto, CA 94304, USA

INTRODUCTION

The epitaxial interface between CaF_2 and Si(111) is a prototype for the study of interface formation between a polar insulator and a non-polar semiconductor. An important question is the nature of the bonding at the interface: whether it is of ionic or covalent character, or intermediate between these extremes. It is also important to address whether the silicon atoms bond to Ca or to F atoms, and whether the stoichiometry is modified at the interface.

RESULTS AND DISCUSSION

The photo-induced electron emission from the Ca 3p, F 2s, F 2p and Si valence band states is shown in Fig. 1. Spectrum 1(a) is characteristic of bulk CaF_2. The binding energy of the Ca 3p states corresponds to Ca atoms surrounded by eight F atoms, and would decrease if F atoms are missing or replaced by Si atoms at the interface. This is seen to be the case for a thin film [see Fig. 1(b)], where a Ca 3p component due to interface Ca atoms is shifted by 2.3 eV to lower binding energy.

Annealing these thin films of CaF_2 at 750 - 800°C leads to a re-evaporation of the film. Below a coverage of one monolayer, a series of reconstructions is observed, 1x1→2x1→5x1→3x1→7x7, with progressively smaller F : Ca ratios. Spectrum 1(c) is taken from a 5x1 surface, and the bottom spectrum from a 3x1 surface. The binding energy of the Ca 3p on the 5x1 surface is the same as that at the CaF_2-on-Si(111) interface. The Ca 3p state for the Si(111):Ca 3x1 surface is also close to this energy. The 5x1 structure likely involves bonding of the form Si-Ca-F, among others, while the 3x1 structure contains only Si-Ca or Si-Ca-Si bonding. The similarity in binding energy between the interface Ca and that on the 5x1 surface suggests that the bonding environment is similar in both cases. If the CaF_2 molecule is intact at the interface, then the interface Ca environment differs from bulk CaF_2 only by interchanging one of 8 fluorine atoms with a Si atom. It is unlikely that this would lead to a 2.3 eV shift in the Ca 3p binding energy. If the F layer between the Ca and Si atoms were removed, however, the interface Ca would be in an environment equivalent to Si-Ca-F.

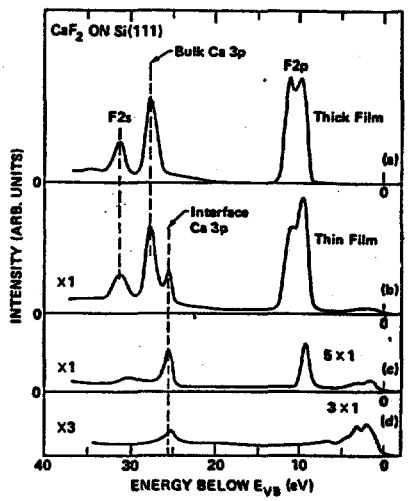

Fig. 1: Shallow core levels for (a) >50 Å film of CaF_2 on Si(111) (T_{dep} = 500°C); (b) 11 Å film (T_{dep} = 700°C); (c) submonolayer film (5x1) obtained upon annealing (b); (d) Si(111):Ca 3x1 surface obtained upon annealing (b). (a: $h\nu$ = 130 eV; b,c,d: $h\nu$ = 135 eV).

Further information can be obtained from the Si 2p core level, shown in Fig. 2. In addition to the bulk Si contribution, there are components shifted to both higher and lower binding energy. The primary interface component is shifted by 0.36 eV to lower binding energy, the direction expected for Si-Ca bonding. There are also two smaller components, shifted by ~0.45 eV and ~0.85 eV to higher binding energy. The larger value might be expected for Si-F bonding at the interface, with the F atoms directly above the Si dangling bonds.

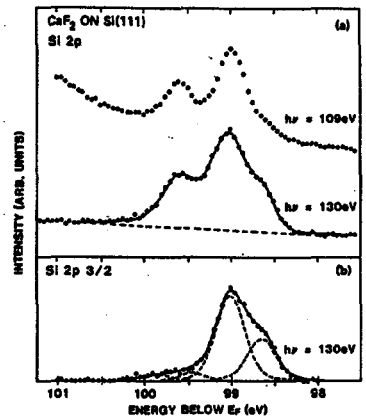

Fig. 2: Si 2p core level for the same film as for Fig. 1(b). a) Top: Bulk sensitive spectrum. Bottom: Surface sensitive spectrum. Solid line is a least squares fit which is deconvolved in (b). b) Spin-orbit deconvolution of surface sensitive spectrum. The dashed curves are the components of a least squares fit to the data.

An explanation consistent with the above results is that at least 90% of the interface consists of Ca atoms directly above Si dangling bonds, and that most of the fluorine layer between the Ca and Si layers is removed. The F atoms which remain may sit in the hollow site or between the first and second silicon layers. The Si 2p components shifted to higher binding energy could be due to either of these geometries. Another possible source for the component shifted to higher binding energy is a small portion of the interface (<10%) with direct Si-F bonding. Varying amounts of either this second type of interface or the amount of F remaining near the interface may account for the differences between this work[1] and that recently reported by Himpsel *et al.*[2]

ACKNOWLEDGEMENTS

We are grateful for the assistance of L.-E. Swartz. Part of this work was performed at SSRL which is supported by the DOE; and the NSF Division of Materials Science.

REFERENCES

*Present address: Dept. of Physics, Univ. of California, Berkeley, CA 94720 USA.

**Present address: Dept. of Physics and Measurement Technology, Linköping Institute of Technology, S-581 83 Linköping Sweden.

1. M. A. Olmstead, R. I. G. Uhrberg, R. D. Bringans, and R. Z. Bachrach, J. Vac. Sci. Technol A4, 1123 (1986); Phys. Rev. B35, in press.

2. F. J. Himpsel et al., Appl. Phys. Lett. 48, 596 (1986); D. Rieger et al., Phys. Rev. B34, 7295 (1986).

Surface and Interface Aspects of Si on GaAs(100)

R.Z. Bachrach, R.D. Bringans, Marjorie A. Olmstead*, and R.I.G Uhrberg**

Xerox Palo Alto Research Center
3333 Coyote Hill Rd., Palo Alto, Ca 94304

1. Introduction

The motivation of our work was to investigate the surface microchemistry of silicon deposited on GaAs at the stage prior to its diffusion into the bulk. Under suitable conditions, silicon will diffuse rapidly and this diffusion has also proven useful for semiconductor laser processing because it induces layer-disordering of superlattices.[1] Silicon has also been introduced inside lasers at high concentrations by MOCVD growth and the creation of a phase of $GaAs_{(1-x)}$-$(Si_2)_x$ has been deduced.[2] These experiments, however, warrant further clarification.

One further motivation for our work was the possibility to investigate a (100) surface single domain 1x2 reconstruction in an overlayer thickness regime which spanned the adsorbate induced to epitaxial coverages. Results of Zalm et al found that single domain surfaces were obtained for thicknesses up to 10 monolayers (ml) and thus one would have a metastable single domain Si(100) surface.[3] Our initial investigation of the interfacial chemistry indicates that the specific models for the reconstruction may be complex, particularly in the 0.5-1.5ml range. We will therefore present the analysis of the angle resolved UPS data at a later time.

2. Experimental Details

Silicon was deposited with a thermal evaporation source. The source consisted of a resistively heated silicon filament shaped by etching. Use of molybdenum radiation shield behind the filament and around the assembly was crucial to achieving the desired evaporation rates. Deposition was monitored by an in-situ quartz crystal monitor which was calibrated with some test step depositions. Deposition rates of up to 5 A/min were achieved with filament currents of 5-6 amps. Typically the deposition rate saturated as a function of input power and depended upon micro-filament formation in the specific filament. These rates were adequate for the current experiments. The source was kept warm during As_4 exposures and then outgassed prior to depositions.

The experiments reported here have been carried out on GaAs(100) substrates prepared by standard techniques and then sputter cleaned and annealed in an As_4 beam. We have also started from regrown GaAs layers, and in general these result in better ordered surfaces. Subsequent annealing of the surfaces in vacuum was used to prepare specific surface conditions. In this work, we have concentrated on the two ends of the surface phase diagram, the Ga rich 4x6 and the As rich c(4x4) and c(2x8). Once the samples were prepared, core and valence band photoemission spectra were obtained at the Stanford Synchrotron Radiation Laboratory using the Grasshopper monochromator. All the measurements were made in a p-polarized geometry where the light was incident at about 85^{o} and the axis of the cylindrical mirror analyzer was approximately 5^{o} with respect to the surface normal.

3. Results and Discussion

Silicon was deposited in a sequence of staged experiments consisting of deposition followed by annealing. The depositions onto room temperature surfaces resulted in disordered surfaces. Subsequent annealing at 450^{o}C produced ordered 1x2 structures for coverages above 0.5ml starting from the GaAs(100) 4x6 and 1.0ml starting from the GaAs(100) c(2x8) surfaces. Annealing to 600^{o}C produced sharper LEED patterns with less background. In general, silicon deposition with the substrate held at 600^{o}C produced better LEED patterns than those obtained after room temperature deposition and subsequent annealing. Annealing of depositions in the 0.5-2 monolayer range in this study resulted in ordered surfaces with a single domain 1x2 reconstruction. In some cases a minority second domain was observed, but a second anneal was found to reduce it.

The period doubling direction, (i.e. the "2" direction of the 1x2 reconstruction) was along the "8" direction for a starting GaAs(100) c(2x8) surface and in the "6" direction for the GaAs(100) 4x6 surface. Thus if the period doubling is due to dimerization of the surface atoms, the dimers are in the orthogonal direction to the arsenic dimers thought to exist on the arsenic-rich surfaces. The simplest explanation of this result implies that the surface atoms occupy the equivalent of next layer gallium sites and as the layer builds up, the preference is for double layer growth. This can occur for example if Si atoms form an outer layer of Si-Si dimers on the surface. It is also possible that the surface layer consists of Ga or As dimers which "float" on top of the Si atoms. The LEED results only show that the surface layer atoms occupy only the Ga sublattice site of an extended GaAs crystal.

The deposition and annealing sequence is presented in Figure 1 for the Si, As, and Ga core level ratios as a function of Si deposition determined from the quartz crystal monitor. The data are plotted to exhibit the annealing history for a GaAs(100) 4x6 and GaAs(100) c(2x8) starting surface. The As/Ga 3d core level area ratio of the clean surfaces is consistent with previously obtained data.[4,5] The individual As and Ga peaks attenuate with the coverage, but interestingly, the ratio remains approximately constant with silicon coverage. In each case, annealing temperatures of 450^{o}C or 600^{o}C resulted in a decrease in the silicon signal relative to both the arsenic and the gallium by 30% at each initial annealing stage while the surface As/Ga ratio increased slightly. The fact that the As/Ga ratio remained approximately constant as a function of deposition, although of course the absolute intensities decreased, constrains some of the possible structural interpretations.

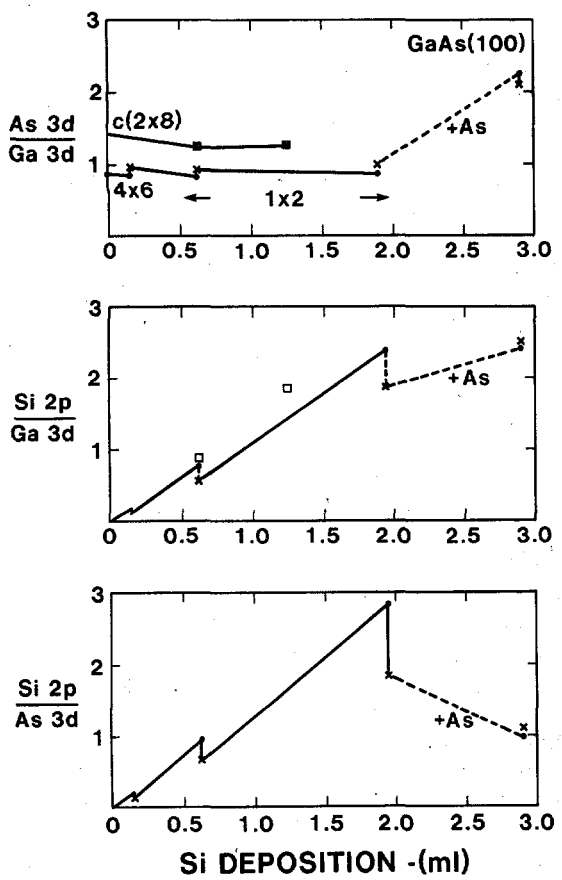

Fig 1. Core level ratios as a function of silicon deposition. a) As-3d/Ga-3d for starting surfaces of As rich c(2x8) and Ga rich 4x6. In the case of the 4x6 surface, the Si was deposited onto a room temperature substarte and then annealed. b) Si-2p/Ga-3d ratio versus Si deposition for the same surfaces. c) Si-2p/As-3d ratio versus Si deposition for the same surfaces.

A surprising aspect of the annealing experiments is that the annealing of the surface in the presence of silicon approximately maintains the effective surface As/Ga ratio. Annealing the As rich native surfaces to 600°C would convert them to the more Ga rich 4x6. Thus the silicon appears to be constraining the evaporation of surface arsenic. We have observed similar behaviour for the arsenic terminated silicon surfaces where the strong bonds formed between Si and As require temperatures greater than 700°C to desorb the arsenic.[6] In the case of the data for the 4x6 starting surface, there is a 10% rise in the As/Ga ratio upon annealing. This indicates that either the Si covers Ga atoms more effectively or that As atoms come nearer the surface after interaction with Si. The As/Ga ratio still remains substantially below that for the GaAs(100) c(2x8) starting surface. The fact that the 1x2 surfaces have different As/Ga ratios in the presence of similar amount of deposited Si and that the orientation remains 1x2 as the coverage is increased is significant. Note that we are still getting a linear uptake with 2 ml coverage. Further experiments are required to extend this data to saturation coverages.

We have explored various yield models to simulate the data in figure 1 , although more data is required to determine a unique model. A promising model which would explain the 1x2 structure on As-rich starting surfaces is generated by replacing the As vacancies in the outermost As layer of the clean surface with Si atoms and then adding a complete layer of silicon atoms. The outermost layer of this arrangement will then consist of Si atoms occupying only Ga sublattice sites. Dimerization of these Si atoms then leads to the observed 1x2 reconstruction.

There are two possible models for the 4x6 that are consistent with the observed arsenic coverage of approximately 25%.[4] This could be 25% of arsenic adatoms on a complete Ga layer or 25% Ga vacancies in an outer Ga layer as depicted in Fig 2a and 2b. The Ga vacancy representation shown in Fig 2a is more consistent with the Si coverage data. Once the 25% of Ga vacancies are filled with Si the 1x2 pattern will occur if Ga-Ga and Ga-Si dimers form. In our experiments the 1x2 pattern was found to develop with deposition between 0.25 and 0.5 monolayers. For the As adatom case, one would not expect to observe the onset of the 1x2 at such a low coverage. For the As-rich GaAs(100) c(2x8), the surface is thought to consist of a 75%-90% complete layer of As and one would expect the 1x2 to arise at coverages of around 1 monolayer and this was observed. The interaction of Si with this surface has not yet been explored in enough detail to make definitive conclusions.

As the silicon layer thickness increases, the 1x2 orientation is preserved. Thus above one monolayer, the silicon growth must proceed in bilayer steps which preserve the single domain structure observed. Otherwise an alternation of 1x2 and 2x1 patterns should be observed as a function of thickness.

3.1 Core Line Shapes

The core level spectroscopy line shape investigation is consistent with models where the Si is bonded in a number of inequivalent sites. We present below data on the Ga 3d, Si 2p, and As 3d cores.

3.1.2 Si- 2p Core line

Figure 4 presents Si 2p core level spectra for 0.63ml Si as-deposited onto GaAs(100) 4x6 (dashed curve) and after annealing at 450°C to a 1x2 reconstruction. Annealing in general sharpened the features without producing better resolved spectra as shown by the change from the as-deposited dashed curve to the solid curve. The spectra are plotted on an energy scale relative to the As 3d 5/2 component in the spectra. This procedure was considered to provide the best reference level.

A Si(100):As 2x1 surface is presented as a reference. Investigation of arsenic terminated silicon has produced a specific structural model where the As forms a dimerized surface on the outer layer of silicon.[10] The Si(100):As Si 2p spectra is interpretable in terms of two distinct components, one the bulk silicon and the other for the outer silicon layer bonded to arsenic and a distinct core level shift of [xx] eV.[6] Deposition of Ga onto Si(100) produces a small shift to lower binding energy. Thus the signature for Si-Ga bonds is not very distinct from Si-Si bonds. The resulting alignment of Si 2p levels for the Si(100):As and the GaAs(100):Si surfaces seen in figure 4 indicates the core shifts are dominated by Si-As and Si-Si bonds after annealing into the ordered structure.

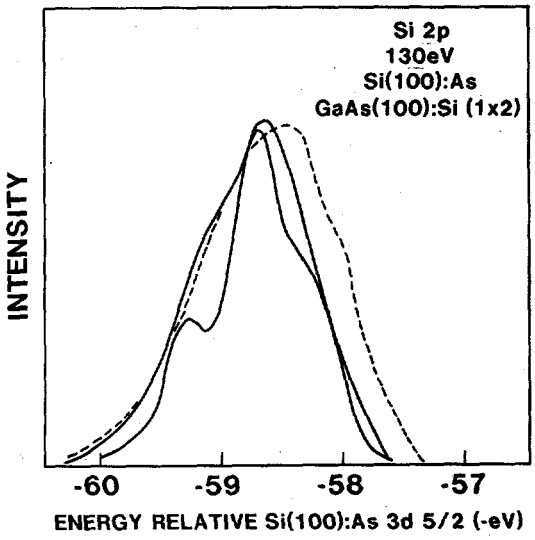

Fig 2. Si 2p core level spectra for a Si(100):As 2x1 surface, and 0.63ml Si as deposited onto GaAs(100) 4x6 and after annealing at 450 °C to a 1x2 reconstruction. The spectra have been plotted relative to the As 3d 5/2 component energy.

Unlike the deposition of As, Ga, or GaAs onto Si(100)[4], the deposition of silicon onto GaAs(100) produced silicon 2p core level spectra with poorly resolved structure. The overall width of the lines for the annealed surfaces however are comparable to that found for As terminated silicon as shown in figure 4. Deconvoluting these Si 2p spectra is problematic because of the trade off that can be made between broadening and the number of peaks. In general, distinct lattice sites should give distinct core level shifts, while disorder associated with specific sites will lead to broadening. With the parameters from the Si(100):As Si 2p spectra as a lineshape guide, a 5 spin-orbit pair fit is required for either the GaAs(100) 4x6 or c(2x8) starting surface. The deconvolution for the 0.63 monolayer deposition does show that the spectrum is determined by a combination of Si-Ga, Si-Si, and Si-As bonds and as expected the starting c(2x8) has a proportionally stronger Si-As component. The higher coverage lineshapes were not distinguishable probably because of the preponderance of Si-Si components. Although we have explored these deconvolutions, we do not feel the fits are as unique as we have found for As or Ga on silicon surfaces and we have therefore chosen not to show deconvoluted spectra.

To explore some of the co-ordination issues, we intentionally grew a thick silicon rich alloy by codepositing GaAs and silicon. This is thought to produce an alloy of $GaAs_{(1-x)}$-$(Si_2)_x$. For the specific case obtained, x = 0.9, annealing at 600°C produced an ordered 1x2 surface, but the LEED pattern indicated a highly strained system. This compares with the distinct 1x2 pattern obtained for the Si deposited and annealed samples. Remarkably, the Si 2p core level spectra were essentially identical with the annealed above 1ml overlayer case. Thus for Si deposited onto GaAs(100), this is also evidence for the silicon having diffused into the surface in addition to the silicon participating in the reconstruction and rules out a major phase separation.

4. Summary

Investigation of the evolution of the GaAs(100) structure with the deposition of Si on As and Ga rich starting surfaces has shown that different atomic configurations are likely involved. In each case, however, the 1x2 surface would be generated by dimerization of the Ga and/or Si in the outer layer. Analysis of the core level spectra shows evidence of Si-Si, Si-As, and Si-Ga bonds indicating silicon is sitting in a number of sites. Some silicon is deduced to diffuse into the bulk even at low annealing temperatures of 450-600 °C.

ACKNOWLEDGEMENTS

We are pleased to acknowledge the skillful assistance of Lars Erik Swartz. We thank Robert Thornton and Robert Burnham for conversations which motivated this work and D.J. Chadi and R.M. Martin for discussions concerning the structural models. Part of this work was performed at SSRL which is supported by the DOE Office of basic Energy Sciences; and the NSF Division of Materials Research. R.I.G.U. was partially supported by the Swedish Natural Science Research Council.

*Present address: Dept. of Physics, U.C. Berkeley, Ca, 94720

**Present address: Dept of Physics and Measurement Technology, Linkoping Institute of Technology, S-581 83 Linkoping, Sweden.

REFERENCES

1. R.L. Thornton, R.D. Burnham, T.L. Paoli, N. Holonyak,Jr, and D.G. Deppe, Appl. Phys. Lett, **49**, 133, July (1986).
2. R.D. Burnham, N. Holonyak,Jr., K.C. Hsieh, R.W. Kaliski, D.W. Nam, R.L. Thornton, and T.L. Paoli, Appl. Phys. Lett, **48**, 800, March (1986).
3. P.C. Zalm, P.M.J. Maree and R.I.J. Olthof, Appl Phys. Lett, **46**, 597, (1985).
4. R.Z. Bachrach, R.S. Bauer, P. Chiaradia, and G.V. Hansson, J. Vac Sci. Tech, **18**, 797, (1981).
5. R.Z. Bachrach, R.S. Bauer, P. Chiaradia, and G.V. Hansson, J. Vac Sci. Tech, **19**, 335, (1981).
6. R.D. Bringans, R.I.G. Uhrberg, M.A. Olmstead, R.Z. Bachrach, and J.E. Northrup, Physica Scripta, (1987), to be published.
7. D.J. Chadi, C. Tanner, and J.S. Ihm, Surf. Sci. **120**, L425 (1982); J. Ihm, D.J. Chadi, and J.D. Joannopoulos, Phys Rev B **27**, 5119, (1983).
8. T. Narusawa, K.L.I. Kobayashi, and H. Nakashima, Japan Journal of Applied Physics, **24**, L98, (1985).
9. R.Z. Bachrach, R.S. Bauer, and J.C. McMenamin, Inst Phys. Conf Ser. **43**, 1073-1076, (1979).
10. R.I.G. Uhrberg, R.D. Bringans, R.Z. Bachrach, and J.E. Northrup, Phys Rev Let, **56**, 520, (1986); J. Vac Sci. Tech, **A4**, May/Jun (1986).

STRUCTURE/FUNCTION STUDIES OF OXIDASES, PEROXIDASES AND CATALASES

B. Chance, M. Chance, G. Bunker, A. Naqui, Y.-H. Zhou
Institute for Structural & Functional Studies, Philadelphia, PA

L. Powers
AT&T Bell Labs, Murray Hill, NJ

Project I

Cytochrome oxidase studies have been the main feature of this group's activities at SSRL and, as a consequence, a large "data bank" has been obtained over the years employing Beam Line I-5 for copper studies and Beam Line II-2 for iron studies. The occasional simultaneous use of these two lines has made for effective data gathering, adequate optical sample monitoring and optimal efficiency of personnel deployment.

The main achievement in current work, has been the documentation of the properties of the membrane-bound oxidase which are readily studied in terms of their copper signal on Beam Line I-5 (1), while for iron studies, cytochromes b and c are removed to non-interfering levels, and studies are made on line II-2 (2). Since the dilute preparations require one or two shifts of averaging under normal beam conditions, optical measurement of sample damage has become of paramount importance in this study. To this point, several criteria have been developed in optical scans from 400 to 700 nm, among them; 1) appearance of absorption at 445 nm indicates reduction, 2) disappearance of the 655 nm band and 3) appearance of greater intensity at 600 nm indicates an altered state of the enzyme. Only by frequent optical monitoring of these parameters have we been able to ensure that the data accumulated are of an identifiable state of the oxidase. A paper on the structure of copper sites has been accepted for publication in the Journal of Biological Chemistry (3).

Project II

The EXAFS study of peroxidase intermediates as background data for the study of compounds A,B and C of cytochrome oxidase has lead to a number of results, many of which have been published (2,4) which indicate different structures for compounds I and II of a variety of peroxidases. These compounds are kinetically distinct, typically reacting with electron and proton donors at rates that differ by a factor of over 100 in favor of compounds of type I. Other's data that indicate identical structures for these two compounds are puzzling since it negates the possibility that structure/function relationships exist in these metalloenzymes (5). There is a possibility that mixtures of compounds I and II are obtained at high optical criteria for identifying high levels of purity of these compounds have been further developed, which are applicable to highly concentrated samples employed in these studies and which have ensured us of the homogeneity of those samples already tested. However, to further document the purity of the compounds, Dr. S. Saigo has been invited to this country from the Photon Factory in Japan to develop his freeze-quench apparatus specifically for studies on Beam Line II-2. One data set has already been acquired and in the most recent runs, further data sets are in process under rigidly controlled conditions where authenticated occupancies of compound II of over 90% are achieved, together with adequate EXAFS data collection time. Other peroxidase intermediates are under study and have been reported on (6), but the nature of compound II in relation to compound I is of utmost importance for establishing structure/function relationships among these key models. A scientific question is whether the pulsed peroxide compound of cytochrome oxidase is structurally related to compound I or compound II. This also affords a firm base for studies of the functional cytochrome oxidase peroxidase compound, compound B, which we also expect to trap in Saigo's apparatus (see below).

Hypothesis B was that altered structures of cytochrome oxidase of different subunit and amino acid constitutions can be produced and will reveal further structure/function relationships. Since the alterations can only be effectively carried out in microorganisms, Dr. Robert Poyton's studies with yeast cells are of the greatest interest, and collaborative activities have been undertaken together with several studies of baseline structures of the yeast cytochrome oxidase. Preliminary data sets were obtained in June, and further work in the current activity. The yeast oxidase may have a different structure from that of beef heart, and at the same time, it is capable of a 10 times greater turnover number. Thus, already a comparision of these two oxidases has given further insights in the structure/function relationships in cytochrome oxidase. It should be noted, at the same time, that previous studies of the paracoccus enzyme, which has an activity similar to that of the beef heart enzyme, have shown no structure differences as yet determinable.

Future Plans. The pursuit of structually altered forms of cytochrome oxidase that have different functional activity seems paramount in the pursuit of generalized structural/functional relationships in the peroxidases and cytochrome oxidases. The EXAFS technique seems ideally suited to this purpose and information relevant to current theories of cytochrome oxidase function is expected to emerge.

References

1. Powers, L. Chance, B., Ching, Y.-C. and Angiolillo, P. Biophys. J. 34, 465-498 (1981).
2. Chance, M., Powers, L., Poulos, T. and Chance, B. Biochem. 25, 1266-1270 (1986).
3. Powers, L., Chance, B., Ching, Y.-C. and Lee, C.-P. Structure of the Copper Sites in Membrane-Bound Cytochrome c Oxidase. J. Biol. Chem. (1987) (in press).
4. Chance, B., Powers, L. Ching, Y.-C., Poulos, T., Schonbaum, G.R., Yamazaki, I. and Chance, B. Arch. Biochem. Biophys. 235, 596-363 (1984).
5. Penner-Hahn, J.E., McMurry, T.J., Renner, M., Latos-Grazynsky, L., Smith Eble, K., Davis, I.M., Balch, A.L., Groves, J.T., Dawson, J.H., Hodson, K.O. J. Biochem. 12761-12764 (1983).
6. Chance, B., Kumar, C., Powers, L. and Ching, I.-Y. Biophys. J. 44, 353-363 (1983).

This work was supported by NIH grant GM-33165

EXTRACTION OF SHORT RANGE ORDER (SRO) PARAMETERS FROM EXAFS SECOND SHELL AMPLITUDES IN OXIDE AND SILICATE SOLID SOLUTIONS

G.A. Waychunas
Center for Materials Research, Stanford University
Stanford, Ca. 94305

W.A. Dollase and C.R. Ross
Department of Earth and Space Sciences, U.C.L.A.
405 Hilgard Avenue, Los Angeles, Ca. 90024

SRO parameters in solid solutions are difficult to measure by conventional techniques if the differences in the scattering power of the species in question is small, or if the species are minor constituents. One way around this difficulty is to compare the observed neighbor shell backscattering amplitude from the EXAFS with that calculated using a model structure where the composition and SRO parameters may be varied. If the species being examined for ordering-clustering have large differences in either or both the backscattering amplitude or phase, then a large change in the total amplitude will be observed as a function of the shell composition. A neighbor shell composition is directly related to the Warren-Cowley SRO parameter for that neighbor shell. It appears from model calculations, that a large enough phase difference is present in species whose atomic number differs by only 4 to 5. Normally, anomalous scattering or combined X-ray and neutron scattering work would be required for successful SRO determinations in such cases.

Species which have a large phase difference as well as a backscattered amplitude difference are important in geochemical systems. For example, Na-Ca ordering is important in the feldspar and pyroxene minerals, Fe-Mg ordering is important in the olivine, pyroxene and other silicate minerals. Particularly in the pyroxenes ($ABSi_2O_6$) the A sites may have ordered species distinct from the B sites, and there may be A-B ordering as well. Knowledge of such ordering schemes can lead to determination of the temperatures and possibly, pressures, of the minerals formation.

An example of a simple test system is the MgO-FeO (rocksalt structure) solid solution. In this system the second shell about the probe Fe atom contains only Fe and Mg at similar distances. Figure 1 shows the observed second shell amplitudes compared with calculations based on a random arrangement of second shell atoms and using backscattering amplitudes and phases as given by Teo and Lee (1). The distances between the absorber and the backscatterers strongly affect the phase and must be accurately modeled. This effect is shown by the two theoretical curves in figure 1. The curve produced by a Distance Least Squares (DLS) model which suggests a near Vegard-type bond length variation fits the data points better (2). The DLS model allows for site compliance in the structure, i.e. adjustment of the host structure for the incorporation of solute species. Hence at low FeO concentrations the MgO bond length is inappropriate, rather the solution adjusts its bonds to take up about 50% of the ionic radius mismatch (2).

In the MgO-FeO system the agreement with theory is good, the dip in the curve coming from the large phase difference in the Mg versus Fe second shell backscattering. The calculated curves can be adjusted to fit more precisely if empirical Mg and Fe backscattering factors and phases are used. In the case of a strongly clustered system, the second shell amplitude would approximate the FeO amplitude at most compositions. Thus the system (synthesis temperature 1353 K) has very little short range order. Analogous examination of the fourth shell gives a similar result, though with larger relative errors.

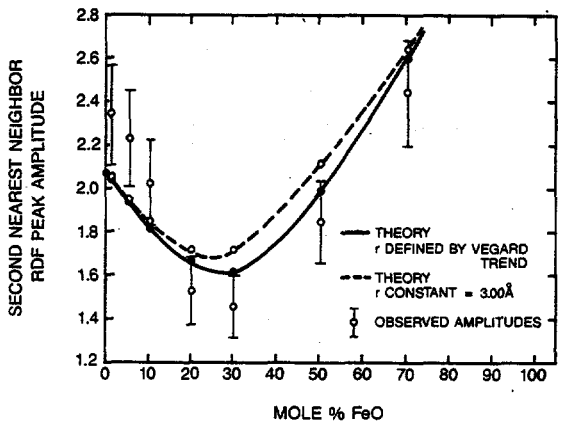

Figure 1. Second shell backscattering amplitudes in MgO-FeO solid solutions.

Our study includes the charge coupled solution $MgO\text{-}LiFeO_2$ (which may show the effects of simultaneous ordering and clustering) and several synthetic pyroxene solutions: $CaMgSi_2O_6\text{-}CaFeSi_2O_6$, $CaMgSi_2O_6\text{-}NaFeSi_2O_6$ and $CaFeSi_2O_6\text{-}NaAlSi_2O_6$.

At the present time we have partial results for two of the pyroxene solutions with Fe edge data collected at room and liquid nitrogen temperature. Figure 2 shows the observed mean Fe-O bond length in $CaMgSi_2O_6\text{-}CaFeSi_2O_6$ (diopside-hedenbergite). In this pyroxene system the Ca is ordered into the larger M2 site and the Fe for Mg substitution occurs in the M1 sites which are octahedra sharing edges to form a kinked chain in the pyroxene structure. The bond distances appear to be about constant from 30% to 100% Hd. Additionally, the near edge structure of the Fe K-edge for these materials changes dramatically from 2% to 30% Hd but is then unvarying up to 100% Hd. Both of these observations suggest clustering of the Fe in the M1 chains. The calculated versus observed second shell amplitudes are shown in figure 3. Despite the fact that the Fe and Mg neighbors in the M1 sites adjacent to a probe Fe atom in M1 make up only part of the second shell, there is a large variation in the backscattered amplitude for the random variation as a function of composition. This trend is similar to the observed trend, but indicates smaller backscattering

than is observed at all synthetic compositions. Since the backscattering amplitude increases with Hd component or more numerous second shell Fe, this comparison also indicates clustering. However, it must be noted that errors in the phase and amplitude factors used in generating the calculated values can strongly affect the results in the pyroxene systems. The second shell also contains the Ca atoms in M2, as well as Si and O. Since all of the distances of these species from the absorber vary with composition, and presumably degree of order, simulations of the structure are essential for the backscattering amplitude calculations.

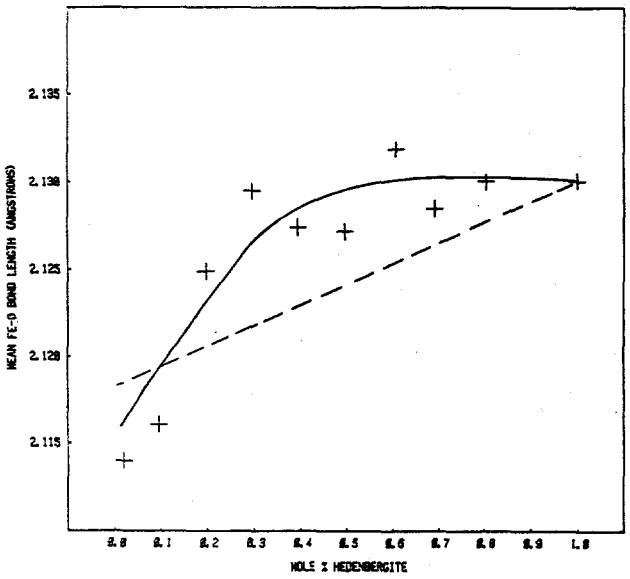

Figure 2. Mean Fe-O bond distances in Di-Hd solid solutions contrasted with the DLS model of the structure (dashed line).

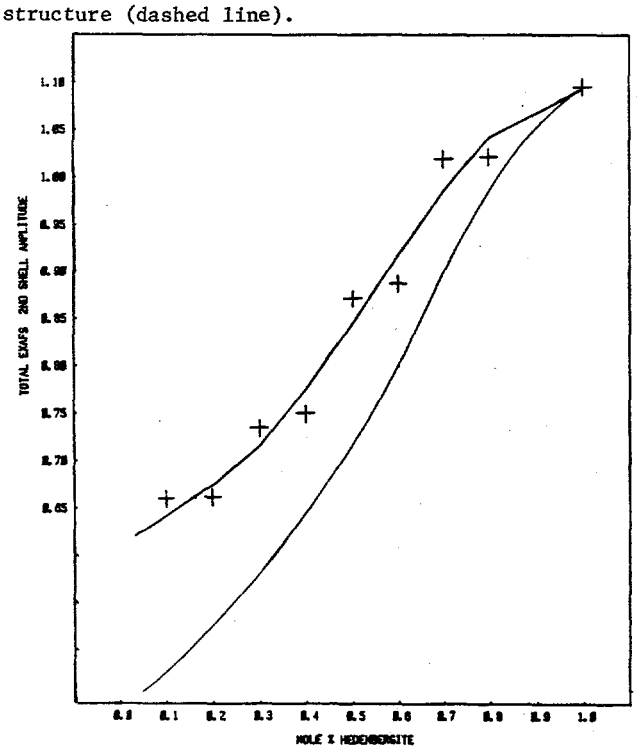

Figure 3. Comparison of EXAFS second shell amplitudes in Di-Hd solid solutions. Upper curve is the observed amplitudes, lower curve the calculated.

Our present effort is concerned with the modeling of the pyroxene and oxide solution structures as a function of both composition and short range order.

In the $NaAlSi_2O_6$-$CaFeSi_2O_6$ system there is the possibility of M2-M2 and M2-M1 ordering as well as M1-M1. Compositions about the midpoint of this system are observed to have varying degrees of short range order (3). Our first results are shown in figure 4.

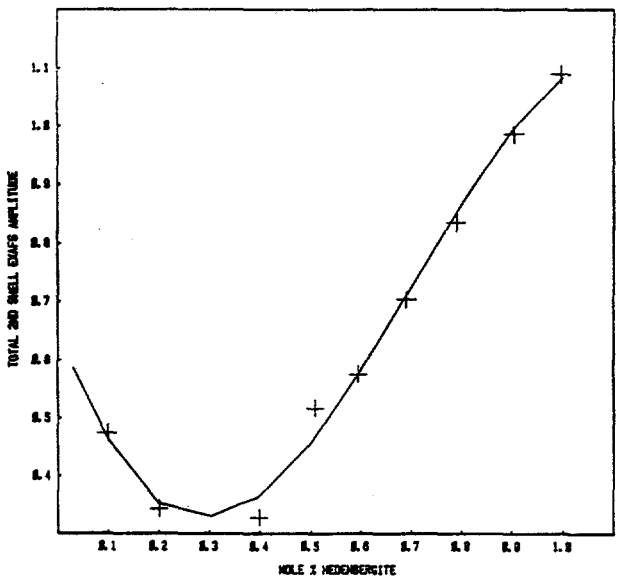

Figure 4. Second shell backscattering amplitudes for Jd-Hd ($NaAlSi_2O_6$-$CaFeSi_2O_6$) solid solutions.

The trend observed is clearly inconsistent with much clustering, but indicates behavior between a completely random and an ordered second shell. In order to quantify the results and determine the SRO parameters we will need to calculate rather complex structural models and the backscattering from a second shell containing six different species (Ca,Na,Fe,Al,Si and O) with two SRO parameters (M2-M1), (M1-M1). This work is in progress along with the analysis of the Ca EXAFS for the Ca-containing pyroxene solutions.

References.

1. B.-K. Teo and P.A. Lee (1979) J. Amer. Chem. Soc., 101, 2815
2. W.A. Dollase (1980) Phys. Chem. Minerals, 6(4), 295
3. M.E. Fleet, C.T. Herzberg, G.M. Bancroft and L.P. Aldridge (1978) Amer. Mineralogist, 63, 1100

X-RAY ABSORPTION SPECTROSCOPY OF SUBSTRATE INTERACTION WITH NITROGENASE FeMo PROTEIN

A. Lawrence Roe(1), Britt Hedman(1,2),
Steve Vaughn(3), Barbara Burgess(3), Keith O. Hodgson(1)

(1) Department of Chemistry, Stanford University, Stanford, CA 94305
(2) SSRL, SLAC, Bin 69, P.O. Box 4349, Stanford, CA 94305
(3) Department of Molecular Biology and Biochemistry, UC Irvine, CA 92717

Nitrogenase is the molybdenum containing enzyme system responsible for the reduction of dinitrogen in nitrogen fixation. A molybdenum and iron containing cofactor that is essential for this reduction can be extracted from the molybdenum protein . While a variety of experiments indicate that molybdenum is involved in the reduction, direct ligation of dinitrogen, or any other substrate, has not been demonstrated. The intent of these experiments was to determine possible substrate binding to molybdenum by measuring the K and L edges and the K EXAFS of molybdenum in the protein and in the extracted cofactor.

Kinetic experiments show that several small molecules inhibit the reduction of dinitrogen, and many of these are themselves reduced by nitrogenase. Molybdenum ENDOR experiments indicate a change in the molybdenum environment in the presence of methyl-isocyanide (MIC), so this was chosen as a good candidate for molybdenum ligation. The molybdenum K and L edge spectra of nitrogenase in the presence of: MIC, acetylene, carbon monoxide, bromide, and cyanide show absolutely no effect caused by the addition. The cofactor spectra also show no effect. There is a difference between the molybdenum edge spectra of cofactor and the protein: extraction of the former causes a shift of 0.8 eV to higher energy and a broadening of the principal maximum. These changes are caused by the replacement of 2-3 of the sulfurs around molybdenum in the protein by oxygens upon extraction. In contrast, the shifts in the molybdenum K edge positions in the protein caused by MIC or cyanide are less than 0.1 eV. Similarily, the L3 edge should shift and change in shape with a change in the ligand field around molybdenum or the effective charge of molybdenum. It does not change.

The K edge EXAFS (figure 1) and Fourier transforms of these samples are also indistinguishable. A comparison of the low k region of the protein EXAFS is presented to show the effect of a adding a single extra low Z ligand to the fitted spectrum (figure 2). A fit to this filtered data over the range 4 1/Å to 13.5 1/Å gives sulfur and iron parameters in good agreement with those previously reported. The addition of the contribution from a single low Z ligand at 2.0 Å shows that there would be a small but measurable change in the phase of the first two EXAFS peaks. This shift is not observed, hence the EXAFS gives no indication of bonding of any of these small molecules to molybdenum in nitrogenase.

Research supported by NIH Grant RR 01209 and NSF Grant CHE 85-12129.

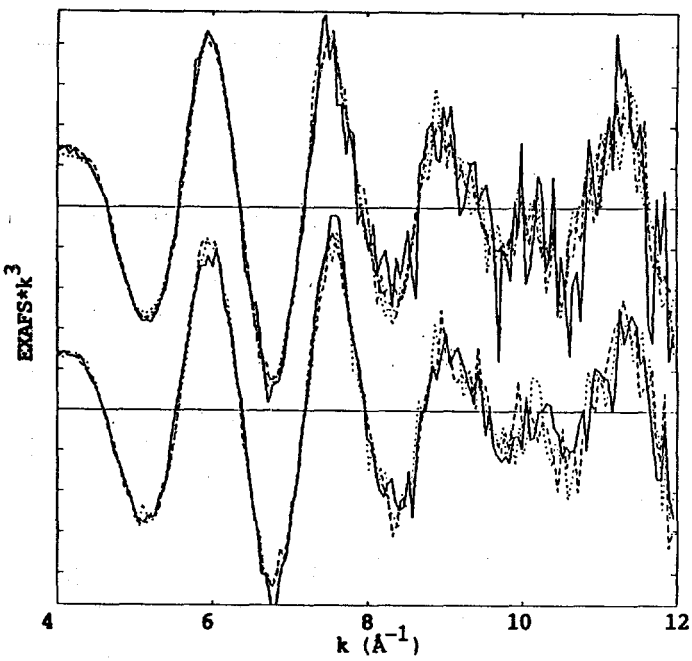

Figure 1. EXAFS of Semi-reduced nitrogenase MoFe protein in the presence of substrates and nitrogen reduction inhibitors. Top: methyl-isocyanide (-----), acetylene (.....), carbon monoxide (.-.-.), bromide (——); bottom: pure semi-reduced protein (——), methyl-isocyanide (----), and cyanide (.....).

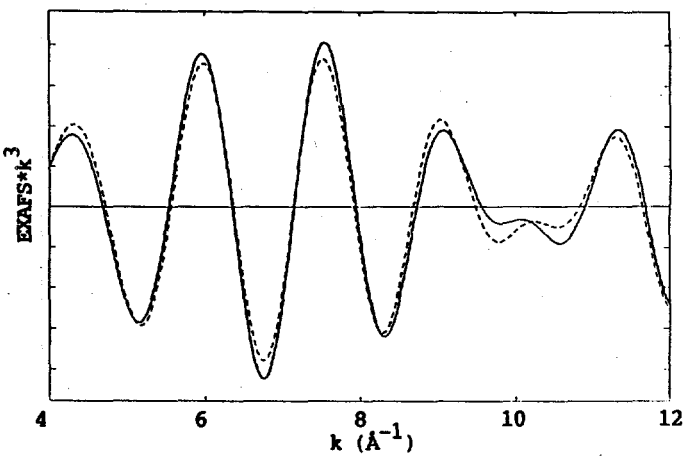

Figure 2. Fitted EXAFS of semi-reduced nitrogenase (——) and the same fit with one extra oxygen at 2.0 Å (-----).

X-ray Absorption Spectroscopic Studies of Nickel Containing Metalloenzymes

R. A. Scott and M. K. Eidsness
School of Chemical Sciences, University of Illinois, Urbana, IL 61081

To aid in the characterization of Ni metalloenzyme active site structures, we have examined the Ni X-ray absorption edges of a number of Ni compounds [1]. Edges can be utilized as indicators of electronic and molecular structure given appropriate, structurally characterized model compounds. In such cases, edge features may be correlated with Ni oxidation state, ligand type, and site geometry. The approach we have taken is to attempt to correlate edge changes to changes in a single characteristic (*i. e.* oxidation state, ligand type or site geometry) between pairs of model compounds.

Oxidation state. At present, we have examined a single pair of model complexes which differ in Ni oxidation state while preserving the coordination sphere at the Ni site. We have compared the Ni(II) and Ni(III) edges of $[Ni(mnt)_2]^{2-/-}$ (mnt = maleonitriledithiolate). Their edge spectra are structurally similar except for a shift of 1.1 eV in the edge inflection points. The inflection point of the Ni(III) complex occurs at higher energy, and this may be explained by an increase in the ionization energy due to the greater effective nuclear charge at the Ni(III) ion.

Ligand type. We have found that the shape of the Ni edge is sensitive to the coordination environment of the Ni ion. To date, we have examined the edges of model complexes containing Ni-N, Ni-O, or Ni-S ligation. An edge comparison of Ni-N and Ni-S ligated complexes of octahedral geometry (Figure 1a) and square planar geometry (Figure 1b) shows that the main difference is the overall larger edge jump for the Ni-N complexes. The edge jump of the Ni-O octahedral complex is very similar to that of the Ni-N complex. The same effect was observed in a comparison of Ni-N and Ni-S complexes of approximately tetrahedral geometry. Such differences in edge height only allow distinction between coordination spheres dominated by either N or S ligands. We expect a continuous gradation of edge heights for mixed (N, S) ligand sets, and this has been observed in two Ni model compounds having a 2N, 2S coordination sphere.

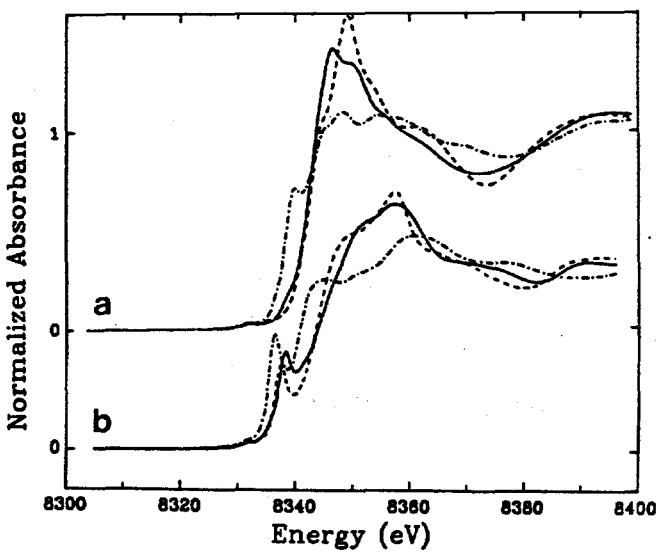

Figure 1. Ni K edge spectra of (a) pseudo-octahedral complexes $[Ni(en)_3]Cl_2 \cdot 2H_2O$ (en = ethylenediamine) (—), $[Ni(phen)_3]Cl_2 \cdot 7H_2O$ (phen = 1,10-phenanthroline) (- - -), $[Ni([9]aneS_3)_2](ClO_4)_2$ ([9]aneS$_3$ = 1,4,7-trithiacyclononane) (·····), and (b) square planar complexes [Ni(Pc)] (Pc = phthalocyanine) (—), [Ni(m-TPP)] (m-TPP = meso-tetraphenylporphyrin) (- - -), and $[(n\text{-}Bu)_4N]_2[Ni(mnt)_2]^{2-}$(·····).

Coordination geometry. The most useful aspect of Ni X-ray absorption edges is the presence of electronic transitions from 1s to valence levels which give rise to pre-edge peaks. The intensity of the assigned transitions can yield information about the symmetry of the Ni site. We have examined Ni(II) complexes having approximate local site symmetries of square planar (D_{4h}), octahedral (O_h), and tetrahedral (T_d) geometries. Although Ni enzyme active site structures are not expected to demonstrate any of these limiting geometries, the edge features should at least be sufficient to indicate the approximate geometrical arrangement of ligands.

The Ni edges of three Ni-S containing complexes of approximate T_d, D_{4h}, and O_h geometries are shown in Figure 2. In the case of T_d symmetry, the pre-edge peak at *ca.* 8332 eV is assigned to the forbidden 1s → 3d transition which becomes allowed through p-d mixing in the noncentrosymmetric site. The intensity of this transition relative to the other geometries is illustrated in the Figure 2 inset. Square planar geometry is characterized by a striking pre-edge transition at *ca.* 8336 eV. This peak is assigned to the 1s → $4p_z$ transition, by analogy to square planar Cu(II) complexes [2]. Both NiS_6 and NiN_6 complexes with local O_h symmetry yield edges that are devoid of any readily noticeable pre-edge absorption peaks. The absence of a significant 1s → 3d transition at *ca.* 8332 eV and the intense 1s → $4p_z$ transition at *ca.* 8336 eV can be used to infer a (pseudo-) octahedral coordination geometry.

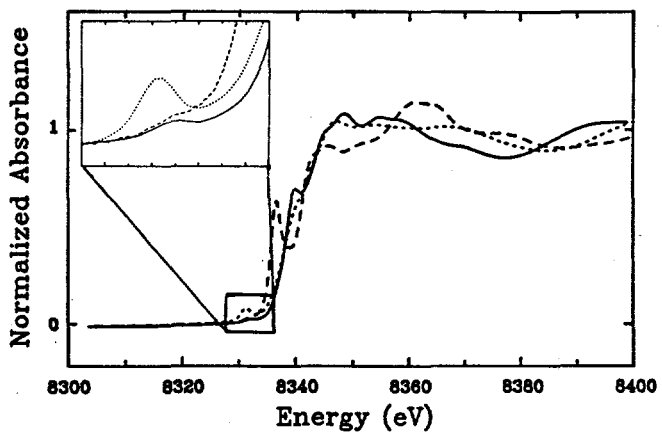

Figure 2. Ni K edge spectra of complexes differing in Ni site geometry: octahedral, $[Ni([9]aneS_3)_2]^{2+}$ (—); square planar, $[Ni(mnt)_2]^{2-}$ (- - -); and tetrahedral, $[Ni(SC_6H_5)_4]^{2-}$ (· · ·). The figure inset energy range is 8328-8336 eV.

References.
1. Eidsness, M. K.; Sullivan, R. J.; Scott, R. A. In "Bioinorganic Chemistry of Nickel", Lancaster, J. R. Ed.; VCH: Deerfield Beach, 1987, in press.
2. Smith, T. A.; Penner-Hahn, J. E.; Berding, M. A.; Doniach, S.; Hodgson, K. O. *J. Am. Chem. Soc.* **1984**, *107*, 5945-5955.

MULTIPLE WAVELENGTH CRYSTALLOGRAPHY ON SULFITE REDUCTASE AND PHOTOACTIVE YELLOW PROTEIN

Duncan E. McRee*, Wayne A. Hendrickson**, John A. Tainer*, and Elizabeth D. Getzoff*
*Molecular Biology Department, Research Instititute of Scripps Clinic, La Jolla, CA 92037
**Molecular Biophysics Department, Columbia University, New York, New York 10032

Multiple wavelength crystallographic studies have been initiated on sulfite reductase and photoactive yellow protein. The use of multiple wavelengths will allow the structure factor intensities to be phased by anomalous differences and thereby overcome problems in obtaining multiple heavy atom derivatives for these two proteins.

Sulfite reductase is an enzyme that catalyzes the 6-electron reduction of sulfite to sulfide, a necessary step in the assimilation of sulfur from the biosphere. The native enzyme from *E. coli* has two subunits, one of which can carry out the reaction by itself, the hemoprotein subunit. We have crystallized this subunit (1) and are determining the atomic structure using x-ray diffraction. The hemoprotein subunit is especially interesting because it contains both a heme and an Fe_4S_4 cluster for a total of 5 Fe. The K absorption edge of Fe is easily obtainable with synchrotron radiation, making this protein an excellent candidate for phasing by measuring the difference in Fe absorption at several wavelengths.

The data were collected on the area detector for crystallography station (Beam line I-5). All techniques were the same as were used for conventional data collection (1) except that the wavelength was varied. The differences in absorption are on the order of a few percent and require optimal conditions for measurement. The strategy used takes advantage of the ease of changing wavelengths at the synchrotron. Each frame of data is collected sequentially at each of four wavelengths: above, below and at the Fe edge, and one far removed. Each reflection is thus measured close in time and in the same geometry at 4 different wavelengths. minimizing experimental error due to crystal decay, slippage, etc. The data are collected on two-dimensional area detector of the Hamlin type. Preliminary work using conventional Cu Kα radiation showed that the signal is large enough to measure, and resultant Patterson maps revealed the positions of the 5 Fe. The additional wavelengths are needed for complete phasing. In our first trip we were not able to collect a complete data set, and we expect to finish during the next run.

In a second, preliminary experiment, we initiated studies on a photoactive yellow protein (PYP) complexed with $PtCl_4$. PYP was purified from the phototrophic bacterium *Ectothiorhodospira halophila* and crystallized. The hexagonal crystals are in space group $P6_3$ with unit cell dimensions a=b=66.89, c=40.68 Å and appear to have one 15,000 dalton protein in the asymmetric unit (2). PYP contains a chromophore with retinal-like properties; its color can be reversibly bleached by visible light with kinetics similar to that of sensory rhodopsin. The crystals can also be bleached by an intense visible light source without cracking, but are not bleached by x-rays. This suggests that structures can be obtained for both bleached and colored conformations of the protein-bound chromophore. The crystals diffract strongly to at least 1.5 Å resolution, are resistant to radiation damage, and are suitable for a high resolution structure determination. The covalently bound chromophore and photobleaching characteristics of the protein offer unique opportunities to study protein conformational change and refolding as well as to understand the mechanisms of light-induced conformational change at atomic resolution.

EXAFS of PYP crystals showed a strong Pt edge that was significantly shifted from a control, uncomplexed $PtCl_4$ solution, indicating the $PtCl_4$ has bound to the protein. These crystals diffract very strongly and last well in the beam, making an ideal candidate for future experiments with multiple wavelength measurements.

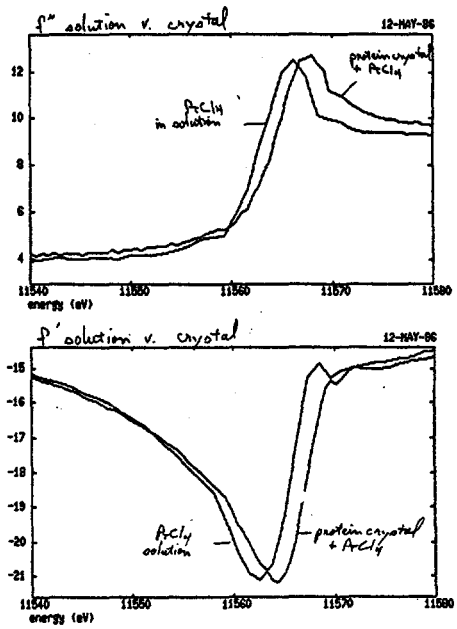

Fig. 1. EXAFS scan of PYP Pt derivative done at SSRL to determine the feasibility of collecting multiple wavelength data at the Pt absorption edge. The scan shows that the Pt edge has been shifted relative to free K_2PtCl_4 in solution and this is taken as evidence of binding to the protein. Data collection at multiple wavelengths around the Pt absorption edge should allow an atomic structure determination of PYP.

References

1. McRee, D.E., Siegel, L.M., and Richardson, D.C. (1986) *J. Biol. Chem.* 261, 10277-10281.
2. McRee, D.E., Meyer, T., Cusanovich, M. Getzoff, E. (1986) *J. Biol. Chem.*, 261, 13850-13851.

ANOMALOUS SMALL ANGLE X-RAY SCATTERING FROM IONOMERS

Y.S. Ding, R.A. Register, and S.L. Cooper
Chemical Engineering Department, University of Wisconsin
Madison, WI 53705

S. Hubbard and K.O. Hodgson
Chemistry Department, Stanford University
Stanford, CA 94305

We have used anomalous small-angle x-ray scattering to study the peak and zero-angle upturn in the characteristic scattering pattern of ionomers. This preliminary investigation has shown that cations are the source of the zero-angle scattering, but that the zero-angle and peak scattering have different origins.

Ionomers are polymers containing a small amount of acid comonomer, neutralized with various cations. Regardless of the ionomer's chemical structure, the small-angle x-ray scattering patterns all exhibit two characteristic features: a broad peak at a Bragg spacing of 2-5 nm, and a dramatic increase in scattered intensity near zero angle. Various models of ionomer microstructure have been proposed, all based on the idea that the ionic groups aggregate into microdomains (1). To date, the most satisfying interpretation of the scattering pattern has been that the peak arises from interparticle scattering between aggregates having a liquid-like order, while the upturn is due to impurities or voids in the sample (2).

In this investigation, we have used a sample of sulfonated polystyrene (6.9 mole percent sulfonated repeat units), neutralized with Ni^{2+}. By tuning the x-ray energy to 5 and 100 eV below the Ni^{2+} absorption edge, we were able to selectively vary the scattering power of the cation while leaving the scattering power of the other elements (H,C,O,S) virtually unchanged. The diffference between the scattering patterns at the two energies then reflects the scattering due to the cations only.

The data were collected on SSRL Beamline II-2, using a 50 cm camera length. The data were corrected for transmittance by normalizing to the counting rate of a photodiode placed in the main beam after the sample. The difference spectrum was then obtained by first correcting for fluorescence by matching the tails of the patterns at high q ($q = 4\pi\sin\theta/\lambda$) and then subtracting the two. The original and difference patterns are shown in Figure 1, where the difference pattern has been scaled to have the same number of integrated counts as the original. Two points are apparent from this figure: 1) the sources of both the peak and the upturn scattering contain Ni, since both features are present in the difference pattern, and 2) the difference pattern does not have the same shape as the original. Specifically, the lower intensity of the upturn indicates that its source is more dilute in Ni than the aggregates, which are the source of the peak scattering. However, the upturn scattering is not due to voids.

The peak in the difference pattern is well-described by a hard-sphere interparticle scattering model (2), with an aggregate core radius of 0.67 nm, a radius of closest approach of 1.56 nm, and a volume per particle of 76 nm^3. This model, however, does not predict any zero-angle scattering. One possible source of this scattering is embodied in the Debye-Bueche random two-phase model (3), which predicts a scattering intensity decaying exponentially with q. This would be superimposed on the peak scattering to give the observed pattern. A good fit to the upturn in the difference pattern is obtained with a correlation length of 300 nm and an electron density contrast equal to 2% of that between the aggregates and the matrix. Possible sources of this heterogeneity include ions dispersed in the hydrocarbon matrix, or the breakup of the material into aggregate-rich and aggregate-poor zones, as is known to occur in colloids (4). However, additional data and modelling efforts will be necessary to truly determine the source of the zero-angle scattering.

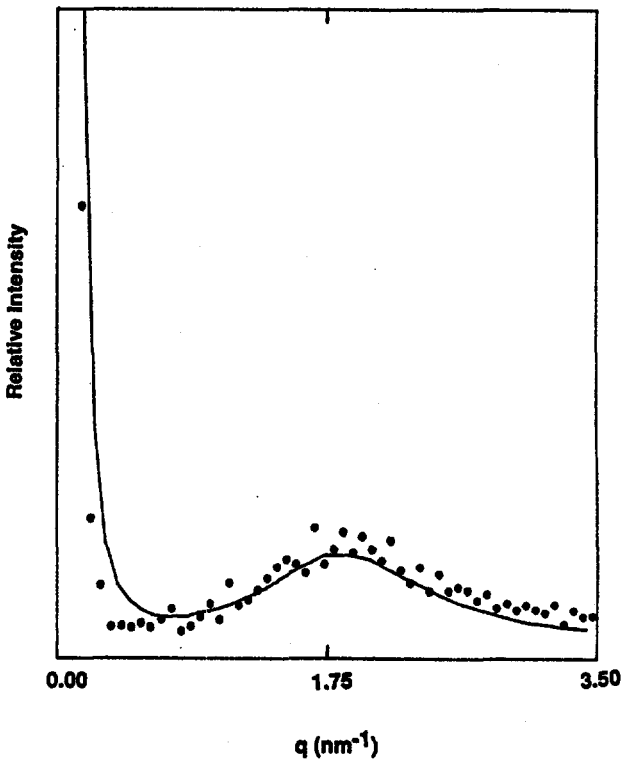

Figure 1. The scattering pattern taken 100 eV below the Ni^{2+} edge (——) and the difference pattern, scaled to be equal in integrated intensity (o).

We have just completed the collection of a large body of anomalous small-angle x-ray scattering data on a wide variety of nickel-neutralized ionomers, again using SSRL Beamline II-2. This data should help to settle some of the issues raised in this preliminary investigation.

References

1. A. Eisenberg, Macromolecules, 3, 147 (1970).
2. D.J. Yarusso and S.L. Cooper, Macromolecules, 16, 1871 (1983).
3. P. Debye and A.M. Bueche, J. Appl. Phys., 20, 518 (1949).
4. N. Ise, Agnew. Chem. Int. Ed. Engl., 25, 323 (1986).

ANOMALOUS DISPERSION CRYSTALLOGRAPHY OF A FERREDOXIN

Proposal 976B

H.M.Krishna Murthy,J.L.Smith and W.A.Hendrickson,
W.H.Orme-Johnson E.A.Merritt and R.P.Phizackerley

Columbia University,Massachusetts Institute of Technology
and Stanford Synchrotron Radiation Laboratory

Introduction

As has been detailed in the past few years (1), the availibility of tunable X-radiation at synchrotrons presents one with the opportunity of solving the phase problem using an approach that is radically different from those conventionally used for this purpose in macromolecular crystallography. The method uses the anomalous scattering effects from suitable centres present in native crystals of macromolecules or centres that can be introduced into crystal lattices of macromolecular crystals. The power and elegance of the method have been demonstrated by using the previously solved structure of lamprey haemoglobin as a test problem (2). Here we report the attempted application of this procedure to Clostridium acid-urici Ferredoxin.

Ferredoxins (Fd) are small Iron/Sulphur proteins that mediate electron transfer reactions in a variety of bacterial systems by virtue of posessing Fe-S clusters of suitable redox potentials (for a review see ref 3). The molecular structure of the Fd from Peptococcus aerogenes has been elucidated (5) and that of the Fd from Desulphovibrio gigas is being worked on (6) using conventional single wavelength techniques. the Fd from Clostridium acidi-urici, which is a protein of 55 amino acid residues, exhibits strong homology (42 out of 55 residues being identical in the two sequences) to P.aerogenes Fd and like the latter incorporates two tetrameric Fe-S clusters as the active prosthetic groups. we have chosen this Fd as an example of a protein with native metal centres the anomalous scattering from which may be exploited in a multiple wavelength experiment.

Crystallization and Data Collection

Crystals were obtained by equilibation of droplets of protein, containing approximately 20-25 mgs of protein and 10-20 percent saturated ammonium sulphate (SAS) solution at Ph 7.8 (200 mM TRIS), against approximately 60-70 percent SAS solutions in vapour diffusion plates. The largest crystals that could be grown were approximately 0.4 x 0.15 x 0.15 mm. Subsequent X-ray photographic and diffractometric analysis showed that these crystals belong to the tetragonal space groups P4(1)2(1)2 or P4(3)2(1)2 and had lattice dimensions of a = 34.56 and c = 75.27 Angstroms. It was also evident that these were not single crystals, yielding split peaks at the positions of diffraction maxima. Nevertheless, since a limited exploration of the reciprocal lattice showed the split peaks to be relatively uniformly distributed, it was decided to continue with the experiment using these crystals.

The precise knowlwdge of anomalous scattering factors which are derived from absorption edge measurements are extremely important in a multiple wavelength experiment. Since the absorption edge measurements themselves are critically depedent on the chemical environment of the absobing species, flourescence measurements were made on the crystal intended to be used for the collection of diffraction data. From these measurements absorption coefficients were derived after scaling and background corrections. The anomalous scattering factor f" could then be obtained by direct relationship and f' by Kramers-Kronig transformation.

For the diffraction measurements five X-ray wavelengths were chosen so as to maximize the phasing power in the experiment. A wavelength of 1.7390 A was chosen to maximize the Bijvoet differences and one of of 1.7419 A to maximize the dispersive differences from the Fe anomalous scattering centres in the protein. Two more baseline wavelengths of 1.8000 A (a remote pre- edge point) and 1.5000 A (a remote high energy point) were chose... A fifth wavelength 1.9000 A was chosen to simultaneously measure the anomalous scattering from the sulphur atoms in the clusters.

The diffraction measurements were made on the area detector diffractometer after careful alignment of a crystal so as to be able to measure the Bijvoet pairs related by mirror symmetry simultaneously on the face of the detector. Data at the series of five wavelengths were measured in frames 0.15 degrees apart. A complete set of diffraction data to a nominal resolution of 2.5 A were accumulated on two crystals in different orientations.

Data Processing and Analysis

The data are in the process of being reduced to a set of integrated intensities after application of various geometric correction factors. After having done this and applying scaling corrections, the data would be ready for further steps in the procedure for the determination of the Fe structure factors, location of the Fe-S centres from a Patterson function and the eventual computation of a protein electron density map as detailed in (1).

References

1) W.A.Hendrickson,J.L.Smith and S.Sheriff, Methods in ENZYMOLOGY 115,41-55 (1985).
2) W.A.Hendrickson, Trans. of the Amer. Cryst. Assn. 21, 11-21, 1985.
3) W.H.Orme-Johnson, Ann. Rev. of Biochem. 38, 159-204 (1973).
4) E.T.Adman,L.C.Sieker and L.H.Jensen, J. Biol. Chem. 248, 3987-3996 (1973).
5) L.C.Sieker,E.T.adman,L.H.Jensen and J.Legall, J. Mol. Biol. 179,151-155 (1984).

CHEMICAL MICRO-TOMOGRAPHY AT SSRL

J. H. Kinney, Q. C. Johnson and R. A. Saroyan
Lawrence Livermore National Laboratory
Livermore, CA 94550

U. Bonse and R. Nusshardt
Dept. of Physics, Dortmund University
Dortmund, FRG

and
M. C. Nichols
Sandia National Laboratory
Livermore, CA 94550

Our research at SSRL has been aimed at developing a rapid computed tomography (CT) capability for the non-destructive elemental and chemical-state characterization of small samples.[1,2] The key word in this description is rapid, as other researchers have used pin-hole rastering techniques to achieve high resolution CT reconstructions.[3] Rastering techniques are ponderously slow, however, and cannot be used in many situations of practical interest.

Bonse[4], et al., suggested the use of CCD array detectors for application in high-resolution CT. These commercially available detectors have excellent noise characteristics, large dynamic range and high spatial resolution. Furthermore, by allowing simultaneous measurements of both multiple slices and x-ray projection paths, the speed with which CT can be accomplished is greatly increased.

Figure 1 shows the experimental apparatus developed for performing synchrotron CT. In this configuration, nearly monochromatic x-rays passing through a sample are converted to visible light in a rare-earth phosphor. The visible light is imaged onto a fiber optics face plate which is coupled to a thermoelectrically cooled CCD array detector.[5] The CCD is operated in a charge integrating mode. The charge accumulated during an exposure is read out via a camera controller and stored in a Microvax II computer. This data is Fourier transformed and then back projected to obtain CT reconstructions. A typical scan of a 2mm high by 1 cm wide volume with better than 10% sensitivity and resolution of 20 microns takes about two hours.

The system tested at SSRL during the past year used the focussing lens in a 1:1 imaging configuration. This limits our spatial resolution to no better than 20 microns. Our sensitivity, better than 10%, is limited by counting statistics. Longer counting times, more efficient phosphors and wider aperture lenses will greatly improve this figure. There has been insufficient time to determine the contrast-detail-dose diagram for this system. However, for elemental concentrations less than 20mg/cm^3, no loss in resolution has been observed.

Figure 2 shows a typical test specimen. The specimen consists of a Debye-Scherrer capillary tube, 500 microns in diameter, which has been filled with a dilute solution of $CuSO_4$. A 200 micron capillary has been placed in the solution so as to be concentric with the larger capillary. The smaller capillary contains only air. The capillary walls have been measured and found to be between 1 and 2 microns in thickness.

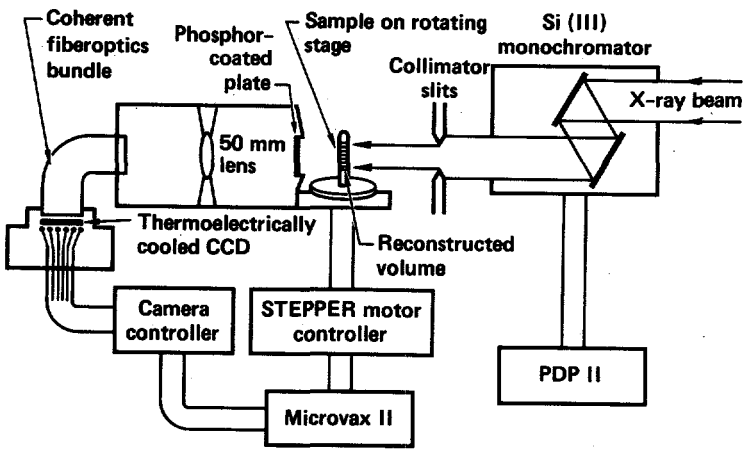

Figure 1. Experimental apparatus

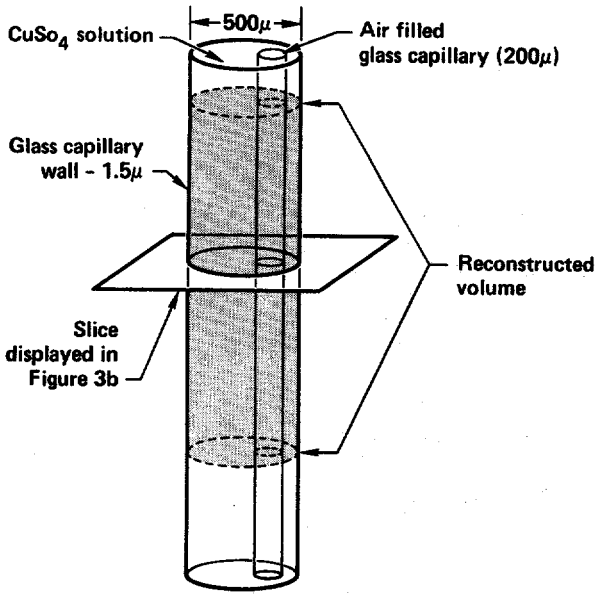

Figure 2. A typical CT test specimen: chemical and air-filled Debye-Scherrer capillaries.

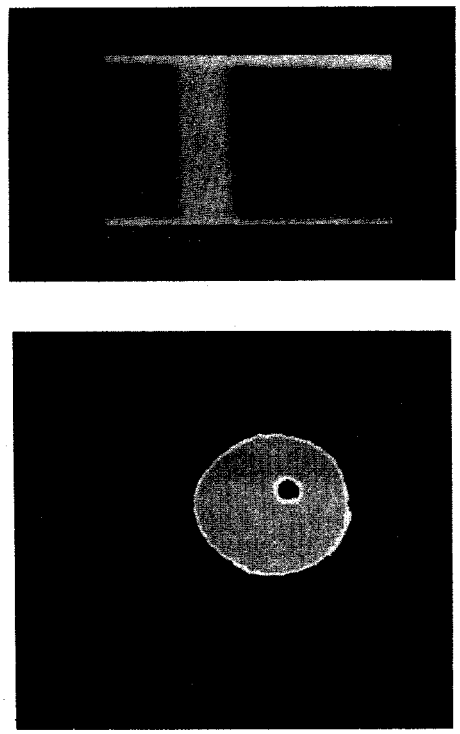

Figure 3. a) A transmission radiograph of the test specimen shown in Figure 2. Note that in transmission the presence of the inner capillary is obscured by the surrounding media. b) A reconstruction of a slice through the CT test specimen which clearly shows the two capillaries and the regions containing air.

Figure 3a shows a radiograph taken with the CCD camera of the concentric capillaries. A series of radiographs such as this was made while rotating the capillaries about 180° in one degree increments. A typical reconstructed slice through the capillaries made from these data is shown in Figure 3b. We can clearly resolve the concentric capillaries. Furthermore, the reconstruction clearly shows the regions containing the air and copper solution. Reconstructions obtained by subtracting data taken above and below the Cu K-edge enhance these contrasts even further.

It is tempting to interpret the edge definition as resolving the glass walls. This is not the case. The appearance of the edge definition is due to edge enhancement in the display. In our present configuration, it is impossible to resolve low-contrast objects as small as one micron.

Further work calls for adding a short focal length lens in a magnifying geometry to increase resolution to approximately one micron. This can be done with no loss in efficiency.

References:

1. Q. C. Johnson, et al. (1986) Mat. Res. Soc. Symp. Proc., 69, 203.

2. J. H. Kinney, Q. C. Johnson, M. C. Nichols, U. Bonse and R. Nusshardt (1986) Applied Optics, 25, 4583.

3. For example: Yu. I. Borodin, et al. (1986) Nuc. Inst. Meth., A246, 649.

4. U. Bonse, et al. (1986) Nuc. Inst. Meth., A246, 644.

5. J. H. Kinney, Q. C. Johnson, U. Bonse, R. Nusshardt and M. C. Nichols (1986) SPIE, 691, 43.

X-RAY ABSORPTION STUDY OF PRESSURE INDUCED VALENCE INSTABILITIES

R. Ingalls
Department of Physics, University of Washington, Seattle, WA 98195

K.R. Bauchspiess and E.D. Crozier
Department of Physics, Simon Frazer University, Burnaby, B.C., CANADA

During this reporting period we have continued our high pressure study of the mixed valent compound, SmSe. It should be recalled that this material is an insulator at atmospheric pressure but undergoes an isostructural transition to the conducting mixed valent state between approximately 32 and 38 kbar. Previously we have reported that the Sm valence, as measured via the Sm L_3-edge structure, appears to change more gradually then the pressure-volume discontinuity would indicate [1]. In fact, although the Sm valence appears to increase from 2+ around 20 kbar, it only seems to reach 3+ at 70 or 80 kbar.

Other somewhat puzzling behavior is that in the mixed-valent region, only one Sm-Se distance is observed in the EXAFS data. Also, despite a shift of 7 eV in the Sm L_3-edge white line, the EXAFS parameter, E_0, does not appear to shift. Similar observations have been made for mixed valence $Sm_{1-x}Y_xS$ [2].

In order to understand this problem, a low temperature press has been constructed in order to extend this work down to liquid nitrogen temperature [3]. Excellent EXAFS data have been obtained for both the Se K-edge as well as the Sm L_3-edge. Analysis of the former indicate that the mean-square fluctuation in the Se-Sm bond length increases in the mixed valence transition region [4]. The most recent results from the Sm L_3-edge are still undergoing careful analysis. The picture that emerges from this work evidently must include the effect on the spectra of a variation of the valence fluctuation time with pressure.

This work was supported in part by the U.S. D.O.E. Grant #DE-FG06-84ER45163 and by the Natural Sciences and Engineering Research Council of Canada.

References

1. R. Ingalls, E.D. Crozier, N. Alberding, K.R. Bauchspiess, P. Viren, and B. Houser, SSRL Rpt. 85/01, K. Cantwell, ed., p. IX-5.
2. J.B. Boyce, R.M. Martin, and J.W. Allen, In EXAFS and Near Edge Structure, A. Bianconi, L. Incoccia and S. Stipcich, eds., (Springer Verlag, Berlin).
3. E.D. Crozier, et al., See entry under Proposal No. 100, this current Annual Progress Report.
4. K.R. Bauchspiess, E.D. Crozier, and R. Ingalls, Proc. of the Int. Conf. EXAFS and Near Edge Struc. IV; (to be published, J. de Phys.).

Synthesis and Structural Characterization of $CaTiO_3$ Doped with 0.05-7.5 Mole Percent Gadolinium(III)

Elizabeth M. Larson, P. Gary Eller,* John D. Purson and Charles F. Pace
Isotope and Nuclear Chemistry Division
Los Alamos National Laboratory
Los Alamos, NM 87545

R.B. Greegor and F.W. Lytle
Boeing Corporation
Seattle, WA 98124

Michael P. Eastman
Department of Chemistry
University of Texas
El Paso, TX 98124

INTRODUCTION

Calcium titanate, $CaTiO_3$, is one constituent of several ceramic composites which have been proposed as hosts for long-term disposal of high-level nuclear wastes.[1-2] Originally transuranic and fission product elements (including lanthanides) were expected to enter these phases by random substitution, with specific site selectivity being determined by ionic size. A variety of structure techniques have been used to show that complicated cation ordering, shear effects, and even twinning on a unit cell basis can occur, in addition to formation of distinct but closely related phases.[3-8] Because of the similarities of the ionic radii of Ca^{+2} and trivalent/tetravalent actinides and lanthanides, for many titanate waste formulations the calcium site in $CaTiO_3$ is expected to be the major host site for fission product and transuranium elements.[1-3, 9-11] Calcium titanate containing gadolinium, which occupies the middle position of the lanthanide series, thus affords an ideal site substitution model not only for the lanthanide fission products but also for tri- and tetravalent transuranic elements.

X-RAY DIFFRACTION

$CaTiO_3$ with 7 mole percent Gd was prepared by ballmilling the appropriate stoichiometric ratios of Gd_2O_3, CaO and TiO_2 for one hour, followed by coldpressing and firing at 1450 C for two weeks. Pale brown crystals formed during a two-week cooling process. X-ray diffraction was collected on a representative sample. Lattice constants and crystallographic symmetry corresponded with the reported $CaTiO_3$ structure.[12] The structure was solved using published positions for Ca, Ti and O and Patterson methods. All atoms refined anisotropically to give R= 8.3% and unreasonably small thermal parameters for Ca . Substantial electron density at the Ca site was observed in a difference fourier map. Upon refining the coupled occupancy factors of gadolinium and calcium at the Ca site, the refinement converged with Ca and Gd occupancies of 92.5(3)% and 7.5(3)% respectively. Final R= 4.0%.

X-RAY ABSORPTION

Extended X-ray absorption fine structure (EXAFS) data were collected at room temperature in both the absorption and fluorescence modes on powdered samples contained in plastic envelopes, at SSRL. Gadolinium doped perovskite and Gd_2O_3 (C-type) were examined. Details of the data workup procedures were as described in earlier publications.[13] The EXAFS curves were obtained after application of a cubic spline fitting routine to the raw gadolinium L_{III} edges. The Gd_2O_3 was used as a model compound for phase extraction. Figure 1 exhibits the EXAFS results for the Gd-doped perovskite as well as the Gd_2O_3 standard.

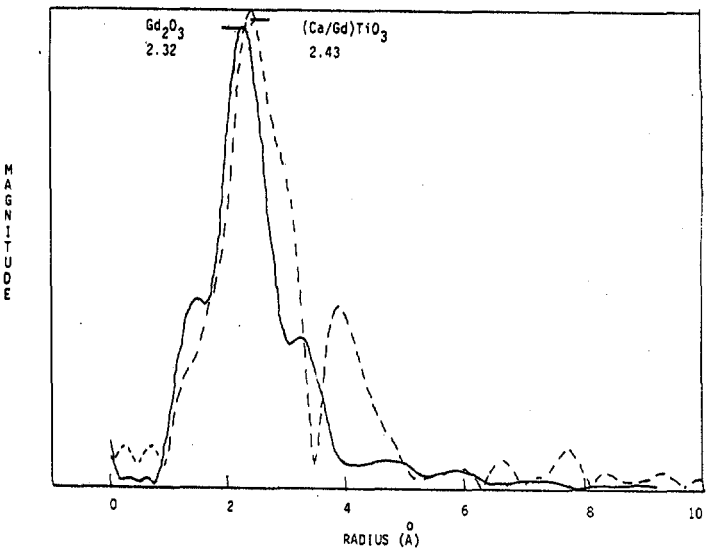

Figure 1. Phase corrected radial distribution curves for Gd_2O_3 (solid) and $(Ca_{.925}/Gd_{.075})TiO_3$ (dashed). Transforms were calculated with K^1 weighting.

DISCUSSION

The single crystal X-ray refinement shows conclusively that, as predicted, Gd^{+3} enters the Ca^{+2} site of $CaTiO_3$ and that the Ca(Gd) site is surrounded by eight near-neighbor oxygens (2.36-2.67 Å, mean 2.52 Å). The X-ray diffraction results, of course, give the average of these parameters over the structure. The first shell Gd-O distance as determined by EXAFS (Figure 1) is 2.43 Å, shorter by about the difference in ionic radii of Ca^{+2} and Gd^{+3} in eight coordination (1.12 and 1.07 Å respectively)[10]. Since the EXAFS technique gives the average Gd-O distance at specific Gd sites, the discrepancy between X-ray diffraction and absorption results suggest that the coordination shell is slightly contracted about the Gd^{+3} ions compared to the Ca^{+2} sites. This effect should produce local inhomogeneities in the structure, especially at high doping levels , as observed by Raman and EPR methods.

REFERENCES

1. A.E. Ringwood, A.M. Oversby, S.E.Kesson, W. Sinclair, N.G. Ware, W.O. Hibberson & A. Major, Nucl.Chem.Waste Mgt. 2, 287 (1981).
A.E. Ringwood, Amer.Sci., 70, 201 (1982).
2. E.R.Vance & D.K. Agrawal, Nucl.Chem. Waste Mgt., 3, 229 (1982).
3. T.J. White, R.L.Segall & P.S. Turner, Angew.Chem.Int.Ed., 24, 357 (1985).
4. F. Mazzi & R.Munno, Amer.Mineral., 68, 262 (1983).
5. N. Ishizawa, F. Marumo, S. Iwai, M. Kimura & T. Kawamura, Acta.Cryst., B38, 368 (1962).
6. G.V. Bauzuev & G.P. Shveikin, Dokl.Akad.Nauk SSSR, 226, 393, Engl. Trans. (1983).

7. M.Nanot, F.Queyroux, J.C.Gilles & R.Portier, J.Solid Statw Chem., 38, 74 (1981).
8. C.R.A. Catlow, A.V. Chadwick, G.N. Greaves & L.M. Moroney, Nature, 312, 601 (1984).
9. R.A. Penneman & P.G. Eller, Radiochim.Acta, 32, 81 (1983).
10. R.D. Shannon, Acta Cryst., A32, 751 (1976).
11. W.H. Zachariasen, J.Less-Common Met., 62, 1 (1978).
W.H. Zachariasen & R.A. Penneman, J.Less-Common Met., 69, 369 (1980).
12. H.J.A. Koopmans, G.M.H. van de Velde & P.J. Gellings, Acta Cryst., C39, 323 (1983).
13. F.W. Lytle, G.H. Via & J.H. Sinfelt, " X-ray Absorption Spectroscopy of Catalyst Applications. ", Synchrotron Radiation Research. (I.Winick & S. Doniach, eds.), Plenum; New York, pp. 401-24.

A Copper XAS Study of Dopamine β-Hydroxylase

R.A. Scott , R.J. Sullivan
School of Chemical Sciences, University of Illinois, Urbana, IL 61801

L.I. Kruse, W.E. Dewolf, R.E. Dolle
Smith Kline & French Laboratories, Philadelphia, PA 19101

Dopamine β-Hydroxylase (DBH) is a copper -containing mixed function oxidase which catalyzes the benzylic hydroxylation of dopamine to norepinepherine. DBH is inactive in the Cu(II) form and requires reductive priming by a one electron donor to convert it to the enzymatically active Cu(I) form. Although there has been some debate in the past about the exact copper content of DBH, it is accepted that maximal enzymatic activity is achieved with a copper to subunit ratio of 2:1. A copper binuclear active site would seem to be favored in light of the facts that DBH has a net two electon reaction stoichiometry, a 2:1 copper to subunit ratio, and a functional similarity to tyrosinase and hemocyanin which both contain a copper binuclear active site. However, EPR studies of the resting Cu(II) form of DBH show no evidence for a magnetic interaction between the copper atoms. Here we report the results of a copper EXAFS analysis of bovine DBH in the Cu(I) and Cu(II) forms with a 2:1 copper to subunit ratio.

The copper k x-ray absorption edge spectra for the oxidized and abscorbate-reduced forms of DBH are compared in Figure 1 with the oxidized and dithionite-reduced forms of bovine plasma amine oxidase and for the "model compound" $Cu(imidazole)_4^{+2}$. The edge comparisons demonstrate that the oxidized form of DBH consists of copper in only the +2 oxidation state and the reduced form of the enzyme consists of copper in the +1 oxidation state. The shape of the edge of the oxidized form of DBH is consistent with predominantly imidazole ligation. No evidence is available regarding the possible differences in the two copper sites since the edge spectra represent only an average copper environment.

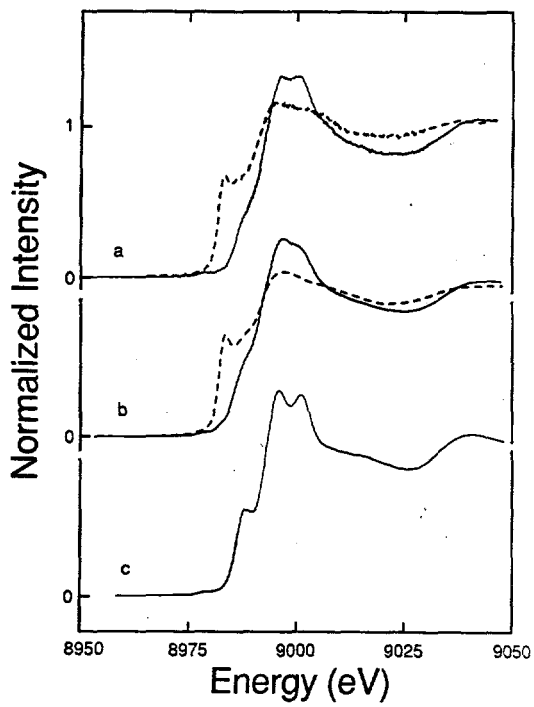

Figure 1: Comparison of Cu K absorption edges for: (a) oxidized (——) and dithionite-reduced (- - -) bovine plasma amine oxidase; (b) oxidized (——) and ascorbate-reduced (- - -) bovine DBH; and (c) $[Cu(imidazole)_4]^{+2}$.

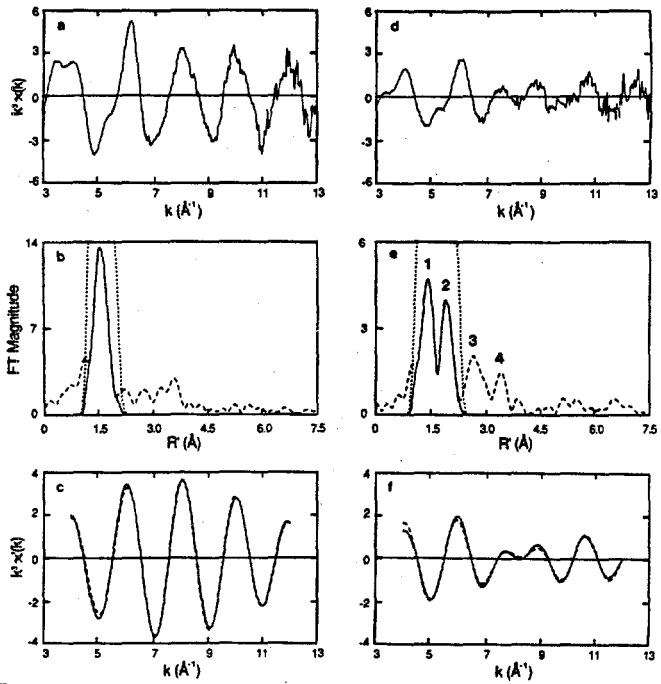

Figure 2: Comparison of Cu EXAFS analysis for Cu(II) (left) and Cu(I) (right) forms of DBH. Fourier transforms of the raw Cu EXAFS data in (a) and (d) are shown in (b) and (e), respectively. The filter windows (· · ·) in (b) and (e) were used to extract the first shell contributions which are shown as back-transforms in (c) and (f). The best curve-fitting results are shown as dashed lines in (c) and (f).

Figure 2 summarizes our analysis of the copper EXAFS of oxidized and ascorbate-reduced forms of DBH. The copper EXAFS and Fourier transform (FT) of oxidized DBH (Figure 2a,b) have appearances reminiscent of data obtained from $Cu(imidazole)_4^{+2}$. FT peaks between R'~ 2.0-3.8 Å (Figure 2b) are most likely due to scattering by carbon and nitrogens in the outer shells of imidazole rings, indicating coordination by histidine. Curve-fitting analysis of the extracted first- shell FT peak (Figure 2c) yields the result of 4 ± 1 (N,O)-containing ligands at 1.98 ± 0.02 Å.

Comparison of Figures 2a,d indicate that a very significant structural change occurs upon ascorbate reduction. More specifically, the copper EXAFS FT of ascorbate-reduced DBH exhibits two main (first shell) peaks at R'~ 1.5 and 1.9 Å (peaks 1 and 2 in figure 2e). Extraction and curve-fitting analysis of peaks 1 and 2 (Figure 2f) indicate that they arise from Cu-(N,O) and Cu-S interactions, respectively. The best fits are obtained assuming two or three (N,O)-containing ligands with Cu-(N,O) distances of 1.94 ± 0.02 Å and one S-containing ligand with a Cu-S distance of 2.30 ± 0.02 Å.

In conclusion, our results have shown that the copper sites in the oxidized and ascorbate-reduced form of the enzyme are structurally distinct. The significant structural rearrangement of the copper active sites that accompanies ascorbate reduction is suggested by our results to be at least partially responsible for the reductive activation of DBH. Further studies of the copper sites should now be directed towards the ascorbate- reduced form of DBH.

High Temperature X-ray Absorption Study of Iron Sites in Crystalline, Glassy, and Molten Silicates and Oxides

Glenn A. Waychunas, Gordon E. Brown, Jr., Carl W. Ponader, and William E. Jackson
Center for Materials Research and Department of Geology
Stanford University, Stanford, CA 94305

Introduction

The general objective of this study is to obtain direct structural information on the local environment of iron in silicate melts at high temperatures. Iron is the most important transition element in natural silicate melts, glasses, and minerals, in some glass-ceramic systems, and in many slags. Its presence can cause significant changes in phase properties, yet little is known about its local structural environment in melts from these systems. Most past structural studies related to such melts have been performed on quenched samples (glasses) which do not necessarily have the same average structure as the corresponding melt. EXAFS spectroscopy was utilized in this work because it yields direct structural information involving only those pair correlations relevant to the element of interest. High x-ray intensities were required to permit in situ data collection through the furnace and sample holder. In order to assess the feasibility of obtaining EXAFS structural information from oxide and silicate melts at high temperatures, high-temperature EXAFS studies of crystalline oxides and silicates with well-characterized structures are required. This step is also essential for assessment of thermal versus static disorder effects. The iron-bearing samples chosen for study are listed in Figure 1 next to their XANES spectra, and iron coordination number and oxidation state are indicated in each case. The liquidus temperatures of the sodium-iron and potassium-iron silicate melts are 1023°K and 1173°K, respectively.

Experimental Details

EXAFS/XANES spectra were collected on powdered samples using fluorescence detection methods at temperatures ranging from 90 to 1173°K. Low temperature data were collected with an LN_2-cooled sample holder. High temperature data were collected using a Lytle-type, water-cooled, evacuated (10^{-3} torr) furnace assembly consisting of a Ta- or Mo-wound resistance furnace containing a thin-walled BN sample holder. Data for the crystalline model compounds were collected during two dedicated runs on wiggler side station IV-1 (90 to 523°K on model compounds) and bending magnet line II-3 (298 to 1173°K) using Si (111) monochromator crystals and a 1 mm high entrance slit. High temperature results for the model compounds were sufficiently good to warrant detailed EXAFS work on the glasses and melts at high temperature. Glass/melt data were collected in the same manner on beam line II-3, and at least three clear EXAFS oscillations were observed for the glasses and melts in the k range 4 to 11 $Å^{-1}$. The highest temperature attainable with our furnace assembly for extended periods (> 2 hours) was 1200°K. At this temperature, however, oxidation of the resistance elements occurred slowly and caused eventual failure. As a result, seven different furnaces were required to complete our experiments. Optical and electron microprobe examination of the glasses quenched from the melts after data collection showed no evidence of reaction between melt and sample holder. Some oxidation of iron in one of the quenched melts was detected by subsequent Mossbauer spectroscopy on samples of the glasses.

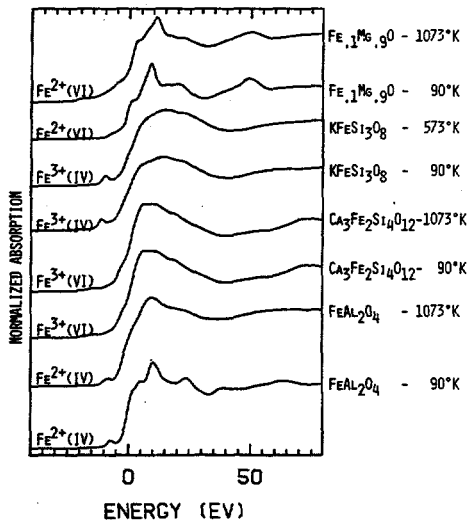

Fig. 1a. Comparison of Fe K-NEXAFS for model compounds at different temperatures.

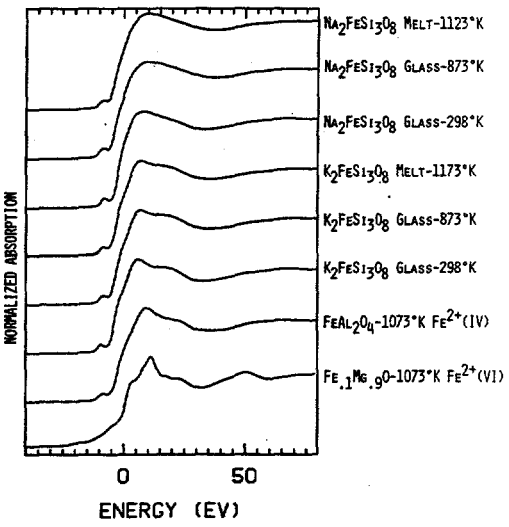

Fig. 1b. Comparison of Fe K-NEXAFS for Na-Fe and K-Fe silicate glasses and two model compounds.

Results and Discussion

Selected Fe K-XANES spectra of model compounds, glasses, and melts are shown in Figure 1. The pre-edge feature of Fe is sensitive to its coordination environment [1,2], with tetrahedral coordination producing about an order of magnitude intensification relative to octahedral coordination (cf. 90°K spectra of $Mg_{.9}Fe_{.10}$ and $FeAl_2O_4$ in Fig. 1a). Comparison of the height of the pre-edge feature relative to the height of the edge step among the glasses, melts, and model compounds indicates that the majority Fe species in the glasses and melts is tetrahedral iron (>90%). The relative positions of pre-edge and edge features of Fe in oxides are sensitive to oxidation state, with features for Fe3+ shifted 2 to 3 eV higher than features for Fe^{2+} [1]. A comparison of Fe edge positions in the glasses indicates that the majority of Fe is 2+, as would be expected from charge balance considerations.

Fitting the Fe K-EXAFS spectra of the glasses and melts over the k range 4 to 11 $Å^{-1}$, using $Mg_{.9}Fe_{.10}$ and $FeCaSi_2O_6$ as model compounds for phase and amplitude calibration, yielded the following results (CN = number of oxygens around Fe, R = Fe-O distance in Å, DW = Debye-Waller-type parameter in Å, estimated standard errors in parentheses referring to the least significant decimal place quoted):

Composition		CN	R	DW
$K_2FeSi_3O_8$	(glass @ 298°K)	4.1(3)	1.99(1)	0.035(9)
$K_2FeSi_3O_8$	(glass @ 673°K)	3.1(4)	1.97(1)	0.05(1)
$K_2FeSi_3O_8$	(supercooled melt @ 1073°K)	3.1(5)	1.93(1)	0.08(1)
$K_2FeSi_3O_8$	(melt @ 1173K°)	5.0(9)	1.96(1)	0.11(1)
$Na_2FeSi_3O_8$	(glass @ 298°K)	3.3(4)	2.02(1)	0.04(1)
$Na_2FeSi_3O_8$	(glass @ 673°K)	2.7(4)	1.95(1)	0.06(1)
$Na_2FeSi_3O_8$	(glass @ 873°K)	2.8(5)	1.93(1)	0.07(1)
$Na_2FeSi_3O_8$	(melt @ 1123°K)	3.2(6)	1.94(1)	0.08(1)

Fitting the high temperature EXAFS spectrum of crystalline $FeAl_2O_4$ (@ 1173°K), using $FeCaSi_2O_6$ as a model compound, yielded the following results: CN = 3.9(5), R = 1.97(1); DW = .08(1). Selected radial distribution functions, uncorrected for phase shifts, are shown in Figure 2.

The following conclusions can be drawn from our results:

(1) The average coordination of Fe in the glasses and melts examined at most of the temperatures appears to be tetrahedral, based on both EXAFS and XANES results. This conclusion is also supported by ^{57}Fe Mossbauer analyses of glasses quenched from the melts after high temperature EXAFS data collection.

(2) The observed Fe-O distances in the glasses and melts range from 1.93 to 2.02 Å, which includes the distance predicted for tetrahedral Fe^{2+} - oxygen bonds from radii summation (1.99 Å). Distances expected for octahedral Fe^{2+} - oxygen bonds and tetrahedral Fe^{3+} - oxygen bonds are 2.14 and 1.85 Å, respectively. The major peaks in the RDF's for hercynite ($FeAl_2O_4$ @ 1073°K) and $K_2FeSi_3O_8$ melt (@1173°K) centered at 1.6 Å are asymmetric. The lower R contribution is thought to be significant and may represent tetrahedral Fe^{3+} - oxygen distances. This suggestion is supported by our Mossbauer analyses of quenched K-Fe silicate melt, which show that 32% of the iron is Fe^{3+}, probably in tetrahedral coordination. Two shell fits of the EXAFS spectra of these samples will be attempted. In contrast, the major peak in the RDF of Na-Fe silicate melt (@ 1123°K) is symmetric, and Mossbauer analyses of the quenched glass show no evidence of Fe^{3+}. There is the hint of a second feature at about 3.1 Å in the RDF of the K-Fe silicate glass at 298°K, which we tentatively interpret as due to an Fe-Si correlation. If correct, this interpretation supports an average local structure around an oxygen bonded to Fe^{2+} in this glass consisting of one tetrahedral silicon, one tetrahedral iron, and one or more Na atoms, which would approximately satisfy local charge balance requirements. Higher quality data, particularly for the melts, are required to test this hypothesis.

(3) Values of the Debye-Waller-type parameters for the glasses and melts increase smoothly with temperature and are comparable to values for the crystalline model compounds at high temperatures.

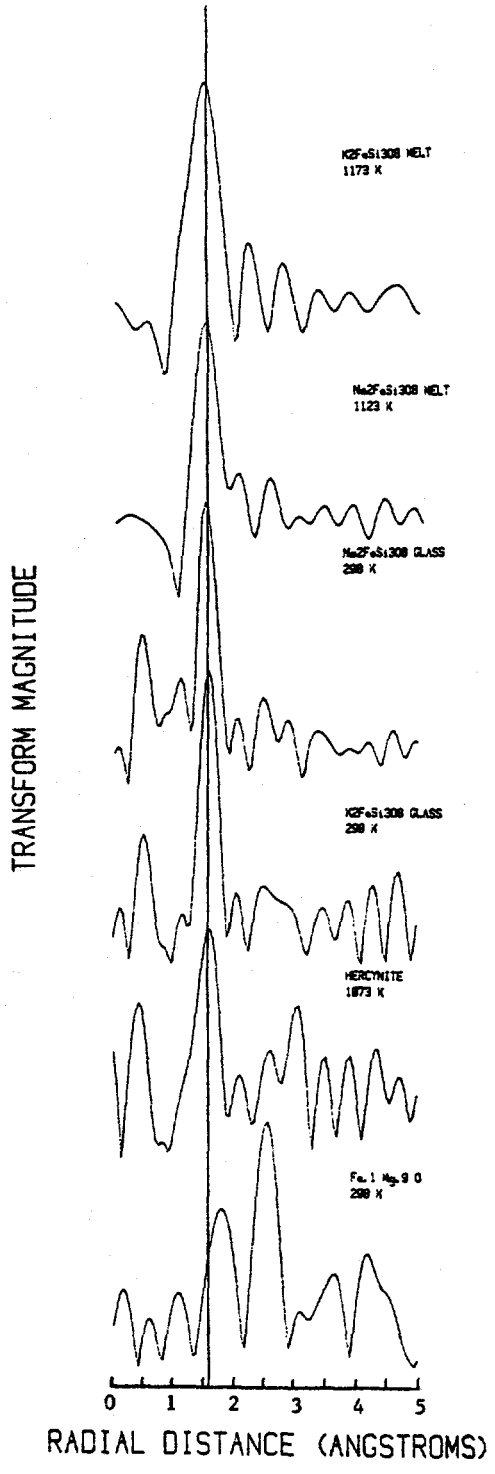

Fig. 2. Selected radial distribution functions for model compounds, glasses, and melts.

We suggest that this observation indicates little difference in static disorder around iron in the glasses and melts relative to the well-ordered, crystalline compounds.

(4) The average iron environment in the melts is similar to that in the glasses at lower temperatures.

(5) Our observations lead to the suggestion that iron in the glasses and melts examined acts as a "network former". This suggestion differs from that of most published spectroscopic studies of Fe^{2+} in glasses and melts, which assumes Fe^{2+} to be a "network modifier".

(6) Our study has demonstrated the feasibility of high temperature x-ray absorption studies of transition metal cations in glasses and melts with melting points of 1200°K or less. Such studies can yield direct structural information which is complementary to that from x-ray and neutron scattering. Additional, higher quality EXAFS/XANES data on these and other glass/melt compositions are needed to examine the structural role of iron and other transition metals in silicate and oxide melts. Improved furnace design and a higher quality vacuum environment should increase the maximum temperature attainable in such work, and thereby make higher melting temperature systems accessible to structural study.

Acknowledgements

This work was supported by NSF Grant EAR-8513488. DOE and NIH support of SSRL is also gratefully acknowledged. We thank J. Stebbins (Stanford) for helpful discussions.

References

1. G.A. Waychunas, G.E. Brown, Jr., and M.J. Apted, Phys. Chem. Minerals 10, 1 (1983).
2. F.W. Lytle and R.B. Greegor, Mat. Res. Soc. Symp. Proc, Vol. 61, 259 (1986).

XAS STUDY OF ION ADSORPTION AT AQUEOUS/OXIDE INTERFACES

A. Lawrence Roe(1), Kim F. Hayes(2), Catherine J. Chisholm(3), Gordon E. Brown,Jr.(3), Keith O. Hodgson(1), George A. Parks(3), James O. Leckie(2)

(1) Department of Chemistry, (2) Department of Civil Engineering, (3) School of Earth Sciences, Stanford University, Stanford, CA 94305

Introduction.

Aqueous adsorption models are applicable in many diverse fields: low temperature aqueous geochemistry (ore deposition, ore prospecting), chemical oceanography (oceanic trace metal transport), environmental engineering (design of trace metal removal processes for industrial wastestreams, transport of trace metals and radionuclides in groundwater), electronic engineering (modeling behavior of ion sensitive field effect transistors (ISFETS)), chemical engineering (design of catalytic systems and corrosion control). These models have been formulated from bulk properties of aqueous/solid systems and it is often difficult to predict behavior outside the range over which the initial experiments were performed. They have reached a level of sophistication, however, where knowledge of the structure of surface complexes can be used to constrain fitting parameters to improve the models' predictions. In order to provide such knowledge, we have measured the EXAFS of two different systems over a range of pH and initial species concentrations: plumbous cation partitioned on α-FeOOH and selenium oxyanions partitioned on α-FeOOH.

Experimental Details.

All of the experimental measurements for the partitioned materials were done in situ the presence of water; the lead data were measured on centrifuged pastes or suspensions and all of the selenium data were measured on suspensions. Teflon cells with mylar windows were used to ensure that the samples retained water during the measurements. The XAS data were measured as the fluoresence spectra of bulk solutions in a 90 degree orientation. The XAS of model compounds with known structures were all collected in transmission mode.

All partitioned samples discussed below were prepared by adjusting the pH to a value that would produce substantial partitioning of the sorbate to the solid phase. The stock α-FeOOH suspension contained 30 grams/liter with a surface area of 50 sq.meters/gram; the effective concentration of binding sites on α-FeOOH was 20mM. Lead system 1 represents a surface coverage of roughly 10%; lead system 2 has 50% surface coverage and an equal amount of lead that may or may not be sorbed. In both cases the supernatant contained negligible lead. Both of the selenium suspensions are near the maximum loading of selenium.

Plumbous Cation.

Comparison of the Pb L3 x-ray absorption edge spectra of oxygen-ligated model compounds and lead partitioned with α-FeOOH (Pb/FeOOH) yields structural information for the local lead environment. Pb/FeOOH samples were generated from a series of α-FeOOH suspensions (with initial lead concentrations of 30 mM, 15 mM, and 2 mM) by the adjustment of the pH until the solution lead concentration decreased to a minimal value. The two extremes of this series will be discussed: 1, 2 mM lead nitrate solution /α-FeOOH, and 2, 30 mM lead nitrate solution/α-FeOOH. System 2 is characterized by a sharp increase in the total amount of lead partitioned as a function of pH.

The edge regions of several models and of Pb/FeOOH systems 1 and 2 (figure 1) show marked variability. The spectrum of Pb(II)aq has a significantly larger principal maximum than the other materials. All of the other spectra are characterized by a low energy shoulder and principal maxima that are variable in energy and amplitude. A qualitative comparison leads to the following conclusions:

- The local environment of lead in 2 is not that of an oxide or hydroxide precipitate, but has the same shoulder and maxima energies as plumboferrite. This observation is consistent with the formation of a layer of adsorbed lead covering portions of the oxide surface, since plumboferrite consists of sheets of lead-oxygen octahedra sandwiched between iron spinel structures (figure 2). Extending this argument there should be iron in the second shell of atoms surrounding lead.
- The edge spectrum of 1 is significantly different from 2; 1 has only one maximum and it has increased amplitude relative to 2. In 1 the principal maximum has shifted to lower energy and it like that of aqueous lead, because of the amplitude change coupled with the energy shift. Note that 1 has a unique spectrum, different from all of the models. The implication for the lower concentration of lead on the oxide surface is that there is little aggregation of lead on the surface, and the coordination environment around lead has high symmetry and few or no second-shell metals.

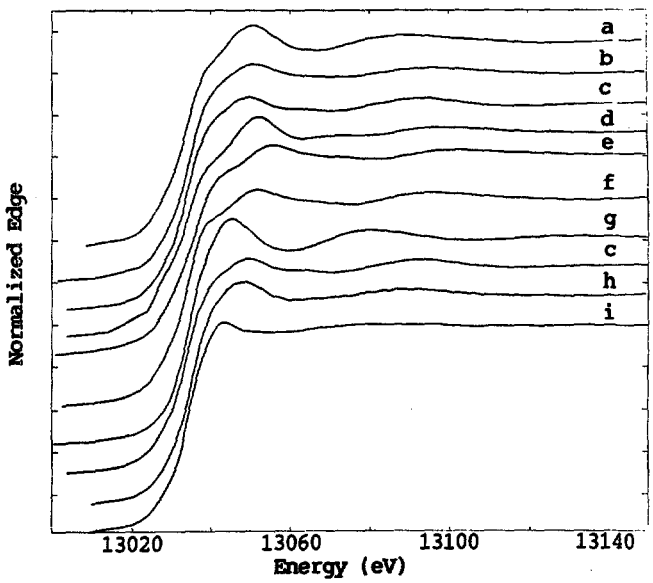

Figure 1. Lead L3 edges of Pb partitioned with α-FeOOH and lead model compounds: (a) $K_2Pb_4Si_8O_{21}$, (b) Pb/FeOOH 2, (c) $PbFe_4O_7$, (d) PbO (ortho.), (e) $Pb(OH)_2$, (f) $[Pb_6O(OH)_6](ClO_4)_4.H_2O$, (g) aqueous $Pb(NO_3)_2$, (h) Pb/FeOOH 1, (i) $PbFe_{12}O_{19}$.

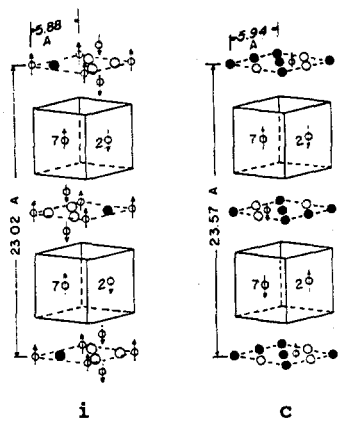

Figure 2. Structures of $PbFe_{12}O_{19}$, (i), and $PbFe_4O_7$, (c). Lead atoms are represented by filled circles, oxygens by open circles, and iron by circles crossed with arrows. The planes containing lead are separated by iron spinel blocks. Structure (c) is proposed by A.J. Mountvala and S.F. Ravitz (1962), J. Amer. Ceramic Soc., 45, 285-288.

The EXAFS spectra are not in obvious agreement with the interpretations of the edge, however, EXAFS curve-fitting analyses are still being performed. All of the models show a beat pattern in the EXAFS between k=6 $Å^{-1}$ and k=10 $Å^{-1}$, except for the small lead cluster, which does not display a beat until k=9.5 $Å^{-1}$ (figure 3). By this criterion 2 is certainly not identical to plumboferrite, since 2 does not display any beat. Note, however that the EXAFS of 2 matches that of the $Pb_6O(OH)_6$ cluster and the noise in 2 may be obscuring any beat region. The EXAFS of 1 is unique; note especially the position of the first two maxima in the EXAFS. These peaks are at low energy and they only match plumboferrite and a potassium-lead silicate, but both of these models have a pronounced beat pattern.

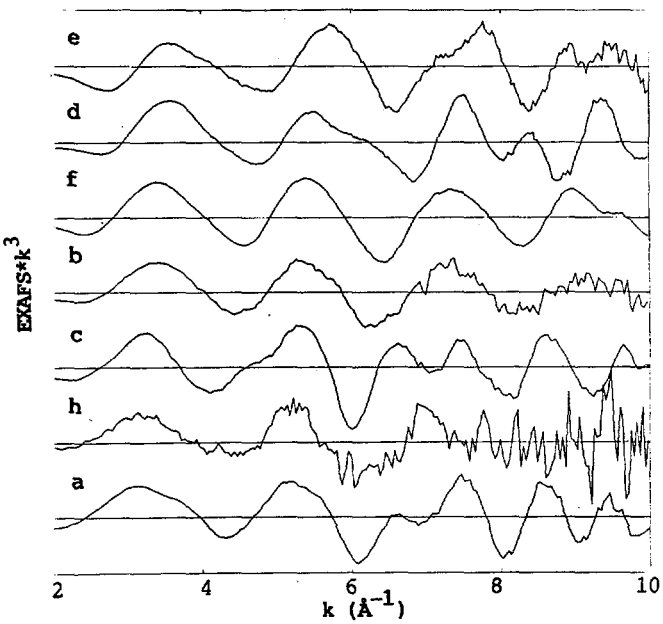

Figure 3. Lead L3 EXAFS of Pb partitioned with α-FeOOH and lead model compounds. The curve labels are the same as for figure 1.

Selenium Oxyanions.

XAS spectra of the oxyanions in water were compared with the spectra of the anions partitioned with α-FeOOH. In comparison to the lead data, the interpretation of the XAS data for the selenium oxyanions is straightforward. The edges are dependent only on the oxidation state: all of the selenite spectra have the same edge position and shape, and there is a constant shift in energy relative to the selenate spectra. There is no evidence for surface complexes in the edge region.

The EXAFS of the two species partitioned with α-FeOOH are dramatically different. The Fourier transforms of the selenate (figure 4) show no change caused by the partitioning with the α-FeOOH. The opposite is true for selenite: The Fourier transform shows a second shell contribution to the EXAFS at 2.9. EXAFS fits of the backtransformed curves with parameters obtained from solid sodium selenite (Na_2SeO_3), soild sodium selenate (Na_2SeO_4), and a selenium iron cubane cluster (Se-Fe parameters) give the fits shown in figure 5. The first shell of oxygens are unchanged from the solids and there is a calculated value of 1.2 irons at 3.33 Å for the selenite/α-FeOOH. These results are not consistent with structural models in which selenite groups share an edge with two adjacent surface oxygens (figures 6a and 6b). They are consistent with the model shown in figure 6c, in which a single oxygen is shared between the surface of α-FeOOH and the selenite group.

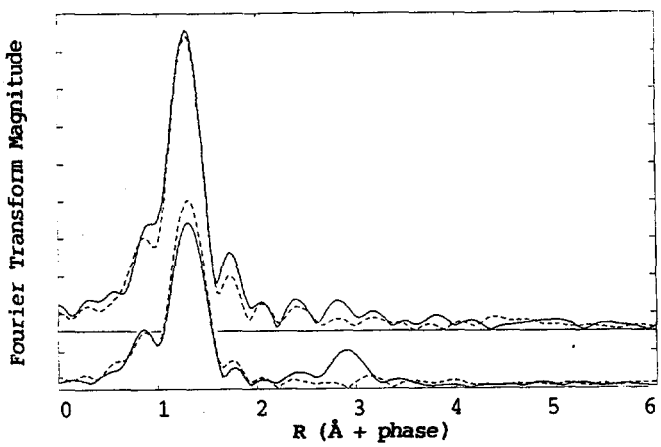

Figure 4. Fourier transforms of the selenium K edge EXAFS of selenium oxyanions in solution (dashed lines) compared with selenium oxyanions partitioned with α-FeOOH (solid lines). The upper curves are for selenate (SeO_4^{2-}) and the lower curves for selenite (SeO_3^{2-}).

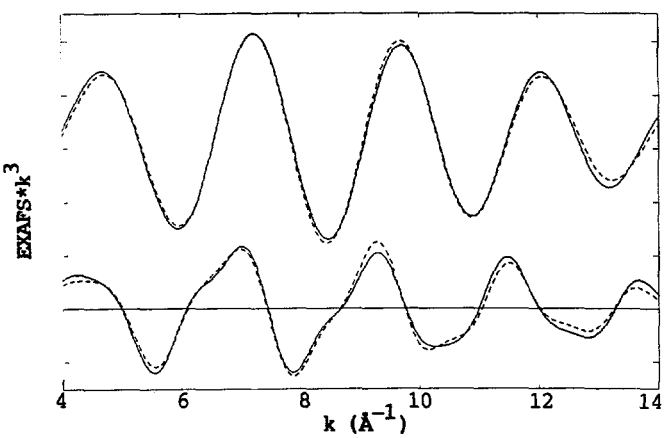

Figure 5. Fits to the Fourier filtered EXAFS of SeO4/FeOOH (upper curve) and SeO3/FeOOH (lower curve). The fits are shown as dashed lines.

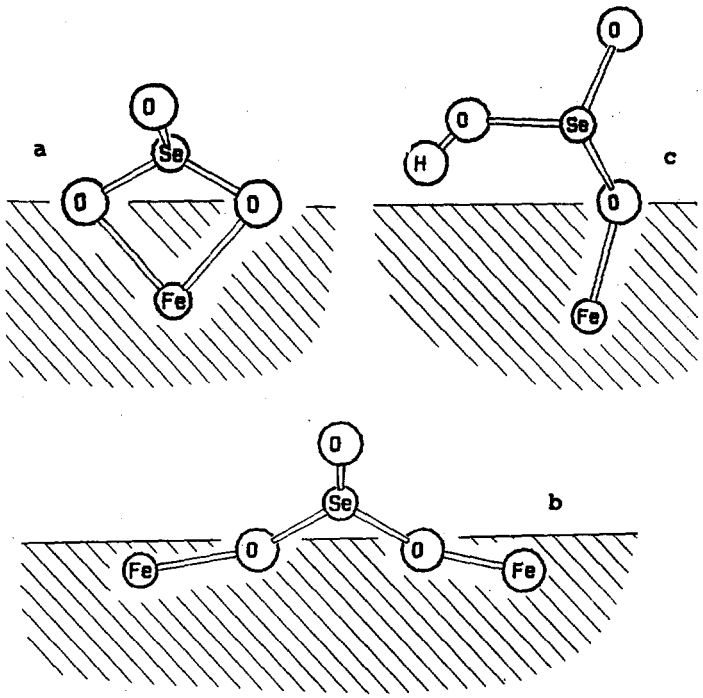

Figure 6. Representations of possible adsorption complexes for SeO3/FeOOH. The oxide is designated as the shaded area.

Conclusions.

Our selenium results allow us to discriminate among several potential models for selenite coordination to the α-FeOOH surface. In contrast, selenate appears to retain its hydration sphere in the SeO4/FeOOH system. Although our results for Pb/FeOOH are not as conclusive, they do permit us to reject certain surface complexation models. Our study has shown that useful and unique structural data can be obtained for adsorbed metal species in situ at solid/aqueous interfaces using x-ray absorption spectroscopy. This new application of XAS should be useful in distinguishing among metal environments for a range of adsorbates.

Acknowledgements.

This research was supported, in part, by NSF grants CHE-85-12129 and EAR-85-13488. We gratefully acknowledge the experimental assistance of Britt Hedman, Carl Ponader, and William Jackson, and the support of SSRL through DOE and NIH.

Ordering of a-Si at a Si(111) Interface

I. K. Robinson, W. K. Waskiewicz and R. T. Tung
AT&T Bell Laboratories
Murray Hill, NJ 07974, U.S.A.

J. Bohr
Riso National Lab, Denmark

In our June 1986 run we measured a Si(111)/a-Si interface prepared by cold deposition of 50 Å of Si onto a clean MBE-grown Si(111) surface. The 7x7 reconstruction of the substrate was preserved underneath the amorphous layer, as evidenced by previous transmission electron diffraction experiments[1]. We also found strong 1/7th order diffraction peaks, supporting this claim, and were able to collect an accurate set of 70 structure factors and are in progress of structural analysis. We find many significant differences between these data and those from the clean surface which agree so well with the Takayanagi model[2] of Si(111)7x7, so conclude there is considerable modification upon deposition of the amorphous layer.

To gain an understanding of the nature of this modification, without the complication of the detailed atomic structure of the large unit cell, we then measured the intensity profiles of the (1,0,l) and (0,1,l) crystal truncation rods, as shown in fig 1[3]. We use a hexagonal definition of the unit cell with (0,0,1) as the surface normal. Each point in the figure is angle-integrated and background subtracted, then corrected for Lorentz factor and sample area and finally divided by the Si form factor so that it corresponds to the interface structure factor alone.

The fit to these data was obtained with the model of fig. 2, adjusting 12 parameters to minimize a least-squares residual. The most important deviations from the ideal truncation rod profile (dashed in fig. 1) are the broad peaks at l=1 and l=4. Because these are the positions of Bragg peaks in the diamond lattice with reversed stacking order, we are immediately informed of the presence of reversed regions in the interface, as shown in the model. Three such layers overall had to be included to get a good fit.

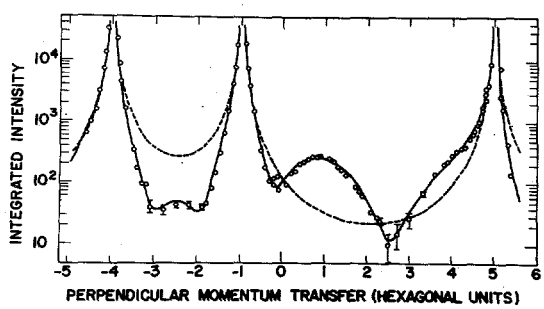

Figure 1. (1,0,l) and 0,1,l) crystal truncation rods of the Si(111)/a-Si interface. Hexagonal coordinates have been used. The two rods have been joined together by use of the (1,0,l) = (0,1,-l) crystallographic identity. The divergences at l=-4, -1 and 5 are bulk Bragg peaks.

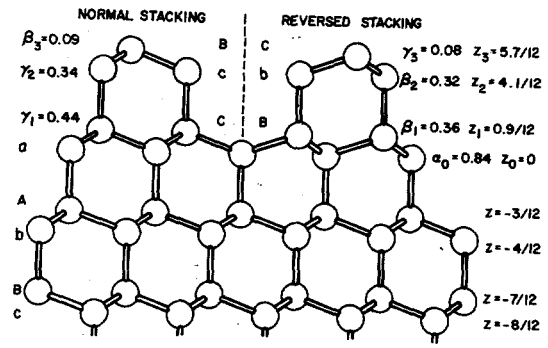

Figure 2. Model of the Si(111)/a-Si interface used to fit the data of Fig. 1. No significance is attached to the lateral placement of regions of normal and reversed stacking, only the fractional occupancies of each: $\alpha\beta$ and γ corresponding to A B and C sites respectively. Parameters Z_j are layer heights in fractions of the hexagonal unit cell parameter, $\sqrt{3}\,a_0$=9.41Å.

Casual inspection of the Takayanagi model[2] reveals the role of the a-Si in the formation of this interface: the abrupt beginning of the reversed stacking region locates the "stacking fault" layer of the clean surface as no. 1 in the model without ambiguity. Above this we would expect from the Takayanagi model a layer of adatoms at height Z=2/12, but these have been replaced by an ordered layer at height Z_2 =4/12 which must partly originate from the a-Si. Finally there is one more partly ordered layer at Z_3 =5/12.

References

1. J. M. Gibson, H. J. Gossmann, J. C. Bean, R. T. Tung, L. C. Feldman Phys. Rev. Lett. *56* 355 (1986)
2. K. Takayanagi, Y. Tanishiro, S. Takahashi, M. Takahashi, Surface Sci. *164* 367 (1985).
3. I. K. Robinson, W. K. Waskiewicz, R. T. Tung, J. Bohr, Phys. Rev. Lett. *57* 2714 (1986).

EXAFS Study of Trace Element Environments in Quenched Silicate Melts of Geochemical Interest

Proposal 999Mp

C.W. Ponader, G.E. Brown, Jr., and W.E. Jackson
Department of Geology, Stanford University
Stanford, California 94305

Trace metal partitioning in crystal-melt systems of geological interest is a complex phenomenon which, if understood, could contribute unique information on magma genesis and evolution. The major purpose of our work on the nature of structural environments of trace metals in quenched silicate melts is to gain a more fundamental understanding of how these environments vary with bulk compositional changes in silicate melts and to test the hypothesis that the transport of certain elements at low concentrations is influenced by the formation of metal–halogen complexes. We have collected EXAFS and XANES spectra for several trace metals in silicate glasses in order to examine the changes in the metal site as the glass composition varies. The metals (edges) studied include La, Gd, and Yb (L_{III}); U (L_{III}, M_V); and Zr and Mo (K). They were present at 2000ppm concentration in three glass compositions: albite ($NaAlSi_3O_8$) (ab), sodium trisilicate ($Na_2Si_3O_7$) (ts) and a peralkaline composition on the join approximately midway between albite and sodium trisilicate ($Na_{3.3}AlSi_7O_{17}$) (pr). Despite the low concentrations of the metals studied, the data are quite good up to a k of at least 10 (Fig. 1). Previous EXAFS studies have been done on U and Zr in silicate glasses [1,2,3,4]; however, the glass compositions differed from those studied here and the metals studied were present at much higher concentrations. EXAFS spectra of the metals in our glasses were also determined with 2 wt. percent F or Cl added in order to identify and examine possible metal-halogen complexes in the glass. Spectra were collected in fluorescence mode on BL VII-3 and BL IV-1 during dedicated runs in April, 1986 and January, 1987. Strong amplitude reductions were observed in fluorescence EXAFS of model compounds used for the rare earths (RE oxides, RE chlorides and RE fluorides). These reductions were probably due to self-absorption and were overcome by collecting spectra of model compounds in transmission mode.

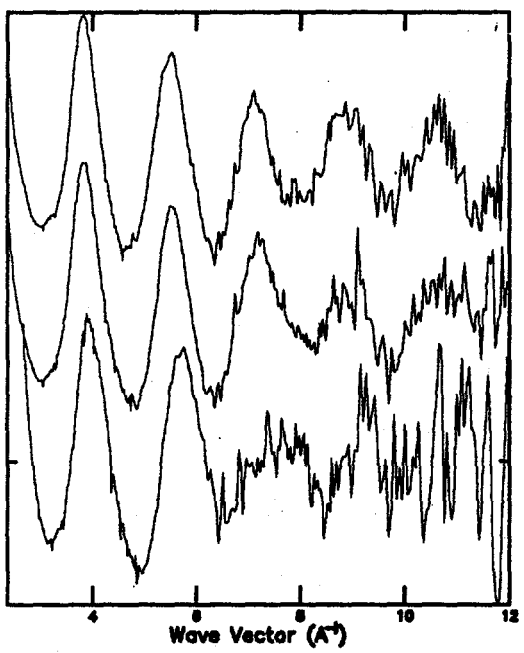

Fig. 1. $k^3\chi(k)$ functions for Yb in albite (bottom), sodium trisilicate (middle) and albite + F (top) glasses.

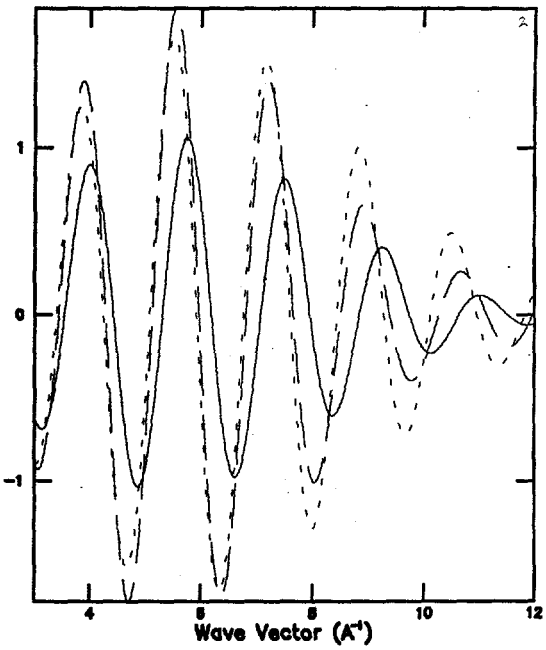

Fig. 2. Back-transformed chi functions for Yb in albite (solid), sodium trisilicate (long dashed) and albite + F (short dash) glasses. Note the large phase and amplitude differences between the polymerized (albite) and the relatively depolymerized (sodium trisilicate and albite + F) glasses.

EXAFS of the rare-earths demonstrate that the sites occupied by the metals are approximately octahedral with average RE-O bond distances of 2.43Å (La), 2.37Å (Gd), and 2.22Å (Yb). Based on the value of the thermal and static disorder parameter σ^2, the site appears to become more distorted as the glass becomes more polymerized in the order ts < pr < ab. The distortion of the site also appears to increase as the size of the cation increases (Yb < Gd < La). There is no evidence for any interaction between chlorine and the rare-earths in the

glasses; and, although the similarity between the back- scat tering and the phase-shift parameters of F and O makes it difficult to rule out a small interaction, there is also no evidence for RE-F bonding. The major effect of the halogens appears to be to depolymerize the glass and thus to decrease the distortion of the rare-earth site (Fig. 2). The significance of the differences between fits involving different numbers of shells of one ligand or two different ligands can be evaluated by calculating the normalized standard deviation (R) for each fit and then calculating the test statistic $\Re = R_1/R_0$. In general, R_0 is the NSD of the unrestricted fit and R_1 is the NSD of the restricted fit. Use of this test is similar to the familiar F-test. Values of $\Re$ for various significance levels and degrees of freedom have been tabulated by Hamilton [5].

In order to fully evaluate the metal-halogen complex hypothesis it is also important to examine the local structure around the halogen atom. We attempted to collect data for fluorine on the old Grasshopper line (I-1) during dedicated run in collaboration with J. Stohr. However, the low resolution of the 1200 line/mm grating at the fluorine K-edge and interference from the Fe L_{III} edge combined to reduce the data quality and make it unusable. We plan to collect chlorine K-EXAFS and XANES spectra on chlorine-bearing glasses during the Spring, 1987 run.

Acknowledgements

This work was supported by NSF Grand EAR-8513488. DOE and NIH support of SSRL is also gratefully acknowledged.

References

1. T. Dumas and J. Petiau (1984) *EXAFS and Near-Edge Structure III*, eds. K.O. Hodgson, B. Hedmann, and J.E. Penner-Hahn, Springer-Verlag, New York, 311.
2. J. Petiau, G. Calas, T. Dumas, and A.M. Heron (1984) *EXAFS and Near-Edge Structure III*, eds. K.O. Hodgson, B. Hedmann, and J.E. Penner-Hahn, Springer-Verlag, New York, 291.
3. J. Petiau, G. Calas, D. Petitmaire, A. Bianconi, M. Benfatto, and A. Marcelli (1986) *Phys. Rev. B*, **34**, 7350.
4. G.E. Brown, Jr., C.W. Ponader, and K. Keefer (1986) Int. Mineral. Assoc. Abstr. Prog., 14th General Meeting, 64.
5. W. Hamilton (1965) *Acta Cryst.*, **18**, 502.

ANOMALOUS SMALL ANGLE X-RAY SCATTERING STUDY ON Tb TITRATED BACTERIORHODOPSIN

[1]S. Wakatsuki, [1]K. O. Hodgson, [3]R.M. Stroud, and [2]S. Doniach

[3] Departments of [1]Chemistry and [2]Applied Physics, Stanford University
[3]Dept. of Biochemistry and Biophysics, Univ. of California, San Francisco

BacterioRhodopsin (bR) molecules contain Mg(II) and Ca(II) which are believed to play an important role in photocycling. These cations can be removed by using a cation exchange column. The color of the membrane is changed from purple to blue upon removal of the cations[1]. This color change is restored if any cation is added to the blue form of bR. In this study, a strong anomalous scatterer, Tb(III), was added to the blue form. Partially oriented bR samples were prepared by centrifuging bR suspensions at 50,000 rpm for 10 hours. A pellet contains layers of membrane sheets which are randomly rotated about the axis perpendicular to the membrane plane. Data were collected at beamlines IV-2 and II-2 at SSRL. Energies were around 7515 eV, the L_{III} edge of Tb.

The electron density distribution along the direction normal to the membrane plane can be obtained from the meridional intensity data. The intensity difference profiles (Fig.1), I(7515)-I(7505), I(7525)-I(7505) and I(7525)-I(7515), have a distinctive feature at 0.028 (1/Å). As expected, the sign of the feature changes according to $\Delta f'$. Further analysis should answer the question, where cation binding sites are located relative to the center of the membrane.

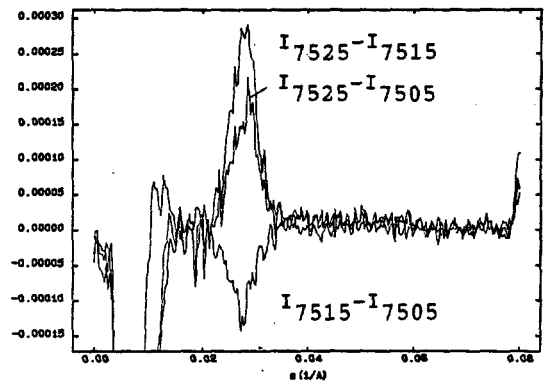

Fig.1 Meridional intensity difference profiles, $I_{7525}-I_{7515}$, $I_{7525}-I_{7505}$, and $I_{7515}-I_{7505}$.

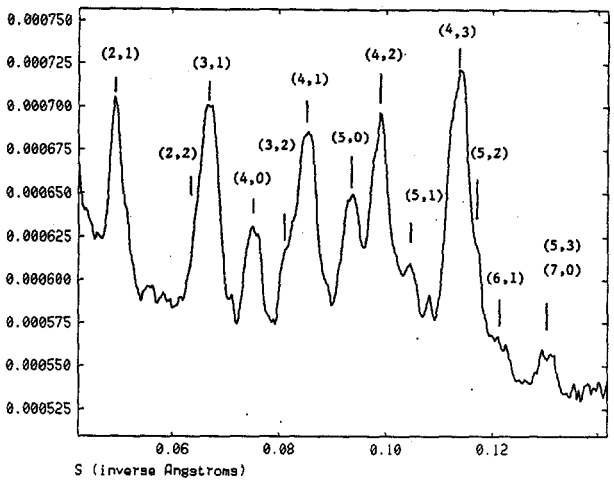

Fig.2 Diffraction peaks in the equatorial direction. Peaks used for the in-plane 2D electron density map are indexed.

In the equatorial direction, intensity profiles (Fig.2) show in-plane diffraction peaks which were used to generate a 2D electron density map (Fig.3). Now we can obtain additional reflections, (5,2), (6,1), (5,3), and (7,0). This is partly due to improvement of the sample preparation, and leads to a higer resolution electron density map with the resolution of 8.8 Å. The difference profiles, I(7465)-I(7515) and I(7505)-I(7515), are still slightly noisy, but show peaks corresponding to the diffraction peaks.

Background scattering was subtracted by using least square slpine of the flat parts of the scattering profiles. Some of the overlapping peaks were resolved by deconvolution with a gaussian desmearing function. Intensities were corrected for membrane misorientation by multiplying by $2\pi S^2$. Then, each corrected I(h,k) was divided into F(h,k) and F(k,h) using the ratios of F(h,k) and F(k,h) obtained from electron diffraction data. In case of the reflections (5,3), (3,5) and (7,0), the corresponding ratios were used because these three peaks overlap. Electron density map (Fig.3) was generated using the phase information from the electron diffraction work[2]. Preliminary Fourier difference maps show similar peaks as the Pb(II) work by N.V. Katre, et al[3] indicating the positions of cation binding sites.

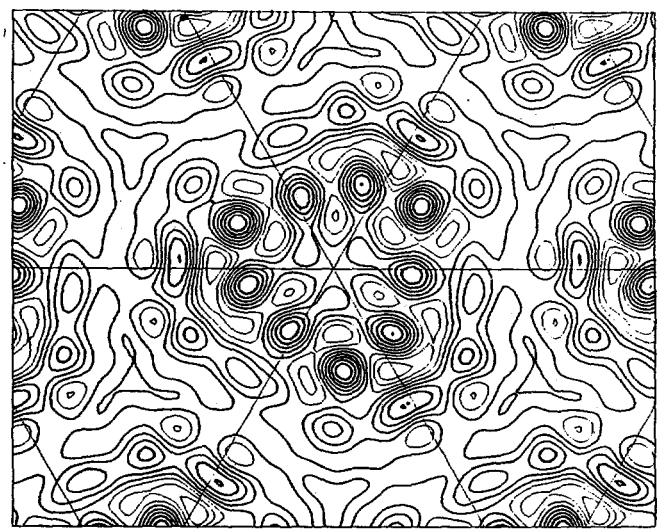

Fig.3 Electron density map of bacterioRhodopsin calculated from in-plane diffraction peaks in Fig.2.

Research supported by NIH Grant RR 01209 and NSF Grant CHE 85-12129.

REFERENCES:

1. Kimura, Y., Ikegami, A. and Stoeckenius, W. (1984), Photochem. Photobiol., 40, 641-646.
2. Unwin, P.N.T. and Henderson, R. (1975), J. Mol. Biol., 94, 425-440.
3. Katre, N.V., Kimura, Y. and Stroud, M. (1986), Biophysics J., 50, 277-284.

FLOW APPARATUS TESTS OF HEMOPROTEIN REACTIONS AT HIGH BEAM INTENSITIES

B. Chance G. Bunker, G. Zhang S. Khalid G. Rosenbaum
Institute for Structural & Functional Studies, Philadelphia, PA

The regenerative flow apparatus has been continuously developed in order to optimize it for the study of rapid reactions (1). The observation chamber has been enlarged so as to accommodate not only a focused beam, characteristic of II-2, but also unfocused beams; the solid angle available from the flow apparatus has been enlarged so that both sides of the apparatus can be viewed by detectors, and finally, the flow apparatus itself has been revised so as to deliver concentrated enzyme intermediates over long periods of time. A test system consists of 0.75 mM horseradish peroxidase with one equivalent of H_2O_2 and two equivalents of ascorbate. This mixture gives a lifetime of the compound II intermediate of 100 msec which allows a 1 sec discharge of the contents through the sample chamber for X-ray observation (Figure 1). Preliminary tests of this observation chamber verify the capability for 0.75 mM detection, but further improvement is necessary to optimize the signal-to-noise ratio. A current difficulty is that the high concentrations of protein coat the stainless-steel cylinders of the driving pistons and compromise the gas-water O-ring seal.

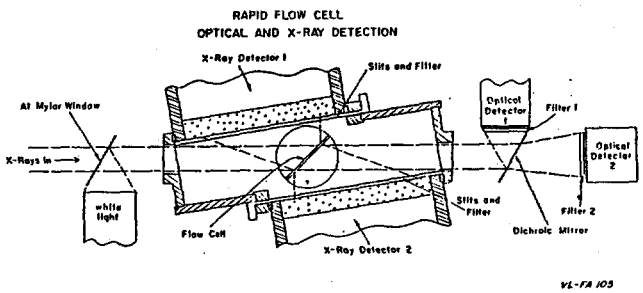

(Figure 1)

The optically pumped flow-flash apparatus has been completed and tested in detail prior to studies at SSRL (2). The lifetime of the flash lamps (1 kilowatt average power) has perenially been a problem, but four days of continuous flashing with X-ray data accumulation have been obtained. Sample damage appears to be minimal using flow through of 5 mM hemoglobin solution. A profile of signal output vs. the sample chamber number shows that 50% of the signal is obtained from the first 100 micron sample chamber (both sides are employed) and that 3-4 chambers are sufficient. The four chambers of 100 microns thickness are sufficient since these are placed at 45° with respect to the beam; the thickness is 0.5 mm.

In this apparatus, X-ray absorption data are acquired during the flash and the effective measuring time depends upon the rapidity of recombination. It is estimated that the time performance is in the microsecond to nanosecond region. The duty ratio of the flow flash apparatus as now employed is 1:60. The duty ratio is 50%, the data being acquired during the flow when the observation chamber is filled with the intermediate, and during the recycle when the observation chamber is filled with the free enzyme.

The application of these apparatuses to specific scientific problems are exemplified by the ability to study compound II horseradish peroxidase at room temperature, on the one hand, and the ability to study the structure of the late stages of the RT transition in hemoglobin and seem to be projects of significant utility.

References

1. Chance, B., Kumar, C., Legallais, V., Pennie, W., Sorge, J. and Khalid, S. Nuclear Instruments & Methods, 222, 180-184 (1984).

2. Chance, B., Korszun, R., Khalid, S., Alter, C. Sorge, J. and Gabbidon, E. in Structural Biological Applications of X-Ray Absorption, Scattering and Diffraction (B. Chance and H. Bartunik eds.) Academic Press, NY pp. 44-69 (1986).

This work was supported by NIH grant GM-31992

LOW TEMPERATURE PHOTOLYSIS/RECOMBINATION OF HEMOPROTEINS UNDER CONDITIONS OF NUCLEAR TUNNELING

B. Chance, Y.-H. Zhou, G. Bunker, G. Zhang, M. Chance, S. Khalid, G. Rosenbaum
Institute for Structural & Functional Studies, Philadelphia, PA

L. Powers
AT&T Bell Labs, Murray Hill, NJ

Goal. To track the trajectory of the ligand to the heme-iron active site by trapping intermediate states of recombination at helium temperatures. Previous work at 4° K showed the photoproduct to have the ligand 0.05 Å displaced from the bound position (1). Work in July at 40° K shows the average ligand position to be 0.7 Å farther away. The goal of the January study was to determine the average ligand position at 60° K.

Method. Because several hours of data acquisition is necessary for adequate EXAFS analysis of 1.2 mM myoglobin samples, it is necessary at the temperatures above 4° K to ensure by continuous illumination and by continuous optical monitoring that the composition of the sample was either constant throughout the EXAFS scan or falling in a known manner.

Methodological Improvement. In order to ensure the possibilities of continuous illuminating of the sample and, at the same time, observing its spectral properties, time-sharing of actinic and measuring wavelengths was employed with approximately 2 msec for each in a continuous manner, the total period of 8 msec. This method provided sufficient photolysis to obtain 80% at 40° and 60% at 60° and 100% at 7°.

Caveat. Photolysis illumination with a light pulse creates a thermal transient which may raise the sample well above the average temperature and create new structural states. Illumination with a high power lamp can cause rises of sample temperature of dozens of degrees. The conditions of our illumination raise the sample 1.4° K as directly measured with a diode embedded in the sample.

Experimental Results. EXAFS spectra acquired in the recent beam time allotments at all three temperatures under conditions where the sample temperature was precisely known as was the extent of photolysis as measured by optical transmission through the sample and as computed from the observed appearance of the "geminate state" band at 764 nm.

Data Analysis. Analysis of the data for mixtures of species are difficult in principle and practice. However, the optical measure of the sample composition is accurate to better than ±2% and is readily calibrated by varying the sample composition under photolysis conditions from 130° to 7° and back again. The unphotolyzed MbCO is therefore accurately known, and under the conditions of this experiment corresponds to 0% at 7°, 20% at 40° and 40% at 60°. Analysis is in progress on this new data set and will be reported shortly.

Publications. A paper on the 40° study completed in July is in the process of publication (2).

Reference

1. Chance, B., Fischetti and Powers, L. Biochemistry, 22, 3820-3829 (1983).

2. Powers, L., Chance, B., Chance, M., Campbell, B., Freedman, J., Khalid, S., Kumar, C., Naqui, A., Reddy, K.S. and Zhou Y.-H. Kinetic, Structural and Spectroscopic Identification of Geminate States of Myoglobin: A Ligand Binding Site on the Reaction Pathway. Biochem. (1987) (submitted).

This work was supported by NIH grant GM-31992

PARTIAL STRUCTURE FACTOR DETERMINATION IN BINARY LIQUIDS BY ANOMALOUS SCATTERING

W.K. Warburton*, K.F. Ludwig+, & A.I. Binenstock#

*The Institute of Physics, USC, Marina del Rey, CA
+IBM Watson Research Labs, Yorktown Heights, NY
#Dept.Appl.Physics, Stanford Univ., Stanford, CA

Introduction:

During the year, data were collected on both Aq-$ZnCl_2$ and Aq-ZnI_2 solutions for comparison with earlier data taken on Aq-$ZnBr_2$ solutions in order to investigate the role of anion size on local solution structure. The bulk of the year's effort, however, was spent analyzing data previously collected on concentrated Aq-$ZnBr_2$, Aq-$CuBr_2$, Aq-$NiBr_2$, and Aq-RbBr solutions, which were studied to examine the effect of cation variation upon local solution structure. These samples are well suited to this study for several reasons. First, all the K absorption edges involved are readily accessible. Second, the chosen progression of atoms should directly illuminate the (often dominant[1]) role of the splitting of cation d-orbitals in the field of the coordinating atoms as d goes from 8 (Ni) to 10 (Zn). This "ligand field stabilization energy" (LFSE) favors octahedral coordination, but is zero for a d^{10} atom. Here size and electrostatic energy effects should determine the structure. Third, the latter term, which favors ordering, varies inversely with cation charge, a difference which should be observed between the 1-1 alkalai bromide and the 2-1 transition metal bromides.

Both EXAFS and Differential Anomalous Scattering (DAS)[2] data were taken at each edge for each sample. In a binary Aq-MX_n (M=metal, X=halide) aqueous solution, six partial structure factors (M-O, M-M, M-X, X-X, X-O, & O-O) contribute significantly to the total x-ray scattering. DAS at the M and X edges breaks this into the two simpler sets (M-O, M-M, & M-X) and (X-O, X-M, & X-X), but the EXAFS data, which are sensitive to nearest neighbor chemical identities and coordination distances, are then extremely useful in their interpretation.[3]

Aq-$ZnBr_2$: (8.0M and 2.7M)

Good fits to the Zn EXAFS data require both O and Br shells, at distances which are concentration independent. The Br EXAFS data require shells of O and Zn. Values are given in Table 1. Figure 1 shows the radial distribution function (RDF) and differential distribution functions (DDFs) obtained by DAS. At low r, they should approach the dashed lines, which are $-r\rho_0$ (ρ_0 being the mean solution density). The rRDF and rDDF functions are approximately represented by:

$$\rho(r) = 0.353\,\rho_{Zn-Zn} + 0.790\,\rho_{Br-Br} + 0.152\,\rho_{O-O} + 0.746\,\rho_{Zn-Br} + 0.236\,\rho_{Zn-O} + 0.500\,\rho_{Br-O} \quad (1a)$$

$$\rho_{Zn}(r) = 1.30\,\rho_{Zn-Zn} + 1.77\,\rho_{Zn-Br} + 0.52\,\rho_{Zn-O} \quad (1b)$$

$$\rho_{Br}(r) = 1.59\,\rho_{Br-Br} + 1.59\,\rho_{Br-Zn} + 0.54\,\rho_{Br-O} \quad (1c)$$

Consider the first peak in the 2.0-2.8A region. The EXAFS suggests Zn-O and Zn-Br distances of 1.95A and 2.37A. Pure water has 2.82A O-O distances.[4] All three could occur in this peak. However, only Zn-O and Zn-Br are included in $\rho_{Zn}(r)$ and only Br-Zn in $\rho_{Br}(r)$ at this distance. Using $X_a S_{ab} = X_b S_{ba}$, with first peak areas of 4.84 and 1.90, Eqns 1b & 1c may be solved for $N_{Zn-Br} = 2.2$ and $N_{Zn-O} = 1.8$. Being unmixed with the Zn-O contribution, the Br rDDF produces the best Zn-Br distance estimate, 2.40A, identical to the anhydrous crystal distance.[5] r_{Br-O}, N_{Br-O}, r_{Br-Br}, and N_{Br-Br} are found similarly. (Table 1) The Zn cations are thus tetrahedrally coordinated, since $N_{Zn-Br} + N_{Zn-O} = 4.0$ and the values r_{Zn-Br} and r_{Br-Br} are correctly related by (3.99A = (8/3) r_{Zn-Br}).

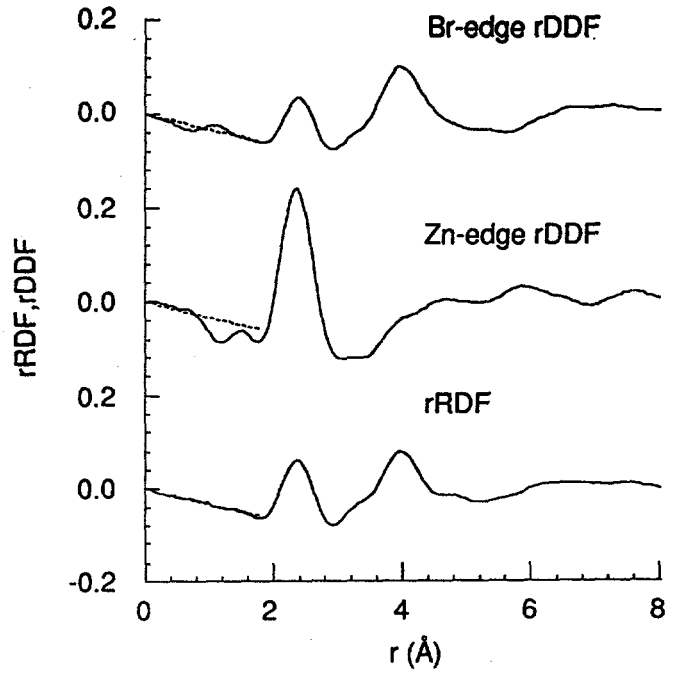

Fig. 1: Distribution functions from 8.0M Aq-$ZnBr_2$.

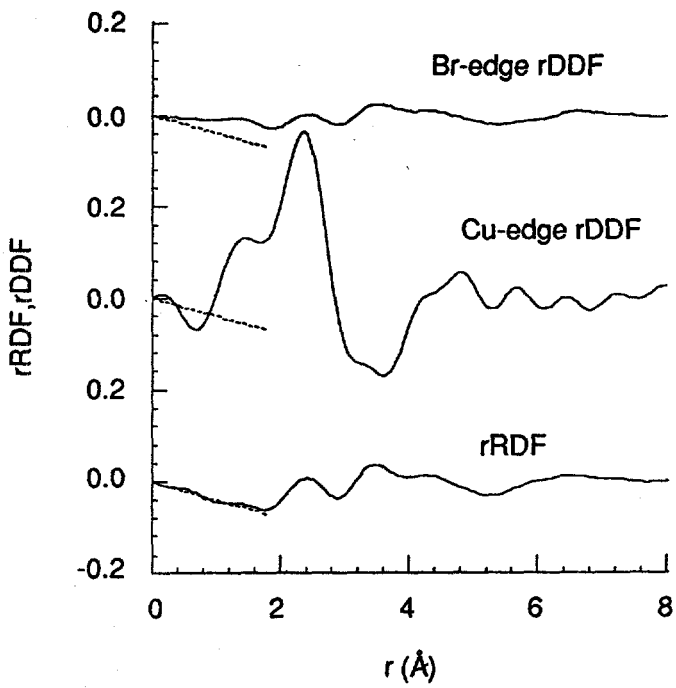

Fig. 2: Distribution functions from 4.5M Aq-$CuBr_2$.

Aq-$CuBr_2$: (4.5M)

Good fits to the EXAFS data, required both O and Br shells about Cu, and both Cu and O shells about Br. (Table 1). Figure 2 shows the RDF and DDFs for both Cu and Br. The rDDFs show some unphysical correlations at low r. Several sources could cause this behavior, including inaccurate anomalous scattering factors and poor normalization constants. Luckily, such problems usually only vary slowly with k, affecting the low r results much more than the high r results, which should therefore be more reliable. Using the peak areas and EXAFS distance and neighbor identity clues, we find the coordinating atoms distances and numbers. (Table 1) In particular, the Cu atoms are octahedrally coordinated by about 2 Br atoms and 4 O atoms. The Br rDDf has a poorly resolved set of peaks in the region of 3.3-4.6A, which almost certainly includes Br-O pairs at their usual 3.3-3.4A distance, but for which we have yet to develop a convincing interpretation.

The observation of octahedral coordination of the Cu^{++} ions suggests the presence of $Cu(H_2O)_4Br_2$ complexes, in concord with the work of Fontaine et al.[6] These authors, by analogy to the chain structures found in the crystal hydrate $CuCl_2.2H_2O$ and the anhydrous $CuCl_4$ and $CuBr_4$ crystals, suggested that the liquid's local structure might resemble chains of $CuBr_x(H_2O)_{1-x}$ planar units sharing edges. This structure would result in a definite next-nearest neighbor Cu-Cu peak in the Cu rDDF at about 3.45A, however, of which no trace is to be seen in our data.

Aq-$NiBr_2$: (4.0M)

The EXAFS data at both the Ni and Br K edges required two shell fits, (O & Br) and (O & Ni). (Table 1) Figure 3 shows the rRDF and dDDF functions. Analysis of the curve peak areas, taken with the EXAFS results, show that Ni ions are octahedrally coordinated by 5.5 O atoms at 2.06A and 0.5 Br ions at about 2.50A. Bromine ions are principally coordinated by 7 $\pm$1 O atoms. The Aq-$NiBr_2$ solution also shows strong evidence for outer shell complexing in the large peak at 4.6A in both the Ni and Br rDDFs, which can only arise from the Ni-Br term. Since ion-O and Br-Br separations may also lie in this region, however, it is not currently possible to extract a reliable next-nearest neighbor coordination number.

Aq-RbBr: (4.0M)

Both the Rb and Br K edge EXAFS data could be fit assuming only a single O shell, implying complete hydration. (Table 1) The scattering rRDF and rDDFs are shown in Figure 4. Less beam time was available to take these data and they clearly suffer at low r values. Our conclusions are therefore only tentative. Each DDF shows only a single major peak, at 2.90A for Rb and 3.35A for Br. Since the sum of the Rb^+ and Br^- radii is 4.43A, the existance of Rb-Br neighbors cannot be completely ruled out, but, considering the EXAFS result, the dominant ion neighbors appear to be water. There is no evidence of outer shell complexing.

Conclusions:

The three transition metal bromides which were studied all showed strong complexing behavior, with Aq-$ZnBr_2$ showing tetrahedral complex geometry while Aq-$CuBr_2$ and Aq-$NiBr_2$ show octahedral geometry. The difference between the two is that for Aq-$CuBr_2$ (as in Aq-$ZnBr_2$) most of the anions are directly bonded to cations near saturation, while in Aq-$NiBr_2$ there is little direct anion-cation contact. Both these results and the trends exhibited are in good agreement with thermodynamic measurements as well as the predictions of ligand field theory.[7]

Table 1: Aqueous solution results:

	Ion Pair	r_{M-X} (DAS)	r_{M-X} (EXAFS)	N_{M-X}
Aq-$ZnBr_2$:	Zn-O		1.95	1.8
	Zn-Br	2.40	2.35	2.2
	Br-O	3.25	3.26	1.6
	Br-Br	3.99		4-6
Aq-$CuBr_2$:	Cu-O		1.96	3.6
	Cu-Br	2.42	2.43	1.9
	Br-O	3.3-3.4	3.30	
Aq-$NiBr_2$:	Ni-O	2.06	2.04	5.5
	1st Ni-Br	2.50	2.51	0.5
	Br-O	3.36	3.23	
	2nd Ni-Br	4.6		
Aq-RbBr:	Rb-O	2.90	2.84	
	Br-O	3.35	3.30	

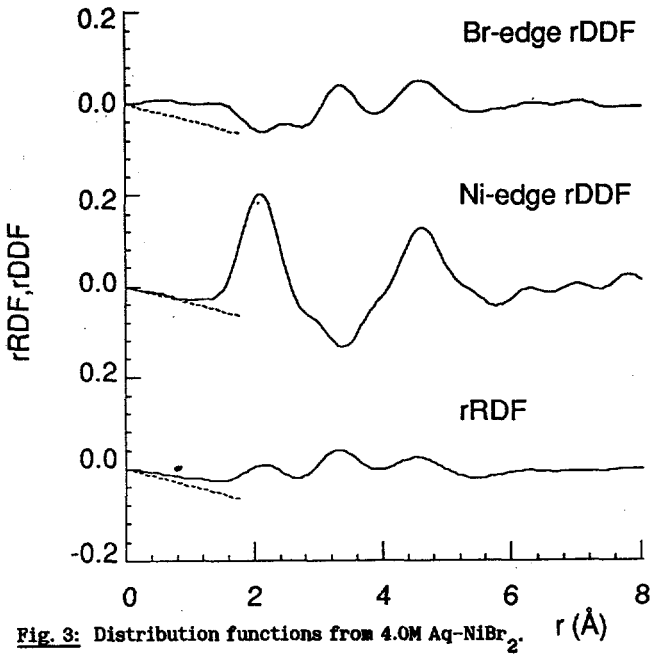

Fig. 3: Distribution functions from 4.0M Aq-$NiBr_2$.

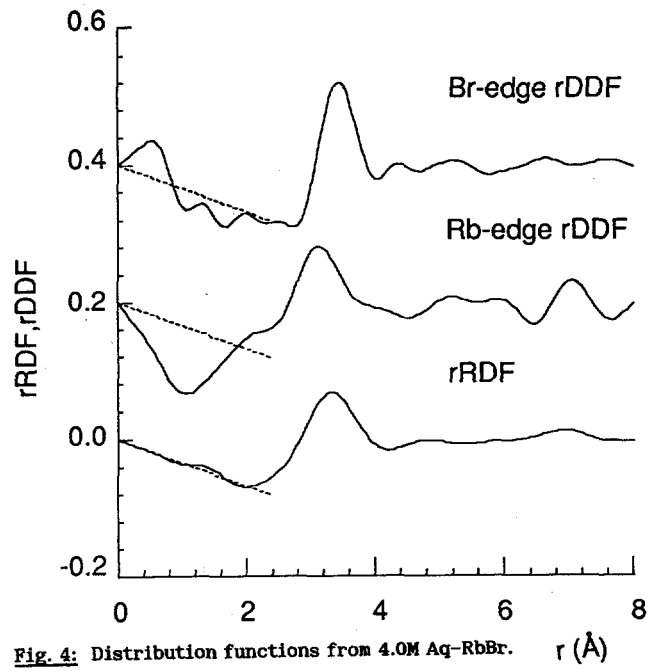

Fig. 4: Distribution functions from 4.0M Aq-RbBr.

References:

1. F.A. Cotton and G. Wilkinson, Advanced Inorganic Chemistry, (Wiley & Sons, New York, 1980) 4th Ed.
2. P.H Fuoss, P. Eisenberger, W.K. Warburton & A. Bienenstock, Phys.Rev.Lett. 46,1537 (1981).
3. J. Kortright and A. Bienenstock, J.Non.Cryst.Solids 61/62,273 (1984).
4. A. Narten, W.E. Thiessen and L. Blum, Science 217,1033 (1982).
5. H.M. Balyuzi, Acta Cryst. A31,600 (1975).
6. A. Fontaine, P. Lagarde, D. Raoux, M.P. Fontana, G. Maisano, P. Migliardo and F. Wanderlingh, Phys.Rev.Lett. 41,504 (1978).
7. Z. Libus and G. Kowalewska, Polish J. Chem. 52,709 (1978).

MEMBRANE X-RAY DIFFRACTION STUDIES OF THE ACETHLCHOLINE RECEPTOR*

R.H. Fairclough[1], D.P. Richman[1], S. Doniach[2], S. Hubbard[2], S. Wakatsuki[3] and K.O. Hodgson[3].

Department of Neurology[1], University of Chicago, Chicago, IL 60637

Departments of Applied Physics[2] and Chemistry[3], Stanford University, Stanford, CA 94305

Membrane X-ray diffraction of oriented acetylcholine receptor (AChR) enriched membranes in concert with anomalous scattering from Tb(III) ions bound to membrane multivalent cation binding sites has illuminated the distribution of these sites along an axis normal to the membrane plane (1). We have continued these experiments at small angles ($0.004 < S < .08$ Å^{-1}) with AChR enriched membranes in one of several metastable states: 1. the closed resting state; 2. the carbamylcholine induced desensitized state; 3. the tetraphenylphosphonium blocked state; 4. the tubocurarine blocked state; and 5. the α-bungarotoxin (α-BgTx) blocked state. Since Tb(III) competes with carbamylcholine and acetylcholine for binding sites on the receptor, we hope to learn about the location of the ACh binding site as well as about the availability of other Tb(III) binding sites in membranes with the AChR locked in one of the several metastable states. At least one anomalous diffraction data set has been collected for membranes with the AChR in each of the different states, and three or more data sets have been collected on the AChR in the desensitized and α-BgTx blocked states. A typical reduced anomalous scattering (I_{off}-I_{on}) data set is presented in Fig. 1. In this data set we have used the raw

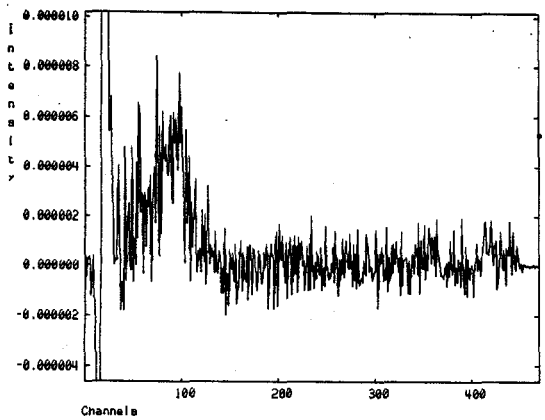

Figure 1. Intensity differences $\Delta I(s) = I_{off} - I_{on}$ of scattered X-rays measured for 7505eV (off) and .7515ev (on) for a sample of oriented acetylcholine receptor enriched membranes treated with 50 μM Tb(III).

equatorial profiles at each of the two X-ray energies as a background which accounts for the rather noisy pattern. We have not routinely recorded as many total counts on the equatorial profiles as on the meridional. This data illustrates the need for better counting statistics despite the appearance of a characteristic anomalous scattering pattern (1).

We have recently begun collecting small angle membrane diffraction data sets on AChR enriched membranes complexed to monoclonal antibodies (mAb) directed against different sites on the AChR. We wish to first determine the location of the relative height of the antibody combining site relative to the membrane bilayer. For some of the antibodies we wish to merely know to which side of the bilayer the antibody is binding. Secondly we wish to determine the effect of the antibodies on the Tb distribution in the AChR.

We have collected diffraction data sets on six different AChR-mAb complexes. We've carried one data set through the analysis to obtain electron density profiles for membranes with and without mAb 383C which are presented in Fig. 2.

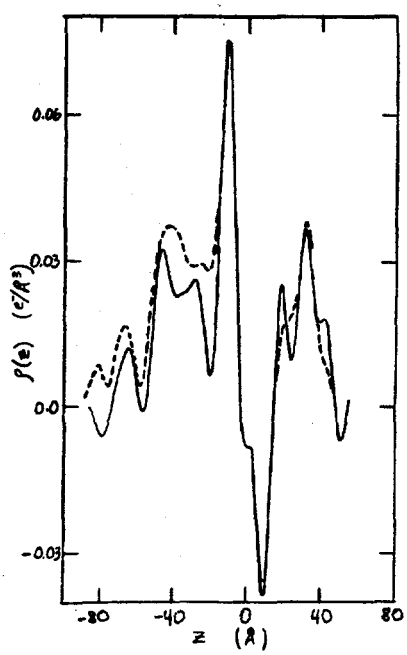

Figure 2. Electron density profiles normal to the membrane plane for AChR enriched membranes with (---) and without (-) mAb383C complexed to the AChR.

This antibody binds 2:1 to the AChR, inhibiting the binding of α-BgTx and carbamylcholine to the AChR. Furthermore binding of α-BgTx and carbamylcholine to the AChR blocks the binding of mAb 383C to the receptor (2). We feel the added electron density seen in the presence of the antibody represents the location of the Fv region of the mAb bound to the receptor, the remainder of the antibody being sufficiently flexible to be "smeared out" in the electron density profile.

REFERENCES

1. Fairclough, R.H., Miake-Lye, R.C., Stroud, R.M., Hodgson, K.O. and Doniach, S. J. Mol. Biol. 189:673-680 (1986).
2. Mihovilovic, M. and Richman, D.P. J. Biol. Chem. (in press).

*Research supported by NIH grants: NS 19779, NS 15462, NS 24304, and RR01209

EXAFS Studies of Impurities in Semiconductors

F. Sette, J. E. Rowe and J. M. Poate

AT&T Bell Laboratories
Murray Hill, New Jersey 07974

Various models for defects associated with impurities in semiconductors have been proposed but very little direct structural information is available. We have used the EXAFS technique on the JUMBO beamline at SSRL coupled with a custom made soft X-ray fluorescence detector to examine S impurities in single crystal GaAs(100) wafers prepared by ion implantation of the S impurities at 150 keV with subsequent annealing in an As atmosphere to maintain stoichiometry. The impurity concentration ranged from $5x10^{14}cm^{-2}$ to $10^{16}cm^{-2}$ which corresponds to mean bulk doping densities of $10^{19} - 2x10^{20}cm^{-3}$.

The fluorescence detector, used to monitor the Sulphur K_α photon intensity was a custom-made energy-dispersive proportional counter with a thin 125 micron Be window and an energy resolution of 800 eV FWHM. The atomic profiles of S in the samples were measured by secondary ion mass spectrometry (SIMS) and the electrical activity of the S was determined by Hall effect and electrochemical capacitance-voltage (CV) profiling.[1] Remnant damage was studied by ion channeling; samples showed a high degree of crystallinity after annealing, with backscattering yields ($\approx$ 4%) close to those of virgin GaAs.

In Fig. 1 we show the S(K-edge) photoabsorption spectra and the EXAFS signal in k-space of two S implanted GaAs samples with mean S concentration, $\bar{n}=2x10^{19}at/cm^3$ and $\bar{n}=2x10^{20}at/cm^3$ respectively. These samples correspond to implantation doses of $1x10^{15}$ and $1x10^{16}at/cm^2$, and were annealed at 900 °C after implantation. The mean concentrations were calculated assuming Gaussian-like implantation distributions which agreed with SIMS measurements. The S atoms were distributed over a mean depth of $\approx$5000Å from the surface and no surface enrichment was detected by comparing the FY S(K-edge) photoabsorption spectra with the S(KLL) Auger yield (probing depth $\approx$30Å) spectra.[2] From the data in Fig. 1, we estimate the detection limit of the FY technique to be $5x10^{17}at/cm^3$. This limit is obtained from signal to background (STB) ratio of 10% defined as the edge-jump divided by the background.[2] In Fig. 1(a), for the $2x10^{19}at/cm^3$ sample, the STB ratio is 220%. Therefore, because typical photoabsorption lengths of medium atomic number materials in the energy range between 1500 and 3000eV are $\approx 1\mu m$, we can estimate the detection limit of soft x-ray FY $\approx(2x10^{19}/20x(0.5/1))=5x10^{17}at/cm^3(\approx 10ppm)$.

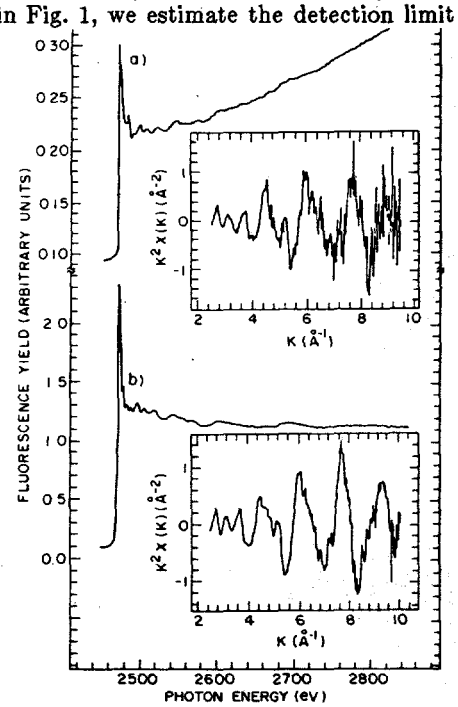

The S first shell distance for samples annealed at temperatures above 700 °C and $\bar{n}$ ranging between $2x10^{19}$ and $2x10^{20}at/cm^3$ is 2.33 $\pm$0.03Å, 0.12Å shorter than GaAs (2.445Å). However the S second and third shell distances (3.98 $\pm$0.03 and 4.68$\pm$0.03 Å) are identical to bulk GaAs (3.990 and 4.679 Å). These results demonstrate that the S atoms are substitutional and rule out models with interstitial or clustered S atoms behaving as non-electrically active defects.[3] The contraction of the S first-neighbor distance may be expected because the S-Ga or S-As bonds are typically $\approx$0.15Å shorter than the Ga-As bondlength, however the first shell EXAFS parameters shows some anomalies respect to those of the outer shells. In fact the number of first-shell neighbors is 2.6 instead of 4 as expected for substitutional S atoms and the first-shell Debye-Waller factor is physically too large when compared with that of second and third shells.[4] Another unusual feature is the width of the first-shell peak in the |F(r)| transform function which has FWHM 0.13Å wider than the second and third-shell width. This compares with the width of EXAFS peaks in the |F(r)| of Ga and As in GaAs[5] where second and third-shell widths are 0.55Å FWHM, consistent with our results, but the first-shell width is 0.45Å FWHM, which is 0.23Å narrower than our case. We explain this effect by two different substitutional configurations for the S atoms: (1) substitutional on the As site, (2) substitutional with an As vacancy on the second shell (S_{As}or(S_{As},V_{As})). In fact a missing As atom on the second shell implies four broken bonds one on a Ga atom of the first shell, two on two Ga atoms of the third shell and one on a Ga atom on the fifth shell. Therefore the As vacancy is a weak perturbation on the eleven second-shell As atoms and on ten of the twelve third shell Ga atoms, which do not have broken bonds.

Our new technique measures the detailed atomic structure around dopant-impurities in semiconductors with detection sensitivitv of $\sim 5x10^{17}at/cm^3$.

REFERENCES

[1] C. M. Wolfe and G. E. Stillman, App. Phy. Lett. *27*, (1975) 564.

[2] J. Stöhr, E. B. Kollin, D. A. Fisher, J. B. Hastings, F. Zaera and F. Sette, Phys. Rev. Lett. *55*, 1468 (1985).

[3] See for example: "New Developments in Semiconductor Physics," edited by F. Beleznay, G. Ferenczi and J. Giber (Springer-Verlag, Berlin 1980) and "Ion Implantation and Beam Process" edited by J. S. Williams, J. M. Poate (Academic Press, New York 1984).

[4] P. A. Lee, P. H. Citrin, P. Eisenberger, B. M. Kincaid, Rev. Modern Physics *53*, (1981), 769.

[5] J. C. Mikkelsen and J. B. Boyce, Phys. Rev. B *28*, (1983) 7130. The same results are found for Germanium: E. A. Stern, B. A. Bunker and S. M,. Heald, Phys. Rev. B *21*, (1980) 5521.

CHARACTERIZATION OF V, CR, NI, AND AS COMPOUNDS FOUND IN OIL-FIRED POWER-PLANT ASH AND FERROCHROME SMELTER DUST USING X-RAY ABSORPTION SPECTROSCOPY--POTENTIAL CARCINOGENIC COMPOUNDS

J.E. Silk, D.J. Eatough, L.D. Hansen, M.W. Hill and N.F. Mangelson
Brigham Young University, Departments of Chemistry and Physics
Provo, Utah 84602
and
F.W.Lytle and R.B. Greegor
The Boeing Company, Seattle, WA 98124

Oil-fired power-plant fly ash has been shown to be cytotoxic [1.2]. Since the cytotoxicity of many toxic metals (e.g. V, Cr, As, Cd) is dependent on the specific chemical species present, it is necessary to identify the exact chemical species in the power-plant ash in order to make meaningful risk assessment analyses. The toxicity of vanadium, chromium and arsenic is dependent on the oxidation state of the element and only certain inorganic compounds of chromium, arsenic and nickel are known to be carcinogenic. Vanadium and nickel concentrations in oil-fired power-plant fly ash are one to five percent, while chromium and arsenic are found in the range of ten to one thousand parts per million. Combustion conditions within power plants are not well enough understood or maintained to predict with certainty the chemical state of the above elements. In addition ambient conditions may lead to changes in chemical state.

The objective of a series of current studies is to determine the chemical species of the above listed elements in power-plant fly ash as it is emitted from the plant and after it has been transported for a time in the ambient environment. While EXAFS analysis cannot be used as a routine analytical technique for the analysis of environmental samples, it can provide bench mark data with which to compare the validity of other analytical procedures. A short series of measurements were made to show the feasibility of studying elements and samples noted above.

Two samples were obtained from the stacks of an oil-fired power plant (plant #1) and two samples were obtained in the ambient environment 20 km from a power plant (plant #2) while the plume was impacting upon the sampling site. Another sample was collected from the baghouse of a ferrochrome smelter [3]. The EXAFS measurements were made on beam line station IV-1 using a Si(220) double crystal monochrometer. Most of the data were collected in the fluorescence mode.

Vanadium and Nickel K-edge data were obtained from the power-plant and smelter samples. Data analysis was carried out as reported for a previous set of data [4].

Chromium K-edge data were obtained for all five samples and for nine chromium reference compounds which included Cr(0), Cr(III) and Cr(VI) oxidation states. The fluorescence detector absorption spectra for three samples and two reference compounds [$PbCr(VI)O_4$ and $Cr(III)_2O_3$] are given in Figure 1. Preliminary analysis, based on comparisons such as those seen in Figure 1., suggests that all three samples contain chromium primarily in the III oxidation state. Note, for example the strong, pre-edge peak in the Cr(VI) compound which is absent in all three sample spectra. More data will be needed in order to make a full analysis on the fly-ash samples.

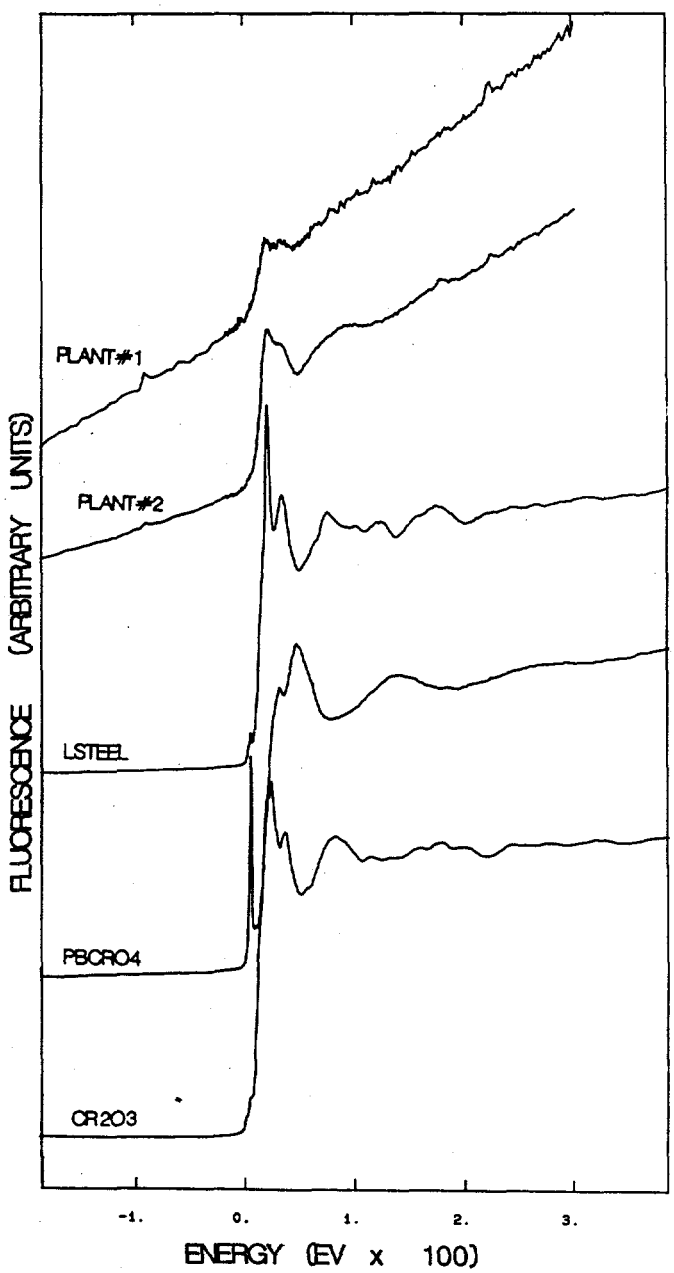

Figure 1. Chromium K-edge, fluorescence detector X-ray absorption spectra for two oil-fired power-plant fly-ash samples (PLANT #1 and PLANT #2), a ferrochrome smelter sample (LSTEEL) and two chromium reference compounds (Cr_2O_3 and Cr_2O_5).

Arsenic K-edge data were obtained for the four fly ash samples and for six arsenic reference compounds which included both the As(III) and As(V) oxidation states. The fluorescence detector absorption spectra for a plant #1 sample and three reference compounds [$As(III)_2O_3$, $As(III)_2S_3$ and $As(V)_2O_5$] are shown in Figure 2. Preliminary observations suggest that arsenic in the power plant sample is As(V). The sharp peak aligns with that in As_2O_5 which is shifted to higher energy than the peaks in the As(III) compounds. Because of the low arsenic concentration, additional data will be required before complete analysis can be made.

This study provided sufficient X-ray absorption data to confirm that vanadium, nickel, chromium and arsenic can be studied in oil-fired power-plant fly ash collected in the stack and in the environment. Baghouse dust from a ferrochrome smelter was also successfully studied. Sufficient data were collected for EXAFS analysis of a few cases. Additional data collection will be required for complete characterization of the elements in the samples studied.

This research project is supported by Southern California Edison and is being carried out in a cooperative study with research programs of the U.S. EPA and the California State Air Resources Board.

References.

1. G.L. Fisher, K.L.McNeill, B.A. Prentice and A.R. McFarland, Environ. Health Perspect. 51 (1983) 181-6.

2. C. Wei, O.G. Raabe and B.J. Kimble, Bull. Environ. Contam. Toxicol. 32 (1984) 179-86.

3. X.B. Cox, III, R.W. Linton and F.E. Butler, Environ. Sci. Technol. 19 (1985) 345-52.

4. N.W. Lytle, D.J. Eatough, L.D. Hansen, M.W. Hill, N.F. Mangelson, F.W. Lytle and R.B. Greegor, in Fly Ash and Coal Conversion By-products: Characterization, Utilization, and Disposal II, ed. G.J. McCarthy, P.F. Glasser and D.M. Roy, Materials Res. Soc. Symp. Proc. 65 (1986) 141-50.

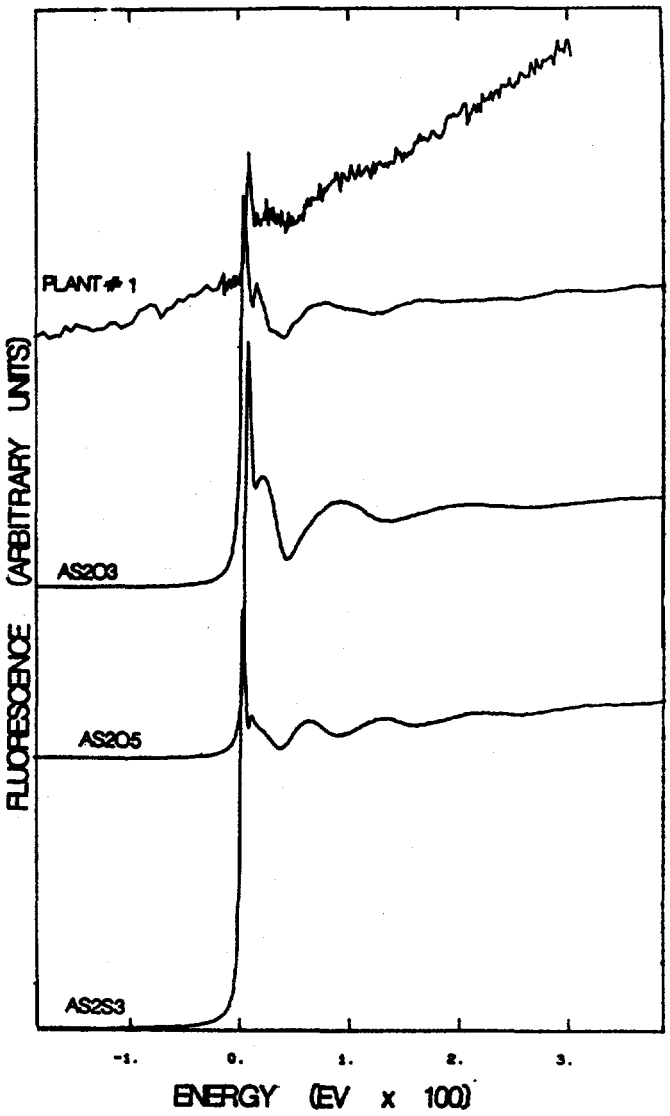

Figure 2. Arsenic K-edge, fluorescence detector X-ray absorption spectra for an oil-fired power-plant fly-ash sample (PLANT #1) and three arsenic reference compounds (As_2O_3, As_2S_3, and As_2O_5).

THE ORIENTATION OF SURFACE CARBONATE ANION ON Ag(110)

J. Solomon and R.J. Madix*
C.M. Friend**
J. Stöhr***

*Department of Chemical Engineering, Stanford University, Stanford, CA 94305
**Department of Chemistry, Harvard University, Cambridge, MA 02138
***IBM Almaden Research Center, 650 Harry Road, San Jose, CA 95120

Surface carbonate has been studied previously with temperature programmed reaction spectroscopy, X-ray photoemission and high resolution electron loss vibrational spectroscopy on Ag(110) [1,2,3]. The species is readily formed by reaction of preadsorbed atomic oxygen with CO_2 at or below 400K in vacuum. Formation of the surface carbonate results in substantial reorganization of the long range order on the surface, as shown by low energy electron diffraction. The vibrational spectra suggest that the species is tilted upward slightly from the surface plane. XPS results give the C(1s) and O(1s) binding energies as 287.2 and 529.9 eV, respectively. In the carbonate anion in metallic salts the C-O bonds are equivalent, and the bond length is 1.23-1.33 Å. With the use of NEXAFS the orientation of the plane of the anion and the C-O bond lengths were determined on beam line I-1 at SSRL with the end station of Jo Stöhr.

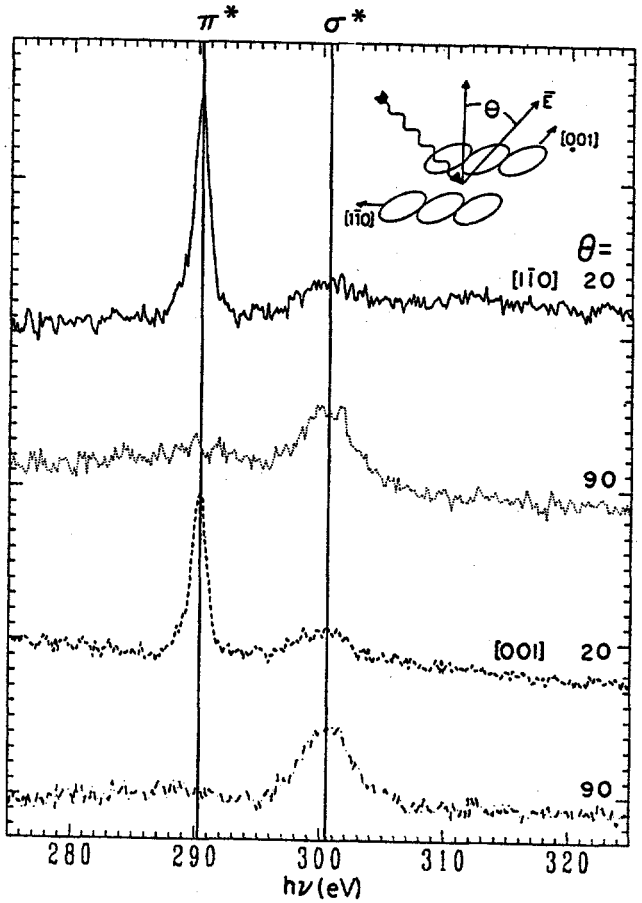

Figure 1. Carbon K edge NEXAFS spectra of surface carbonate on Ag(110) at 300 K.

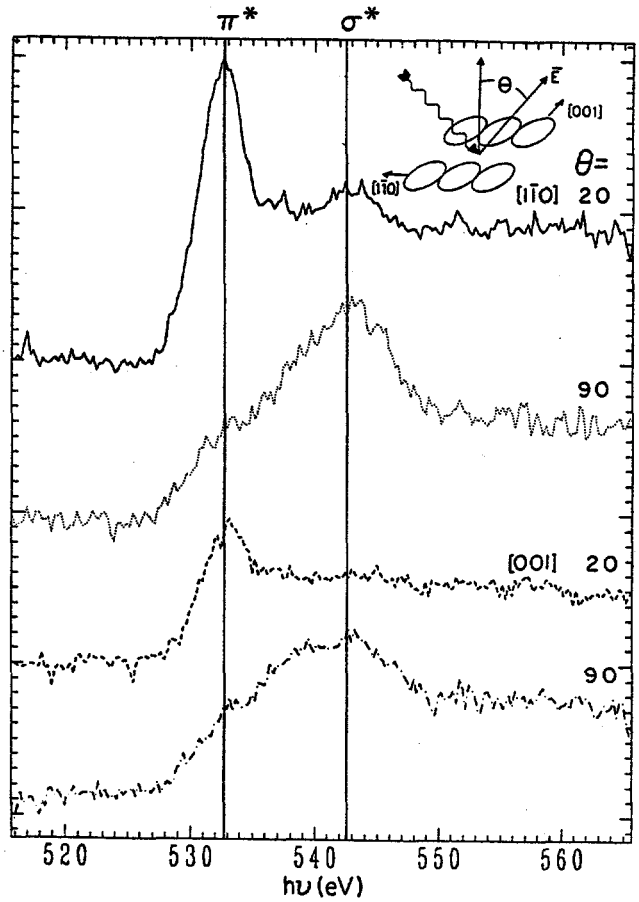

Figure 2. Oxygen K edge NEXAFS spectra of surface carbonate on Ag(110) at 300 K.

The angle dependence of the near edge resonances indicate that the anion is oriented parallel to the plane of the surface. At normal incidence (electric field vector in the plane of the surface) only the σ^* shape resonance is evident in either the C(1s) or O(1s) spectra (figs. 1 and 2); the dominance of this resonance and the absence of the π^* resonance is expected if the C-O bonds lie in the plane of the surface. The**σ resonances are found at 300.5 and 542.6 eV, respectively, and the π^* resonances are at 290.1 and 532.9 eV, respectively. From the positions of both the O(1s) and the C(1s) σ^* resonances the bond length is calculated to be 1.32 Å compared to the value observed in bulk metal carbonates given above.

The orientation obtained in this study agrees well with that deduced from angular resolved photoemission studies [4] and is in disagreement with the deductions from EELS. The EELS result was based on the appearance of the umbrella mode in the spectrum and the application of the dipole selection rule that mitigates against the observation of this mode for the planar geometry found here. The origin of this discrepancy is not understood and is currently under study.

[1] M.A. Barteau and R.J. Madix, J. Chem. Phys 74 (1981) 4144.

[2] M.A. Barteau and R.J. Madix, J. Elec. Spect. 31 (1983) 101.

[3] E.M. Stuve, R.J. Madix, and B.A. Sexton, Chem. Phys. Lett. 89 (1982) 48.

[4] A. Bradshaw, private communication.

π BONDED ALKOXIDE INTERMEDIATES IN ALCOHOL OXIDATION: ORIENTATIONS OF ALLYL AND PROPARGYL BY NEXAFS

R.J. Madix and J. Solomon*
J. Stöhr**

*Department of Chemical Engineering, Stanford University, Stanford, CA 94305
**IBM Almaden Research Center, 650 Harry Road, San Jose, CA 95120

It is now well established that preadsorbed atomic oxygen on Ag(110) will react with alcohols to form surface alkoxides in near monolayer concentrations [1]. In alkyl alcohols the alkyl group generally points away from the surface, and there is no evidence for hydrogen bonding of the backbone to the surface from either NEXAFS or surface vibrational spectroscopy. We may anticipate that carbon-carbon unsaturation in the backbone can cause the species to tilt due to π bonding of the double or triple bond with the surface, since ethylene and acetylene do form weak π bonds with the Ag(110) surface [2,3]. The question of orientation of such species is important to the formation of strongly adhering polymer films on metals. Consequently we have studied the structure and bonding of the alkoxides of allyl and propargyl alcohols (2-propen-1-ol and 2-propyn-1-ol) to determine if, indeed, the unsaturated bonds cause these alkoxyl groups to preferentially align on the surface.

The alkoxides, allyloxide (2-propenyloxide) and propargyloxide (2-propynyloxide), were prepared as previously determined by reacting the parent alcohols with atomic oxygen preadsorbed on meticulously cleaned Ag(110). Care was taken to react away all the atomic oxygen as water in their formation. The stabilities of these intermediates was characterized by temperature programmed reaction spectroscopy in concurrent work [4]. NEXAFS spectra were taken at the carbon edge with the surface at 100K on beam line I-1 at SSRL.

The spectra taken for allyloxide clearly indicate that the intermediate is π-bonded with the plane of the π orbital perpendicular to the plane of the surface. Figure 1 shows spectra taken for both normal and glancing incidence of the radiation along the [100] and [1$\bar{1}$0] azimuths. The orientation of the double bond is easily recognized by the dependence of the π^* resonance on the polar angle. The absence of this resonance (except for the small component due to non-perfect polarization of the beam) at normal incidence and the dominance of this resonance at glancing incidence clearly shows that the lobes of the antibonding π orbitals lie perpendicular to the surface. The lack of azimuthal ordering is also apparent in the intensities of the π^* resonances along the two azimuths. The $*\sigma$ resonances were deconvoluted using Gaussian peak shapes with a best fit at the energies expected for the unperturbed bond lengths in the parent alcohol.

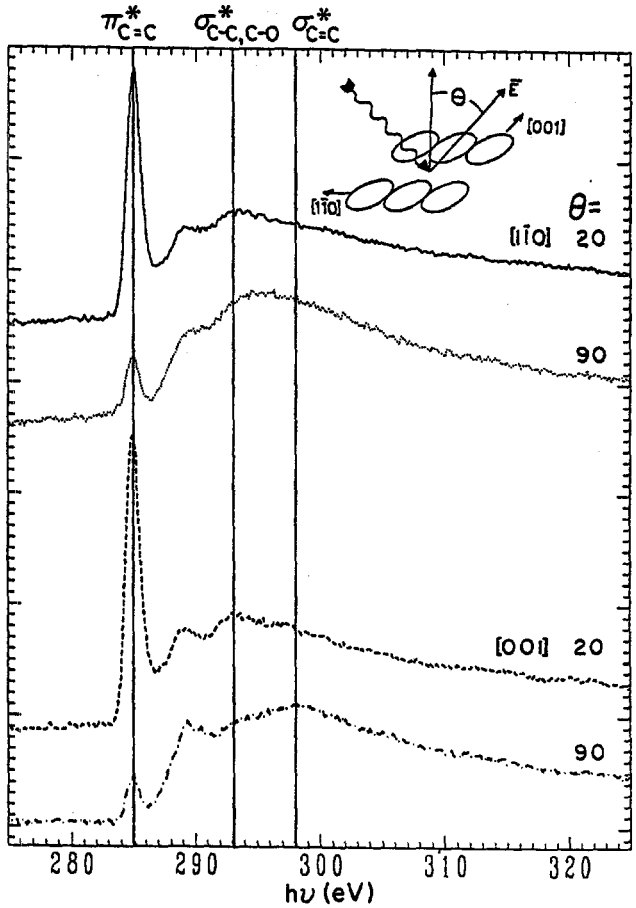

Figure 1. Carbon K edge NEXAFS spectra for allyloxide on Ag(110) at 100 K.

The spectra for propargyloxide show evidence for a strongly preferred azimuthal ordering (fig. 2). It is evident that the π^* resonance at 285.5 eV vanishes at normal incidence with the electric field vector along the [1$\bar{1}$0] azimuth, indicating that the C-C bond axis lies perpendicular to the close-packed direction. The σ^* resonance appears to grow in this orientation also, and the position of the σ^* resonance is nearly the same as that for acetylene [5], indicative of retention of the triple bond.

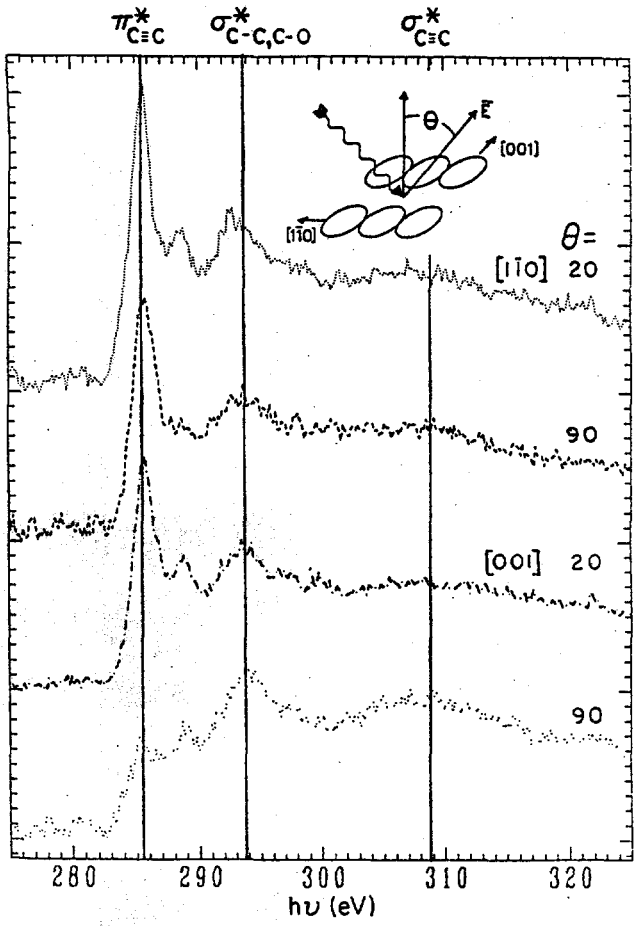

Figure 2. Carbon K edge NEXAFS spectra for propargyloxide on Ag(110) at 100 K.

The results of these studies clearly show that bond unsaturation in the backbone of surface alkoxides can cause preferential orientation of a species which is strongly bound at another site in themolecular framework, even on a weakly interacting metal such as silver. In neither allyloxide or propargyloxide is the unsaturated C-C bond significantly perturbed. The bond lengths of 1.41 and 1.22 Å are very close to those for ethylene (1.34 Å) and acetylene (1.20 Å), respectively. Thus no loss of the allylic hydrogen is observed, unlike that commonly observed in organometallic complexes of allylic species. In agreement with these observations, no complicating reactions due to the presence of the double bond are observed with allyl alcohol oxidation reactions studied elsewhere.

[1] R.J. Madix, Science **233** (1986) 1159.
[2] M.A. Barteau and R.J. Madix, Surf. Sci. **103** (1981) L171.
[3] E.M. Stuve, R.J. Madix and B.A. Sexton, Surf. Sci. **123** (1982) 491.
[4] J.L. Solomon and R.J. Madix, to be published.
[5] P. Stevens, R.J. Madix and J. Stöhr, to be published.

BONDING AND ORIENTATION OF ACETONITRILE AND ITS OXYGEN INTERMEDIATES ON Ag(110)

P. Stevens and R.J. Madix*, C.M. Friend**, J. Stöhr***

*Department of Chemical Engineering, Stanford University, Stanford, CA 94305
**Department of Chemistry, Harvard University, Cambridge, MA 02138
***IBM Almaden Research Center, 650 Harry Road, San Jose, CA 95120

In heterogeneous catalysis silver shows unique selectivity for the oxidation of organic molecules. Among the reactions so selectively conducted by silver is the oxidation of amines to nitriles [1]. The oxidation of ethylamine ($CH_3CH_2NH_2$) to acetonitrile (CH_3CN) can be completely understood on the basis of the strong nucleophilicity of adsorbed oxygen and the gas phase acidity of the amine [2]. In previous work we have shown that the product, CH_3CN, also reacts further, since the C-H bond can be ruptured by adsorbed atomic oxygen. The metastable intermediates formed in this reaction have been identified by temperature programmed reaction spectroscopy to be $-CH_2CN$ and -CHCN. The existence of the triple bond in these species affords the study of their bonding and orientation on the surface by NEXAFS. This work was performed on beam line I-1 at SSRL.

Multilayers of CH_3CN were first formed by condensation at 100K. The NEXAFS results show no dependence on the angle of incidence of the radiation, indicating random orientation of the molecule in the multilayer. The nitrile, however, appears to orient itself in the submonolayer state preferentially with the C-N bond parallel to the surface, as shown in fig. 1. The prominence of the σ^* resonances at normal incidence attests to this preferred geometry. The magnitude of the π^* resonance at both polar angles is currently under further study. The energy of the $^*\sigma$ resonances at 292 and 309 eV indicate that the bond lengths in the monolayer state are not significantly different from the gas phase value of 1.16 Å. Indeed, the resonances are not shifted from the condensed state (fig. 1).

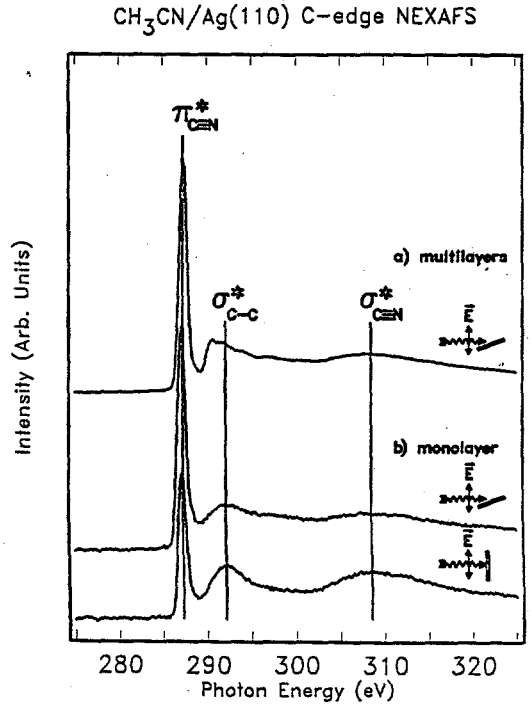

Figure 1.

In contrast the spectra for $-CH_2CN$ indicate a strong azimuthal as well as polar orientation of the species. This intermediate was synthesized to one-quarter monolayer coverage by coadsorbing acetonitrile and one-eighth monolayer of preadsorbed atomic oxygen at 100 K and annealing to 340 K. The presence of the strong σ^* resonances for normal incidence with the electric field vector along the [001] azimuth is a clear indication of alignment of the C-C and C-N bonds perpendicular to the close-packed direction on the (110) surface. This preferential orientation is obviously caused by π-bonding to the surface, yet the bond lengths of 1.16 Å are unperturbed from the gas phase value of CH_3CN. The values of these bond lengths clearly reveal that the species is bonded to the surface strongly via the methyl carbon and that the C-N bond is not significantly rehybridized.

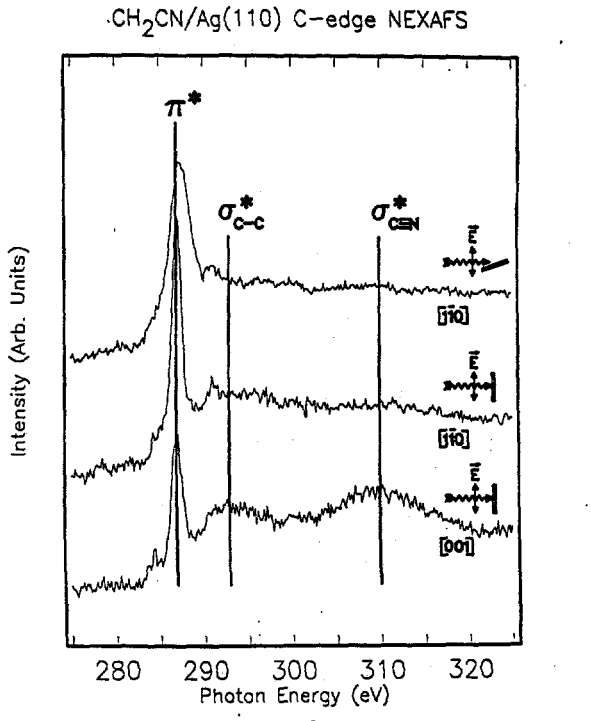

Figure 2.

[1] M. Thornburg and R.J. Madix, to be published.
[2] M.A. Barteau and R.J. Madix, Surf. Sci. 120 (1982) 262.

XAS OF GAS PHASE METAL-CONTAINING CHEMICAL SYSTEMS

E. C. Marques, D. R. Sandstrom, F. W. Lytle and R. B. Greegor
Boeing Aerospace Company, Seattle, WA 98124

Our experimental program utilizes x-ray absorption spectroscopy (XAS) to study metal-containing chemical systems, such as metal electrolyte solutions, metal complexes and metal cluster systems. Objectives include the direct experimental measurement of chemical structure in dynamic transient phases and in non-condensed phases. In 1986, emphasis was placed on development of capabilities for detecting metal-containing gas phase XAS. This report describes our progress.

A new gas-phase x-ray absorption detector, illustrated in figure 1, was developed. It combines two distinct elements: a long-path x-ray detection chamber (similar to ionization type) and a high temperature vacuum evaporation cell. Both components can be evacuated to 10^{-5} Torr base pressure. A uniform electric field was maintained between two opposing plate electrodes, mounted parallel to the x-ray beam path, for total electron-yield detection. The source aperture for the metal vaporization cell was oriented at an oblique angle close to the x-ray path.

Experimental time on SSRL beam line IV-1 was utilized for tests of the apparatus during high temperature vaporization of Cu metal (source temperatures at approximately 2300 C). Estimates of a Cu vapor density of 10^{13}-10^{14}/cm^3 were based on vaporization rate, source emission profile, and mean thermal velocity. Sensitivity of electron yield detection measurements to this level for some non-metal gas phase systems has been established by Lytle.[1] His results suggested that detectability of x-ray absorption in metal vapors like Cu effluent should be adequate.

Our preliminary data were quite noisy but useful because they revealed a requirement for a more practical scheme of electrical isolation in the detection circuit near a noisy thermal source. The noise was understood to arise from both a thermionic background component (source temperature dependent) background in the vapor and leakage current (time dependent) due to evaporant condensation on electrical insulating components in the chamber. The latter effect was mitigated by installation of a complex baffled insulator system, resulting in a much reduced total noise level. It was then possible to observe a Cu gas absorption edge feature, shown in figure 2. High quality XAS data for a number of volatile metal complexes were measured in the gas chamber detector. For these data there was no thermionic component, suggesting that good quality data can be obtained for high temperature metal vapors, with improved thermionic shielding.

We plan to extend this XAS measurement technique to study structure in metal gas phase reaction species. This will be accomplished by introducing a small partial pressure of reaction gas (CO, Cl_2, NH_3 etc.) diluted by an inert carrier gas. Mixing occurs in the vaporization cell so that in the vicinity of the detection electrodes the reaction will be approaching equilibrium. In the long term, our plans include investigation of gas phase specie discrimination in XAS detection using mass sensitive and trapping schemes such as ion cyclotron resonance.

Work supported by the Office of Naval Research

References

1. F. W. Lytle and R. B. Greegor, "GAS PHASE X-RAY ABSORPTION SPECTROSCOPY WITH AN ELECTRON YIELD DETECTOR", presented at IVth Int. EXAFS Conf., Fontevraud, FR, July 1986.

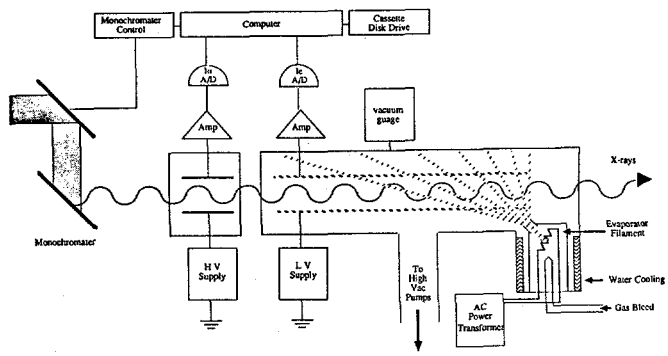

Fig. 1 Gas Phase XAS Detector - Evaporation Cell Concept

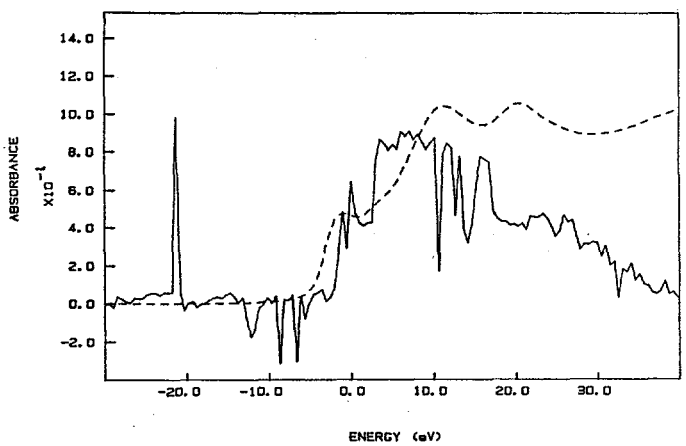

Fig. 2 Cu XAS K-edge spectra, with zero of energy scale referenced to 8.979 keV, for vaporized Cu metal (solid line: Note - large thermionic noise spikes) and Cu foil calibration (dotted line).

HIGH-PHOTON FLUX PHOTOEMISSION STUDIES IN NARROW BAND MATERIALS

J.W. Allen*, J.-S. Kang*†, W.P. Ellis**, B.B. Pate††
M.B. Maple†, M.S. Torikachvili†, I. Lindau††

*Xerox Palo Alto Research Center, Palo Alto, CA. 94304
†University of California, San Diego, La Jolla, CA. 92093
**Los Alamos National Laboratory, Los Alamos, NM. 87545
††Stanford Synchrotron Radiation Laboratory, Stanford, CA. 94305

5f SPECTRAL WEIGHT IN DILUTED HEAVY-FERMION URANIUM MATERIALS

The 5f spectral weights of heavy Fermion uranium materials contrast sharply with the 4f weights of heavy-Fermion Yb and Ce materials. For the latter group, the 4f spectrum measured in photoemission (PES) and bramstrahllung isochromat (BIS) spectroscopies is dominated by single-site energetics and the impurity Anderson Hamiltonian gives a unified description of the 4f spectrum and such low energy properties as the specific heat and the magnetic susceptibiltiy, which can be characterized by a spin fluctuation energy, the Kondo temperature T_K [1]. As predicted theoretically, for heavy materials, which have small T_K, there is very little 4f weight at the Fermi energy E_F. For uranium, there is very much weight around the Fermi level, with a somewhat band-like appearance, and the importance of Coulomb interactions can be inferred [2] only from the fact that the total BIS/PES width is greater than in local density-functional (LDA) calculations. We have given reasons to hope that calculations for the impurity Anderson Hamiltonian made realistic for uranium will be as successful as those for Ce and Yb [1]. Alternatively [3] it has been argued that the ligand-U 5f hybridization is sufficiently large that lattice interactions dominate the 5f spectrum so that the proper zeroeth order description is provided by an LDA calculation.

To determine experimentally whether single-site or lattice effects are more important for the main features of the 5f spectrum, we have measured the photoemission spectrum of dilute uranium systems. The high flux beam line V is not yet ready and so we have done these studies on beam line III-1, although for systems not as greatly diluted as we would like to study. Nonetheless the results permit meaningful conclusions, and show that uranium as dilute as 0.1% can certainly be measured when beam line V is available.

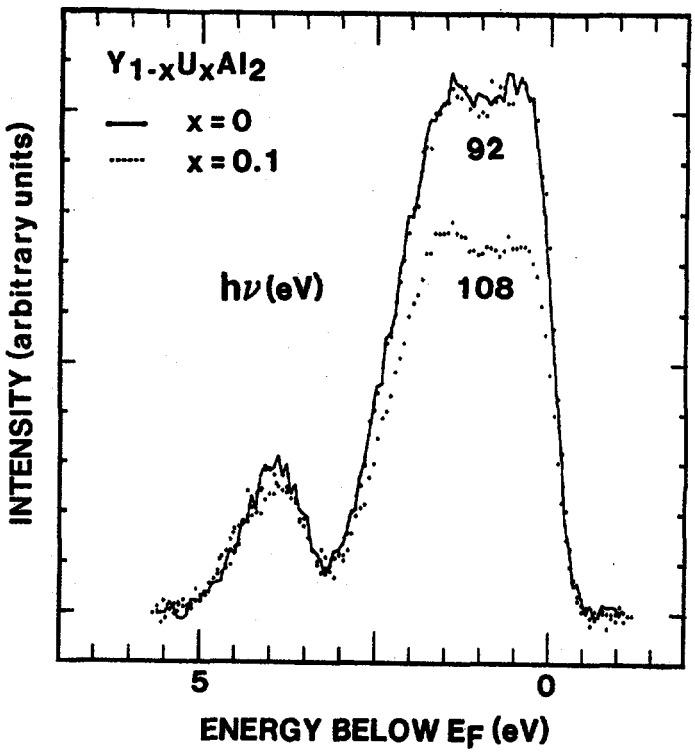

Fig. 1

UAl_2 is a typical heavy Fermion material, which we have studied previously [2]. The alloy system $U_xY_{1-x}Al_2$ has the same crystal structure for all x. We have measured the valence band photoemission spectra for x = 0, 0.02 and 0.1 for photon energies in the vicinity of the uranium 5d edge, where the U 5f emission resonates. The spectra are normalized to a photon flux monitor. Fig. 1 shows that the spectra for x = 0 and 0.1 are identical at a photon energy $h\nu = 92$ eV, the Fano minimum where the U 5f emission is suppressed. Fig. 1 also shows that for the Fano maximum energy $h\nu = 108$ eV, the x = 0 spectrum (shown dotted) has the same shape but less intensity by a factor $\alpha \sim 0.7$, reflecting a modest cross-section decrease.

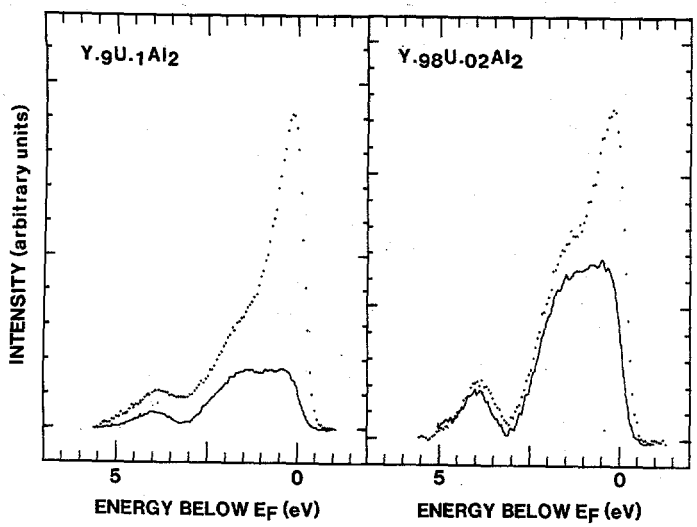

Fig. 2

Fig. 2 shows for x = 0.02 and 0.1 the spectra for $h\nu = 92$ eV and 108 eV. The 92 eV spectrum as been scaled by α so that the difference between the two spectra gives the uranium spectrum. Taking the off-resonance spectrum as an amplitude reference, *the areas under* the two difference spectra are roughly in the ratio 5 to 1. Fig. 3 compares the 5f spectra thus obtained for x = 1, 0.1 and 0.02, scaled to have the same magnitude. It is obvious that the spectra are essentially identical, and we conclude that the spectrum is not dominantly determined by lattice effects. A paper describing these results is in preparation.

REFERENCES

1. J.W. Allen, S.-J. Oh, O. Gunnarsson, K. Schönhammer, M.B. Maple, M.S. Torikachvili and I. Lindau, Adv. in Physics **35**, 275 (1986).

2. J.W. Allen, S.-J. Oh, L.E. Cox, W.P. Ellis, M.S. Wire, Z. Fisk, J.L. Smith, B.B. Pate, I. Lindau and A.J. Arko, Phys. Rev. Letters **54**, 2635 (1985).

3. D.D. Sarma, F.U. Hillecrecht, W. Speier, N. Martensson and D.D. Koelling, Phys. Rev. Letters 57, 2215 (1986).

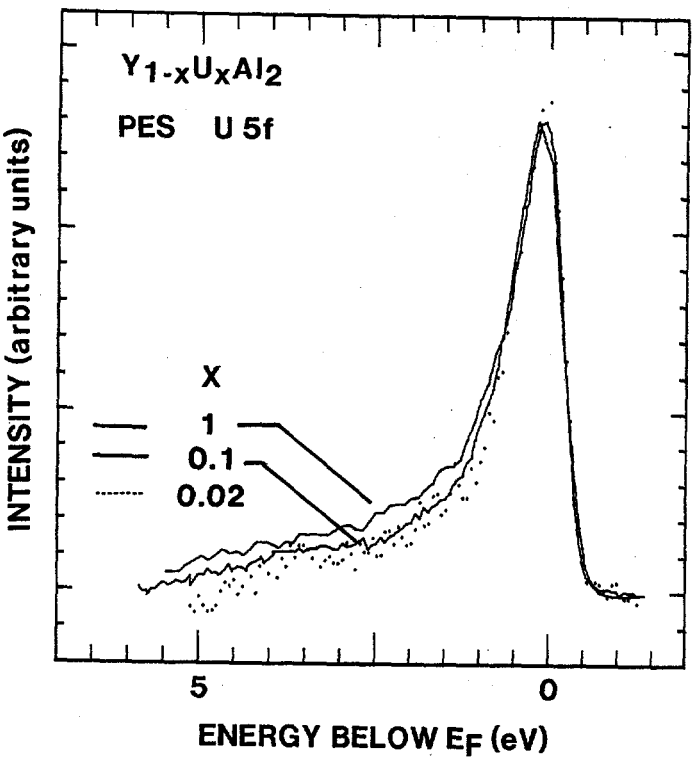

Fig. 3

SOFT X-RAY SPECTROSCOPY OF MOLYBDENUM ENZYMES, CO-FACTORS AND MODEL COMPOUNDS

S. P. Cramer[1,6], M. W. W. Adams[1], G. N. George[1], E. I. Stiefel[1], V. Minak[1], J. Enemark[1], W. Cleland[2,3], B. E. Smith[4], L. S. Solomonson[5]

[1]Exxon Research and Engineering, Annandale, New Jersey 08801
[2]Department of Chemistry, U. Arizona, Tucson, Arizona 85721
[3]Department of Chemistry, U. Mississippi, University, Mississippi 38677 (current address)
[4]AFRC Unit of Nitrogen Fixation, U. Sussex, Brighton, UK
[5]Department of Biochemistry, U. South Florida, Tampa, Florida 33612
[6]Schlumberger-Doll Research, Ridgefield, Connecticut 06877 (current address)

Although frequently used by surface scientists, the 2-3 keV region has seen relatively few biochemical or geochemical applications (1). The object of this proposal is to develop techniques for probing phosphorus and sulfur K edges, as well as molybdenum L edges, under dilute biological conditions. Beam line VI in undulator mode (2) is ideal for this purpose, and we have prompted SSRL to reduce the Be window thickness on this beam line first from 20 to 15 and now to 10 mils on this beamline.

To better understand the physics of Mo L-edge splittings, we have examined a series of Mo compounds with systematic variation of ligands and geometry. We have found that the x-ray splittings are close to the optical splittings of the corresponding Tc analogs. For example, the splitting in the MoO_4^{2-} L_2 and L_3 edges is 2.2 and 2.4 eV respectively. The optical splitting in MoO_4^{2-} is only 1.7 eV, whereas the optical splitting in TcO_4^{2-} is 2.35 eV. For more complicated structures, we find that 2nd derivative plots of the L-edges reveal a wealth of structure hidden in the raw absorption spectrum (Figure 1). We have also done preliminary single crystal L-edge experiments on MoO_3 crystals, for which we see dramatic orientation effects (Figure 2). Finally, we have observed changes in the L-edge spectra of molybdenum enzymes such as xanthine oxidase, which should eventually address the symmetry of the active site (Figure 3).

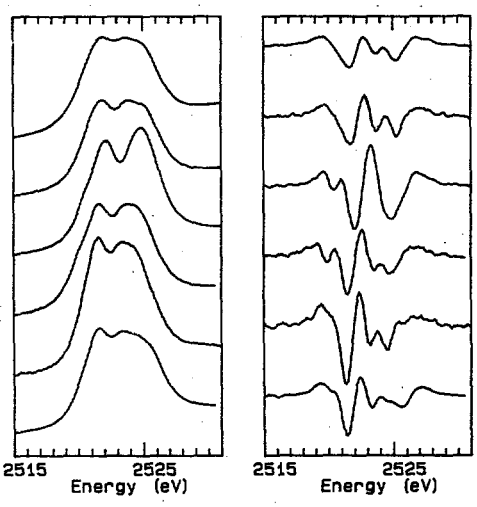

Figure 1. L_3 absorption edges (left) and 2nd derivatives (right) for a series of Mo(V) complexes based on the hydrotris (3,5-dimethyl-1-pyrazoyl) borate ligand, L. Compounds are of the form LMoO(X,Y), where the donors X and Y are (top to bottom): (Cl^-,Cl^-), (Cl^-,^-OMe), ($^-O^-CH_2CH_2O^-$), ($^-SCH_2$-CH_2O^-), (PhS^-, PhS^-), and (N_3^-,N_3^-).

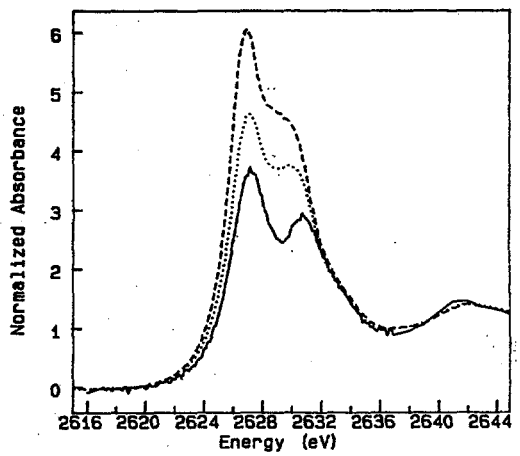

Figure 2. L_2 absorption edge region for a MoO_3 single crystal at 3 different angles with respect to the electric field polarization.

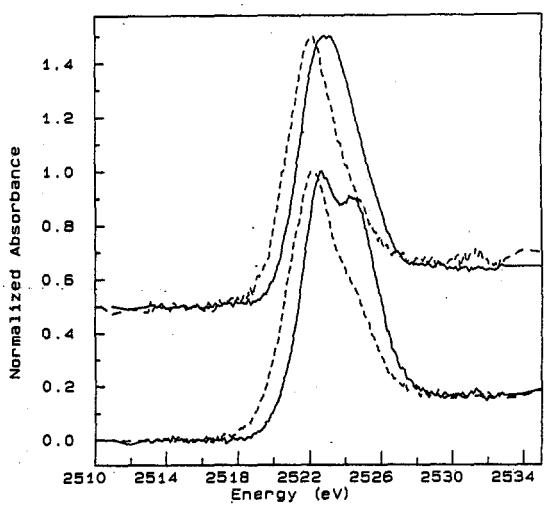

Figure 3. L_3 absorption edge region for xanthine oxidase in active (top) and desulfo (bottom) forms. (—) oxidized enzyme, (- - -) reduced enzyme.

References

1. Lytle, F. W.; Greegor, R. B.; Sandstrom, D. R.; Marques, E. C.; Wong, J.; Spiro, C. L.; Huffman, G. P.; Huggins, *Nucl. Inst. Meth.* **1984**, *226*, 542-9.

2. Hedman, B.; Frank, P.; Penner-Hahn, J. E.; Roe, A. L.; Hodgson, K. O.; Carlson, R. M. K.; Brown, G.; Cerino, J.; Hettel, R.; Troxel, T.; Winick, H.; Yang, J. *Nucl. Inst. Meth.* **1986**, *A246*, 797-800.

XAS INVESTIGATIONS OF RIESKE-LIKE IRON SULFUR CENTERS

Proposal 1035B

C.J. Batie[1], D.P. Ballou[1], and J.E. Penner-Hahn[2]

[1]Department of Biological Chemistry, University of Michigan, Ann Arbor, MI 48109
[2]Department of Chemistry, University of Michigan, Ann Arbor, MI 48109

The phthalate oxygenase (PO) from Pseudomonas cepacia catalyzes the dioxygenation of phthalate to a dihydrodiol (Eq. 1). PO contains two Fe atoms in a

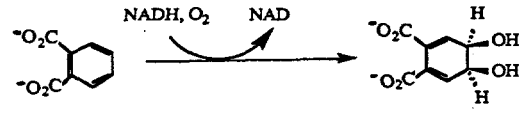

binuclear site and a third, dissociable iron in a mononuclear site. The binuclear site is a [2Fe-2S] cluster, however it has electrochemical and spectroscopic properties distinct from other (e.g. ferredoxin) [2Fe-2S] clusters. The PO cluster is spectroscopically similar to the binuclear site in the "Rieske" respiratory electron transfer protein. In Thermus thermophilus, the Rieske-like cluster contains at most two terminal thiolate ligands. Recent ENDOR measurements demonstrate that at least one, and more likely two, different types of nitrogen atoms are directly coordinated to the Fe/S cluster in Rieske proteins [1]. Possible structures for the Rieske-like cluster are shown below (X is a low-Z, probably N, ligand).

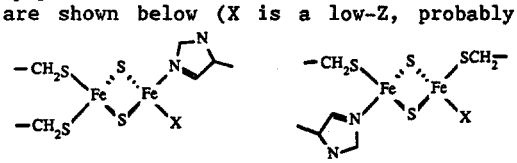

We have used EXAFS spectroscopy to characterize the Rieske-like and the mononuclear sites in PO. In order to study selectively the Rieske-like site, we measured data for PO in which the mononuclear Fe had been removed. In order to study selectively the mononuclear site, we measured Zn EXAFS data for PO in which the mononuclear site was reconstituted with Zn.

Experimental

X-ray absorption data were measured on beam-line 7-3 using Si(220) monochromator crystals. Energy calibration was referenced to the first inflection point of an Fe foil absorption spectrum (7111.2 eV) measured at the same time as the data. A Stern-Heald detector was used to monitor protein X-ray fluorescence. Protein concentrations were ca. 4 mM. All spectra were measured at 4K. The samples which were examined include the native (3Fe) protein (fully reduced), the 2 Fe (Rieske-like cluster only) in both oxidized and reduced forms, and the reconstituted protein (2Fe+Zn) in the presence and absence of phthalate.

Results

Fourier transforms of the EXAFS data for oxidized and reduced forms of the Rieske-like cluster are shown in Figure 1. These data are dominated by Fe-S and Fe-Fe EXAFS, confirming the general features of the proposed structures. Data analysis is in progress to determine the bond lengths and coordination numbers and to investigate the low-Z ligands. The EXAFS data (not shown) for the Rieske-like cluster indicate that a structural change occurs on reduction. From Figure 1, it would appear that this involves a change in the Fe-Fe distance.

The EXAFS data for the Zn reconstituted mononuclear site (not shown) is consistent with predominantly low-Z ligation. There is no evidence for an EXAFS detectable interaction with the Rieske-like site. In order to address the question of whether the structure of the Zn substituted mononuclear site is the same as that of the native (Fe containing) site, we have calculated the difference between the EXAFS data for the 3Fe and the 2Fe forms of the protein. This difference should reflect the structure at the mononuclear Fe site. Although the signal/noise ratio for the difference data is worse than that for the Zn data, preliminary analysis suggests that the structure of the mononuclear site does not change significantly on substitution of Zn for Fe.

Interestingly, XANES spectra for the Zn site (Figure 2) suggest that the structure of this site is substrate dependent. This is consistent with the suggestion that catalytic activity takes place at the mononuclear site. The nature of this change is not immediately obvious, however the EXAFS data (not shown) contain no substrate dependent changes for k> 4Å^{-1}. This would suggest that the effects observed in the XANES reflect orientation changes rather than a gross change in ligation. We are attempting to interpret these spectra in terms of structural parameters.

References

1. Cline, J.F.; Hoffman, B.M.; Mims, W.B.; LaHaie, E.; Ballou, D.P.; Fee, J.A., 1985, J. Biol. Chem., 260, 3251-3254.

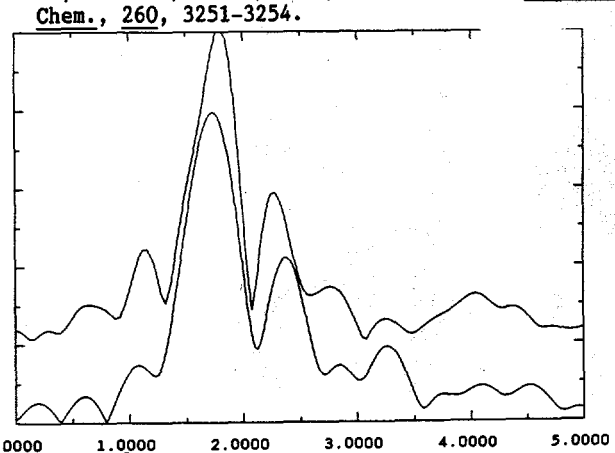

Figure 1. k^3 weighted Fourier transforms of EXAFS for 2Fe PO. Top) Reduced Rieske center. Bottom) Oxidized Rieske center. Contributions of Fe-S and Fe-N to the first shell are not resolved in this figure.

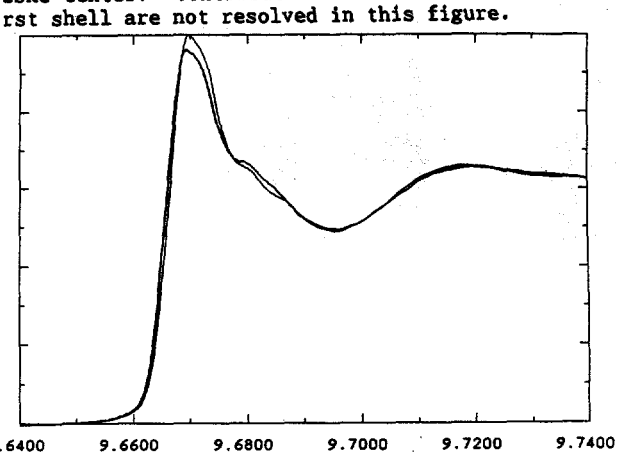

Figure 2. Normalized Zn XANES spectra for 2Fe+Zn protein. Light) without phthalate. Dark) with phthalate.

X-RAY ABSORPTION OF ORIENTED CYTOCHROME OXIDASE

G.N. George[1], R.C. Prince[1], T.G. Frey[2], and S.P. Cramer[3]

[1]Exxon Research and Engineering, Annandale, New Jersey 08801
[2]Dep't of Biology, San Diego State University, San Diego, California 92182
[3]Schlumberger-Doll Research, Ridgefield, Connecticut 06877

Cytochrome oxidase, the mitochondrial enzyme which reduces O_2 to H_2O, contains two types of iron, in heme *a* and heme a_3, and two different coppers, Cu_A and Cu_B. The EXAFS analyses for this enzyme have been the subject of interminable discussion (1,2), in part because of the presence of multiple forms of the enzyme (3,4). To approach the problem in a fresh manner, we have recorded the x-ray absorption spectra of cytochrome Fe and Cu on the enzyme in an oriented hydrated membrane multilayer preparation (5). Not only is this closer to the true physiological conditions, but the angular dependence of the XANES and EXAFS allows us to distinguish between the different types of iron and copper and to define their orientations.

The angular dependence of the copper K edge (Figure 1), is dominated by the variation of a feature at 8987 eV which maximizes at $\theta = 90$ degrees. This feature is a well known marker for Cu(II) complexes with tetragonal symmetry, and is known to be polarized along the long Cu *z*-axis. Analysis of the amplitude variation shows that this particular copper *z*-axis is oriented nearly perpendicular to the membrane normal; separate chemical information tells us that this is Cu_B.

The angular dependence of the iron K edge EXAFS (Figure 2) is also significant. A feature at $R + \Delta = 2.1$ Å grows stronger in the 90 degree data and is suggestive of an axial sulfur ligand to iron. We are currently truing to distinguish this from possible Fourier transform artifacts.

Because much of the water is removed from the sample, the quality of data obtainable on membrane multilayers is superior to solution spectra. We expect the use of such samples to become more common in future biochemical EXAFS.

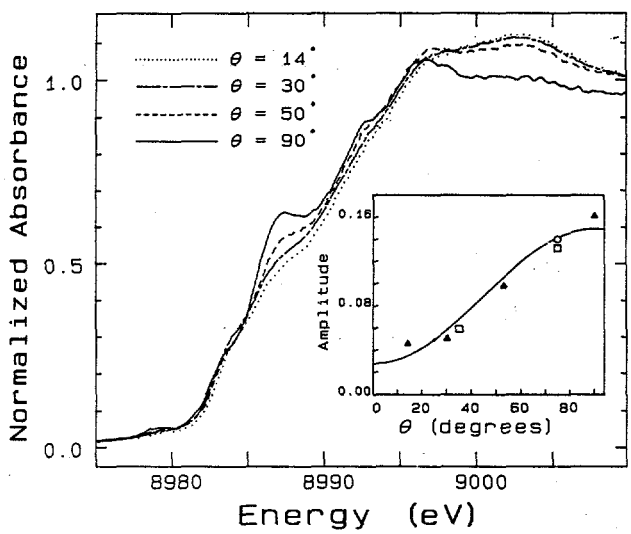

Figure 1. Orientation dependence for oxidized cytochrome oxidase Cu K edge. θ is the angle between the $\vec{E}$-polarization and the membrane normal.

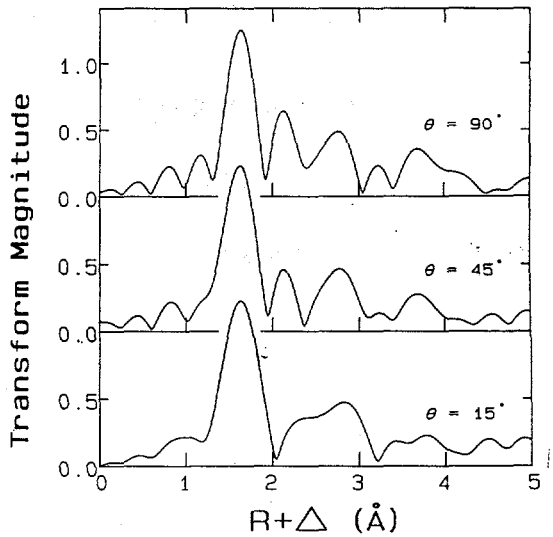

Figure 2. Orientation dependence for oxidized cytochrome oxidase Fe K edge EXAFS.

References

1. Powers, L.; Chance, B.; Ching, Y.; Angiolillo, P. *Biophys. J.* **1981**, *34*, 465-98.

2. Scott, R. A.; Schwartz, J. R.; Cramer, S.P. *Biochemistry* **1986**, *25*, 5546-55.

3. Naqui, A.; Chance, B.; Cadenas, E. *Ann. Rev. Biochem.* **1986**, *55*, 137-166.

4. Young, L. J.; Palmer, G. *J. Biol Chem.* **1986**, *261*, 13031-3.

5. George, G. N.; Cramer, S. P.; Frey, T. G.; Prince, R. C. *Adv. Mem. Biochem. Bioenerg.* Kim, C. H. ed., Plenum, N.Y. (1987) - in press.

X-RAY CRYSTALLOGRAPHY OF β-LACTAMASE ENZYME

J. R. KNOX, P. C. MOEWS, H. ZHAO and J. K. M. RAO
Department of Molecular and Cell Biology and
Institute of Materials Science
The University of Connecticut
Storrs, CT 06268

β-Lactamase is a bacterial enzyme which inactivates β-lactam antibiotics (penicillins and cephalosporins).[1] Its presence in pathogens is a clinical problem which makes β-lactam therapy ineffective. A knowledge of the three-dimensional structure of this enzyme could aid the design of newer, β-lactamase-resistant antibiotics. X-ray diffraction data from β-lactamase crystals have been collected on the rotation camera facility for protein crystallography during the period June 12-16, 1986.

The β-Lactamase from Enterobacter cloacae P99. This 39,000-dalton enzyme, which is particularly active against cephalosporins, crystallizes[2] in the orthorhombic space group $P2_12_12$ with cell dimensions 77.4 x 69.4 x 63.6 A. The crystals grow from polyethylene glycol as long, flat prisms with very small cross section (0.02 x 0.15 mm) which makes the use of conventional x-ray sources impractical. On the rotation camera at SSRL we were able to record 3° 15' oscillation films with 3 minute exposures. A pinhole collimator 0.200 mm in diameter was used at a crystal-to-film distance of 70 mm. Crystal translation between film packs was necessary to reduce radiation damage. In total, 138 film packs were recorded from six crystals. Of these crystals, two were native enzyme crystals diffracting to 2.2 A resolution, three were heavy atom derivative crystals ($TbCl_3$, $K_3UO_2F_5$, K_2PtCl_4), and one was an active-site bound complex with boronic acid. For each crystal, a total rotation range of about 95° could be recorded before crystal deterioration. Data were indexed with the ALIGN program[3] on an E&S PS330 graphics. Scaling and merging of integrated intensities using OSCMGR produced R(I) factors between 7% and 9 % for the 2.2 A native data and 10.8% for the $TbCl_3$ derivative data.

A Method for the Indexing of Oscillation Films from Large Unit Cells.[3] An interactive graphics program for the PS330 has been written to display and index screenless x-ray oscillation films from macromolecular crystals with unit cells edges of at least 500A. ALIGN, a Fortran program which works in conjunction with M. G. Rossmann's program OSCMGR, accurately displays densitometered reflection intensities, provides the required transformation between predicted and observed relection coordinates, and is useful in determining crystal mosaicity and detecting unit cell changes.

We have used ALIGN to index data sets of the tetragonal form of TEM β-lactamase. The unit cell is large and each 2° oscillation film contains five thousand reflections to 3.0 A resolution. With a well-focused beam (λ = 1.5A) and a crystal-film distance of 100 mm there are about three reflections per mm along the c* direction; the spots measure about 200-250 μm in this direction and are separated by a gap of 50-75 μm. Originally, with the use of fiducial marks, 6 - 8 hours were required to predict the pattern, plot the positions of reflections, locate the fiducial marks, and obtain the two-dimensional rotation matrix and translation necessary to start refinement. Using ALIGN and OSCMGR together, an inexperienced user was able to align and index a film with the last of three predicted patterns in only 15 minutes. We have also used ALIGN with the smaller P99 β-lactamase unit cell (75 - 100 A) where alignment and indexing was much easier.

Conclusions. Diffraction films from native and derivative P99 β-lactamase crystals are being densitometered and indexed in our laboratory. Patterson and molecular replacement methods are being used to solve the structures.

Acknowledgement. This work is supported by grant AI-10925 from the NIH.

References

(1) J. M. T. Hamilton-Miller and J. T. Smith, Beta-Lactamases. Academic Press, London (1979).
(2) P. Charlier, O. Dideberg, J.-M. Frere, P. C. Moews and J. R. Knox, J. Mol. Biol. 171, 237-238 (1983).
(3) P. C. Moews, T. Sakamaki and J. R. Knox, J. Appl. Cryst. (1986), 19, 101-104.

PRELIMINARY STUDIES OF VARIOUS VIRUSES AND VIRUS COMPLEXES

The following crystals were examined during the visit by members of the laboratories of J. E. Johnson and M. G. Rossmann, May 7 - 9, 1986.

1) SV40 Crystals (J. Tsao, M. Luo, M. G. Rossmann)

Diffraction patterns extending to 6 Å resolution were observed. Crystals were small (0.2 mm). This is the first time that crystals of SV40 have been examined that diffracted as well as these crystals. The data were sufficient for a tentative space group determination.

2) Bean Pod Mottle Virus (Y. Li, C. V. Stauffacher, J. E. Johnson)

Two different crystals were examined which diffracted to about 10 Å resolution only.

3) Mengo Virus - Receptor Attachment Site (M. Luo, M. G. Rossmann)

Sialic acid was diffused into Mengo virus crystals in the hope that it would bind to the receptor attachment site. A partial data set to high (2.6 Å) resolution was collected. The films were processed and showed that no sialic acid was bound.

4) Human Rhinovirus 14 - Receptor Attachment Site (M. Luo, M. G. Rossmann)

Sialic acid was diffused into rhinovirus crystals in the hope that it would bind to the receptor attachment site. A partial data set to high (2.6 Å) resolution was collected. The films were processed and showed that no sialic acid was bound.

5) N. β Capensis Virus (B. Wu, J. E. Johnson, C. V. Stauffacher)

Crystals did not survive the journey to California.

6) Flockhouse Virus (R. C. Tucker, J. E. Johnson, C. V. Stauffacher)

Crystals did not survive the journey to California.

7) Cowpea Mosaic Virus (C. V. Stauffacher, J. E. Johnson)

Limited data to 2.6 Å resolution was taken to standardize the wavelength and cell dimensions with respect to these well characterized crystals. The wavelength was found to be accurately stated to the third decimal place.

CRYSTALLOGRAPHIC STUDIES OF ANTIGEN-ANTIBODY COMPLEXES

P.M. Colman, W.G. Laver[†], G.M. Air[*] and R.G. Webster[**]

CSIRO, Division of Protein Chemistry, Parkville 3052, Australia.

[†]John Curtin School of Medical Research, Australian National University, Canberra.

[*]Department of Microbiology, University of Alabama, Birmingham, Alabama.

[**]St. Jude Children's Research Hospital, Memphis, Tennessee.

X-ray diffraction data were collected from crystals of influenza virus neuraminidase complexed with various Fab fragments of monoclonal antibodies. Data were measurable to 2.5Å resolution, compared to a limit of 2.9Å with a rotating anode X-ray source.

Full datasets on two different complexes were collected. The Fab fragment NC41 when complexed with the neuraminidase from an avian influenza virus crystallises in space group $P42_12$ with a=b=167Å, c=124Å (1). Isomorphous crystals of a single site mutant of neuraminidase complexed with the same Fab fragment have also been grown (1), although the affinity of the Fab for the mutant antigen is slightly lower than for wild type.

The data demonstrate that the Fab binds to the two neuraminidases isosterically, i.e. no rearrangement of the antibody on the antigen results from the mutation (Asn→Asp) although the affinity is lowered. The structure of this antibody-antigen complex has now been determined from the Rotating Anode Datasets (2).

1. Laver, W.G., Webster, R.G., and Colman, P.M. (1987) Virology, in press.
2. Colman, P.M. et al. in preparation.

DATA COLLECTION ON CD,ZN METALLOTHIONEIN AT [illegible] WAVELENGTHS

S.A. Collett and C.D. Stout
Department of Molecular Biology,
Research Institute of Scripps Clinic,
La Jolla, CA 92037

We are currently refining the structure of Cd,Zn metallothionein (MT) starting from a 2.3A resolution data set and preliminary structure (1). The protein, MW 6500 daltons, contains $Cd_4(cys)_{11}$ and $Cd_1Zn_2(cys)_9$ clusters. From the 2.3A analysis it is clear that higher resolution data is required to study the details of the Cd and Zn coordination, protein stereochemistry and solvation in this novel structure.

The crystals are intrinsically good diffracting but difficult to grow large (space group $P4_12_12$, a=b=30.9A, c=120.4A, one molecule per asymmetric unit). In June, 1986, with the x-ray beam tuned to λ=1.54A we collected a complete 1.9A resolution data set using the oscillation camera facility on beam line VII-1. During six shifts data were successfully collected from four crystals mounted on either a* or c* and maintained at 4°C. Oscillation angles ranged from 2.7° to 4.5° depending on crystal mount, and exposure times were 1.5 to 2.5 minutes ($\sim 5 \times 10^6$ total counts in dose mode). The crystals diffracted strongly to 1.9A, the limit of resolution with flat cassettes at crystal-to-film distance of 5.5 cm. The crystals were observed to decay relatively rapidly (20 min. total exposure), as indicated by an increase in mostacity, and the diffraction pattern exhibited thermal diffuse scattering effects. Trial experiments using V-shaped cassettes to sample the data beyond 1.9A were unsuccessful due to the camera geometry, but one exposure with a modified flat cassette indicated that data were present to 1.65A.

In November, 1986 a trial data set was collected with the wavelength tuned to λ=1.08A, at the suggestion of Dr. P. Phizackerley. At the shorter wavelength the expectation is that the relative signal-to-noise will be increased due to reduced background scattering during equivalent exposure times. At the same time, absorption effects will be smaller and the absorbed dose in the crystal should be smaller, reducing decay (2). Qualitatively these advantages appear to be born out in the MT films at 1.08A vs. 1.54A.

Data were collected with the oscillation camera on beam line VII-1 using similar experimental conditions as for λ=1.54A. At crystal-to-film of 5.5cm reflections along the 120.4A c axis were adequately resolved using a 0.2mm collimator. At this crystal-to-film distance reflections to 1.35A are recorded on a flat cassette, facilitating data processing. For MT crystals the diffraction pattern extended isotropically to 1.5-1.6A resolution. During three shifts data were collected on two crystals, one mounted on (110) (3° oscillations, 24° of data), and one mounted on (001) (35° oscillations, 42° of data). Reflections to 1.5A were not overlapped on the films. Cassettes were loaded with 6 layers of Al foil between films with three films per cassette, this being the limit in thickness allowable. This gave reasonable attenuation of strong high angle reflections, but strong low angle reflections remained saturated on the C film. In the future it is planned to use Au foils. Exposures were $\sim 1.0 \times 10^7$ total counts in dose mode or twice that used at λ=1.54a. In other words, at the shorter wavelength the same signal-to-noise is achieved, although the exposure is doubled; at the same time data to higher resolution are recorded on flat cassettes and decay and absorption effects are minimized. For the MT crystals, decay and thermal diffussion scattering were no worse at λ=1.08A in spite of the greater total exposure per crystal. A further advantage of the 1.08A wavelength is the enhanced anomalous scattering for Zn (K-edge 1.20A) vs. 1.54A. The objective of further experiments is to complete the 1.5A resolution data collection using the 1.08A wavelength.

Supported by NIH grant GM-36535.

References

1. W.F. Furey, A.H. Robbins, L.L. Clancy, D.R. Winge, B.C. Wang and C.D. Stout (1986) Science 231, 704-710.
2. U.W. Arndt (1984) J. Appl. Cryst. 17, 118-119.

X-RAY CRYSTALLOGRAPHIC STUDIES ON SINGLE CRYSTALS OF *N. GONORRHOEAE PILIN*

Hans E. Parge, Elizabeth D. Getzoff, Duncan E. McRee, and John A. Tainer

Department of Molecular Biology, Research Institute of Scripps Clinic, La Jolla, California 92037

Introduction

Pili, long filamentous appendages found on the cell surface, mediate the attachment of many pathogenic bacteria to host cells. Each pilus is assembled primarily from multiple copies of one major structural protein, pilin, which varies with serotype. In *Neisseria gonorrhoeae*, pilin has a molecular weight of 18,000 and consists of approximately 160 amino acids with a highly conserved N-terminal and an antigenically variable C-terminal sequence (1).

Experimental

Crystals of pilin have been grown by conventional vapour diffusion techniques (2,3,4). These crystals, though small (60-100 microns thick and up to 1.5 mm long), diffract to better than 2.8 Å resolution using 1.54 Å wavelength Cu Kα radiation and to better then 2.4 Å resolution using 1.08 Å wavelength synchrotron radiation.

Crystals were mounted in glass capillaries (0.5 mm) along with some of their mother liquor from the crystallization solution. Diffraction data were collected on an Arndt Wonacott oscillation camera from a number of native and potential heavy atom derivatives of pilin in three different crystal orientations. A crystal-to-film distance of 100 mm, a 0.2 mm collimator, and oscillation ranges of 2.0° to 4.5° with exposure times of 1.5 to 3.0×10^7 counts/degree were used. The dimensions of these crystals usually permitted the collection of large portions of the data from a single crystal by repeated translation to expose fresh material after every 6 to 8 oscillation photographs. Data were collected at 5 and -15°C.

Data Processing

Data films were digitized on a P-1000 Optronics drum scanner linked to a VAX 11/750 computer. A 50-micron raster was used for all films and provided good resolution of the diffraction spots. Digitized data were processed using a combination of programs: MOSCO (5) to provide the initial rough alignment and the determination of exact spindle position and Rossman's (6) package for the refinement of orientation, and the integration, merging, and scaling of reflections.

Results

For data collection, we find that significant increases in crystal lifetimes in the x-ray beam can be achieved by collecting at low temperatures (-15°) and shorter wavelengths (1.08 Å). Analysis of a native data set on pilin (approximately 85% complete) to 3.5 Å resolution, which was collected about the long axis of the needle-shaped crystals, has provided confirmation of our proposed model for the structure of pilin (2,3,4) and has thrown some light on the possible modes of assembly of pilin to form the pilus fiber.

References

1. Hagblom, P., Segal, E., Billyard, E., and So, M. (1985) *Nature* **315**, 156-158.
2. Parge, H.E., McRee, D.E., Capozza, M.A., Bernstein, S.L., Getzoff, E.D., and Tainer, J.A. (1987) *In* The Pathogenic Neisseriae, American Society of Microbiology, in press.
3. Parge, H.E., McRee, D.E., Deal, C.D., So, M., Getzoff, E.D., and Tainer, J.A., (1987) *Nature*, in preparation.
4. Deal, C.D., Tainer, J.A., So, M., and Getzoff, E.D. (1985) *In* The Pathogenic Neisseriae (ed. G.K. Schoolnik) American Society for Microbiology, Washington, D.C., 302-308.
5. Nyborg, J., Wonacott, A. J., Thierry, J.-C., Champness, J. N., (1975) MRC Laboratory of Molecular Biology, Hills Road, Cambridge.
6. Rossman, M.G., (1985) *In* Methods in Enzymology (eds. Colowick, S.P. and Kaplan, N.O.), **114**, Part A, 237-281.

X-RAY DIFFRACTION DATA COLLECTION OF PROTEINS

A. de Vos, L. Tong, M. Milburn, and S.-H. Kim
Department of Chemistry, University of California
Berkeley, CA 94720

We have collected 2.0 Å resolution diffraction data on native crystals and 3.0 Å diffraction data on two heavy atom derivatives of a nucleotide binding protein. In addition we have tested the limit of diffraction from several small crystals including allophycocyanine and J-protein, a histadine binding protein in E. coli. We have also collected 2.7 Å resolution diffraction data on monellin, an intensely sweet protein. All the data have been recorded on X-ray films. The films for monellin have already been scanned and processed and the rest of the films are in the process of being scanned by an optical scanner. The monellin data will be used to refine the crystal structure of the protein solved at 3 Å resolution using diffractometer data.

DEVELOPMENT of an X-RAY MICROPROBE USING MULTILAYER MIRRORS

A.C. Thompson, J. Underwood, and Y. Wu
Center for X-Ray Optics

R. Giaque
Applied Science Division
of
Lawrence Berkeley Laboratory
Berkeley, CA 94720

A multilayer mirror system has been developed to focus 10 keV x-rays from a synchrotron source to produce a beam with enough intensity to easily measure trace element concentrations. This high spatial resolution, high intensity x-ray microprobe provides a powerful new method to measure the concentrations and spatial distribution of many elements quickly and simultaneously in a sample area of less than 100 square microns. With our present instrument, sub-picogram quantities of elements from potassium to zinc can be measured in a 300 second counting time.

Since the samples do not have to be put under a vacuum, the microprobe can accommodate a wide variety of samples that cannot be studied with an electron microprobe; biological samples in an aqueous environment are a good example. The sensitivity to trace elements is also better than that of an electron microprobe.

The geometry of the system is shown in figure 1. The LBL-EXXON beamline at SSRL was used with a wiggler field of 0.8 Tesla. The beamline monochromator was equipped with Silicon <111> crystals and tuned to 10 keV. The system used a pair of mirrors in a Kirkpatrick-Baez geometry to focus the beam to a spot 16 μm wide by 6 μm high. The two multilayer mirrors were fabricated from a pair of concave spherical mirrors that were coated with W-C multilayers using a new multilayer coating facility at LBL. With SSRL operating at 3 GeV and 80 mA a beam intensity of 8 x 10^7 photons/sec was measured. The sample was placed on a two dimensional precision scanning stage which was scanned to produce one and two-dimensional images. When the x-ray beam strikes the sample, elements in it are caused to fluoresce with characteristic spectral lines, which are recorded by a Si(Li) detector placed perpendicular to the beam.

A variety of samples were scanned to demonstrate the capability of the instrument. Figure 2 shows energy spectra obtained at different positions along an algae filament by stepping the sample in 10 micron increments. While the concentration of most elements remains relatively constant, the iron concentration varies dramatically along the filament. Figure 3 shows the results of two-dimensional scan of a microscopic inclusion containing aqueous calcium chloride solution in a 200 micron thick section of quartz. The contour lines give the relative concentration of calcium in the area. This instrument may provide a method to assay the elements dissolved in the water within these inclusions non-destructively, a measurement that is impossible with existing techniques. Since minerals are transported through the earth's crust by water seepage, this instrument will be a valuable tool for geologists studying rock and ore formation.

Further experiments are planned to utilize the present system and to improve the spot size and elemental sensitivity. Presently the major factor limiting the final spot size is the relatively large emittance of the SPEAR electron beam. As the emittance and beam stability are improved the quality and spatial resolution of our images will also improve.

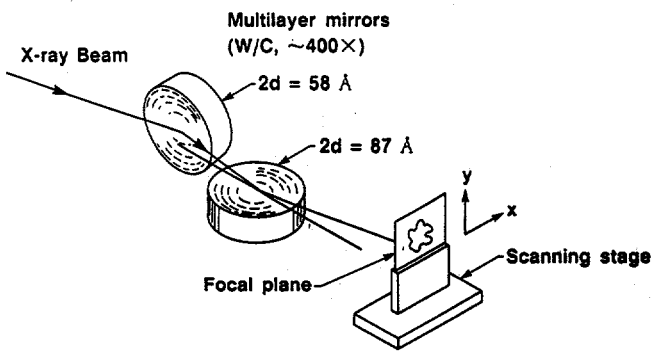

Figure 1. Geometry of x-ray microprobe.

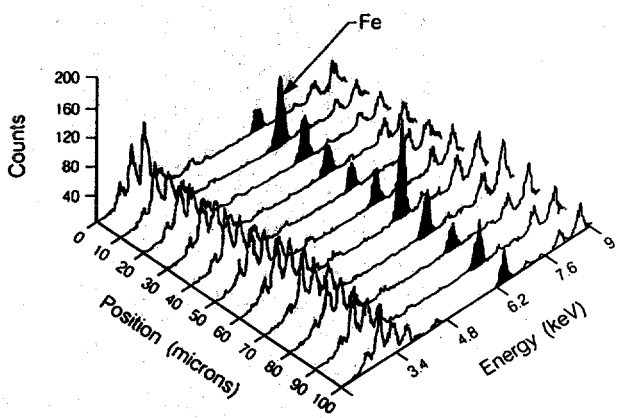

Figure 2. The energy spectrum obtained at 10 micron intervals along a filament of blue-green algae. The variation of iron along the filament is highlighted. Using the x-ray microprobe it is possible to measure the elemental composition of cells along the filament and to correlate elemental gradients with cell types and cell function.

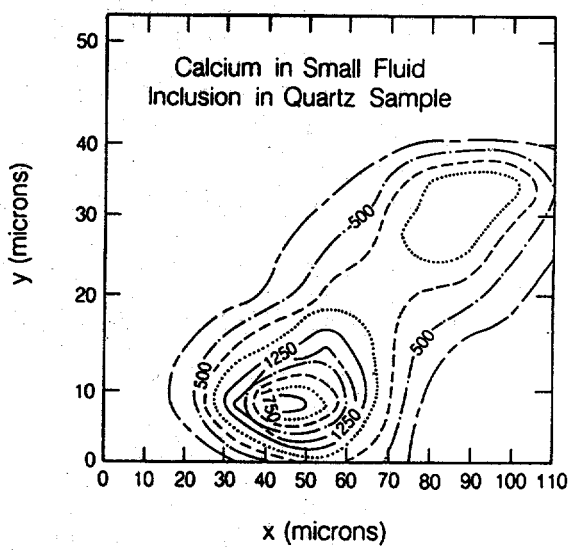

Figure 3. Relative calcium concentration in a small water inclusion (bubble) in a thin quartz sample. The x-ray microprobe provides a non-destructive method to measure the elemental concentrations of many elements simultaneously. Study of these small water inclusions will help provide an understanding of mineral transport through the surrounding rock.

GaAs ON Si(100) STUDIED WITH GRAZING INCIDENCE SCATTERING

J.B. Kortright
Lawrence Berkeley Laboratory
Berkeley, California 94720
and
S.L. Laderman, M.P. Scott and A. Fischer-Colbrie
Hewlett-Packard Laboratories
Palo Alto, California 94304

GaAs grown by MBE on Si(100) substrates is an example of a heteroepitaxial system under wide investigation as a prototypical large lattice mismatch system, as well as for its technological promise. Empirical approaches to improved crystal growth currently appear limited by a lack of reliable detailed models of the epitaxial process in this system [1]. This work is the first reported instance attempting to use x-ray scattering experiments to directly measure physical properties of the defect structures in epitaxial GaAs/Si with the idea of developing better structural models for strain relaxation and epitaxial quality. In these experiments we set out to explore the strength and symmetry of the scattering due to key defect types.

We employed the grazing incidence geometry in order to maximize the signal from the GaAs layer, to measure the depth dependence of the defect concentration and to study the scattered intensity in the vicinity of in-plane GaAs reflections.

Two samples grown by MBE were the primary objects of study. In both, the GaAs deposition consisted of a 400 deg. C growth of a 1000 A thick "low temperature" buffer layer followed by a 575 deg. C growth of a 2000 A thick "high temperature" layer. This two step growth is typical of procedures used today to optimize the technical usefulness of the epitaxial film [2]. The two samples differed significantly in two ways, the degree and direction of substrate off orientation and method of surface preparation. At the outset of this work, it was known that the average epitaxial crystal quality, as measured by conventional double crystal x-ray rocking curve analysis, was substantially higher in the case of sample 1 than in the case of sample 2. Two samples prepared using the MOCVD technique were also investigated, though time has not allowed for a thorough study of these samples. Data presented here are from the MBE samples.

X-ray scattering experiments were performed in two parts. The bulk of the data was collected with 10.0 keV photon energy and scattering vector nearly in the plane of the sample surface on B.L. VI-2 during dedicated conditions. Some data with photon energy 7.0 keV and scattering vector strongly out of the sample surface plane were studied on B.L. VII-2 during parasitic conditions. Selected observations are presented here.

Limiting penetration into the GaAs layer by tuning the incident angle near the critical angle, we learn of the depth dependence of certain defects. With the scattering vector strongly out of the plane of the thin films, we see twins in just the buffer layer of sample 1 and twins in sample 2 which extend throughout the buffer and high-T growth layer. Twins are seen in only one azimuthal orientation for sample 1 and in two perpendicular azimuthal orientations for sample 2.

The first figure shows scans near the twinned 111 reflection for sample 2. Here the scattering plane was normal to the sample surface, and for different, fixed incidence angles the detector was scanned to vary the scattering angle. These scans reveal a streak in reciprocal space emanating from the twin 111 spot. This streak has an angle with respect to the reciprocal lattice of the untwinned material characteristic of a 111 direction. The length of this streak suggests that the twinned regions have spacial extent of order 100 A along these directions.

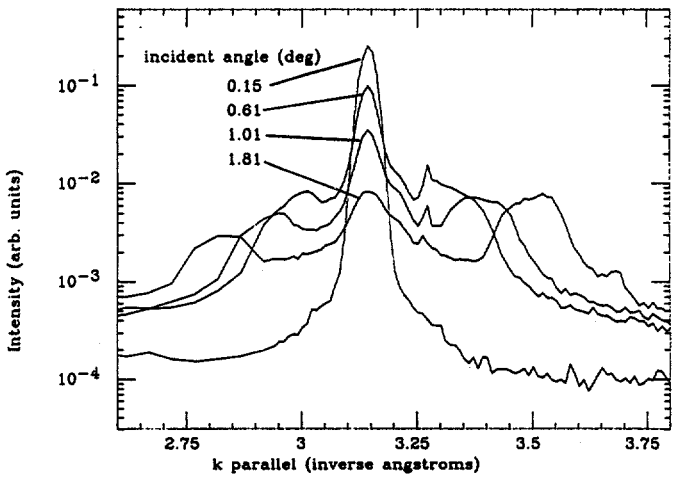

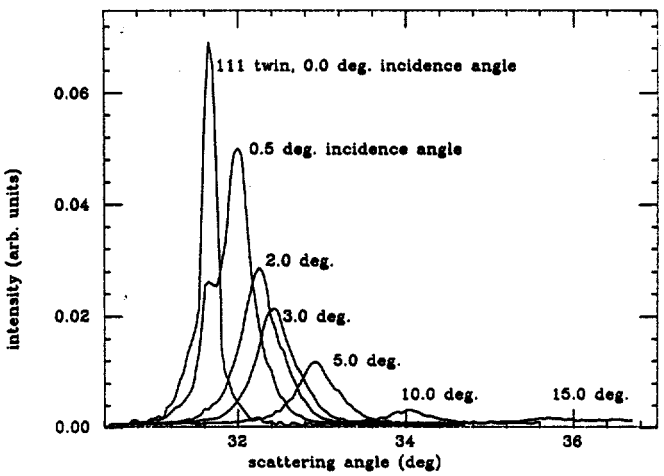

The second figure shows scans in the vicinity of the GaAs 220 reflection of GaAs which is oriented with respect to the Si substrate. These scans have scattering vector almost in the plane of the sample for different, fixed incidence angles near the critical angle as noted. We see the truncation rod of the GaAs 220 reflection. A slight shoulder on the high-k side of the GaAs 220 peak indicates strained GaAs at the interface with the Si. Side-lobes about the 220 peak appear when x-rays penetrate the buffer layer, and change with grazing angle. These streaks originate from the 220 reciprocal lattice point roughly along 111 directions. Comparing the intensity of these streaks with that of the truncation rods of the 220 reflections leads us to conclude that a significant volume of material is present in these regions giving rise to the streaks. Planar defects such as stacking faults are interpreted as the cause of these streaks.

These results demonstrate the grazing incidence scattering technique to be very useful in learning about defects in very thin films in a depth-sensitive way. We learn that microtwin formation is a significant feature of GaAs/Si heteroepitaxial growth. The directions along which microtwins form appear correlated to the precise substrate off-orientation. Small domains of untwinned material are observed to be delineated by planar defects lying along 111 directions. Some GaAs at the Si interface is strained. We are investigating the extent to which these x-ray scattering techniques can be used to obtain quantitative information about the density and characteristic size of the observed defect signals.

Acknowledgements.

The preparation of sample 1 by S. Koch was, in part, made possible by support from the NSF through the Center for Materials Research at Stanford. We thank P.H. Fuoss for use of his grazing incidence diffractometer. One of us (JK) was supported by the U.S. Department of Energy under contract DE-AC03-76SF00098.

References.

1. S.J. Rosner, S. Koch, S. Laderman and J.S. Harris, Proc. MRS, Heteroepitaxy on Si, 67, 1986.
2. S.M. Koch, S.J. Rosner, R. Hull, G. W. Yoffe, J.S. Harris, to be published in J. Crystal Growth.

INTERATOMIC STRUCTURAL CHARACTERIZATION OF W-C MULTILAYERS USING GRAZING INCIDENCE SCATTERING

J.B. Kortright and J. Denlinger
Center for X-ray Optics
Lawrence Berkeley Laboratory
Berkeley, California 94720

Tungsten-carbon periodic multilayer structures were some of the first multilayers to demonstrate utility as x-ray optical devices [1]. Even so, very little has been known about the local interatomic arrangements which make up the ultra-thin layers of these structures. We have applied the grazing incidence scattering (GIS) technique to learn more about the in-plane interatomic arrangements in this multilayer system as a function of layer thickness and annealing.

Multilayer samples were prepared by magnetron sputtering at LBL onto uncooled, highly polished optical flats. As-prepared samples with five different multilayer periods were studied: 8.3 A, 19.0 A, 37.0 A, 59.4 A and 108.8 A. Based on sputtering rates of the individual elements, the W-rich layers in each of these multilayers would be roughly 0.4 of the total period, assuming no intermixing at the interfaces. This is typical of the relative thickness of the W- and C-rich layers used in x-ray optical applications. The sample with as-prepared period of 37 A was also studied after annealing at 300 C for 18 hrs.

The GIS geometry adopted had the scattering vector very close to the plane of the multilayers, so that in-plane interatomic correlations yielded the measured scattering. The photon energy was 10.000 keV. The incident angle of about 0.70 degree (slightly above the critical angle) allowed us to avoid contributions from the substrate to the scattered intensity. We probe primarily in-plane W-W correlations in these structures, since the scattered intensity from W-C and C-C correlations are roughly one and two orders of magnitude less that from W-W correlations.

The multilayer Bragg scattering was measured separately in the laboratory using Cu K-alpha radiation. The intensity in the first order multilayer Bragg peak was found to decrease with decreasing period. Extremely weak but measurable composition modulation exists in the 8.3 A period sample. Because the modulation is so weak, we can use the interatomic scattering from this multilayer as a standard representative of scattering from a largely intermixed amorphous structure of W and C in the same proportions as the average all of the samples. Annealing of the sample with initial period 37.0 A caused an expansion of the multilayer period by 3.2 percent.

The in-plane, GIS intensity from the multilayers are shown in the first figure. For multilayer periods 59.4 A and less interatomic correlations are amorphous. The sample with period 108.8 A shows a superposition of a diffuse amorphous profile with polycrystalline peaks at positions expected for bcc W. These sharp peaks are really the tails of polycrystalline, in-plane Bragg peaks which are relaxed normal to the layers because of the finite extent of the layers. Scans with scattering vector perpendicular to the multilayer reveal that this crystalline W is highly textured with 110 planes parallel to the multilayer planes. The diffuse amorphous intensity is significant compared to the intensity from the crystalline part of the W-rich layers, suggesting a significant amount of amorphous W-rich material compared to the polycrystalline, textured bcc W. We infer that W-rich layers of this sample consist of poly-crystalline, bcc W at the center of the layers surrounded on at least one side (perhaps both) by W-rich amorphous "interface layers" between the

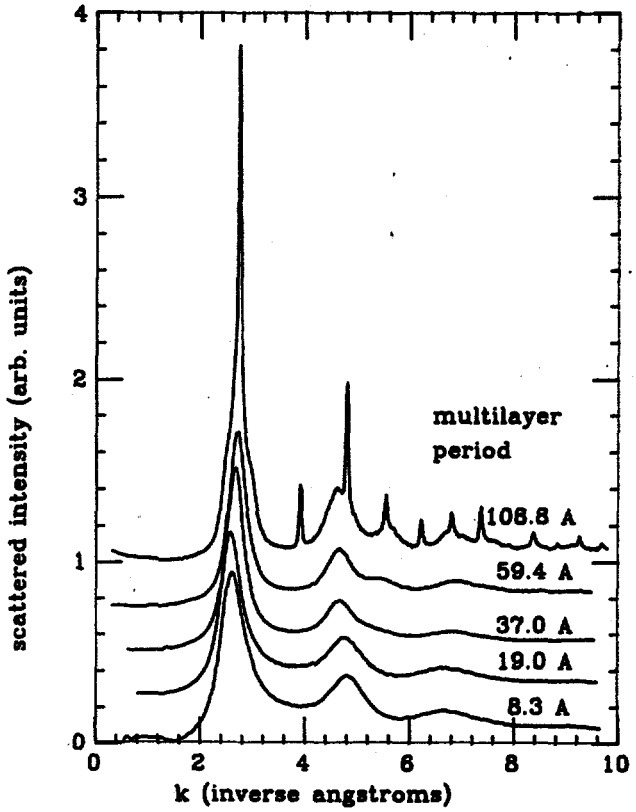

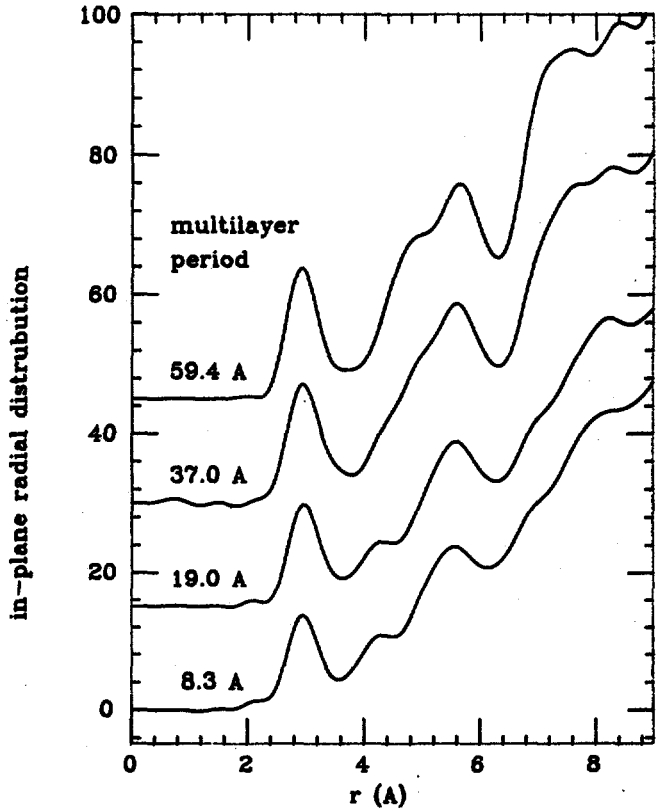

adjacent C-rich layers. The amorphous part of the scattered intensity from the 108.8 A period sample is more similar to that of the 59.4 A period sample than to amorphous profiles of multilayers with smaller period.

Normalization of the amorphous scattering patterns and Fourier transformation into real space to obtain radial distribution functions for these layered samples is somewhat more complicated than for nominally homogeneous binary amorphous alloys because of the layered nature of the samples. The density is poorly defined, and we must consider cylindrical as well as spherical symmetry as that properly describing the distribution of interatomic scattering. We obtain an estimate of the best apparent density of the W-rich layers, during analysis of the data. We have assumed both spherical and cylindrical coordinates in the analysis, and have found that trends with multilayer period and annealing are very similar in each case. Results presented here assume spherical symmetry.

Radial distribution functions (RDFs) for the amorphous samples are shown in the second figure. RDFs show subtle but real changes with thickness. The RDF for the 59.4 A period sample is characteristic of RDFs for typical glassy metals, with a single pronounced first peak and split second peaks. The 8.3 and 19.0 A period samples show rather different RDFs than the 59.4 A period sample, indicating significant structural change in the W-rich layers with thickness. The RDF for the 37.0 A period sample shows features intermediate between the thicker and thinner amorphous samples. As the period decreases we observe a decrease in the second nearest neighbor distance and the increase of a very small shoulder on the low-r side of the first peak. In the W-C intermetallic compounds, mixing of W and C is characterized by short W-C first neighbors at this distance, which would appear as a weak feature in the RDFs due to the small scattering factor of C. Also in the compounds, second neighbor W-W distances are shorter than the shortest second neighbor distances in both bcc W and the RDF from the 59.4 A period multilayer. Observation of the development of these features with decreasing period leads us to the interpretation that as the period decreases, the in-plane structure of the W-rich layers becomes increasingly dominated by short-range order more like that of the intermetallic compounds. Annealing of the 37.0 A period sample causes the RDF to develop features more characteristic of the thinner samples, suggesting increased intermixing with annealing.

In conclusion, the GIS technique reveals a variety of changing local atomic arrangements with thickness and annealing in the W-rich layers of W/C multilayers. Interface layers between the W- and C-rich layers are identified by their distinct scattering patterns and are seen to change with layer thickness. Generally increased intermixing of W and C with decreasing layer thickness are observed. Changes in interatomic arrangements with thickness and annealing are in qualitative agreement with the changing multilayer x-ray optical performance.

Acknowledgements.

This work was supported both by the U.S. Dept. of Energy under contract DE-AC03-76SF00098 and by an Air-Force Office of Scientific Research contract with the Regents of the University of California for performance at the Lawrence Berkeley Laboratory, which is operated under DoE contract DE-AC03-76SF00098.

References.

1. Barbee, T.W., Jr, and D.C. Keith, in proc. of Workshop on X-ray Instrumentation for Synchrotron Radiation, SSRL Report 78/04

SOLID STATE EFFECTS ON THE 4d PARTIAL CROSS SECTION AND THE ASYMMETRY PARAMETER OF METALLIC Ag

M. Ardehali, P. H. Mahowald, and I. Lindau
Stanford Electronic Laboratories
Stanford University, Stanford CA 94305

The purpose of the present work is, first, to demonstrate that there is in general a modification of the partial cross section (Σ) and the asymmetry parameter[1] (β) of polycrystalline Ag compared with the atomic Ag due to the solid-state effects; second, to show that there is a strong correlation between the behavior of Σ and the solid-state effects on the 4d initial state wave functions; third, to demonstrate that the behavior of β for polycrystalline Ag is strongly influenced by the solid-state effects on both the initial and the final state wave functions; and finally to point out that the energy dependence of β can be used as a powerful technique to establish the validity of Bloch type wave for the final state wave function at all photon energies.

We measured the Σ and the β of metallic Ag and of semi-isolate Ag atoms deposited on Si around Cooper[2] Minima. Although the behavior of the cross section appears to be competely determined by the characteristic of the initial state wave function, the asymmetry parameter seems to be very sensitive to the nature of both the initial and the final state wave functions. The 4d partial cross section of polycrystalline Ag exhibits significantly less energy dependence than the atomic Ag, due to the d-d interaction of the initial state wave function. In comparison, the decrease in the oscillation of the β of the 4d asymmetry parameter of metallic Ag is attributed to the solid-state effects on both the initial state and the final state wave functions.(Fig 1)

At lower photon energies near the threshold, the behavior of the asymmetry parameter is almost entirely determined by the energy dependence of the final state wave function[3]. The energy dependence of the β of Ag atoms deposited on Si substrate copmpares favorably with atomic calculations. Thus the final state wave function of the Ag 4d at Ag/Si interface is very much atomic like. In contrast, the asymmetry parameter of the metallic Ag is shifted up toward 2. From this we can infer that the final state wave function of the polycrystalline Ag is a near plane wave type even at very low photon energies.

We finally wish to point out that for a plane wave type final state wave function the asymmetry parameter is exactly equal to 2. Thus any deviation of β from 2 can be used as a powerful tool to identify the dissimilarity of the final state from a plane wave for all photon energies.

REFERENCES

1. C. N. Yang, Phys. Rev. **74**, 764 (1948)
2. J. W. Cooper, Phys. Rev. **128** (1962) 681
3. J. Cooper and R. N. Zare, in lectures in Theoretical Physics, Vol. IIC, edited by S. Geltman, K. Mahanthappa, and W. Brittin (Gordon and Breach, New York, 1968), p. 317

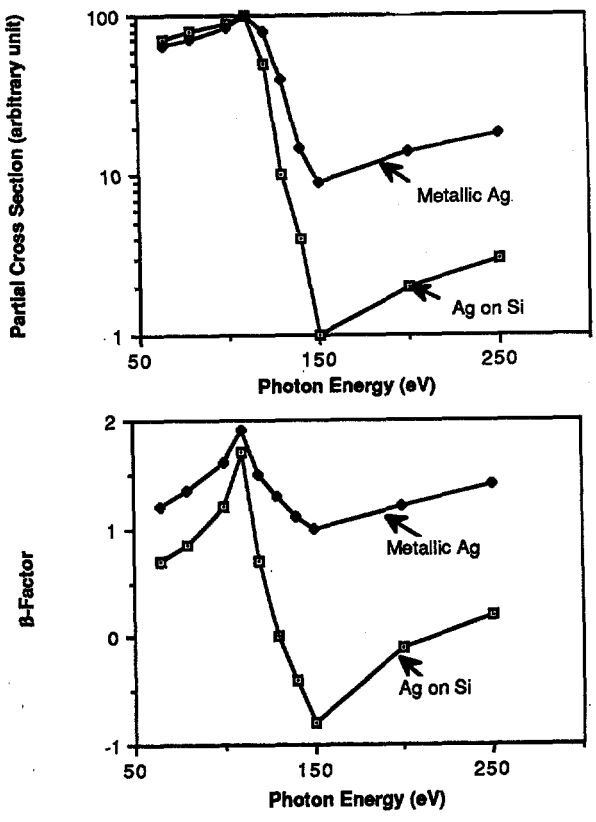

X-ray Scattering Studies of Strained-Layer InGaAs/GaAs and InGaAs/AlGaAs

S. Brennan
Stanford Synchrotron Radiation Laboratory, Stanford, CA 94305

A. Fischer-Colbrie, S. Laderman, and M.P. Scott
Hewlett-Packard Laboratories, Palo Alto, CA 94303

The InGaAs/AlGaAs and InGaAs/GaAs epitaxial systems are potentially important for use in high-speed electronic and opto-electronic devices. A practical difficulty with the AlGaAs/InGaAs system is that the lattice parameters differ by ~1%. This lattice mismatch can result in unacceptably high defect densities. Another difficulty with the AlGaAs/InGaAs system is that the thermodynamics (e.g. ideal growth temperatures) for the two materials are quite different. To make high-quality materials for these devices, the dependence of the critical thickness for defect generation on composition, thermodynamic and kinetic factors must be understood.

In this work, we have used BL VII-2 to make x-ray scattering studies of very thin layers (100-500 Å) of InGaAs on GaAs, AlGaAs/(100 Å)-InGaAs/GaAs MODFET structures, and AlGaAs/InGaAs multilayers on GaAs grown by MBE at different substrate temperatures. We have taken advantage of both the intensity and collimation provided by synchrotron radiation to study the very thin layers as well as obtain a long range of scattering data with high resolution in order to study subtle changes in the superlattice structures.

In the study of the single layers, the component perpendicular to the films was measured (l-scans of the (204) reflection). For 100, 200, 300 and 500 Å $In_{0.25}Ga_{0.75}As$ on GaAs, there is a displacement in |K| to lower values of 0.091 (+/-0.002), 0.082 (+/-0.005), 0.080 (+/-0.001), and 0.080 (+/-0.001) $Å^{-1}$ respectively, with respect to the GaAs value. This compares to a theoretical difference of 0.088 $Å^{-1}$ for a dislocation- free material and 0.043 $Å^{-1}$ for a relaxed material. These results show a gradual relaxation (from initially coherent) of the InGaAs lattice with respect to the GaAs substrate with increasing layer thickness.

The dependence of multilayer quality on substrate temperature was measured for temperatures between those ideal for InGaAs and AlGaAs growth. Fig. 1 shows the scattering near the (004) reflection (perpendicular to surface) from multilayers of 10 layer pairs of (100Å)-$Al_{0.3}Ga_{0.7}As$/(30 Å)-$In_{0.15}Ga_{0.85}As$ (total film thickness 1300 Å) grown on GaAs at 500, 550, and 600 °C. From these spectra, we see strong oscillations for all three samples, which are most strongly damped for the 500 °C sample. Overall, the 550 and 600 °C data are quite similar. One feature which is clearly different in all three samples is the strength of the peak near 3.73 $Å^{-1}$. In addition, there is a secondary intensity modulation between the primary peaks (especially the higher |K| peaks) in the 550 and 600 °C data, and not in the 500 °C sample. The secondary modulation frequency is consistent with the overall film thickness of 1300 Å. These data suggest that the 550 and 600 °C samples are of reasonably high quality while the 500 °C sample is less uniform and of overall poorer quality. TEM studies showed that the layers were planar and that the films were very similar. Modelling studies are planned to compare calculated and measured peak intensities to determine the structural origin of the small changes in scattering.

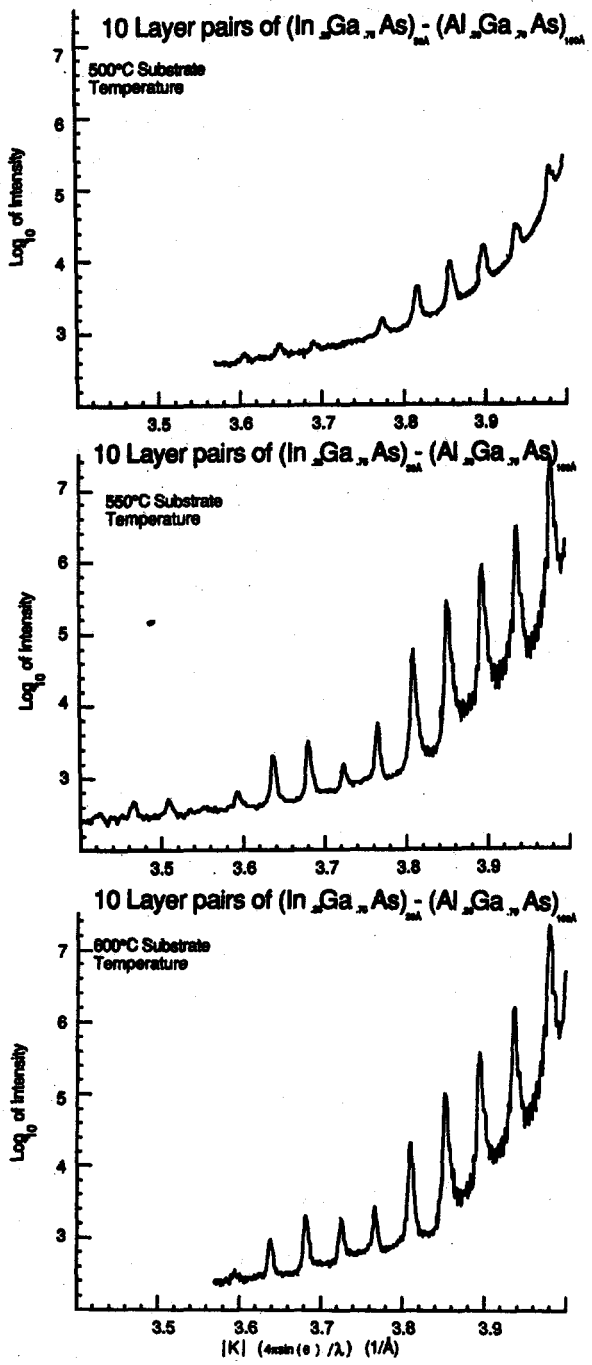

Fig. 1 X-ray scattering patterns near the GaAs (004) reflection for AlGaAs/InGaAs multilayers grown on GaAs at different substrate temperatures.

X-ray Optics Experiments on Beam Line V

Staff Priority Time 8005

R. Tatchyn
Stanford Synchrotron Radiation Laboratory
Stanford, CA 94305

P.L. Csonka, H. Kilic, H. Watanabe
Department of Physics, University of Oregon
Eugene, OR 97403

A. Toor
Lawrence Livermore National Laboratory
Livermore, CA 94550

A. Fuller
Department of Materials Science
Stanford University
Stanford, CA 94305

We have performed four experiments on the Beam Line V undulator line: a) focusing of undulator light with an ellipsoidal mirror[1] b) on axis streak camera measurements of undulator pulses c) lithographical studies of PMMA, and d) power measurements of undulator light [1,2]. In the first experiment, characterizations of the mirror's power distribution in the focal plane, were done both with resist (PMMA) photography and with a scanning x-y slit. A demagnified image of the electron beam source was obtained; the SPEAR source dimensions of about 1 mm (vertical) and 6 mm (horizontal) were demagnified to a spot size of about 15μ x 15μ (FWHM), resulting in a estimated peak power density of about 10^9 W/cm^2. The streak camera measurements utilized a specially constructed UHV chopper to provide both synchrotron pulse isolation and grating of the streak camera electronics. Gaussian pulses of about 570×10^{-12} sec FWHM were observed.

Resist (PMMA) exposures were taken with different gap settings of the 10 period and 24 period undulators. These exposures were taken through a thin gold transmission grating placed .001" away from the resist surface, an optimal spacer distance for recording Fresnal diffraction effects. The exposures were taken through Beryllium and aluminized mylar filters for harmonic isolation and for suppression of visable and UV light.

Power measurements of the undulator output light were taken with a specially constructed calorimeter (figure1). The UHV chopper referred to above was used to extend the dynamic range. The limiting aperture for the undulator light was a 1cm^2 circular cross section of a differential pumping section. In view of the fact that the undulator's output light profile was significantly larger than1 cm, especially in the horizontal plane, a geometrical correction factor had to be applied in estimating the total output power from the calorimeter readings. The calorimeter itself was calibrated using a precision resistor and a known voltage source. Comparing the corrected measurements with theoretically predicted output power level[3], we can assign a 70% probability that the measurements were within 25% of those predicted by theory. These estimates hold for both the 10 period and 24 period undulators, the only two that were used during our experimental run. The principal uncertainly underlying the quoted figures is in the accuracy with which the beam line's output light was centered on the differential pumping system's axis. For both undulators an approximately linear variation in output power with storage ring current was observed.

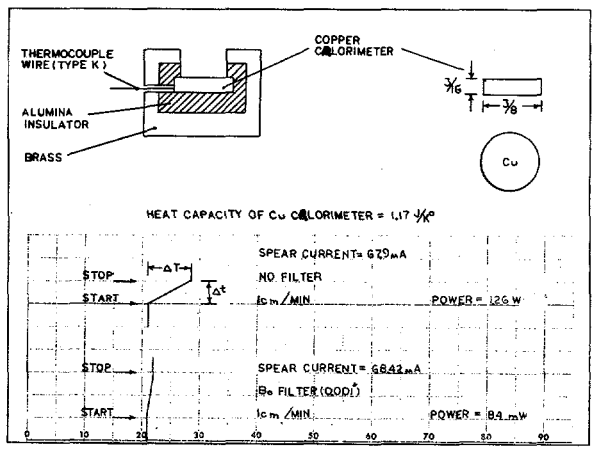

Reference

1) R. Tatchyn, P.L. Csonka, H. Kilic, H. Watanabe, A. Fuller, M. Beck, A. Toor, J. Underwood, R. Catura, (1987), to appear in SPIE Proceedings No. 733

2) R. Tatchyn, A. Toor, H. Kilic, J. Hares, J. Kilkenney, P.L. Csonka, H. Watanabe, A. Fuller, (1987), to appear in SPIE Proceedings No. 733.

3) R.Z. Bachrach, R.D. Bringans, B.B. Pate, R.G. Carr, (1986), SPIE Proc. No. 582.

Structural Investigations of Layered Synthetic Microstructures and Binary Amorphous Alloys

Staff Priority Time 8101

Marybeth Rice
Department of Electrical Engineering
Stanford University

Arthur Bienenstock
Stanford Synchrotron Radiation Laboratory

In May of 1986 we performed scattering experiments on a-WGe. This investigation is part of a program to study layered synthetic microstructures (LSMs) of WGe and a-WGe alloys. This program builds on the work of Kortright on a-MoGe[1] and of Wilson on MoGe LSMs[2].

This project was inspired by the unusual structures discovered in the MoGe LSMs. The outstanding feature of the MoGe LSMs is the strong influence of the interface on the structure of very thin (~10 A) layers. We suspect that the strength of this influence is a function of the affinity the component materials have for one another i.e., their tendency to form compounds. To check this hypothesis we will perform experiments substituting W for Mo. W is nearly identical to Mo in some aspects- size and outer shell electron configuration- but very different in its interaction with Ge. W unlike Mo does not form compounds with Ge. We shall investigate the types of structures that form when the constituent components are not interactive. An understanding of the structure of the LSMs will be supported by an understanding of the structure of the amorphous alloys. These are interesting in their own right. The weak W-Ge interaction should manifest itself in different atomic arrangements than those found in the other systems studied (a-MoGe, a-FeGe[3]).

Our preliminary experiment was a study of an amorphous thin film of 8 atomic % W-92 atomic % Ge. The sample was prepared by sputtering in the Vapor Phase Synthesis Laboratory at CMR. Scattering experiments were performed in transmission geometry on wiggler beam line IV-3. These yielded radial distribution functions (RDFs) and differential distribution functions (DDFs). The RDF has a first peak at 2.56 A with an area of 6.08. This area represents the average number of atoms about an average atom. In contrast, the RDF for a-MoGe at 8 atomic % Mo has a peak area of 5.2 at 2.54 A. Of greater interest is the W edge DDF which has a first peak area of 8.9 at 2.73 A. This is very close to the W-W distance (2.74 A) and may indicate a clustering of W atoms. This result is quite different from the Mo edge DDF of a-MoGe at low Mo concentrations. At 14 atomic % Mo, the Mo edge DDF has a first peak at 2.68 A with an area of 8.6. The a-WGe system is apparently quite different from the a-MoGe system. Further investigation should prove interesting especially with regard to the structural changes that accompany the metal-semiconductor transition in a-WGe and the types of structures present in the WGe LSMs at small layer spacings.

1. Kortright, J. B., Ph.D. Thesis, Stanford University and SSRL Report 84/05 (1984)
2. Wilson, L. C., Ph.D. Thesis in progress, Stanford University.
3. Lorentz, R. D., Ph.D. Thesis, Stanford University (1986).

W edge DDF

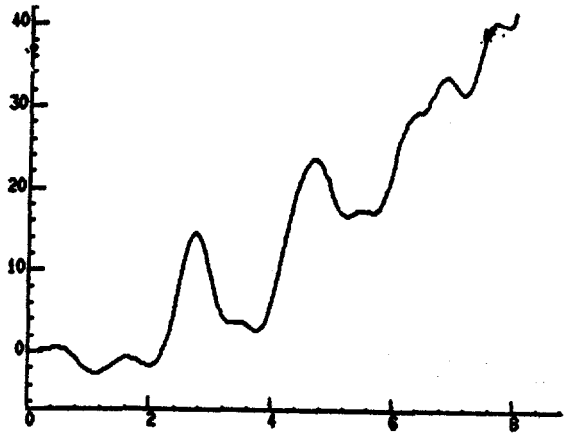

Mo edge DDF

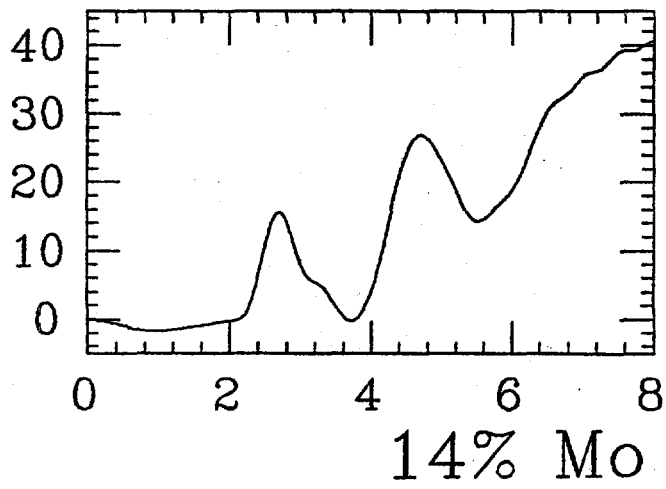

ANOMALOUS SCATTERING STUDIES OF AMORPHOUS Zr-Fe ALLOYS

H. U. Krebs
Institut für Metallphysik, University of Göttingen, 34 Göttingen, West Germany

A. Bienenstock
Stanford Synchrotron Radiation Laboratory, Stanford, CA 94305

INTRODUCTION

By using the differential anomalous X-ray scattering technique[1], we have investigated amorphous Zr-Fe alloys over a broad composition range. The aim of this research was to get structural information about the supposed phase separation in the middle of the concentration range and especially about the local environment of the Fe atoms, where significant changes at about 33 at%Fe were determined by earlier Mössbauer experiments [2].

EXPERIMENTAL PROCEDURE

Amorphous Zr-Fe alloys were prepared over a composition range of $20 \leq x \leq 90$ at%Fe by three different methods: by meltspinning near the two eutectica in the phase diagram, by magneton sputtering on Si substrates and by solid state reaction - annealed for 1 h at 350°C - of sputtered Zr/Fe-element multilayers. Anomalous scattering experiments were performed in reflection at energies of 10 and 160 eV below the Fe- and the Zr-absorption edges. The experimental setup and the data analysis was performed as described by Kortright [3]. The anomalous scattering factors were determined from absorption measurements using the Kramers-Kronig relation [1].

RESULTS AND DISCUSSION

Between the two measurements at 10 and 160 eV below the Fe absorption edge the anomalous term f' (Fe) changes from -3.38 to -6.9 electrons. In Fig.1 the reduced radial and differential distribution functions (RDF and DDF) taken near the Fe-edge are shown for Zr-Fe samples with different compositions. The average nearest neighbor distance of the atoms - determined from these RDFs and DDFs - significantly changes near 33 and 62 at%Fe. This indicates that an amorphous two-phase region exists between these two concentrations. Furthermore it is obvious from the peak positions of the DDFs that in the amorphous alloys below 33 at%Fe no Fe-Fe neighbors exist with direct contact and the occurence of Fe-rich phase with Fe atoms in contact leads to a reduction of the peak position above 33 at%Fe. This explains the second Fe-environment earlier seen in the Mössbauer experiments [2] and why this is the lowest Fe concentration, where ferromagnetism at low temperature exists in melt spin samples or annealed sputtered films. The comparison of co-sputtered and solid state reacted films with anomalous scattering, magnetization measurements and transmission electron microscopy showed that 62 at%Fe is the concentration of the second amorphous phase within the two phase region [4]. Therefore the anomalous scattering experiments were helpful to clarify the structural changes in these amorphous Zr-Fe alloys.

REFERENCES

1. P. H. Fuoss, P. Eisenberger, W. K. Warburton and A. Bienenstock, Phys. Rev. Lett. 46, 1537, 1981.

2. C. Michaelsen, H. A. Wagner and H. C. Freyhardt, J. Phys. F 16, 109, 1986.

3. J. Kortright, Ph. D. Thesis, Stanford University.

4. H. U. Krebs, D. J. Webb and A. F. Marshall, will be published in Phys. Rev. B, 1987.

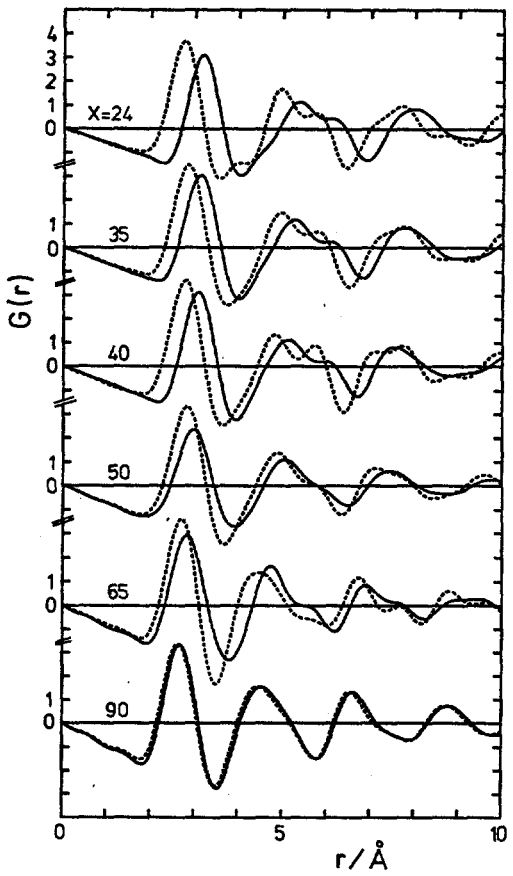

Fig. 1: RDFs and DDFs of amorphous $Zr_{100-x}Fe_x$ alloys of different compositions.

CHANGE OF LAYER STRUCTURE IN A W(15 Å)/C(15 Å) MULTILAYER FILMS BY VACUUM ANNEAILNG

Y. Takagi* and A.I. Bienenstock

Stanford Synchrotron Radiation Laboratory, Stanford, CA 95305
*Present address: R & D Laboratories-I, Nippon Steel Corporation, Kawasaki 233, JAPAN

Introduction

Some of the W/C multilayer films are known to be good x-ray reflectors[1]. Recently, there have been several studies of the change of their reflectivities with annealing[2,3]. Large d-spacing increases (8-15%) were observed in those having thin W-layers (d<20Å)[2,3].

The purpose of this experiment is to measure the change of the reflectivity with annealing, and to clarify the origin of the d-spacing increase. For this purpose, the well collimated, parallel synchrotron radiation beam is desirable for measuring the low-order multilayer peaks. This experiment is preliminary to in-situ annealing measurements which we are planning as the next stage and which are expected to yield definitive answers.

Experimental procedure

The samples were prepared by magnetron sputtering at Energy Conversion Devices, Inc. Sample annealing was performed at 730° C for 2.5 hrs. in a diffusion pump vacuum. BL IV-3 was used, and 5.5 keV was chosen as the incident x-ray energy. K-space and rocking curve scans of the peaks were performed.

Results and discussion

The results of the 1st order peaks are shown in the figure. Although the rocking curves look almost identical to each other, there are some dramatic differences between the k-space scans before and after annealing. The peak positions are shifted to lower k, without reduction of the peak intensity, after annealing. This result agrees with our previous investigation using Cu K-alpha radiation[2]. It was confirmed that, after further annealing, the intensity decreased significantly and the rocking curves became broader. In addition, some alpha-W crystalline peaks appeared in the higher k-region.

Schuller and co-workers concluded that this layer expansion originated from the crystallization of alpha-W and the agglomeration of the crystallites in the W-layer. However, in the present experiments the d-space expansion occurred long before the peak intensity started to drop and the rocking curve became broader, both of which are believed to be related to the crystallization and the agglomeration. Although final judgement should be delayed until the results of the in situ measurement have been obtained, we believe the agglomeration of the W-crystallites is the result of layer expansion rather than its cause.

This work is supported by Energy Conversion Devices, Inc.

References
1. See, for example, papers in Proc. SPIE Vol. 563.
2. Y. Takagi et al., MRS Symp. Proc. Vol. 55, p. 441.
3. E. Ziegler et al., Appl. Phys. Lett., 48 (1986) 1354.

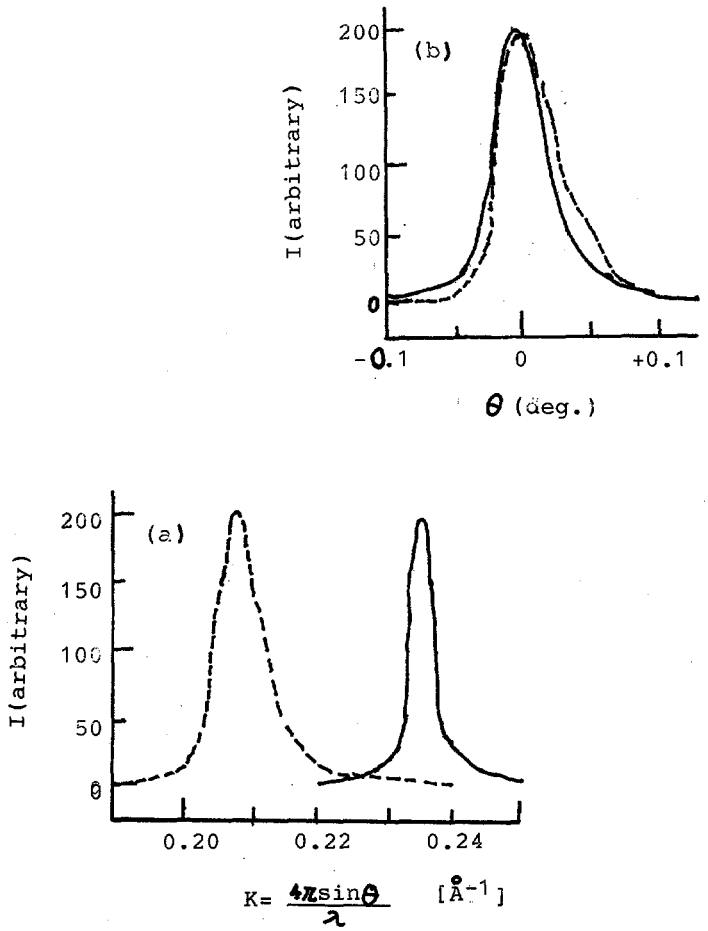

Figure X-ray diffraction patterns of 1st order reflections from the layer structure in a W(15 Å)/C(15 Å) multilayer films before and after annealing. The curves in (a) show K-space scans; (b), rocking curves. The solid lines are those from the as-prepared samples; the dashed, those from the samples annealed for 2.5 hrs. at 730 °C in a vacuum better than 1×10^{-4} torr. The incident energy, 5.5 keV was used for the experiment.

Compton Scattering in Germanium and Silicon

C. A. Kilbourne
Stanford University, Department of Materials Science and Engineering

S. M. Brennan, A. I. Bienenstock
Stanford Synchrotron Radiation Laboratory

This research has two goals, which are:

1) to obtain high resolution Compton profiles using the high flux available at PEP.

2) to study how the total Compton intensity, the integrated profile, changes as the incident photon energy passes through a characteristic energy of the material studied.

The work to be performed on PEP is in its initial stages, with emphasis on evaluation of various options for the spectrometer system. With PEP unavailable, the expermental focus was the second part of the program, using SPEAR.

The integrated Compton scattering work is motivated by the need to know accurately the intensity of the Compton scattering as function of angle in anomalous scattering experiments on amorphous materials. This scattering must be subtracted from the total scattering, leaving the coherent scattering information used in structural determination. In these experiments, tabulated values for the incoherent intensity have been used, which has been assumed to be invariant with incident photon energy. This has been justified by the claim that the Compton scattering arrises only from the A^2 term in the Hamiltonian, which is true for unbound electrons and for cases in which the the electrons can be treated as unbound, as in the impulse approximation. A requirement for the validity of the impulse approximation is that the incident photon energy be much greater than the electron binding energy. This is clearly not applicable near a characteristic energy of the sample. Since anomalous scattering experiments involve scans very near an absorption edge, we sought to monitor any change in the total Compton scattering as the incident photon energy drops below such a characteristic energy.

We measured the intensity of the Compton scattering in a germanium single crystal above and below the germanium k-edge (11103 eV). We worked at a scattering angle of 160° with the scattering vector normal to the (111) face. Since this is not near a Bragg reflection, measured elastic scattering resulted from thermal diffuse scattering only. Data were taken with a solid state detector and multichannel analyzer combination. Initial data taken with an intrinsic germanium detector did not resolve the Compton and elastic peaks sufficiently so a silicon-lithium detector with 170 eV resolution was employed. Data were collected at energies ranging from 10500 eV to 13900 eV. We are still in the process of analysis, but a brief qualitative description of results at three energies follows.

Figure 1 presents spectra resulting from incident energies of 10500, 11090, and 13000 eV. In order to show all the relevant peaks, a logarithmic scale has been chosen. At 10500, we see three defined peaks, the k-α Raman, the Compton, and the elastic. The k-β Raman lies between the latter two. The position of the Raman peaks should be as far below the flourescence energies (α_1= 9886 eV, α_2 = 9855 eV, β = 10982 eV) as the incident energy is below the k-edge. At 10500, the α Raman seems about 100 eV too low, an effect noted by Eisenberger, Platzman, and Winick and explained as the result of the convolution of the assymetrical Raman peak with the experimental resolution function[1]. At 11090, the strength of the Raman peaks is notable, with the α now dominating the spectrum and the β obscuring the separation between the Compton and the elastic. Far above the edge, at 13000, the α and β flourescence lines dominate the spectrum, but are clearly distinct from both the Compton and the elastic. We will use a curve fitting routine to separate the Compton and elastic at high energy, and will determine an α/β ratio in order to remove the β contribution from those peaks at lower energy.

Attempts to obtain Compton profiles on germanium and silicon using an improvised curved crystal scanning spectrometer were not fruitful.

Reference

[1] P. Eisenberger, P.M. Platzman, H. Winick, Phys. Rev. B 13 2377 (1976)

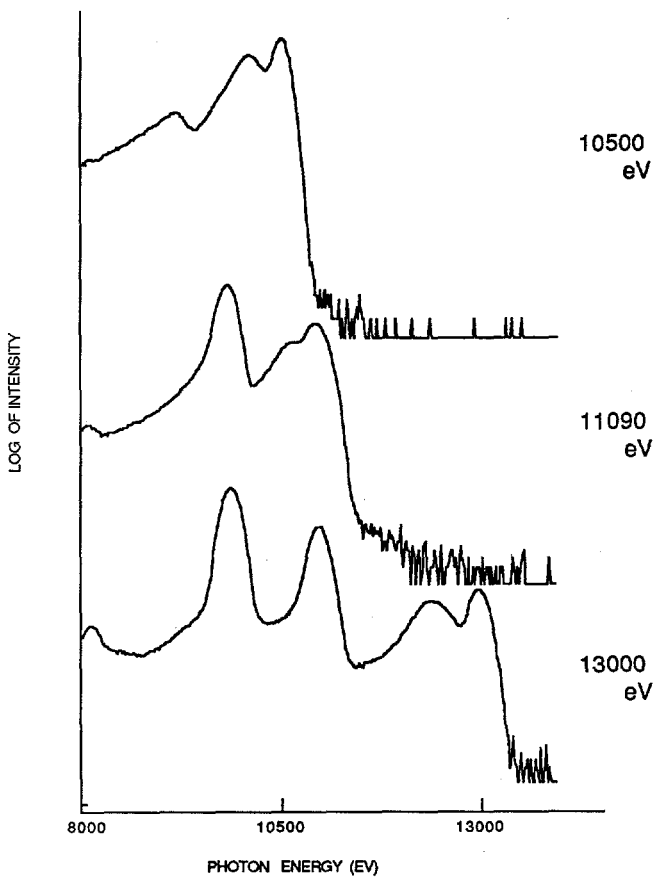

Figure 1. Elastic and inelastic scattering from germainium for incident energies above and below the germanium k-edge

Grazing Incidence X-ray Studies using the new PEP Beamline 5-B

Paul Fuoss

AT&T Bell Laboratories, Holmdel, NJ. 07733.

Sean Brennan

Stanford Synchrotron Radiation Laboratory, Stanford, Ca. 94305.

Alice Fischer-Colbrie

Hewlett-Packard Laboratories, Palo Alto, Ca. 94304.

Karl Ludwig

Dept. Materials Science, Stanford Univ., Stanford, Ca. 94305.

The new general purpose beamline 5-B on the PEP storage ring has been used to study the structure of thin amorphous films using Grazing Incidence X-ray Scattering (GIXS). Due to the high brilliance of the PEP source data were collected in a previously impractical scattering geometry. These results demonstrate the utility of high brightness sources for the study of weakly scattering samples such as amorphous thin films.

The source of radiation from PEP is an undulator which is described in more detail elsewhere in this volume. Its salient feature for GIXS (other than high flux) is extremely low horizontal and vertical divergence (approximately 35 μrad. in both directions). In prior experiments involving GIXS from thin amorphous films at SPEAR a horizontal scattering geometry has been used. In the horizontal scattering geometry (2θ rotating about a nearly vertical axis) the large sample size is coupled to the large spot size and higher horizontal divergence of the incident beam. This results in an increase in signal of roughly 50 over scattering in the vertical plane on a SPEAR beamline. Due to the highly polarized nature of the synchrotron light in the horizontal direction however, the scattering at 2θ values near 90° is quite low. This causes great difficulty in normalization and analysis of the resultant data. Because the horizontal and vertical divergence for PEP are the same, no increase in scattered intensity is gained by scattering in the horizontal plane. The added scattered intensity at high k when a vertical scattering geometry is used is a significant advantage.

Figure 1 compares scattering data from the same sample obtained in the two different scattering geometries on two different beamlines, PEP 5-B and SPEAR IV-2. The SPEAR data were taken at 11000 eV in the horizontal geometry. The PEP data was obtained using the vertical scattering geometry at an energy of 12550 eV. Note that while the data are similar for the first two peaks, above k=3 $Å^{-1}$ the data from SPEAR is much lower intensity, decreasing to zero intensity at k=8 $Å^{-1}$ because of the polarized nature of the source. No such restriction exists for scattering in the vertical plane, so the PEP data shows much stronger scattered intensity around k=8 $Å^{-1}$.

Due to the limited extent of the experimental running on PEP we were unable to collect the complete set of data necessary for a full analysis, but we can expect from these preliminary results that PEP will open up a whole range of experiments in surface structural physics.

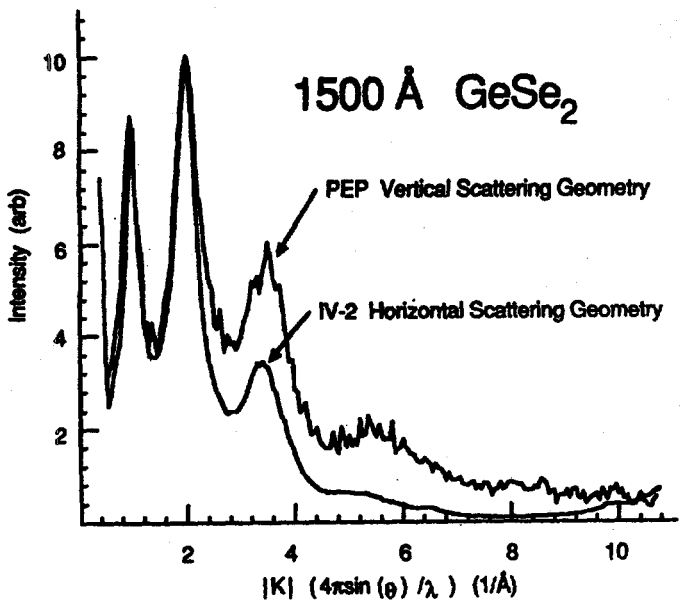

SYNCHROTRON DIFFRACTION STUDY OF Co-DOPED IRON OXIDE FILMS

T. C. Huang and M. F. Toney
IBM Almaden Research Center, San Jose, CA. 95120

S. Brennan and Z. Rek
Stanford Synchrotron Radiation Laboratory, Stanford, CA. 94305

INTRODUCTION

Thin γ-Fe_2O_3 films are candidates for high density magnetic recording media. They can be prepared in a number of ways. One of the most effective methods involves the direct formation of an intermediate cubic iron oxide phase, presumable Fe_3O_4, by reactive sputtering of an Fe target in a carefully controlled Ar-O_2 atmosphere, and a subsequent high temperature oxidation in air to complete the conversion to γ-Fe_2O_3.[1] Recently, a polarized neutron reflection depth profile analysis of sputtered Co-doped iron oxide thin films revealed previously unreported magnetic behavior of a post-oxidized film.[2] A thin magnetic dead-layer was found at the top 150Å surface of the post-oxidized "γ-Fe_2O_3" film, whereas an as-deposited "Fe_3O_4" sample was magnetically constant throughout its 2600Å depth. One of the key steps for the understanding of this effect is the identification of the surface and bulk structures of the films.

With its remarkable properties such as high intensity, easy X-ray wavelength selection, and highly collimated beam, synchrotron radiation is most suitable for the depth profiling diffraction analysis of thin films. In this study, synchrotron radiation was used for surface and bulk structure analysis of both the as-deposited "Fe_3O_4" and the post-oxidized "γ-Fe_2O_3" films. By correlating the synchrotron results with the magnetic data, a better understanding of the film properties and the iron oxide oxidation process has been obtained.

EXPERIMENTAL

The experiments were done at the Wiggler station VII-2.[3] 1.38Å radiation was used in the initial stage of the experiment. Subsequently, a longer wavelength of 1.83Å was chosen to eliminate Fe X-ray fluorescence from the films and improve the peak to background ratios.

Unlike the grazing incidence scattering technique which is widely used for studying long-range order of single-crystal surfaces and thin films,[4] a combination of Seemann-Bohlin scanning technique[5] and grazing incidence diffraction arrangement is more suitable for structural depth profiling of polycrystalline thin films. In the Seemann-Bohlin geometry, the horizontal specimen is fixed at a small incident angle θ with respect to the incident beam. The detector is scanned along the 2θ circle in a vertical plane of a Huber 5020 goniometer to record the diffracted X-rays from crystal planes which are inclined to the surface of the specimen (see Fig. 1). At grazing incident angles less than the critical angle for total reflection (~ 0.3°), the penetration depth of X-rays is limited to the top 100Å or less surface. It may be increased gradually by increasing the incident angle. The diffracted beam, which originates from this region of variable depth, can be used for structure determination of polycrystalline thin films.

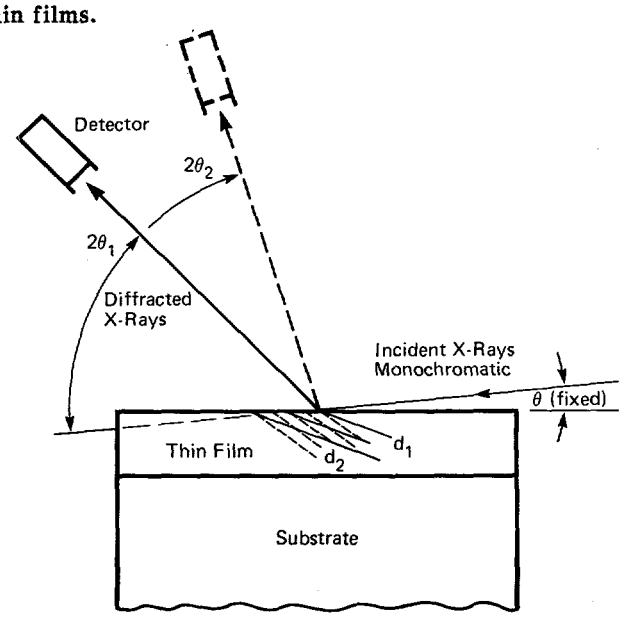

Fig. 1. Geometry of Seemann-Bohlin diffraction arrangement in the vertical plan of a Huber 5020 goniometer.

RESULTS

Post-Oxidized "γ-Fe_2O_3" Film

Synchrotron polycrystalline diffraction patterns with various penetration depths were obtained with incident angles θ ranging from 0.12° to 8.0°. Diffraction patterns recorded at θ=0.12° and 8.0° are plotted in Fig. 2. The patterns show two different sets of polycrystalline thin film peaks indicating a difference in the structures at the surface and the bulk of the film. A search of the standard powder diffraction file[6] identified a hexagonal α-Fe_2O_3 structure at the surface and a tetragonal γ-Fe_2O_3 structure in the bulk.

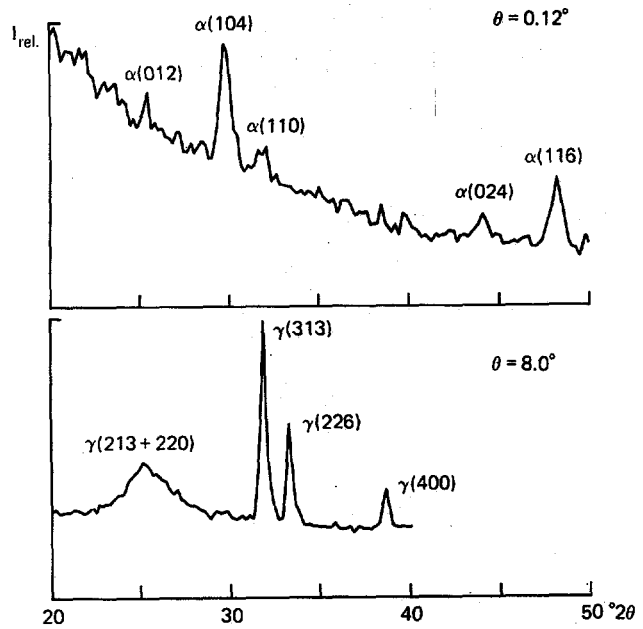

Fig. 2. Synchrotron polycrystalline diffraction patterns of the post-oxidized "γ-Fe_2O_3" film (λ=1.38Å).

Diffraction patterns near the critical angle of total reflection θ_c have also been obtained. As shown in Fig. 3, patterns recorded at θ=0.312°, 0.319° and 0.325° show a gradually change in intensity from α-Fe_2O_3 to γ-Fe_2O_3. The decrease in α to γ ratio indicates a transition from anti-ferromagnetic α-Fe_2O_3 to ferromagnetic γ-Fe_2O_3 as the X-rays penetrated deeper into the film.

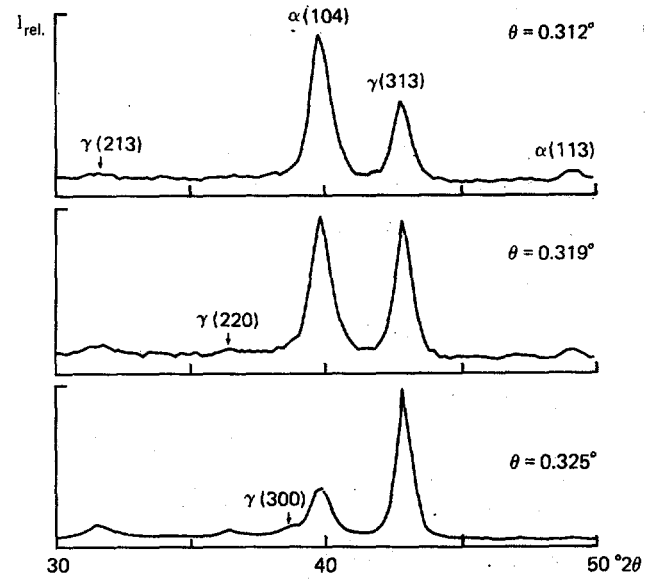

Fig. 3. Synchrotron polycrystalline diffraction patterns of the post-oxidized "γ-Fe_2O_3" obtained with 1.83Å radiation and incident angles near θ_c.

As-Deposited "Fe_3O_4" Film

Diffraction patterns from surface and bulk of the as-deposited "Fe_3O_4" film have also been recorded. Patterns obtained at θ=0.25°, 0.5° and 5.0° are plotted in Fig. 4. The similarity indicates the structure remains constant throughout the depth of the as-deposited film. The presence of the "superlattice" (300) reflection shows that the "Fe_3O_4" film is not a face-centered cubic Fe_3O_4 but a simple cubic iron oxide and/or a tetragonal γ-Fe_2O_3.

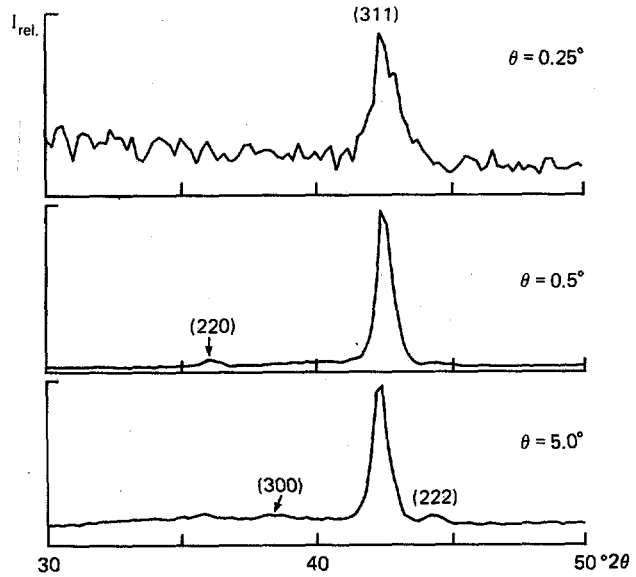

Fig. 4. Synchrotron polycrystalline diffraction patterns of the as-deposited "Fe_3O_4" film (λ=1.83Å).

CONCLUSION

A new synchrotron diffraction method combining the Seeman-Bohlin and the grazing incidence techniques has been used successfully to determine the surface and bulk structures of polycrystalline films. Analysis showed that the post-oxidized "γ-Fe_2O_3" film has α-Fe_2O_3 at the surface and γ-Fe_2O_3 in the bulk. The formation of the anti-ferromagnetic α-Fe_2O_3 caused the magnetically dead layer observed by neutron measurement. The as-deposited "Fe_3O_4" film was found to be actually a simple cubic iron oxide and/or a tetragonal γ-Fe_2O_3, and the film structure remains unchanged throughout the depth of the film.

REFERENCES

1 Y. Ishii, A. Terada, I. Ishii, S. Ohta, S. Hattori, and K. Makino, IEEE Trans. Magn., MAG-16 (1980) 1114.
2 S. S. Parkins, R. Sigsbee, R. Felici, and G. P. Felcher, Appl. Phys. Lett., 48 (1986) 604.
3 D. E. Moncton and G. S. Brown, Nucl. Instr. and Meth., 208 (1983) 579.
4 S. Brennan, Surface Sci., 152/153 (1985) 1.
5 R. Felder and B. S. Berry, J. Appl. Cryst. 3 (1970) 372.
6 Powder diffraction file of the Joint Committee on Powder Diffraction Standards (International Centre for Diffraction Data, Swarthmore, PA, 1986).

WHITE BEAM SECTION TOPOGRAPHY OF DEFORMATION FIELDS SURROUNDING LASER-DRILLED HOLES IN SILICON

Y. H. Chung[1], Z. U. Rek[2], B. Coulman[3], and S. R. Stock[1]

[1]School of Materials Engineering, Georgia Institute of Technology
Atlanta, Georgia 30332-0245

[2]Stanford Synchrotron Radiation Laboratory

[3]Signetics Corporation, 811 Arques Avenue, P. O. Box 3409
Sunnyvale, California 94088

Introduction

X-ray diffraction topography is a powerful technique for characterizing defects in crystals. Synchrotron radiation eliminates the inordinately long exposures required for laboratory topography, and its continuous spectrum allows images from many different diffraction planes to be recorded simultaneously.

Projection topography is useful for surveying the defect content of crystals, but depth information is lost and defects can sometimes be obscured. Continuously varying deformation fields lead to striking contrast in projection topography, but it is very difficult and computation-intensive to convert the diffracted intensities to strains or strain gradients[1].

Section topography, however, preserves depth information, at the cost of sampling smaller volumes, and provides better defect visibility. The presence of Pendellosung fringes (PF) in section topographs is a sensitive indication perfection, and a number of other groups [2,3] have also observed PF in synchrotron white beam section topographs. Wave propagation is profoundly affected by strain gradients: extra PF can be introduced or the PF pattern can be completely disrupted. Providing that the strain gradient β is constant within the Borrmann triangle, closed-form relations exist between $|\beta|$ (e.g. $\partial^2 u_i/\partial x^2_j$) and the number of extra PF [4,5]. Section topographs of crystals deformed elastically by a uniform temperature gradient [4] and of diametrically compressed crystals [6] have shown the usefulness of the Eikonal formulation for quantifying strain gradients.

We report preliminary results of quantitative strain mapping of the elastic deformation surrounding laser-drilled holes in silicon crystals. Our goals are to identify the drilling conditions which lead to minimum strain and to extend the range of applicability and spatial resolution of section topographic strain mapping.

Experimental Methods

The white radiation topography apparatus on Beamline II-4 was used to produce the topographs. It consisted of an adjustable, tantalum vertical slit (from a Lang camera) and a Huber two-circle goniometer with goniometer head. Slit widths were between 5 and 25 μm. Both the slit assembly and the sample could be translated along the two axes perpendicular to the incident beam with precision of 2.5 μm; this was important for the section step scanning and for superimposing section and projection topographs so that the exact position of the section on the specimen could be determined.

Kodak SR5 single-sided emulsions and 10 μm thick Ilford L4 nuclear emulsions were used, and exposure times were on the order of five minutes. The film was mounted perpendicular to the incident beam, and a thin aluminum cover and a lead beam stop were used to minimize background. Generally, sets of seven or eight section patterns were recorded on a single piece of film by translating the specimen and film in tandem. The spacing between section topographs was 1.0 mm, so as to preventing overlap of adjacent images.

Results

Figure 1 shows the transmission Laue pattern obtained with section step scanning (1 mm steps) of a laser-drilled, 0.5 mm thick (001) Si crystal. The pattern has been significantly demagnified, and the shadow of the beam stop is clearly visible. The optimum reflections for observing the structure within the section topographs are those with diffraction vectors perpendicular to the slit: otherwise the width of the Borrmann triangle is too narrow.

Figure 2 is a white beam projection topograph showing the deformation field around a laser-drilled hole (two surface scratches labeled A are present). The dark vertical stripe is the overexposed image of a section topograph. The diffraction vector was $\underline{h} = [33\bar{1}]$ and the fundamental wavelength diffracted was $\lambda = 0.605$Å. The lobes of enhanced diffracted intensity are not exactly symmetric which probably reflects inhomogeneities in the incident laser beam or in the exact pattern of solidification within the hole.

Figure 3 shows a set of section topographs obtained with step scanning. These topographs were recorded with 1 mm step sizes, and they bracket the hole. As one would expect from the beam profile in the vertical direction, there is considerably less intensity at the upper and lower edges of these diffraction spots. The PF pattern is quite clear away from the hole, extra periods are introduced as one approaches the hole and adjacent to the hole, in the very high gradient region, the PF pattern has been completely disrupted. Figure 4 shows an enlargement of a section topograph with additional fringes introduced by the deformation gradient.

Continuing Research

Conversion of the number of extra P.F. to values of $\partial u_i/\partial x_j$ are currently underway as is mapping of $\partial u_i/\partial x_j$ as a function of position. We are also investigating methods of increasing the rate at which we can produce sets of step scanned section topographs.

Acknowledgements

We acknowledge support from the Georgia Institute of Technology (SRS and YHC) and from Signetics Corporation (BC). This work was done at SSRL which is supported by the Department of Energy, Office of Basic Energy Sciences; and the National Institutes of Health, Biotechnology Resource Program, Division of Research Resources.

References

1. Y. Epelboin and A. Soyer, in: Application of X-ray Topographic Methods to Materials Science, Weissmann, Balibar and Petroff, eds. (Plenum, New York, 1984) p. 161.

2. K. Naukkarinen and M. Blomberg, J. Mat. Sci. Letters 2 (1983) 111.

3. Y. Sugita, S. Iida, H. Sugiyama, K. Matsui, M. Miyazaki and H. Kawata, in: Photon Factory Activity Report (1984/5) p. VI-184.

4. M. Hart, Z. Phys. 189 (1966) 269.

5. N. Kato and Y. Ando, J. Phys. Soc. Japan 21 (1966) 964.

6. Y. Ando and N. Kato, J. Appl. Cryst. 3 (1970) 74.

7. A. L. Andersen and L. Gerward, Phys. Stat. Sol. (A) 23 (1974) 537.

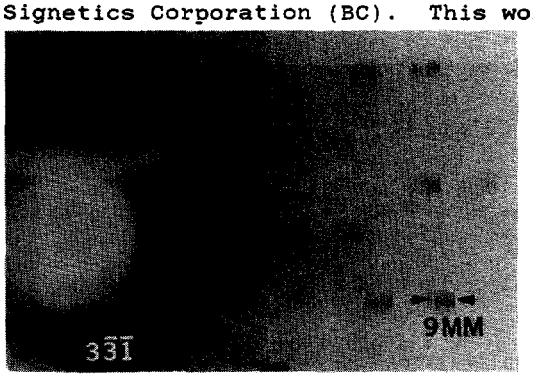

Figure 1. White Beam Section Topographs of a Laser-Drilled (001) Silicon Crystal. Nine section topographs are recorded using step scanning and steps of 1.0 mm. The beam stop is visible at the left.

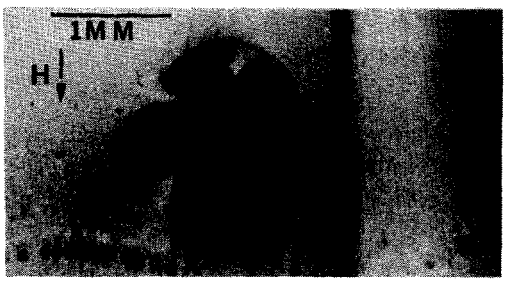

Figure 2. White Beam Projection Topograph. The diffraction vector is $\underline{h}$ = [3$\bar{3}$1] and the fundamental wavelength is 0.605 A. The laser-drilled hole is centered between the lobes of enhanced diffracted intensity. A superimposed section topograph is seen to the right of the hole and surface damage is labeled by A.

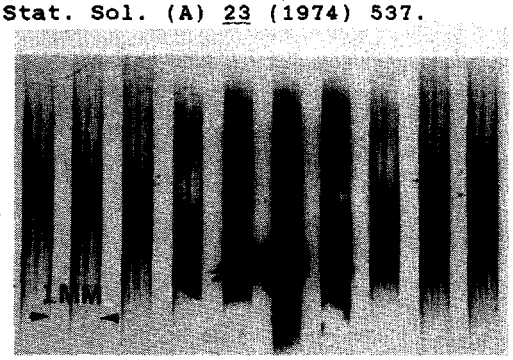

Figure 3. Set of Section Topographs Obtained with Step Scanning. The strain field associated with this typical laser-drilled hole is evident from the extra PF introduced. The diffraction vector is $\underline{h}$ = [3$\bar{3}$1] and the wavelength is 0.65 A.

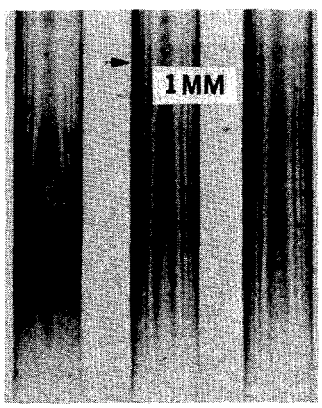

Figure 4. Enlargement of Some of the Section Topographs shown in Fig. 3.

APPLICATION OF WHITE RADIATION SECTION TOPOGRAPHY TO STUDY OXYGEN PRECIPITATION AND STRAINS IN CZ SILICON

Z. U. Rek[1], S. Hahn[2], B. Coulman[3], S. R. Stock[4]

1. Stanford Synchrotron Radiation Laboratory, Stanford,Ca94305
2. Siltec Corp.,Mt. View, Ca 94043
3. Signetics Corp., 811 Arques Ave, Sunnyvale, Ca 94086
4. School of materials Engineering, Georgia Inst. of Technology Atlanta, Georgia 30332-0245

White radiation section topography is an extremely useful tool to study structural quality of Si single crystals. The unique features of this technique are the following: 1. high sensitivity to strain caused by the microdefects or thin layer presence in the crystal; and 2. inherent depth resolution;

One of the problems we have studied concerns oxygen precipitation in Czochralski grown Si. An important unresolved issue related to thermal donors (TD's) is their role in oxygen precipitation, especially during nucleation stages near 700°C. While various researchers have found that TD generation by annealing at 450° significantly enhances precipitation rates, the path or paths from TD formation to oxygen precipitation are unclear and have not been separated from effects of other impurities.
In this study [1] we investigated the effect of a 450°C pre-anneal upon oxygen precipitation during subsequent low(700°C) - medium (950°C) temperature two-step anneals of silicon with heavy B- and Sb-doping. We observed very different precipitation behaviors in the two cases. Sb-doped material exhibits a continous increase in oxygen precipitation with time. We observe in the case of B-doped material that the suppression of oxygen precipitation is associated with an increase in material perfection during thermal anneal at 450°C for up to 52h. (Fig.1). Pendellosung fringes' appearance is a direct indication of improved quality of the material. The explanation of this effect can be found in [1].

Section topography was helpful in understanding dislocations in crystals. The LOCOS technique [2] for growing field oxide isolation is widely used in Si device construction. Strain produced at the mask edges can be large enough to exceed critical levels for dislocation motion into substrate, with the potential for degraded device performance. Very large (mm scale) oxide structures were grown for topographic study. Section topographs were stepped along a Si(110) oriented edge (Fig.2). For a 1μm thick oxide grown at 1150°C, long parallel dislocations propagate under the oxide and assume a configuration determined by the balance of forces acting upon them.

We have recently started work on strain associated with Si/SiO_2 interfaces. The first collected data for MOS capacitor test devices structure, where the 100Å oxide layer was coverd by 4000Å of polysilicon, reveal complex fringe patterns (Fig.3). One set of fringes is characteristic of a perfect crystal, while the other sets of fringes may be due to the edges of the SiO_2-polysilicon layers. The work on this problem is in progress.

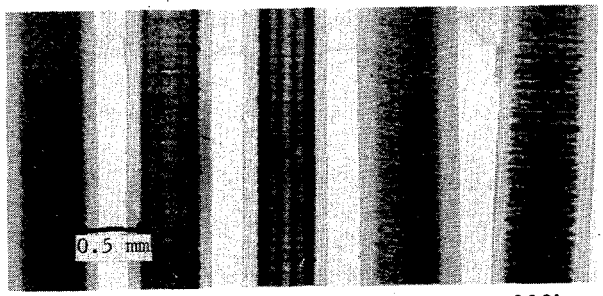

Fig.1. Section topographs for heavily B-doped wafers after annealing at 450°C for various periods of time.

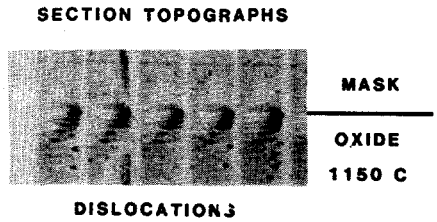

Fig.2. Section topographs of dislocations originated during field oxide growing.

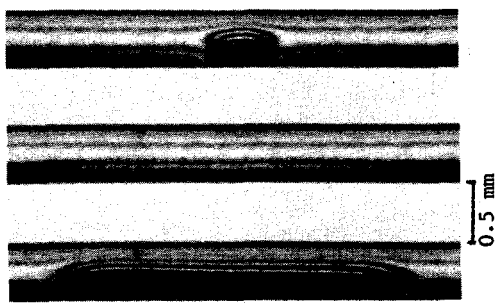

Fig.3. Three section topographs taken during crystal scanning with 0.5mm step, horizontal slit.

References:
1. S.Hahn,M.Arst,Z.U.Rek,V.Stojanoff, W.T.Tiller, Appl. Phys. Letters, 50, no 3,(1987), 401
2. J.A.Appels,E.Kooi,M.M.Paffen, J.J.Schatorje,W.H.C.G.Verkuylen, Phillips Res. Rep. 25,(1970),118

RADIATION DAMAGE IN BORON NITRIDE X-RAY LITHOGRAPHY MASKS

Paul King, Lawrence Pan, Piero Pianetta
Stanford Synchrotron Radiation Laboratory
Stanford, CA

Alex Shimkunas, Philip Mauger
Micronix Corporation
Los Gatos, CA

Daniel Seligson
Intel Corporation
Santa Clara, CA

Membrane materials are a critical element in the technology of x-ray lithography as they form the substrate for the x-ray mask. Although chemical vapor deposited (CVD) hydrogenated boron nitride has performed satisfactorily with conventional x-ray sources, we have observed significant degradation in both the optical and mechanical properties after exposure to high doses in the synchrotron environment.

Boron nitride membranes were exposed under vacuum to synchrotron radiation (0.8 to 3 keV) on the lithography beam line (III-4). Membranes were typically 4um thick and had a built-in tensile stress of 5E8 dyne/cm2. In-situ measurements of the optical transmissivity of the membranes were performed during the x-ray exposure with a HeNe laser. As shown in Figure 1 the transmission at 633nm fell to 50% of its original value after the membranes absorbed doses of 200kJ/cm3 and to 35% after 400kJ/cm3. A dose of 200kJ/cm3 would be absorbed after fewer than 5000 exposures of a resist with a 100mJ/cm2 sensitivity. No time delay was observed between the beginning of the x-ray exposure and the decrease in the optical transmission. Damage depended simply on the dose absorbed and appeared to be independent of the incident spectrum and incident power.

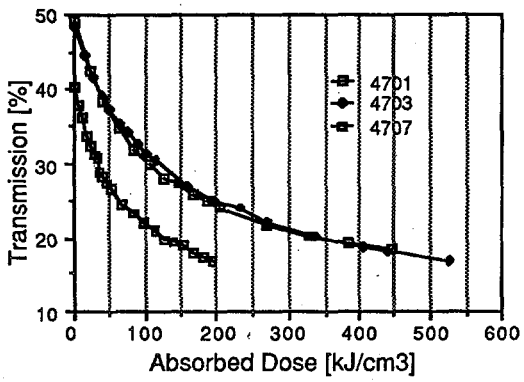

Figure 1. Transmission vs dose in three samples of 4.7um CVD BN membranes

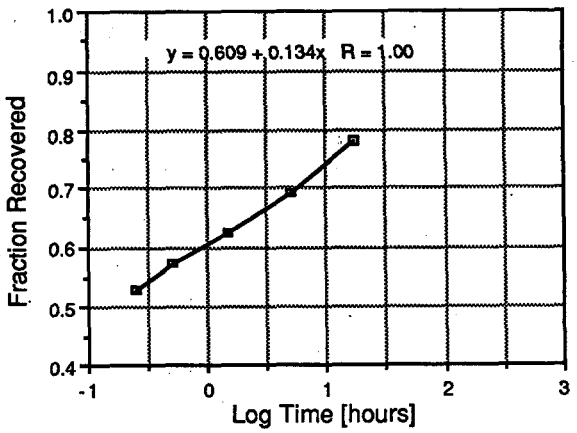

Figure 2. Transmission annealing behavior 4.7 um CVD BN membrane at 200C

The dimensional stability of the membranes was characterized by scanning a stylus profilometer over the damaged area at different absorbed doses. The membranes strained linearly with increasing x-ray dose and showed no evidence of saturation up to doses of 450 kJ/cm3. The measured strain can be associated with a decrease in film tension on the order of 3E8 dyne/cm2 and is large enough to cause severe pattern distortions in an x-ray mask.

Both forms of damage responded well to annealing. Some self annealing was observed (on the order of 20% recovery after four weeks) and essentially full recovery was obtained at elevated temperatures. Figure 2 shows the recovery in transmission at 633nm of samples annealed in air at 200C. At 300C there was complete recovery in the transmissivity and nearly complete (98%) recovery of the original pre-exposure tension.

Other candidate materials (silicon and silicon nitride) were also studied and showed no degredation after absorbed doses of over 2000kJ/cm3.

SULFUR K EDGE X-RAY ABSORPTION STUDIES OF SULFATE-VANADIUM INTERACTIONS WITHIN LIVING PLASMA CELLS FROM ASCIDIA CERATODES

Patrick Frank[1,4], Britt Hedman[1,2], Robert M.K. Carlson[3], Trevor A.Tyson[1,4], A. Lawrence Roe[1], and Keith O. Hodgson[1,2]

1 Department of Chemistry, Stanford University, Stanford CA,94305
2 Stanford Synchrotron Radiation Laboratory, SLAC, Bin 69, P.O. Box 4349, Stanford CA, 94305
3 Chevron Oil Field Research Co., P.O. Box 446, La Habra CA 90631 USA
4 Department of Applied Physics, Stanford University, Stanford CA 94305 USA

Introduction. The highly unusual aspects of the biological chemistry characteristic of the blood cells from ascidians (tunicates, or more commonly 'sea squirts') was first described more than 75 years ago [1]. These include extraordinary concentrations of vanadium, sulfur and acidity now known to be contained primarily within morula cells termed 'vanadocytes'[2]. These green cells, here obtained from Ascidia ceratodes, commonly make up 60-80% of the cells present within the plasma and do not play any role in transport of oxygen [3,4]. The biological function of vanadocytes remains obscure. As an approach to understanding however, we have been carrying out x-ray absorption near edge spectroscopic (XANES) studies on sulfur within living, intact vanadocytes using the 54-pole wiggler at SSRL in undulator mode[5,6]. Comparison of this data with biologically appropriate model solutions has permitted evaluation, here reported for the first time, of in situ interactions between vanadium and sulfate within vanadocytes.

Experimental. The experiments were performed on beam line VI-2 during dedicated conditions (3 GeV, 35-80 mA, focussed, Si(111) double-crystal, monochromator). Details of the experimental conditions have been described previously[5]. Solutions of vanadium(III) sulfate and methane sulfonate were prepared by reduction of the appropriate salt under hydrogen using a Pd/C catalyst[2].

Results. Sulfur edge spectra have shown themselves to be sensitive to oxidation state, symmetry and overall structure (within the same formal oxidation state) of the absorbing atom[5,6,7]. In Figure 1 XANES spectra are shown of sulfate in the presence of sodium and vanadium(III) respectively as Na_2SO_4 and $V_2(SO_4)_3$, in pH 1.5 sulfuric acid. The presence of vanadium(III) has clearly broadened the sulfate edge transition with respect to sodium. The full widths at half height are 2.9 eV and 2.2 eV respectively. In addition, a shift of about 0.2eV to higher energy is seen in the position of the maximum of the vanadium sulfate absorption feature. This finding is at the limits of spectrometer resolution, however the observed shift titrates in a regular manner with increasing [V(III)] in acidic sulfate solutions (at nearly constant total [SO_4^{2-}]) [7], lending credibility to this result.

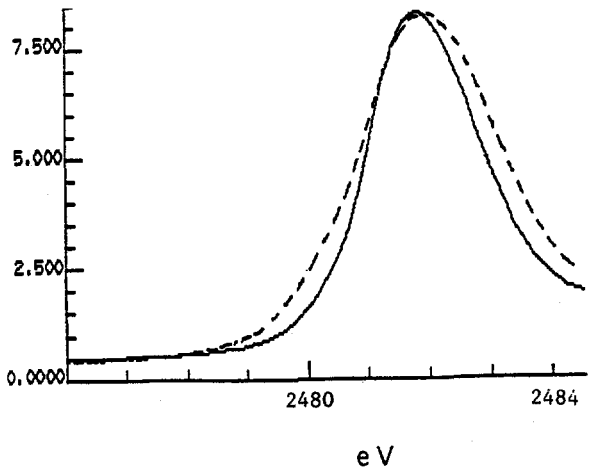

Figure 1. Normalized K-edge x-ray fluorescence spectra of 1M sodium sulfate in pH 1.5 sulfuric acid (full line); and of 1M $V_2(SO_4)_3$, pH 1.5 (dashed line). Ordinate is in arbitrary units.

By way of comparison, spectra of manganese(II) sulfate and sodium sulfate are shown in Figure 2. Manganese is very close to vanadium in Z but differs critically in its chemistry with sulfate in that divalent manganese does not form a complex ion with sulfate. This is in contrast with vanadium(III) [2,6]. Inspection of figure 2 shows that no significant differences exist in the state of sulfate in solutions of Mn(II) and Na^+. Since these solutions were comparable to that of the vanadium sulfate in terms of total sulfate concentration, the possibility that self-absorption of the sulfate fluorescence photon contributes to the enhanced line width of the V(III)-containing solution is eliminated.

It is therefore clear that sulfate XANES spectra are sensitive to physically subtle but chemically important changes in state. Interestingly and by way of corroboration, similar effects to that of vanadium(III) were noted in sulfate solutions of serially increasing acidity. That is, as solution pH dropped from 5 to 0, sulfate edge spectra broadened and shifted slightly to higher energy[7]. Over this range of pH the chemical state of sulfate changes monotonically from SO_4^{2-} to HSO_4^-, one of the four tetrahedrally disposed oxygens becoming protonated. In this event, the T_d symmetry of sulfate changes to C_{3v}, leading to the expectation of shifting transition probabilities within the no-longer triply degenerate HOMO (T_2 becomes E and A_1).

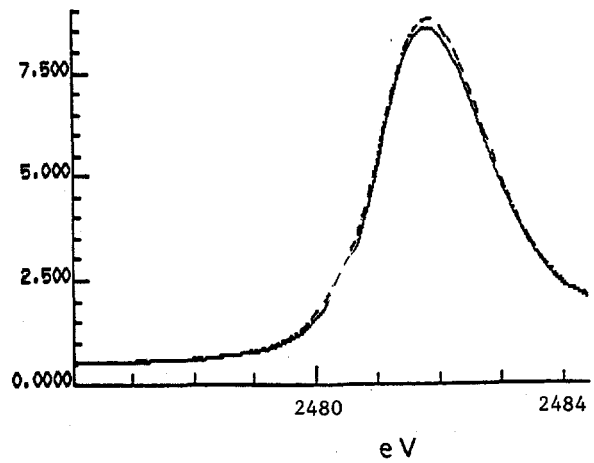

Figure 2. Normalized K-edge x-ray flourescence spectra of 1M $MnSO_4$ in pH 1.5 sulfuric acid (full line); and of 1M sodium sulfate (dashed line) as in Figure 1.

Thus in acidic solutions of vanadium(III) sulfate the predominent species is seen to be VSO_4^+, that is the complex cation. In Figure 3 are shown plots of sulfur edge spectra of: a solution of sodium sulfate and cysteic acid (the latter contains the group $-CH_2SO_3^-$); vanadium(III) sulfate and methane sulfonate; and living, intact vanadocytes. Of the two model solutions, that containing vanadium(III) matches the cellular spectrum both in peak position, and in line width. This is particularly obvious at the high energy side of the flourescence band where the two spectra are nearly superposed. The solution containing sodium sulfate fails to reproduce the cellular spectrum on both these counts. Consideration of the sulfonic acid portion of the spectrum (i.e. the low energy shoulder near 2480.5eV) [5,6] is at this point less unambiguous, both because of the difficulty in resolving this feature away from the sulfate maximum, and because data analysis is as yet unadvanced.

Conclusions. XANES sulfur edge data of intact, living blood cells fram Ascidia ceratodes has been explicated with respect to a specific V(III)-sulfate interaction for the first time, through comparison with spectra of biologically appropriate model solutions. The hypothesis put forward previously [2,8,9] that the vanadium exists intracellularly primarily as a simple inorganic aquosulfate complex is strongly corroborated.

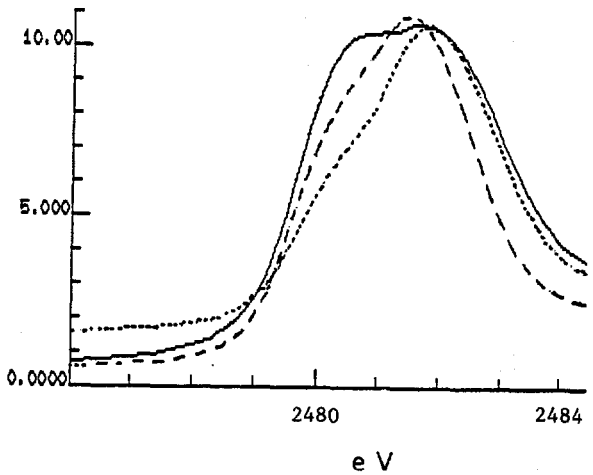

Figure 3. Normalized K-edge x-ray fluorescence spectra of 1M $V(SO_4)(CH_3SO_3)$, pH 1.3 (full line); of 1M sodium sulfate with 1M cysteic acid (dashed line); and living, intact vanadocytes (see text) (dotted line). Ordinate in arbitrary units.

References.

[1] Henze, M. Hoppe Seyler's Z. Physiol. Chem. (1911), 72, 494

[2] Frank, P., Carlson, R.M.K., and Hodgson, K.O. Inorg. Chem. (1986), 25, 470

[3] Biggs, W.R. and Swinehart, J.H Experientia (1979), 35, 1047

[4] Macara, I.G., McLeod, G.C. and Kustin, K. Comp. Biochem. Physiol. (1979), 62A, 821

[5] Hedman, B., Frank, P., Penner-Hahn, J.E., Roe, A.L., Hodgson, K.O., Carlson, R.M.K., Brown, G., Cerino, J., Hettel, R., Troxel, T., Winick, H., and Yang, J. Nucl. Instr. Meth. (1986), A246, 797

[6] Frank, P., Hedman, B., Carlson, R.M.K., Tyson, T.A., Roe, A.L. and Hodgson, K.O. (1987) submitted

[7] unpublished results

[8] Carlson, R.M.K. Proc. Natl. Acad. Sci. USA (1976), 72, 2217

[9] Tullius, T.D., Gillum, W.O., Carlson, R.M.K. and Hodgson, K.O. J. Am. Chem. Soc. (1980), 102, 5670

Research supported by NIH Grant RR 01209 and NSF Grant CHE 85-12129.

EXPERIMENTAL AND THEORETICAL XAS EDGE STUDIES AT THE SULFUR K, MOLYBDENUM L AND CHLORINE K EDGES

Trevor A. Tyson[1], Britt Hedman[1,2], A. Lawrence Roe[1], Stephen F. Gheller[3], William E. Newton[3] and Keith O. Hodgson[1]

[1]Department of Chemistry, Stanford University, Stanford, CA 94305, USA
[2]SSRL, SLAC, Bin 69, P.O. Box 4349, Stanford, CA 94305, USA
[3]Western Regional Research Center, USDA-ARS, Albany, CA 94710; and Department of Biochemistry and Biophysics, University of California, Davis, CA 95616, USA

Introduction. X-ray absorption near edge structure is sensitive to the electronic structure and geometric arrangement of ligands around an absorbing site. It is potentially very useful for addressing structural questions both in biological and other systems. This is particularly so at lower energies, where the energy resolution is enhanced due to monochromator resolution and core hole life-time effects. Molybdenum L, sulfur K and chlorine K edges, all of which are of significant chemical and biological relevance, occur at energies (2.4-2.9 keV) which are not easily accessible either with UHV or hard x-ray beam lines. By using the SSRL/LBL/EXXON 54-pole wiggler beam line at SSRL in undulator mode, we can, as previously reported [1], obtain more than an order of magnitude increase in flux at the S K-edge as compared to that obtainable on an SSRL 8-pole wiggler beam line. To further improve the flux, the downstream beam line 10 mil Be window was replaced by a 5 mil window, and the exit beam pipe Kapton window replaced by 1/4 mil polypropylene. Studies of low concentration samples (as low as a few millimolar) have thereby been enabled, making experiments on biological materials possible. Since these measurements are normally performed with the beam line focused, we have recently also been able to perform polarized XAS measurements on oriented single crystals at these energies, for sample sizes on the order of $(0.1\ mm)^3$.

Oriented Single Crystals. In order to probe the electronic structure of low-Z molecules, polarized sulfur and chlorine K-edge spectra of single crystals containing the oxyanions SO_4^{2-}, ClO_3^-, $S_2O_3^{2-}$ and $S_2O_6^{2-}$ were measured. In concert with these measurements, the well-developed X-α MSW model [2] was used to obtain the ground state and relaxed-excited state energy levels of the molecular orbitals involved in the excitation processes. As a result of our analysis of the experimental data and interpretation of our calculations have been able to draw some general conclusions. First of all, the K-edge excitation spectra of these molecules is governed by single particle quasi-vertical excitations which obey dipole selections rules (no clear evidence of multiple excitations was found). Secondly, nearly complete transfer of the central sulfur or chlorine 3p electrons to the ligands was evident. As an example of this we show (Figure 1) the polarized absorption spectrum of $KClO_3$. Removal of most of the 3p electrons from the central chlorine atom makes possible excitations from Cl 1s to e-symmetry (spectrum A) molecular orbitals (Cl $3p_x$-$3p_y$) and from Cl 1s (spectrum B) to the a1-symmetry (Cl $3p_z$) molecular orbital. Last of all, the spacings and ordering of the levels is consistent with that of our calculations and can be used to determine oxyanion specific optical and ultraviolet absorption properties.

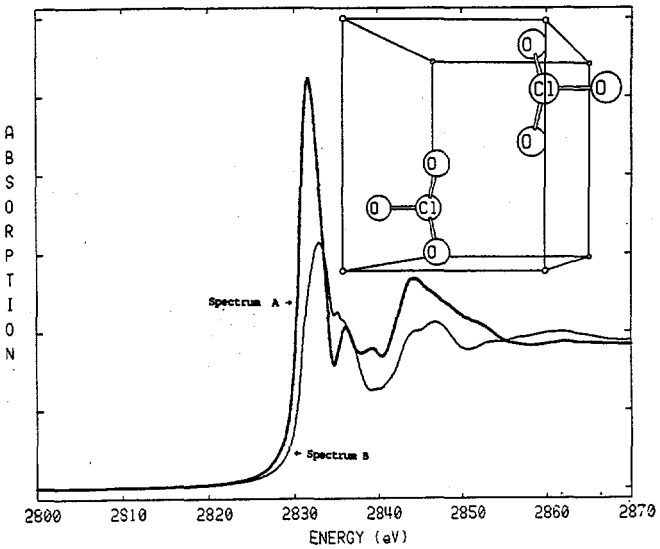

Fig. 1. Chlorine K-edge spectra of $KClO_3$ with the C_3 symmetry axis of the ClO_3^- anion (A) perpendicular and (B) parallel to the electrical field polarization vector of the X-ray beam. The inset figure is an ORTEP plot of the unit cell of $KClO_3$ [3] (Potassium atoms left out for clarity.).

Biological Applications. We have widened our previous systematic study of sulfur, molybdenum and thio-coordinated molybdenum compounds at the S K and Mo L edges. Results from determination of the forms of sulfur present in living cells from tunicates are presented in a separate report. In two consecutive runs we have shown the feasibility of measuring S K and Mo L XAS edge spectra for both the enzyme nitrogenase (from Azotobacter vinelandii) and its FeMo cofactor in semi-reduced form. The edge spectrum of the cofactor is consistent with a mixed S/O/N coordination sphere with Mo in an oxidation state higher than +IV, when compared to relevant model compounds. Further analysis of the data, as well as that of the oxidized form of FeMoco is in progress.

References.

[1] B. Hedman, P. Frank, J.E. Penner-Hahn, A.L. Roe, K.O. Hodgson, R.M.K. Carlson, G. Brown, J. Cerino, R. Hettel, T. Troxel, H. Winick, J. Yang, Nucl. Instr. Meth. **A246** (1986) 797.
[2] K.H. Johnson, Int. J. Quantum Chem., 5 (1971) 429.
[3] J.W. Wats, Acta Cryst. **B34** (1978) 1679.

Research supported by NIH Grant RR 01209 and NSF Grant CHE 85-12129.

APPLICATION OF X-RAY POWDER DIFFRACTION TO THE CHEMICAL CHARACTERIZATION OF ATMOSPHERIC AEROSOLS

J. M. Jaklevic, R. D. Giauque, and W. F. Kolbe
Lawrence Berkeley Laboratory
University of California
Berkeley, CA 94720

The current technology for the characterization of atmospheric particulate samples is not well adapted to the identification of specific chemical species in the ambient aerosol. Although numerous methods are available to determine the elemental composition of samples, a more complete characterization including the chemical form of the particles is necessary before the origin and possible atmospheric transformation of the ambient aerosol can be studied. Powder diffraction is a powerful technique for the identification of crystalline compounds but is limited in sensitivity in its normal laboratory implementation, particularly for those cases in which it is important to identify minor chemical constituents in the presence of dominant species.

Recently Parrish, et al. [1] have demonstrated the capabilities of monochromatic synchrotron radiation for x-ray powder diffraction studies. The improved angular resolution which can be achieved with the synchrotron beam opens up the possibility of performing chemical analysis with improved specificity and sensitivity relative to laboratory measurements. The increased sensitivity of synchrotron x-ray powder diffraction measurements to artifacts arising from particle size and preferred alignment effects is reduced in the case of atmospheric aerosol samples because of the controlled particle size distribution established by the filter sampling procedures. Both the laboratory standards and ambient samples were acquired using an aerosol sampler which limited the particle sizes collected on the filter substrate to less than 2.5 μm diameter.

Measurements were performed on bending magnet beamline I-5 using the (220) silicon double crystal monochrometer. The energy was fixed at 8 keV for the data presented here although other energies were evaluated for specific applications. The goniometer was equipped with 0.15° Soller slits. Scans were taken for both standards and ambient samples in 0.04° steps over an angular range of 20 to 50° in 2θ. Typical data acquisition periods were 20 to 60 min.

Figure 1 is a plot of the diffraction pattern obtained for a 1 mg/cm^2 Na_2SO_4 standard prepared by filtering a laboratory-generated aerosol onto a 2 μm pore size Teflon filter. The measured angular resolution is 0.14° which is consistent with the Soller slit dimensions. Comparison of the relative intensities of the reflections with those observed in our laboratory and those listed in the standard diffraction files indicates that no significant artifacts attributable to particle size statistics or preferential alignment are present.

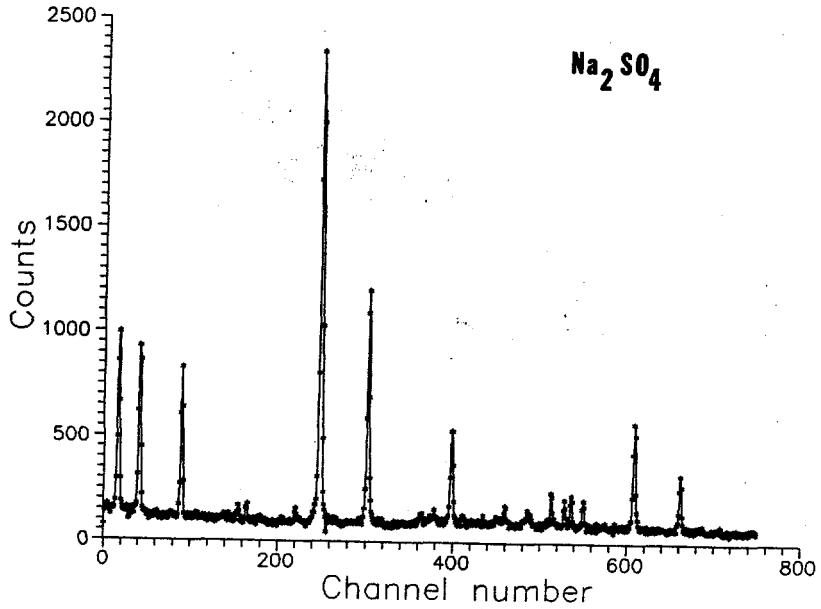

Additional data were obtained on ambient samples acquired in a field study of cities in the eastern U.S. These samples were lightly loaded with total particle mass of 100 μg/cm^2 or less. Diffraction peaks from the major aerosol constituents such as mascagnite $(NH_3)_2SO_4$ were easily measured in a 20 min counting period. Due to the low beam intensity and limited time available, no attempt to observe minor constituents was made.

Careful evaluation of the data indicated that the improvement in peak to background relative to laboratory measurements obtained with a Bragg-Brentano instrument was not as great as that anticipated from the improvement in angular resolution. This was primarily due to our inability to eliminate the scattering background in this preliminary setup. Nevertheless, the quality of the data indicates the potential for dramatic improvements over laboratory measurements particularly if larger fluxes could be used in an experimental setup where spurious scattering was reduced.

References

1. W. Parrish, M. Hart, C. G. Erickson, N. Masciocchi, and T. C. Huang (1986) Adv. X-Ray Anal., Vol. 29, 243, Plenum Press, NY.

Acknowledgments

This work was supported by the Director's Office of Energy Research, Office of Health and Environmental Research, U.S. Department of Energy Contract No. DE-AC03-76SF00098.

CRYSTALLOGRAPHIC ANALYSIS OF SELENOBIOTINYL STREPTAVIDIN FROM MEASUREMENTS OF MULTIWAVELENGTH ANOMALOUS DIFFRACTION

Arno Pähler, Janet L. Smith and Wayne A.Hendrickson
Columbia University, New York
Ethan A. Merritt and R. Paul Phizackerley
Stanford Synchrotron Radiation Laboratory, Stanford

Previous studies on lamprey hemoglobin (1) have shown that anomalous dispersion at multiple wavelengths offers a feasible method to overcome the phase problem in X-ray crystallography and to solve protein crystal structures. The present report summarizes the progress made so far in applying this method to a complex between the tetrameric protein streptavidin and selenobiotin,an analog of its natural ligand.

Streptavidin is a bacterial protein that forms a very tight, noncovalent complex with its ligand biotin. We have grown three crystal forms of streptavidin. The orthorhombic modification in spacegroup I222, which has two core streptavidin subunits per asymmetric unit, has been used for the work reported here. Neither streptavidin nor biotin contain atoms that produce reasonably strong anomalous dispersion at any accessible wavelength. However, the sulfur atom in biotin can be replaced by selenium, which has its K-absorption edge at a readily accessible energy (12.7 keV). Since biotin and selenobiotin crystallize isomorphously, we had little doubt that this analog of biotin would bind to streptavidin and our synchrotron studies confirm that it does.

DIFFRACTION MEASUREMENTS

Diffraction data to 3.0 A spacing were collected at SSRL's area-detector diffractometer (BL I-5) at four wavelengths (0.9000 A, 0.9789 A, 0.9792 A and 1.1000 A) from a single crystal with approximate dimensions of 1.04 x 0.42 x 0.17 mm. Bijvoet pairs were measured at each wavelength. Cell dimensions derived from this crystal were a=95.20, b=105.63 and c=47.41 A. Anomalous contributions to the atomic form factor were evaluated from X-ray absorption across the Se K-edge, measured from the data crystal, and revealed a marked dichroism . Since the crystal cracked as a result of soaking in the selenobiotin solution, reflection profiles were rather broad and highly asymmetric with FWHM of about 1.0 degree. During data reduction no corrections were made for radiation damage. Empirical absorption corrections were made on the basis of psi-scans of the data crystal using Cu K-alpha (1.5418 A) radiation after the data collection. These measurements also showed that the crystal still diffracted well and two data sets, to 5.0 A and to 3.0 A spacings, were subsequently collected with Cu K-alpha radiation.

DATA ANALYSIS AND RESULTS

Bijvoet pairs were locally scaled to eliminate systematic errors in the data as were measurements at the four wavelengths, and the data were put on an approximately absolute scale. Multiple-wavelength phase determination using up to eight measurements per reflection resulted in refined values for the total normal structure factor amplitude, the Se normal structure factor amplitude and the phase difference between these two structure factors . The 10481 phased reflections were merged to produce 5047 unique reflections in the 3 A sphere. Despite the comparatively poor quality of the data it was possible to identify the positions of the expected two Se atoms from Patterson maps based on coefficients using the Se normal structure factor amplitudes. These two sites also obeyed the molecular twofold symmetry derived from self-rotation function calculations using data from uncomplexed streptavidin crystals. Least-squares refinement of these two sites against 1187 reflections gave an R-factor of 37.4 % with a reflection-to-parameter ratio of about 130.

Amplitudes and phases for calculation of electron-density maps were obtained by a modification of the phasing procedure. The normal structure factor amplitudes calculated from the Se atomic positions were included and not refined, the Cu K-alpha data were included as a fifth wavelength and formulae were developed to calculate figures-of-merit. A figure-of-merit weighted electron density map showed the least amount of noise. Selenium positions are a dominant feature in the electron density map, as can be seen in Fig. 1. When a least-squares refinement of the molecular twofold axis is carried out in this map, twofold related densities agree with a correlation coefficient of about 0.67. Suppressing the selenium electron density leads to a correlation coefficient of about 0.34. Though being low, the value is statistically significant, indicating a less than 1% probability, that the electron density is not twofold symmetric.

Molecular averaging as well as the availability of data from the monoclinic crystal form, which contains a full tetramer in the asymmetric unit, will enable us to improve the quality of the phases. We anticipate that it will be possible to obtain a map in which the streptavidin structure can be interpreted starting from multiple-wavelength anomalous-dispersion phases and proceeding in this fashion.

1. Wayne A. Hendrickson, Janet L. Smith, R. Paul Phizackerley, Ethan A. Merritt, Warner E.Love SSRL Report 1985, p. IX-31

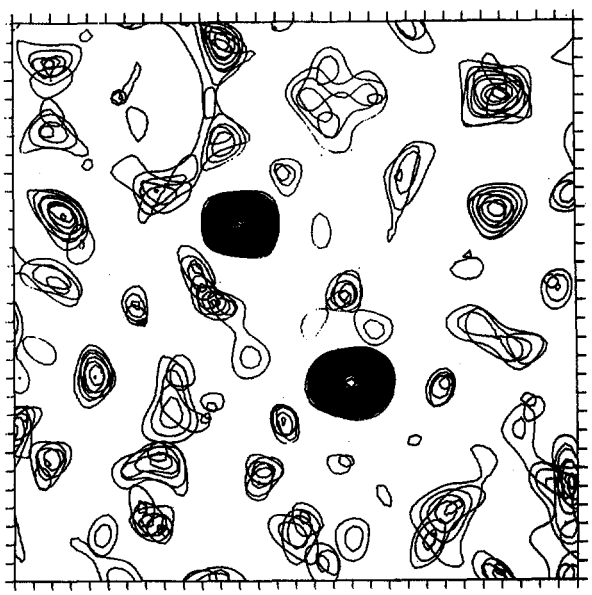

ABSORBED DOSE AS A UNIQUE DETERMINANT OF X-RAY RESIST PERFORMANCE

Daniel Seligson
Intel Corp.
Santa Clara, Ca. 95051
and
Paul King, Lawrence Pan, and Piero Pianetta
SSRL, Bldg. 120

Today's R&D on x-ray lithography (XRL) employs no standard source and no standard spectrum. Instead, electron impact guns, laser and gas plasmas, synchrotron and even transition radiation are all being developed. These various sources have their spectra peaked between 1 and 3 keV. The usual method of specifying resist sensitivity is in terms of incident dose (mJ/cm2), but because of the strong energy dependence of absorption, the apparent sensitivity of the same resist measured with the different sources could easily vary by a factor of 10. We undertook to determine the energy dependence of resist sensitivity over the energy range currently considered relevant for XRL. Our findings have allowed us to develop a source-independent definition of resist sensitivity based on absorbed dose (J/cm3). This will have important applications in research and manufacturing. It immediately enables a quantitative comparison of different resists and sources.

Several different photoresists were exposed to narrowband (50 eV, FWHM) x-ray radiation using a wide bandpass monochromator on beam line III-4. For each resist, the graph of thickness remaining versus absorbed dose density falls along a universal curve independent of energy (Fig. 1), indicating that the chemistry of resist exposure is independent of energy. Based on these measurements, we propose a simple macroscopic model of resist behavior and we make use of the demonstrated universality to predict the sensitivity of these resists for other x-ray sources. We also generalize the results to UV and e-beam exposures. Future experiments for comparing e-beam and x-ray data are planned.

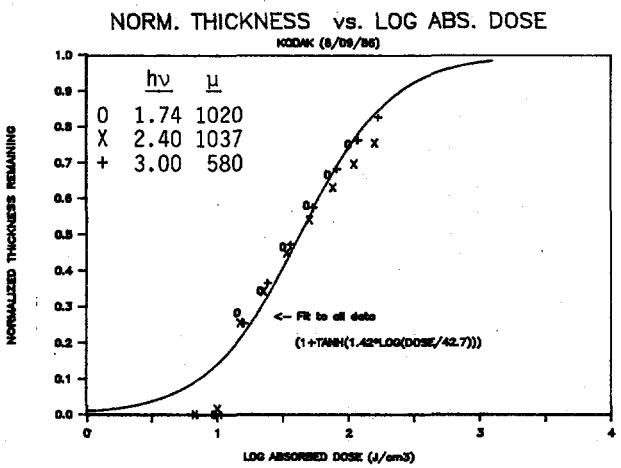

Figure 1. The 1st experimental evidence of source independent resist performance is observed in this graph of normalized thickness remaining vs. log absorbed dose. The resist is a Br-polystyrene derivative.

The monochromatic experiments are too time consuming to be practical for screening large numbers of resists. For that purpose we must use the broadband spectrum 1 to 3 keV. We have implemented hardware and software that enable us to expose a single resist coated Si wafer with 60 different exposure doses over a 3 decade range. At present the cycle time for this for this procedure is <30 minutes. Using the results of the model developed to explain the monochromatic experiments, we analyzed these broadband exposure data and obtained contrast and universal sensitivity for each resist. A comprehensive sample of x-ray and e-beam resists were screened in this way.

The small dose increments obtainable revealed some new phenomena about resist behavior. A series of molecular fractions of a chlorinated polystyrene were examined for sensitivity and contrast (Fig. 2). The heavier fractions were faster, as expected, but they also swelled at low dose (near the gel point). This method of investigating swelling is both simple and quantitative, whereas other methods rely on qualitative observations of wrinkling of high resolution resist patterns. Also, by studying the molecular weight series we have clearly demonstrated the limitation of achieving good sensitivity by increasing the molecular weight without limit. We believe that the mechanism of swelling is solvent penetration of the weakly crosslinked (underexposed) polymer network. Following development, the swollen structure remains intact when the solvent is removed.

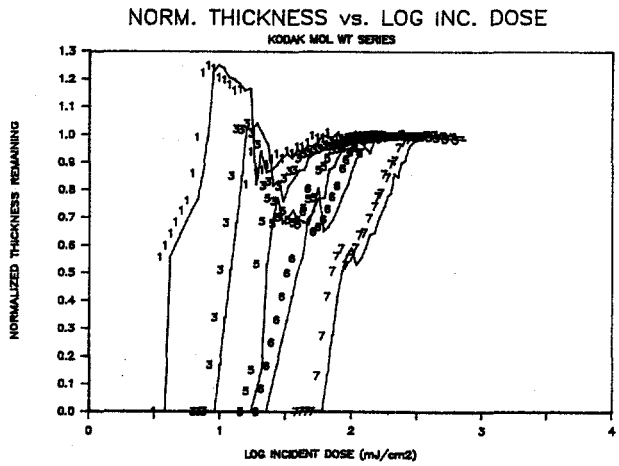

Figure 2. Normalized thickness vs. log incident dose for a molecular weight series of Cl-polystyrenes. The heavier fractions (smaller numbers) are more sensitive, but are prone to swelling and have lower contrast.

We gratefully acknowledge Charlie Anderson of Kodak Research Laboratories for supplying us with experimental resists, Troy Barbee Jr. of LLNL for providing the multilayer crystals used in the monochromator, and Don Rose of Intel Corp. for inititiating this collaboration.

DIFFERENTIAL ANOMALOUS X-RAY SCATTERING OF LACCASE

J.E. Penner-Hahn[1], A.M. Schmidt[2], D.R. McMillin[2], and R.D. Lorentz[3]

[1]Department of Chemistry, University of Michigan, Ann Arbor, MI 48109
[2]Department of Chemistry, Purdue University, West Lafayette, IN 47907
[3]Basic Technologies, Electronic & Information Sector Laboratories, 3M, St. Paul, MN 55144

Introduction

Recently we have shown that differential anomalous X-ray scattering (DAS) can be used to probe long distance (5-10 Å) solute structure in dilute solutions [1]. In order to test the potential of this technique for studying metal-metal interactions in metalloproteins, we have recently collected DAS data for laccase.

Laccase is a multi-copper oxidase containing copper in three distinct sites. These sites are identified as Type 1, Type 2 and Type 3. EXAFS studies [2] have shown that the Type 3 site, which contains a binuclear Cu pair, has a Cu-Cu distance of ca. 3.4 Å. Recent azide binding studies suggest that the Type 2 and Type 3 sites form a trinuclear cluster, with the Type 2 site within 5.2 Å of one of the Type 3 Cu atoms [3]. There has been however no direct evidence concerning the relative location of the Type 1 site within the protein. Recently a new derivative of laccase has been prepared in which the Type 1 Cu is selectively replaced with Hg. We have collected Cu edge differential anomalous X-ray scattering data for both native (Cu_4) and Hg substituted (Cu_3Hg) laccase.

Experimental

All protein solutions were 1.7 mM in protein and were prepared in 0.100 M pH 6.0 phosphate buffer. This corresponds to a Cu concentration of 0.0036 atomic % in the native sample. The scattering experiment was performed on Beamline 4-3 using coupled θ-2θ scans and a reflection geometry. Data were collected at 8880 eV and 8975 eV (100 eV and 5 eV below the Cu K absorption edge, respectively). The total data collection time was ca. 8 hrs/sample

Discussion

The normalized difference (-100 minus -5 eV) for the native (Cu_4) data is shown in Figure 1. From this Figure it is clear that the present data are not of sufficient quality to allow calculation of the Cu differential distribution function. This is due to a combination of the low Cu concentration and the limited data collection period.

The most striking result, however, is seen on examination of the radial distribution functions (RDFs). The RDFs for Cu_4 and for Cu_3Hg laccase are compared in Figure 2. Since these functions are dominated by protein and water scattering, they are expected to be nearly identical. Although this is true over most of the data range, the RDF for the Cu_3Hg protein is significantly larger than the RDF for the Cu_4 protein at ca. 5 Å. Identical results are observed for both the -5 eV data and the -100 eV data, ruling out any systematic errors in one data set. This feature would seem to suggest the presence of a 5 Å inter-atomic vector in the Cu_3Hg protein which is absent in the Cu_4 protein.

At least two possibilities exist to explain the 5 Å feature. One is that there is an unusually high density of protein atoms at 5 Å from the Type 1 site. When the Cu in this site is replaced with Hg, enhanced Hg-ligand scattering would be observed. Alternatively, the 5 Å feature could represent inter-site metal-metal scattering. This would again be stronger when the Type 1 Cu was replaced with Hg. In the latter case, the present data would be providing information on the relative location of the Type 1 copper within the protein. In order to resolve this question, we plan to collect higher quality data for RDFs and to attempt DAS measurements at both the Cu and Hg edges.

References

1. Lorentz, R.D.; Bino, A.; Penner-Hahn, J.E., J. Am. Chem. Soc., 1986, 108, 8116-8117.
2. Wollery, G.L.; Powers, L.; Peisach, J.; Spiro, T.G., Biochemistry, 1984, 23, 3428-3434.
3. Allendorf, M.D.; Spira, D.J.; Solomon, E.I., Proc. Natl. Acad. Sci., USA, 1985, 82, 3063-67.

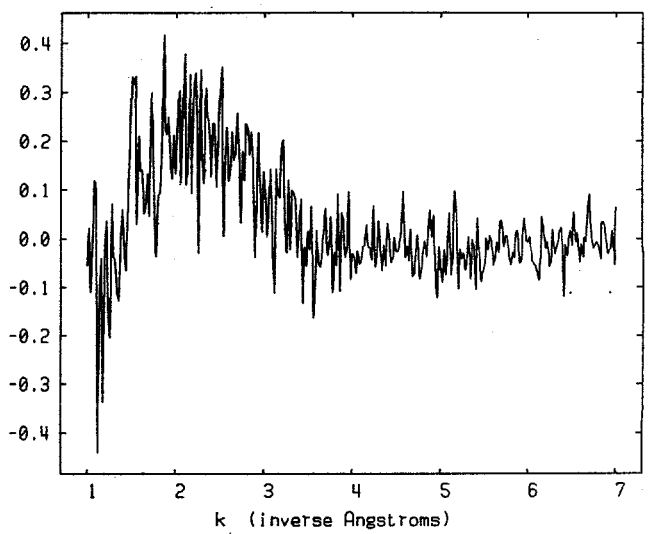

Figure 1. Normalized difference (-100 minus -5 eV) for native laccase.

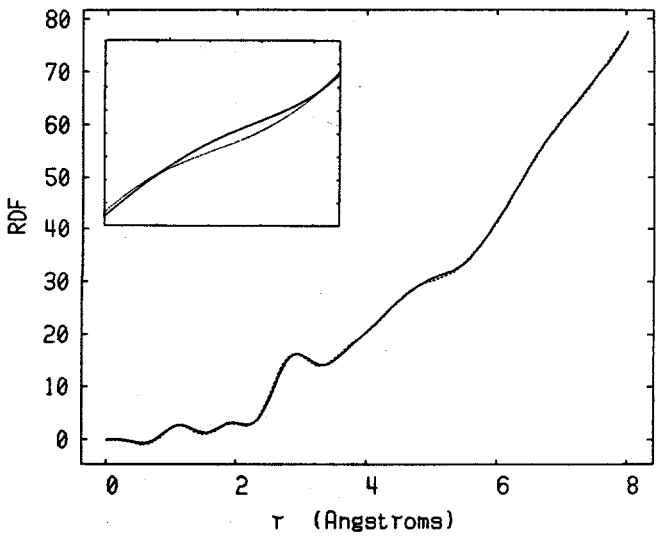

Figure 2. Radial distribution functions for laccase (at -100 eV). Dash) native (Cu_4). Solid) substituted ($HgCu_3$) laccase. Inset) Expansion showing difference at ca. 5 Å.

TIME AND FREQUENCY DOMAIN RESPONSE OF SILICON PIN PHOTODIODE

Andrew P. Sabersky
SAB Partners
1836 17th Avenue, Suite D
Santa Cruz, CA 95062

PIN Silicon photodiodes are widely used as receivers in lightwave communications systems and as detectors in a variety of pulsed laser experiments. Physically small diodes, processed for low capacitance and having temporal impulse responses less than a nanosecond, are commercially available. Detailed time and frequency response characteristics of these devices are seldom available, and since we need these for our purposes, we use the pulsed structure of synchrontron light as a test source to measure our detectors.

When the response of a fast photodetector coupled to an electronic instrument is measured, the output includes factors due to the entire measurement system, including:

(1) The photodetector device
(2) The electrical coupling between detector and instrument (the mount)
(3) The electronic measuring instrument
(4) The optical test pulse

The photodetector is Advanced Detector Corp's AD101 Silicon PIN photodiode. It has an effective sensitive surface area of .036 sq. cm., and is operated with a bias of 50v.

The mount (fig. 1) is coaxial, impedance matched at 50 ohms. This mount, similar to the one used with vacuum photodiodes for SPEAR and PEP bunch length measurement, (Ref. 1), has an external bias decoupling capacitor, this making internal bias resistors and leads unnecessary. The time domain results show the benefits of this design, very little parasitic overshoot or ringing.

Time domain response is measured with a sampling oscilloscope, H/P 1810A plug-in. The response of the scope is down 3dB at 1 GHz, this corresponding to a sigma(time) of 187 ps. The power spectral density (PSD) of the output is measured with a Tektronix 7L13 spectrum analyzer plug-in.

A well-known problem in timing with a storage ring is that beam-derived timing signals arrive later than optical signals. We used internal triggering on the sampling oscilloscope, finding that we could trigger stably on the largest-amplitude bunch in the ring while observing bunches in the next group of four, approx. 200 ns later.

SPEAR was operating at 3.0 GeV, current = 40 (+/- 5) mA total stored current, 16 bunches stored in 4 groups of 4 bunches, and RF gap voltage approx. 3.0 MV. The sigma(time) of bunch length, the bunch being approximated as a Gaussian in time, is 210 (+/- 50) ps.

We ran on Beam Line 8, with the monochromator set to zero degrees to pass visible light. The exit window is Pyrex. We used the full available spectrum in this experiment.

The time domain response of the system is an approximately triangular pulse (no photo available) with rise time (10% to 90%) 500 ps and fall time 1500 ps. Ringing and overshoot are $<$ 2% peak amplitude. Full width half max. of the diode + mount response is 1300 (+/- 100) ps, with scope and optical pulse corrections subtracted.

The PSD of the optical pulse pattern is complex, depending in detail on the spacing and amplitude of the electron bunches. Only the single-bunch mode yields a spectrum which is smooth and predictable. Nevertheless, by considering the peak values in the PSD at the output of the mount, we estimate the frequency response of the system to be 3 dB down at 400 MHz, consistent with the time domain response.

References

1. P.B. Wilson et al, "Bunch lengthening and related effects in SPEAR II", IEEE Trans. Nucl. Sci. 24, 1211-1214.
2. I.H. Munro and A.P. Sabersky, "Synchrontron radiation as a modulated source.." in Synchrotron Radiation Research chapter 9, ed. Winick and Doniach, Plenum (1980).

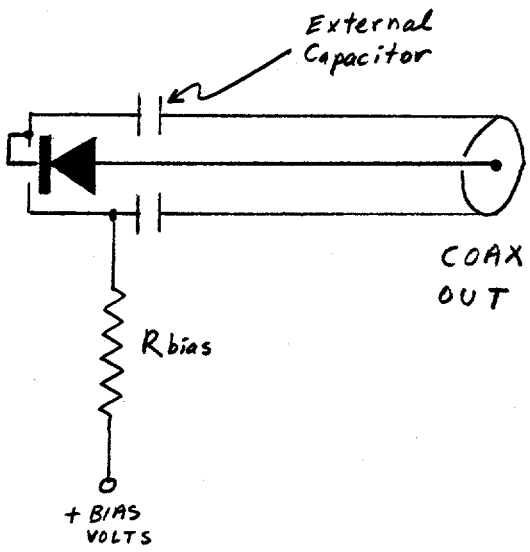

FIG. 1

SYNCHROTRON X-RAY POLYCRYSTALLINE DIFFRACTOMETRY-III

W. Parrish, M. Hart [a], M. Bellotto [b], C. Erickson and G. Will [c]
IBM Almaden Research Center, San Jose, California, 95120-6099

a. Department of Physics, The University, Manchester M13 9PL, U.K.
b. Politecnico di Milano, 20133 Milan, Italy
c. Mineralogisches Institut der Universitat Bonn, D-5300 Bonn, F.R.G.

Instrumentation. A major improvement in the resolution decreased the profile width (FWHM) from 0.17° to 0.05° (2Θ) *(5)*. This was done with a new design long parallel slit collimator to define the diffracted beam. The foil length was increased to 365 mm and spacing kept at 0.2 mm. The peak intensities of the reflections were the same as our previous 100x0.2 mm collimator. Precise alignment is essential to avoid profile asymmetry. An example of the improved resolution is shown in Fig. 1 for a secton of the quartz powder diffraction pattern for the d-range 1.31 to 0.83Å. The upper pattern was recorded with 0.17° resolution and λ = 1Å, and the lower with 0.05° and 1.28 Å. A perfect crystal analyzer can give somewhat higher resolution but the intensities are greatly reduced and some techniques involving wavelength changes become far more difficult to implement. A high speed Rigaku scintillation counter and pulse height analyzer with linearity exceeding 10^5 c sec^{-1} was used.

Profile fitting. The sharp symmetrical single profiles have a large advantage in precise measurements of peak diffraction angles, intensities, resolving overlapping reflections and determining profile broadening arising from the specimen. The profile widths are the same as the collimator aperture at small 2Θs and increase as tanΘ due to wavelength dispersion. The instrument function is constant except for the width.

The high resolution profiles could be fitted with a symmetrical pseudo-Voigt function consisting of a sum of Gaussian (G) and Lorentzian (L) curves *(7)* :

$$p\text{-}V = xG + (1-x)L$$
$$= xI_p\left[1 + 4\,\frac{(2\theta - 2\theta_p)^2}{FWHM(L)^2}\right]^{-1} + (1-x)I_p \exp\left[-4\ln 2\,\frac{(2\theta - 2\theta_p)^2}{FWHM(G)^2}\right]$$

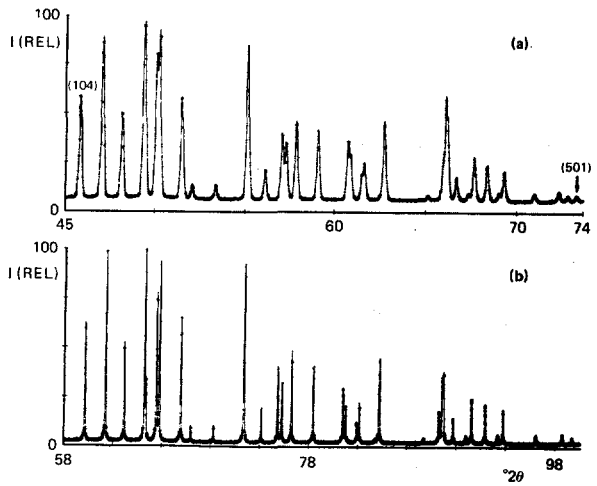

where x is the ratio of the peak intensities of G and L, I_p the maximum peak intensity, $2\Theta_p$ the peak angles and FWHM the width at one-half net peak height of the G and L components. We found the ratio was not critical and used x = 0.25. The differences between the unsmoothed experimental points and the calculated profile is shown at half height in Fig. 2. Fig. 2(a) is the W(111) powder profile, FWHM = 0.063°, and 2(b) is Si(422), FWHM = 0.102°, both recorded with λ = 1.54 Å radiation.

Profile Broadening Analysis. The determination of particle size, microstain, disorder and stacking faults by the Warren-Averbach method is greatly simplified by the uniform symmetrical instrument function *(3)*. The easy selection of short wavelengths (about 1Å) provides additional reflection pairs and allows analyses along different crystallographic directions. Plots of the crystallite size coefficients A_L^S as a function of the distance L in a (hkl) direction are shown in Fig. 3. The solid dots are for strained Pd powder and the circles for the annealed powder.

Precision Lattice Parameter Determination. The absence of instrument aberrations which cause systematic errors, the measurement of 2Θs with profile fitting to about 0.0001° and least squares refinement to determine the 0° diffractometer calibration correction and lattice parameter, provide the possibility of making measurements in the ppm range which is more than an order of magnitude better than conventional methods *(6)*. Precision measurements were made on a number of cubic, rhombohedral and orthorhombic inorganics. The wavelengths were determined from absorption edges and a better method will be tried on the next run.

Crystal Structure Refinement. Structure analysis was done on high resolution powder runs of quartz to 115° with λ = 1.28 Å, and orthorhombic Mg_2GeO_4 to 85° with λ = 1.74 Å *(7,9)*. The integrated intensities were determined by profile fitting and the refinements done with the POWLS program. An improved method for handling the problem of incomplete random particle distributions in the specimen preparation was developed. We obtained R_{Bragg} = 1.6% for quartz and the positional and thermal parameters closely matched the best published single crystal data.

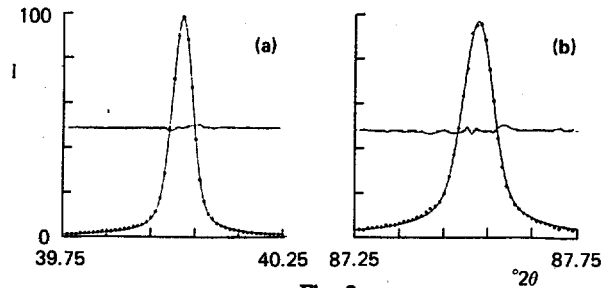

Fig. 2

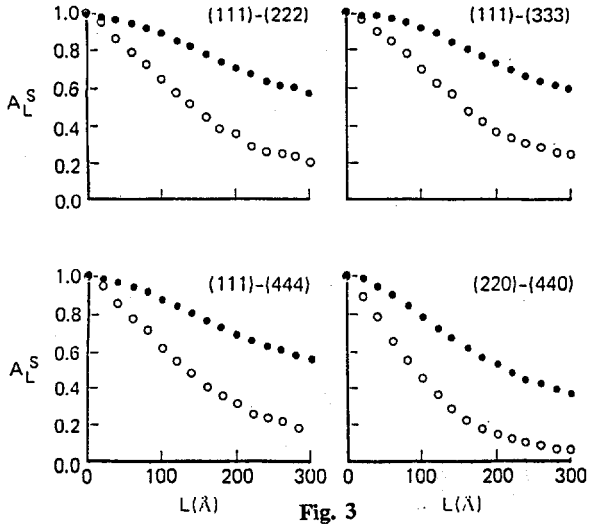

Fig. 3

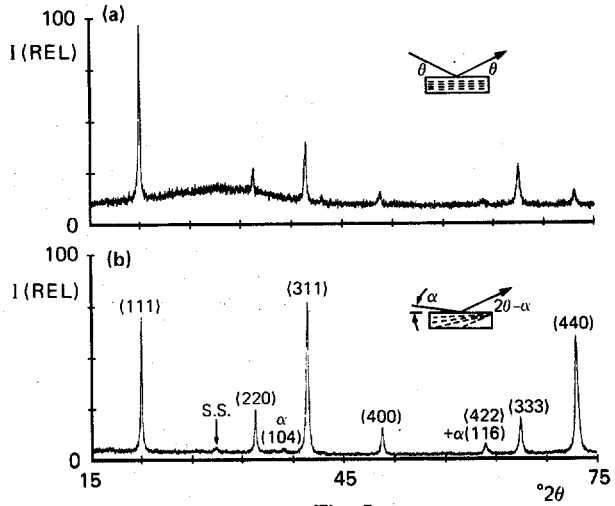

Fig. 5

The Mg_2GeO_4 data contained a number of impurity peaks which were removed in the analysis. The R_{Bragg} was 4.9%. Fig. 4 is a typical Fourier map showing the electron density. The method is flexible and precise and will be compared to the Rietveld method.

Four full powder data sets of Yb_2O_3 were obtained at four wavelengths slightly longer than the Yb L-III absorption edge using the same experimental conditions *(8)*. The structure data were refined to R_{Bragg} = 1.3% to 1.7%, and the anomalous scattering factor f determined.

Methods for Thin Films Studies. In conventional Θ:2Θ scanning the beam usually penetrates the entire film thickness and the pattern contains reflections only from planes parallel to the surface and the substrate scattering as shown in Fig. 5(a). The parallel beam optics permit decoupling of the Θ:2Θ specimen:detector angular relation without distorting the profiles, loss of resolution or precision. In this geometry the specimen can be set at a small grazing angle of incidence and only the detector is step-scanned (in the vertical plane as in powder pattern scans). Reflections occur from planes inclined to the surface, and if the angle is small enough the substrate scattering is avoided, Fig. 5(b). This makes it possible to use methods to characterize thin films which cannot be done with conventional focussing methods.

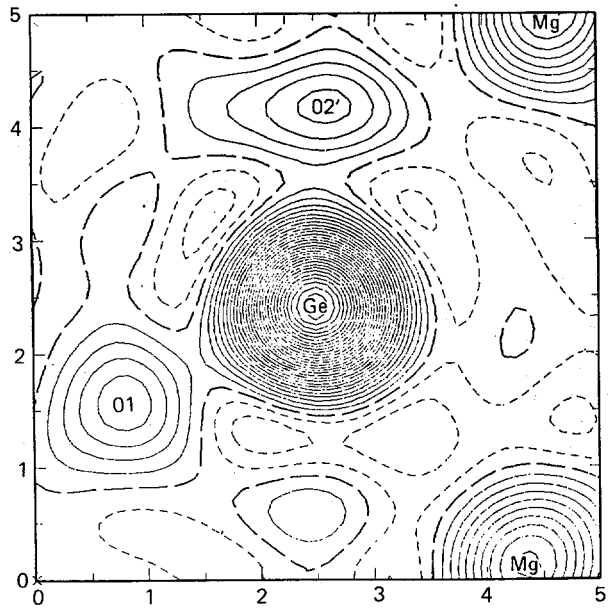

Two methods were developed: 1) grazing incidence depth profiling, and 2) texture analysis with energy dispersive diffraction. Both methods use the same instrumentation as for powder diffraction.

Grazing incidence studies of 5000 Å iron oxide films were made with 1.75 Å radiation to avoid FeK fluorescence *(1)*. Below the critical angle (about 0.3°) the phases and lattice parameters could be determined as a function of depth in the top 45 to several hundred Angstroms by selecting an incidence angle. Above the critical angle the penetration depth increases to several thousand Angstroms and profiling cannot be sensitively controlled. A method for correcting the peak shifts due to X-ray refractve index was developed. Weak peaks from the top 60 Å of the film were detected and identified as a superstructure reflection (S.S.) of γ-Fe_2O_3 and reflections from α-Fe_2O_3.

High resolution energy dispersive diffraction can be done by step-scanning the incident beam channel monochromator with the specimen and scintillation counter fixed at selected angles *(4)*. It was used in a study of texture in a 4100 Å Pd/Xe film which had strong (111) orientation parallel to the surface *(2)*. The highest intensity is obtained when the lattice plane is in the symmetric Bragg reflecting position. Rotating the specimen through the interplanar angle between (111) and another plane brings the latter to its symmetrical reflecting position. By measuring the intensities at small angular steps around this position, the distribution of the planes with respect to (111) and the film surface can be mapped.

References

1. G. Lim, M. Bellotto, M. Hart, W. Parrish, and C. Ortiz, in preparation
2. M. Hart, W. Parrish, N. Masciocchi, Appl. Phys. Letters, in press, 1987
3. T.C. Huang, M. Hart, W. Parrish and N. Masciocchi, J. Appl. Phys., in press, 1987
4. W. Parrish and M. Hart, Trans. Am. Cryst. Assoc. 21, 51-55, 1985
5. W. Parrish and M. Hart, Z. Krist., in press, 1987
6. W. Parrish, M. Hart, T.C. Huang and M. Bellotto, Adv. X-Ray Anal. 30, in press, 1987
7. G. Will, M. Bellotto, W. Parrish and M. Hart, in preparation
8. G. Will, N. Masciocchi, M. Hart and W. Parrish, Acta Cryst. A, in press, 1987
9. G. Will, N. Masciocchi, W. Parrish and M. Hart, J. Appl. Cryst., in press, 1987

BONDING OF HCN AND CO ON W(100)-(5x1)-C USING NEAR EDGE X-RAY ABSORPTION FINE STRUCTURE MEASUREMENTS

C.M. Friend and E.K. Baldwin*
R.J. Madix and P.A. Stevens**

*Department of Chemistry, Harvard University, Cambridge MA 02138
**Department of Chemical Engineering, Stanford University, Stanford, CA 94305

The molecular orientation and approximate bond lengths of CO and HCN adsorbed on W(100)-(5x1)-C were derived from near edge X-ray fine structure measurements. The objective of this investigation was to correlate reactivity and bonding structure on W(100)-(5x1)-C for molecules with related electronic structure. In addition, these experiments demonstrated that high quality near edge X-ray fine structure data can be understood even for systems with a high background intensity from surface atoms: in this case the carbide carbon. Carbon K-edge spectra were in good correspondence with nitrogen and oxygen K-edge spectra in the case of HCN and CO, respectively. The study of transition metal surfaces modified with carbon, sulfur or oxygen is key to understanding reactions of catalytic importance. The W(100)-(5x1)-C surface is of particular interest because of the fact that the energetics for bond breaking/making and the relative product distributions for many molecules is dramatically different than clean W(100) [1,2]. Comparison of HCN and CO bonding and reactivity are a means of systematically varying the electronic structure of adsorbates in order to gain a broader understanding of surface reactivity on early transition metals. The structural information derived from these experiments was also used as input for semiemperical, tight-bonding slab calculations performed in order that bonding to the carbide surface be more fully understood [3].

Near edge data obtained at glancing and normal photon incidence on beam line III-1 and the user's end station at SSRL in parasitic mode are depicted in Figure 1. The near edge X-ray fine structure data was fit with Gaussian line shapes using a curve-fitting routine. This allows for accurate determination of integral peak intensities and the energy of σ^* resonances in order to determine molecular orientation [4] and bond length [5]. The ratios of the integral intensities of both the π^* and σ^* resonances at normal to glancing photon incidence demonstrate that the C-O bond axis is normal to the surface plane ±10°. The position in energy of the σ^* resonance results in a C-O bond length of 1.13 Å, identical to the C-O bond length in gas phase $W(CO)_6$ within experimental error. These results are in accord with vibrational data: the C-O stretching frequency is the same for CO adsorbed on W(100)-(5x1)-C and in gaseous $W(CO)_6$. The correspondence in the vibrational and near edge X-ray fine structure results demonstrate the reliability of the conclusions based on C K-edge data obtained in the presence of large quantities of background carbon.

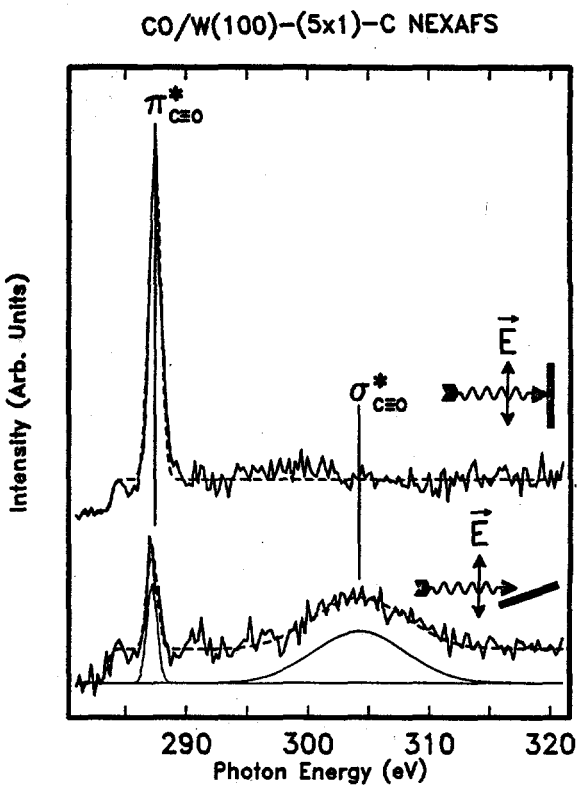

Figure 1.

In the case of HCN, reversible hydrogenation/dehydrogenation competes with complete decomposition and reversible desorption [1]. High resolution electron energy loss spectroscopy has previously established that the HCN is hydrogenated at 475 K on the W(100)-(5x1)-C surface, resulting in formation of HCNH [6]. Temperature-dependent near edge X-ray fine structure data were obtained in order to establish the molecular geometry of the chemically distinct states derived from HCN. Near edge spectra obtained for HCNH adsorbed on W(100)-(5x1)-C are shown in Figure 2a. The polar and angular dependence of the π^* and σ^* resonance intensity demonstrates that the C-N bond axis is oriented parallel to the surface plane. The C-N bond length is determined to be 1.38 Å, compared to a gas-phase C-N bond length of 1.16 Å for HCN. All data support a model where the C-N bond is rehybridized to a bond order of 1.5. Vibrational data further support this contention via comparison with structurally characterized transition metal cluster analogs, which have a C-N bond length of 1.34 Å.

Near edge X-ray fine structure data for HCN annealed to 275 K, prior to hydrogenation, are shown in Figure 2b. These data can be interpreted in terms of tilted HCN or a mixture of species. Preliminary N(1s) X-ray photoemission and high resolution electron energy loss data suggest that at least two species are present on the surface at 275 K.

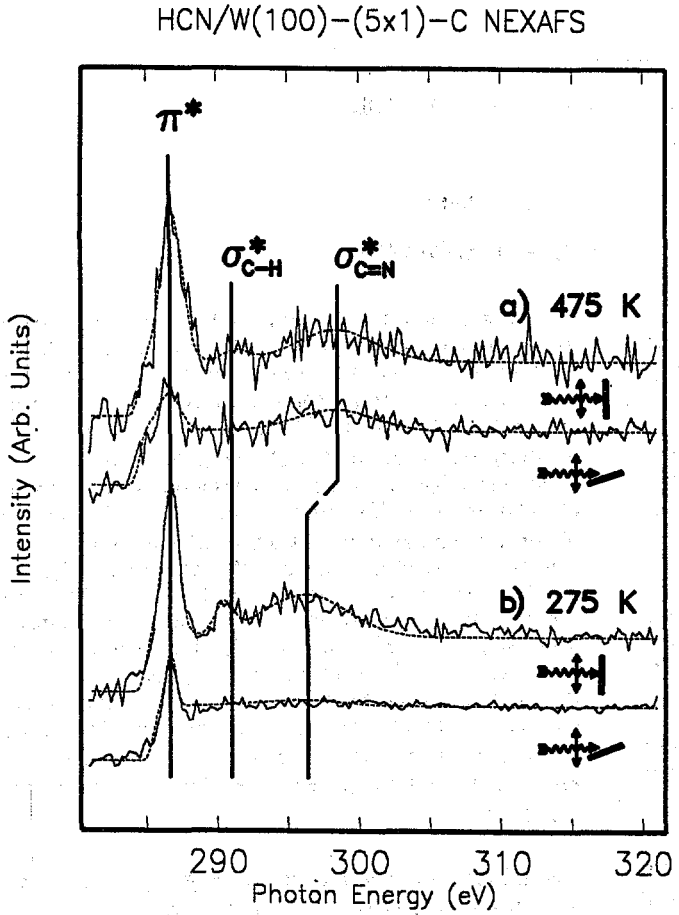

Figure 2.

In summary, the near edge X-ray fine structure method has been successfully used to define key features of the bonding geometry of adsorbates exhibiting complex thermal chemistry. This work exemplifies the utility of the near edge X-ray fine structure technique in the characterization of the structure of chemically complex reaction systems of importance in heterogeneous catalysis.

[1] See, for example, K.A. Pearlstine, C.M. Friend, J. Phys. Chem **90** (1986) 4341.
[2] E.I. Ko and R.J. Madix, J. Phys. Chem. **85** (1981) 4019.
[3] S.A. Jansen, R.S. Hoffmann and C.M. Friend, in preparation.
[4] J. Stöhr, R. Yeager, Phys. Rev. B, **26** (1982) 4111.
[5] F. Sette, J. Stohr, A.P. Hitchcock, J. Chem. Phys. **81** (1984) 4906.
[6] C.M. Friend, J.G. Serafin, P.A. Stevens, E.K. Baldwin, in preparation.

Valence Band Structure of GaAs(001) / $In_{.2}Ga_{.8}As$(001) Strained-Layer Superlattices

Letter of Intent

Jennchang Hwang , and Piero Pianetta

Stanford Synchrotron Radiation Laboratory, Stanford, CA 94305

L. Ralph Dawson

Sandia National Laboratories, Albuquerque, NM 87185

Glenn D. Kubiak, and Richard H. Stulen

Sandia National Laboratories, Livermore, CA 94550

Strained-layer superlattices (SLS's) represent a new class of "synthetic" materials having electrical and optical properties which can be tailored [1]. The successful growth of these materials using molecular beam epitaxy (MBE) has made it possible to control the interlayer lattice mismatch and the resulting strain profile in the SLS through compositional variation of the group III elements. By varying the strain within the SLS, control of important electronic properties can be achieved.

As yet, detailed experimental band structures have not been fully determined for any of the SLS ternary or quaternary alloys. It is well known that the valence band structure of the individual layers will shift as a function of composition. In addition, due to the lattice mismatch between layers, there will be a shift in the valence bands from the resulting strain. The intent of this study has been to determine the valence band dispersion for these materials and attempt to separate strain-induced effects from compositional-induced effects.

To examine the band structure of GaAs/$In_{.2}Ga_{.8}As$ strained-layer superlattices, we have employed angle-resolved photoemission using photon energies between 15 eV and 27 eV with an overall instrumental resolution of 0.25 eV. Both GaAs(001) and $In_{.2}Ga_{.8}As$(001) terminated SLS's have been examined. To separate the effects of compositional-induced shifts in the valence band structure from strain-induced shifts, photoemission from thick, strain-free GaAs(001) has been compared to photoemission from SLS's having 50 Å thick layers terminated either with GaAs(001) or $In_{.2}Ga_{.8}As$(001). The strain profile of the GaAs(001) terminated SLS [2-4] is comprised of tensile strain in the surface plane and compressive uniaxial strain along the surface normal direction, [001]. In contrast, the $In_{.2}Ga_{.8}As$(001) terminated layer has compressive strain in the surface plane and tensile uniaxial strain along [001].

Four representative samples were examined: (1) a 1.5 micron thick, strain-free, MBE-grown GaAs(001) layer on top of bulk n-type GaAs(001), (2) a GaAs(001) terminated SLS, (3) a $In_{.2}Ga_{.8}As$(001) terminated SLS, and (4) a single 50 Å thick layer of $In_{.2}Ga_{.8}As$(001) on bulk GaAs(001). Both of the superlattice samples consisted of alternating 50 Å thick layers of GaAs and $In_{.2}Ga_{.8}As$ grown on top of a thick $In_{.1}Ga_{.9}As$(001) buffer layer. These samples are characterized by an alternating 0.7% in-plane strain for each layer. For sample number 4, the $In_{.2}Ga_{.8}As$(001) layer has a 1.4% in-plane compressive strain.

Normal emission spectra using light incident at 45° with respect to the surface normal for strained and unstrained GaAs(001) are shown in Fig. 1. The two peaks near the valence band maximum which disperse with photon energy correspond to primary cone emission for the valence bands Δ_3,Δ_4, and Δ_1 [5,6]. The broad nondispersive peak at -6.8 eV (referenced to the valence band maximum), has been assigned previously [5-7] to transitions originating from X_3 critical point. Normal emission spectra obtained from the strained GaAs(001) terminated SLS layer are similar to those of unstrained GaAs. The subtle difference due to this 0.7% strain can be seen from the energy dispersion curves shown in Fig. 2. These dispersion curves were obtained from the data using the free electron-like final state model with an inner potential of - 7.7 eV [8,9]. The energy of the valence band maximum has been set equal to 0 for all samples represented in this figure. The dispersion curves show that the Δ_3, Δ_4 band of the strained layer is shifted up by as much as 0.2 eV near $k \sim 0.3\ k_{\Gamma-X}$, but is relatively unchanged further from the zone center near $k \sim 0.7\ k_{\Gamma-X}$.

Normal emission spectra for the $In_{.2}Ga_{.8}As$ strained-layers at two different strains, 0.7% and 1.4%, were also recorded. Dispersion curves for these samples are shown in Fig. 2. Notice that as the strain is increased, the Δ_3,Δ_4 band is shifted to lower energy relative to the Δ_1 band. Moreover the shifted Δ_3,Δ_4 band of the 1.4% strained layer exhibits nearly parallel dispersion to the same band seen in 0.7% strained GaAs(001). As yet, measurements of unstrained $In_{.2}Ga_{.8}As$ have not been completed

In summary, we have examined the valence band dispersion for GaAs(001)/$In_{.2}Ga_{.8}As$(001) SLS's. The relative positions *and* the dispersion of the bands are observed to change as a function of strain for both GaAs(001) and $In_{.2}Ga_{.8}As$(001). The 0.7% in-plane tensile strain in the GaAs(001) layer causes an upward shift of the Δ_3,Δ_4 band relative to the Δ_1 band. In contrast, the in-plane compressive strain in the $In_{.2}Ga_{.8}As$(001) layer causes an energy lowering of the the Δ_3,Δ_4 band relative to the Δ_1 band. In both cases, strain seems to reduce the effective mass characterizing the dispersion of the Δ_3,Δ_4 band.

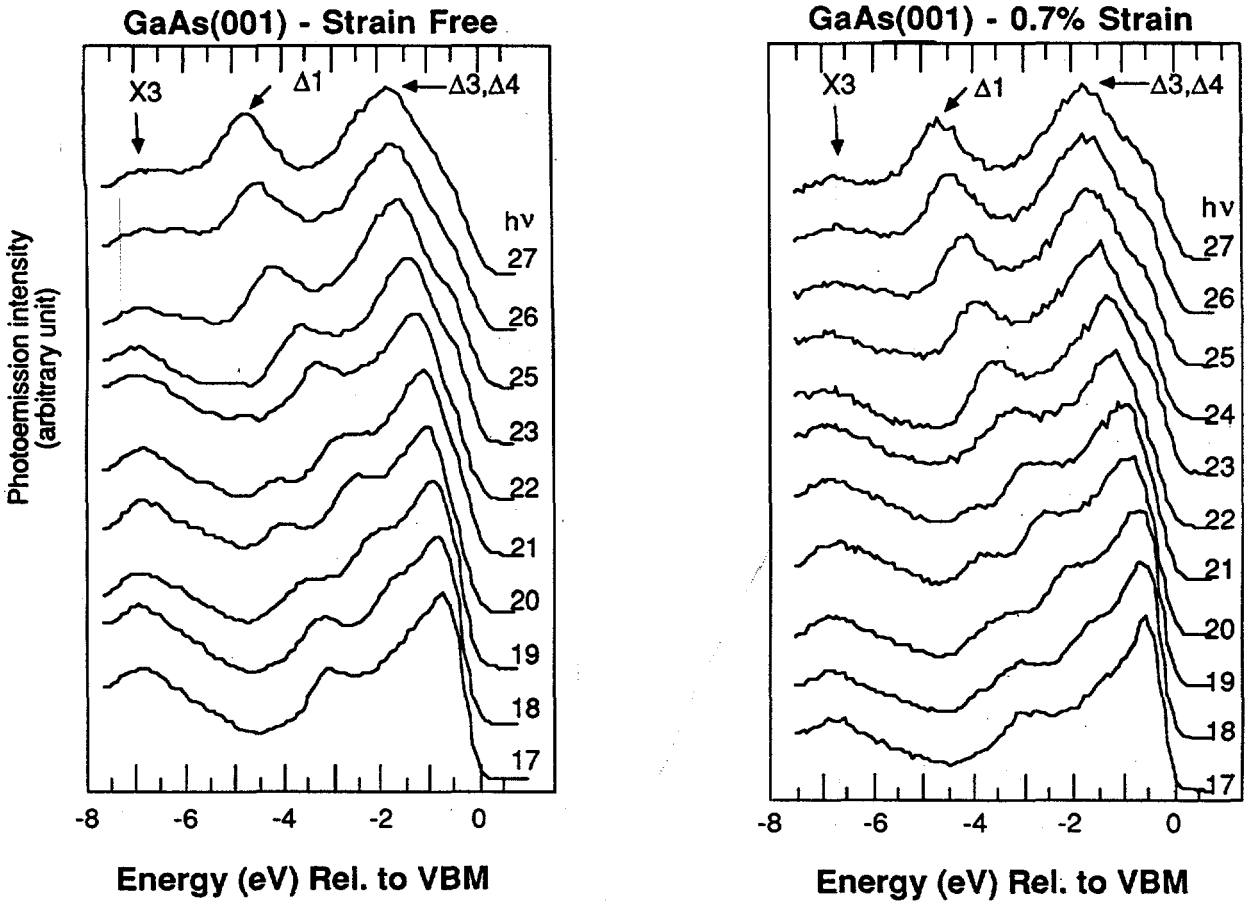

Figure 1

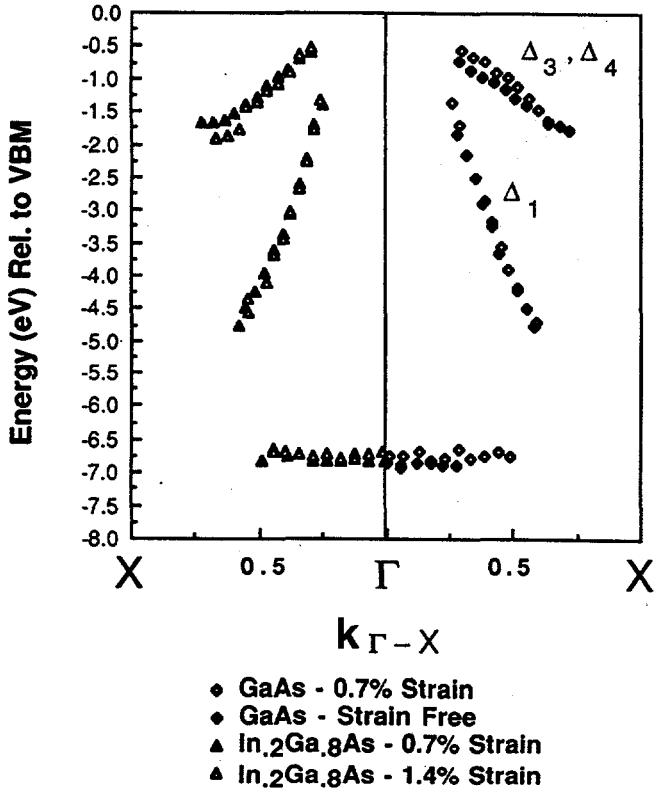

Figure 2

Acknowledgments

We sincerely acknowledge helpful discussions with Dr. C. Van Der Walle and Prof. R.M. Martin. The assistance of K. Shih during the experiment and the technical support of the staff at Stanford Synchrotron Radiation Laboratory is appreciated. This work was supported in part by the U. S. Department of Energy under contract #DE-AC04-76DP00789.

References

1. G.C. Osbourn, J. Vac. Sci. Technol. **B1**(2), 379 (1983)
2. S.T. Picraux, L.R. Dawson, G.C. Osbourn, R.M. Biefield, and W.K. Chu, Appl. Phys.Letter **43**(11),1020 (1983)
3. S.T. Picraux, L.R. Dawson, G.C. Osbourn, Appl. Phys. Letter **43**(10), 930 (1983)
4. W.D.Laidig, C.K. Peng, and Y.F. Lin, J. Vac. Sci. Technol. **B2**(2), 181 (1984)
5. J.R. Chelikowsky and M.L. Cohen, Phys. Rev. **B14**,556 (1976)
6. T.C. Chiang, J.A. Knapp, M. Aono, and D.E. Eastman, Phys. Rev. **B21**, 3513 (1980).
7. G.P. Williams, F. Cerrina, J.Anderson, G.J. Lapeyre, R.J. Smith, J. Hermanson, and J.A. Knapp, Physica **117B&118B** , 350 (1983).
8. P.K. Larsen J.H. Neave, J. Phys. C., **12**, L869 (1979)
9. P. K. Larsen and J. F. Van Der Veen, Sol. State Comm. **40**,459(1981).

X THESES BASED ON RESEARCH AT SSRL

The following is a partial list of Ph.D theses based on experimental research at SSRL. It represents 114 theses from 19 universities.

	INSTITUTION	TITLE/ADVISOR
1986		
S.W. Robey	UC-Berkeley	"Local Surface Structures of c(2x2)S/Ni (011) and (2x2) S/Ge(111) Determined using ARPES" - (advisor - D.A. Shirley)
J. Nogami	Stanford University	"Rare Earth Metal/Semiconductor Interfaces and Compounds" - (advisor - E.I. Lindau)
E.B. Sirota	Harvard University	"X-ray Scattering Study of the Thickness Dependent Phase Diagram of Liquid Crystal Films" (advisor - P.S. Pershan)
A.L. Johnson	UC-Berkeley	"Platinum Surface Chemistry Studied by Thermal Desorption Spectroscopy and Near Edge X-ray Absorption Fine Structure: Absorbate Effects" (advisor - D.A. Shirley)
R.D. Lorentz	Stanford Unversity	"Structural Investigations of Amorphous Iron-Germanium Alloys using Synchrotron Radiation" (advisor-A.I. Bienenstock)
J.J. Hoyt	UC-Berkeley	"An Anomalous Small Angle X-ray Scattering Study of Phase Separation in the Al-Zn-Ag System" (advisor - D. DeFontaine)
J.C. Levin	Univ of Oregon	"Auger Transitions in Noble Gases Following Inner-Shell Ionization by Electron Bombardment and by Synchrotron Radiation" (Advisor - B. Crasemann)
N.W. Lytle	Brigham Young Univ	"Proton-Induced X-ray Emission, Proton-Induced Gamma-ray Emission, and X-ray Absorption Spectroscopy: Application to Environmental Analysis" (Advisor - N.F. Mangelson)
C.C. Bahr	UC-Berkeley	"Chemisorption Geometries of Sulfur on Copper and Molybdenum Surfaces: A Photoelectron Diffraction Study" (Advisor - D.A. Shirley)
T.A. Ferrett	UC-Berkeley	"Photoionization of Atoms and Small Molecules Using Synchrotron Radiation" (Advisor - D.A. Shirley)
P.A. Heimann	UC-Berkeley	"Near Threshold Studies of Photoelectron Satellites " (Advisor - D.A. Shirley)

M.G. Samant	Stanford University	"Atomic and Electronic Structure of Supported Monometallic and Bimetallic Clusters " (Advisor - M. Boudart)
D.J. Sajkowski	Stanford University	"Catalysis by Metals: Single Crystals, Supported or Unsupported Polycrystals, and Co-ordination Complexes" (Advisor - M. Boudart)
S.L. Cohen	Stanford University	"Variable Energy Photoelectron Spectroscopic Studies of d9 and d10 Metal Chloride and Oxide Surfaces" (Advisor - E.I. Solomon)
E.D. Specht	MIT	"Synchrotron X-ray Diffraction Studies of Translational and Orientational Order in Monolayer Krypton on Graphite" (Advisor - R.J. Birgeneau)
J.A. Silberman	Stanford University	"A Photoemission Study of the Electronic Structure and Oxidation Properties of Mercury Cadmium Telluride" (Advisors - I.Lindau/W.E. Spicer)
K.K. Chin	Stanford University	"Initial Stage of the Schottky Barrier Formation of Metal/III-V Semiconductor Interfaces" (Advisor - I. Lindau)
M.D. Williams	Stanford University	"The Effect of Chemical Reactivity and Charge Transfer on Gallium Arsenide (110) Schottky Barrier Formation" (Advisors - W.E.Spicer/ I.Lindau)

1985

K. Kim	Univ of Wash	"A Study of Basic Properties and Applications of EXAFS" (advisor - E.A. Stern)
R. Pro	UC-Berkeley	"Development of a Linear Gas-Proportional X-ray Detector System for Determination of Partial Structure Function in Al, Ag and Zn Alloys" (advisor - D. DeFontaine)
W.G. Petro	Stanford University	"Metal and Oxygen Interactions with III-VCompound Semiconductor Surfaces" (advisors - W. E. Spicer and I. Lindau)
E.N. Keller	Univ of Washington	"Magnetic X-ray Study of a Gadolinium-Iron Amorphous Alloy" (advisor - E.A. Stern)
G. Zhang	Stanford University	"Molybdenum Carbide Catalysts" (partially based on SSRL) (advisor - M. Boudart)
T.A. Smith	Stanford University	"Single Crystal Polarization X-ray Absorption Studies of Copper Complexes" (advisor - K.O. Hodgson)
J. R. Schoonover	Arizona State Univ	"Application of Time-Resolved X-ray Diffraction to Solid State Chemical Reactions" (advisor -S.H. Lin)

L.E. Klebanoff	UC-Berkeley	"Photoelectron Spectroscopy Studies of Cr(001) Surface Ferromagnetism and Near-Surface Antiferromagnetism" (advisor - D.A. Shirley)
J.G. Nelson	UC-Los Angeles	"The Electronic Structure of Gold Gallium Two and Gold Indium Two Intermetallic Compounds" (advisor - R.S. Williams)
J.J. Barton	UC-Berkeley	"Angle-Resolved Photoemission Extended Fine Structure" (advisor - D.A. Shirley)
T.A. Gibson	Stanford University	"Single Crystal Polarized X-Ray Absorption Edge Studies of Copper Complexes" (advisor - K.O. Hodgson)
M.A. Berding	Stanford University	"Calculation of Cu K-Edge Photoabsorption Spectra Using an Extended Continuum Multiple Scattered Wave Method" (advisors - K.O. Hodgson/S. Doniach)
1984		
D.A. McKeown	Stanford University	"Spectroscopic Study of Silica-Rich Glasses and Selected Minerals within the Sodium Aluminosilicate System" (advisor - G.E. Brown, Jr.)
C. E. Bouldin	Univ of Wash	"An EXAFS Study of Amorphous Ge and of the Fe Impurity in Silicon Nitride" (advisor - E.A. Stern)
J.S. Lee	Stanford University	"Catalysis of the Oxidation of Dihydroen by Supported Gold" (partially based on work at SSRL) (advisor - M. Boudart)
K.M. Choudhary	Stevens Institute	"Surface Sensitive Photoemission EXAFS: A New Structural Tool" (advisor - G.M. Rothberg)
S.G. Mochrie	MIT	"Structures and Transitions in Systems with Competing Interactions"(advisor - R.J.Birgeneau)
J.E. Penner-Hahn	Stanford University	"X-ray Absorption Studies of Metalloprotein Structure: Cytochrome P-450, Horseradish Peroxidase, Plastocyanin, and Laccase" (advisor - K.O. Hodgson)
M.K. Eidsness	Univ of Cincinnati	"EXAFS and XANES Studies of Gold in Complexes of Biological Significance" (advisor - R.C. Elder)
J. B. Kortright	Stanford University	"Structural Studies of Amorphous Mo-Ge Alloys Using Synchrotron Radiation" (advisor - A. Bienenstock)
R. S. Moog	Stanford University	"Fluorescence Quenching of Chlorophyllide- and Protoporphyrin-Protein Complexes by Electron Transfer" (advisor - S. G. Boxer)
J.A. Guest	Stanford University	"Studies of Molecular Photoion and Photofragment Alignment" (advisor - R. N. Zare)

B.B. Pate	Stanford University	"The Diamond Surface: Atomic and Electronic Structure" (advisors - W.E. Spicer/I. Lindau)
R.S. Weber	Stanford University	"Structure and Reactivity of Platinum Clusters Supported on Y-Type Zeolites" (advisor - M. Boudart)
G.D. Meitzner	Stanford University	"Characterization of Gold/Y-Zeolite and its Catalytic Activity in the H2 - O2 Reaction" (advisor - M. Boudart)
G.B. Bunker	Univ of Washington	"An X-ray Absorption Study of Transition Metal Oxides" (advisor - E.A. Stern)
1983		
J. Sanchez-Arrieta	Stanford University	"Structural Studies of Hydrodesulfurization Catalysts" (advisor - M. Boudart)
P.H. Kobrin	UC-Berkeley	"Atomic Photoelectron Spectroscoy Studies using Synchrotron Radiation" (advisor - D.A.Shirley)
J. Collett	Harvard University	"X-ray Scattering Study of Liquid Crystal Thin Films" (advisor - P.S. Pershan)
D.W. Lindle	UC-Berkeley	"Inner-Shell Photoemission from Atoms and Molecules using Synchrotron Radiation" (advisor-D.A. Shirley)
P.M. Stefan	Stanford University	"A Photoemission Study of the Electronic Structure and Surface Chemical Properties of Tungsten Carbide and of a Carbonized Tungsten Model Surface for Tungsten Carbide" (advisor - W.E. Spicer)
A.N. Mansour	N. Carolina State	"X-ray Absorption Studies of Silica-Supported Platinum Catalysts" (advisor - D.E. Sayers)
J.G. Tobin	UC-Berkeley	"Dimensionality and Its Effects Upon the Valence Electronic Structure of Ordered Metallic Systems" (advisor - D.A. Shirley)
C. Marques	Washington State U	"Thermal Motion of Surface Atoms in Silica Supported Platinum and Iridium Catalyst Clusters: An EXAFS Spectroscopy Study" (advisor -D.R. Sandstrom)
P.R. Findley	UC-Santa Barbara	"Optical Properties of PbF2 and PbCl2 at High Temperatures" (advisor - W.C. Walker)
M.R. Antonio	Michigan State	"Extended X-ray Absorption Fine Structure Studies of the Iron-Molybdenum Cofactor of Nitrogenase, the Three-Iron Ferredoxin II of Desulfovibrio Gigas, and of Synthetic Molybdenum- and Tungsten-Iron-Sulfur and Iron-Sulfur Model Systems (Part I) and Intercalation of Tetrathiafulvalene into Iron Oxycholoride (Part II)" (advisor - H. Eick)

G.B. Stephenson	Stanford University	"Early-Stage Phase Separation in Amorphous Solids: A Time-Resolved SAXS Study" (advisor - A.I. Bienenstock)
J.M. Tranquada	Univ of Washington	"X-ray Absorption Studies of Solids at High Pressure" (advisor - R. Ingalls)
D. Stearns	Stanford University	"Early Photo Luminescence Decay in Amorphous Hydrogenated Silicon" (advisor -A.I.Bienenstock)
S. Laderman	Stanford University	"Structural Studies of Amorphous Semiconductors Containing Transition Metals" (advisor A.I. Bienenstock)
M.S. Co	Stanford University	"X-ray Absorption Spectroscopy of Hemocyanin and Hemerythrin" (advisor - K.O. Hodgson)
S.D. Conradson	Stanford University	"X-ray Absorption Studies of the Molybdenum Site of Nitrogenase" (advisor - K.O. Hodgson)
R. Miake-Lye	Stanford University	"Anomalous X-ray Scattering as a Probe of Biological Structure" (advisor - K.O. Hodgson)
C.C. Parks	UC-Berkeley	"The Auger Decay Mechanism in Photon Stimulated Desorption of Ions from Surface" (advisor -D.A. Shirley)
D.B. Goodin	UC-Berkeley	"The Local Structure of Manganese in the Photosynthetic Apparatus and Superoxide Dismutase: An X-ray Absorption Study" (advisor -M. Klein)
1982		
M.G. Durrett	Rice University	"Study of KrCl/Kr2Cl Excited State Kininetics Using Synchrotron Radiation Excitation" (advisor - G.K. Walters)
M.L. Shek	Stanford University	"Electronic Structure of Platinum-Copper Surfaces and Chemisorption of Carbon Monoxide" (advisors - I. Lindau, W.E. Spicer)
P.R. Skeath	Stanford University	"Chemical Bonding Phenomena of Column 3 and 5 Adsorbates and Fermi Energy Stabilizaion Mechanisms on GaAs (110)" (advisors -I.Lindau/ W.E. Spicer)
M.H. Hecht	Stanford University	"Synchrotron Radiation Measurements of Subshell Photoionization Cross Sections: Techniques and Applications" (advisor - I. Lindau)
S.-J. Oh	Stanford University	"Resonance and Relaxation Effects in Photoemission Spectroscopy" (advisor - I. Lindau)
S.M. Brennan	Stanford University	"Surface EXAFS of Sulphur on Nickel" (advisor -A.I. Bienenstock)

R.O. Tatchyn	Stanford University	"The Introduction and Developmentof a New Method for Measuring the Optical Constants of Metals in the Soft X-ray Range" (advisor - I. Lindau)
P.A. Heiney	MIT	"Phase Transitions of 2D Atomic and Molecular Crystals" (advisor - R.J. Birgeneau)
D.H. Rosenblatt	UC-Berkeley	"High Resolution Electron Energy Loss Spectroscopy and Photoelectron Diffraction Studies of the Geometric Structure of Adsorbates on Single Crystal Metal Surfaces" (advisor - D.A.Shirley)
J.E. Pollard	UC-Berkeley	"Photoelectron Spectroscopy of Supersonic Molecular Beams" (advisor - D.A. Shirley)
S.H. Southworth	UC-Berkeley	"Atomic and Molecular Photoelectron and Auger Electron Spectroscopy Studies Using Synchrotron Radiation" (advisor - D.A. Shirley)
K. Jackson	Stanford University	"Photoion Fluorescence Polarization: A Study of Molecular Ionization Dynamics" (advisor - R.N. Zare)
V. Yachandra	Princeton University	"EXAFS Studies of Carbonic Anhydrase and Resonance Raman Spectroscopy of Iron-Sulfur Proteins" (advisor - T. Spiro)
1981		
J.M. Fine	Washington State U	"Structure and Stoichiometry in Highly Concentrated Aqueous Solutions of CuBr2" (advisor - D.R. Sandstrom)
C.-Y. Su	Stanford University	"Photoemission Studies of the Interaction of Oxygen with Solid Surfaces" (advisor - I.Lindau)
D.L. Weissman	Stanford University	"Oxygen Chemisorption and Water Synthesis on Palladium and Palladium-Gold; A Study by Thermal Desorption and Photoemission " (advisor - W.E. Spicer)
R.F. Davis	UC-Berkeley	"Angular Distribution and Atomic Effects in Condensed Phase Photoelectron Spectroscopy" (advisor - D.A. Shirley)
F. Kutzler	Stanford University	"Electronic Structure Calculations of Germanium, Molybdenum Chromium and Erbium Compounds Predicted K and L Edge Absorption Spectra" (advisor - K.O. Hodgson)
1980		
B. Bunker	Univ of Washington	"An X-ray Absorption Study of Tetrahedral Semiconductors" (advisor - E. Stern)

J.M. Lornston	Univ of Delaware	"Characterization of Pt/Al2O3 Catalysts by Extended X-ray Absorption Fine Struture" (advisors - J.R. Katzer/J.M. Schultz)
P.H. Fuoss	Stanford University	"Structural Studies of Amorphous Materials Using X-ray Anomalous Scattering" (advisor - A.I. Bienenstock)
D.J. Trevor	UC-Berkeley	"Photoelectron Photoion Molecular Beam Spectroscopy" (advisor - D.A. Shirley)
S.D. Kevan	UC-Berkeley	"Normal Emission Photoelectron Diffraction: A New Technique for Determining Surface Structure" (advisor - D.A. Shirley)
R.V. Taylor	UC-Santa Barbara	"Matrix Spectroscopy of Rare-Gas Oxides and Sulfides" (advisor - W.C. Walker)
P. Frank	Stanford University	"The Biochemistry of Transition Metals: Copper, Vanadium, and Iron" (advisor - K.O. Hodgson)
1979		
M. Breining	Univ of Oregon	"Precision Determining of Atomic Level Energies by Absorption Spectrometry with Synchrotron Radiation" (advisor - B. Crasemann)
F.A. de Parente	Univ of Oregon	"Measurement of the Inelastic Scattering Cross Section of Neon with Synchrotron Radiation" (advisor - B. Crasemann)
T.D. Bonifield	Rice University	"Time Resolved Spectroscopy of Krypton and Xenon Molecules Excited by Electron Impact and by Monochromatic Synchrotron Radiation" (advisor - G.K. Walters)
J.N. Miller	Stanford University	"Photoemission Studies of Adsorption and Oxidation of Selected Metals and Semiconductors" (advisor - I. Lindau)
D.T. Ling	Stanford University	"Angle-Integrated and Angle-Resolved Photoemission Studies of Chemisorption on Copper and Copper/Nickel" (advisors - I. Lindau/W.E.Spicer)
K.A. Mills	UC-Berkeley	"The Determination of Electronic States in Crystalline Semiconductors and Metals by Angle-Resolved Photoemission" (advisor - D.A.Shirley)
D.R. Denley	UC-Berkeley	"Determination of Morphology and Electronic Structure in Solids with 20-1000 eV Radiation" (advisor - D.A. Shirley)
E.D. Poliakoff	UC-Berkeley	"Time-Resolved Spectroscopy Using Synchrotron Radiation" (advisor - D.A. Shirley)
M.G. White	UC-Berkeley	"Photoelectron Spectroscopy of Heavy Molecules" (advisor - D.A. Shirley)

R.A. Rosenberg	UC-Berkeley	"Studies of Electron Correlation in the Photo-ionization Process" (advisor - D.A. Shirley)
T.D. Tullius	Stanford University	"Structures of Metal Complexes in Biological Systems: EXAFS Studies of Blue Copper Proteins, Xamthine Oxidase and Vanadocytes" (advisor - K.O. Hodgson)
1978		
C.M. Garner	Stanford University	"Surface and Interface Studies of Oxygen on Silicon, III-V Heterojunctions, Schottky Barriers" (advisors - I. Lindau, W.E. Spicer)
J.C. Phillips	Stanford University	"Crystal Structure Determination Using Synchrotron Radiation" (advisor - K.O. Hodgson)
P.W. Chye	Stanford University	"Photoemission Studies of the Oxidation of and Schottky Barrier Formation on GaSb, InP, and GaAs" (advisor - W.E. Spicer)
S.P. Cramer	Stanford University	"Chemical Application of X-ray Absorption Spectroscopy-Nitrogenase and Cytochrome P-450" (advisor - K.O. Hodgson)
T. Eccles	Stanford Universtiy	"X-ray Absorption Studies of Hemocyanin" (advisor - K.O. Hodgson)
R.S. Williams	UC-Berkeley	"Angle-Resolved Photoelectron Spectroscopy Applied to the Determination of the Surface Electronic Structure of Crystalline Metals" (advisor - D.A. Shirley)
P.S. Wehner	UC-Berkeley	"Valence Band Photoemission Studies of Clean Metals" (advisor - D.A. Shirley)
1977		
G.E. Ice	Univ of Oregon	"Measurements of X-ray Scattering Cross Sections of Hydrogen and Helium with Synchrotron Radiation" (advisor - B. Crasemann)
P.A. Pianetta	Stanford University	"Photoemission Studies of Solids Using Synchrotron Radiation" (advisor - W.E. Spicer)
S.H. Hunter	Stanford University	"A Structural Study of Amorphous Copper-Arsenic Triselenide Alloys using EXAFS" (advisor - A.I.Bienenstock)
G.R. Apai II	UC-Berkeley	"Photoemission Studies of Clean and Adsorbate Covered Metal Surfaces Using Synchrotron and UV Radiation Sources" (advisor - D.A. Shirley)

1976

K.Y. Yu	Stanford University	"Photoemission and Thermal Desorption Studies of the Adsorption of Simple Molecules on Transition Metals and Alloys" (advisor - W.E. Spicer)
F.R. McFeely	UC-Berkeley	"Relaxation and Cross Section Effects in Valence Band Photoemission Spectroscopy" (advisor - D.A. Shirley)

1975

P.E. Gregory	Stanford University	"Ultraviolet Photoemission Studies of the Surface States and Properties of the (110) Gallium Arsenide Surface, and of the Oxidation of Cesium" (advisor - W.E. Spicer)
B.M. Kincaid	Stanford University	"Synchrotron Radiation Studies of K-edge X-ray Photoabsorption Spectra: Theory and Experiment" (advisor - S. Doniach)

1974

C.A. Ashley	Stanford University	"Extended X-ray Absorption Fine Structure" (advisor - S. Doniach)

XI ACTIVE PROPOSALS

As of December 31, 1986 there were 137 active SSRL proposals. Proposals remain active for two years after their initial rating by the Proposal Review Panel. Since October 1974 SSRL has received a total of 1062 proposals. The Spokesperson for each proposal is underlined and their institution shown in parentheses. The letter suffix appended to the proposal number indicates the sub-panel of the Proposal Review Panel to which the proposal is assigned: Materials (M), Biology (B) or Vacuum Ultra-Violet (V). The small p indicates a program proposal.

No.	Received	Experimenters	Title
100M	9/7/83	*DARYL CROZIER* NEIL ALBERDING ROBERT B GREEGOR P VIRAN K R BAUCHSPIESS J E WHITMORE FARREL W LYTLE ROBERT L INGALLS ANDREW J SEARY (Simon Fraser University)	X-ray Absorption Studies of Disordered Systems
754Mp	6/13/82	*ROBERT B GREEGOR* R F HAAKER R C EWING FARREL W LYTLE (Boeing Company)	X-ray Spectroscopic Investigation of Metamict Minerals
761Bp	8/31/82	*ROBERT A SCOTT* STEPHEN CRAMER (University of Illinois)	XAS Studies on the Active Sites of Cytochrome c Oxidase
801Vp	2/4/83	*JOACHIM STOHR* ROBERT J MADIX D A OUTKA (IBM Research Laboratory)	Surface NEXAFS and EXAFS Studies of Complex Molecules
806Mp	3/1/83	*RICHARD C ELDER* WILLIAM R HEINEMAN (University of Cincinnati)	XASEGS: X-ray Absorption Spectroscopy of Electrochemically Generated Species, A New Technique
810Vp	3/7/83	*WOLFGANG EBERHARDT* E W PLUMMER (Exxon Research & Engineering)	Fragmentation of Organic Molecules Following Soft X-Ray Excitation
814Mp	3/14/83	*ROBERT D LORENTZ* ARTHUR I BIENENSTOCK (3M Central Research Laboratory)	Structural Investigations of Amorphous Fe(x)Ge(1-x) Alloys
833Mp	9/1/83	*MICHEL BOUDART* J SANCHEZ ARRIETA (Stanford University)	In Situ Characterization of Hydroprocessing Catalysts by X-Ray Absorption Spectroscopy

837Mp 9/1/83	*J D LITSTER* S KUMAR J D BROCK B D LARSON (MIT)	Structure of Micellar Liquid Crystals
839Mp 9/1/83	*S H LIN* T GROY A HOLLADAY L EYRING (Arizona State University)	X-ray Diffraction from Specimens Undergoing Solid State Chemical Reactions
840Bp 9/1/83	*MELVIN P KLEIN* VITTAL I YACHANDRA RALPH D BRITT ANN MCDERMOTT R GUILES KENNETH SAUER S UN (Lawrence Berkeley Laboratory)	X-Ray Spectroscopy of Manganese and Iron in Chloroplasts
844Mp 9/6/83	*GOPAL K SHENOY* D L PRICE TIMOTHY I MORRISON S SUSMAN (Argonne National Laboratory)	Structural Study of Silicon and Germanium Chalcogenide Glasses
846Bp 9/8/83	*STEVEN G BOXER* RICK MOOG LARRY TAKIFF ATSUO KUKI PAT SANTANGELO (Stanford University)	Time Resolved Fluorescence Studies of Photosynthetic Reaction Centers and Models
849Mp 9/19/83	*ALAIN FONTAINE* LANE C WILSON KARL F LUDWIG WILLIAM K WARBURTON JEFF J HOYT (Universite de Paris-Sud)	Determination of F' in Semiconductors Using a Prism
857Mp 9/23/83	*FABIO COMIN* J M PHILLIPS PAUL H CITRIN (Istituto di Struttura Della Materia)	Structure and Nucleation Mechanism of Transition Metal Silicide Using SEXAFS
868M 2/24/84	*JAMES B BOYCE* THEODORE H GEBALLE T CLAESON (Xerox)	Local Distortions and Atomic Displacements in A-15 Compounds and Alloys
882Mp 3/1/84	*MATI BLOCH* PETER M EISENBERGER (Argonne National Laboratory)	Structural Studies of Organic Thin Films on the Solid Gas and Liquid Gas Interface

897Vp	4/3/84	*GERALD M ROTHBERG* MARTIN L DENBOER INGOLF LINDAU (Stevens Institute of Technology)	Spin Polarized Photoelectron Studies of Magnetism in Solids (SPEXAFS)
898Mp	5/3/84	*L D GIBBS* JOHN D AXE DAVID MONCTON KEVIN L D'AMICO JAKOB BOHR (Brookhaven National Laboratory)	Magnetic X-Ray Scattering from HO
906Bp	8/29/84	*DALE E SAYERS* E A STERN PAULINE HARRISON ELIZABETH C THEIL KENNETH RAYMOND (North Carolina State University)	X-Ray Absorption Studies of the Protein-Iron Interaction in Ferritin
908Vp	8/31/84	*ROSS D BRINGANS* ROGER I G UHRBERG J E NORTHRUP ROBERT Z BACHRACH (Xerox)	Influence of Surface Reconstruction on Electronic Properties of Semiconductor Surfaces
910Mp	8/31/84	*CHARLES E BOULDIN* M I BELL R A FORMAN (National Bureau of Standards)	Structural Studies of Ion Implants in III-V Semiconductors with Reflectance EXAFS
922Bp	9/6/84	*RICHARD C ELDER* KATHERINE TEPPERMAN (University of Cincinnati)	Gold-Based Antiarthritis and Anticancer Drugs and Metabolites: XAS, WAXS, DAS
925B	9/6/84	*STEVE D CONRADSON* J A KOVACS RICHARD H HOLM J K BASHKIN (Los Alamos National Laboratory)	Characterization of the Mo Site in Nitrogenase by XAS Studies of Relevant Synthetic Compounds
928Mp	9/11/84	*PETER M EISENBERGER* KENG S LIANG (Exxon Research & Engineering)	Grazing-Incidence X-ray Scattering Program
935Vp	9/20/84	*INGOLF LINDAU* N NEWMAN S J EGLASH JOE WOICIK WILLIAM E SPICER K SHIH TOMAS F KENDELEWICZ KRISTINE BERTNESS EZIO PUPPIN DANIEL FRIEDMAN K K CHIN M D WILLIAMS PETER MAHOWALD	Electronic Structure, Chemistry, and the Fermi Level at Semiconductor Surfaces and Interfaces

		J J YEH JOEL SILBERMAN C MCCANTS T CHIANG S LIST CARLO R CARBONE JUN NOGAMI C BOWMAN (SSRL)	
940M	9/26/84	*KENG S LIANG* KARL F LUDWIG JOHN H SINFELT RUSSELL R CHIANELLI ARTHUR I BIENENSTOCK (Exxon Research & Engineering)	Anomalous X-ray Scattering of Supported Catalysts
941Vp	9/26/84	*LUCIO BRAICOVICH* O BISI STEFANO NANNARONE IVANO ABBATI MASSIMO SANCROTTI EZIO PUPPIN UMBERTO DEL PENNINO Z SHEN INGOLF LINDAU WILLIAM E SPICER CARLO CALANDRA (University of Milan)	Study of the Formation of Rare Earth/Elemental Semiconductor (Ge, Si) Interfaces and Compounds
943Vp	9/6/84	*DAVID A SHIRLEY* LAURA MEDHURST STEVEN W ROBEY LOUIS J TERMINELLO ALLEN L JOHNSON PHILIP A HEIMANN TONG LEUNG MARIA NOVELLA PIANCASTELLI JOHN J BARTON SHIHONG LIU BAOHUA NIU LAISHING WANG DENNIS W LINDLE XUN-SHENG ZHANG CHARLES C BAHR SEHUN KIM ALEXIS SCHACH V WITTENAU ERNESTO PAPARAZZO ZHENG-QING HUANG TRICIA FERRETT (Lawrence Berkeley Laboratory)	Electron Spectroscopy of Gases, Solids, and Surfaces
947V	10/15/84	*PAUL H CITRIN* FABIO COMIN (AT&T Bell Laboratories)	Proposal to Perform SEXAFS from Substrate Surfaces

954Mp	12/18/84	*R PETKOVIC-LUTON* JULIA WEERTMAN PETER M EISENBERGER (Exxon Research & Engineering)	A SAXS Study of Grain Boundary Cavitation in Internally Oxidized Copper Using Anomalous Scattering
956Mp	2/27/85	*G P HUFFMAN* ROBERT B GREEGOR F E HUGGINS FARREL W LYTLE (University of Kentucky)	Applications of EXAFS Spectroscopy in the Steel and Coal Industries
957Bp	2/28/85	*DAVID H TEMPLETON* L K TEMPLETON (Lawrence Berkeley Laboratory)	Anomalous Scattering of X-rays
958V	3/1/85	*ROSS D BRINGANS* MARJORIE A OLMSTEAD ROBERT Z BACHRACH ROGER I G UHRBERG (Xerox)	Initial Formation of a Compound/Element Semiconductor Heterojunction
959Vp	3/1/85	*ROBERT Z BACHRACH* MARJORIE A OLMSTEAD ROSS D BRINGANS ROGER I G UHRBERG (Xerox)	Core Level and Near Edge Structure Study of Interface Formation
960Bp	3/4/85	*E A STERN* R H FELTON JOANN SANDERS-LOEHR JOSEPH GILBOA (University of Washington)	EXAFS Investigation of Metalloproteins
961Bp	3/4/85	*BRITTON CHANCE* Y ZHOU ALI NAQUI MARK CHANCE GRANT BUNKER LINDA S POWERS (UCSC/ICFS)	Structure/Function Studies of Oxidases, Peroxidases and Catalysts
962M	3/5/85	*MICHEL BOUDART* D J SAJKOWSKI (Stanford University)	An EXAFS Investigation of the Interaction of Silver Clusters with Dioxygen
963Vp	3/6/85	*JOACHIM STOHR* (IBM Research Laboratory)	NEXAFS and SEXAFS Studies by Means of X-ray Fluorescenc Detection: Local Structure Around Low-Z Atoms
964M	3/7/85	*GLENN A WAYCHUNAS* WAYNE A DOLLASE CHARLES R ROSS (Stanford University)	EXAFS Study of Short Range Order (SRO) in Chain Silicates
965B	3/8/85	*KEITH O HODGSON* BARBARA K BURGESS A LAWRENCE ROE (Stanford University)	Mo X-ray Absorption Spectroscopy Studies of Substrate of Nitrogenase

966B	3/11/85	*ROBERT A SCOTT* DAVID M DOOLEY (University of Illinois)	Cu XAS Studies of Enzymes Involved in Denitrification
967M	3/11/85	*A REFIK KORTAN* ROBERT J BIRGENEAU S G J MOCHRIE PAUL M HORN (AT&T Bell Laboratories)	Melting of a Two Dimensional Stripe Domain System
968M	3/14/85	*SEAN BRENNAN* PAUL H FUOSS PAUL L COWAN (SSRL)	Structure of Sub-Monolayer Sn on Ge(111) Using GIXS and XSW
969Bp	3/14/85	*ROBERT A SCOTT* STEPHEN P CRAMER (University of Illinois)	X-ray Absorption Spectroscopic Studies of Nickel-Containing Metalloenzymes
970B	3/19/85	*KEITH O HODGSON* CHARLES R CANTOR A GAAL S WAKATSUKI (Stanford University)	Time Resolved Small Angle X-ray Scattering of DNA Molecules During Pulsed Field GEL Electrophoresis
971Bp	3/19/85	*F SCOTT MATHEWS* R PAUL PHIZACKERLEY ETHAN A MERRITT PAUL H BETHGE N SHAMALA LOUIS LIM (Washington University)	Flavocytochrome B(2) Structure Analysis by Anomalous Scatterin Using Synchrotron Radiation
972M	3/25/85	*ZOPHIA U REK* W N CATHEY A D COX N SALIBI (SSRL)	EXAFS and XANES in TiCu(y)Fe(1-y)H(x) (y=0 to 1 and x=0 and 1)
973Mp	4/12/85	*CHARLES E BOULDIN* G K HUBLER E D DONOVAN R A FORMAN M I BELL (National Bureau of Standards)	EXAFS Study of Damage and Annealing of Ion Implanted Semiconductors
974B	5/9/85	*DUNCAN E MCREE* WAYNE A HENDRICKSON ELIZABETH D GETZOFF (Research Institute of Scripps Clinic)	Crystallographic Structure of Sulfite Reductase by Multiple Wavelength Measurements
975M	5/13/85	*STUART L COOPER* Y SAMUEL DING (University of Wisconsin)	Anomalous Small Angle X-ray Scattering Study of Ion Containing Polymers

976B	6/28/85	*W H ORME-JOHNSON* R PAUL PHIZACKERLEY WAYNE A HENDRICKSON ETHAN A MERRITT (MIT)	Anomalous Scattering Crystallography of a Bacterial Ferredoxin
977Mp	7/29/85	*MICHEL BOUDART* M SAMANT (Stanford University)	Anomalous Wide Angle X-ray Scattering Studies of Bimetallic Clusters on Amorphous Supports
978Mp	8/29/85	*EKKEHARD SINN* KEITH O HODGSON (University of Virginia)	Binuclear Metalloenzymes: Purple Acid Phosphatases and Urease
979M	8/30/85	*QUINTIN C JOHNSON* JOHN H KINNEY MONTE NICHOLS ULRICH BONSE (Lawrence Livermore National Laboratory)	High Resolution Tomography: Imaging of Crystalline Phases
980M	8/30/85	*JOHN H KINNEY* C E VIOLET L E TANNER M J FLUSS R J BORG (Lawrence Livermore National Laboratory)	EXAFS Study of Atomic Short-Range Order in Au-Fe Alloys
981Bp	9/3/85	*JAMES O ALBEN* FRANK G FIAMINGO ALLAN A CROTEAU CRAIG F HEMANN STEPHEN P CRAMER KIMBERLY A POWELL (Ohio State University)	High Resolution EXAFS Spectroscopy of Iron and Copper Proteins
982M	9/3/85	*ROBERT L INGALLS* B HOUSER NEIL ALBERDING DARYL CROZIER (University of Washington)	X-ray Absorption Measurements of Bond Bending at High Pressures
983M	9/3/85	*ROBERT L INGALLS* M. LAUCKS DARYL CROZIER (University of Washington)	EXAFS Study of Compressed Amorphous Semiconductors
984M	9/3/85	*ROBERT L INGALLS* K R BAUCHSPIESS DARYL CROZIER (University of Washington)	X-ray Absorption Study of Pressure Induced Valence Instabilities
985M	9/3/85	*GRAYSON H VIA* AMAL K GHOSH JAMES M BROWN (Exxon Research & Engineering)	EXAFS Study of Pt/Y Zeolite Catalyst

986B	9/3/85	*MELVIN P KLEIN* RALPH D BRITT R GUILES VITTAL I YACHANDRA JAMES A FEE ANN MCDERMOTT SUSAN DEXHEIMER (Lawrence Berkeley Laboratory)	X-ray Spectroscopy of Manganese and Iron in Superoxide Dismutases
987M	9/3/85	*ROBERT R RYAN* E M LARSON FARREL W LYTLE P G ELLER ROBERT B GREEGOR A SATTELBERGER (Los Alamos National Laboratory)	XAFS Study of Heterobimetallic Actinide-Transition Metal Complexes
988M	9/3/85	*P G ELLER* E M LARSON J D PURSON ROBERT B GREEGOR ROBERT R RYAN FARREL W LYTLE (Los Alamos National Laboratory)	XAFS Study of Actinide Site Speciation in Nuclear Waste Storage Media
989M	9/3/85	*P G ELLER* ROBERT R RYAN D CURTIS FARREL W LYTLE E M LARSON ROBERT B GREEGOR (Los Alamos National Laboratory)	XAFS Study of Fission Product Behavior at the Oklo Natural Fission Reactor
990B	9/3/85	*THOMAS G SPIRO* TAKASHI YONETANI LINDA S POWERS B M HOFFMAN (Princeton University)	EXAFS Studies of Fe, Mn and Fe, Co Hybrid Hemoglobins
991Bp	9/4/85	*RICHARD C ELDER* EDWARD A DEUTSCH (University of Cincinnati)	Technetium and Rhenium Imaging Agents and Therapeutic Radiopharmaceuticals
992B	9/4/85	*ROBERT A SCOTT* WARREN KAPLAN (University of Illinois)	Use of Temperature Dependent EXAFS to Improve Coordination Number Determination
993B	9/4/85	*ROBERT A SCOTT* LAWRENCE I KRUSE (University of Illinois)	Copper EXAFS Spectroscopy of Non-Blue Copper Proteins. Dopamine Beta-Monooxygenase
994Mp	9/5/85	*GLENN A WAYCHUNAS* GORDON E BROWN, JR (Stanford University)	High Temperature EXAFS Study of Fe and Ca in Silicate Crystals and Melts

995Mp	9/6/85	*A LAWRENCE ROE* JAMES O LECKIE GLENN A WAYCHUNAS KEITH O HODGSON GEORGE A PARKS GORDON E BROWN, JR KIM F HAYES (Stanford University)	XAS Study of Cation Adsorption at Aqueous/Oxide Interface
996M	9/10/85	*I K ROBINSON* PAUL H FUOSS W K WASKIEWICZ P A BENNETT (AT&T Bell Laboratories)	X-ray Structure Determination of Si(111) 7X7
997M	9/10/85	*I K ROBINSON* ROBERT J BIRGENEAU P J ESTRUP M ALTMAN (AT&T Bell Laboratories)	The Surface Phase Transition of Clean W(100)
998M	9/10/85	*K K CHAN* KENG S LIANG G J HUGHES PETER M EISENBERGER (Brookhaven National Laboratory)	Order-Disorder Transition of Adsorbates on Nickel
999Mp	9/10/85	*GORDON E BROWN, JR* W A JACKSON GLENN A WAYCHUNAS C W PONADER S ROTHFUS (Stanford University)	EXAFS Study of Trace Element Environments in Quenched Silicate Melts of Geochemical Interest
1000Mp	9/11/85	*FARREL W LYTLE* ROBERT B GREEGOR (Boeing Company)	Characterization of Surfaces by Electron Yield EXAFS at Atomspheric Pressure
1001Mp	1/1/86	*PETER M EISENBERGER* J M NEWSAM S K SINHA KENG S LIANG C R SAFINYA DAVID MONCTON JOHN H SINFELT GRAYSON H VIA (Exxon Research & Engineering)	EXXON PRT Proposal - Beam Line VI
1002M	9/11/85	*IAN D RAISTRICK* FARREL W LYTLE (Los Alamos National Laboratory)	EXAFS Studies of Perfluorinated Ion Exchange Membranes
1003B	9/24/85	*JAMES E PENNER-HAHN* W D FRASCH V L PECORARO (University of Michigan)	Manganese XAS of Purified Photosynthetic Oxygen Evolving Complexes

1004B	10/4/85	*KEITH O HODGSON* R PAUL PHIZACKERLEY ETHAN A MERRITT BRITT HEDMAN HANS C FREEMAN (Stanford University)	Crystallographic Studies of the Cucumber Basic Protein Using Synchrotron Radiation
1005B	10/4/85	*SEBASTIAN DONIACH* A MITRA S WAKATSUKI KEITH O HODGSON ROBERT M STROUD (Stanford University)	Cation Binding in Bacteriorhodopsin
1006B	10/4/85	*BRITTON CHANCE* L PARKHURST B VALLEE S M KHALID LINDA S POWERS GRANT BUNKER GERD ROSENBAUM GUANG ZHANG HERMAN WINICK (UCSC/ICFS)	Flow Apparatus Tests of Hemoprotein Reactions at High Beam Intensities
1007B	10/4/85	*BRITTON CHANCE* L PARKHURST MARK CHANCE LINDA S POWERS S M KHALID Y ZHOU GERD ROSENBAUM GRANT BUNKER R LOBRUTTO (UCSC/ICFS)	Low Temperature Photolysis/Recombination of Hemoproteins Under Conditions of Nuclear Tunneling
1008Mp	10/4/85	*WILLIAM K WARBURTON* KARL F LUDWIG ARTHUR I BIENENSTOCK (University of Southern California)	Binary Liquid Structures Determined by Anomalous X-ray Scattering
1009M	10/4/85	*ZOPHIA U REK* R K ROUTE R S FEIGELSON (SSRL)	A Study of the Defect Structure in CdTe Crystals Using Synchrotron Radiation Topography
1010M	10/14/85	*C R SAFINYA* G SMITH N A CLARK BILL VARADY (Exxon Research & Engineering)	Synchrotron Studies of Freely Suspended Discotic and Ordered Microemulsion Strands
1011M	10/14/85	*J D BROCK* J D LITSTER ROBERT J BIRGENEAU (MIT)	Bond Orientational Order in Tilted Hexatic Liquid Crystal Films

1012B	11/4/85	*ROBERT H FAIRCLOUGH* SEBASTIAN DONIACH KEITH O HODGSON STEVEN R HUBBARD D RICHMAN (University of Chicago)	Membrane X-Ray Diffraction Studies of the Acetylcholine Receptor
1013Vp	11/18/85	*FRANCESCO SETTE* J E ROWE JOHN M POATE (AT&T Bell Laboratories)	NEXAFS and EXAFS Studies of Shallow Inpurities in Semiconductors by Soft X-ray Fluorescence
1014M	12/27/86	*NOLAN MANGELSON* FARREL W LYTLE (Brigham Young University)	Identification of Chemical Compounds in Airborne Particulates by X-Ray Absorption Spectroscopy
1015Vp	2/28/86	*JOHN L GLAND* FRANCISCO ZAERA DANIEL A FISCHER (Exxon Research & Engineering)	The Structure and Reactivity of Adsorbed Intermediates Using NEXAFS and SEXAFS
1017M	3/3/86	*JAMES B BOYCE* FRANK G BRIDGES J C MIKKELSON (Xerox)	Local Structure of Icosahedral Materials
1018Mp	3/3/86	*D DE FONTAINE* B CLARK JEFF J HOYT M KRAITCHMAN B E C DAVIS (University of California)	Diffusion in Ternary Multilayer Thin Films
1019B	3/3/86	*F SCOTT MATHEWS* R PAUL PHIZACKERLEY LOUIS LIM ETHAN A MERRITT (Washington University)	Crystallographic Study of Amicyanin by Anomalous Scattering Using Synchrotron Radiation
1020M	3/3/86	*OWEN MELROY* LESSER BLUM JOSEPH G GORDON GARY BORGES (IBM Research Laboratory)	In Situ Surface EXAFS of Monolayers on Silver Electrodes
1021Mp	3/3/86	*WILLIAM PARRISH* GEORGE WILL CURT ERICKSON MAURIZIO BELLOTTO MICHAEL HART TING C HUANG (IBM Research Laboratory)	Synchrotron X-ray Polycrystalline Diffractometry
1022Vp	3/3/86	*EDWARD I SOLOMON* KRISTINE BUTCHER STEVE V DIDZIULIS JIAN-YI LIN (Stanford University)	UPS Studies of the Coordination Chemistry of Metal Oxides, Chlorides and Sulfides

1023Vp 3/4/86	*ROBERT J MADIX* J SOLOMON PAUL STEVENS C M FRIEND E BALDWIN (Stanford University)	Structure and Bonding of Molecules and Intermediates on Metal Surfaces
1024M 3/4/86	*J V ACRIVOS* S C WEAVER M CHEN LEI A D COX S S P PARKIN P ZIA (California State University)	Study of Organic Metal Anion Structure
1025M 3/4/86	*S C WEAVER* M CHEN LEI A D COX J V ACRIVOS P ZIA (California State University)	Structure of Multiple Valence Compounds such as Prussian Blue vs Temperature
1026M 3/4/86	*DONALD R SANDSTROM* FARREL W LYTLE (Boeing Company)	Transition Metal Ion Complexes in the Gas Phase
1027Bp 3/5/86	*STEVE D CONRADSON* BASIL SWANSON WILLIAM WOODRUFF (Los Alamos National Laboratory)	Dispersive XAS Development: Time Resolved and Diamond Anvil Applications
1028Vp 3/5/86	*JIM ALLEN* INGOLF LINDAU (Xerox)	High-Photon Flux Photoemission Studies of Narrow Band Materials
1029B 3/5/86	*MICHAEL SEUL* SRIRAM SUBRAMANIAM (AT&T Bell Laboratories)	X-ray Diffraction by Molecular Films on Solid Substrates in Aqueous Environment
1030Bp 3/17/86	*STEPHEN P CRAMER* W CLELAND E I STEIFEL GRAHAM N GEORGE L S SOLMONSON B E SMITH M WW ADAMS V MINAK J ENEMARK (Schlumberger-Doll Research)	Soft X-ray Spectrocopy of Molybdenum Enzymes, Cofactors and Model Compounds
1031M 3/18/86	*JAMES E PENNER-HAHN* LEVI THOMPSON M DAVID CURTIS OSWALDO BARALT (Univeristy of Michigan)	XAS of Synthetic Models for Hydrodesulfurization Catalysts

1032M 3/19/86	*CHARLES E BOULDIN* P BOOLCHAND (National Bureau of Standards)	EXAFS Study of Local Chemical Coordination of Cation and Anion Sites in Chalcogenide Glass
1033M 3/19/86	*JAMES E PENNER-HAHN* GEOFFREY WALDO ROBERT MK CARLSON (University of Michigan)	XAS Determination of the Chemical Forms of Sulfur in Petroleums
1034Mp 3/4/86	*PETER S PERSHAN* ERIC SIROTA SUZANNE AMADOR L B SORENSEN (Harvard University)	Structure and Phase Transitions of Hexatic Phases in Thin Liquid Crystal Films
1035B 4/14/86	*JAMES E PENNER-HAHN* HIM-TAI TSANG DAVID P BALLOU JAMES A FEE CHRISTOPHER J BATIE (University of Michigan)	XAS Investigations of Rieske-Like Iron Sulfur Centers
1036M 4/14/86	*BERND CRASEMANN* ROGER CARR S L SORENSEN S B WHITFIELD GEORGE S BROWN W JITSCHIN G BRADLEY ARMEN U WERNER (University of Oregon)	Coster-Kronig Transition Probabilities
1037M 5/19/86	*TIMOTHY M HAYES* D L WILLIAMSON G KRAUSS (Colorado School of Mines)	Grain Boundary Segregation of Impurities in Iron and Steel
1038M 5/19/86	*TIMOTHY M HAYES* P GIBART D L WILLIAMSON (Colorado School Mines)	Deep Donors in Gallium Aluminum Arsenide Semiconductor Alloys
1039B 6/3/86	*STEPHEN P CRAMER* ROBERT A SCOTT GRAHAM N GEORGE TERRENCE G FREY ROGER C PRINCE (Schlumberger-Doll Research)	Polarized XANES and EXAFS of Cytochrome Oxidase in Hydrated, Oriented Mitochondrial Multilayers
1040B 6/3/86	*RUSSELL HILLE* STEPHEN P CRAMER (Ohio State University)	X-Ray Absorption Spectroscopy of Xanthine Oxidase
1041B 9/3/86	*ROBERT A SCOTT* MARLY EIDSNESS (University of Illinois)	Measurement of Metal-Metal Distances in Proteins by X-ray Anomalous Scattering

1042B 9/3/86	*BRITTON CHANCE* DAVID AULD BARTON HOLMQUIST JAMES RIORDAN MARK CHANCE LINDA S POWERS B VALLEE (UCSC/ICFS)	Studies of Intermediates in the Mechanism of Carboxypeptidase-a
1043B 9/3/86	*BRITTON CHANCE* PETER REICHARD GUANG ZHANG S M KHALID ALI NAQUI GRANT BUNKER BRITT-MARIE SJOBERG (UCSC/ICFS)	X-Ray Absorption Spectroscopy of Iron-Iron Interactions: Ribonucleotide Reductase
1044M 9/3/86	*MATTHEW A MARCUS* CHING-LONG TSAI J BEVK (AT&T Bell Laboratories)	Structural Effects of Ultrahigh Strains and Dislocatio Densities
1045M 9/3/86	*MATTHEW A MARCUS* CHING-LONG TSAI (AT&T Bell Laboratories)	Multiple and Unusual Siting in Dilute Solid Solutions
1046B 9/3/86	*EDWARD RUBENSTEIN* JOHN GIACOMINI GEORGE S BROWN HERBERT D ZEMAN ROBERT HOFSTADTER W THOMLINSON JOHN OTIS ALBERT C THOMPSON DONALD C HARRISON ROBERT KERNOFF HELEN GORDON (Stanford University)	Iodine Dichromography with Monochromatic X-ray Beams for Angiography
1047M 9/3/86	*ROBERT L INGALLS* J FREUND DARYL CROZIER (University of Washington)	High Pressure Transition Mechanisms via EXAFS
1048Mp 9/11/98	*CAROLINE KILBOURNE* SEAN BRENNAN ARTHUR I BIENENSTOCK (Stanford University)	High Resolution Compton Profiles of Iron and Silicon
1049Mp 9/11/86	*ROBERT B GREEGOR* R C EWING B C CHAKOUMAKOS FARREL W LYTLE (Boeing Company)	X-ray Spectroscopic Investigation of Radiation Damaged Materials

1050Mp	9/11/86	*GLENN A WAYCHUNAS* MICHAEL J APTED JAMES E PENNER-HAHN GREG J EXARHOS (Stanford University)	X-ray Anomalous Scattering and EXAFS Study of Heavy Metal Complexes in Aqueous Solutions
1051M	9/11/86	*GLENN A WAYCHUNAS* LAWRENCE R BERNSTEIN (Stanford University)	Crystal and Aqueous Chemistry of Germanium in Geochemically Important Systems
1052M	9/11/86	*IVAN SELLIN* D A CHURCH H CEDERQUIST J LEVIN S B ELSTON C S O (Oak Ridge National Laboratory)	Measurement of Recoil Energies of Multiply Charged Recoil Ions and Molecular Fragments
1053B	9/15/86	*ROBERT A SCOTT* DAVID M DOOLEY (University of Illinois)	Copper EXAFS Spectroscopy of Non-Blue Copper Proteins. Amine Oxidases
1054M	9/15/86	*RICHARD W RYON* SUZANNE FLETCHER JOHN H KINNEY HARRY E MARTZ ROBERT A DAY (Lawrence Livermore National Laboratory)	X-Ray Induced Photoacoustic Emission
1055B	9/15/86	*KEITH O HODGSON* A LAWRENCE ROE W E NEWTON FRANK A SCHULTZ BRITT HEDMAN STEPHEN F GHELLER (Stanford University)	XAS of Iron-Molybdenum Cofactor of Nitrogenase under Electrochemical Control
1056Mp	9/16/86	*S R STOCK* ZOPHIA U REK B COULMAN Y H CHUNG (Georgia Institute of Technology)	Section Topographic Strain Mapping Using Synchrotron White Radiation
1057B	1/16/86	*DOUGLAS S CLARK* GREGG A MARG (University of California)	The Role of Metals in the Mechanism of Glucose Isomerase
1058M	9/16/86	*PAUL M HORN* GLENN HELD (IBM Research Laboratory)	Roughening Transition of Metal Surfaces
1059M	9/16/86	*MURLI H MANGHNANI* L C MING (University of Hawaii)	In Situ High P-T Equation-of-State, Phase Transformations and Kinetics Studies on Mantle Mineral Phases using Synchrotron Radiation

1060Mp 9/16/86	*MARYBETH RICE* ARTHUR I BIENENSTOCK (Stanford University)	Structural Investigations of Layered Synthetic Microstructure and Binary Amorphous Alloys
1061Bp 9/16/86	*JAMES O ALBEN* CRAIG F HEMANN ALLAN A CROTEAU KIMBERLY A POWELL FRANK G FIAMINGO (Ohio State University)	Iron Porphyrin Models for EXAFS Analysis
1062Vp 10/1/86	*DONALD C LORENTS* R L SHARPLESS (SRI International)	Spectroscopy and Kinetics of Excited Gases

ROTATION CAMERA PROPOSALS

Access to the rotation camera facility for protein crystallography is through the submittal of a brief application which is reviewed by the Biology Sub-panel of the PRP on a short turnaround basis. The 37 rotation camera proposals active in 1986 are listed below.

1A15	3/21/85	*B. HEDMAN* K. O. HODGSON J. R. HELLIWELL R. P. PHIZACKERLEY E. A. MERRITT (SSRL)	Protein Micro-Crystal Diffraction and the Effects of Radiation Damage using Synchrotron Radiation
1A16	3/22/85	*J. R. RUBIN* T. KOSSIAKOFF (Genentech, Inc.)	High Resolution X-ray Data Collection on Human Recombinant Gamma-Interferon
1A17	4/01/85	*I. WILSON* E. STURA (Research Institute of Scripps Clinic)	Structure of Anti-Peptide Antibodies
1A18	4/05/85	*F. JURNAK* (University of California)	Rapid Transfer Colelction for EF-Tu
1A19	4/10/85	*S. KIM* B. GRAVES (University of California)	Structure of Metal-Binding Proteins
1A20	4/23/85	*M. H. HATADA* C. BYSTROFF (University of California)	Dihydrofolate Reductase Complexes

1A21	5/23/85	*C. CHANG* M. SCHIFFER D. TIEDE J. NORRIS (Argonne National Laboratory)	X-ray Analysis of a Membrane Protein of Photosynthetic Reaction Center from Rhodopseudomonas Sphareoids
1A22	6/24/85	*R. M. STROUD* J. F. MOORE (University of California)	A Natural, Membrane Active, Insecticidal Bacillus Thuringiensis Toxin at 1.5 A
1A23	10/15/85	*I. WILSON* E. STURA (Research Institute of Scripps Clinic)	Structures Determination of an Antibodies Selected Mutant DV5 of Influenza haemagglutinin A-PR-8-34
1A24	4/07/86	*B. LOW* P. W. CORFIELD W. RADDING R. T. LEE (Columbia University)	Cobrotoxin - X-ray Crystal Structure Data Collection
1A25	4/07/86	*C. E. BUGG* V. K. SENADHI (University of Alabama-Birmingham)	Data Collection of Modified Form of Human Gamma Interferon Crystal
1A26	4/15/86	*W. J. COOK* C. E. BUGG S. EALICK S. V. KUMAR (University of Alabama-Birmingham)	High Resolution Diffraction Studies of Ubiquitin
1A27	4/15/86	*P. M. FITZGERALD* N. B. MADSEN M. N. JAMES (University of Alberta)	Glycogen Debranching Enzyme
1A28	4/30/86	*J. M. SOWADSKI* S. S. TAYLOR X. NGUYEN-HUU (University of California)	Determination of Diffraction Limits for Two Crystal forms of Catalytic Subunit of Camp Dependent Protein Kinase
1A29	4/30/86	*L. WEAVER* S. RODERICK (University of Oregon)	Data Collection for Bacterial Luciferase
1A30	4/30/86	*P. B. SIGLER* R. SCHEVITZ Z. OTWINOWSKI C. LAWSON A. JOACHIMIAK (University of Chicago)	Data Collection for a Trip Repressor/Operator Complex
1A31	4/30/86	*M. G. ROSSMANN* C. STAUFFACHER M. LUO (Purdue University)	Diffraction Measurements from Virus Crystals

1A32	5/07/86	*A. YONATH* M. SAPER F. FROLOW I. MAKOWSKI (Weizmann Institute)	Diffraction Measurements from Ribosome Crystals
1A33	5/09/86	*D. E. MCREE* E. D. GETZOFF H. E. PARGE J. A. TAINER (Research Institute of Scripps Clinic)	Diffraction Photos of Pilin Protein Crystals
1A34	5/14/86	*R. O. FOX* H. M. MCCONNELL T. HYNES D. LEAHY (Stanford University)	Monoclonal Fab Fragment Data Collection
1A35	5/19/86	*P. M. COLMAN* W. G. LAVER (CSIRO)	Neuraminidase-Antibody Complexes
1A36	5/23/86	*C. D. STOUT* S. A. COLLETT A. ROBBINS (Research Institute of Scripps Clinic)	High Resolution Data Collection on Metallothionein
1A37	6/03/86	*E. D. GETZOFF* D. E. MCREE H. E. PARGE J. A. TAINER (Research Institute of Scripps Clinic)	Data Collection on Pilin Protein Crystals
1A38	6/18/86	*P. PHIZACKERLEY* E. A. MERRITT G. TIMOTHY G. MORGAN D. SLATER (SSRL)	Test of a Multi-Anode Microchannel Array (MAMA) Detector for Protein Crystallography on the SSRL Rotation Camera Facility
1A39	7/01/86	*W. T. WOLODKO* M. N. JAMES W. A. BRIDGER (University of Alberta)	Succinyl-CoA Synthetase
1A40	7/15/86	*S. EALICK* W. J. COOK S. V. NARAYANA (University of Alabama-Birmingham)	Molecular Structure of Uridine Phosphorylase
1A41	10/07/86	*P. B. SIGLER* R. SCHEVITZ R. MARMORSTEIN D. SCOTT (University of Chicago)	Diffraction Measurements on TRP Repressor - DNA Complex

1A42	10/07/86	*R. O. FOX* H. MCCONNELL T. HYNES D. LEAHY (Stanford University)	X-Ray Crystallography of ANO2 Fab: Hapten Complexes
1A43	10/07/86	*I. WILSON* E. STURA J. AREVALO J. RINI G. LAMBERT (Research Institute of Scripps Clinic)	The Structure of Antibodies, Antigens and Antibody-Antigen Complexes
1A44	10/07/86	*P. FITZGERALD* N. B. MADSEN M. N. JAMES (University of Alberta)	Data Collection for Glycogen Debranching Enzyme
1A45	10/07/86	*A. SZOKE* J. MADEY A. TORR (Lawrence Livermore National Laboratory)	X-Ray Holography
1A46	10/07/86	*S. KIM* Z. LI (University of California)	Native Diffraction Data Collection of Allophycocyanine
1A47	10/07/86	*S. KIM* C. H. KANG (University of California)	High Resolution Diffraction Data Collection of Thaumatin
1A48	10/07/86	*S. KIM* A. DEVOS (University of California)	Native and Derivative Diffraction Data Collection of F Protein
1A50	10/09/86	*C. E. BUGG* S. EALICK (University of Alabama-Birmingham)	Data Collection on Modified Form on Human Gamma Interferon Crystal
1A51	10/16/86	*M. H. HATADA* S. OATLEY (University of California)	Diffraction Measurements from Interleukin 2 and Interferon Alpha
1A52	12/12/86	*C. D. STOUT* S. A. COLLETT A. ROBBINS (Research Institute of Scripps Clinic)	High Resolution Data Collection on Aconitase

XII SSRL EXPERIMENTERS AND PROPOSALS BY INSTITUTIONS

As of December 31, 1986 there were 438 experimenters from 101 institutions officially involved with active proposals at SSRL. In addition, over a 100 others (graduate students, etc.) participated in work at the laboratory in collaboration with these scientists. United States institutions included 53 Universities, 14 private corporations and 12 government laboratories.

U.S. CORPORATIONS: 3M Central Research Laboratory, AT&T Bell Laboratories, Boeing Company, Chevron Oil Field Research Company, EXXON Research & Engineering, IBM Research Laboratory, MACROATOM, Inc., Palo AltoVeterans Hospital, Schlumberger Doll Research, Signetics Corporation, Smith Kline & French Laboratories, SRI International, UCSC/ICFS XEROX

U.S. LABORATORIES: Argonne National Laboratory, Brookhaven National Laboratory, Lawrence Berkeley Laboratory, Lawrence Livermore National Laboratory, Los Alamos National Laboratory, National Bureau of Standards, Naval Research Laboratory, Oak Ridge National Laboratory, Pacific Northwest Laboratory, Sandia National Laboratory, SSRL, Western Regional Research Center

U.S. UNIVERSITIES: Amherst College, Arizona State University, Brigham Young University, Brown University, California Institute of Technology, California State University, Carnegie Institute, Colorado School of Mines, Columbia University, Florida-Atlantic University, Georgia Institute of Technology, Harvard Medical School, Harvard University, Hunter College, CUNY, MIT, North Carolina State University, Northwestern University, Ohio State University, Oregon Graduate Center, Princeton University, Research Institute of Scripps Clinic, Stanford University, Stevens Institute of Technology, Texas A&M University, University of Alabama-Birmingham, University of Arizona, University of California (7 campuses), University of Chicago, University of Cincinnati, University of Colorado, University of Hawaii, University of Illinois, University of Kentucky, University of Michigan, University of Nebraska, University of Nevada, University of New Mexico, University of Oregon, University of Pennsylvania, University of Puerto Rico, University of South Florida, University of Southern California, University of Virginia, University of Washington, University of Wisconsin, Washington University

FOREIGN INSTITUTIONS: Chalmers Institute of Technology, CNRS, Istituto di Fisica del Politecnico, Istituto di Struttura della Materia, Karolinska Institute, King's College, Linkoping University, LNB, Medical Nobel Institute, Simon Fraser University, Universita di Milano, Universita di Modena, Universita di Roma, Universitat Bielefeld, Universitat Bonn, Universite de Paris-Sud, University del Zulia, University of Dortmund, University of Sheffield, University of Sussex, University of Sydney, Weizmann Institute

SSRL EXPERIMENTERS AND PROPOSALS BY INSTITUTIONS

UNITED STATES INSTITIONS

AMHERST COLLEGE

D.M. DOOLEY	966,1053

ARGONNE NATIONAL LABORATORY

M. BLOCH	882
T.I. MORRISON	844
D.L. PRICE	844
G.K. SHENOY	844
S. SUSMAN	844
J. VICCARO	1074
E. ZIEGLER	1074

ARIZONA STATE UNIVERSITY

P.A. BENNETT	996
L. EYRING	839
T. GROY	839
A. HOLLADAY	839
S.H. LIN	839

AT&T BELL LABORATORIES

J. BEVK	1044
M. CHANCE	961,1007,1042
P.H. CITRIN	857,947
P.H. FUOSS	968,996
A.R. KORTAN	967
M.A. MARCUS	1044,1045
S.G.J. MOCHRIE	967
J.M. PHILLIPS	857
J.M. POATE	1013
L.S. POWERS	961,990,1006, 1007,1042
I.K. ROBINSON	996,997
J.E. ROWE	1013
F. SETTE	1013
M. SEUL	1029
W.K. WASKIEWICZ	996

BOEING COMPANY

R.B. GREEGOR	100,754,956, 987,988,989, 1000,1049
F.W. LYTLE	100,754,956, 987,988,989, 1000,1002, 1014,1026, 1049,1069
D.R. SANDSTROM	1026

BRIGHAM YOUNG UNIVERSITY

M.W. HILL	1069
N. MANGELSON	1014,1069

BROOKHAVEN NATIONAL LABORATORY

J.D.AXE	898
J. BOHR	898

BROOKHAVEN NATIONAL LABORATORY - (Continued)

K.K. CHAN	998
H. CHEN	1072
K.L. D'AMICO	898
D.A. FISCHER	1015
L.D. GIBBS	898
S.M. HEALD	1072,1073, 1074
M. SUENAGA	1073
W. THOMLINSON	1046
J.M. TRANQUADA	1073
F. ZAERA	1015

BROWN UNIVERSITY

M. ALTMAN	997
P.J. ESTRUP	997

CALIFORNIA INSTITUTE OF TECHNOLOGY

S.I. CHAN	1067
P.M. LI	1067

CALIFORNIA STATE UNIVERSITY

J.V. ACRIVOS	1024,1025
M. CHEN LEI	1024,1025
S.C. WEAVER	1024,1025
P. ZIA	1024,1025

CARNEGIE INSTITUTE

H.K. MAO	1064

CHEVRON OIL FIELD RESEARCH COMPANY

R. CARLSON	1033

COLORADO SCHOOL OF MINES

T.M. HAYES	1037,1038
G. KRAUSS	1037
D.L. WILLIAMSON	1037,1038

COLUMBIA UNIVERSITY

C.R. CANTOR	970
W.A. HENDRICKSON	974,976

EXXON RESEARCH & ENGINEERING

M.W.W. ADAMS	1030
J.M. BROWN	985
R.R. CHIANELLI	940
W. EBERHARDT	810
P.M. EISENBERGER	882,928,954, 998,1001
G.N. GEORGE	1030,1039
A.K. GHOSH	985
J.L. GLAND	1015
G.J. HUGHES	998

EXXON RESEARCH & ENGINEERING - (Continued)

K.S. LIANG	928,940,998, 1001
V. MINAK	1030
D. MONCTON	898,1001
J.M. NEWSAM	1001
R. PETKOVIC-LUTON	954
R.C. PRINCE	1039
C.R. SAFINYA	1001,1010
J.H. SINFELT	940,1001
S.K. SINHA	1001
E. SIROTA	1034
E.I. STEIFEL	1030
B. VARADY	1010
G.H. VIA	985,1001

FLORIDA-ATLANTIC UNIVERSITY

F.A. SCHULTZ	1055

GEORGIA INSTITUTE OF TECHNOLOGY

Y.H. CHUNG	1056
R.H. FELTON	960,1068
S.R. STOCK	1056

HARVARD MEDICAL SCHOOL

D. AULD	1042
B. HOLMQUIST	1042
J. RIORDAN	1042
B. VALLEE	1006,1042

HARVARD UNIVERSITY

S. AMADOR	1034
E. BALDWIN	1023
J. BASHKIN	925
C.M. FRIEND	1023
R.H. HOLM	925
J.A. KOVACS	925
P.S. PERSHAN	1034

HUNTER COLLEGE CUNY

M.L. DENBOER	897

IBM RESEARCH LABORATORY

M. BELLOTTO	1021
G. BORGES	1020
C. ERICKSON	1021
J.G. GORDON	1020
G. HELD	1058
P.M. HORN	967,1058
T.C. HUANG	1021
K.F. LUDWIG	849,940,1008
O. MELROY	1020
D.A. OUTKA	801
S.S.P. PARKIN	1024

IBM RESEARCH LABORATORY - (Continued)

W. PARRISH	1021
M. SAMANT	977
J. STOHR	801,963

LAWRENCE BERKELEY LABORATORY

C.C. BAHR	943
J.J. BARTON	943
R.D. BRITT	840,986
S. DEXHEIMER	986
T. FERRETT	943
R. GUILES	840,986
P.A. HEIMANN	943
A.L. JOHNSON	943
M.P. KLEIN	840,986
A. MCDERMOTT	840,986
E. PAPARAZZO	943
M.N. PIANCASTELLI	943
S.W. ROBEY	943
K. SAUER	840
D.A. SHIRLEY	0943
D.H. TEMPLETON	957
L.K. TEMPLETON	957
L.J. TERMINELLO	943
A.C. THOMPSON	1046
S. UN	840
A. SCHACH V WITTENAU	943
V.I. YACHANDRA	840,986

LAWRENCE LIVERMORE NATIONAL LABORATORY

J. AKELL	1064
R.J. BORG	980
R.A. DAY	1054
S. FLETCHER	1054
M.J. FLUSS	980
Q.C. JOHNSON	979,1064
J.H. KINNEY	979,980,1054
H.E. MARTZ	1054
R.W. RYON	1054
G.S. SMITH	1064
L.E. TANNER	980
G. TIRSELL	9901
C.E. VIOLET	980
M.J. WEBER	9901

LOS ALAMOS NATIONAL LABORATORY

S.D. CONRADSON	925,1027
D. CURTIS	989
P.G. ELLER	987,988,989
J.A. FEE	986,1035
E.M. LARSON	987,988,989
J.D. PURSON	988

LOS ALAMOS NATIONAL LABORATORY - Continued)

I.D. RAISTRICK	1002
R.R. RYAN	987,988,989
A. SATTELBERGER	987
B. SWANSON	1027
W. WOODRUFF	1027

MACROATOM, INC

F.E. HUGGINS	956

MIT

R.J. BIRGENEAU	967,997,1011
J.D. BROCK	837,1011
S. KUMAR	837
B.D. LARSON	837
J.D. LITSTER	837,1011
W.H. ORME-JOHNSON	976

3M RESEARCH CENTER

R.D. LORENTZ	814
C.-L. TSAI	1044,1045

NATIONAL BUREAU OF STANDARDS

M.I. BELL	910,973
C.E. BOULDIN	910,973,1032
P.L. COWAN	968
R.A. FORMAN	910,973
D.W. LINDLE	943

NAVAL RESEARCH LABORATORY

E.D. DONOVAN	973
G.K. HUBLER	973

NORTH CAROLINA STATE UNIVERSITY

D.E. SAYERS	906,1074
E.C. THEIL	906

NORTHWESTERN UNIVERSITY

B.M. HOFFMAN	990
J. WEERTMAN	954

OAK RIDGE NATIONAL LABORATORY

H. CEDERQUIST	1052
S.B. ELSTON	1052
J. LEVIN	1052
C. S O	1052
I. SELLIN	1052

OHIO STATE UNIVERSITY

J.O. ALBEN	981,1061
A.A CROTEAU	981,1061
F.G. FIAMINGO	981,1061
C.F. HEMANN	981,1061

OHIO STATE UNIVERSITY - (Continued)

R. HILLE	1040
K.A. POWELL	981,1061

OREGON GRADUATE CENTER

J. SANDERS-LOEHR	960

PACIFIC NORTHWEST LABORATORY

M.J. APTED	1050
G.J. EXARHOS	1050

PALO ALTO VETERANS HOSPITAL

J. GIACOMINI	1046
H. GORDON	1046

PRINCETON UNIVERSITY

T.G. SPIRO	990

RESEARCH INSTITUTE OF SCRIPPS CLINIC

A. AREVALO	1A61
S.A. COLLETT	1A52
E.D. GETZOFF	974,1A53, 1A58
G. LAMBERT	1A61
D.E. MCREE	974,1A53
H.E. PARGE	1A58,1A60
J. RINI	1A61
A. ROBBINS	1A52
U. SCHULZE-GAHMEN	1A61
C.D. STOUT	1A52
E. STURA	1A61
J.A. TAINER	1A53,1A58, 1A60
I. WILSON	1A61

SANDIA NATIONAL LABORATORY

M. NICHOLS	979

SCHLUMBERGER DOLL RESEARCH

S.P. CRAMER	761,969,981, 1030,1039, 1040

SIGNETICS CORPORATION

B. COULMAN	1056

SMITH KLINE & FRENCH LABORATORIES

L.I. KRUSE	993

SRI INTERNATIONAL

D.C. LORENTS	1062
R.L. SHARPLESS	1062

SSRL

A.I. BIENENSTOCK	814,849,940, 1008,1048, 1060
S. BRENNAN	968,1048
G.S. BROWN	1036,1046
R. CARR	1036
A.D. COX	972,1024,1025
B. HEDMAN	1004,1055
I. LINDAU	897,935,941, 1028
E.A. MERRITT	971,976,1004, 1019,1A38
R.P. PHIZACKERLEY	971,976,1004, 1019,1A38
Z.U. REK	972,1009,1056
H. WINICK	1006

STANFORD UNIVERSITY

L.R. BERNSTEIN	1051
K. BERTNESS	935
M. BOUDART	833,962,977, 1065,1071
C. BOWMAN	935
S.G. BOXER	846
G.E. BROWN, JR	994,995,999
K. BUTCHER	1022
C.R. CARBONE	935
T. CHIANG	935
K.K. CHIN	935
R.J. DAVIS	1065
S.V. DIDZIULIS	1022
S. DONIACH	1005,1012
S.J. EGLASH	935
R.S. FEIGELSON	1009
D. FRIEDMAN	935
T.H. GEBALLE	868
D.C. HARRISON	1046
K.F. HAYES	995
K.O. HODGSON	965,970,978, 995,1004,1005 1012,1055
R. HOFSTADTER	1046
S.R. HUBBARD	1012
W.A. JACKSON	999
T.F. KENDELEWICZ	935
R. KERNOFF	1046
C. KILBOURNE	1048
A. KUKI	846
J.O. LECKIE	995
J.-Y. LIN	1022
S. LIST	935
R.J. MADIX	801,1023
P. MAHOWALD	935
C. MCCANTS	935
R. MOOG	846

STANFORD UNIVERSITY - (Continued)

G. MORGAN	1A38
N. NEWMAN	935
J. NOGAMI	935
J. OTIS	1046
G.A. PARKS	995
C.W. PONADER	999
E. PUPPIN	935,941
M. RICE	1060
A.L. ROE	965,995,1055
S. ROTHFUS	999
R.K. ROUTE	1009
E. RUBENSTEIN	1046
D.J. SAJKOWSKI	962
P. SANTANGELO	846
Z. SHEN	941
K. SHIH	935
J. SILBERMAN	935
D. SLATER	1A38
E.I. SOLOMON	1022
J. SOLOMON	1023
W.E. SPICER	935,941
P. STEVENS	1023
S. SUBRAMANIAM	1029
L. TAKIFF	846
G. TIMOTHY	1A38
G.P. VALENCA	1071
S. WAKATSUKI	970,1005
G.A. WAYCHUNAS	964,994,995, 999,1050, 1051
M.D. WILLIAMS	935
L.C. WILSON	849
J. WOICIK	935
J.J. YEH	935
H.D. ZEMAN	1046

STEVENS INSTITUTE OF TECHNOLOGY

G.M. ROTHBERG	897

TEXAS A&M UNIVERSITY

D.A. CHURCH	1052

UCSC/ICFS

G. BUNKER	961,1006, 1007,1043
B. CHANCE	961,1006, 1007,1042, 1043
S.M. KHALID	1006,1007, 1043
G. ROSENBAUM	1006,1007

UNIVERSITY OF ALABAMA-BIRMINGHAM

W.J. COOK	1A49
S. EALICK	1A49

UNIVERSITY OF ARIZONA

W. CLELAND	1030
J. ENEMARK	1030

UNIVERSITY OF CALIFORNIA

F.G. BRIDGES	1017
B.K. BURGESS	965
B. CLARK	1018
D.S. CLARK	1057
B.E.C. DAVIS	1018
D. DE FONTAINE	1018
B. DEVOS	1A54,1A56
W.A. DOLLASE	964
J.J. HOYT	849,1018
Z.-Q. HUANG	943
C. KANG	1A55
S. KIM	943
S.-H. KIM	1A54,1A55, 1A56
M. KRAITCHMAN	1018
T. LEUNG	943
S. LIU	943
G.A. MARG	1057
P. MATIAS	1A54,1A56
L. MEDHURST	943
M. MILBURM	1A54,1A56
A. MITRA	1005
B. NIU	0943
M.A. OLMSTEAD	958,959
J. PANDIT	1A54,1A56
K. RAYMOND	906
C.R. ROSS	964
R.M. STROUD	1005
L. TONG	1A54,1A55, 1A56
L. WANG	943
X.-S. ZHANG	943

UNIVERSITY OF CHICAGO

R.H. FAIRCLOUGH	1012
C. LAWSON	1A59
Z. OTWINOWSKI	1A59
D. RICHMAN	1012
R.W. SCHEVITZ	1A59
D. SCOTT	1A59
P.B. SIGLER	1A59

UNIVERSITY OF CINCINNATI

P. BOOLCHAND	1032
E.A. DEUTSCH	991
R.C. ELDER	806,922,991, 1066
W.R. HEINEMAN	806,1066
K. TEPPERMAN	922

UNIVERSITY OF COLORADO

N.A. CLARK	1010
G. SMITH	1010

UNIVERSITY OF HAWAII

M.H. MANGHNANI	1059,1064
L.C. MING	1059,1064

UNIVERSITY OF ILLINOIS

M. EIDSNESS	1041
W. KAPLAN	992
R.A. SCOTT	761,966,969, 992,993,1039, 1041,1053, 1067

UNIVERSITY OF KENTUCKY

G.P. HUFFMAN	956

UNIVERSITY OF MICHIGAN

D.P. BALLOU	1035
O. BARALT	1031
C.J. BATIE	1035
M.D. CURTIS	1031
W.D. FRASCH	1003
V.L. PECORARO	1003
J.E. PENNER-HAHN	1003,1031, 1033,1035, 1050
L. THOMPSON	1031
H.-T. TSANG	1035
G. WALDO	103323

UNIVERSITY OF NEBRASKA

L. PARKHURST	1006,1007

UNIVERSITY OF NEVADA

W.N. CATHEY	972
N. SALIBI	972

UNIVERSITY OF NEW MEXICO

T. BEIN	1070
B.C. CHAKOUMAKOS	1049
R.C. EWING	754,1049
R.F. HAAKER	754
K. MOLLER	1070

UNIVERSITY OF OREGON

G.B. ARMEN	1036
B. CRASEMANN	1036
B.W. MATTHEWS	1A57
S. RODERICK	1A57
S.L. SORENSEN	1036
L. WEAVER	1A57
S.B. WHITFIELD	1036

UNIVERSITY OF PENNSYLVANIA

T.G. FREY	1039
R. LOBRUTTO	1007
A. NAQUI	961,1043
E.W. PLUMMER	810
T. YONETANI	990
G. ZHANG	1006,1043
Y. ZHOU	961,1007

UNIVERSITY OF PUERTO RICO

L. BLUM	1020

UNIVERSITY OF SOUTH FLORIDA

L.S. SOLMONSON	1030

UNIVERSITY OF SOUTHERN CALIFORNIA

W.K. WARBURTON	849,1008

UNIVERSITY OF VIRGINIA

E. SINN	978

UNIVERSITY OF WASHINGTON

J. FREUND	1047
B. HOUSER	982
R.L. INGALLS	100,982,983, 984,1047
M. LAUCKS	983
L.B. SORENSEN	1034
E.A. STERN	906,960,1068
P. VIRAN	100
J.E. WHITMORE	100

UNIVERSITY OF WISCONSIN

S.L. COOPER	975
Y.S. DING	975

WASHINGTON UNIVERSITY

P.H. BETHGE	971
L. LIM	971,1019
F.SCOTT MATHEWS	971,1019
N. SHAMALA	971

WESTERN REGIONAL RSCH. CTR.

S.F. GHELLER	1055
W.E. NEWTON	1055

XEROX

J. ALLEN	1028
R.Z. BACHRACH	908,958,959
J.B. BOYCE	868,1017
R.D. BRINGANS	908,958,959
J.C. MIKKELSON	1017
J.E. NORTHRUP	908

SSRL EXPERIMENTERS AND PROPOSALS BY INSTITUTIONS
FOREIGN INSTITUTIONS

CHALMERS INSTITUTE OF TECHNOLOGY(Sweden)
T. CLAESON 868

CNRS(France)
P. GIBART 1038

ISTITUTO DI FISICA DEL POLITECNICO(Italy)
I. ABBATI 941
M. SANCROTTI 941

ISTITUTO DI STRUTTURA DELLA MATERIA(Italy)
F. COMIN 857,947

KAROLINSKA INSTITUTE(Sweden)
B.-M. SJOBERG 1043

KING'S COLLEGE(England)
M. HART 1021

LINKOPING UNIVERSITY(Sweden)
R.I.G. UHRBERG 908,958,959

LKB(Sweden)
A. GAAL 970

MEDICAL NOBEL INSTITUTE(Sweden)
P. REICHARD 1043

SIMON FRASER UNIVERSITY(Canada)
N. ALBERDING 100,982
K.R. BAUCHSPIESS 100,984
D. CROZIER 100,982,983, 984,1047
A.J. SEARY 100

UNIVERSITA DI MILAN(Italy)
L. BRAICOVICH 941

UNIVERSITA DI MODENA(Italy)
O. BISI 941
C. CALANDRA 941
U. DEL PENNINO 941

UNIVERSITA DI ROMA(Italy)
S. NANNARONE 941

UNIVERSITAT BIELEFELD(Germany)
W. JITSCHIN 1036
U. WERNER 1036

UNIVERSITAT BONN(Germany)
G. WILL 1021

UNIVERSITE DE PARIS-SUD(France)
A. FONTAINE 849

UNIVERSITY DEL ZULIA(Venezuela)
J. SANCHEZ ARRIETA 833

UNIVERSITY OF DORTMUND(Germany)
U. BONSE 979

UNIVERSITY OF SHEFFIELD(England)
P. HARRISON 906

UNIVERSITY OF SUSSEX(England)
B.E. SMITH 1030

UNIVERSITY OF SYDNEY(Australia)
H.C. FREEMAN 1004

WEIZMANN INSTITUTE(Israel)
J.G. GILBOA 960

XIII PUBLICATIONS BASED ON WORK AT SSRL

The following is a partial list of papers published or submitted in 1986 based on work at SSRL. The list represents 236 publications.

Abbati, I., Braicovich, L., Carbone, C., Nogami, J., Lindau, I., del Pennino, U., **"Synchrotron Radiation Study of the Photoionization Cross Section for the Whole Valence Band of 2H-MoS(2)"**: J Electron Spectrosc Relat Phenom 37, 389 (1986)

Abbati, I., Braicovich, L., Carbone, C., Nogami, J., Lindau, I., Iandelli, A., Olcese, G.L., Palenzona, A., **"Photoemission Studies of Si(111)-Yb Interface: What Can Be Learned from Mixed Valence"**: to be published

Abbati, I., Braicovich, L., del Pennino, U., Carbone, C., Nogami, J., Yeh, J.J., Lindau, I., **"Photoemission Spectroscopy of Yb(3)Si(5) and its Connection with Si-4b Interfaces"**: Phys Rev B 34, 4150 (1986)

Abbati, I., Braicovich, L., Carbone, C., Nogami, J., Lindau, I., Johansson, L.I., Majni, G., **"Combination of L(2),(3) and M(2),(3) X-ray Absorption Spectra in Electron States Studies of Heavy d-Metal Silicides: The Case of PtSi"**: to be published

Abbati, I., Braicovich, L., Carbone, C., Nogami, J., Lindau, I., Iandelli, I., Olcese, G., Palenzona, A., **"Photoemission Studies of Mixed Valence in Yb Yb(3)Si(5), YbSi, and Yb(5)Si(3): Equivalent Versus Inequivalent Yb Sites"**: to be published

Alberding, N., Crozier, E.D., Ingalls, R., Houser, B., **"Focussed Multiple Scattering in Compressed ReO(3)"**: submitted J Phys

Allen, J.W., Allen, J.W., Oh, S.J., Gunnarsson, O., Schonhammer, K., Maple, M.P., Torikachvilli, M.S., Lindau, I., **"Electronic Structure of Ce and Light Rare Earth Intermetallics"**: Adv Phys 35, 275 (1986)

Allen, J.W., Kang, J.-S., Lassailly, Y., Maple, M.B., Torikachvilli, M.S., Ellis, W., Pate, B., Lindau, I., **"Electron Spectroscopy Study of the Heavy Fermion Compound URU(2)Si(2)"**: accepted Solid State Comm

Arvanitis, D., Dobler, U., Wenzel, L., Baberschke, K., Stohr, J., **"Position of sigma-Shape and pi-Resonances of C(2)H(2), C(2)H(4) and C(2)H(6) on Cu(100) at 60K: A NEXAFS Study"**: Surf Sci 178, 686 (1986)

Bachrach, R.Z., Bringans, R.D., Pate, B.B., Carr, R.G., **"The SSRL Insertion Device Beam Line "Wunder"**: SPIE 582, 251 (1986)

Bahr, C.C., Barton, J.J., Hussain, Z., Robey, S.W., Tobin, J.G., Shirley, D.A., **"Geometry of (2x2)S/Cu(001) Determined using Angle-Resolved Photoemission Extended Fine Structure"**: submitted Phys Rev B

Bahr, C.C., Robey, S.W., Hussain, Z., Terminello, L.J., Leung, K.T., Lou, J-R, Schach von Wittenau, A.E., Shirley, D.A., **"Chemisorption Geometry of c(2x2)S/Mo(001) Determined with Angle-Resolved Photoemission Extended Fine Structure"**: submitted Phys Rev B

Barton, J.J., Bahr, C.C., Robey, S.W., Hussain, Z., Umbach, E., Shirley, D.A., **"Adsorbate Geometry Determination by Measurement and Analysis of ARPEFS Data: Application to c(2x2)S/Ni(001)"**: Phys Rev B34, 3807 (1986)

Barton, J.J., Robey, S.W., Shirley, D.A., **"Theory of Angle-Resolved Photoemission Extended Fine Structure"**: Phys Rev B 34, 778 (1986)

Bauchspiess, K.R., Crozier, E.D., Ingalls, R., **"High Pressure Studies of SmSe at 77K"**: submitted J Phys

Beard, B.C., Ross, P.N., **"Characterization of a Titanium-Promoted Supported Platinum Electrocatalyst"**: submitted J Electrochem Soc

Beard, B.C., Ross, P.N., **"The Structure and Activity of Pt-Co Alloys as Oxygen Reduction Electrocatalysts"**: submitted J Electrochem Soc

Beard, B.C., Ross, P.N., **"Pt-Ti Alloy Formation from High Temperature Reduction of a Titania Impregnated Pt Catalyst: Implication for SMSI"**: submitted J Phys Chem

Becker, U., Kerkhoff, H.G., Lindle, D.W., Kobrin, P.H., Ferrett, T.A., Heimann, P.A., Truesdale, C.M., Shirley, D.A., **"Orbital-collapse Effects in Photoemission from Atomic Eu"**: Phys Rev A 34, 2858 (1986)

Bertness, K.A., Friedman, D.J., Mahowald, P.H., Yeh, J.J., Wahi, A.K., Lindau, I., Spicer, W.E., **"Oxygen Chemisorption on GaAs (110): Surface or submitted surface Growth"**: J Vac Sci Technol B4, 1102 (1986)

Bertness, K.A., Kendelewicz, T., List, R.S., Williams, M.D., Lindau, I., Spicer, W.E., **"Fermi Level Pinning During Oxidation of Atomically Clean n-InP (110)"**: J Vac Sci Technol A4, 1424 (1986)

Bohr, J., Gibbs, D., Moncton, D.E., D'Amico, K.L., **"Spin Slips and Lattice Modulations in Holmium: A Magnetic X-Ray Scattering Study"**: Phys A 16, (1986)

Bonse, U., **"High Resolution Tomography with Chemical Specificity"**: Nucl Instrum & Methods A246, 644 (1986)

Boudart, M., Samant, M.G., Ryoo, R., **"Atomic and Electronic Strucuture and Chemical Reactivity of Metal Clusters"**: Ultramicroscopy 20, 125 (1986)

Boxer, S.G., Bucks. R.R., **"Fluorescence Lifetimes with a Synchrotron Source"**: Methods in Enzymology 130, 484 (1986)

Boyce, J.B., Mikkelsen, J.C., Bridges, F., Egami, T., **"Extended X-ray Absorption Fine-Structure Study of Quasicrystalline Al-Mn Alloys"**: Phys Rev B33, 7314 (1986)

Braicovich, L., Abbati, I., Carbone, C., Nogami, J., Lindau, I., **"Synchrotron Radiation Studies of the Effect of Thermal Treatment on the Si (111)-Yb Interfaces"**: Surf Sci 168, 193 (1986)

Brennan, S., Fuoss, P.H., Eisenberger, P., **"X-ray Crystallographic Studies of Pb Monolayers on Cu(110) Surfaces"**: Phys Rev B 33, 1986

Brennan, S., Cowan, P.L., Jach. T., LaVilla, R., Perera, R.C.C., Winick, H., **"Optical and Spectral Characteristics of an Insertion Device Used Both As a Wiggler and an Undulator"**: Nucl Instrum Methods A246, 37 (1986)

Brennan, S., **"Surface Structure Analysis using Grazing Incidence X-ray Scattering"**: SPIE 690, 124 (1986)

Bringans, R.D., Uhrberg, R.I.G., Bachrach, R.Z., **"Surface and Bulk Electronic Structure of Ge(111) c (2x8) and Ge(111):As 1x1"**: Phys Rev B34, 2373 (1986)

Bringans, R.D., Uhrberg, R.I.G., Olmstead, M.A., Bachrach, R.Z., Northrup, J.E., **"Model Semiconductor Surfaces: Arsenic Termination of the Ge(111), Si(111), and Si(100) Surfaces"**: accepted Physica Scripta

Bringans, R.D., Uhrberg, R.I.G., Olmstead, M.A., Bachrach, R.Z., **"Surface Bands for Single-Domain 2x1 Reconstructed Si(100) and Si(100):As: Photoemission Results for Off-Axis Crystals"**: Phys Rev B34, 7447 (1986)

Bringans, R.D., Uhrberg, R.I.G., Bachrach, R.Z., Northrup, J.E., **"Surface Band Dispersion of Ge(111)c(2x8) and Ge(111):As 1x1"**: J Vac Sci Technol A4, 1380 (1986)

Brion, C.E., Lindle, D.W., Heimann, P.A., Ferrett, T.A., Piancastelli, M.N., Shirley, D.A., **"Photoelectron Branching Ratios and Partial Photoionization Cross Sections for Production of the (2a(1))(-1) State of H(2)O up to 200 eV"**: Chem Phys Lett 128, 118 (1986)

Brown, G.S., **"The PEP Beam Line"**: Nucl Instrum Methods A246, 147 (1986)

Carbone, C., Nogami, J., Lindau, I., Abbati, I., Braicovich, L., Johansson, L.I., Majni, G., **"X-Ray Absorption Spectroscopy of Pt Silicides: The L(2),(3) and M(2),(3) Edges of Pt"**: Thin Solid Films 140, 105 (1986)

Carbone, C., Nogami, J., Lindau, I., **"Chemisorption of Gd on Si (111): A Photon Energy Dependent Photoemission Study"**: to be published

Carr, R.G., **"Near Edge X-ray Absorption Fine Structure Spectroscopy in Materials Analysis"**: SPIE 690, 38 (1986)

Carr, R.G., **"A New Ultrahigh Vacuum Cleaver for Brittle Materials"**: submitted Rev Sci Instrum

Chance, B., Schick, D., Hettel, R., Powers, L., **"Beam Intensity and Position Compensation Circuits"**: Nucl Instrum Methods A246, 400 (1986)

Chin, K.K., Kendelewicz, T., Newman, N., Lindau, I., Spicer, W.E., **"Chemical Reaction at the In on GaAs (110) Interface"**: J Vac Sci Technol B4, 955 (1986)

Chin, K.K., McKernan, P., Lindau, I., **"Design of an Ultra Low Coverage Metal Evaporator Based on a Geometric Factor"**: J Vac Sci Technol A4, 1949 (1986)

Chin, K.K., Kendelewicz, T., McCants, C., Cao, R., Miyano, K., Lindau, I., Spicer, W.E., **"Kinetic Study of Schottky Barrier Formation of In on GaAs (110) Surface"**: J Vac Sci Technol A 4, 969 (1986)

Coffer, M.T., Shaw, C.F., Eidsness, M.K., Watkins, J.W., Elder, R.C., **"On the Reactions of Auranofin and Et(3)PAuCl with Bovine Serum Albumin"**: Inorg Chem 25, 333 (1986)

Cole, J., Yachandra, V.K., Guiles, R.D., McDermott, A.E., Britt, R.D., Dexheimer, S.L., Sauer, K., Klein, M.P., **"Assignment of the g=4.1 EPR Signal to Manganese in the S2 State of the Photosynthetic Oxygen-Evolving Complex: An X-Ray Absorption Edge Spectroscopy Study"**: submitted Acta

Cox, L.E., Ellis, W.P., Cowan, R.D., Allen, J.W., Oh, S.-J., Lindau, I., Pate, B.B., Arko, A.J., **"Valence-Band Photoemission in UO(2)(111) Near the 5d Resonant Photon Energy"**: submitted Phys Rev B

Cramer, S.P., Flank, A-M, Weininger, A., Mortenson, L.E., **"Single Crystal EXAFS of Nitrogenase"**: J Am Chem Soc 108, 1049 (1986)

Cramer, S.P., Pan, W.-H., Eidsness, M.K., Morton, T., Ragsdale, S., DerVartanian, D.V., Ljungdahl, L.G., Scott, R.A., **"X-Ray Absorption Characterization of Clostridium Thermoaceticum CO Dehydrogenase. Evidence for a Unique Nickel Environment"**: submitted Inorg Chem

Dawson, J.H., Kau, L-S, Penner-Hahn, J.E., Sono, M., Eble, K.S., Bruce, G.S., Hager, L.P., Hodgson, K.O., **"Oxygenated Cytochrome P-450-CAM and Chloroperoxidase: Direct Evidence for Sulfur Donor Ligation Trans to Dioxygen and Structural Characterization using EXAFS Spectroscopy"**: accepted J Am Chem Soc

Del Pennino, U., Nannarone, S., Braicovich, L., Abbati, I., Rossi, G., Lindau, I., **"Optical Corrections in the Measurements of Photoionization Cross Sections from Solids in the Soft X-ray Range"**: J Electron Spectros Relat Phenom 37, 389 (1986)

Dewald, H.D., Watkins, J.W., Heinemann, W.R., Elder, R.C., **"Development of Extended X-ray Absorption Fine Structure Spectroelectrochemistry and Its Aqueous Solution"**: Anal Chem 58, 2968 (1986)

DiGennaro, R., **"Predicting Thermal Distortion of Synchrotron Radiation Mirrors with Finite Elements Analysis"**: SPIE 582, 582 (1985)

Dimon, P., Sinha, S.K., Weitz, D.A., Safinya, C.R., Smith, G.S., Varady, W.A., Lindsay, H.M., **"The Structure of Aggregated Gold Colloids"**: submitted Phys Rev Lett

Doniach, S., Chin, K.K., Lindau, I., Spicer, W.E., **"Microscopic Metal Cluster and Schottky Barrier Formation"**: to be published

Duivenvoorden, F.B.M., Koningsberger, D.C., Uh, Y.S., Gates, B.C., **"Structures of Alumina-Supported Osmium Clusters [HOs(3)(CO)(10){OAl}] and Complexes [Os(II)(CO)(n=2 or 3){OAl}]. Determined by Extended X-ray Absorption Fine Structure Spectroscopy"**: accepted J Am Chem Soc

Eberhardt, W., Plummer, E.W., Chen, C.T., Carr, R., Ford, W.K., **"New Experiments Using a Soft X-ray Undulator"**: Nucl Instrum Methods A 246, 825 (1986)

Eberhardt, W., Plummer, E.W., Lyo, I.W., Reiniger, R., Carr, R., Ford, W.K., Sondericker, D., **"Auger-electron Ion Coincidence Studies to Determine the Pathways in Soft X-ray Induced Fragmentation of Isolated Molecules"**: submitted Aus J Phys

Eidsness, M.K., Sullivan, R.J., Schwartz, J.R., Hartzell, P.L., Wolfe, R.S., Flank, A.-M., Cramer, S.P., Scott, R.A., **"Structural Diversity of F(430) from Methanobacterium Thermoautotrophicum. A Nickel X-Ray Absorption Spectroscopic Study"**: J Am Chem Soc 108, 3120 (1986)

Eidsness, M.K., Flank, A-M, Smith, B.E., Flood, A.C., Garner, C.D., Cramer, S.P., **"EXAFS of Klebsiella pneumoniae Nitrogenase Mo-Fe Protein from Wild-type and nifv Mutant Strains"**: J Am Chem Soc 108, 2746 (1986)

Elder, R.C., Watkins, J.W., III , **"Structure of Trichloro(diethylene-triamine) gold (III), Au(dien)Cl(3), "Determined by Single-Crystal X-ray Diffraction, Raman, and EXAFS Spectroscopies: an EXAFS Caveat"**: Inorg Chem 25, 223 (1986)

Ellis, W.P., Albers, R.C., Allen, J.W., Lassailly, Y., Kang, J.-S., Pate, B.B., Lindau, I., **"Valence-Band Densities of State in NiAs"**: submitted Solid State Commun

Fairclough, R.H., Stroud, R.M., Miake-Lye, R.C., Hodgson, K.O., Doniach, S., **"Terbium/Calcium Binding Sites on the Acetylcholine Receptor"**: submitted NY Acad Sci

Feldman, J.L., Skelton, E.F., Ehrlich, A.C., Dominquez, D.D., Qadri, S.B., Elam, T., Lytle, F., **"Polarized X-ray Absorption Studies of Graphite Intercalated Bromine Compounds"**: Phys Rev B 33, 7961 (1986)

Ferrett, T.A., Lindle, D.W., Heimann, P.A., Kerkhoff, H.G., Becker, U.E., Shirley, D.A., **"Sulfur 1s Core-Level Photoionization of SF(6)"**: Phys Rev A34, 1916 (1986)

Fischer, D.A., Hastings, J.B., Zaera, F., Stohr, J., Sette, F., **"X-ray Fluorescence Proportional Counter for SEXAFS Studies"**: Nucl Instrum Methods 246, 561 (1986)

Fischer, D.A., Dobler, U., Arvanitis, D., Wenzel, L., Baberschke, K., Stohr,J., **"Carbon K Edge Structure of Chemisorbed Molecules by Means of Fluorescence Detection"**: Surf Sci 177, 114 (1986)

Frank, P., Hedman, B., Carlson, R.M.K., Tyson, T.A., Roe, A.L., Hodgson, K.O., **"A Large Reservoir of Sulfate and Sulfonate Resides within Vanadocytes from Ascidia Ceratodes, Revealed by X-ray Absorption Spectroscopy"**: in press Biochemistry

Frank, P., Carlson, R.M.K., Hodgson, K.O., **"Vanadyl Ion EPR as a Non-invasive Probe of pH in Intact Vanadocytes"**: Inorg Chem 25, 470 (1986)

Friedman, D.J., Carey, G.P., Lindau, I., Spicer, W.E., Wilson, J.A., **"Role of Hg Bonding in Metal/Hg(1-x)Cd(x)Te Interface Formation"**: J Vac Sci Technol B4 980, (1986)

Friedman, D.J., Carbone, C., Bertness, K.A., Nakamura, H., Cao, R., Lindau, I., **"Resonant Photoemission at the 5p Threshold in La, Pr, Sm, and Tb"**: J Electron Spectrosc Relat Phenom 41, 59 (1986)

Friedman, D.J., Carey, G.P., Lindau, I., Spicer, W.E., Wilson, J.A., **"Effect of Diffent Cation-Anion Bond Strengths on Metal-Ternary-Semiconductor Interface Formation": Cu/Hg(0.75)Cd(0.25)Te and Cu/CdTe"**: Phys Rev B34, 5329 (1986)

Friedman, D.J., Carey, G.P., Shih, C.K., Lindau, I., Spicer, W.E., Wilson, J.A., **"Diffusion of Ag and Hg at the Ag/(Hg,Cd)Te Interface"**: Appl Phys Lett 48, 44 (1986)

Friedman, D.J., Carey, G.P., Lindau, I., Spicer, W.E., Wilson, J.A., **"Overlayer-Cation Reaction at the Pt/Hg(1-x)Cd(x)Te Interface"**: to be published

Friend, C.M., Stevens, P.A., Serafin, J.G., Baldwin, E.K., Madix, R.J., **"Bonding and Absorption Structure of CO on W(100)-(5x1)-C"**: submitted J Chem Phys

George, G.N, Winge, D., Stout, C.D., Cramer, S.P., **"X-Ray Absorption Studies of the Copper-Beta Domain of Rat Liver Metallothionein"**: J Inorg Biochem 27, 213 (1986)

Giauque, R.D., Jaklevic, J.M., Thompson, A.C., **"Trace Element Determination Using Synchrotron Radiation"**: Anal Chem 58, 940 (1986)

Gibbs, D., Carey, G.P., Shih, C.K., Lindau, I., Spicer, W.E., Wilson, J.A., **"The Ag/(Hg,Cd)Te Interfaces"**: J Vac Sci Technol A 4, 1977 (1986)

Gibbs, D., Bohr, J., Axe, J.D., Moncton, D.E., D'Amico, K.L., **"Magnetic Structure of Erbium"**: submitted Rapid Comm

Guiles, R.D., Yachandra, V.K., McDemott, A.E., Britt, R.D., Cole, J., Dexheimer, S.L., Sauer, K., Klein, M.P., **"The Effect of Hydroxylamine on the Mn-Containing Oxygen Evolving Complex of Photosystem II from Spinach: An X-Ray Absorption Study"**: submitted

Guiles, R.D., Yachandra, V.K., McDermott, A.E., Britt, R.D., Dexheimer, S.L., Sauer, K., Klein, M.P., "Evidence for a Tetranuclear Manganese Cluster in the Photosynthetic Oxygen Evolving Complex. An EXAFS Analysis": submitted

Hahn, S., Wong, C-C. D., Ponce, F.A., Rek, Z.U., "Interaction Between Deposited Film Extrinsic Gettering and Intrinsic Gettering in CZ Silicon During Simulated CMOS Process Cycles": submitted MRS

Hamada, H., Samant, M.G., Boudart, M., "X-Ray Absorption Spectroscopy of Silica-Supported Ir-Ru Bimetallic Cluster": Chem Lett 6, 885 (1986)

Hart, M., Parrish, W., Masciocchi, N., "Studies of Texture in Thin Films Using Synchrotron Radiation and Energy Dispersive Diffraction": submitted

Hecht, M.H., Grunthaner, F.J., Pate, B.B., Pianetta, P., Engelhardt, M., Jansen, W., Bryson, C., "Soft X-Ray Photoemission with the SSX-100 Spectrometer": Nucl Instrum Methods A246, 806 (1986)

Hedman, B., Co, M-S, Armstrong, W.H., Hodgson, K.O., Lippard, S.J., "EXAFS Studies of Binuclear Iron Complexes as Models for Hemerythrin and Related Proteins": Inorg Chem 25, 3708 (1986)

Hedman, B., Frank, P., Penner-Hahn, J., Roe, A, Hodgson, K., Carlson, R., Brown, G., Cerino, J., Hettel, R., Troxel, T., et al, "Sulfur K-edge X-ray Absorption Studies Using the 54-Pole Wiggler at SSRL in Undulator Mode": Nucl Instrum Methods A246, 797 (1986)

Hitchcock, A.P., Horsley, J.A., Stohr, J., "Inner Shell Excitation of Thiophene and Thiolane: Gas, Solid and Monolayer States": J Chem Phys 85, 4835 (1986)

Hogrefe, H., "Application of Spherical Gratings in Synchrotron Radiation Spectroscopy": to be published

Hoyt, J.J., Lyon, O., Simon, J.P., Clark, B., Davis, B.E.C., de Fontaine, D., "The Determination of Partial Structure Functions in an Al-Zn-Ag Alloy": Solid State Commun 57, 155 (1986)

Huang, T.C., Hart, M., Parrish, W., Masiocchi, N., "Line Broadening Analysis of Synchrotron X-ray Diffraction Data": accepted Jour Appl Phys

Huffman, G.P., Huggins, F.E., Shoenberger, R.W., Walker, J.S., Lytle, F.W., Greegor, R.B., "Investigation of the Structural Forms of Potassium in Coke by Electron Microscopy and X-ray Absorption Spectroscopy": FUEL 65, 621 (1986)

Huffman, G.P., Huggins, F.E., "Reactions and Transformations of Coal Mineral Matter at Elevated Temperatures": ACS 301, 100 (1986)

Huffman, G.P., Huggins, F.E., Jenkins, R.G., Piotrowski, A., Lytle, F.W., Greegor, R.B., "Investigation of Alkali and Alkaline Earth Coal Gasification Catalysts by EXAFS Spectroscopy": in press FUEL

Hughes, E.B., Rubenstein, E., Zeman, H.D., Brown, G.S., Buchbinder, M., Harrison, D.C., Hofstadter, R., Kernoff, R.S., Otis, J.N., Thompson, A.C., **"The Angiography Program at Stanford"**: Nucl Instrum Methods A246, 719 (1986)

Ingalls, R., Crozier, E.D., Seary, A.J., **"X-ray Absorption Spectrum of Compressed Copper"**: Physica 139/140B, 505 (1986)

Ingalls, R., Crozier, E.D., Bauchspiess, K.R., Houser, B., **"High Pressure EXAFS Study of SmSc"**: Bull Am Phys Soc 31, 499 (1986)

Ismail, A., Ben Brahim, A., Lassabatere, L., Lindau, I., **"A Study of the Electronic Properties of Cleaved InP Surfaces Induced by Oxygen Exposures"**: J Appl Phys 59, 485 (1986)

Ismail, A., Ben Brahim, B., Palau, J.M., Lassabatere, L., Lindau, I., **"The Interaction of Ag, In, and Al Overlayers with InP (110)": Surface and Diode Studies of the Effect of Indium Interlayers"**: J Vac Sci Technol 36, 217 (1986)

Jiang, D., Alberding, N., Seary, A.J., Crozier, E.D., **"A Reflectivity and EXAFS Study of Layered Structures"**: submitted J Phys
erding, N., Seary, A.J., Crozier, E.D., **"A Reflectivity and EXAFS Study of Layered Structures"**: submitted J Phys

Johnson, R.W., Price, D.L., Susman, S., Arai, M., Morrison, T.I., Shenoy, G.K., **"The Structure of Silicon-Selenium Glasses: I. Short Range Order"**: J Non-Cryst Solids 83, 251 (1986)

Kalkowski, G., Kaindl, G., Brewer, W.D., Krone, W., **"Near Edge X-ray Absorption Fine Structure in Uranium Compounds"**: submitted Phys Rev B

Kallne, E., Tatchyn, R.O., Csonka, P.L., Lindau, I., **"Applications of Transmission X-ray Optics"**: Nucl Instrum Methods A 246, 327 (1986)

Kau, L.S., Solomon, E.I., Hodgson, K.O., **"XANES/EXAFS Study of the Copper Active Site in Methanol Synthesis Catalyst"**: accepted J Phys

Kau, L.S., Spira-Solomon, D.J., Penner-Hahn, J.E., Solomon, E.I., Hodgson, K.O., **"X-ray Absorption Edge Determination of the Oxidation State and Coordination Number of Cu: Application to the T3 Site in Lacceptedase and its Reaction with Oxygen"**: submitted J Am Chem Soc

Kau, L.S., Penner-Hahn, J.E., Solomon, E.I., Hodgson, K.O., **"Quantitative Cu X-Ray Absorption Edge Studies: Oxidation State and Site Structure Determination"**: accepted J Phys

Kau, L.S., Svastits, E.W., Dawson, J.H., Hodgson, K.O., **"Iron-Sulfur Bond Length in Ferrous-Co Heme Complexes as a Function of Sulfur Donor Type"**: Inorg Chem 25, 4307 (1986)

Kau, L.S., Svastits, E.W., Sono, M., Dawson, J.H., Hodgson, K.O., **"EXAFS Study of Active Intermediates: Heme Enzymes and Model Compounds"**: accepted J Phys

Kendelewicz, T., Williams, M.D., Chin, K.K., McCants, C.E., List, R.S., Lindau, I., Spicer, W.E., **"Temperature Dependent Pinning at the Al/n-GaAs (110) Interface"**: Appl Phys Lett 48, 919 (1986)

Kendelewicz, T., Newman, N., Williams, M.D., Lindau, I., Spicer, W.E., **"A Spectroscopic and Electrical Study of the Pd/GaAs Interface"**: to be published

Kendelewicz, T., List, R.S., Lindau, I., **"Frenkel Exciton Induced Resonant Photoemission at the In 4d Edge of InP(110)"**: Phys Scripta

Kendelewicz, T., List, R.S., Bertness, K.A., Williams, M.D., Lindau, I., Spicer, W.E., **"Photoemission Study of the Reactive Pd/Inp (110) Interface"**: J Vac Sci Technol B4, 959 (1986)

Kendelewicz, T., List, R.S., Williams, M.D., Bertness, K.A., Lindau, I., Spicer, W.E., **"Soft X-ray Photoemission Study of Co/n-InP (110) Interface"**: Phys Rev B 34, 558 (1986)

Kendelewicz, T., Mahowald, P.H., Bertness, K.A., McCants, C.E., Lindau, I., Spicer, W.E., **"Surface Shifts in the In 4d and 2p Core Level Spectra of InP (110)"**: to be published

Kinney, J.H., **"The Performance of CCD Array Detectors for Application in High-Resolution Tomography"**: SPIE 691, 43 (1986)

Kip, B.J., Duivenvoorden, F.B.M., Koningsberger, D.C., Prins, R., **"Determination of Metal Particle Size of Highly Dispersed Rh, Ir, and Pt Catalysts by Hydrogen Chemisorption and EXAFS"**: J Am Chem Soc 108, 5633 (1986)

Klebanoff, L.E., Shirley, D.A., **"Surface Dependence of the Cr(001) 3s Photoemission Line Shape"**: Phys Rev B 33, 5301 (1986)

Klebanoff, L.E., Robey, S.W., Liu, G., Shirley, D.A., **"Photoelectron Spectroscopy Studies of Cr(001) Near-Surface and Surface Magnetism"**: J Magn Magn Mater 54, 728 (1986)

Koningsberger, D.C., Martens, R.H.A., Prins, R., Short, D.R., Sayers, D.E., **"The Structure of a Rh/TiO(2) Catalyst in the Sms I State as Determined by EXAFS"**: J Phys Chem 90, 3047 (1986)

Lassailly, Y., Allen, J.W., Ellis, W., Cox, L., Pate, B., Fisk, Z., Lindau, I., **"Electron Spectroscopy Study of the Heavy Fermion Compound U(2)Zn(17)"**: accepted J MMM

Levin, J.C., Sorensen, S.L., Crasemann, B., Chen, M-H, Brown, G.S., **"Krypton L-MM Auger Spectra": New Measurements and Analysis"**: Phys Rev A 33, 968 (1986)

Lindau, I., **"Concluding Remarks - International Conference on the Formation of Semiconductor Interfaces"**: Surf Sci 168, 860 (1986)

Lindau, I., Kendelewicz, T., **"Schottky Barrier Formation on III-V Semiconductor Surfaces: A Critical Evaluation"**: Crit Rev Solid State Mater Sci 13, 27 (1986)

Lindau, I., **"Interfacial Properties of Metal Overlayers on III-V Compounds"**: to be published

Lindle, D.W., Heimann, P.A., Ferrett, T.A., Kobrin, P.H., Truesdale, C.M., Becker, U., Kerkhoff, H.G., Shirley, D.A., **"Photoemission from the 3d and 3p Shells of Kr"**: Phys Rev A 33, 319 (1986)

Lindle, D.W., Ferrett, T.A., Heimann, P.A., Shirley, D.A., **"Increasing Quantum Yield of Sodium Salicylate Above 80 eV Photon Energy: Implications for Photoemission Cross Sections"**: Phys Rev A 34, 1131 (1986)

Lindle, D.W., Heimann, P.A., Ferrett, T.A., Kobrin, P.H., Truesdale, C.M., Becker, U., Kerkoff, H.G., Shirley, D.A., **"Photoemission from the 3d and 3p subshells of Kr"**: Phys Rev A 33, 319 (1986)

List, R.S., Woicik, J., Mahowald, P.H., Lindau, I., Spicer, W.E., **"The Si/GaAs (110) Heterojunction Discontinuity: Amorphous Versus Crystalline Overlayers"**: to be published

Lorentz, R.D., Bino, A., Penner-Hahn, J.E., **"Differential Anomalous X-ray Scattering Evidence for the Existence of m-H(3)(O) (2)(-) Bridging Ligands in Solution"**: accepted J Am Chem Soc

Lytle, N.W., Eatough, D.J., Hansen, L.D., Hill, M.W., Mangelson, N.F., Lytle, F.W., Greegor, R.B., McCarthy, G.J., Glasser, P.F., Roy, D.M., **"Identification of Chemical Compounds in Fly Ash by X-ray Absorption Spectroscopy & Proton Induced X-ray & Gamma-Ray Emission Analysis: in Fly & Coal Conversion By-Products: Characterization, Utilization"**: Mat Res Soc Symp Proc 65, 141 (1986)

McDermott, A.E., Yachandra, V.K., Guiles, R.D., Britt, R.D., Dexheimer, S.L., Sauer, K., Klein, M.P., **"The State of Iron and Manganese in the Photosynthetic Apparatus Determined by X-Ray Spectroscopy"**: submitted Springer

McDermott, A.E., Yachandra, V.K., Guiles, R.D., Britt, R.D., Dexheimer, S.L., Sauer, K., Klein, M.P., **"The S1 and S2 States of Manganese in the Oxygen-Evolving Complex from Synechococcus. Similarities to Spinach"**: submitted

Moncton, D.E., Gibbs, D., Bohr, J., **"Magnetic X-ray Scattering with Synchrotron Radiation"**: Nucl Instrum Methods A246, 839 (1986)

Montano, P.A., Shenoy, G.K., Alp, E.E., Schulze, W., Urban, J., **"Structure of Copper Microcluster Isolated in In Solid Argon"**: Phys Rev Lett 56, 2076 (1986)

Moon, D.W., Cameron, S., Zaera, F., Eberhardt, W., Carr, R., Bernasek, S.L., Dwyer, D.J., **"A Titled Precursor for CO Dissociation on the Fe(100) Surface"**: submitted Sur Sci Ltr

Newman, N., Spicer, W.E., Kendelewicz, T., Lindau, I., **"On the Fermi Level Pinning Behavior of Metal/III-V Semiconductor Interfaces"**: J Vac Sci Technol B4 931 (1986)

Newton, W.E., Schultz, F.A., Gheller, S.F., Lough, S., McDonald, J.W., Conradson, S.D., Hedman, B., Hodgson, K.O., **"Iron-Molybdenum Cofactor of Azotobacter Vineladii Nitrogeanse": Oxidation-Reduction Properties and Structural Insights"**: Polyhedron 5, 567 (1986)

Newton, W.E., Gheller, S.F., Schultz, F.A., Burgess, B.K., Conradson, S.D., McDonald, J.W., Hedman, B., Hodgson, K.O., **"Redox and Compositional Insights into the Iron-Molybdenum Cofactor of Azotobacter Vineladii Nitrogenase as a Guide to Synthesis of New Mo-Fe-S Clusters"**: submitted Intl Symp

Nogami, J., Kendelewicz, T., Lindau, I., Spicer, W.E., **"Binding Energy Shifts from Alloying at Metal/Compound-Semiconductor Interfaces"**: Phys Rev B34, 669 (1986)

Nogami, J., Williams, M.D., Kendelewicz, T., Lindau, I., Spicer, W.E., **"Chemical Reaction and Anion Trapping at the Yb/GaAs (110) Interface"**: J Vac Sci Technol A 4, 808 (1986)

Nogami, J., Lindau, I., **"Rare Earth Metal/Semiconductor Interface Formation"**: to be published

Nogami, J., Carbone, C., Friedman, D.J., Lindau, I., **"The Electronic Structure of the Yb/Ge (111) Interface"**: Phys Rev B 33, 864 (1986)

Olmstead, M.A., Uhrberg, R.I.G., Bringans, R.D., Bachrach, R.Z., **"Arsenic Overlayer on Si(111): Removal of Surface Reconstruction"**: Phys Rev B34, 6041 (1986)

Olmstead, M.A., Uhrberg, R.I.G., Bringans, R.D., Bachrach, R.Z., **"Initial Formation of the Interface Between a Polar Insulator and a Nonpolar Semiconductor: CaF2 on Si(111)"**: J Vac Sci Technol B4, 1123 (1986)

Olmstead, M.A., Uhrberg, R.I.G., Bringans, R.D., Bachrach, R.Z., **"Photoemission Study of Bonding at the CaF(2)-on-Si(111)"**: accepted Phys Rev B

Outka, D.A., Madix, R.J., **"Structural Characterization of Molecules and Reaction Intermediates on Surfaces Using Synchrotron Radiation"**: submitted Surf Sci

Outka, D.A., Stohr, J., Rotermund, H.H., Madix, R.J., Solomon, J., Hermsmeier, B., **"NEXAFS Studies of Complex Alcohols and Carboxylic Acids on the Si(111)(7x7) Surface"**: to be published Surf Sci (1987)

Parrish, W., Hart, M., Huang, T.C., **"Synchrotron X-ray Polycrystalline Diffractometry"**: J Appl Cryst 19, 92 (1986)

Parrish, W., Hart, M., **"Parallel Beam Powder Diffractometry Using Synchrotron Radiation"**: Material Science Forum 9, 39 (1986)

Parrish, W., Hart, M., Erickson, C.G., Masciochhi. N., Huang, T.C., **"Instrumentation for Synchrotron X-ray Powder Diffractometry"**: Adv in X-ray Anal 29, 243 (1986)

Pate, B.B., **"The Diamond Surface": Atomic and Electronic Structure":** Surf Sci 165 (1986)

Penner-Hahn, J.E., Smith, T.A., Hedman, B., Hodgson, K.O., Doniach, S., **"Polarized X-ray Absorption Near Edge Structure":** accepted J Phys

Penner-Hahn, J.E., Eble, K.S., Dawson, J.H., Hodgson, K.O., **"Structural Characterization of High Valent Intermediates in Horseradish Peroxidase":** accepted J Phys

Penner-Hahn, J.E., Eble, K.S., McMurry, T.J., Renner, M., Balch, A.L., Groves,J.T., Dawson, J.H., Hodgson, K.O., **"Structural Characterization of Horseradish Peroxidase using EXAFS Spectroscopy. Evidence for Fe=O Ligation in Compounds I and II":** J Am Chem Soc 108, 7819 (1986)

Penner-Hahn, J.E., Benfatto, M., Hedman, B., Takahashi, T., Doniach, S., Groves, J.T., Hodgson, K.O., **"Polarized X-ray Absorption Near-Edge Structure of Highly Oxidized Chromium Porphyrins":** Inorg Chem 25, 2255 (1986)

Petro, W.G., Kendelewicz, T., Lindau, I., Spicer, W.E., **"The Au-GaAs (110) Interface: Photoemission Studies of the Effects of Temperature":** Phys Rev B 34, 7089 (1986)

Phizackerley, R.P., Cork, C.W., Merritt, E.A., **"An Area Detector Data Acquisition System for for Protein Crystallography Using Multiple-Energy Anomalous Dispersion Techniques":** Nucl Instrum Methods A246, 579 (1986)

Pianetta, P., Redaelli, R., Jaeger, R., Barbee, T.W., **"X-Ray Lithography at the Stanford Synchrotron Radiation Laboratory":** Nucl Instrum Methods A246, 641 (1986)

Pianetta, P., Barbee, T.W. Jr., Redaelli, R., **"Performance of Layered Synthetic Microstructures in Monochromator Applications in the Soft X-Ray Region":** Nucl Instrum Methods A246, 352 (1986)

Prince, R.C., Savas, J.C., George, G.N., Cramer, S.P., Patel, R.N., **"Spectroscopic Properties of Hydroxolase of Methanemonooxygenase":** submitted BPA

Qadri, S.B., Skelton, E.F., Webb, A.W., Kennedy, J., **"The Effect of Zn and Mn on Cd-Te Bond Strength in Cd(1-x)Zn(x)Te and Cd(1-x) Mn(x)Te":** Physica 139-140B, 341 (1986)

Qadri, S.B., Elam, W.T., Ayers, J.D., Vold, C.L., Skelton, E.F., Webb, A.W., **"Rapid EDXD Studies of Isothermal Crystallization of Metallic Glasses":** Nucl Instrum Methods A246, 817 (1986)

Qadri, S.B., Skelton, E.F., Webb, A.W., Kennedy, J., **"Structural Studies of Cd(0.95)Zn(0.05)Te and Cd(0.90)Mn(0.10)Te":** J Vac Sci Technol 4, 1971 (1986)

Robey, S.W., Barton, J.J., Bahr, C.C., Liu, G., Shirley, D.A., **"An ARPEFS Investigation of c(2x2) S/Ni(001)":** submitted Phys Rev B

Robey, S.W., Bahr, C.C., Hussain, Z., Leung, K.T., Lou, J., Schach von Witenau, A.E., Shirley, D.A., **"The Surface Structure of (2x2) S/Ge(111) Determined Using ARPEFS"**: submitted Phys Rev B

Robinson, I.K., Waskiewicz, W.K., Fuoss, P.H., Stark, J.B., Bennett, P.A., **"X-ray Diffraction Evidence of Adatoms in the Si(111)7x7 Reconstructed Surface"**: Phys Rev B 33, 7013 (1986)

Robinson, I.K., **"Symmetry of the Si(111)7x7 at an a-Si Interface"**: submitted Phys Rev B

Robinson, I.K., Waskiewicz, W.K., Tung, R.T., Bohr, J., **"Ordering at Si(111)/a-Si and Si(111)/SiO(2) Interfaces"**: Phys Rev Lett 57, 2714 (1986)

Rowen, M., Waldhauer, A., Pianetta, P., **"Crystal Heating on the Jumbo Double Crystal Monochromator at SSRL"**: Nucl Instrum Methods A246, 440 (1986)

Rubenstein, E., Hofstadter, R., Zeman, H.D., Thompson, A.C., Otis, J.N., Brown, G.S., Giacomini, J.C., Gordon, H.J., Kernoff, R.S., Harrison, D.C., Thomlinson, W., **"Transvenous Coronary Angiography in Humans using Synchrotron Radiation"**: Natl Acad Sci (USA) 83, 9724 (1986)

Safinya, C.R., Roux, D., Smith, G.S., Sinha, S.K., Dimon, P., Clark, N.A., Bellocq, A.M., **"Steric Interactions in a Model Multimembrane System: A Synchrotron Radiation X-ray Study"**: submitted Phys Rev Lett

Savborg, O., Schoonover, J.R., Lin, S.H., Eyring, L., **"Time-Resolved X-ray Diffraction Study of Decomposition of Cd(OH)(2) using Synchrotron Radiation"**: accepted Solid State Chem

Schiferl, D., Katz, A.I., Mills, R.L., Schmidt, L.C., Vanderborgh, C., Skelton, E.F., Elam, W.T., Webb, A.W., Qadri, S.B., Schaerfer, M., **"A Novel Instrument for High Pressure Research at Ultra-High Temperatures"**: Physica 139-140B, 897 (1986)

Schmitz, H.A., J.C. Bilello, Z.U. Rek, **"Energetics of Dislocation Relaxation Associated with Cleavage in Cd-doped Zn Crystals as Probed by Synchrotron Topography"**: Mater Sci Eng 81, 293 (1986)

Scott, R.A., Schwartz, J.R., Cramer, S.P., **"Structural Aspects of the Copper Sites in Cytochrome c Oxidase. An X-Ray Absorption Spectroscopic Investigation of the Resting-State Enzyme"**: Biochem 25, 5546 (1986)

Sette, F., Pearton, S.J., Rowe, J.E., Stohr, J., **"Local Structure of S Impurities in GaAs"**: Phys Rev Lett 56, 2637 (1986)

Shih, C.K., Friedman, D.J., Bertness, K.A., Lindau, I., Spicer, W.E., Wilson, J.A., **"Electron Beam Induced Hg Desorption and the Electronic Structure of the Hg Depleted Surface of Hg(1-x)Cd(x)Te"**: J Vac Sci Technol A4, 1997 (1986)

Short, R.T., O, C-S, Levin, J.C., Sellin, I.A., Liljeby, L., Huldt, S., Johansson, S-E, Nilsson, E., Church, D.A., **"Production of Very Low-Energy Highly Charged Ions by Synchrotron Radiation"**: Phys Rev Lett 56, 2614 (1986)

Sirota, E.B., Pershan, P.S., Amador, S., Sorensen, L.B., **"Synchrotron X-ray Observation of Surface Smectic-I Hexatic Layers on Smectic-C Liquid Crystal Films"**: to be published Phys Rev A (1987)

Skelton, E.F., Elam, W.T., Webb, A.W., Qadri, S.B., **"Magnetic Stirrer for Diamond-Anvil Cells"**: Physica 139-140B, 919 (1986)

Skelton, E.F., Qadri, S.B., Webb, A.W., Dinan, J., **"High Pressure Studies of Hg(0.8)Cd(0.2) Te"**: J Vac Sci Technol 4, 1974 (1986)

Skelton, E.F., **"Energy Dispersive Diffraction at Elevated Pressures using Synchrotron Radiation"**: Trans Am Cryst Assn 21, 33 (1986)

Skelton, E.F., Webb, A.W., Schaefer, M.W., Schiferl, D., Katz, A.I., Hochheimer, H.D., Qadri, S.B., **"X-ray Diffraction Studies Under Extremely Non-Ambient Conditions": Application to Transition Metal Dichalcogenide Solid Lubricants"**: Adv X-ray Anal 30, 1986

Skelton, E.F., Elam, W.T., Webb, A.W., Qadri, S.B., Schiferl, D., **"Energy Dispersive Spectroscopy using Synchrotron Radiation": Intensity Considerations"**: Physica 139-140B, 499 (1986)

Smith, T.A., Lerch, K., Hodgson, K.O., **"Structural Study of the Cu Sites in Metallothionein from Neurospora Crassa"**: Inorg Chem 25, 4677 (1986)

Spicer, W.E., Kendelewicz, T., Newman, N., Chin, K.K., Lindau, I., **"The Mechanisms of Schottky Barrier Pinning in III-V Semiconductors": Criteria Developed from Microscopic (Atomic Level) and Macroscopic Experiments"**: Surf Sci 168, 240 (1986)

Spiro, C.L., Wong, J., Lytle, F.W., Greegor, R.B., Maylotte, D.H., Lamson, S.H., **"Forms of Potassium in Coal and Its Combustion Products"**: Fuel 65, 327 (1986)

Tabe, M., Chiang, T.T., Lindau, I., Spicer, W.E., **"Initial Stage of Thermal Oxidation of the Si(111) 7x7 Surface"**: Phys Rev B34, 2706 (1986)

Tatchyn, R., Csonka, P., Kallne, E., Toor, A., Gillespie, C., Lindau, I., Fuller, A., **"Surface Heating in a Lacquer-Coated Mirror Irradiated with Undulator Light"**: SPIE 582, 291 (1986)

Tatchyn, R.O., Csonka, P.L., **"Attainment of submillimeter Periods and a 0.3 Tesla Peak Field in a Novel Micropole Undulator Device"**: submitted J App Phys

Templeton, D.H., Templeton, L.K., **"X-Ray Birefringence and Forbidden Reflections in Sodium Bromate"**: Acta Crystallogr A42, 478 (1986)

Teng, T.Y., Huang, H.W., **"Hemoglobin and Myoglobin Embedded in Dry Poly(vinyl alcohol) Film for X-ray Absorption Studies"**: Biochem Biophys Acta

Thompson, A.C., Zeman, H.D., Rubenstein, E., Otis, J.N., Hofstadter, R., Brown, G.S., Harrison, D.C., Kernoff, R.S., Giacomini, J.C., Gordon, H.J., Thomlinson, W., **"Transvernous Cornonary Angiography in Dogs Using Synchrotron Radiation"**: J Cardiac Imaging

Thompson, A.C., Wu, Y., Underwood, J.H., Barbee, T.W., **"Focusing of Synchrotron Radiation X-Ray Beams Using Synthetic Multilayer Mirrors"**: submitted NIM

Tranquada, J.M., Ingalls, R., **"X-ray Absorption Study of CuBr at High Pressure"**: Phys Rev B 34, 4267 (1986)

Tulkki, J., Armen, G.B., Aberg, T., Crasemann, B., Chen, M-H, **"Quantum Theory of Post-Collision Interaction in Inner-Shell Photoionization"**: accepted Z Physik D

Uhrberg, R.I.G., Bringans, R.D., Bachrach, R.Z., Northrup, J.E., **"Electronic and Atomic Structure of Arsenic Terminated Si(100)"**: J Vac Sci Technol A 4, 1259 (1986)

Uhrberg, R.I.G., Bringans, R.D., Olmstead, M.A., Bachrach, R.Z., **"Electronic Structure, Atomic Structure and the Passivated Nature of the Arsenic Terminated Si(111) Surface"**: accepted Phys Rev B

Uhrberg, R.I.G., Bringans, R.D., Bachrach, R.Z., Northrup, J.E., **"Symmetric Arsenic Dimers on the Si(100) Surface"**: Phys Rev Lett 56, 520 (1986)

Van't Blik, H.F.J., Koningsberger, D.C., Prins, R., "Characterization **of Bimetallic CoRh/SiO(2) Catalysts with TPR, TPO and EXAFS Spectroscopy"**: submitted J Catal

Vijay-Kumar, S., Senadhi, S.E., Ealick, S.E., Nagabhushan, T.L., Trotta, P.P., Kosecki, R., Reichert, P., Bugg, C.E., **"Crystallization and Preliminary X-Ray Investigation of a Recombinant Form of Human Gamma Interferon"**: in press J Bio Chem

Walton, J.T., Sommer, H.A., Thompson, A.C., Hughes, E.B., Zeman, H.D., **300-Element Silicon-Lithium Position-Sensitive Imaging Detector for Angiography"**: IEEE Trans NS-33, 537 (1986)

Warburton, W.K., Iwancyzk, J.S., Dabrowski, A.J., Hedman, B., Penner-Hahn, J.E., Roe, A.L., Hodgson, K.O., Beyerle, A., **"Development of Mercuric Iodide Detectors for XAS & XRD Measurements"**: Nucl Instrum Methods A 246, 558 (1986)

Warburton, W.K., Ludwig, K.F., Jr., **"Absorption Effects in the Determination of Anomalous Scattering Factors using X-ray Refraction through a Prism"**: Phys Rev B 33, 8424 (1986)

Watkins, J.W., Greene, B., Darnall, D.W., Elder, R.C., **"Determination of Gold Binding in an Algal Bi Biomass using EXAFS and XANES Spectroscopies"**: in press, Inorg Chem

Waychunas, G.A., Brown, G.E., Jr., Apted, M.J., **"X-ray K-edge Absorption Spectra of Fe Minerals and Model Compounds: II. EXAFS"**: Phys Chem Minerals 13, 31 (1986)

Weatherill, T.D., Rauchfuss, T.B., Scott, R.A., **"Structural Evidence Concerning the Frontier Orbitals in [Fe(2)E(2)CO(6)](2) E=S,Se": Redox Active Dichalcogen Ligands"**: Inorg Chem 25, 1466 (1986)

Webb, A.W., Skelton, E.F., Qadri, S.B., Cannon, J.F., **"Compressibility of Ni(3)In"**: Physica 139-140B, 311 (1986)

Whitfield, S., Carr, R.G., Armen, B., Sorensen, S.L., Levin, J.C., Crasemann, B., **"Four-Hole Final States in L-Shell Auger Decay of Ni and Cu"**: submitted Phys Rev A

Wiedemann, H., **"Design of Low Emittance Storage Rings Beam Choppers for Line-Scan"**: Nucl Instrum Methods A246, 4 (1986)

Will, G., Masciocchi, N., Parrish, W., Hart, M., **"Crystal Structure Refinement of Synchrotron Powder Diffraction Data"**: submitted

Williams, M.D., Nogami, J., Kendelewicz, T., List, R.S., Bertness, K.A., Lindau, I., Spicer, W.E. ,**"Yb/GaAs (110) Pinning Behavior of the the Rare Earth GaAs Interface"**: Solid State Commun 58, 15 (1986)

Winick, H., **"Present and Future Synchrotron Radiation Facilities in Japan"**: Nucl Instrum Methods A251, 177 (1986)

Wong, J., Slack, G.A., **"EXAFS and XANES Studies of Vanadium in Rhombohedral beta-Boron"**: J Solid State Chem 61, 203 (1986)

Wong, J., **"EXAFS: A Modern Structural Tool in Materials Science"**: Mat Sci & Eng 80, 107 (1986)

Y.-C. Lu, R.S. Feigleson, R.K. Route, Z.U. Rek, **"A Study of the Defect Structures in CdTe Crystals Using Synchrotron X-Ray Topography"**: J Vac Sci Technol A, Vol 4, 2190 (1986)

Yachandra, V.K., Guiles, R.D., McDermott, A.E., Cole, J., Britt, R.D., Dexheimer, S.L., Sauer, K., Klein, M.P., **"Comparison of the Structure of the Manganese Complex in the S1 and S2 States of the Photosynthetic Oxygen Evolving Complex: An X-Ray Absorption Spectroscopy Study"**: accepted Solid State Commun

Yachandra, V.K., Guiles, R.D., McDermott, A.E., Britt, R.D., Cole, J., Dexheimer, S.L., Sauer, K., Klein, M.P., **"The State of Manganese in the Photosynthetic Apparatus Determined by X-Ray Absorption Spectroscopy"**: accepted J Phys

Yeh, J.J, Nogami, J., Friedman, D.J., Cao, R., Hwang, J., Koch, S., Lindau, I., **"An Illustration on the Measurement of the Net Yield of the SSRL Beamline I-I Monochromator"**: Nucl Instrum Methods A246, 286 (1986)

Yeh, J.J., Bertness, K.A., Cao, R., Hwang, J., Lindau, I., **"Bonding Characteristics of the Ag/Si Interface Identified by the Energy Dependence of the Photoemission Cross Section"**: to be published

Zaanen, J., Sawatzky, G.A., Allen, J.W., **"The Electronic Structure and Band Gaps in Transition Metal Compounds"**: J Magn & Magn Mater 54, 607 (1986)

BOOKS AND CONFERENCE PROCEEDINGS

Bienenstock, A., "Stanford University Synchrotron Radiation Laboratory: Universities, Government, and Industries Strongly Linked" in Emerging National R&D and Management Trends, S. A. Johnson (edited) University Press of America, p. 145 (1986)

Bienenstock, A., "Next-Generation X-ray Synchrotron Radiation Facilities" in Communications on the Materials Science and Engineering Study Materials Research Society, 1986 pp. 119-122

Gewirth, A.A., Cohen, S.L., Solomon, E.I., "Spectroscopic Studies of Active Sites: Blue Copper and Electronic Structural Analogues" in Excited States and Reactive Intermediates: Photochemistry, Photophysics, and Electrochemistry, A.B.P. Lever (editor) ACS Symposium Series 307, June 1986

Lytle, F.W., Gland, J.L., Greegor, R.B.., Marques, E.C., Sandstrom, D.R., Horsley, J.A., Via, G.H., Sinfelt, J.H., "Determination of the Atomic and Electronic Structure of Platinum Catalysts by X-ray Absorption Spectroscopy" in Catalyst Characterization Science, Deviney, M.L. (editor) (American Chemical Society)

Lytle, F.W., Greegor, R.B. "Identification of Transition Metal Sites in Fused SiO(2) by X-ray Absorption Spectroscopy" in Defects in Glasses, Galeener, F. et al. (Materials Research Society, 1986)

Penner-Hahn, J.E., Hodgson, K.O. "X-Ray Absorption Spectroscopy of Iron Porphyrins" in Physical Bioinorganic Chemistry A.B.P. Lever and H.B. Gray (editors) (Addison Wesley, in press 1986)

Penner-Hahn, J.E., Hodgson, K.O., "Polarized X-ray Absorption of Biomolecules" in Structural Biological Applications of X-ray Absorption, Scattering and Diffraction, Bartunik, H.D. (editor) (Academic Press 1986. p. 35)

S. Hahn, "Effect of 450(o)C Thermal Annealing Upon Oxygen Precipitation in B-Doped C2 Si Wafers" in Defects in Semiconductor H.Y. von Bardeleben (editor) (Materials Sci Forum 10-12 1986))

Schiferl, D., Fritz, J.N., Katz, A.I., Skelton, E.F., Qadri, S.B., Ming, L.C., Manghnani, M.H., "Ultra-High Temperature Diamond-Anvil Cell for X-ray Diffraction: Application to the Comparison of the Gold and Tungsten High Temperature/High Pressure Scales" in High Pressure Research in Geophysics, S. Akimoto and M.H. Manghnani (editors)

Solomon, E.I., Gewirth, A.A., Cohen, S.L., "Recent Developments in Inorganic Spectroscopy" in Understanding Molecular Properties, A. E. Hansen et al (editors) (Reidel, Dordrecht)

Warburton, W.K., Ludwig, K.F., Wilson, L., Bienenstock, A., "Differential Anomalous X-ray Scattering Techniques for Determination of Liquid and Amorphous Structures" in Turnbull Symposium Proceedings (Materials Research Society, 1986)

Yeh, J.J., Friedman, D.J., Cao, R., Nogami, J., Lindau, I., "Oxidation Behavior of the divided 3 x divided 3 Ag and Au/Si (111) Surfaces at Room Temperature Studied by Photoemission" in Thin Films-Interfaces and Phenomena, R.J. Nemanich et al (editors) (MRS Symp Proc 54, North-Holland 1986) pp 605-610

☆U.S. GOVERNMENT PRINTING OFFICE: 1987 787 702/79153